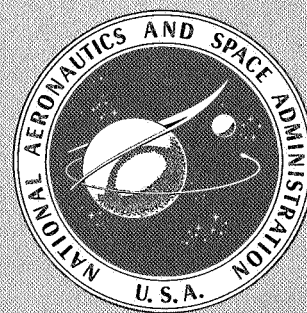# WAKE VORTEX

# MINIMIZATION

A symposium held at
WASHINGTON, D.C.
February 25–26, 1976

NATIONAL AERONAUTICS AND SPACE ADMINISTRATION

# WAKE VORTEX

# MINIMIZATION

*A symposium held at Washington, D.C.,
on February 25-26, 1976*

The long–lasting turbulence associated with trailing vortex systems of an aircraft in flight is a documented and demonstrated hazard to following aircraft, particularly if it is in the final approach to landing. Establishment of minimum separation distances between successive aircraft operations from airports has effectively reduced the hazard, but at the expense of reduced runway utilization rates at high–traffic–density air terminals and of increased aircraft operating costs. These safety considerations and resulting limitations in airport utilization, which will become more severe in the years ahead with the projected growth of aircraft sizes and aircraft traffic, have led organizations such as the Department of Transportation, Federal Aviation Administration (FAA), National Transportation Safety Board, Aircraft Owners and Pilots' Association, and the Air Transport Association of America to declare that wake turbulence is a major operational problem, particularly in the final approach and landing phase of aircraft operation.

In response to an urgent FAA request for assistance on the problem, NASA intensified its ongoing wake vortex research program in the summer of 1972 to seek a solution at the source (i.e., through aerodynamic means), both through the development of workable devices that could be applied to existing aircraft and through new design considerations for future aircraft. The immediate objective of the intensified effort was to report to the FAA early in 1974 as to whether such a solution appeared feasible. NASA's assessment of the situation would then be an important consideration in the decision the FAA subsequently would make as to the necessity for developing and installing wake monitoring and avoidance systems at major airports around the country.

Guided by available background studies, the coordinated and focused program performed at several of the NASA Centers investigated the effectiveness of such aerodynamic schemes as spoilers, vortex generators, trailing drag devices, steady and pulsed mass injection, and span load variations. The effectiveness of the schemes was determined by vortex velocity measurements

and flow visualization techniques (e.g., hot wire, laser Doppler, hydrogen bubble, and smoke flow), as well as by measurements of the rolling moment imposed on an aircraft model positioned at various distances behind the wake of the generator aircraft model. Tests were completed in various NASA ground facilities (such as the 7- by 10-ft, vertical short takeoff and landing, and 40- by 80-ft wind tunnels in a specially constructed towing facility), in a number of contractor water channels, and in flight operations.

By January 1974, work had progressed to the point where NASA was able to state that it was guardedly optimistic that an aerodynamic solution was feasible; i.e., that it was possible to eliminate the wake vortex hazard as a constraint to airport operations by new aerodynamic designs or by retrofit modifications to large transport aircraft.

Since that time, further understandfng of the phenomenon has been gained, and a number of the more promising approaches have been explored in more detail. Although a "final" solution is not yet in hand, the progress that has been made is most encouraging and the program is continuing. The purpose of the symposium is to summarize and document the progress made thus far.

Alfred Gessow
*Chief, Fluid and Flight Dynamics*
*NASA Headquarters*

CONTENTS

# INTRODUCTION

### Alfred Gessow
### NASA Headquarters

On behalf of NASA, I would like to welcome you and to extend our hope that you will find the sessions informative and worthwhile.

The large turnout we see here for a technical conference on a narrow subject area is a measure of the impact the vortex turbulence problem has had on all of the groups involved in air transportation— including the Department of Transportation, the Federal Aviation Administration **(FAA),** the aircraft manufacturers, the airline operators, the pilots' organizations, the traveling public, the National Transportation Safety Board (NTSB), and, of course, on NASA itself, whose mission is to provide technical information for problems such as the one that concerns us today.

The purpose of my remarks is to-try to set the stage for the technical program that follows; that is, to clarify the relation of the vortex minimization work which we will be discussing to the total problem of wake vortex turbulence, to review briefly the significance of the problem as it relates to various aspects of aircraft operations, and, finally, to describe the structure of the conference agenda *so* that it will be more coherent and useful.

Although the primary impact of the wake vortex problem is not safety, as such, the cause of the problem lies, of course, in the hazard potential of trailing vortexes, as shown in figure 1. The hurricanelike air motions associated with the long–lived, invisible, vortex–wake system trailing behind an aircraft in flight are a real hazard to an aircraft encountering the system. The severity of the hazard is dependent on the size, geometry, and operating conditions of the generator and following aircraft; the distance between the

two aircraft; the angle and altitude of encounter; the atmospheric conditions existing at the time; and perhaps on other factors of which we are not aware.

It is of interest to examine the severity of the safety problem. Some answers are provided by the results of an FAA-funded study of aviation accidents that occurred over the 10-year period from 1964-73, using NTSB data. The results of the study, which does not cover "near-miss" cases or military accidents, show that "probable vortex-related accidents" constitute less than one-half percent of all single aircraft accidents; that the vortex problem has been largely confined to small-weight (less than 5700 kg (12 500 lb)) general aviation aircraft operating under visual flight rules (VFR) conditions; that landing behind another landing aircraft on the same runway was the most frequent cause of vortex-related accidents, with the problem concentrated close to the touchdown zone (within about 1070 m (3500 ft) of the runway); that the takeoff/takeoff condition (with both aircraft starting their roll from the threshold) seems to be free of the vortex problem; and that there were no IFR landing accidents when full IFR separations were provided.

A prime reason for the extremely small accident rate is the FAA-imposed instrument flight rules (IFR) separation standards and the increasing awareness of the wake vortex problem on the part of operating personnel in both VFR and IFR conditions. Until March 1970, 9-km (5-n.-mi.) separation distances were required for nonheavy aircraft (less than 140 Mg (300 000 lb)) following heavy aircraft (greater than or equal to 140 Mg (300 000 lb)), and 5½ km (3 n. mi.) for all other separations. These distances have recently (March 1976) been increased as shown in table 1, with the maximum being an 11-km (6-n.-mi.) separation distance for small aircraft following a heavy aircraft.

Although separation standards seem to be adequate from a safety point of view, they significantly reduce current airport operating capacities and impose costly delays affecting the airlines and the general public. The penalties for continuing with the present separation standards will become increasingly severe in the years ahead, with the projected growth in air traffic operating from essentially the same number of airports as we have today.

TABLE 1.— Terminal Radar Minimum Separatioii

| Type of following aircraft | Generator | | | | | |
|---|---|---|---|---|---|---|
| | Small[a] | | Large[b] | | Heavy[c] | |
| | Separation | | | | | |
| | Kilometers | Nautical miles | Kilometers | Nautical miles | Kilometers | Nautical miles |
| Small. ▪ ▪ ▪ | 5½ | 3 | 7 | 4 | 11 | 6 |
| Large. ▪ ▪ ▪ | 5½ | 3 | 5½ | 3 | 9 | 5 |
| Heavy. ▪ ▪ ▪ | 5½ | 3 | 5½ | 3 | 5 | 4 |

Some quantitative measures of the penalties imposed by wake vortex separation distances have been generated in a recent economic study for FAA. Shown in table 2 is the effect of different spacings and mixes in terms of landings per hour on a single runway. If standard 5½-km (3-n.-mi.) IFR radar spacing is assumed to provide 30 operations per hour at full capacity of the runway, then capacity would be cut by a third with 9-km (5-n.-mi.) separation between all aircraft. If a 13-km (7-n.-mi.) separation were to be applied —

TABLE 2.— Effect of Aircraft Spacing on Single Runway Arrival Capacity

| Operations per hour | Spacing | |
|---|---|---|
| | Kilometers | Nautical miles |
| 40 . . . . . . . . . . . . . ▪ | All 4 | All 2 |
| 30 . . . . . . . . . . . . . ▪ | All 5½ | All 3 |
| 28[a]. ▪ . ▪ . ▪ . . ▪ . . . ▪ | 1.1 | 3/5 |
| 27[a]. ▪ . ▪ . . ▪ . ▪ . . . ▪ | .8 | 3/7 |
| 27[b]. . ▪ . ▪ . ▪ . ▪ . ▪ . ▪ | 1.1 | 3/5 |
| 25[b]. ▪ . ▪ . ▪ . ▪ . . . . ▪ | .8 | 3/7 |
| 20 . . . ▪ . . ▪ . . . ▪ . . ▪ | All 9 | All 5 |
| 16 . . . ▪ . . . . ▪ . . . . ▪ | All 13 | All 7 |

3

as has been proposed for certain circumstances — then capacity would be cut in half. Conversely, if spacing could be reduced to 4 km (2 n. mi.) ,then standard capacity could be increased by a third, and doubled with a 2.8-km (1.5-n.-mi.) spacing.

The same economic study showed the dollar and fuel savings that would result if the vortex-imposed 5%- to 9-km (3- to 5-n.-mi.) separation matrix could be replaced by a single 5½-km (3-n.-mi.) standard. The annual savings with 5½-km (3-n.-mi.) separation at one runway at Chicago-O'Hare Airport during the period from 1964 to 1973 are as follows:

(1) Airline cost savings:  $2½ million

(2) Airline fuel savings:  215 000 barrels

(3) Passenger cost savings: $5 million

Thus, as we are all aware, there are strong incentives to remove wake vortex turbulence as an impediment to air traffic operations in and about our airports. Figure 2 shows that the problem is being attacked in two ways. One approach is to alter the vortex pattern shed by the generator aircraft *so* that its effects on other aircraft would be minimal. NASA has the responsibility for this approach, following a request for help by FAA in the summer of 1972, and it is this program that is the subject of the present symposium.

The other approach, being pursued by the Department of Transportation (DOT) and FAA with some help from NASA, is to develop and install a wake vortex avoidance system that would increase runway capacity by varying the separation distance to conform to the aircraft and the meteorological condi- tions present. A complete system would involve many factors, such as the detection or prediction of the presence and strength of the vortexes present at a given time; an evaluation of the threat on the basis of vortex strength, location, and following aircraft characteristics; and the determination of the proper hazard avoidance action. Such a system would be complicated and costly. DOT is currently evaluating a much simpler and less costly approach that shows much promise; however, if the NASA minimization program is completely success- ful, then an avoidance system of any kind would not be needed. Nevertheless, it seems reasonable to pursue the technology for both programs in parallel *so*

that the relative cost/benefits can be evaluated on a rational basis.  The ultimate solution may involve a mix of both approaches.

The program for this symposium is divided into three parts.  First is a theoretical session that forms a basis for the experimental program.   The second part describes the experimental facilities and techniques used, and the third presents key experimental findings grouped according to technique. Although a great deal of research has been done on determining the character and behavior of vortexes, the emphasis in this symposium is on the practical effectiveness of schemes to minimize vortex effects on following aircraft.

In consonance with the safety statistics discussed earlier, the minimization work concentrates on the landing approach condition and on the effectiveness of the minimization schemes in reducing vortex effects on small, general aviation aircraft,   The symposium will conclude with a panel discussion on future prospects (not provided herein).
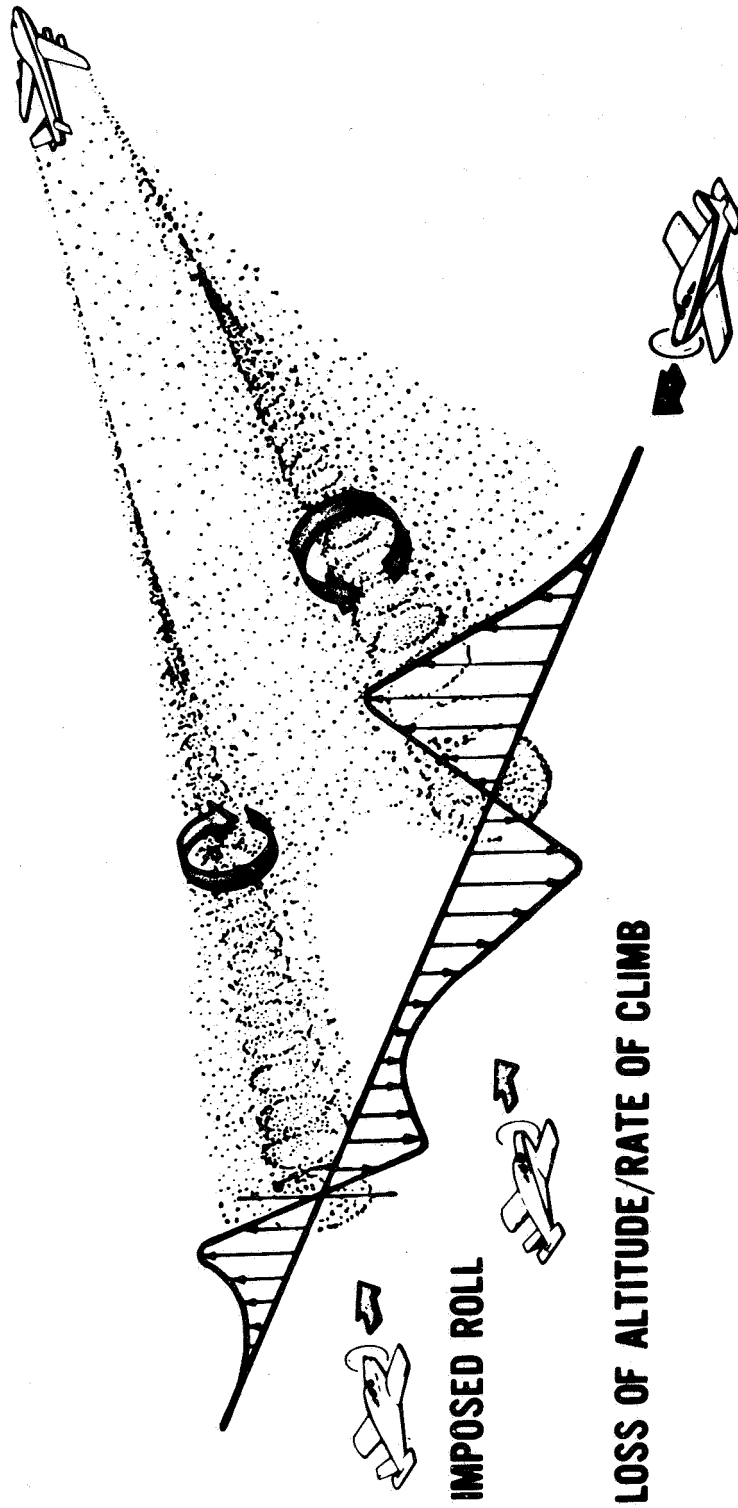
**STRUCTURAL LOAD FACTORS**

**IMPOSED ROLL**

**LOSS OF ALTITUDE/RATE OF CLIMB**

Figure     hazards of wake vortex encounters.

MINIMIZE
WAKE
VORTEX

DEVELOP
AVOIDANCE
SYSTEM

MINIMIZE
AND/OR
AVOID
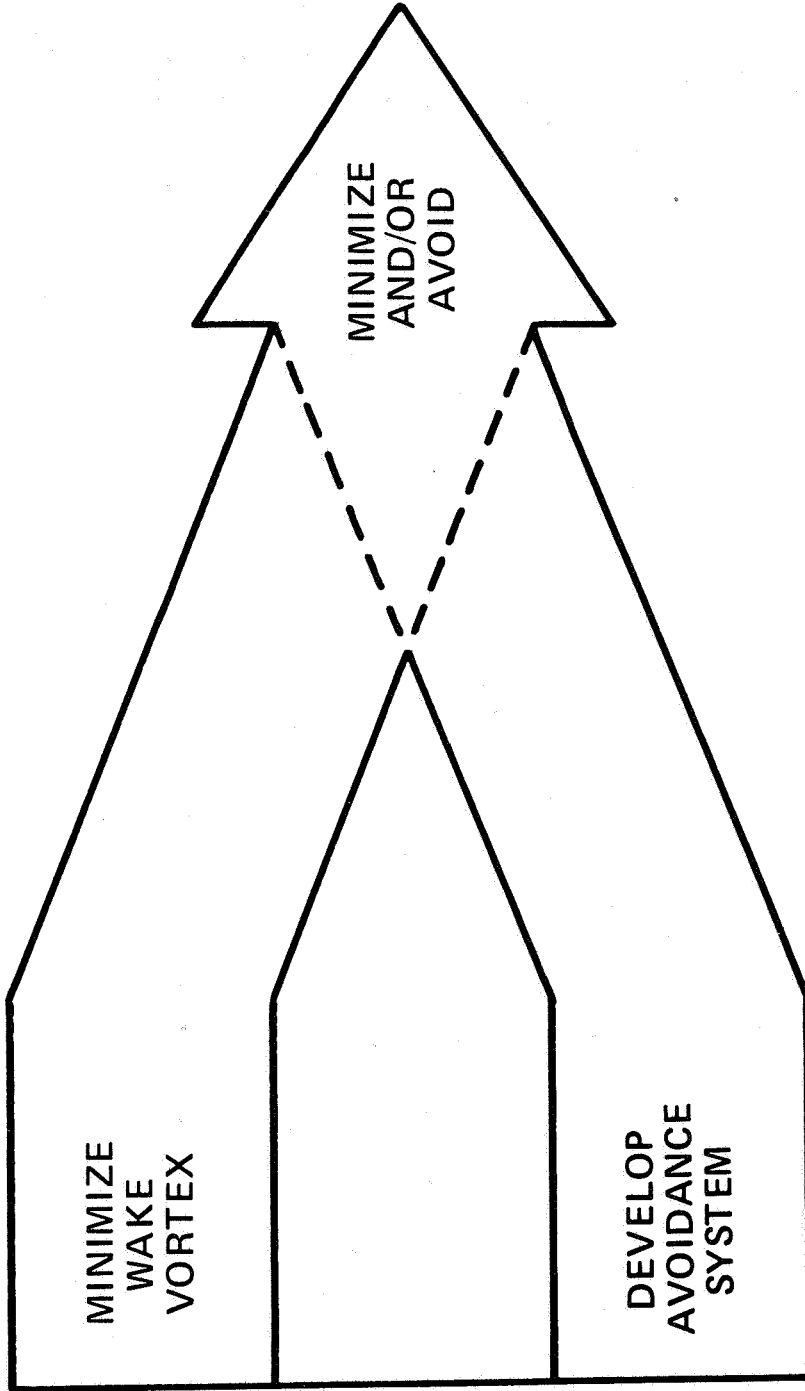
Figure 2 —Aircraft wake vortex program approach: remove impairment of wake vortex aircraft operation

# INVISCID MODELING OF AIRCRAFT TRAILING VORTICES

Vernon J. Rossow

Ames Research Center

## SUMMARY

A survey is presented of inviscid theoretical methods that have proven useful in the study of lift–generated vortices.  Concepts derived using these inviscid theories are then presented which have helped to guide research directed at alleviating the velocities and rolling moments imposed on aircraft entering these wakes.

## INTRODUCTION

The purpose of this conference is to present a status report on research directed at reducing the disturbances to the air behind aircraft as they fly through the atmosphere.  The objective of such a reduction is to minimize the hazard to smaller aircraft that might encounter these wakes.  The general guidelines given this research are that natural atmospheric motions be assumed negligible so that the alleviation schemes will be effective on calm days when the wakes are believed to be most persistent.  A further restriction is that the alleviation is to be achieved by aerodynamic means, hopefully to be accomplished by changes on the wake–generating aircraft that are easy to retrofit onto existing aircraft.

With these guidelines as a background, this paper first presents an overview of inviscid theoretical methods that have been found useful in the study of lift–generated wakes.  Several wake–alleviation schemes developed by use of inviscid theory are then described.  The effect of viscosity and turbulence on these theories is discussed only briefly to indicate the limits of applicability of some of the methods because a survey of theoretical methods that include viscosity and turbulence is the subject of the next paper.  The reader is directed to references 1–8 for other papers that review

9

and summarize research on vortices from a historical or technical point of view not restricted to alleviation.

<div align="center">NOMENCLATURE</div>

$\mathcal{R}$    . aspect ratio

b     span of wing

$C_L$     lift coefficient, $\dfrac{\text{lift}}{(1/2)\rho U_\infty^2 S}$

    local lift coefficient

$C_l$     rolling−moment coefficient, $\dfrac{\text{rolling moment}}{(1/2)\rho U_\infty^2 S b}$

c     wing chord

$\bar{c}$     mean geometric chord

$f(\Gamma_o/\nu)$     Iversen's Reynolds number function

$\ell(y)$     local lift

N     number of vortices

r     radius of vortex

S     wing area

T     dimensionless time $= \dfrac{4t\Gamma_o}{b^2}$

t     time

$U_\infty$     free−stream velocity; alined with x axis

$V_1$     maximum circumferential velocity in vortex

$v_\theta$     circumferential velocity in vortex

| X,Y,Z | dimensionless coordinates, for example, $X = \frac{2x}{b}$ |
|---|---|
| x,y,z | coordinates, x is streamwise and z is vertical |
| $a$ | angle of attack |
| $\Gamma$ | circulation |
| $\gamma$ | circulation in point vortices |
| $\nu$ | kinematic viscosity |
| $\rho$ | air density |

Subscripts

| f | following model that encounters wake |
|---|---|
| g | model that generates wake |
| o | centerline value of circulation |
| v | vortex |

## OVERVIEW OF FLOW FIELD

It is conyenient to divide the flow field into the several regions indicated in figure 1. The rollup region lies immediately behind the wake-generating aircraft where the wake character is changing rapidly with distance. because of self-induced distortions. The plateau region is that axial incre-ment of the wake where the vortices have a nearly constant structure. The decay region includes that part wherein substantial diffusion of vorticity occurs due to viscous and turbulence effects. Various vortex dispersion mechanisms such as vortex instabilities, bursting, or breakdown can occur in any of these three regions and their character may or may not depend on viscosity and turbulence. The boundaries of these regions are determined experimentally.

Since the wake is produced by the lead or wake-generating aircraft, any analysis of the lift-generated wake begins with and depends on the completeness and accuracy of the description of the flow field around the generator aircraft. This aspect of the wake-vortex problem has received considerable attention during the past several decades, but a general method is not yet available for finding the complete flow field in order to precisely define the initial conditions for the wake. However, very good approximations to the lift-distribution and wake-starting conditions may be obtained by use of inviscid vortex-lattice computer programs. The status of these methods can be found in references 9 to 12. Efforts are currently being made to include the effect of the rollup of the wake on the lift distribution (e.g., refs. 12-15). The comparisons in figure 2 (prepared by Maskew using the method of refs, 13 and 14) show that the rollup of the vortex sheet can affect the span loading substantially at the wing tips when the wing is at high angles of attack. The agreement of that prediction with the experimental span-loading measurements of Chigier and Corsiglia (ref. 16) is much better than the result obtained when the vortex wake is assumed to remain flat or in a plane without rolling up from its edges. Such a change in span loading has an effect on total lift, but the much larger effect appears in the distribution of vorticity in the wake. Caution should therefore be exercised when a flat wake is assumed in calculating the span loading on the generating wing because the loading gradients at the wing tip may not represent the correct concentration of vorticity. Most of the wind-tunnel studies at Ames Research Center were made at small angles of attack (i.e., $a \lesssim 12°$) so the accuracy of the flat wake approximation was adequate. For these calculations, a modified version of a program by Hough (ref. 17) was used.

Downstream of the generating aircraft, the vorticity shed by the lifting surfaces usually rolls up into two or more counterrotating (or pairs) vortices in the rollup region shown in figure 1. This process is approximated quite well by inviscid analyses, but as the wake ages (i.e., further downstream) viscosity and turbulence cause differences to increase between the inviscid result and the actual flow field. Flow processes that occur in the so-called rollup and plateau regions (discussed later) may be approximated

12

3

fairly well by inviscid theories, but the decay region requires more complete theories that include viscosity and turbulence.

The wake—vortex problem exists because, at some distance behind the generating aircraft, another aircraft may encounter the wake. The objective of this research program is to first evaluate the loads caused by the wake on this following aircraft and then to reduce them to a tolerable level by some sort of alleviation scheme. Although many types of encounter are possible, the NASA program concentrated on the axial penetration of the wake (indicated in fig. 1) because it seemed the most likely to happen during landing. The flow field over the follower induced by the wake is then approximated by the same inviscid steady—state theories used to model the generator, but an allowance must now be made for the nonuniform properties of the incoming airstream. Another section describes the theories used to analyze the flow over the follower and the comparisons made with experiment.

## WAKE ROLLUP

Several methods are discussed here for predicting how the vorticity distribution in the wake immediately behind the lift—generating surfaces changes from a nearly flat spanwise distribution into two circular regions of vorticity (fig. 3). This reshaping process is usually referred to as the rollup of the wake or vortex sheet shed by the wing. The methods and topics discussed now are:

- Two—dimensional time—dependent motion of point vortices
- Three—dimensional time—dependent motion of vortex filaments
- Direct— and inverse—rollup theories
- Plateau and decay regions for isolated vortex

Ideally, it would be desirable to treat the rollup of the distributed vorticity by a numerical scheme that includes the boundary layer on the wing, fuselage, and other surfaces along with the drag of the landing gear and the

thrust of the engines. Finite–difference methods for the two– and three–dimensional time–dependent aspects of the flow field are being developed and improved upon by several research groups with the hope that such a more complete analysis of the wake can be made. Although these more complex methods make it possible to more accurately represent the structure of the wake, they are not easy to use and require variable grid sizes and larger amounts of computer time. Since these methods usually include viscosity, they will not be discussed further here. Methods specifically designed for reducing wake velocities are discussed in another section.

### Two–Dimensional Time–Dependent Motion of Point Vortices

Since the velocity field of a point vortex is known in closed form, a simple representation of the wake is obtained by replacing the continuous distribution of vorticity with a distribution of point vortices that move with time. This method was applied to vortex sheets by Rosenhead (ref. 18) and Westwater (ref. 19) over 40 years ago and it has been used extensively since then to estimate the reshaping of the vorticity distribution in wakes with time or distance behind the generating wing. The analysis is carried out as a two–dimensional time–dependent problem in the so–called Trefftz plane (fig. 3). An example of an elliptically loaded wing is presented in figure 4 (taken from ref. 20). Estimating the wake restructuring by such a time–dependent method has two principal difficulties. The first is to assess the numerical accuracy of the calculations and the second is to interpret the results.

A variety of papers have elaborated on the shortcomings of the method and have introduced ways to remedy these shortcomings (e.g., refs. 21 to 27). These discussions generally agree that the spiral shape at the edges of vortex sheets is often not well simulated by the vortex array and that the point vortices sometimes undergo excursions believed to be associated with the vortex array and not with the vortex sheet being represented. Several methods have been introduced recently (refs. 25 to 27) to stabilize these vortex motions and to eliminate the excursions believed not to be a part of the vortex–sheet structure. Although these techniques suppress vortex excursions

and sheet kinking, they also introduce another error source. The use of finite cores in the vortices suggested by Chorin **and** Bernard (ref. 25) and Kuwahara and Takami (ref. 26) or the accumulation of vortices at the center of the spiral as suggested by Moore (ref. **27**) all contain arbitrary parameters not related to the conservation equations for the fluid they are to represent. The computed results may then appear more reasonable than those obtained from point vortices, but the quantitative accuracy is uncertain. Finite vortex cores instead of point vortices were used in some of the cases analyzed, and the vortex motions were smoothed. The qualitative nature of the solutions was found not to change if the core radius chosen for the vortices was less than the initial spacing of the vortices. However, the vortex motions were found to depend on the core size chosen. Another method has recently been introduced by Maskew (ref. 14) which enables an improved representation of continuous vortex sheets by breaking the primary discrete vortices used in the representation into subvortices when and where needed.

*Numerical accuracy* - The motion of a number of two-dimensional point vortices in an incompressible fluid is a problem for which numerical calculations are known to be unstable; consequently, any initial error grows with each time step. Fbr this reason, the calculations are usually begun with a large number of significant figures (double precision on most computers) in the hope that the desired result can be achieved before accumulated errors wipe out all the accuracy. It is also essential that the accuracy or error accumulation be monitored during the calculafions to detect an inappropriate choice of mesh size or excessive error growth. For example, Westwater (ref. 19) used the first moment of vorticity as an indicator of accuracy. When suitable error monitors are used, it is possible to determine whether seemingly unrealistic results are attributable to numerical error or to properties of the vortex array being analyzed.

Three error monitoring parameters are used in the calculations made at Ames:

(1)  The first moment of vorticity for each side (to reduce the likeli-
hood of compensating errors due to symmetry):

$$\bar{y}\Gamma_o = \bar{y} \sum_{j=1}^{N/2} \gamma_j = \sum_{j=1}^{N/2} y_j \gamma_j \tag{1}$$

(2)  The second moment of vorticity  **J**  about the center of gravity for
the vortices on each side:

$$J = \sum_{j=1}^{N/2} \left[ \left( y_j - \bar{y} \right)^2 + \left( z_j - \bar{z} \right)^2 \right] \gamma_j \tag{2}$$

(3)  The Kirchhoff–Routh path function  $W_r$  for the entire array of
vortices (e.g., ref. 28):

$$W_r = \sum_{i=1}^{N-1} \sum_{j=i+1}^{N} \left( \frac{\gamma_i \gamma_j}{4\pi} \right) \ln \left[ \left( y_i - y_j \right)^2 + \left( z_i - z_j \right)^2 \right] \tag{3}$$

Note that none of these quantities are used in the time–dependent calculations
nor do they depend on the numerical integration scheme used.   They are period-
ically evaluated (usually after every 10 or 20 steps) to ascertain how much
error has accumulated in the positions of the assembly of vortices.   It was
found that the Kirchhoff–Routh path function was the first to indicate the
presence of errors in the calculat'ions and that the first moment of vorticity
was hardly ever affected; that is, the first moment is the least sensitive of
the three accuracy monitors.   When enough significant figures are retained
in the results to cover the plotting accuracy, the gross aspects and trends
of the vortex sheet observed in various experiments appear to be modeled
correctly.

*Interpretation* of *data* – The interpretation of the point vortex distribu-
tion in terms of a continuous distribution is not straightforward.   A tech-
nique  from reference 20 provided a vortex structure when a group of point
vortices in the wake were known to be associated with a given rotational
motion, for example, vortices on one side of an elliptically loaded wing.

16

Within each such group, the distribution of point vortices was first reinterpreted as a stepwise radial distribution of circulation about the centroid of vorticity for one side of the wing. This was done by assuming that the vorticity associated with a point vortex in the array is spread uniformly on a ring with a radius equal to the distance of the vortex from the centroid. As indicated in figure 5, the resulting stepwise curve for circulation as a function of radius agrees quite well with the variation predicted by Betz' theory (refs. 29 and 30) for elliptic loading even though rollup is not entirely completed (fig. 4(b)). A faired curve through the stepwise variation could then be used to determine the circumferential velocity distribution in the vortex.

An interpretation difficulty does not arise, however, in those situations wherein the observation point lies well outside the vortical region. For example, representation of the wakes of most conventional aircraft in the far field by two point or line vortices is quite adequate for determining their motion in the presence of the ground and a crosswind. Comparisons of theoretical positions measured for vortices (e.g., refs. 31–35) and a predicted unsteady pressure field with that measured on the ground (ref. *36)* provide insight into the adequacy of the approximations for various circumstances.

### Three–Dimensional Time–Dependent Motion of Vortex Filaments

The point vortex representation of quasi–two–dimensional wakes can be extended into the full three–dimensional time–dependent case by use of vortex filaments instead of point vortices. Typical applications of this technique to the analysis of wake vortices has been made in references 37 to 44. Summation of the contributions to the velocity field (e.g., by the Biot–Savart law) must be made along the entire length of each filament rather than just a pointwise summation. The increase in calculation time required becomes cumbersome and introduces further sources for numerical errors and instabilities. Unfortunately, simple conservation relationships are not available for three–dimensional filaments that permit an easy evaluation of error growth as the computation proceeds. A further complication not present in the two–dimensional case is that infinite self–induced velocities occur if the

filament is assumed to have zero core radius. This difficulty is usually circumvented by assuming an artificial core or cutoff radius within which the velocity decreases to zero as the center of the filament is approached. The numerical solution therefore may or may not depend strongly on the core radius or axial flow along the core (e.g., ref. *44).* If the solution is strongly dependent on core diameter, the analysis should probably be carried out by use of a finite-difference method so that a more realistic representation of the vorticity distribution is used in the theoretical model.

Despite the foregoing disadvantages, the vortex-filament approximation has been useful in predicting the more general structure of aircraft wakes as they approach airports. Considerable effort has also been devoted to the investigation of the self-induced instabilities of a vortex pair observed by Scorer (refs. *45, 46)* and others to sometimes be responsible for the breakup of aircraft wakes (e.g., refs. *45-48).* The initiation and growth characteristics of these instabilities (which can lead to breakoff and linking to form loops from two parallel and counterrotating vortices) are reviewed in the section on inviscid alleviation schemes.

## Direct- and Inverse-Rollup Theories

*Direct-rollup theory* - A theoretical tool frequently used to study the circumferential velocity distribution in lift-generated vortices is the simple rollup method of Betz (ref. 29). His theory is based on the conservation equations for inviscid, two-dimensional vortices and relates the circulation in the fully developed vortex to the span loading on the generating wing. The simplicity of the method results from the assumptions that the vortex is completely rolled up and that the rollup process is inviscid. To achieve a unique result, the vortex sheet is assumed to roll up in an orderly fashion from the wing tip inboard, so that successive layers of the sheet are wrapped around the center and over previous wrappings (fig. **3).** Any axial or streamwise variation in the flow velocity is assumed to have a negligible effect on the rollup process. The Betz method does not treat the transition or intermediate stages between the initial vortex sheet behind the wing and the final rolled-up vortex structure. When the derivation is completed

18

(e.g., ref. 30), the vortex structure is related to the span loading on the generating wing by

$$\Gamma_v(r_1) = \Gamma_w(y_1) \qquad (4)$$

where the radius in the vortex $r_1$ is related to a spanwise station on the wing $y_1$ by

$$r_1 = - \frac{1}{\Gamma_w(y_1)} \int_{b/2}^{y_1} \Gamma_w(y)\,dy \qquad (5)$$

The symbol $\Gamma_w$ denotes the bound circulation on the wing and $\Gamma_v$, the circulation in the fully developed vortex. Although the Betz theory does not appear to have been used extensively for a number of years after its first derivation, it has recently been demonstrated by Donaldson et al. (refs. 49, 50) to be useful and often more accurate than more complex methods. The favorable publicity given to the Betz method by Donaldson led to an elabora- tion of the theory and the more examples by Mason and Marchman (ref. 51) and to the use of the rollup theory by Brown (ref. 52) to predict the axial flow velocity in the vortex. A typical example of the good representation provided by the inviscid rollup theory is presented in figure 6. The experimental data (ref. 53) were obtained with a three-component hot-wire probe, and the span loading for the Betz calculation was obtained with a vortex-lattice theory (ref. 17). It appears that viscous effects have not altered the vortex structure appreciably in these cases. Recently, Bilanin and Donaldson (ref. 54) have extended the rollup theory to include the drag of the wing and of turbulence injection devices.

*Inverse rollup theory* - As more experimental velocity data were accumu- lated with the ground-based facilities (refs. 53 and 55), it became desirable to relate the vortex structure backward to the span loading on the wing that generated the vortex. This led to what might be called an inverse-Betz method (ref. 56) based on the same basic equations and assumptions as the direct-Betz method. The derivation is begun with the expression presented previously that relates the radius $r_1$ in the vortex to the spanwise

station on the wing $y_1$ which contains a given amount of circulation. After some simple manipulations and because the vortex is axially symmetric, so that the circulation may be written as $\Gamma_v = 2\pi r_1 v_\theta$, the inverse relationship becomes

$$\frac{b}{2} - y_1 = r_1 + \int_0^{r_1} \frac{d(rv_\theta)}{v_\theta} \tag{6}$$

where $v_\theta$ is the measured circumferential velocity in the vortex.

Two sample cases presented in figures 7(a) and (b) include the measured vortex structure, the span loading inferred from these measurements by the inverse rollup method, and, for comparison, the span loading predicted by vortex-lattice theory. These results show that the inverse rollup theory can recover the span loading on the generating wing fairly accurately. With almost all configurations, a difference occurs near the wing tip as a result of the finite core size and solid-body rotation in the vortex near $r = 0$. The magnitude of the distortion in span loading depends on the size of the core, which is influenced by the character of the boundary layer on the wing and on the viscous and turbulent shear forces in the vortex itself. In most cases, these distortions appear to be small and to occur only near the wing tip.

*Region of applicability of rollup theories* - The simplicity of both the direct and the inverse rollup methods results from the assumptions that the vortex is completely rolled up and that the rollup process is inviscid. These two assumptions then limit the downstream interval over which the theories apply. The upstream end of the region of applicability begins where the rollup of the vortex sheet is largely completed and can be estimated by use of inviscid, time-dependent rollup calculations. Results such as those in figures 6 and 10 of Rossow (ref. 20) indicate that a major part of the rollup process behind many wings can be considered practically complete within as few as 3 to 5 span lengths behind the generating wing.

The downstream end of the region of applicability is the distance at which viscous and turbulent decay of the vortex has modified its structure to the extent that the inviscid theory no longer approximates it. An

estimate for this limit can be obtained from the recent data of Ciffone and Orloff (ref. 55) wherein a so-called plateau region (discussed in the next section) is identified. Within this plateau region, they found that the vortex decays very little, but it is followed by a region where the vortex decays roughly as $t^{-1/2}$. These considerations suggest that the region of applicability of the Betz method lies between about 3 span lengths and the downstream end of the plateau region, which is estimated from the data of Ciffone and Orloff (ref. 55). Another consequence of the inviscid rollup assumption is that excessively high velocities are often predicted at and near the center of the vortex. Nevertheless, comparisons made by Donaldson et al. (refs. 49, 50, and *54)* have shown that outside the core region (radius of maximum circumferential velocity), the Betz rollup theory yields reliable estimates for the vortex structure.

### Plateau and Decay Regions for Isolated Vortex

The accuracy with which both the inviscid direct- and inverse-Betz methods relate the span loading to the vortex structure suggests that either the early history of the vortex is nearly inviscid or that the decay process is very slow. The correct interpretation appeared when the circumferential velocity was measured by Ciffone and Orloff (ref. 55) at a number of stations behind several generating wings. Figure 8, taken directly from their paper, shows that the maximum circumferential velocity is essentially unchanged for approximately *40* span lengths behind those three wings. The expected decay of the vortex, which is inversely proportional to the square root of distance, then begins to occur. The two straight lines for each configuration shown in figure 8 approximate the data in each region. The presence of both a plateau (nearly inviscid) and a decay region is also indicated in Donaldson's analysis (ref. 57) of the decay of a vortex using his second-order closure model for turbulence. Since a wide variety of wing planforms all exhibited the same characteristic plateau and decay regions, Iversen (ref. 58) set about finding an explanation for the onset of decay. By using a self-similar turbulent vortex, he was able to correlate the data obtained in ground-based facilities and in flight into the single curve shown in figure 9 (taken from Iversen, ref. 58).

Iversen's Reynolds number function $f\left(\Gamma_0/\nu\right)$ is conveniently equal to 1.0 for Reynolds numbers over $10^6$. From the data of reference 55 and these correlation functions, Ciffone (ref. 59) has developed an empirical relation-ship that makes it possible to predict easily the end of the plateau region and the peak swirl velocity in vortices. The information gained by Iversen (ref. 58) and Ciffone (ref. 59) was then extended by Iversen (ref. 60) to a numerical analysis of an isolated vortex using a mixing length model for the eddy viscosity. The initial data for the structure of the vortex were obtained using the rollup theory based on span loading. The numerical analy-sis is then able to predict the structure of the vortex in the plateau region, through the transition process, and into the decay region.

The simple Betz rollup theories assumed that each vortex in the pair acts independently of the other (i.e., as if it were isolated). The fact that such an assumption is valid for large distances into the wake was predicted in the theoretical work of Nielsen and Schwind (ref. 2, p. *413*). The very slow decay of an isolated vortex or of a single pair indicates that radical changes must be made in these lift-generated wakes if the hazard to encountering aircraft is to be substantially reduced.

## ROLLING MOMENT ON ENCOUNTERING WING — AXIAL PENETRATION

Another aspect of the wake-vortex problem that is approximated fairly well by inviscid theory 'is the estimation of the rolling moment on a wing as it encounters the wake vortices. A simple and reasonably accurate method is needed to not only evaluate the rolling-moment hazard posed by wakes of exist-ing aircraft but also to compare alleviation schemes. The NASA studies were restricted to axial penetrations and cross-vortex penetrations were not studied. (Refs. 1, 2, 5, 53, and 61-88 present the results of studies of the wake encounter problem.) This is not meant to imply that a cross-vortex encounter is less hazardous, but that entry into the vortex along the axis is probably the most likely to occur during landing and takeoff operations. If the flight path of the following aircraft is along or only slightly off axial, the flow field is approximated by steady-state theories. The schematic diagram in figure 10 indicates the way in which the rolling moment on the

following wing is analyzed.  The axial or streamwise velocity is assumed equal
to the free-stream velocity.  The vertical components of the circumferential
velocities in the vortices are used as the upwash or downwash on the follower
wing by adding the contributions of the one or more pairs of vortices in
the wake.  The torque on the following wing is then reduced to coefficient
form by

$$C_{l_f} = \frac{\text{rolling moment}}{(1/2)\rho U_\infty^2 S_f b_f}$$

In the study at Ames reported in reference 53, the torque or rolling
moment on the encountering wing was calculated by

1.  Two-dimensional strip theory
2.  Strip theory with empirical lift-curve slope correction
3.  Vortex-lattice theory; flat-wake approximation

The two-dimensional strip theory for the rolling moment assumes that the
lift on each spanwise wing element is given by its two-dimensional value or

$$l(y) = C_{L_a} \sin a \frac{1}{2} \rho U_\infty^2 c(y) \tag{7}$$

where $C_{L_\alpha}$ is the two-dimensional lift-curve slope of the airfoil section at
that spanwise station, $\sin a \approx w/U_\infty$ is the flow inclination, and $c(y)$ is
the local chord of the wing.  When the quantity $yl(y)$ is integrated across
the span of the rectangular wings used in reference 53, the rolling-moment
coefficient becomes (e.g., refs. 20 and 53)

$$C_{l_f} = \frac{C_{L_\alpha}}{b_f^2} \int_{-b_f/2}^{b_f/2} (w/U_\infty)y \, dy \tag{8}$$

The values presented in table I were found by integrating equation (8) numeri-
cally after setting $w/U_\infty$ equal to the sum of the measured $v_\theta/U_\infty$ contribu-
tions of the left- and right-hand vortices.  A different form of equation (7)
can be obtained when only one vortex is acting on the following wing by setting
$w/U_\infty = v_\theta/U_\infty = \Gamma(r)/2\pi r U_\infty$ and with $y = r$:

$$C_{l_f} = 2 \left(\frac{C_{L_\alpha}}{2\pi}\right)\left(\frac{b_g}{b_f}\right)^2 \int_o^{b_f/2b_g} \left[\frac{\Gamma(r)}{b_g U_\infty}\right] d\left(\frac{r}{b_g}\right) \tag{9}$$

Although equation (9) is sometimes more convenient, equation (8) is used here because it is believed to be more accurate for the wakes being considered.

For two-dimensional wings, the lift-curve slope, $C_{L_a}$, is usually taken as $2\pi$. As noted in table **I** (reproduced from ref. 53), the predictions made with $C_{L_a} = 2\pi$ are then generally too high because it does not account for the induced angles of attack near the wing tips and near the vortex centerline. An empirical relationship for the lift-curve slope to be used in the calculation of torque may be obtained by use of the formula introduced by R. T. Jones (p. 95 of ref. 89):

$$C_{L_\alpha} = \frac{2\pi \mathcal{R}}{P \cdot \mathcal{R} + 2} \tag{10}$$

where $\mathcal{R}$ is the aspect ratio and $P$ is semiperimeter/span. Maskew* compared the rolling moment calculated by vortex-lattice theory and by the strip theory with several versions of equation (10). He concluded that the span, aspect ratio, and perimeter in equation (10) should be interpreted on the basis of half a wing when the vortex and wing center are aligned. He reasoned that each half wing then acts as a separate wing, and equation (10) should be interpreted accordingly. For the rectangular wings studied here, equation (10) then becomes

$$C_{L_\alpha} = \frac{2\pi \mathcal{R}_f}{\mathcal{R}_f + 6} \tag{11}$$

The strip-theory predictions corrected for $C_{L_\alpha}$ by equation (11) are noted in table **I** to be in good agreement with the vortex-lattice theory and in fair agreement with experiment. The vortex-lattice theory used is a version of

*B. Maskew, Hawker Siddeley Aviation, Ltd. (NRC Associate at Ames Research Center), private communication.

Hough's (ref. 17) and of Maskew's (ref. 13) methods adapted to the present situations. The differences that occur between the vortex–lattice theory and experiment may be due to any of the following: differences in the interpretation of the measured rolling moments; differences in the vortex velocity data (e.g., large axial velocities), a combination of both, or unsteady aspects of the wind–tunnel measurements due to meander of the vortex which were assumed negligible. Nevertheless, the foregoing results indicate that either the vortex–lattice theory or the simple strip theory with $C_{L_a}$ determined by the Jones–Maskew formula provides reasonable estimates for the rolling moment induced by a vortex on a follower wing.

With the empirically adjusted strip theory, the rolling moment and lift on a wing can be simply calculated at a large number of points in the wake. Contours of equal rolling–moment coefficient and lift interpolated from these points are presented in figure 11 for one vortex and one span ratio. Only one quadrant is presented because the flow field is symmetrical vertically and antisymmetrical about the centerplane. Although the contours are not as precise as if determined by vortex–lattice theory, they do indicate the nature of the area over which high values of rolling moment occur. As expected, the maximum rolling moment occurs when the encountering wing is centered approximately on the vortex. Aircraft typically have the control capability to create a rolling–moment coefficient of *0.04* to 0.06 *so* that any imposed torque by a vortex that causes $C_{l_f}$ to exceed about 0.06 will cause the encountering aircraft to roll even when full counterroll control is imposed. The shaded area in figure 11(a) within the contour labeled 0.06 can then be interpreted, for example, as a hazardous region where overpowering rolling moments are to be found. Similarly, the results in figure 11(b) indicate that large values of positive and negative lift are induced on the follower by the vortex wake, depending on its location relative to the vortex pair. As expected, the shapes of the curves of constant torque and lift change with both the vortex structure and with the span of the follower. The dependence of the rolling moment on distance behind the generating aircraft are not discussed because downstream changes in the structure of a two–vortex developed wake depend largely on viscosity and turbulence.

# ALLEVIATION SCHEMES BASED ON INVISCID THEORY

Past research has shown that the wakes of conventional lifting systems on aircraft persist as a single vortex pair for unacceptable distances behind the generating wing. The slow rate at which vorticity is dispersed from such a single pair suggests that changes must be made in the flow field of the generating wing so that the wake is tolerable when it is fully developed. Therefore, the topics to be treated here are:

- Centroid of vorticity consideration
- Span loading for large vortex cores
- Sawtooth loadings for vortex dispersion
- Self-induced vortex excursions
- Convective merging of vortex cores

The alleviation schemes discussed in these subsections are based on modification of the flow over the generator to produce certain flow mechanisms in the near wake which disperse the lift-generated circulation. The first subsection describes one approach for selecting desirable characteristics in the span loading for alleviation. Several conceptual vortex wakes that have been useful in guiding our wake-vortex minimization program are then presented along with some of their characteristics. Although the guidelines presented are still being developed, they serve to indicate a direction for research and to identify desirable features in the flow field that could provide alleviation.

## Centroid of Vorticity Consideration

Since the span loading on the generating wing goes to zero at both wing tips, the wake contains equal amounts of positive and negative vorticity. If the loading falls off monotonically from a maximum at the centerline to zero at the wing tips, the wake rolls up into one vortex per side or a single pair. Although the net circulation in the wake is zero, considerable distance or time behind the generating wing is required (to mix on a two-dimensional basis) before the two concentrations of opposite vorticity combine or diffuse enough to have, in effect, a vanishing circulation

throughout the wake. One way to shorten the distance for complete mixing of circulation is to decrease the effective span by making the net shed circulation zero over a smaller part of the span. One obvious point for such a subdivision is at the wing centerline. The effectiveness of such a consideration is demonstrated by first considering the conservation of the first moment of circulation and the relationship between span loading and shed vorticity. By inviscid theory, the spanwise location of the centroid of vorticity $\bar{y}$ shed by the lifting surface remains fixed for each side of the wing. Hence, far behind the wing, the centroid of shed vorticity is located at the same spanwise station as at the wing, which is given by

$$\bar{y} = \frac{-1}{\Gamma_{C_L}} \int_0^{b_g/2} y \, \frac{d\Gamma(y)}{dy} \, dy = \frac{1}{\Gamma_{C_L}} \int_0^{b_g/2} \Gamma(y) dy$$

where $\Gamma(y)$ is the bound circulation on the wing and $\Gamma_{C_L}$ is the centerline circulation or the final total circulation in each vortex of the pair far downstream (i.e., $\Gamma)_{x=\infty}$). Since the spanwise loading is related to the bound circulation by

$$\ell(y) = \frac{1}{2} \rho U_\infty^2 c C_\ell(y) = -\rho U_\infty \Gamma(y)$$

the spacing between the vortices in the final pair far downstream is then

$$\frac{b_g'}{b_g} = \frac{C_{L_g}}{[cC_\ell(0)/\bar{c}]} \tag{12}$$

independent of the shape of the span loading used to obtain the lift. Since the strength of the final vortices for a given lift is proportional to $(b_g')^{-1}$, the separation between the vortices, the corresponding circulation is

$$\Gamma)_{x=\infty} = \Gamma_{C_L} = \frac{-\text{lift}}{\rho U_\infty b_g'} = \frac{-cU_\infty C_\ell(0)}{2} \tag{13}$$

On the basis of these simple considerations, final weak or low-intensity vortices are therefore obtained by reducing the lift at the wing root or aircraft centerline as much as possible while $C_{L_g}$ is held fixed. Such a

27

possibility has been demonstrated in the data obtained by Ciffone (ref. 90) behind a model of a Boeing 747 in a water tow tank with dye flow visualization. Measured distances between vortices far downstream yielded values for four flap configurations as $b'_g/b_g$ = 1.03, 1.25, 1.50, and 1.72. On the basis of these measurements, the circulation in the final vortex is reduced to 1.03/1.72 (or 60%) by the one flap configuration that has 30 percent of its inboard end cut off as compared with the conventional landing configuration — a substantial reduction. Both configurations shed the same number of vortices, but the latter has a better balance between positive and negative circulation for wake alleviation. Confirmation of the reduced circulation in these cases by measuring the velocity or rolling moment in the wake has not been made. Theoretical span loadings (fig. 12) for the wing alone without a fuselage as centerbody indicate that the far-field separation between the vortices would be $\left. b'_g/b_g \right)_{\text{theory}}$ = 1.22, 1.26, 1.28, and 1.31. Although the order of magnitude of these predicted results is about right, the disagreement between 1.31 and 1.72 is not small. The differences in the configurations used in the theory and experiment probably account for some of the differences in the predicted and measured values of $b'_g/b_g$. Also, some merging of vortices may still be in progress at the farthest downstream station observed.

Other theoretical separation distances can be found by subdividing the span loading differently to approximate different vortex interactions. However, more theoretical and experimental information is needed to guide the theory and the interpretation of the vortex separation distances. The subsections that follow therefore present some mechanisms by which vortices merge or combine and some guidelines for promoting, enhancing, or preventing the merger. This discussion is not concerned with the lifting efficiency or any drag penalty of the alleviation schemes, but the first objective is to determine what can be done. When promising configurations are identified, it will then be necessary to optimize the alleviation concept by including more complete considerations of the entire aircraft.

### Span Loadings for Large Vortex Cores

A variety of wing shapes have been considered experimentally and theoretically as a means to reduce the high circumferential velocity in

lift–generated vortices.  These configurations were studied because it was thought that enlarging the vortex core would reduce the swirl velocity and the rolling moment associated with a given lift.  The direct relationship between span loading and vortex structure provided by the Betz rollup theory suggested that wing planform, twist, or camber be shaped to produce a loading that sheds vortices with large cores (e.g., refs. 20, 51, 52, 55, and 56). Many of these span loadings had the characteristics that they tapered gradually to zero at the wing tips from an increased centerline loading.  The properties of these loadings is illustrated by considering a so–called tailored loading (ref. 20) that produces a vortex sheet which rotates as a unit rather than rolling up from its edges (fig. 13).  In this particular case, the velocity distribution in the wake was specified and the corresponding strengths of the vortex sheet and of the span loading were then found. When the vortex structure was compared with that for elliptic loading, it was found that the higher centerline lift required to maintain a given lift on the generator leads to higher rolling moments when the span of .the follower wing is more than about 0.2 of the span of the generating wing.  This result is apparent in figure 14 when the circulation in the two vortices is compared for various span followers using equation (9) for the rolling moment.

These results and the guidelines developed in the previous subsection suggest that a span loading designed only on the basis of large vortex cores is not the proper direction for wake alleviation because these wings require higher centerline loadings.  The corresponding decrease in $b_g'/b_g$ associated with these loadings also suggests that a direct span loading — vortexcore design is not a good direction to proceed and that another approach should be tried.

Sawtooth Span Loadings for Vortex Dispersion

A second vortex–wake configuration studied theoretically in reference 20 was designed to translate downward as a unit (indicated schematically in fig. 15).  This wake consisted not of a continuous vortex sheet but of a number of discrete vortices.  The two–dimensional time–dependent theory for discrete vortices predicted that the vortex strengths required for such motion

alternate in sign across the span so that the span loading has a stepped or sawtooth shape as illustrated in figure 15. When the time-dependent method discussed previously is used to predict the shape of the wake, it is found to remain flat because all the individual vortices move downward at the same velocity. If, however, a disturbance is given to one of the vortices, the specified uniform motion breaks down and the vortices form pairs that make large excursions across the wake (as shown in fig. 16(a)). Hence, although the shape of the sawtooth loading fluctuates about elliptic loading, the vortices in the wake do not revolve about the edge or tip vortices in the way that they do for elliptic loading (fig. 16(b)). If a similar disturbance is given to the vortices shed by elliptic loading, the general shape of the wake is not altered, although the positions of some of the vortices change slightly.

The numerical result shown in figure 16(a) suggests that wakes with multiple vortex pairs can be designed *so* that they are unstable to disturbances, and convection of vorticity across the wake can be considerably enhanced by the resulting excursions of the vortex pairs. These theoretical results do not indicate whether the various pairs of vortices merge or link with one another to form a dispersed wake with low velocities, or if the vortices remain discrete with high core velocities. Insight into the characteristics of wakes shed by sawtooth loadings was obtained by flow-field observations made on two experimental wings configured to approximate sawtooth loading. The first wing was swept and equipped with seven flap segments per side (refs. 53 and 55). When these segments were deflected alternately up and down across the span, the loading is predicted by vortex-lattice theory to be as shown in figure 17. Tests by Ciffone and Orloff (ref. 55) in a water tow tank showed that the vortices shed by this wing did undergo large excursions in the wake and that various pairs linked in the way described by Scorer (ref. 45 and 46), Crow (ref. 37), and MacCready (ref. 2, p. 289). But when the various excursions and linking were completed, a vortex pair still remained in the wake. These preliminary results indicate that generation of multiple vortex pairs will bring about large vortex excursions that lead to linking, but additional criteria are needed to achieve adequate diffusion of the wake vorticity.

A second wing on which vortex wake alleviation was attempted by span-load modification was that of the Boeing *747* subsonic transport (refs. 80 and **83).** The wing has inboard and outboard flaps (fig. 18) that can be deflected separately *so* that the loading can be enhanced inboard or outboard within the limits indicated in figure 19. If the inboard flaps are deflected their full amount (30° setting), the span loading has a large hump inboard resembling a combination of tailored and sawtooth span loading. Although that loading produces three vortex pairs in the near–field rollup region, the two flap vortices combine, *so* that only two vortices per side persist into the far-field region. Far downstream, these two vortices of the same sign merge into a single diffuse vortex illustrated in figure 20. Tests in a water tow tank and in a wind tunnel indicate that the rolling moment imposed on a following aircraft by the wake of this configuration would be less than half that posed by the wake of the landing configuration at the same lift coef-ficient. Furthermore, this reduced value was below the roll–control capability of a LearJet aircraft which could be used to probe the wake. Flight tests conducted with the Boeing *747,* the LearJet, and a *T-37* aircraft (ref. *80)* confirmed the predictions of the ground–based facilities when the landing gear was retracted. **It** was found, however, that if any of the landing gears were extended or if the aircraft were yawed, the hazard alleviation achieved with the unconventional flap settings was greatly reduced.

These test results indicate that **it** **is** possible to induce large vortex excursions and reduced swirling velocities in the wake **if** substantial oscil-lations occur in the span loading. **A** theoretical estimate of the magnitude required was obtained in reference 20 by trying various types of span–load fluctuations and calculating whether dispersion occurred. **It** was found that the wake had a chaotic character if the loading variations in the loading were 30 percent or more of the maximum and if their spanwise sizes were about the same. The two–dimensional, time–dependent theory predicted that the multiple vortices shed into the wake would then undergo large excursions. Guidelines for whether the several vortex pairs will combine into a single pair in the far field by either a cutoff and linking process, or by a convective merging process, or neither are discussed in the next two subsections.

Before leaving this discussion, note that the vortex wakes of sawtooth loading will generally dissipate more rapidly than those of elliptic-like loadings for two reasons. First, each vortex pair in the wake is more closely spaced. Therefore, since the decay distance for a vortex pair depends on the distance between them (or on their effective span), the actual distance to a given dissipation (as given in figs. 8 and 9) would be decreased by the span ratio. Secondly, the theoretical analysis of Bilanin and Widnall (ref. 91) indicates that the sinusoidal instability is intensified by decreased spacing of vortices as the second power of span. It is not surprising then that the wakes produced by wings with multiple spanwise flap segments are often observed to dissipate more rapidly and to be less hazardous than wakes produced by wings with only one flap or none.

## Self-Induced Vortex Excursions

The vortex pair behind aircraft flying at high altitudes is often observed (e.g., refs. 2, *37, 45, 46, 47,* and *48)* to undergo periodic, anti-symmetrical distortions that increase in amplitude until the vortices either appear to burst at the sharp bends or to link to form a series of loops. The linking process in such a vortex-vortex interaction occurs rapidly when the two equal and opposite vortices in the pair approach each other closely enough that the filaments appear to break in the flight direction and reconnect or link across the wake to form irregularly shaped loops that then disperse and decay. A comparison of the hazard posed by the vortex loops with that posed by the original parallel vortices needs to be made to determine whether a chance encounter with an axial segment of a loop is just as hazardous and whether flight across a segment of the vortex loop would cause unacceptable accelerations or air loads. Whether the loop stage of the wake is more or less hazardous than the original parallel-vortex stage is uncertain, but it seems apparent that the formation of loops enhances the decay and dispersion of the circulation in the wake.

A stability analysis by Crow (ref. *37)* showed that, once started, the wave growth results from the self-induced velocity field of the vortex pair with a preferred wavelength about 8.6 times the distance between the

32

vortices. Other analyses (e.g., ref. 2) extended the analysis to include the effect of core size and axial velocities. A numerical calculation using three-dimensional vortex filaments for the vortex pair has also been made by Hackett and Theisen (ref. 2 or 38) of the time history of the development of a periodic loop.

These research results demonstrate that antisymmetric, periodic, or sinusoidal disturbances on a vortex pair will lead to large self-induced excursions. The mechanism by which the two vortices break from their original streamwise filament and link across to the other vortex in the pair has not been analyzed nor has the decay of the loops been treated adequately. Added data are also needed on the effect of variables such as core size, axial velocity in the core, vortex strength, etc., when linking or bursting of the vortex filaments occurs.

The self-induced or sinusoidal instability for a single vortex pair has not proven to be a viable solution to the wake-vortex alleviation problem for several reasons. First, the beginning of wave growth requires a disturbance from the atmosphere or from some periodic lift modification on the generating aircraft. Introduction of a periodic span-load variation on the generating wing was shown by Bilanin and Widnall (ref. 91) to be an effective way to initiate growing waves that led to bursting when the curves in the vortex filaments reached a small radius of curvature. Implementation of such a scheme on a full-sized aircraft would be difficult, however. A second and more serious drawback is that the waves grow slowly and often become highly sinuous without bursting, linking, or appearing to decay. Lastly, the large vortex cores produced by aircraft in the landing and takeoff configurations do not seem to be conducive to wave growth.

A new approach to stimulation or initiation of self-induced or vortex-vortex instabilities that led to large vortex excursions was suggested by the numerical analysis of wakes produced by the so-called sawtooth loadings studied in reference 20. It was found that a wake with multiple vortex pairs about equally spaced across the span of the generating wing and of about the same magnitude but alternating in sign would undergo large excursions without being stimulated. These self-induced excursions are not periodic, but are

often of the order of the span of the wing when the wake consists of vortices comparable in magnitude and alternating in sign.

As previously discussed, an experimental demonstration of the effectiveness of sawtooth loading for producing large vortex excursions was first made by Ciffone and Orloff (ref. 55) in a water tow tank. The wing was equipped with seven flap segments deflected alternately upward and downward by $15°$ to produce seven vortex pairs. A theoretical estimate of the span loading (fig. 17) indicates that the strengths of the vortices do alternate in sign and are about the same within a factor of 2. In the experiment, large vortex motions and linking occurred, but when the activity died down, a single residue vortex pair remained. Further theoretical and experimental studies are needed to arrange and match the vortex pairs to more completely disperse the wake so that the remaining velocities are tolerable and to possibly optimize the loading, Although the experiment was not completely successful, it did demonstrate that self-induced and rapid growth of vortex motions can be produced with sawtooth-type loadings. Another result found from the experiment was that it showed that linking could occur between opposite but not necessarily equal vortices. Such a partial linking process forms a series of vortex loops connected by vortex filaments. Convection of vorticity by the stronger vortex probably then causes the two vortices to completely merge by a process similar to that discussed in the next subsection (illustrated in fig. 21). An example of such a linking between an unequal vortex pair was observed in some flight experiments of Barber and will be presented by Corsiglia and Dunham in a paper to follow later in this conference. The interaction of the two opposite but unequal vortices from the flap has also been simulated numerically by Leonard (private communication) at ARC. These results indicate therefore that the multiple vortex pairs shed by sawtooth loading may provide a way to initiate the large vortex excursions and linking needed for alleviation. Various aspects of the dispersion and decay mechanisms need to be better defined and understood to make the method effective and to minimize penalties associated with these loadings and their implementation.

## Convective Merging of Vortex Cores

The blending or merging of the several vortices shed by flap edges, pylons, horizontal tail, and the wing tip into a single vortex is a common and well-known occurrence. The merging of two or more vortex cores (i.e., vortical regions) has also been studied theoretically from an inviscid point of view (e.g., refs. 92-97) and with a second-order turbulence theory (ref. 7). Some results are now presented of a current study by the author that extends previous investigations by finding some circumstances under which two-dimensional inviscid vortex cores will or will not merge convectively.

Convective merging of the cores of two Rankine vortices is illustrated in figure 21. The initial distribution of circulation is made approximately uniform over the circular regions of the cores by putting point vortices of the same strength on three circles at uniform intervals. Since they each approximate Rankine cores, the maximum vortex velocity occurs at the outer ring. The inner rings rotate more slowly so that the cores, when isolated, rotate as a solid body. However, as shown in figure 21, when the two cores of the same sign and magnitude are placed in proximity but not touching, their mutual induction causes their shape to become distorted so that the two vortical regions reform into a single'region.

A slightly greater separation between the cores results in the vortices becoming only slightly elongated but not merging (fig. 22). A series of such calculations was then used to determine a boundary between merging and nonmerging cases (fig. 23); that is, a combination of spacing and relative vortex strengths on the merging side of the curves do form a single vortical region from the original two circular regions. In these cases, merger was assumed to have occurred whether one or both of the cores was reshaped in the process. Note that merging occurs for vortices of opposite sign only when their relative strengths differ by a factor of about 5.

When a core structure other than Rankine is used, the merging process becomes more restrictive because the cores become effectively smaller relative to their spacing. The boundaries for two other radial variations of circulation are also presented in figure 23 as dashed curves to show how the merging

region shrinks for more concentrated vortex cores. Since the vortex structures shed by flaps and wing tips are usually more concentrated than that for Rankine cores, and since merging requires a given maximum spacing, merging of two given vortices will be delayed until turbulence and viscosity diffuse the circulation to the degree needed for the convective redistribution to occur. The time-dependent calculations also showed that if convective merging is going to occur, it does so rapidly. Otherwise, the core shapes oscillate about their original circular shape.

Previous theoretical calculations indicate that the structure of a vortex pair consisting of two equal and opposite vortices, whether inviscid or including turbulence, will change very slowly with time (e.g., ref. 2, p. 413 ff; refs. 7 and 60). When the wake contains two or more pairs of vortices, the spacing between the vortices can change so that convective merging that would not occur at the outset does occur later. Another convenient set of guidelines is the vortex domain plots such as those prepared by Donaldson and Bilanin (fig. 2.2 of ref. 7). The boundaries shown for point vortices eliminate vortex combinations that will probably not be matched for convective merging or will not stay near one another long enough to merge. The number of remaining possibilities is still large and specific situations must be analyzed before the development of satisfactory guidelines has been completed.

CONCLUDING REMARKS

Inviscid modeling of lift-generated wakes has provided insight into the structure of the vortices and into means whereby wake velocities can be reduced or minimized. The available theories yield fairly good estimates for the wake-vortex structure (but not the axial flow) produced by the generating aircraft and for the wake dynamics in the so-called rollup and plateau regions. Satisfactory results are also obtained with inviscid theories for the loads induced by the wake on an aircraft as it enters along a near-axial flight path. As more comparisons are made with experiment, it may, however, be found necessary to include unsteady effects and better estimates of the lift curve. Some aspects of self-induced or vortex-vortex instabilities are

approximated by inviscid theories, but analyses and experiments currently in progress may indicate that improved methods are needed.

The survey of alleviation schemes presented here indicates that more complete theories are needed to aid the understanding of and to guide the design of lifting systems that shed wakes which dissipate rapidly. The area of greatest need is for methods that better represent continuous distributions of vorticity so that flow processes such as vortex merging and linking can be more accurately modeled. The most direct approach is probably through numerical analysis of the flow field by a finite−difference scheme, Analytical approaches should, however, not be ruled out because well−defined guidelines can often be developed in this way if that portion of the flow field which is of interest is properly approximated. If a numerical scheme is developed, it should be easy to use and should not require substantial amounts of computer time, because a large number of variables and a wide range of conditions must be systematically considered to find those that provide alleviation and those that will be optimum for various aircraft.

One approach presented here for wake−vortex alleviation suggests that the span loading chosen should shed several vortex pairs of both signs so that the vortices combine quickly to form a single pair low in strength and widely spaced. A way to achieve this is to design the span loading so that the centerline circulation is much lower than the maximum bound circulation on the wing. The vortices must then be spaced and have such magnitudes that they combine by convective merging and linking or both to form a single pair not too far downstream which is relatively weak and with a large separation. It may also be possible to arrange the loading *so* that this final pair is also dispersed by linking. Indications from inviscid theory and from some experiments are that a sawtooth−type loading that sheds multiple vortex pairs of both signs may provide or have built into it the self−induced vortex excursions needed to implement the linking process and the dispersion of vorticity. However, more guidelines and a better understanding of these flow fields, of the linking process, and of the decay of the vortex loops produced are needed to make sawtooth loading a viable alleviation scheme.

Preliminary results from a theoretical two–dimensional study of convective merging of vortical regions indicate that further results will adequately define the conditions when merging will occur. Briefly, convective merging appears to be an effective process for combining vortical regions of the same sign that are relatively close to one another, but it is not particularly powerful for alleviating wake velocities because vortices of opposite sign do not readily merge convectively.

Inviscid theories have played an important role in the wake–vortex research program. Results from these theories should not be taken as final nor should they be considered as too inaccurate to be valid. When the inviscid methods are used where applicable and when the results are properly interpreted, they can continue to be useful for preliminary screening of wake–vortex alleviation schemes.

## REFERENCES

1. Bleviss, Z. O.:   Theoretical Analysis of Light Plane Landing and Take-of€ Accidents Due to Encountering the Wakes of Large Airplanes.   Rept. SM–18647, Douglas Aircraft Corp., Santa Monica Div., Dec. 1954.

2. Olsen, John H.; Goldberg, Arnold; and Rogers, Milton, eds.:   Aircraft Wake Turbulence.   Plenum Publishing Corp., Sept. 1970.

3. El–Ramly, Z.:   Aircraft Trailing Vortices — a Survey of the Problem. Tech. Rept. ME/A 72–1, Carleton Univ., Ottawa, Canada, Nov. 1972.

4. Kurylowich, G.:   Analyses Relating to Aircraft Vortical Wakes.  AFFDL/ FGC–TM–73–23, Feb. 1973.

5. Gessow, A.:   Aircraft Wake Turbulence Minimization by Aerodynamic Means. 6th Conference on Aerospace and Aeronautical Meteorology, El Paso, Texas, Nov. 12–14, 1974.

6. Roberts, L.:   On Wake Vortex Alleviation.  NASA/University Conf. on Aeronautics — Theme:   The Future of Aeronautics, Univ. of Kansas, Oct. 23–24, 1974.

7. Donaldson, C. du P.; and Bilanin, A. J.: Vortex Wakes of Conventional Aircraft. AGARDograph 204, May 1975.

8. Rossow, Vernon J.: Survey of Computational Methods for Lift-Generated Wakes. Aerodynamic Analyses Requiring Advanced Computers, Part II, NASA SP-347, 1975, pp. 897-923.

9. Analytic Methods in Aircraft Aerodynamics. A symposium held at Ames Research Center, Moffett Field, Calif., NASA SP-228, 1969.

10. Aerodynamic Interference. AGARD Conference Proceedings No. 71, AGARD-CP-71-71, 1971.

11. Ashley, H.; and Rodden, W.P.: Wing-Body Aerodynamic Interaction. Ann. Rev. Fluid Mech., vol. 4, 1972, pp. 431-472.

12. Aerodynamic Analyses Requiring Advanced Computers, Parts I and II, NASA SP-347, 1975.

13. Maskew, B.: Numerical Lifting Surface Methods for Calculating the Potential Flow about Wings and Wing-Bodies of Arbitrary Geometry. Ph.D. Thesis, Loughborough Univ. of Tech., Oct. 1972.

14. Maskew, Brian: A Subvortex Technique for the Close Approach to Discretized Vortex Sheet. NASA TM X-62,487, 1975.

15. Kandil, O. A.; Mook, D. T.; and Nayfeh, A. H.: Nonlinear Prediction of the Aerodynamic Loads on Lifting Surfaces. AIAA Paper 74-503, 1974.

16. Chigier, N. A.; and Corsiglia, V. R.: Tip Vortices — Velocity Distributions. NASA TM X-62,087, 1971.

17. Hough, G.: Remarks on Vortex-Lattice Methods. AIAA J. Aircraft, vol. 10, no. 5, May 1973, pp. 314-317.

18. Rosenhead, L.: The Formation of Vortices from a Surface of Discontinuity. Proc. Roy. Soc. (London); vol. A134, 1931, pp. 170-192.

19. Westwater, F. L.: The Rolling Up of the Surface of Discontinuity Behind an Aerofoil of Finite Span. Reports and Memoranda 1692, British A.R.C., 1935, pp. 116-131.

20. Rossow, V. J.: Theoretical Study of Lift–Generated Vortex Wakes Designed to Avoid Roll Up. AIAA J., vol. *13,* no. *4,* April *1975,* pp. *476–484.*

21. Spreiter, J. R.; and Sacks, A. H.: The Rolling–Up of the Trailing Vortex Sheet and Its Effect on the Downwash Behind Wings. J. Aeronaut. Sci., vol. *18,* no. **1,** Jan. *1951,* pp. *21-32.*

22. Hama, F. R.; and Burke, E. R.: On the Rolling–Up of a Vortex Sheet. Tech. Note BN–220, AFOSR–TN *60-1069,* Univ. of Maryland, *1960.*

23. Takami, H.: A Numerical Experiment with Discrete–Vortex Approximation, with Reference to the Rolling Up of a Vortex Sheet. Sudaer 202 (AFOSR 64-1536), Sept. *1964.*

24. Moore, D. W.: The Discrete Vortex Approximation of a Vortex Sheet. Rept. *AFOSR-1084-69,* Calif. Inst. of Tech., *1971.*

25. Chorin, A. J.; and Bernard, P. S.: Discretization of a Vortex Sheet, with an Example of Roll–Up. College of Engineering Rept. *FM-72-5,* Univ. of California, Berkeley, Nov. *1972.*

26. Kuwahara, K.; and Takami, H.: Numerical Studies of Two–Dimensional Vortex Motion by a System of Point Vortices. J. Phys. Soc. Japan, vol. *34,* no. **1,** Jan. *1973,* pp. *247-253.*

27. Moore, D. W.: A Numerical Study of the Roll–Up of a Finite Vortex Sheet. J. Fluid Mech., vol. *63,* pt. 2, *1974,* pp. *225-235.*

28. Lin, C. C.: On the Motion of Vortices in Two Dimensions. No. *5,* Applied Mathematics Series, The Univ. of Toronto Press, Toronto, Canada, *1943.*

29. Betz, A.: Verhalten von Wirbelsystemen. Z.A.M.M., Bd. XII, Nr. *3, 1932,* pp. *164-174* (available as NACA TM *713).*

30. Rossow, V. J.: On the Inviscid Rolled–up Structure of Lift Generated Vortices. AIAA J. Aircraft, vol. 10, no. **11,** Nov. *1973,* pp. *647-650.*

31. Brashears, M. R.; Hallock, J. N.; and Logan, N. A.: Analysis of Predicted Aircraft Wake Vortex Transport and Comparison with Experiment, AIAA Paper *74-506, 1974* (to be published in Journal of Aircraft).

32. Hallock, J. N.; and Goldstone, L.: US/UK Vortex Monitoring Program at Heathrow Airport, AGARD Guidance and Control Panel 20th Symposium on Plans and Developments for Air Traffic Systems, Paper 24, 1975.

33. Hallock, J. N.; Wood, W. D.; and Spitzer, E. A.: The Motion of Wake Vortices in the Terminal Environment, AIAA/AMS Sixth Conference on Aerospace and Aeronautical Meteorology, Preprint Volume, 1974, pp. 393-398.

34. Brashears, M. R.; and Hallock, J. N.: Aircraft Wake Vortex Transport Model, J. Aircraft, vol. 11, no. 5, 1974, pp. 265-272.

35. Brashears, M. R.; and Hallock, J. N.: A Predictive Model of Wake Vortex Transport, AIAA/AMS Sixth Conference on Aerospace and Aeronautical Meteorology, Preprint Volume, 1974, pp. 387-392.

36. Brown, C. E.: Pressure Field of a Vortex Wake in Ground Effect. AIAA J. Aircraft, vol. 12, no. 2, Feb. 1975, pp. 120-121.

37. Crow, S. C.: Stability Theory for a Pair of Trailing Vortices. AIAA J., vol. 8, no. 12, Dec. 1970, pp. 2172-2179.

38. Hackett, J. F.; and Theisen, J. G.: Vortex Wake Development and Aircraft Dynamics, Aircraft Wake Turbulence and Its Detection, edited by J. H. Olsen et al., Plenum Press, New York, 1971, pp. 243-263.

39. Widnall, S. E.; Bliss, D.; and Zalay, A.: Theoretical and Experimental Study of the Stability of a Vortex Pair, Aircraft Wake Turbulence and Its Detection, edited by J. H. Olsen et al., Plenum Press, New York, 1971, pp. 305-338.

40. Saffman, P. G.: The Motion of a Vortex Pair in a Stratified Atmosphere, Studies in App. Math.; vol. LI, 1972, pp. 107-119.

41. Hama, F. R.: Progressive Deformation of a Carved Vortex Filament by its Own Induction, Phys. Fluids, vol. 5, no. 10, Oct. 1962, pp. 1156-1162.

42. Moore, D. W.; and Saffman, P. G.: The Motion of a Vortex Filament with Axial Flow. Phil. Trans. Roy. Soc., series A, vol. 272, 1972, p. 403.

43. Leonard, A.:   Simulation of Unsteady Three-Dimensional Separated Flows with Interacting Vortex Filaments.   Aerodynamic Analyses Requiring Advanced Computers, Part II, NASA *SP-347, 1975,* pp. *925-937.*

44. Moore, D. W.;  and Saffman, P. G.:   A Note on the Stability of a Vortex Ring of Small Cross Section.   Proc. Roy. Soc. London, series A, vol. *338, 1974,* pp. *535-537.*

45. Scorer, R. S.:   Natural Aerodynamics, Pergamon Press, New York, *1958.*

46. Scorer, R. S.; and Davenport, L. J.:   Contrails and Aircraft Downwash, J. Fluid Mech., vol. *43, 1970,* pp. 451-464.

47. Harvey, J. K.; and Fackrell, J. E.:   Observation of a Mechanism Causing a Trailing Contrail Vortex to Break Up, Aero Rept. *70-08,* Imperial College, London, *1970.*

48. Tombach, I.:   Observations of Atmospheric Effects of Vortex Wake Behavior.   AIAA J. Aircraft, vol. 10, no. 11, Nov. *1973,* pp. *641-647.*

49. Donaldson, Coleman du P.:   A Brief Review of the Aircraft Trailing Vortex Problem, A.R.A.P.   Rept. *155,* May *1971.*

50. Donaldson, C. du P.; Snedeker, R. S.; and Sullivan, R. D.:   Calculation of Aircraft Wake Velocity Profiles and Comparison with Experimental Measurements.   AIAA J. vol. 11, no. *9,* Sept. *1974,* pp. 547-555.

51. Mason, H. W.; and Marchman, J. F., III:   The Farfield Structure of Aircraft Wake Turbulence.   AIAA Paper *72-40, 1972.*

52. Brown, C. E.:   Aerodynamics of Wake Vortices.   AIAA J., vol. 11, no. *4,* April *1973,* pp. *531-536.*

53. Rossow, V. J.; Corsiglia, V. R.; Schwind, R. G.; Frick, J. K. D.; and Lemmer, O. J.:   Velocity and Rolling Moment Measurements in the Wake of a Swept Wing Model in the *40-* by 80-Foot Wind Tunnel.   NASA TM *X-62,414, 1975.*

54. Bilanin, A. J.; and Donaldson, C. du P.:   Estimation of Velocities and Roll-Up in Aircraft Vortex Wakes.   AIAA J. Aircraft, vol. *12,* no. *7,* July *1975,* pp. *578-585.*

55. Ciffone, D. L.; and Orloff, K. L.: Far–Field Wake–Vortex Characteristics of Wings. AIAA J. Aircraft, vol. 12, no. 5, May 1975, pp. 464–470.

56. Rossow, V. J.: Prediction of Span Loading from Measured Wake–Vortex Structure — An Inverse Betz Method. AIAA J. Aircraft, vol. 12, no. 7, July 1975, pp. 626–628.

57. Donaldson, C. du P.: Calculation of Turbulent Shear Flows for Atmospheric and Vortex Motions. AIAA J., vol. 10, 1972, pp. 4-12.

58. Iversen, J. D.: Correlation of Turbulent Trailing Vortex Decay Data. AIAA J. Aircraft (to be published).

59. Ciffone, D. L.: Correlation for Estimating Vortex Rotational Velocity Downstream Dependence. AIAA J. Aircraft, vol. 11, no. 11, Nov. 1974, pp. 716-717.

60. Iversen, J. D.: Inviscid to Turbulent Transition of Trailing Vortices. Paper ISU-ERI-Ames-74241, Iowa State Univ., Engineering Research Inst., Nov. 1974.

61. Heaslet, M. A.; and Spreiter, J. R.: Reciprocity Relations in Aerodynamics, TN 2700, 1952, NACA.

62. Rose, R.; and Dee, F. W.: Aircraft Vortex Wakes and Their Effects on Aircraft, RAE Tech. Note Aero 2934, Dec. 1963.

63. McGowan, W. A.: Calculated Normal Load Factors on Light Airplanes Traversing the Trailing Vortices of Heavy Transport Airplanes, NASA TN D-829, March 1969.

64. McGowan, W. A.: Trailing Vortex Hazard. SAE Transactions, Rept. 68–220, vol. 77, 1968, pp. 740-753.

65. Wetmore, J. W.; and Reeder, J. P.: Aircraft Vortex Wakes in Relation to Terminal Operations. NASA TN D-1777, April 1963.

66. Miller, E. R., Jr.; and Brown, C. W.: An Experimental Study of Trailing Vortex Wakes Using a Large Towing Tank, Hydronautics, Inc., Laurel, Md., Aug. 1971.

67.  Jones, W. P.; and Rao, B. M.: Airloads and Moments on an Aircraft Flying over a Pair of Inclined Trailing Vortices, Aircraft Wake Turbulence and Its Detection, Plenum Press, 1971.

68.  Hackett, J. E.; and Theisen, J. G.: Vortex Wake Development and Aircraft Dynamics, Aircraft Wake Turbulence and Its Detection, edited by J. Olsen, A. Goldberg, and M. Rogers, Plenum Press, New York, 1971.

69.  Corsiglia, V. R.; Jacobsen, R. A.; and Chigier, N.: An Experimental Investigation of Trailing Vortices Behind a Wing with a Vortex Dissipator, Aircraft Wake Turbulence and Its Detection, edited by J. Olsen, A. Goldberg, and M. Rogers, Plenum Press, New York, 1971.

70.  Jones, W. P.: Vortex–Elliptic Wing Interaction. AIM J., vol. 10, no. 2, Feb. 1972, pp. 225–227.

71.  Filotas, L. T.: Vortex Induced Wing Loads. AIM J., vol. 10, no. 7, July 1972, p. 971.

72.  Andrews, William H.; Robinson, Glenn H.; and Larson, Richard R.: Exploratory Flight Investigation of Aircraft Response to the Wing Vortex Wake Generated by Jet Transport Aircraft, NASA TN D–6655, March 1972.

73.  Wentz, W. R., Jr.: Evaluation of Several Vortex Dissipators by Wind Tunnel Measurements of Vortex–Induced Upset Loads. Aeronautical Rept. 72–3, Wichita State Univ., Sept. 1972.

74.  Robinson, Glenn H.; and Larson, Richard R.: A Flight Evaluation of Methods for Predicting Vortex Wake Effects on Trailing Aircraft, NASA TN D–6904, Nov. 1972.

75.  Harlan, Raymond B.; and Madden, Stephen J., Jr.: A Hazard Definition for Wake Turbulence Encounter During Terminal Area Operations, MIT–MSL–RE–81, Mar. 1973.

76.  Banta, A. J.: Effects of Planform and Mass Injection on Rolling Moments Induced by Trailing Vortices. M. S. Thesis, Wichita State Univ., Dec. 1973.

77.  Kirkman, K. L.; Brown, C. E.; and Goodman, A.:   Evaluation of Effective-
     ness of Various Devices for Attenuation of Trailing Vortices Based on
     Model Test in a Large Towing Basin.   NASA CR-2202, Dec. 1973.

78.  Nelson, R. C.:   The Response of Aircraft Encountering Aircraft Wake
     Turbulence.   AFFDL TR 74-29, June 1974.

79.  Nelson, R. C.; and McCormick, B. W.:   The Dynamic Behavior of an
     Aircraft Encountering Aircraft Wake Turbulence.   AIAA Paper 74-774,
     Aug. 1974.

80.  Tymczyszyn, J.; and Barber, M. R.:   A Review of Recent Wake Vortex
     Flight Tests.   18th Annual Symposium of Society of Experimental Test
     Pilots, Los Angeles, Calif., Sept. 26, 1974.

81.  Hastings, E. C., Jr.; Shanks, R. E.; Champine, R. A.; and Copeland,
     W. L.:   Preliminary Results of Flight Tests of Vortex Attenuating
     Splines.   NASA TM X-71928, 1974.

82.  Johnson, Walter A.; and Teper, Gary L.:   Analysis of Vortex Wake
     Encounter Upsets, Systems Technology, Inc., Tech. Rept. 1025-2.

83.  Corsiglia, V. R.; Rossow, V. J.; and Ciffone, D. L.:   Experimental
     Study of the Effect of Span Loading on Aircraft Wakes.   AIAA Paper 75-
     885, 1975 (see also NASA TM X-62,431, 1975).

84.  Patterson, J. C., Jr.; and Flechner, S. G.:   An Exploratory Wind-Tunnel
     Investigation of the Wake Effect of a Panel Tip-Mounted Fan-Jet Engine
     on the Lift-Induced Vortex, NASA TN D-5729.

85.  Hastings, E. C., Jr.; Patterson, J. C., Jr.; Shanks, R. A.; Champine,
     R. A.; Copland, W. L.; and Young, D. C.:   Development and Flight Test
     of Vortex Attenuating Splines, NASA TN D-8083, Sept. 1975.

86.  Patterson, J. C., Jr.:   Vortex Attenuation Obtained in the Langley Vortex
     Research Facility.   AIAA J. Aircraft, vol. 12, no. 9, Sept. 1975,
     pp. 745-749.

87.  Iverson, James D.; and Bernstein, Shmuel:   Trailing Vortex Effects on
     Following Aircraft.   AIAA J. Aircraft, vol. 11, no. 1, Jan. 1974,
     pp. 60-61.

88. Iverson, J. D.; and Bernstein, S.:  Dynamic Simulation of an Aircraft
    Under the Effect of Vortex Wake Turbulence, Annales de l'Association
    pour le Calcul Analogique, vol. *14, 1972,* pp. *136-144.*

89. Jones, R. T.; and Cohen, D.:  Aerodynamics of Wings at High Speeds.
    Aerodynamic Components of Aircraft at High Speeds, vol. VII, edited
    by A. F. Donovan and H. R. Lawrence, Princeton Univ. Press, *1957.*

90. Ciffone, Donald, L.:  Vortex Interactions in Multiple Vortex Wakes Behind
    Aircraft.  AIAA Paper *76-62, 1976.*

91. Bilanin, A. J.; and Widnall, S, E.:  Aircraft Wake Dissipation by
    Sinusoidal Instability and Vortex Breakdown.  AIAA Paper *73-107, 1973.*

92. Moore, D. W.; and Saffman, P. G.:  Structure of a Line Vortex in an
    Imposed Strain.  Aircraft Wake Turbulence and Its Detection, edited by
    J. H. Olsen et al., Plenum Press, New York, **1971,** pp. *339-354.*

93. Roberts, K. V.; and Christiansen, J. P.:  Topics in Computational Fluid
    Mechanics.  Computer Phys. Commun, Suppl., vol. *3,* Sept. *1972,* pp. *14-*
    *32.*

94. Christiansen, J. P.:  Numerical Simulation of Hydrodynamics by the Method
    of Point Vortices.  J. Computational Phys., vol. **13,** no. *3,* Nov. *1973,*
    pp. *363-379.*

95. Christiansen, J. P.; and Zabusky, N. J.:  Instability, Coalescence
    and Fission of Finite-Area Vortex Structures.  J. Fluid Mech., vol. *61,*
    pt. *2,* Nov. *6, 1973,* pp. *219-243.*

96. Winant, C. D.; and Browand, F. K.:  Vortex Pairing: the Mechanism of
    Turbulent Mixing-Layer Growth at Moderate Reynolds Number.  J. Fluid
    Mech., vol. *63,* pt. *2, 1974,* pp. 237-255.

97. Moore, D. W.; and Saffman, P. G.:  The Density of Organized Vortices in
    a Turbulent Mixing Layer.  J. Fluid Mech., vol. *69,* pt. *3, 1975,*
    pp. *465-473.*

TABLE I.- COMPARISON OF PREDICTED AND MEASURED ROLLING-MOMENT COEFFICIENTS (from ref. 53).

| Configuration | $\alpha$, deg | $C_{L_g}$ | $b_f/b_g$ | $AR_f$ | Normalized rolling moment, $C_{\ell_f}/C_{L_g}$ | | | |
|---|---|---|---|---|---|---|---|---|
| | | | | | Measured[a] | Strip theory | | Vortex-lattice theory Flat-wake approximation |
| | | | | | | $C_{L_\alpha} = 2\pi$ | Empirical $C_{L_\alpha}$ | |
| Flaps 0° | 8 | 0.75 | 0.29 | 5.84 | 0.092 | 0.222 | 0.110 | 0.109 |
| Flaps 0° plus spoiler | 8 | .70 | --- | --- | .053 | .184 | .091 | .085 |
| Landing | 6 | .85 | --- | --- | .081 | .243 | .120 | .117 |
| Landing plus spoiler | 8 | .86 | --- | --- | .081 | .163 | .081 | .071 |
| Tailor[a] | 10 | .82 | --- | --- | .105 | .246 | .122 | .111 |
| Flaps 0° | 8 | .75 | .14 | 2.82 | .099 | .317 | .101 | .090 |
| Flaps 0° plus spoiler | 8 | .70 | --- | --- | .023 | .154 | .049 | .038 |
| Tailor[a] | 10 | .82 | --- | --- | .074 | .173 | .055 | .042 |

WAKE-GENERATING AIRCRAFT

ROLL-UP REGION

PLATEAU REGION

DOWNWASH

FOLLOWING AIRCRAFT
(AXIAL ENCOUNTER)

DECAY REGION
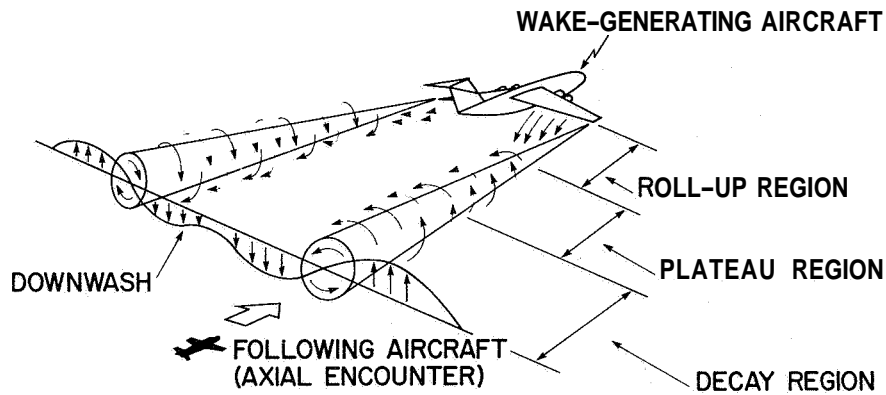
Figure 1.- Flow field produced by lift-generated vortices; distances not
drawn to scale.
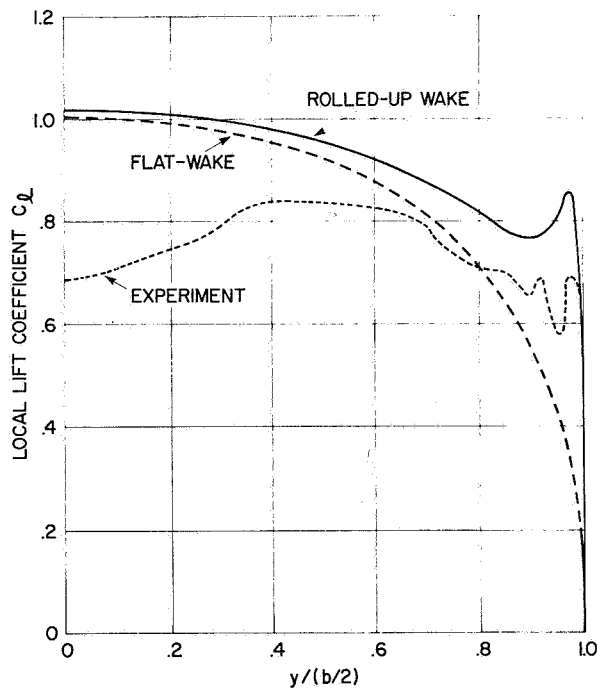


Figure 2.- Measured spanwise lift distribution on rectangular wing compared
with loading predicted by vortex-lattice theory assuming that wake is
flat and that near wake is rolling up; $a = 12°$.  (From B. Maskew, private
communication.)

48

$$y_1 = r_1 + \int_0^{r_1} \frac{d(rv_\theta)}{v_\theta}$$

$$r_1 = -\frac{1}{\Gamma_w(y_1)} \int_{b/2}^{y_1} \Gamma_w(y)\,dy$$

Figure 3.- Schematic diagram of wake rollup and relationships between span loading and vortex structure.



Figure *4*.- Rollup of vortex wake shed by elliptic loading calculated by inviscid two-dimensional time-dependent approximation; W is dimensionless vertical velocity (from ref. 20).

*49*
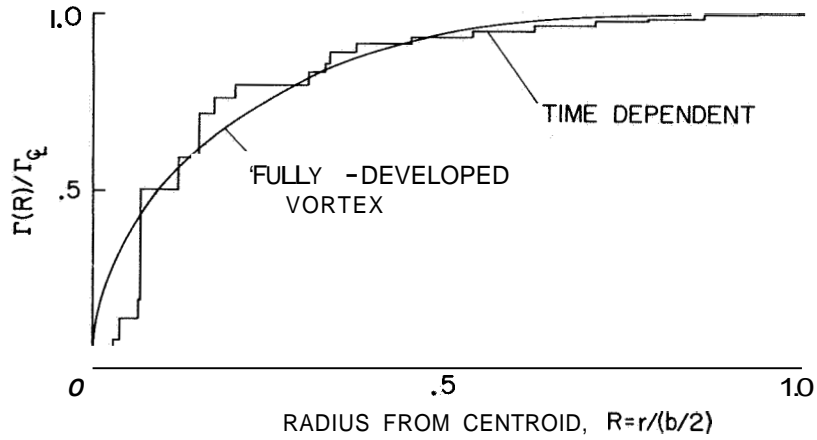
Figure 5.– Comparison of structure of vortex shed by elliptic loading as predicted by time–dependent method with that predicted by the Betz direct rollup theory; $\Gamma_{C_L}$ is circulation on centerline (from ref. 20).
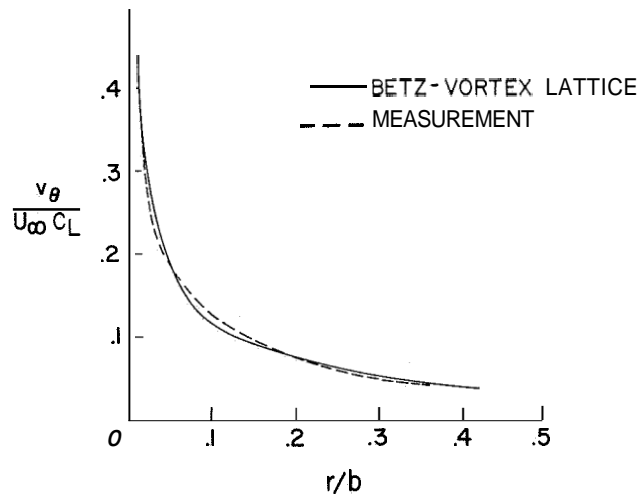


Figure 6.– Comparison of measured vortex structure with prediction made by the Betz rollup theory using span loading predicted by vortex–lattice theory for a swept wing that approximates CV–990 wing (from ref. 53).
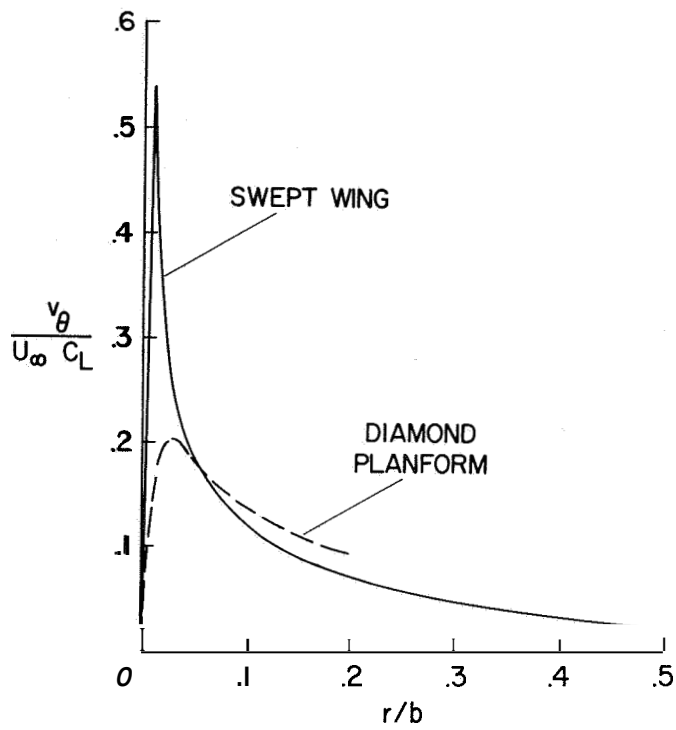
(a) Measured vortex velocity profiles (ref. *53*).
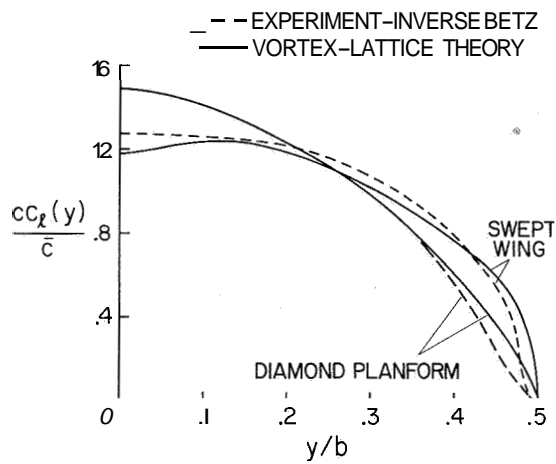


(b) Calculated span loadings.

Figure **7.**– Comparison of inverse rollup theory with vortex–lattice theory (from ref. 56).

51

WATER TANK DATA

$\alpha = 5 \deg$ , $U_\infty = 2.07 \, \text{m/sec}$

WING PLANFORM $(\Gamma_0/U_\infty b)$

O RECTANGULAR .038
a SWEPT .063
□ DIAMOND .050

——— PREDICTION

$\dfrac{V_1}{U_\infty} \sim \left(\dfrac{x}{b}\right)^{-\frac{1}{2}}$
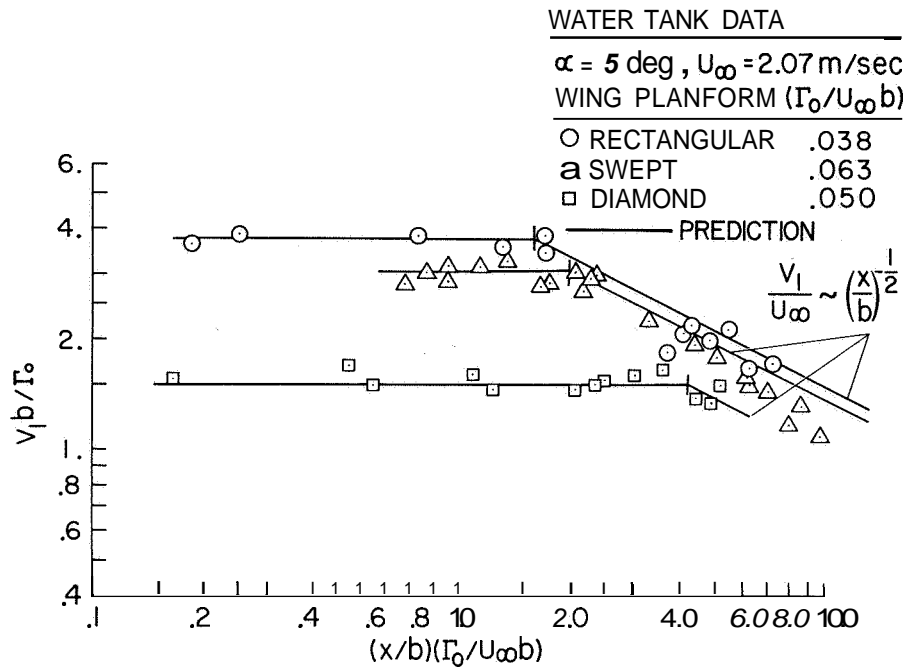
Figure 8.– Maximum circumferential velocity in vortices behind wings as measured in water tow tank (from Ciffone and Orloff, ref. 55).
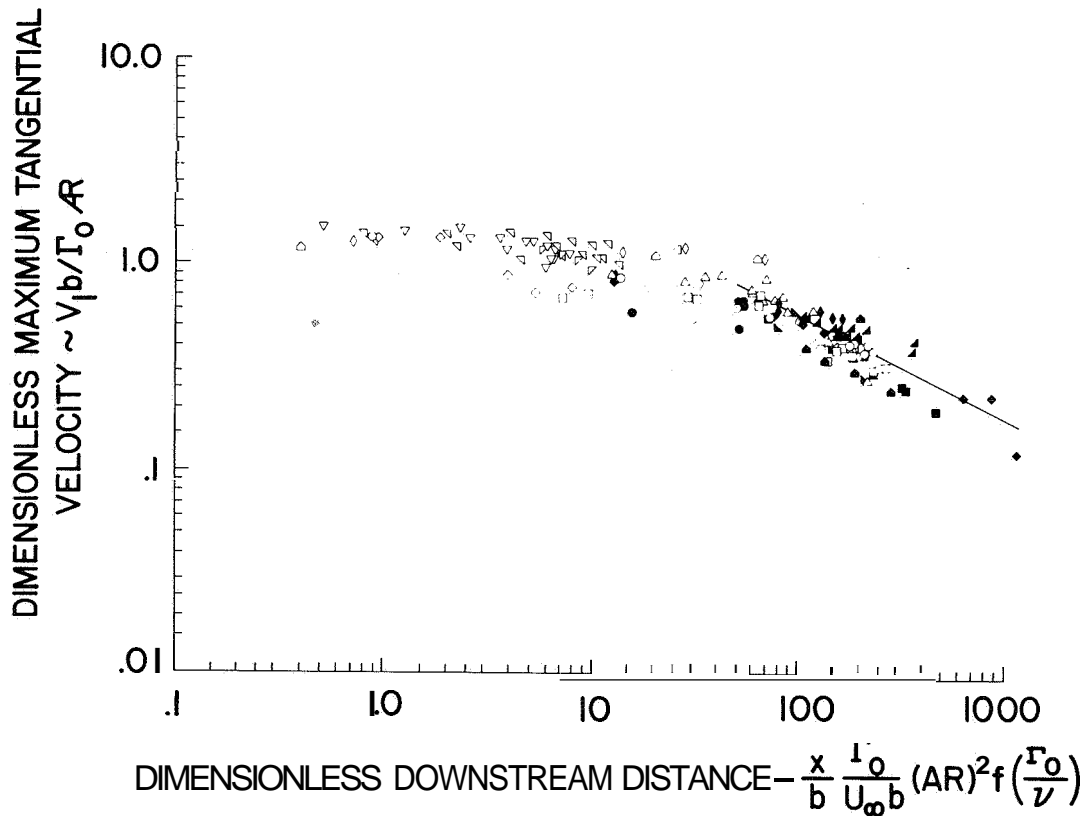


Figure 9.– Correlation of data from ground–based and flight experiments on maximum circumferential velocity in vortices shed by various conventional span loadings (from Iversen, ref. 58).
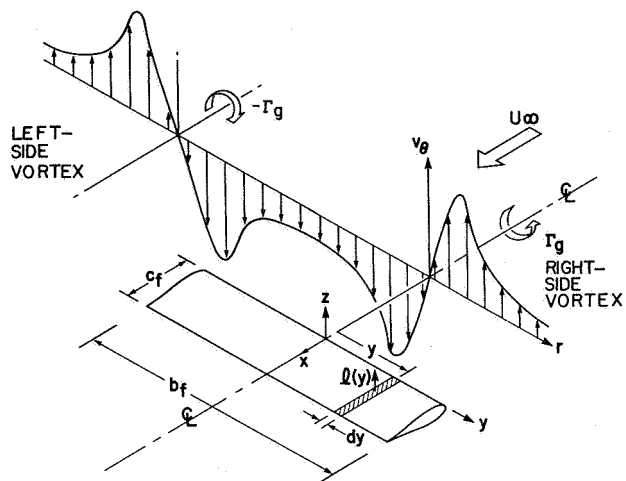
Figure 10.– Wake vortex pair impinging on a follower wing.
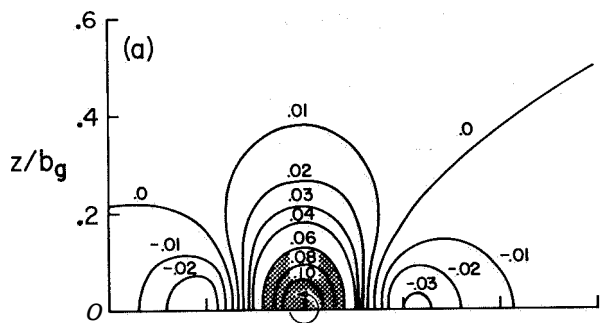


(a) Contours of equal rolling–moment parameter, $C_{l_f}/C_{L_g}$; $C_{l_f})_{max}/C_{Lg} = 0.122$.
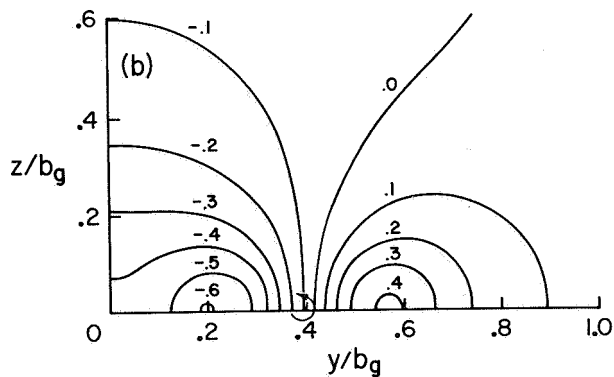


(b) Contours of equal lift parameter, $C_{L_f}/C_{L_g}$; $C_{L_f})_{max}/C_{L_g} = -0.88$.

Figure 11.– Rolling moment and lift induced on the follower wing by the wake of a swept wing; tailored loading, $b_f/b_g = 0.29$ (from ref. *53*).
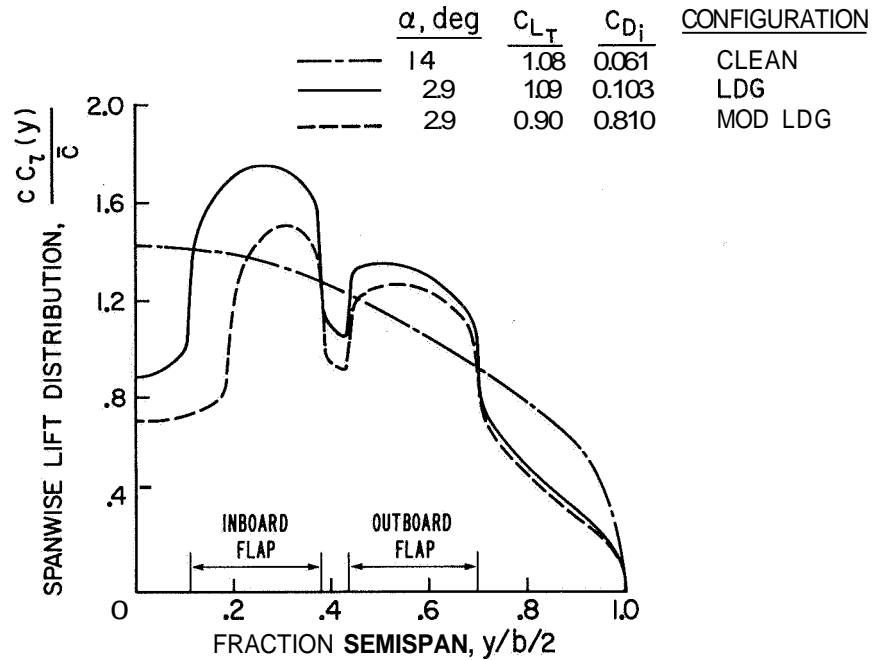
Figure 12.– Span loadings predicted by vortex–lattice theory for Boeing 747 wing without a fuselage (from Ciffone, ref. 90).
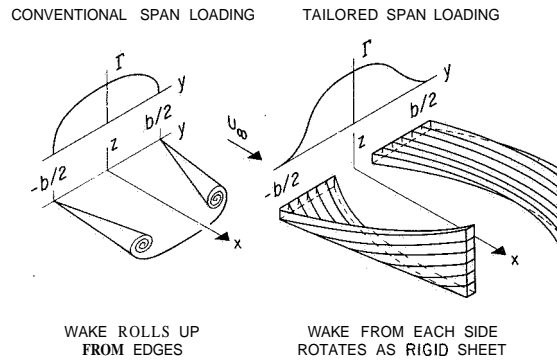


Figure 13.– Comparison of conventional wake with hypothetical wake designed to have parts that rotate as a unit without rolling up from its edges (from ref. 20).

54

3
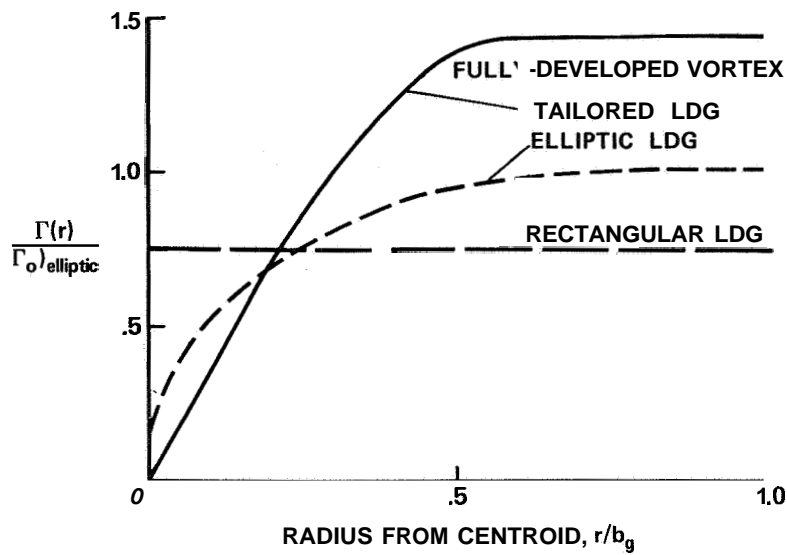
Figure 14.– Radial distribution of circulation in wake vortices shed by .90 percent tailored loading as predicted by Betz' theory for fully developed vortices.
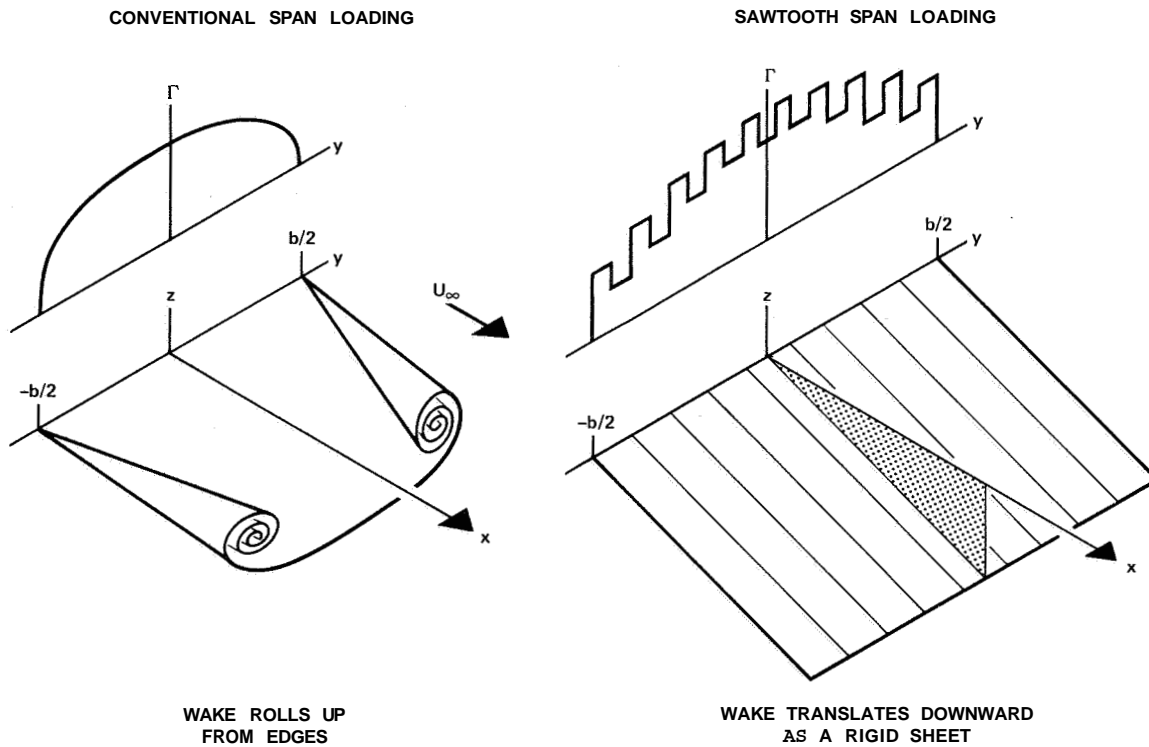


Figure 15.– Comparison of conventional wake with a hypothetical wake designed to translate downward as a unit.

55

SAWTOOTH LOADING                    CONVENTIONAL LOADING
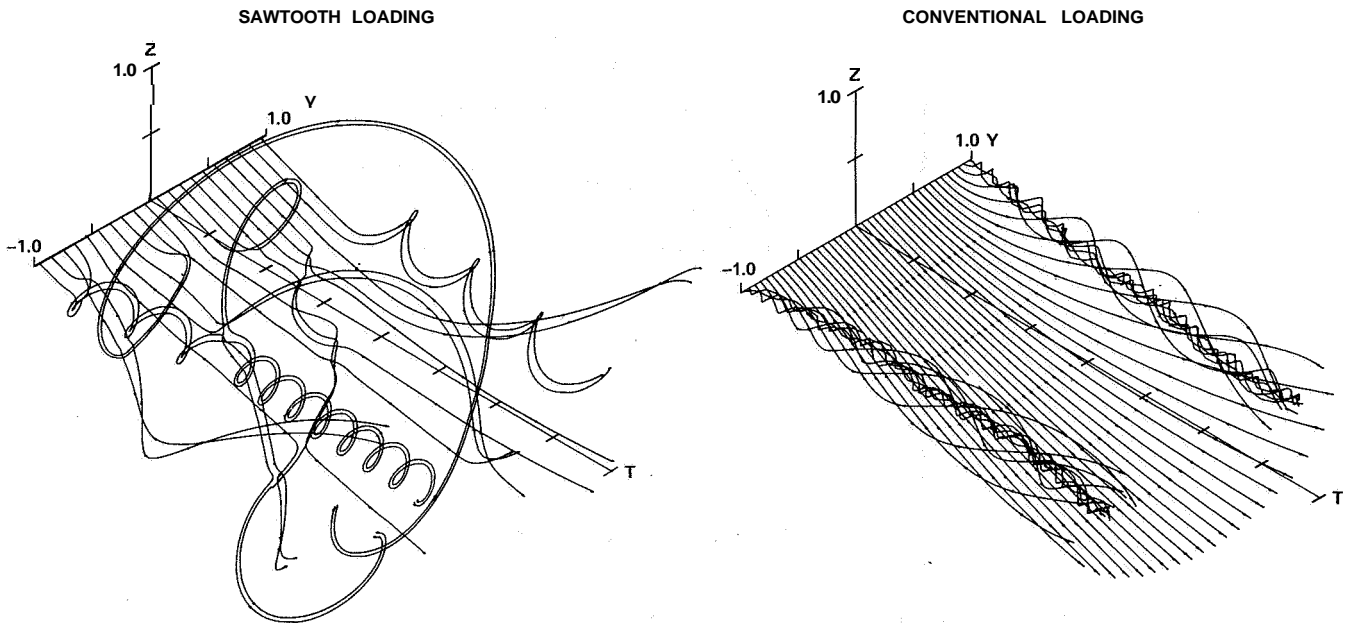
(a) Large–scale wake mixing.          (b) No wake mixing.

Figure 16.– Wake structure predicted by time–dependent vortex calculations
for elliptic and sawtooth span loadings (from ref. 20).



SAWTOOTH LOADING ON CV990 WING
$C_L = 0.7$
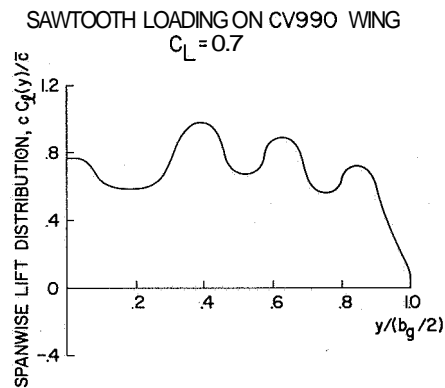
Figure 17.– Span loading predicted by vortex–lattice theory for swept wing
with seven flap segments per side deflected alternately up and down 15°;
$C_L = 0.7$ (from ref. 53).
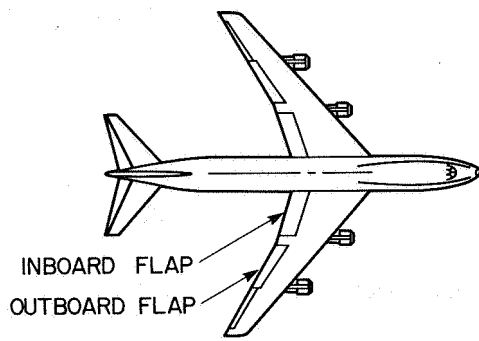
Figure 18.– Plan view of Boeing 747 subsonic transport.
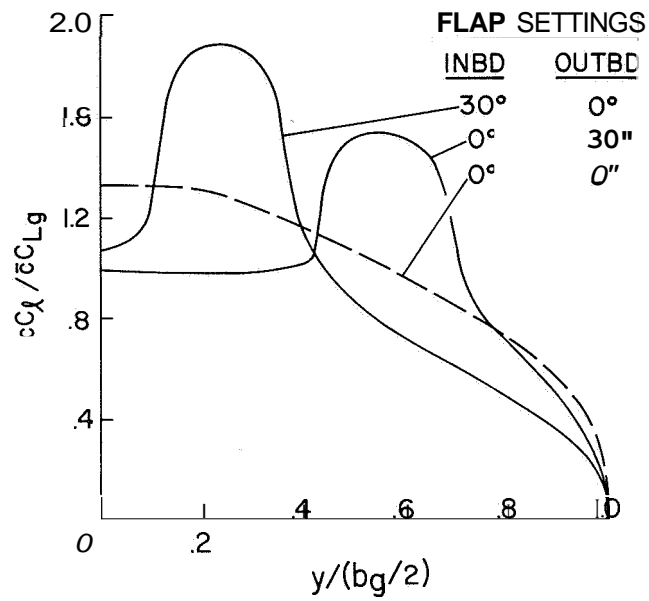


Figure 19.– Span loadings calculated for Boeing 747 wing using vortex–lattice theory (from ref. 83).

CONVENTIONAL LANDING CONFIGURATION

x/b=6

x/b

WAKE VORTICES MERGED
TO FORM SINGLE PAIR
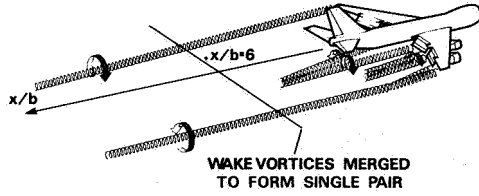
MODIFIED LANDING CONFIGURATION (LDG/0°)

FLAP INBOARD AND
OUTBOARD VORTICES MERGE

FLAP AND TIP VORTICES
MERGE (GEAR UP)

1.5

13

6

x/b
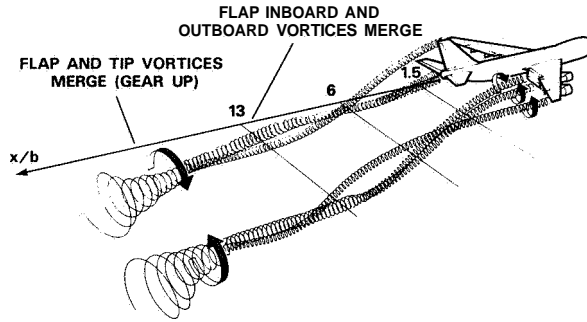
Fig. 20.- Comparison of two wakes of Boeing 747 (from ref. 83).



$\Gamma_1 = \Gamma_2$
$d_s = 1.7 d_c$

$\Gamma_2$

$\Gamma_1$    T = 0

$d_c$

T = 1

$d_s$

VORTEX C.G. LOCATIONS

T = 2

T = 3
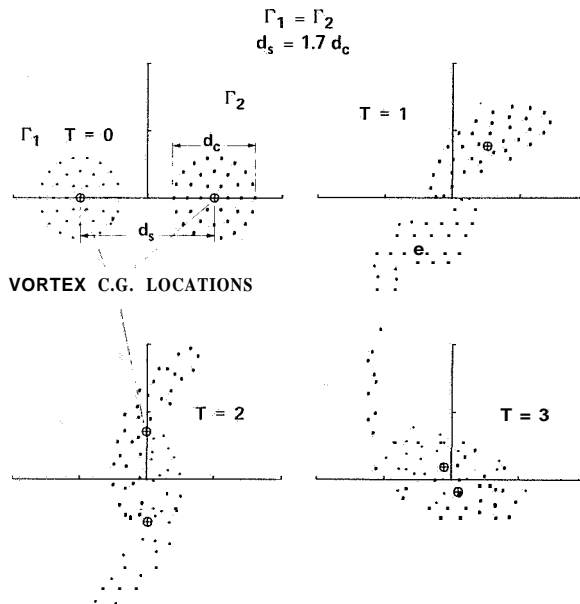
Fig. 21.- Merging sequence predicted numerically for two Rankine vortices of
equal strength, $\Gamma_1 = \Gamma_2$ and $d_s = 1.7 d_c$.
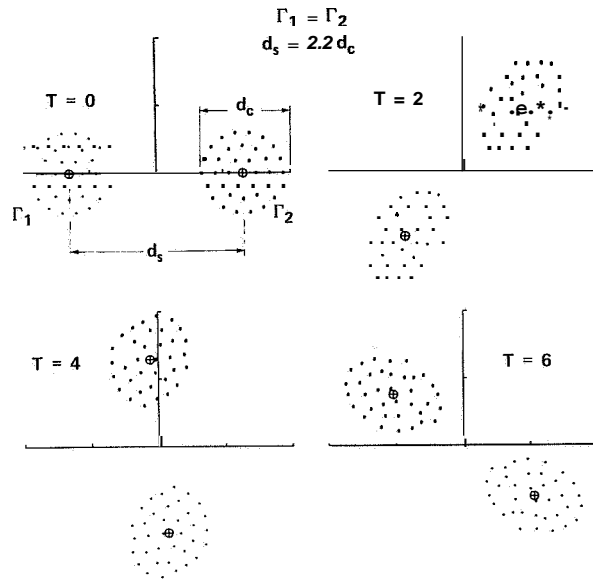
Figure 22.– Case where two Rankine vortex cores do not merge because spacing between them is too large; $d_s = 2.2 d_c$, $\Gamma_1 = \Gamma_2$.
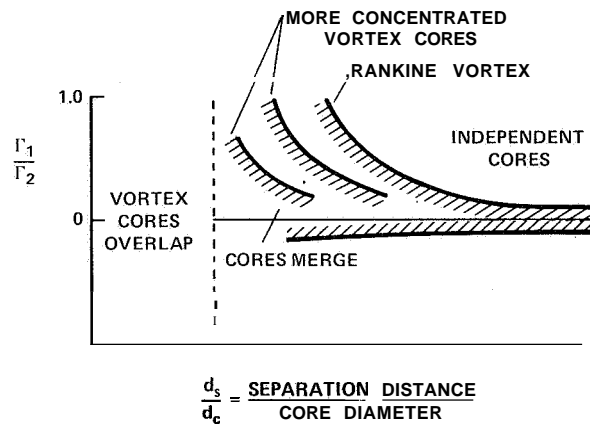


Figure 23.– Combinations of strength and spacing required for Rankine vortex cores to merge.

# VISCOUS EFFECTS IN AIRCRAFT TRAILING VORTICES"

Alan J. Bilanin, Milton E. Teske,
Coleman duP. Donaldson and Richard S. Snedeker
Aeronautical Research Associates of Princeton, Inc.

## SUMMARY

The mechanism of merging of like-signed aircraft vortices leads to a rapid redistribution of trailed vorticity in a wake through both convective and turbulent processes. Merging is investigated experimentally in a small wind tunnel and analytically through the use of a code which computes turbulent transport using a second-order closure turbulent model. Computations are reported which demonstrate the merging phenomenon, and comparisons are made with experimental results. The usefulness of point vortex computations in predicting merging is explored. Limited computations have shown that jet exhaust does not appreciably alter the merging phenomenon. The effect of ambient atmospheric turbulence on the aging of an aircraft wake is investigated at constant turbulent dissipation rate. It is shown that under stable atmospheric conditions, when atmospheric macroscales are less than or equal to the vortex spacing, misleading results may be obtained. This conclusion cautions against using one parameter to characterize the ability of the atmosphere to dissipate aircraft wake vortices.

# I. INTRODUCTION

The hazard associated with an aircraft's trailing vortex wake is generally acknowledged to be the large rolling moments induced on an encountering aircraft. These rolling moments are related to the angular momentum contained in the wake itself. The magnitude of angular momentum can be directly estimated from the Betz roll-up model (ref. 1), which has received widespread use in recent years (refs. 2-5). The Betz roll-up technique specifies how the torque exerted by the lift distribution on a wing (see **rig. 1**) results in a distribution of angular momentum in the trailed vortex through the relationships

$$r = \bar{y}(y) - Y \tag{1}$$

$$\Gamma(r) = \Gamma(y) \tag{2}$$

where $\Gamma(y)$ is the circulation distribution on the wing and $\Gamma(r)$ is the circulation distribution in the downstream vortex. The length $r$ is related to $y$ through Eq. (1), where $\bar{y}(y)$ is the centroid of vorticity shed outboard of wing station $y$ and is defined as

$$\bar{y}(y) = \frac{-1}{\Gamma(y)} \int_{y}^{S} \frac{d\Gamma(\eta)}{d\eta} \eta \, d\eta \tag{3}$$

Equations (1) through (3) are equivalent to

$$\text{Torque} = \int_{Y}^{S} \ell(\eta)[\eta - \bar{y}(y)]d\eta = 2\pi\rho \int_{0}^{r} U_{\infty}V_{\theta}(\chi)\chi 2d\chi \tag{4}$$

where $\ell(\eta) = -\rho_{0}U_{\infty}\Gamma(\eta)$ is the wing sectional loading on the fluid and $s$ is the wing semispan.

The axial flux of angular momentum in a vortex of radius $r$ equals the torque exerted on the fluid (calculated about $\bar{y}(y)$ outboard of wing station $y$). Setting $y = 0$ in Eq. (4) shows that the torque exerted by the wing equals the axial flux of angular momentum in the Betz vortex and is given by

62

$$\text{Torque} = \frac{Lb}{4} \left[ \frac{\bar{y}(0) - \bar{y}_L}{s} \right] \tag{5}$$

where $\bar{y}_L$ is the centroid of the load distribution defined by

$$\bar{y}_L = \frac{\int_0^s \Gamma(\eta)\eta \; d\eta}{\int_0^s \Gamma(\eta) \; d\eta} \tag{6}$$

Since $(\bar{y}(0) - \bar{y}_L)/s$ is a function only of the shape of the load distribution, its value is nearly constant among various aircraft. (For a rectangularly loaded wing and a linearly loaded wing $(\bar{y}(0) - \bar{y}_L)/s = 1/2$ and $1/6$ , respectively.) It is therefore not surprising that the rolling moment hazard is a function of the .generating aircraft's size, since the angular momentum in the Betz vortex (from eq. (5)) is proportional to the product of the lift L and wing span b . If a small aircraft were to encounter the whole of this torque from a jumbo jet, the results would be disastrous.

Fortunately, the torque induced on an encountering aircraft is a fraction of that which might actually be extracted from the wake. This is due simply to the fact that the encountering aircraft's dimensions permit it to span only a portion of the vortex at any one time. This may not however be a saving grace, since the roll control capability of·an aircraft diminishes with diminishing span. What then will permit a small aircraft to fly at a reasonable distance behind a larger generating aircraft? The answer lies in the distribution of angular momentum. First, the conservation of angular momentum would say that the total axial flux of angular momentum in the half–cross plane calculated about the aircraft wing centerline must initially equal the generator's wing root bending moment. Apparently the distribution of angular momentum can be substantially altered by tailoring the generator's lift distribution. Second, the landing or takeoff wake of an aircraft, comprised of multiple vortex pairs (see fig. 2), can undergo an

initially convective instability called vortex merging.  The merging phenomenon results in a redistribution of trailed vorticity in a wake through convective and turbulent processes.  This re-distribution lessens the hazard of the trailed wake in distances which have been observed to be tens of spans behind the generating aircraft.

The convective and turbulent interactions between vortices in distances of up to 30 or 40 spans behind the generator form the subject of this paper.  A qualitative description of the aging process in the near vortex wake and the relevance of multiple vortices and merging are discussed in Section II.  In Section III, A.R.A.P.'s turbulent model is briefly reviewed, and a simple merging computation between two equal strength like-signed vortices is given.  Recent experimental results of the vortex-vortex interaction problem obtained in a small wind tunnel are described in Section IV.  A discussion of how point vortex computations can be used to determine whether strong vortex interactions are likely to occur in vortex wakes is given in Section V.  Numerical calculations of aircraft wakes including the effects of thrust and atmospheric turbulence are presented in Section VI.  Finally, in Section VII, conclusions are offered.

## SYMBOLS

| | |
|---|---|
| $A$ | wing aspect ratio  . |
| $b$ | wing span |
| $b'$ | separation between two oppositely signed vortices |
| $C_D$ | drag coefficient |
| $C_L$ | lift coefficient |
| $C_T$ | thrust coefficient |
| $d$ | separation between like-signed vortices |
| $e$ | circulation box size |
| $h$ | vertical height of vortex pair |
| $\ell$ | sectional lift on the fluid |
| $L$ | lift |

| | |
|---|---|
| P | pressure |
| q | $\sqrt{\overline{uu} + \overline{vv} + \overline{ww}}$ |
| r | radial coordinate |
| $r_c$ | viscous core radius |
| s | wing semispan |
| s' | b'/2 |
| t | time |
| U,V,W | velocity components in the x,y,z Cartesian system |
| $U_\infty$ | flight speed |
| $V_\theta$ | swirling velocity |
| x,y,z | Cartesian coordinate system |
| $\bar{y}(y)$ | centroid of trailed vorticity |
| $\bar{y}_L$ | centroid of the load distribution |
| | |
| $\Gamma$ | circulation |
| $\Gamma_0$ | wing root circulation |
| $\zeta$ | vorticity |
| $\varepsilon$ | turbulent dissipation rate |
| $\Lambda$ | turbulent macroscale or integral scale parameter |
| $\nu$ | kinematic viscosity |
| $\rho_0$ | ambient density |
| $\psi$ | secondary streamline value |
| — | overbar denotes time average |

## II.  A QUALITATIVE DESCRIPTION OF VORTEX WAKE AGING

When an aircraft in a clean (cruise) configuration trails a
wake, two regions of somewhat concentrated vorticity are left in
the fluid, shown schematically in figure 3.  For an encountering
aircraft whose span is less than the semispan of the generating
aircraft, a most desirable piece of information is the intensity
of the swirling flow in a circular area whose diameter is the
wingspan of the encountering aircraft.  If circulation is a

reasonable measure of this intensity, then we must determine how circulation might decrease in this region, If we center the area about the centroid of shed vorticity (as in fig. 3), we see that vorticity cannot be transported from this region by convection since, roughly speaking, streamlines do not leave the circular region. Hence, diffusion is the only mechanism able to spread vorticity and reduce circulation in this area. Unfortunately, the axisymmetric vortex is quite stable and can only sustain low turbulence levels. In fact, turbulence is actually damped in the central region of the vortex (the viscous core). It is just in this region where vorticity is maximum, making it desirable to dis-tribute this vorticity rather extensively over the wake half-plane. Apparently, however, only molecular transport provides any diffusion of vorticity here.

That vortex cores from simply loaded wings are in fact nearly laminar can be seen from figure 4 where smoke released from a tower has been entrained into the wing tip vortex of a large aircraft. The air through which the aircraft flies is discernibly turbulent (as interpreted from the dispersion of smoke) while the vortical fluid making up the viscous core is nearly laminar.

Turbulent computations using second-order closure modeling also confirm this feature of isolated vortices. The swirling velocity for a classical Lamb vortex is given by

$$V_\theta = \frac{\Gamma}{2\pi r} \left( 1 - \exp \frac{r^2}{r_c^2} \right) \tag{7}$$

Taking the equilibrium, nondiffusive, and high Reynolds number limits of the second-order closure model (ref. 6), we obtain the turbulent kinetic energy distribution shown in figure 5. Also shown is the corresponding distribution of vorticity. Note that no turbulent kinetic energy is predicted for $r/r_c \leq 1.25$ . The centrifugal effect of the swirling velocity suppresses the Production of turbulence in this region.

From observations and analytic considerations(refs. 5,7), aircraft vortices do not produce sufficient axial shear to provide a mechanism for any sizable production of turbulence. The vortices from a clean aircraft age quite independently in a calm atmosphere. (The vortex pair from a clean aircraft can undergo a Crow instability excited by the atmosphere (ref. 8). However, time scales for this instability result in distances behind the aircraft far larger than those being considered here.)

In the landing or take-off configuration (flaps deployed), the trailed wake takes on a decidedly more complex structure. Multiple vortex pairs are trailed and interact. Significantly, this interaction may be favorable since the straining effect of vortex upon vortex may destroy the circular symmetry of each vortex. The vortices undergo an initial convective instability leading to a production of turbulent energy and turbulent redistribution of the vorticity (again, see fig. 3). On comparable time scales, the multiple-pair wake can age more than the wake of the cruise aircraft when this favorable interaction is utilized.

Of course, other mechanisms can also act to spread vorticity across the wake. However, only vortex breakdown acts on a time scale commensurate with the merging phenomenon. Unfortunately, our work on the transport processes involved in breakdown is just beginning.

In sum, the merging phenomenon is a naturally occurring mechanism of decay in aircraft multiple-vortex wakes, leading to a more rapid conversion of the kinetic energy of the swirling velocities in the vortices into turbulent kinetic energy. If the merging phenomenon can be understood and predicted, a great potential exists for lessening the hazard associated with vortex wakes through suitably tailored wing lift and drag distributions.

# III. A NUMERICAL COMPUTATION OF MERGING

Dunham (ref. 9) first observed the merging phenomenon between flap and tip vortices of the B-747 aircraft on what has become the LDG/O configuration. That is, inboard flaps are deployed at $\delta_f = 46^o$ and midspan flaps remain undeployed. His sketch of the phenomenon is shown in figure 6, where ink injected at the wing was used to visualize the vortices. He observed that the tip and flap vortices, while quite distinct at fifteen span-lengths behind the B-747, appeared to interact further downstream until only one rather weak (diffuse) vortex remained. The rather rapid diffusion of the ink suggested the mechanism of turbulent transport in the spreading of the trailed vorticity.

To model the convection and turbulent diffusion of vorticity, we at A.R.A.P. have developed a computer code to solve the equations of fluid motion including our invariant turbulent model (ref. 10). This model is based on a closure of the rate equations for the velocity correlations at the second order. Details of the model, its evolution and validation, may be found in references 10 and 11. It suffices here to reproduce the equations. The flow variables are separated into mean and fluctuating components, then averaged and modeled where appropriate. The mean variables satisfy continuity

$$\frac{\partial U_i}{\partial x_i} = 0 \qquad (8)$$

and momentum

$$\frac{\partial U_i}{\partial t} + U_j \frac{\partial U_i}{\partial x_j} = -\frac{\partial \overline{u_i u_j}}{\partial x_j} + \nu \frac{\partial^2 U_i}{\partial x_j^2} - \frac{1}{\rho_o} \frac{\partial P}{\partial x_i} \qquad (9)$$

where the density $\rho_o$ is constant.

The turbulent velocity correlations satisfy the rate equations

$$\frac{\partial \overline{u_i u_j}}{\partial t} + U_k \frac{\partial \overline{u_i u_j}}{\partial x_k} = - \overline{u_i u_k} \frac{\partial U_j}{\partial x_k} - \overline{u_j u_k} \frac{\partial U_i}{\partial x_k}$$

$$\underbrace{\phantom{- \overline{u_i u_k} \frac{\partial U_j}{\partial x_k} - \overline{u_j u_k} \frac{\partial U_i}{\partial x_k}}}_{\text{Production}} \qquad (10)$$

$$+ v_c \frac{\partial}{\partial x_k} \left( q\Lambda \frac{\partial \overline{u_i u_j}}{\partial x_k} \right)$$

pressure and velocity diffusion

$$- \frac{q}{\Lambda}\left( \overline{u_i u_j} - \delta_{ij} \frac{q^2}{3} \right)$$

$$\underbrace{\phantom{- \frac{q}{\Lambda}\left( \overline{u_i u_j} - \delta_{ij} \frac{q^2}{3} \right)}}_{}$$

tendency toward isotropy

$$+ \nu \frac{\partial^2 \overline{u_i u_j}}{\partial x_k^2}$$

viscous diffusion

$$- \delta_{ij} \frac{2bq^3}{\Lambda} - \frac{2a\nu \overline{u_i u_j}}{\Lambda^2}$$

$$\underbrace{\phantom{- \delta_{ij} \frac{2bq^3}{\Lambda} - \frac{2a\nu \overline{u_i u_j}}{\Lambda^2}}}_{}$$

dissipation

where $q = (\overline{u_i u_i})^{1/2}$. The pressure and velocity diffusion, tendency toward isotropy, and dissipation terms are modeled. Models are chosen on the basis of dimensional consistency, tensor invariancy under transformation, and physical considerations (ref. 11). The constants $v_c$ , b , and a have the values 0.3 , 0.125, and 2.5, respectively. These constants have been determined from appropriate experiments so chosen where possible to emphasize the particular effect studied.

Lambda (Λ) is the turbulent integral scale or macroscale parameter gaging the coherent length scale of the turbulent eddies. It is determined from a dynamic equation which models the production, diffusion, and dissipation of the integral scale'of the turbulence. The dynamic scale equation being used (ref. 11) is

$$\frac{D\Lambda}{Dt} = \underbrace{0.35 \; \frac{\Lambda}{q^2} \; \overline{u_i u_j} \; \frac{\partial U_i}{\partial x_j}}_{production} + \underbrace{0.6 \; \frac{\nu}{\lambda^2} \; \Lambda}_{dissipation}$$

$$+ \underbrace{0.3 \; \frac{\partial}{\partial x_i} \left( q\Lambda \; \frac{\partial \Lambda}{\partial x_i} \right) - \frac{0.375}{q} \left( \frac{\partial q\Lambda}{\partial x_i} \right)^2}_{diffusion} \tag{11}$$

where $\lambda = \dfrac{\Lambda}{[a+(bq\Lambda/\nu)]^{1/2}}$ is the dissipation scale.

Equations (8-11) have been programmed to solve either two-dimensional unsteady or three-dimensional steady problems with a parabolic approximation made in one space dimension. The details of the algorithms used can be found in reference 12.

As a first illustration of the numerical computations, we have chosen the simplest merging problem between two like-signed equal strength vortices. The computational region is shown in figure 7. Two Gaussian spots of vorticity of the form

$$\frac{\pi d^2 \zeta}{2\Gamma} = \frac{d^2}{2r_c^2} \exp \left( - \frac{r^2}{r_c^2} \right) \tag{12}$$

have been placed at $y = \pm d/2$ , $z = 0$ . The **radius** $r$ is measured outward from both $y = \pm d/2$ , $z = 0$ . Gaussians of turbulent kinetic energy of the form

$$q^2 = q_o^2 \exp \left( - \frac{r^2}{r_c^2} \right) \tag{13}$$

70

are also placed at  $y = \pm d/2$ , $z = 0$  with

$$q_0^2 = 0.01\left(\Gamma/\pi d\right)^2 \tag{14}$$

The calculation is started with  $\overline{uu} = \overline{vv} = \overline{ww} = q^2/3$  and  $\overline{uv} = 0$.
The integral scale parameter is initially taken equal to 0.2s.
Boundary conditions on velocity are applied via a multipole expansion
of the vorticity field (ref. 12).  Turbulent quantities are set
equal to zero at the computational boundaries.

The results of the computations are shown in figures 8, 9, and
10, where instantaneous distributions of pressure, vorticity, and
turbulent kinetic energy are shown in intensity form.  The counter-
clockwise rotation of the pair is expected.  It is interesting to
note that the mean flow variables, pressure and vorticity, take on
a discernibly more axisymmetric structure at  $t\Gamma/\pi d^2 = 4$  than
the turbulent kinetic energy,  This is expected in a phenomenon in
which the redistribution of vorticity is initially governed by con-
vection.  The initial time scale for turbulent redistribution
through diffusion is of the  $O(\Lambda/q)$  , which is approximately
$t\Gamma/\pi d^2 = 1$ .

A comparison with an equivalent isolated vortex decay compu-
tation illustrates the significance of the merging phenomenon in
terms of aging the vortex flow field.  We have chosen to compute
the decay of an isolated axisymmetric vortex whose initial
vorticity distribution is Gaussian and whose circulation equals
that of the pair.  The core radius  $r_c$  has been chosen to make
the polar moment of the vorticity distribution computed about the
centroid equal to that of the merging pair.  Thus,

$$r_c^2 = r_{c_{pair}}^2 + \frac{d^2}{4} \tag{15}$$

The computation is carried out with an axisymmetric version of the
code (ref. 13) used to compute the merging of the like-signed pair.
The initial turbulence distribution is taken to be  $\overline{uu} = \overline{vv} = \overline{ww} = q^2/3$  where

$$q^2 = 2.0q_o^2 \exp\left[-\left(\frac{r}{r_{c_{pair}}}\right)^2\right] \qquad (16)$$

so that the initial total turbulent kinetic energy in both computations are equal. The integral scale parameter A is taken to be 0.2s ,

Figure 11 shows the total turbulent kinetic energy in the crossplane as a function of time. The level that can be supported by the axisymmetric isolated vortex is far less than initially introduced, as discussed earlier and in reference 6. However, the breakdown of the axisymmetric structure about each vortex in the merging pair results in the production of turbulent kinetic energy and, hence, Reynolds stresses, which diffuse the mean vorticity outward in addition to the convective spreading. The production of turbulence is the transport mechanism which can diffuse vorticity to the wake centerline and result in the decay of circulation in the wake, as was shown schematically in figure 3.

## IV. EXPERIMENTAL OBSERVATIONS OF MERGING AND PAIR INTERACTIONS

A simple experiment was designed to observe the merging phenomenon in a controlled environment.

### Apparatus an& technique

Flow visualization studies of vortex merging and pairing were carried out in A.R.A.P.'s 0.305 m × 0.305 m subsonic wind tunnel. This facility has a 2-m-long test section with an adjustable roof to allow modification of the axial pressure gradient. For these studies the pressure gradient was set at zero.

The tunnel has a maximum velocity capability of 15 m/sec and the test section turbulence level is relatively low -- about 0.2% For the purposes of these studies, the test section was fitted with windows for its full length on one side, and the interior

3

surfaces were painted flat black to improve visibility of the white smoke used for visualization.

Vortex flows were produced by airfoils mounted through opposite sidewalls of the tunnel just upstream of the test section. Each airfoil had a constant chord of 7.62 cm and was mounted so that its angle of attack and length of immersion in the stream could be adjusted. Thus, the strengths of the vortices and their initial spacing could be set to any desired value. The airfoil section was NACA 0012 and the tip was a revolved section. Construction was of molded fiber glass and polyester resin. The airfoils were hollow to permit the flow of smoke from outside the tunnel to holes in the wing tips near the points of initial vortex roll-up. This arrangement produced a quite satisfactory concentration of smoke in the trailed vortex behind each airfoil.

Observation of merging and pairing phenomena was accomplished by illuminating the entrained smoke with a planar beam of light directed across the tunnel normal to the flow. In this way a cross-section of the vortex flow pattern was made visible when viewed from a point upstream or downstream of the light beam. In order to record the patterns photographically, a small mirror was mounted inside the wall of the diffusor downstream of the test section. The mirror was set so as to reflect an image of the illuminated cross-section through a window in the side wall and, finally, to a camera outside the tunnel. With this setup it was possible to photograph patterns between 3 and 23 chord-lengths downstream of the airfoils.

Continuous illumination was provided by the beam from a lantern slide projector and instantaneous illumination was provided by an electronic flash unit. Thus, it was possible to view smoke patterns that were either time averaged (usually 1/2-second exposure) or "frozen" (1/2800 second). The planar beam of desired intensity was produced by passing the light through a vertical slit about 0.95 cm wide.

A sufficient quantity of dense white smoke was produced by a boiled–kerosene smoke generator.

Views of the wind tunnel and airfoil assemblies are shown in figure 12.

## Results

The merging phenomenon between vortices of same sign and strength is visualized in figure 13. Viewed from downstream, the angles of attack for the left and right wings are $-6^{\circ}$ and $6^{\circ}$, respectively. The vortex rotation is then in the clockwise direction. As can be seen, the vortices are quite distinct at $x/d = 18$ but merge quite rapidly between $x/d = 90$ and $114$. By $x/d = 138$, the merged pair is nearing an axisymmetric shape. The straining effect of vortex upon vortex is quite evident at the $x/d = 114$ and $126$ stations.

The photographs suggest that the merging phenomenon is nearly laminar. This is attributed to rather low test Reynolds numbers. Typically, $\Gamma/\nu \simeq 5000$ for these tests, while the Reynolds numbers associated with aircraft wakes are more like $10^7$. This, however, does not limit the usefulness of these tests since the initial stages of the merging phenomenon are convection dominated. The initial redistribution of trailed vorticity can be studied directly.

To again illustrate the importance of turbulent transport, the merging computation presented in Section III is compared with smoke visualization photographs. Figure 14 shows computed vorticity intensity plots and photographs of visualized smoke at comparable downstream positions. The comparison of smoke intensity with vorticity is not quite correct since the smoke particles are not quite the same density as the fluid. The comparisons, however, are qualitatively quite good with the last axial station showing the greatest departure. The turbulent computation shows the vorticity measurably more spread through the fluid and at a substantially lower level. Both effects result from the turbulent diffusion present in the numerical simulation.

The next sequence of photographs, shown in figure 15, explores angle-of-attack change of one wing while holding vortex separation and the angle of attack of the second wing constant. The photographs are taken at downstream station $x/d = 55.4$. Equal sign and strength vortices occur with $\alpha_{ref} = -\alpha_{var} = -6°$. As one vortex is weakened, the stronger vortex begins to strain the weaker vortex and proceeds to wrap the weaker vorticity around itself. When the vortices become of opposite sign, there is less tendency to merge even when one vortex is significantly weaker than the other. Compare, for instance, $\alpha_{ref} = -6°$, $\alpha_{var} = 2°$, and $a_{ref} = -6°$, $a_{var} = -2°$. When both angles of attack are equal the classical vortex pair is produced.

The next sequence of photographs (fig. 16) explores the stability of the counter-rotating pair as the separation between the pair is reduced. At a fixed downstream station, the vortex pair has descended to a lower position in the tunnel as separation is decreased. The last photograph shows how remarkably stable the counter-rotating configuration can be. The physical mechanisms which permit vortices of like sign to merge quite readily while inhibiting the merging of vortices of opposite sign are yet to be explained, Moore and Saffman's work (ref. 14) notwithstanding.

In figure 17 an attempt is made to visualize the structure of the vortex by taking a high-speed photograph (1/2800 sec). Upper right shows the instantaneous smoke pattern of an unmerged pair, while upper left shows the continuously lighted smoke distribution, Lower right shows the instantaneous smoke pattern of a merging pair with equal strength and like sign. This may be compared to the continuously lighted photograph in lower left. A careful inspection of the instantaneously lighted photographs shows the merged pair to be more turbulent than the unmerged pair.

## V.   MERGING COMPUTATIONS USING POINT VORTICES

An important part of the merging phenomenon is the production of turbulence and the subsequent diffusion of trailed vorticity. Before using a program that incorporates all of these effects, we may first obtain some fundamental results using a far simpler inviscid model, namely, the point vortex technique for computing wake structure.   Point vortex computation for wakes is not a new idea, having been used first by Westwater (ref. 15) in 1935.   Since that time, many investigators have used this technique.   The basic idea is to distribute point vortices ip the Treffetz plane of a hypothetical wing, as shown in figure 18, and compute their trajectories in time.   The resulting motion will be produced by the convective interaction between the vortices themselves.

Given two like-signed vortices, the rate of merging should increase as the separation between the vortices decreases.   The simplest interesting wake is made of two vortex pairs; for example, one comprised of flap and tip vortices.

Merging should occur if the subsequently computed trajectories brought the flap and tip vortices closer together, or at least did not increase the distance between vortex centers.   Figures 19 and 20 illustrate the trajectories of two rather differently structured wakes.   The tight orbiting of flap and tip vortices in figure 19 will result in merging while the weak interaction between flap and tip vortices, shown in figure 20, may not result in merging.

For two-vortex-pair wakes a qualitative prediction of whether merging may in fact occur can be obtained from a wake classification chart shown in figure 21.   When vortices are of like sign and fall in the region marked "remain together," one might expect that merging will <u>eventually</u> occur.   On the other hand, wakes which fall in the region denoted "separate" may possibly remain unmerged.   Wakes from real aircraft in a landing or takeoff configuration have far more structure than can be

76

represented simply by two vortex pairs. In fact, the B-747 aircraft in a landing configuration trails six discrete pairs if the tail vortex is included (ref. 6).

At the next level of complexity we consider a third vortex pair which can be used to model a fuselage vortex. We choose as a representative case the wake from the Landing/0 configuration studied by NASA. The load distribution shown in figure 22 has been taken from the work of Ciffone and Lonzo (ref. 16). The Betz roll-up recipe will predict roll-up into three discrete vortices (ref. 2). The trajectories as viewed in the Treffetz plane are shown in figure 23. As can be seen, the distance between the flap and tip vortices continuously increases downstream. Ciffone and Lonzo conducted flow visualization experiments in a towing tank on this configuration and reported that merging did not occur. It is instructive to compute the separation between tip and flap vortices as a function of downstream distance while varying the strength of the fuselage vortex (fig. 24). By weakening the fuselage vortex, it is possible to reduce the separation between flap and tip vortices. The minimum separation between flap and tip vortices occurs when $\Gamma_j \simeq - 0.3 \Gamma_f$ . Further reduction in fuselage vortex strength serves only to again increase the distance between flap and tip vortices.

In figure 25 the sensitivity of distance between flap and tip vortices is investigated as a function of the position of the fuselage vortex. By moving the fuselage vortex from $\bar{y}_j/s = 0.125$ to 0.2 (a shift of 7.5% of the semispan), the flap and tip vortices can be brought to a distance of only 9% of the wing semispan. The dots lying near the curve denoted $\bar{y}_j/s = 0$ correspond to the distance between flap and tip vortices in a fully two-dimensional unsteady solution of the equations of motion with the computer code described in Section 111. This computation is not described in this paper, but may be found in reference 12. It is heartening to see the good agreement between the transportative model and the simple point vortex calculation.

The above computations serve to demonstrate the sensitivity of wake geometry to modest changes in wing load distribution. It is an unfortunate fact that technologies to give accurate predictions of load distributions are somewhat lacking, particularly for wings with flaps and slats deployed. The magnitude of the loss of lift at the wing-fuselage junction quite strongly influences wake geometry. In our opinion, there is now a need to know the wing load distribution more accurately than ever before.

The next level of sophistication of computing roll-up and vortex-vortex interaction discretizes the shed. vorticity with a large number of point vortices. Various investigators have questioned the validity of such a model, particularly when computations proceed for any length of time. These criticisms have been reviewed in reference 6. However, if one is careful with numerics and physical interpretation of the results, it appears that a great deal can be learned from such a computation.

Figure 26 shows the modified Landing/0 configuration at $C_L \cong 0.8$. This load distribution was represented by forty discrete vortices of equal strength. The subsequent positions are shown in figure 27. Plotted also are the positions of the flap, tip and fuselage vortices as obtained from a three-vortex-pair representation. These clusters are in reasonable agreement with the three-vortex-pair computations.

For a second computation we remove the fuselage vortex from the modified Landing/0 configuration as shown by the dashed line on figure 26, still using forty equal strength vortices to represent the trailed vorticity. In figure 28 a comparison of the many vortices representation is made with a two-vortex-pair model. The results are quite acceptable.

Figure 29 shows the distance between the flap and tip vortex centroids, as computed above, with quite good agreement.

The study shown in figure 25 indicates that moving the fuselage vortex to 20% of the semispan of the wing causes the flap

and tip vortices to move into close proximity. The load distri-
bution for the LDG/0 configuration (fig. 22) was altered inboard
to create a fuselage vortex of strength $\Gamma_j = -0.47\Gamma_f$ . As it
turned out, the fuselage vortex centroid was located at $\bar{y}/s = 0.185$ .
The separation between tip and flap vortices as a function of down-
stream distance is shown in figure 30. For this configuration,
minimum separation of $d/s \cong 0.175$ is reasonably well predicted.
However, the distances downstream at which this minimum is achieved
do not compare favorably. When the fuselage vortex is removed,
so that flap and tip vortices move apart, the computation using
a distribution of vortices again compares favorably with compu-
tations using one point vortex to represent each discrete vortex
in the wake. The discrepancy when distributions move together lies
in the incorrect approximation that the centroid of a given distri-
bution of vorticity moves at the velocity induced at its centroid
by other concentrations. In reference 6 we show that the velocity
of the centroid of a bounded region of vorticity in an infinite
fluid is given by

$$\frac{d\vec{r}}{dt} = \frac{\int \vec{U}_o \zeta dA}{\Gamma} \tag{17}$$

where $\vec{U}_o$ is the velocity field induced by the presence of all
other concentrations of vorticity in the fluid other than the one
whose motion is being computed. As two distributions come close
together, $\vec{U}_o$ may vary significantly over $\zeta$ and the motion of
the centroid is not simply the fluid velocity at the centroid in-
duced by all other concentrations of vorticity.

Another significant result from this computation is that the
calculation which used a distribution of point vortices did not
show any tendency to merge. We add without further comment that
the negative fuselage vortex was also in close proximity to the
flap and tip vortices during closest approach.

It has been our purpose in this section to point out that
simple discrete vortex computations can be used to quickly assess

whether particular lift distributions will result in a multiple vortex wake which will merge. When vortices of like sign remain in proximity of each other, the merging process must eventually occur. An estimation of the deintensification as a result of merging requires the use of a transportative fluid model, such as that presented in Section III. In sum, inviscid computations indicate that small changes in aircraft configuration and, hence, wing lift distribution can have a profound effect on wake structure. More accurate knowledge of lift distributions on commercial jet-liners, particularly in the landing and take-off configurations with and without landing gear deployed, would greatly aid in understanding the dynamics of aircraft vortex wakes.


## VI. CALCULATIONS OF AGING IN AIRCRAFT VORTEX WAKES

Computations using the vortex wake code discussed in Section III are presented here to illustrate merging and the significance of engine exhaust and ambient atmospheric turbulence.

### Decay of a simple vortex pair

Figure 31 shows the initial conditions of the computation of the decay of a simple vortex pair. The initial vorticity and turbulent kinetic energy distributions were taken to be Gaussian about $y/s' = \pm 1$. Two computations were made with the viscous core radius $r_c/s' = 0.4$ and $0.8$. The integral scale parameter $\Lambda/s'$ was taken equal to 0.2. The turbulent energy components were again equally distributed with $\overline{uu} = \overline{vv} = \overline{ww} = q^2/3$. The cross-correlations were initially taken to be zero.

The computations are carried out in time and the results transformed to downstream distance through $x = U_\infty t$. Figure 32 shows the circulation computed over the area $y \geq 0$. The constant circulation region for the initially tight vortex ($r_c/s' = .4$) illustrates the situation depicted in figure 3. Circulation cannot decrease until the vorticity has diffused across the wake.

The computation for the initially more diffuse vortex $(r_c/s' = .8)$ has been carried downstream to a distance of $x'/b' = 8\pi Ab'^2/b^2 C_L$ ; at $C_L = 1$ and $A = 7$ and a rectangularly loaded wing, $x/b \simeq 160$ . For a B-747 aircraft this is approximately 10 km. Without ambient atmospheric turbulence, the vortex pair ages quite slowly. Figure 33 compares the maximum root-mean-square turbulence level $q$ between the pair and a computation using a single isolated vortex having the same initial conditions as one vortex of the pair. The level of turbulent intensity in the pair is not significantly different than that computed for an isolated vortex,

In figure 34 we show the $r_c/s' = 0.8$ circulation as a function of downstream distance about a square of side 2e, centered at the centroid of vorticity in the half-plane. As might be expected, the decay of circulation is far more rapid than the half-plane value.

Figure 35 shows the computed descent rate $dh/dt$ of the vertical centroid $\bar{z}$ of the vorticity. The $\bar{z}$ increases as a function of downstream distance since a uniform upwash has been added to the cornputation (of magnitude $\Gamma_o/4\pi s'$) to keep the vortex pair centered in the computational mesh. The descent rate decreases as vorticity diffuses across the aircraft centerline.

In figures 36 and 37 are shown instantaneous streamlines at the beginning and end of the computation for the $r_c/s' = 0.8$ computation. The $y,Z$ coordinate system is one in which the fluid at infinity is at rest; therefore, the pair descends downward.

## Merging of equal strength flap and tip vortices, including engine exhaust

Vortices are positioned at $y/s = - .95$ , $-.4$ , $.4$ and $.95$ , and $z/s = 0$ . In the right-half plane the vortices are of equal strength and of positive sign. In the left-half plane the vortices are of equal strength and negative sign. The vorticity distributions are given by Gaussians

$$\frac{\zeta 2\pi s^2}{\Gamma} = \frac{2s^2}{r_c^2} \exp\left(-\frac{r^2}{r_c^2}\right) \tag{18}$$

and the turbulent kinetic energy distribution about each vortex is given by

$$\left(\frac{2\pi sq}{\Gamma}\right)^2 = 0.01 \quad p\left(-\frac{r^2}{r_c^2}\right) \tag{19}$$

with the turbulent energy components again equally divided initially. Cross correlations are initially taken to be zero.

A second computation uses the above initial conditions but adds the jet exhaust. At a lift coefficient of 1.5 and assuming $C_D = C_T = 0.125 C_L$, the axial velocity excess about each engine is given by

$$\frac{\Delta U 2\pi s}{\Gamma} = 8.0 \exp\left(-52.0 \frac{r^2}{s^2}\right) \tag{20}$$

Taking the aspect ratio equal to 7, the flight speed is $40.0\Gamma/2\pi s$. The engine exhausts are Gaussians of excess axial velocity and are positioned at $y/s = -0.75$, $-0.4$, $0.4$, and $0.75$ and $z/s = -0.08$. Except for a vertical displacement of $z/s = -0.08$, the inboard engines exhaust directly into the flap vortices. Additional Gaussian distributions of turbulent kinetic energy are positioned at each engine with the distribution given by

$$\left(\frac{2\pi sq}{\Gamma}\right)^2 = 0.64 \exp\left(-52.0 \frac{r^2}{s^2}\right) \tag{21}$$

The turbulent energy components are equally partitioned and the cross correlations taken to be zero initially.

Figure 38 shows a comparison of the trailed vorticity in intensity plot form. The darkest areas have intensity equal to unity, since the plots have been made by nondimensionalizing the vorticity with the maximum value at $x/b = 0$. As can be seen, the jet engines do not hinder the merging of flap and tip vortices.

At twelve spans downstream the jet engines give slightly more spreading of the trailed vorticity; hence, the lower maximum value.

Figure 39 shows the intensity of the turbulent kinetic energy. Note that the normalization differs between the run with and without jet exhaust. It is likely that appreciable redistribution of the trailed vorticity is yet to occur owing to the large values of turbulent kinetic energy in the wake. This feature is over-emphasized by taking the initial integral scale parameter $\Lambda/s$ to be 0.2 for both runs. The integral scale parameter in the exhaust jets should be initialized to be somewhat smaller. In any case, the merging phenomenon is not significantly altered by jet exhaust and its accompanying turbulence.

Jet exhaust axial velocity excess intensity plots are shown in figure 40. Note that the inboard engine exhaust which was introduced into the flap vortex is slower to decay than the exhaust from the outboard engine, again demonstrating the suppression of the production of turbulence by swirl.

Wake dissipation by atmospheric turbulent diffusion of vorticity

There has been an attempt (ref. 8) to correlate wake life-time with the turbulent dissipation rate $E$ (our model at high Reynolds number gives $E = 0.125q^3/\Lambda$). Vortices present their greatest hazard under stable atmospheric conditions. Under these conditions, scales can be smaller than the characteristic wake length scale — the vortex spacing. Under these problem atmospheric conditions, the turbulent dissipation rate does not contain sufficient information to estimate the diffusion of trailed vorticity by the atmosphere. The integral- or macro-scale must be known. This fact can be demonstrated by two computations in which $E$ is held constant. For light and light-to-moderate turbulence, we use a value of $E^{1/3} = 2$ $cm^{2/3}/sec$ as suggested in reference 8.

83

If we take $\Lambda/s = 0.2$ and $2.0$ , the corresponding turbulent kinetic energies become $(2\pi s q/\Gamma)^2 = 0.025$ and $0.116$ , respectively. These two values can probably be achieved in a stable atmosphere with conventional jetliners.

The initial conditions are again Gaussians of vorticity at $y/s = \pm 1$ of opposite sign to produce a counter-rotating pair. The viscous core radius is taken to be $r_c/s = 0.5$. The turbulent energy components are again equally distributed so that $\overline{uu} = \overline{vv} = \overline{ww} = q^2/3$ initially. Integral scale parameter and turbulent energy components are held constant on the computational boundaries.

Figure 41 shows the circulation decay computed about a box contour of side 2e centered at the centroid of the vorticity. At the end of the computation (typically a wake age of 60 sec), levels differ by a factor of two. More importantly, the rate of decay differs by approximately a factor of four. These results do well to emphasize the importance of scale and caution against too simple a parameterization of the atmosphere. Obviously, the effects of wind shear and stratification help to make the analysis of the interaction of a vortex wake with the atmosphere a most difficult one.

An indirect comparison can be made between the above results and figure 34, which gives circulation decay of a vortex pair in a quiescent atmosphere. The initial spread of vorticity is different in that $r_c/s = 0.8$ for the pair in the quiescent atmosphere, while $r_c/s = 0.5$ for the above cases. The abscissa on figures 32 and 41 are equal and so time or downstream positions can be compared directly. The slow decay of the pair in a quiescent atmosphere is clearly demonstrated. The dominance of the atmosphere in controlling the ultimate death of a vortex wake is absolute even for low ambient turbulence levels. The turbulent atmosphere may be likened to an infinite reservoir of turbulent kinetic energy which can, for unlimited time, nibble away at the vortex wake.

Work is currently underway at A.R.A.P. to investigate through second–order closure turbulent modeling the fluid dynamics of the lower atmosphere. This work (partially reported in ref. 17) should give those of us concerned with the vortex hazard the tools necessary to access the rate of wake aging which results from interaction with a dynamic atmosphere.

## VII. CONCLUSIONS AND RECOMMENDATIONS

The phenomenon of vortex merging has been investigated experimentally in a wind tunnel and numerically through the use of a computer code, which includes transport via a second–order closure turbulent model. It is shown that the merging phenomenon between like–signed vortices is a mechanism which results in redistribution of the trailed vorticity through convective and turbulent mechanisms. This redistribution is one which extensively spreads the vorticity over the wake and therefore hastens the decay process. Comparisons between experimental observations of vortex merging and numerical simulation of the phenomenon are favorable.

The usefulness of discrete point vortex computations to investigate wake geometry and structure is discussed, It is shown that small changes in the strength and/or initial position of the fuselage vortex can have a profound effect on the structure of the multiple–vortex–pair wake.

Using the transportative code, computations have been run which demonstrate merging between like–signed and strength flap and tip vortices with and without engine jet exhaust. The merging phenomenon does not appear to be significantly altered by the jet exhaust.

The effect of ambient atmospheric turbulence on the aging of an aircraft wake is investigated at constant turbulent dissipation rate. It is shown that under stable atmospheric conditions, when atmospheric macroscales may be less than or equal to the vortex

spacing, misleading results may be obtained if vortex aging is correlated only with the turbulent dissipation rate. This result cautions against using one parameter to characterize the ability of the atmosphere to dissipate aircraft wake vortices.

The technology now exists to investigate the complex convective and diffusive processes in aircraft vortex wakes. However, to use this technology requires an accurate description of the wing load distribution - a quantity not easily predicted for all but cruise-configured wings. It is recommended that accurate load distributions be obtained experimentally for the B-747 aircraft. These data will surely be of use in both understanding the interactions which result in a minimum hazard wake as well as permitting this technology to be transferred to other jumbo jetliners.

There is yet the problem of ground plane-vortex wake interaction. Hopefully, the merging phenomenon with its resulting transportative mechanisms will still be active.

## REFERENCES

1. Betz, A.: Behavior of Vortex Systems. NACA TM 713 (trans. from ZAMM, Vol. XII.3, 1932).

2. Donaldson, C. duP., R.S. Snedeker, and R.D. Sullivan: A Method of Calculating Aircraft Wake Velocity Profiles and Comparison with Full-scale Experimental Measurements. J. Aircraft 11, 9, September 1974, pp. 547-555.

3. Rossow, V.: On the Inviscid Rolled-up Structure of Lift-Generated Vortices. J. Aircraft 10, 11, November 1973, pp. 647-650.

4. Jordan, P.: Structure of Betz Vortex Cores. J. Aircraft 10, 11, November 1973, pp. 691-693.

5. Bilanin, A.J., and C. duP. Donaldson: Estimation of Velocities and Roll-Up in Aircraft Vortex Wakes. J. Aircraft 12, 7, July 1975, pp. 578-585.

6. Donaldson, C. duP., and A.J. Bilanin: Vortex Wakes of Conventional Aircraft. AGARD-AG-204, May 1975.

7. Moore, D.W., and P.G. Saffman: Axial Flow in Laminar Trailing Vortices. Proceedings of the Royal Society: Ser. A: Mathematical and Physical Sciences' 333, 1973, pp. 491–508.

8. Tombach, I.: Observations of Atmospheric Effects of Vortex Wake Behavior. J. Aircraft 10, 11, November 1973, pp. 641-647.

9. Dunham, R.E., Jr.: Model Tests of Various Vortex Dissipation Techniques in a Water Towing Tank. NASA LWP-1146, January 1974.

10. Donaldson, C.duP.: Atmospheric Turbulence and the Dispersal of Atmospheric Pollutants. EPA-R4-73-016a, March 1973.

11. Lewellen, W.S., and M.E. Teske: Turbulence Modeling and its Application to Atmospheric Diffusion. Part 11: Critical Review of the Use of Invariant Modeling. EPA-600/4-75-016a, August 1975.

12. Bilanin, A.J., M.E. Teske, C. duP. Donaldson, and G.G. Williamson: Vortex Interactions and Decay in Aircraft Wakes. A.R.A.P. Report No. 271, May 1976.

13. Sullivan, R.D.: A Program to Compute the Behavior of a Three-Dimensional Turbulent Vortex. ARL-TR-74-0009, December 1973.

14. Moore, D.W., and P.G. Saffman: Structure of a Line Vortex in an Imposed Strain. Aircraft Wake Turbulence and its Detection (J.H. Olsen, A. Goldburg, M. Rogers, eds.), Plenum Press, New York, 1971, pp. 339-354.

15. Westwater, F.L.: Rolling Up of the Surface of Discontinuity Behind an Aerofoil of Finite Span. A.R.C. R&M 1962, 1935.

16. Ciffone, D.L., and C. Lonzo, Jr.: Flow Visualization of Vortex Interactions in Multiple Vortex Wakes Behind Aircraft. NASA TM X-62,459, June 1975.

17. Lewellen, W.S., and G.G. Williamson: Wind Shear and Turbulence Around Airports. A.R.A.P. Report No. 267, January 1976.

18. Bradshaw, P.: The Effects of Streamline Curvature on Turbulent Flow. AGARDograph 169, August 1973.
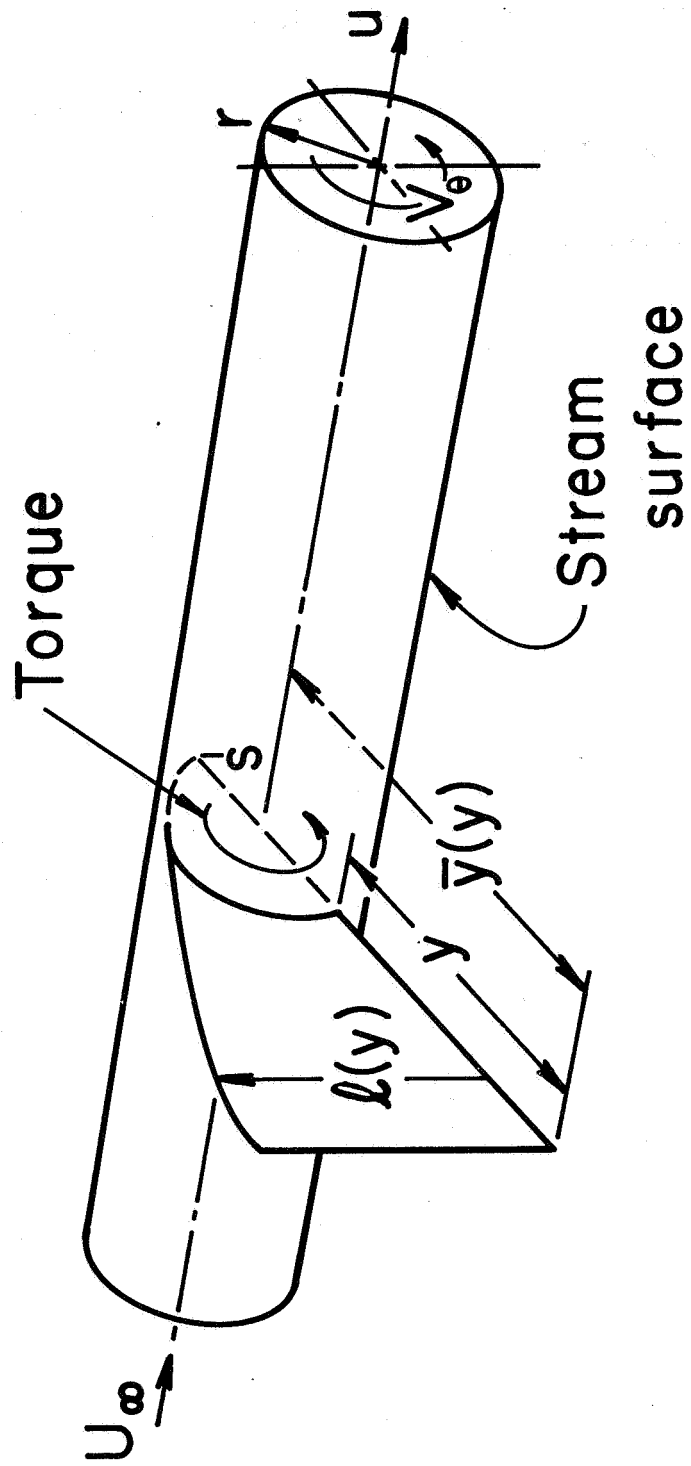
Figure 1. Geometry of the Betz roll-up model
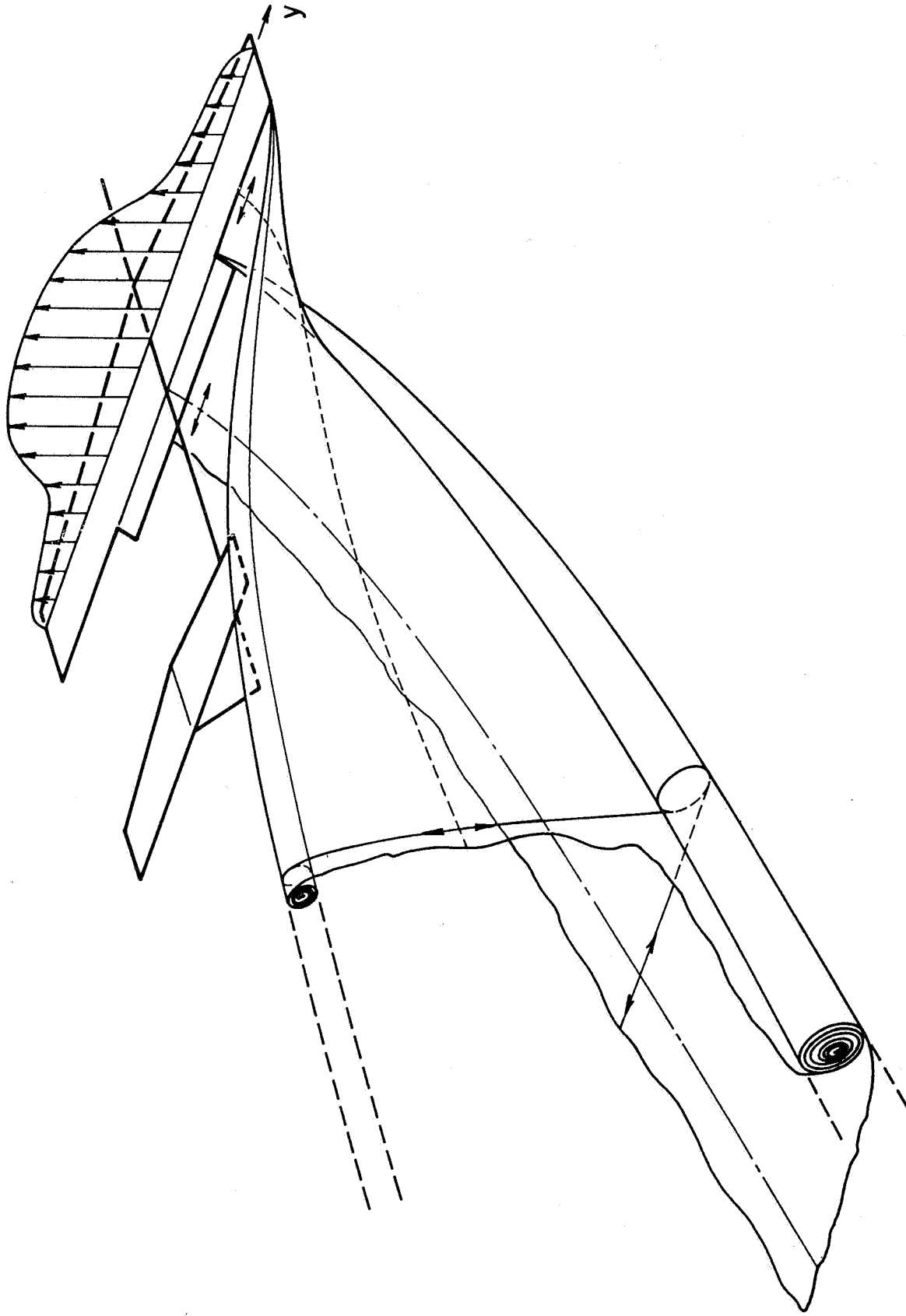
Figure 2. The roll-up of the flap and tip vortices (from ref 6)

/// positive vorticity

\\\ negative vorticity

t = 0
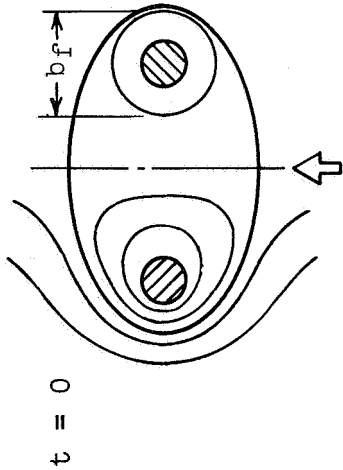
Single vortex pair
(in all figures, a uniform
upward velocity is assumed to
cancel wake descent)

$t = t_1$
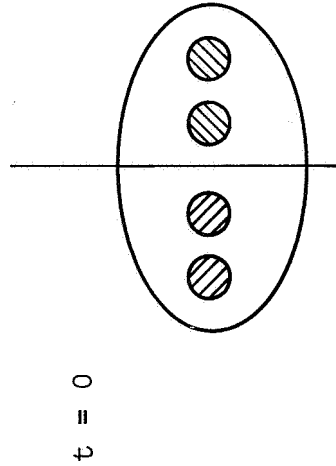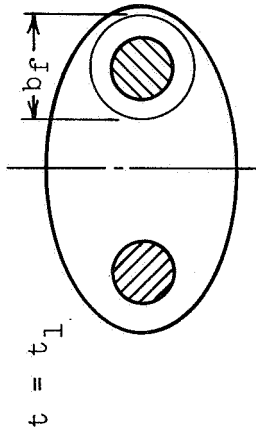
Trailed vorticity slowly
diffused by viscous transport

$t = t_2$

Trailed vorticity still not
extensively diffused throughout
wake

wake
containing
trailed
vorticity

$t = t_2$

cancellation
of vorticity
across wake
centerline
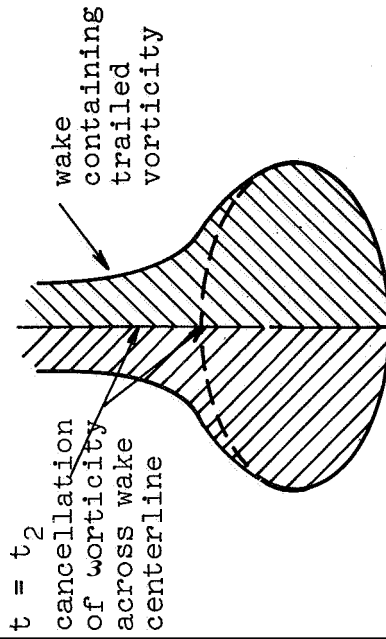
Aged wake; vorticity is sheared in a
wake and also diffuses across wake
centerline

t = 0

Multiple pair vortex wake

$t = t_1$

Turbulent merging resulting
in extensive redistribution
of trailed vorticity

Figure 3. An idealization of the processes which result in the aging of a single- and
multiple-pair vortex wake. The encounter aircraft's span is denoted by $b_f$.

90
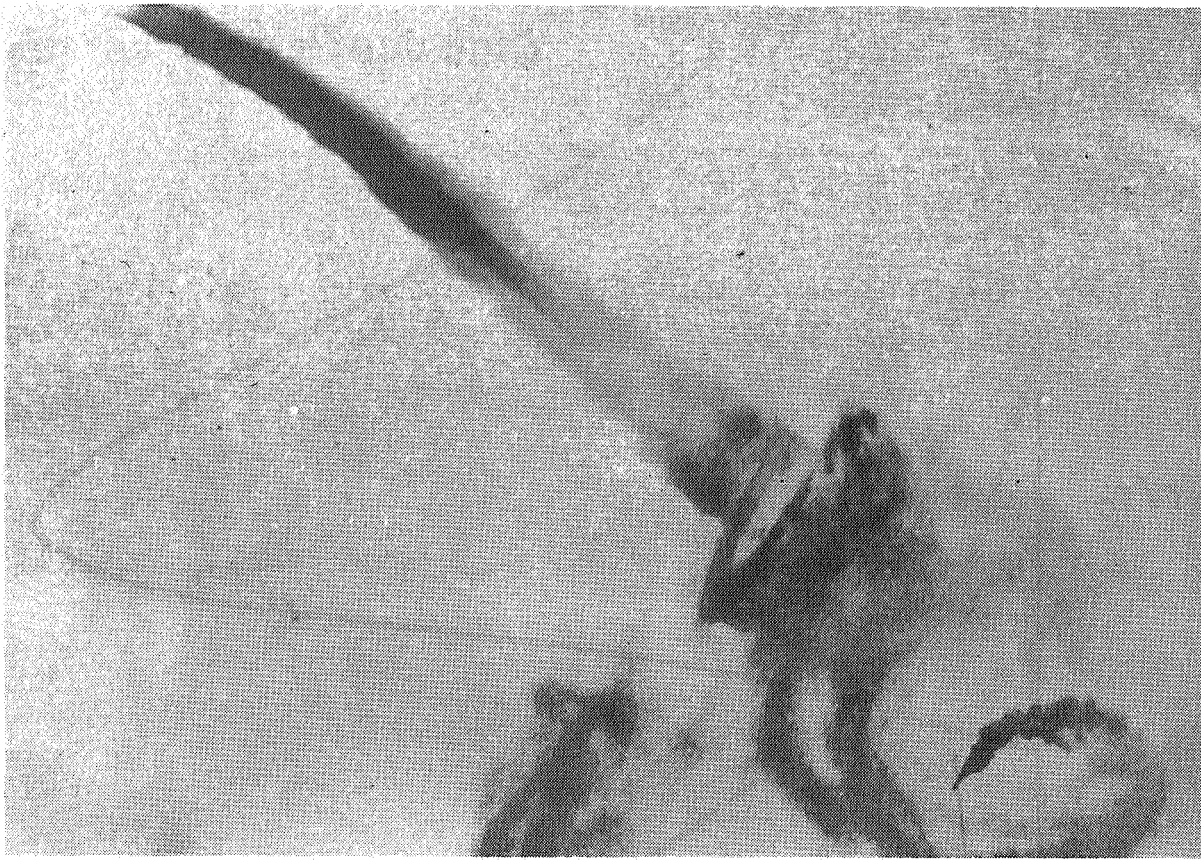
Figure 4.  The laminar viscous core of an aircraft vortex.
The smoke shows the effect of higher turbulence
level in the surrounding atmosphere  (ref. 18.
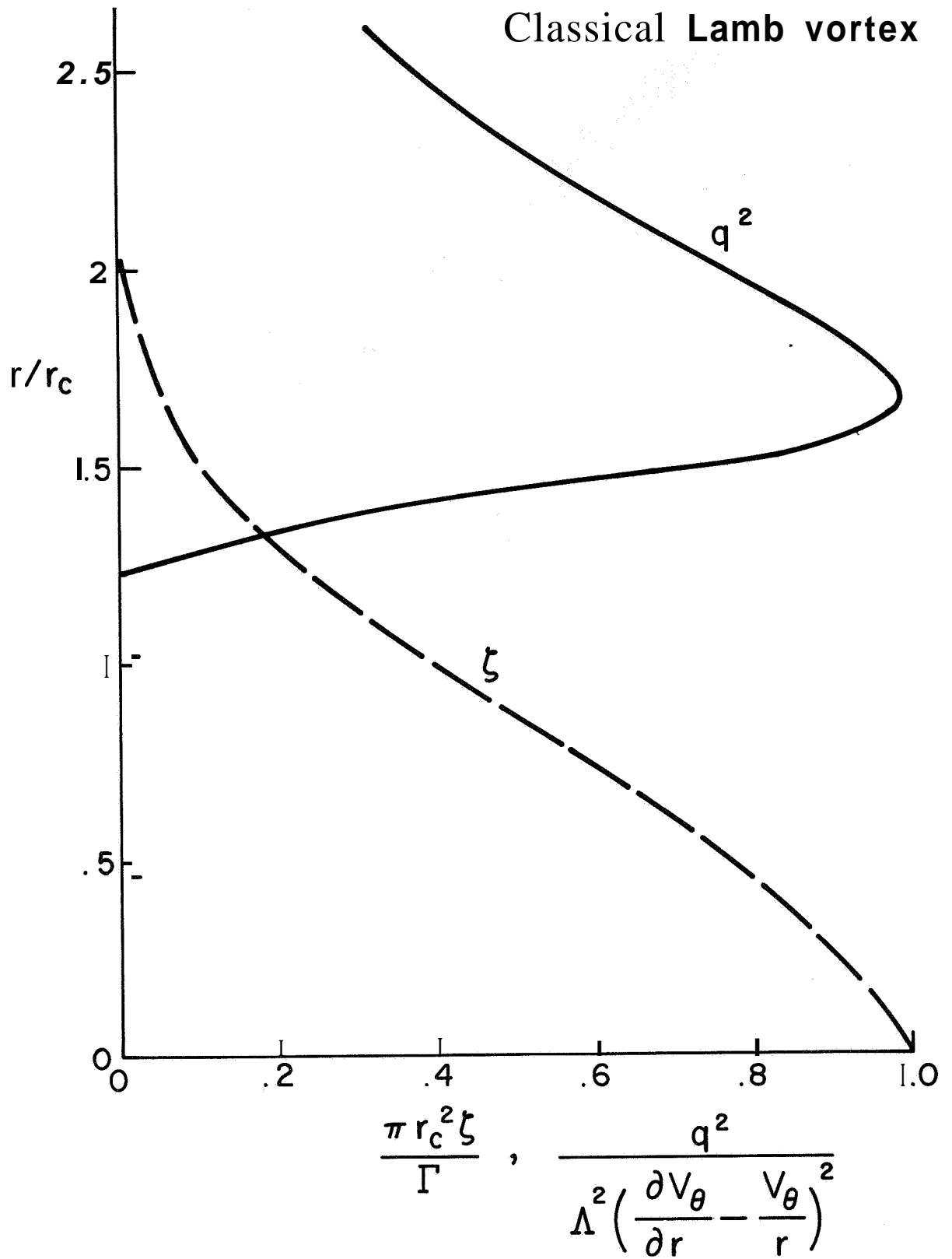
Figure 5.   The superequilibrium turbulent kinetic energy and vorticity distribution in a Lamb vortex.

**Overhead view**

**Side view**

Aircraft
passage

I5 spanlengths
behind
**747** model

Turbulent
interaction

**30** spanlengths
behind
**747** model

**45** spanlengths
behind
**747** model
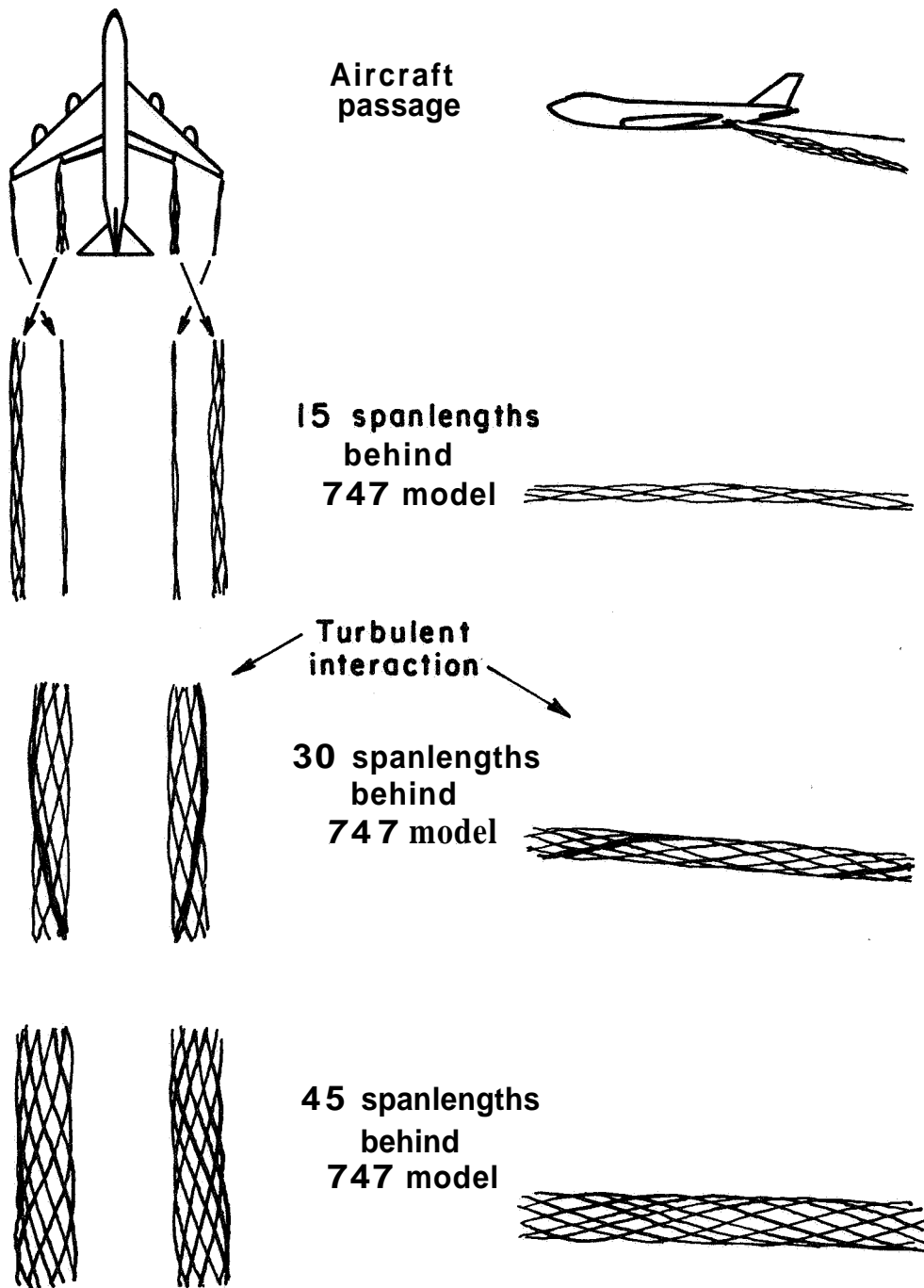
Figure 6.    Merging interaction of a tip and a flap vortex as
sketched by Dunham (ref. 9).

93
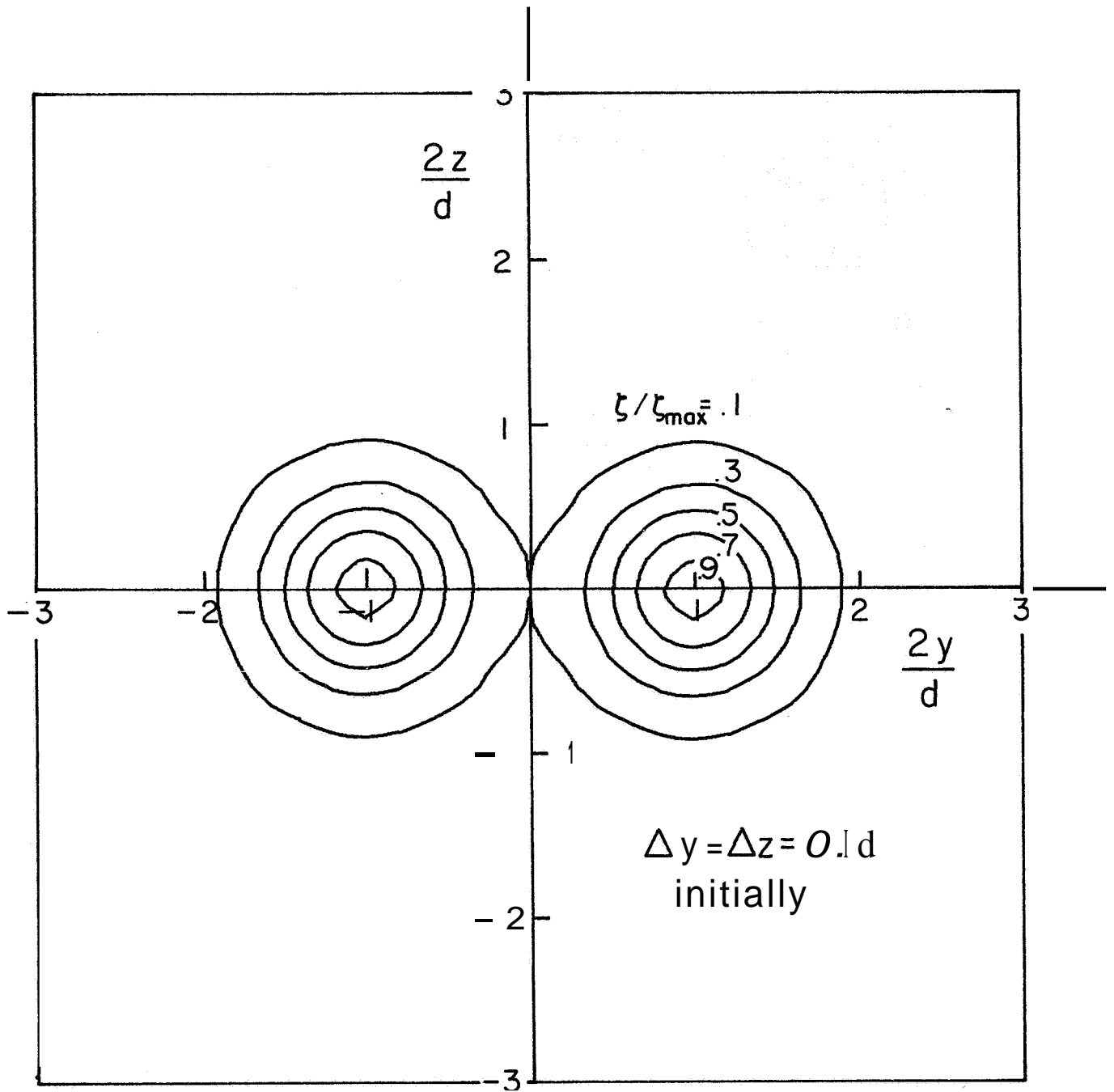
Figure 7.  The computational domain and the isopleths of the initial vorticity distribution.  The computational boundaries are moved outward as the computation proceeds.

$t\Gamma/\pi d^2 = 0.0$ ; $P_{min}/P_n = 1.0$

$t\Gamma/\pi d^2 = 1.33$ ; $P_{min}/P_n = 0.75$

$t\Gamma/\pi d^2 = 2.67$ ; $P_{min}/P_n = 0.52$
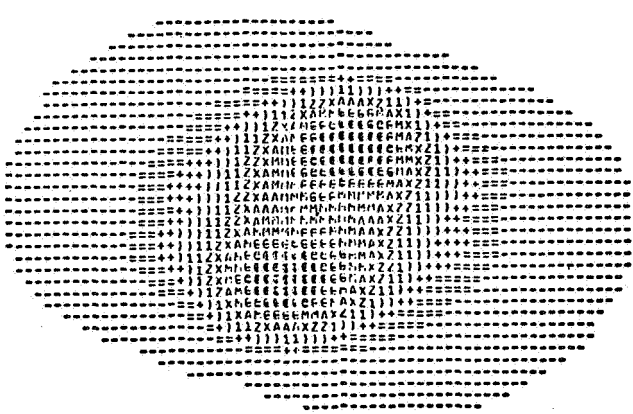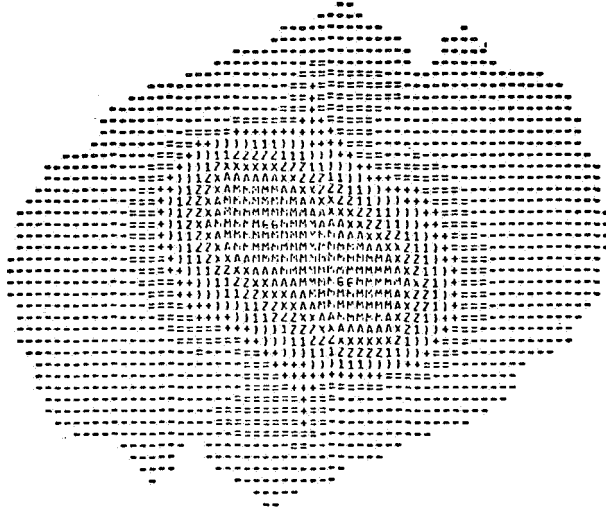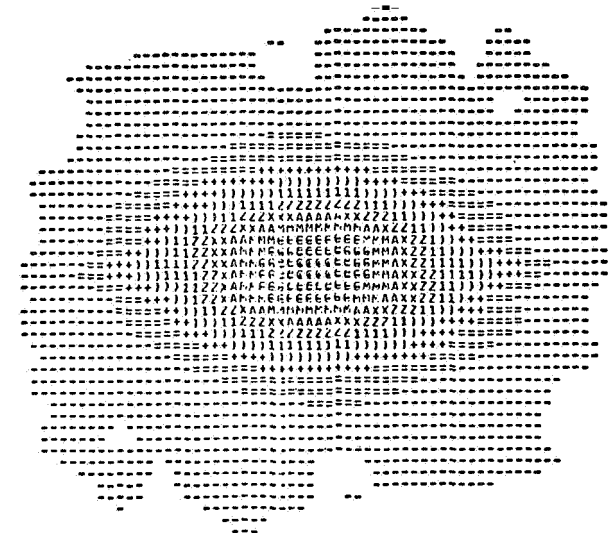
$t\Gamma/\pi d^2 = 4.0$ ; $P_{min}/P_n = 0.65$

Figure 8.  Pressure intensity plots for the merging of two equal strength, like-signed vortices. $P_n = -6.0\rho_o(\Gamma/\pi d)2$ .

$t\Gamma/\pi d^2 = 0.0$ ; $\zeta_{max}/\zeta_n = 1.0$

$t\Gamma/\pi d^2 = 1.33$ ; $\zeta_{max}/\zeta_n = 0.58$

$t\Gamma/\pi d^2 = 2.67$ ; $\zeta_{max}/\zeta_n = 0.35$
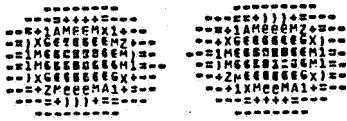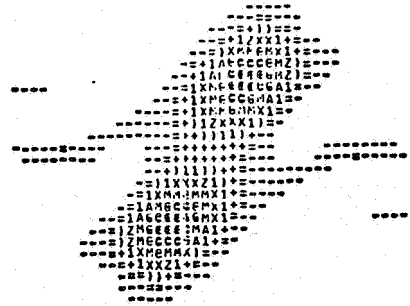
$t\Gamma/\pi d^2 = 4.0$ ; $\zeta_{max}/\zeta_n = 0.34$

Figure 9. Vorticity intensity plots for the merging of two equal strength, like-signed vortices. $\zeta_n = 14.8\Gamma/\pi d2$ .

$$t\Gamma/\pi d^2 = 0.0 \; ; \; q^2_{max}/q^2_n = 0.18$$

$$t\Gamma/\pi d^2 = 1.33 \; ; \; q^2_{max}/q^2_n = 0.3$$

$$t\Gamma/\pi d^2 = 2.67 \; ; \; q^2_{max}/q^2_n = 0.52$$
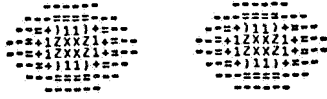
$$t\Gamma/\pi d^2 = 4.0 \; ; \; q^2_{max}/q^2_n = 1.0$$

Figure 10. Turbulent kinetic energy intensity plots for the merging of two equal strength, like-signed vortices. $q^2_n = 0.54(\Gamma/\pi d)^2$ .

97
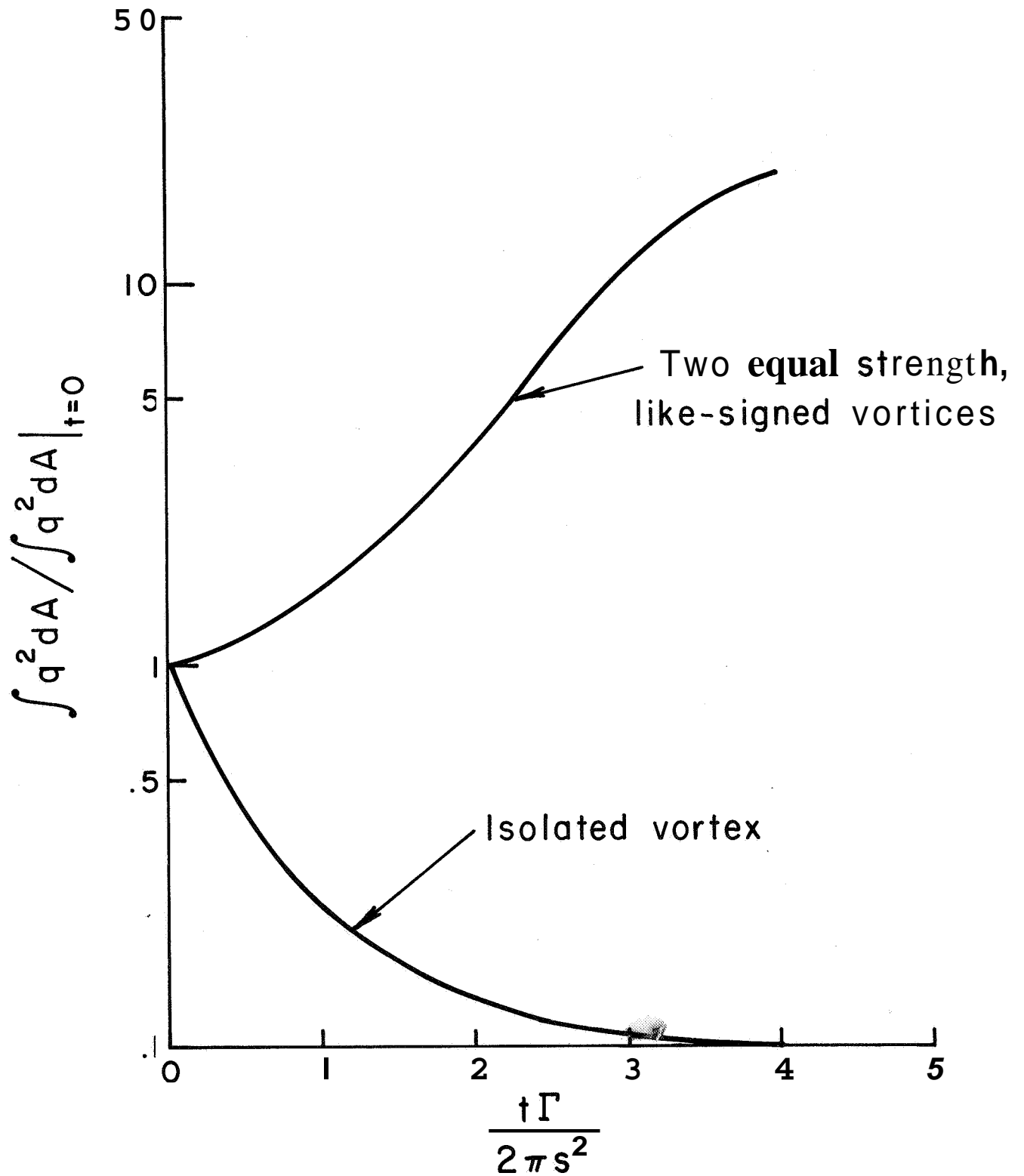
Figure 11. Comparison of the turbulent kinetic energy as a function of time between an isolated vortex and two equal strength, like-signed vortices.
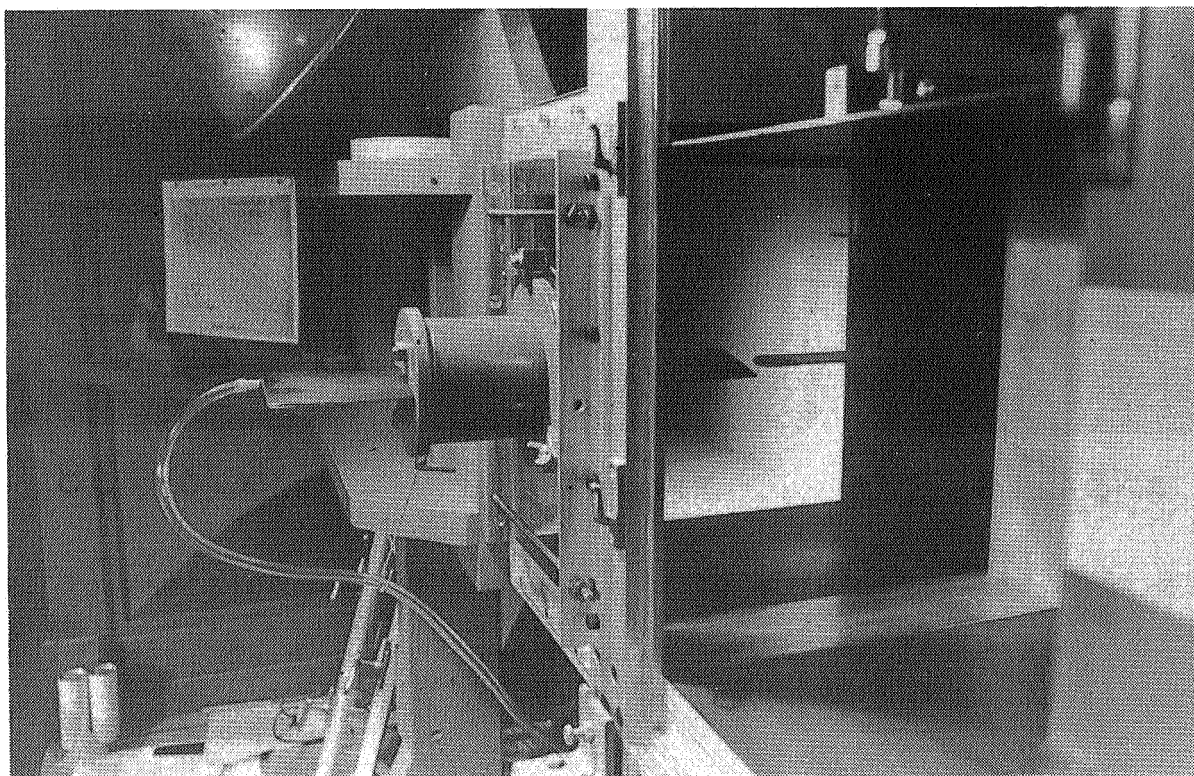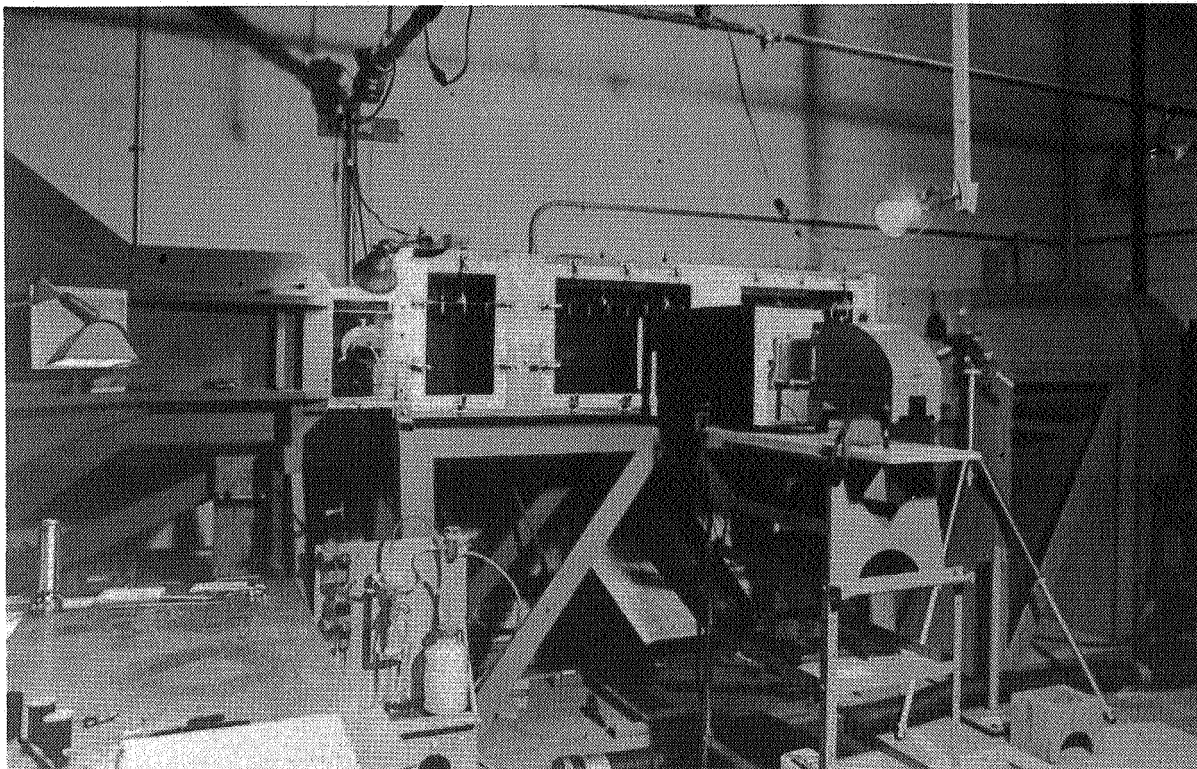
Figure 12.   View of the A.R.A.P.   wind tunnel (top) and the
vortex generator airfoils (bottom).

x/d=18        x/d=30        x/d=54

x/d=66        x/d=78        x/d=90

x/d=114       x/d=126       x/d=138
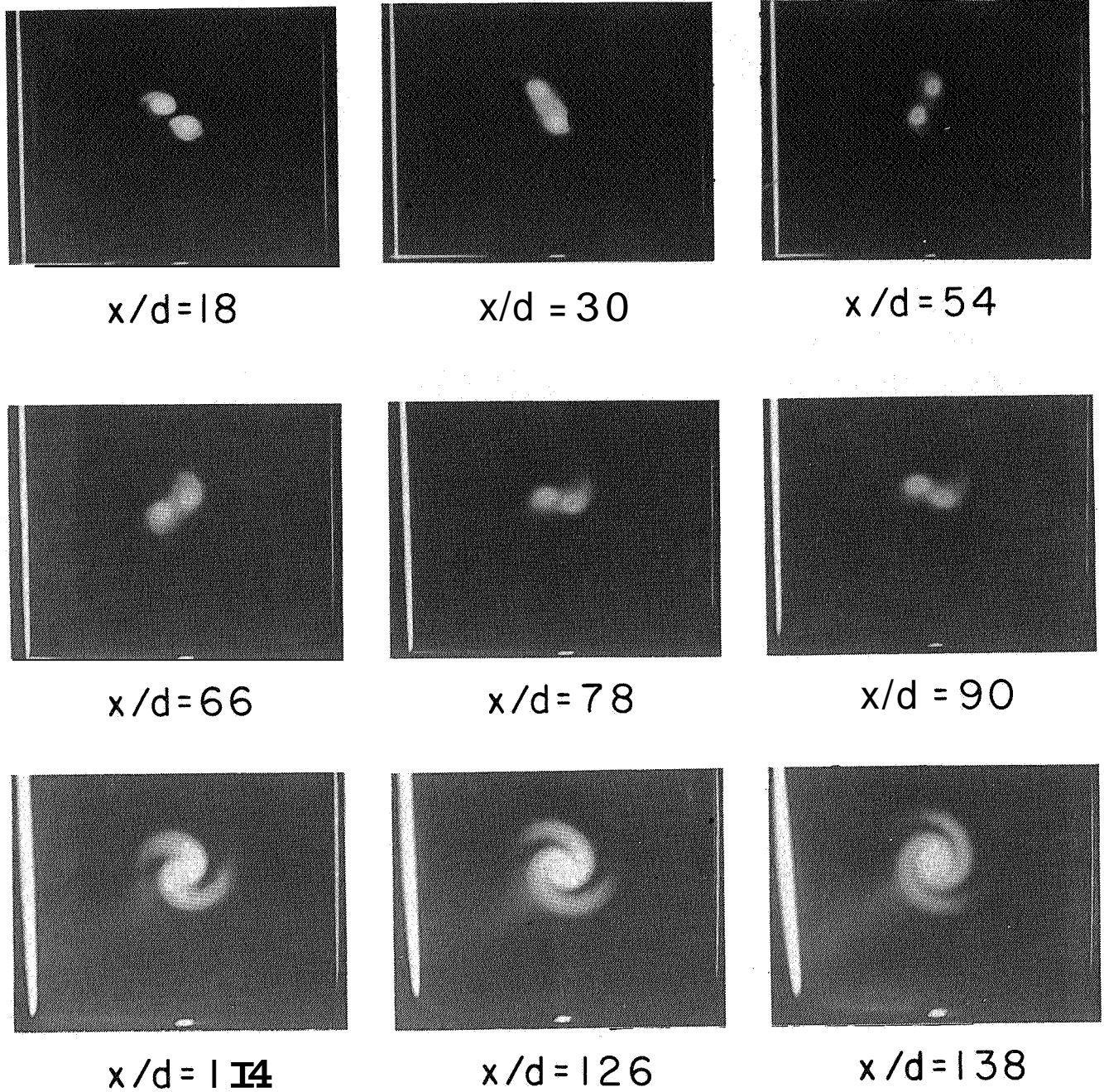
Figure 13.   Smoke pictures of the merging of two vortices of like sign and strength at several downstream locations. The airfoil angles of attack are $\alpha_{left} = -6°$ and $\alpha_{right} = +6°$ and the tip spacing $d = 1.27$ cm.
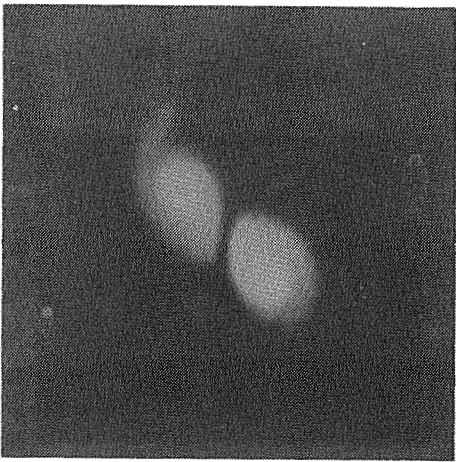
x/d=40

x/d=88

x/d=24
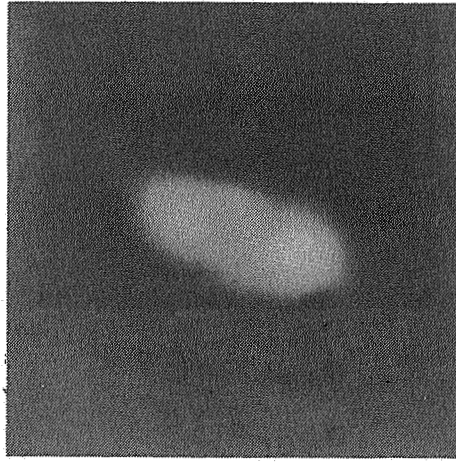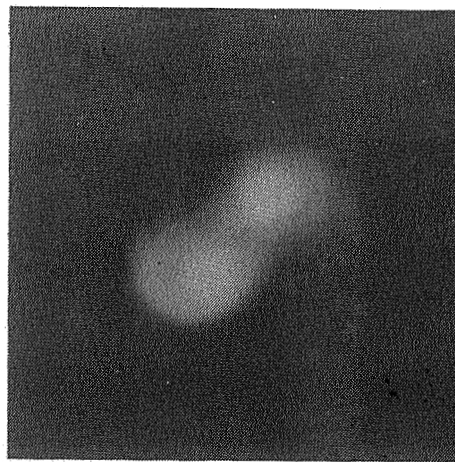
x/d=72
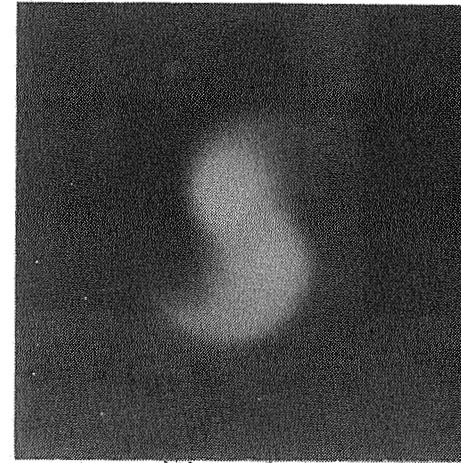
Figure 14. Comparisons of computed merging of vorticity distributions with smoke patterns in vortices of like sign and strength. The airfoil angles of attack are $\alpha_{left} = +6°$ and $\alpha_{right} = -6°$. The tip spacing d = 0.95 cm.

$$\alpha_{ref} = \alpha_U = -6° \qquad \alpha_{ref} = -6° \qquad \alpha_{ref} = -6°$$
$$\alpha_{var} = \alpha_L = 6° \qquad \alpha_{var} = 4° \qquad \alpha_{var} = 3°$$

$$\alpha_{ref} = -6° \qquad \alpha_{ref} = -6° \qquad \alpha_{ref} = -6°$$
$$\alpha_{var} = 2° \qquad \alpha_{var} = 0 \qquad \alpha_{var} = -1°$$

$$\alpha_{ref} = -6° \qquad \alpha_{ref} = -6° \qquad \alpha_{ref} = -6°$$
$$\alpha_{var} = -2° \qquad \alpha_{var} = -4° \qquad \alpha_{var} = -6°$$
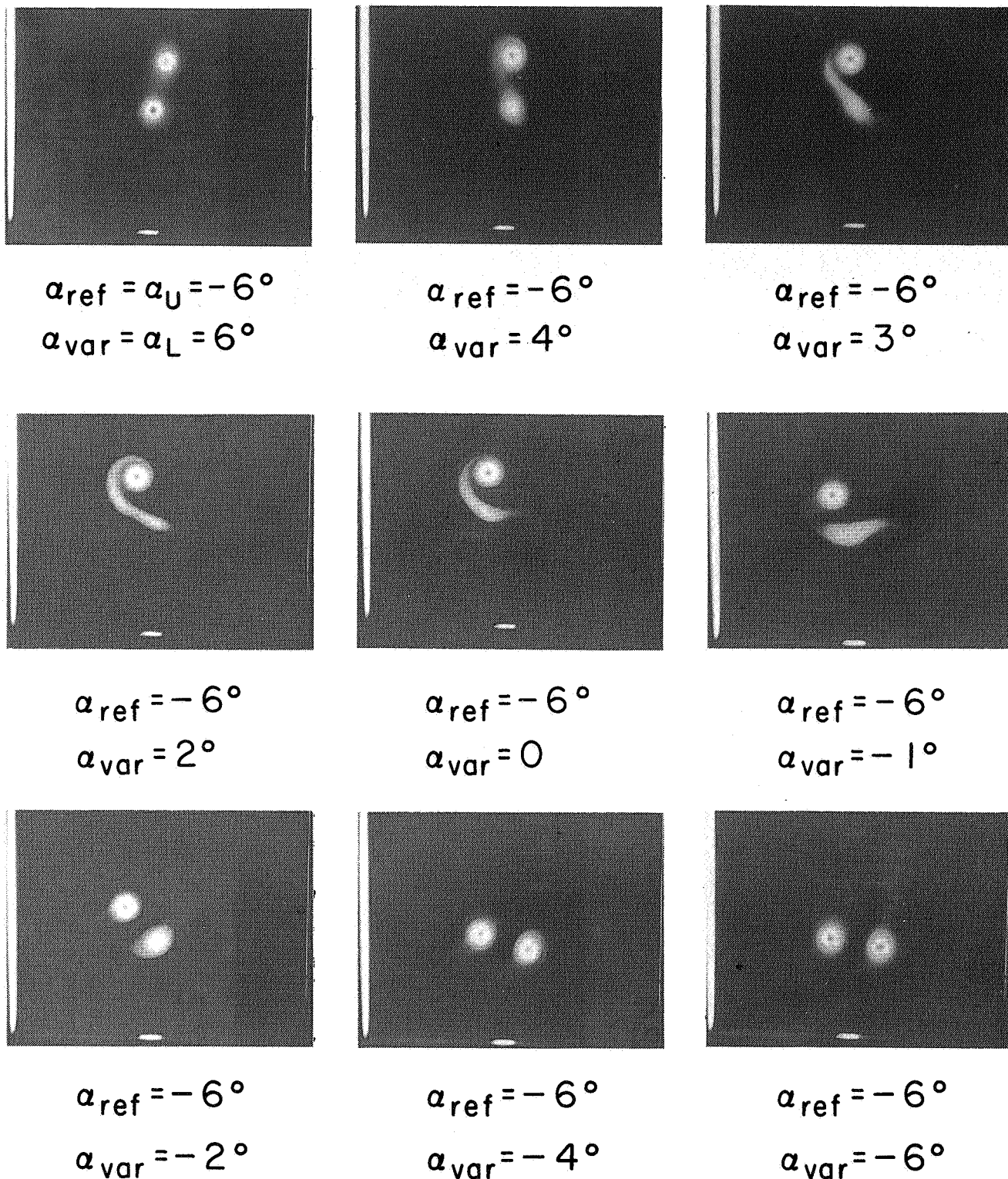
Figure 15.    Smoke pictures of the interaction of one vortex
of constant strength with another of varying strength
and sign.    The axial station is    $x/d = 55.4$    and the
tip spacing    $d = 2.06$    cm.
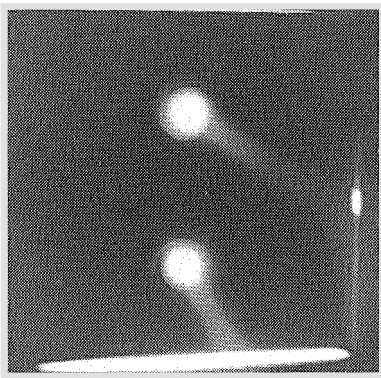
$d/d_0 = .250$
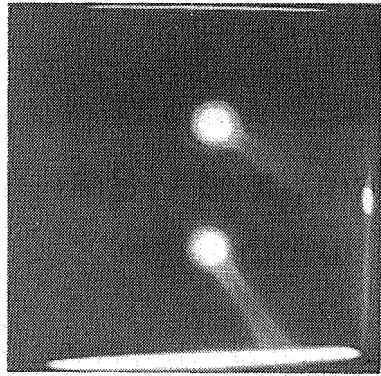
$d/d_0 = .500$

$d/d_0 = .750$
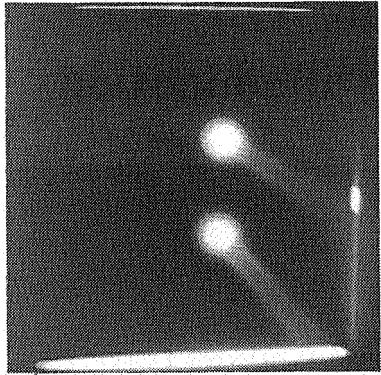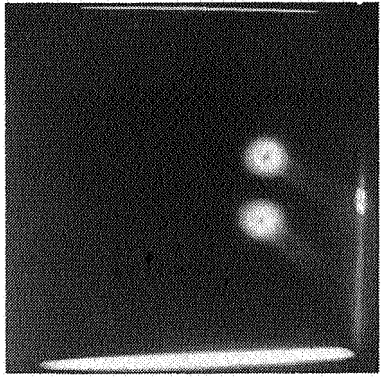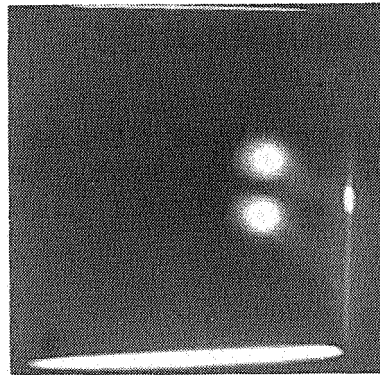
$d/d_0 = 1$

$d/d_0 = 109$

$d/d_0 = .125$

$d/d_0 = 188$
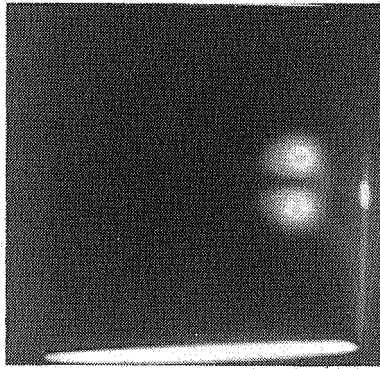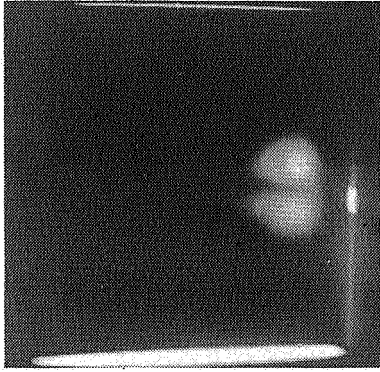
Figure 16   Smoke pictures of a pair of vortices of opposite sign and equal strength. Both airfoils are set at $\alpha = -6°$ and the axial station $x/d_0 = 15.75$. The initial tip spacing $d_0 = 10.16$ cm.
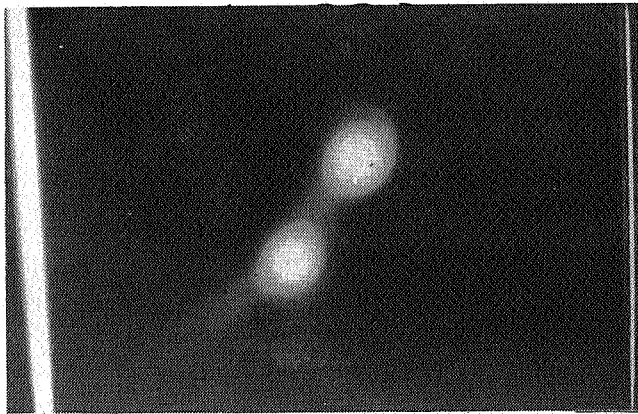
d=2.54 cm, x/d=63

Continuous illumination
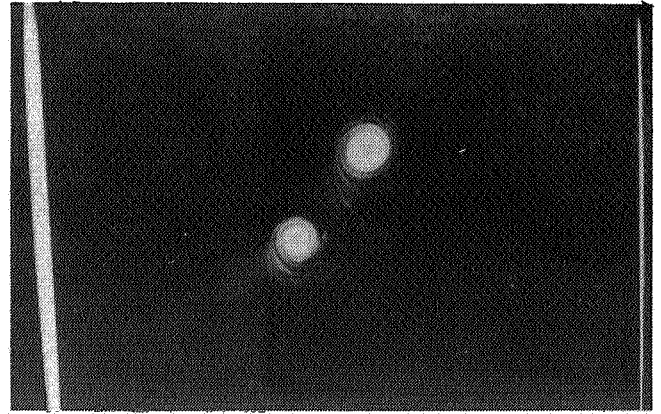
d=2.54 cm, **x/d** = 63

Flash illumination
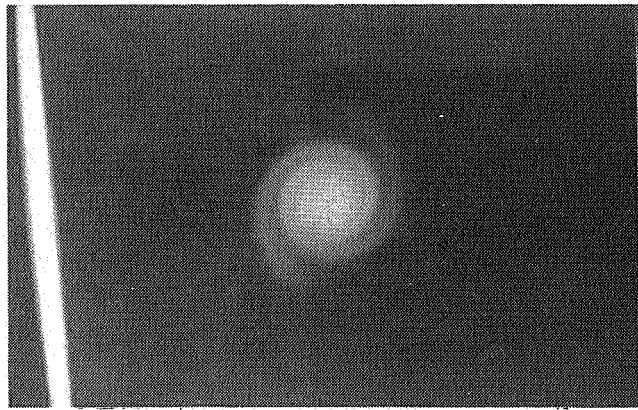
d=0.95 cm, x/d=184

Continuous illumination
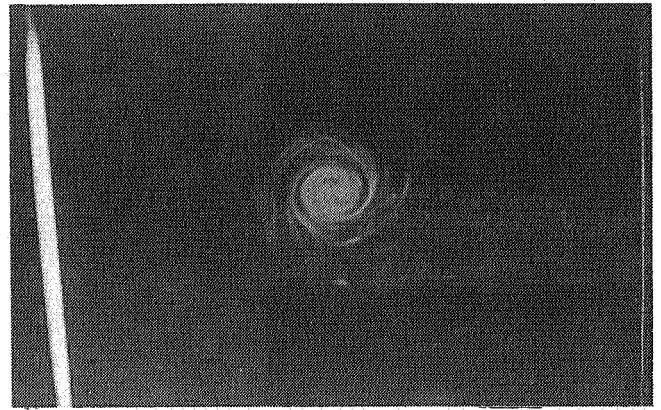
**d**=0.95 cm, x/d=184

Flash illumination

Figure 17.  Illustrations of the smoke patterns under continuous (1/2 sec exposure, left) and flash (1/2800 sec exposure, right) illumination.
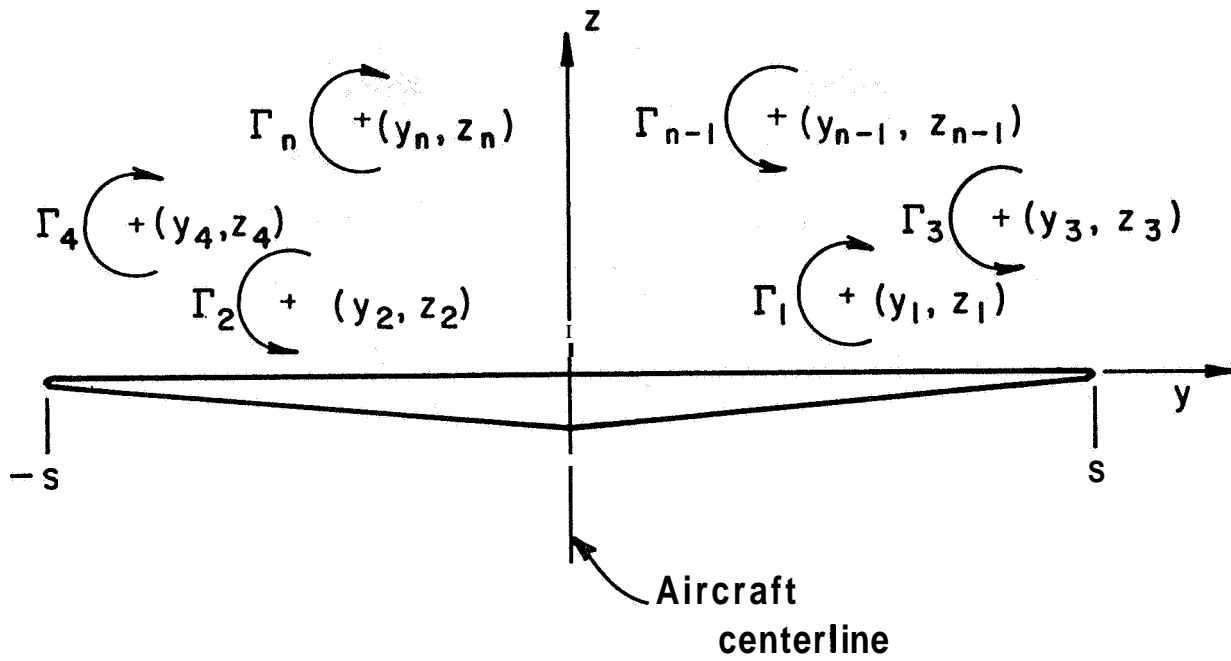
Figure 18. Geometry for the calculation of the downstream location of vortex centroids.
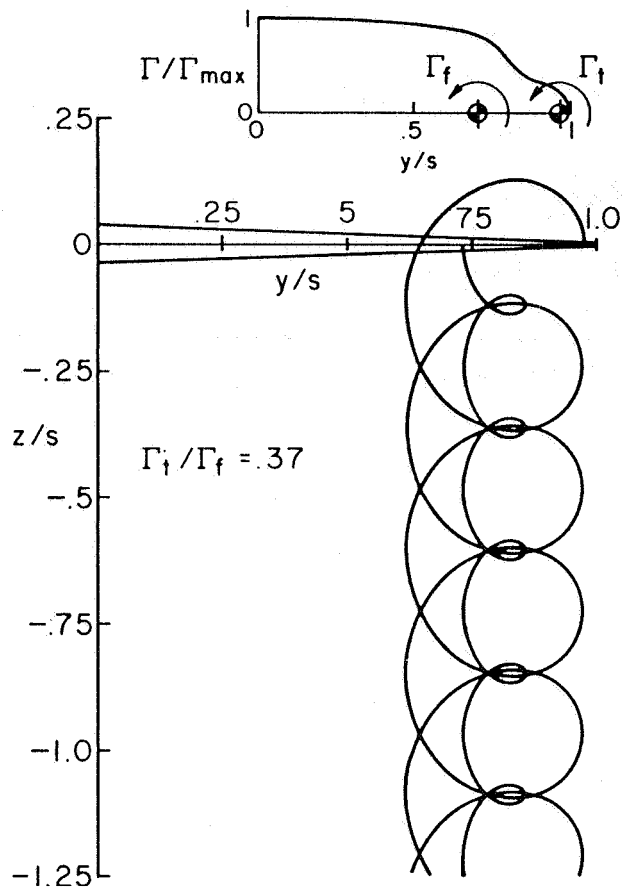
Figure 19.  Vortex centroid locations as seen from down-
stream with strong interaction between
neighboring vortices (ref. 6).
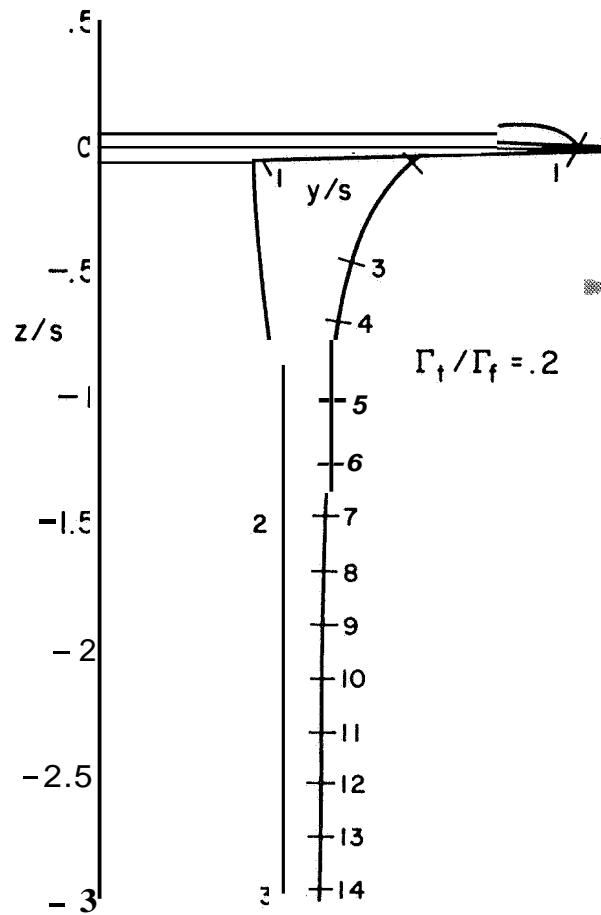
Figure 20. Vortex centroid locations as seen from down-
stream with weak interaction between like-
signed vortices – pairs diverge. The time
interval between consecutive integers is a
constant (ref. 6).

THE BEHAVIOR OF TWO
INITIALLY PLANAR VORTEX
PAIRS HAVING A COMMON
PLANE OF SYMMETRY

$y_1$ is measured to the
largest positive vortex
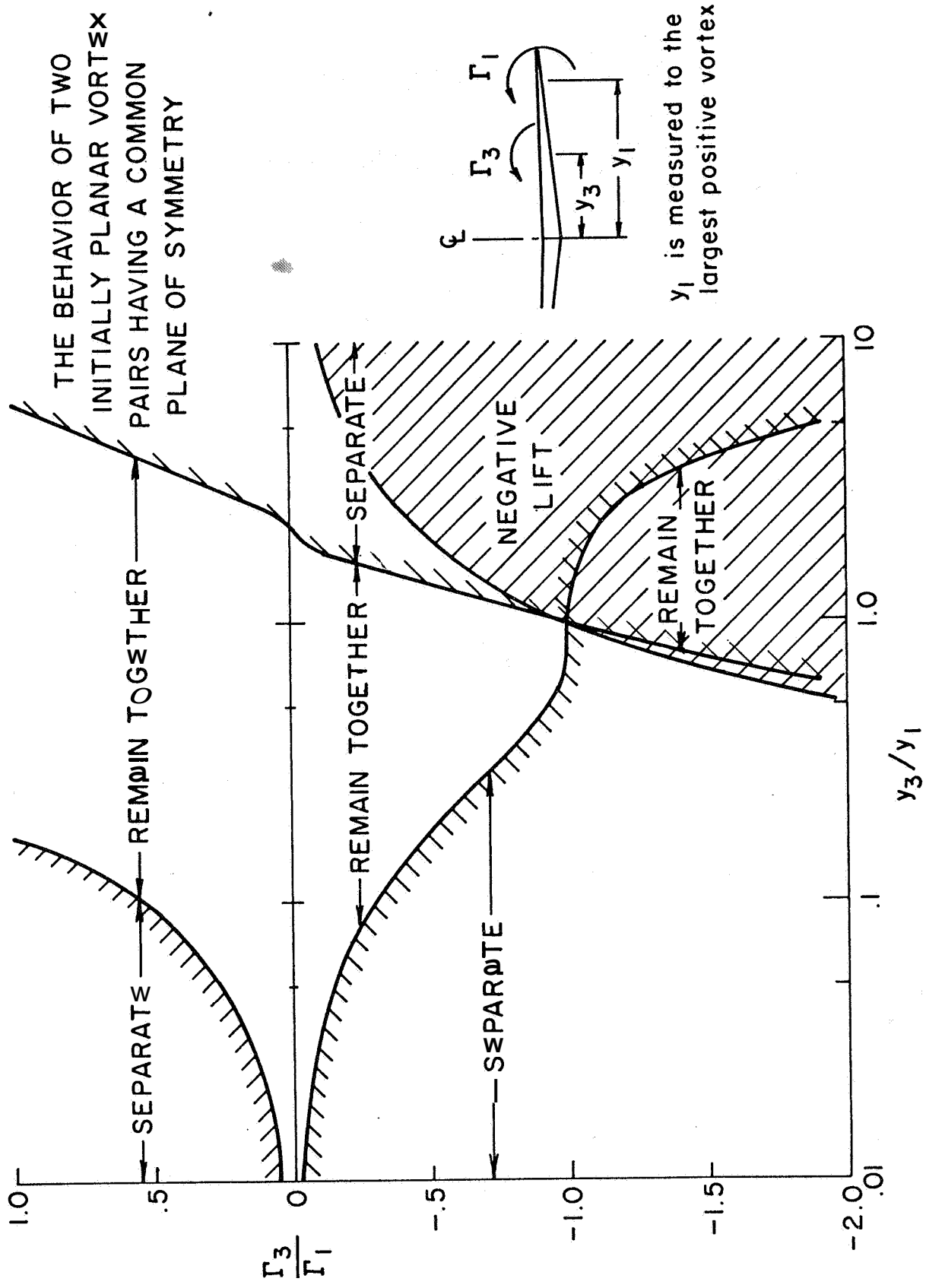
Figure 21.   Wake classification chart for two-vortex-pair wakes

108
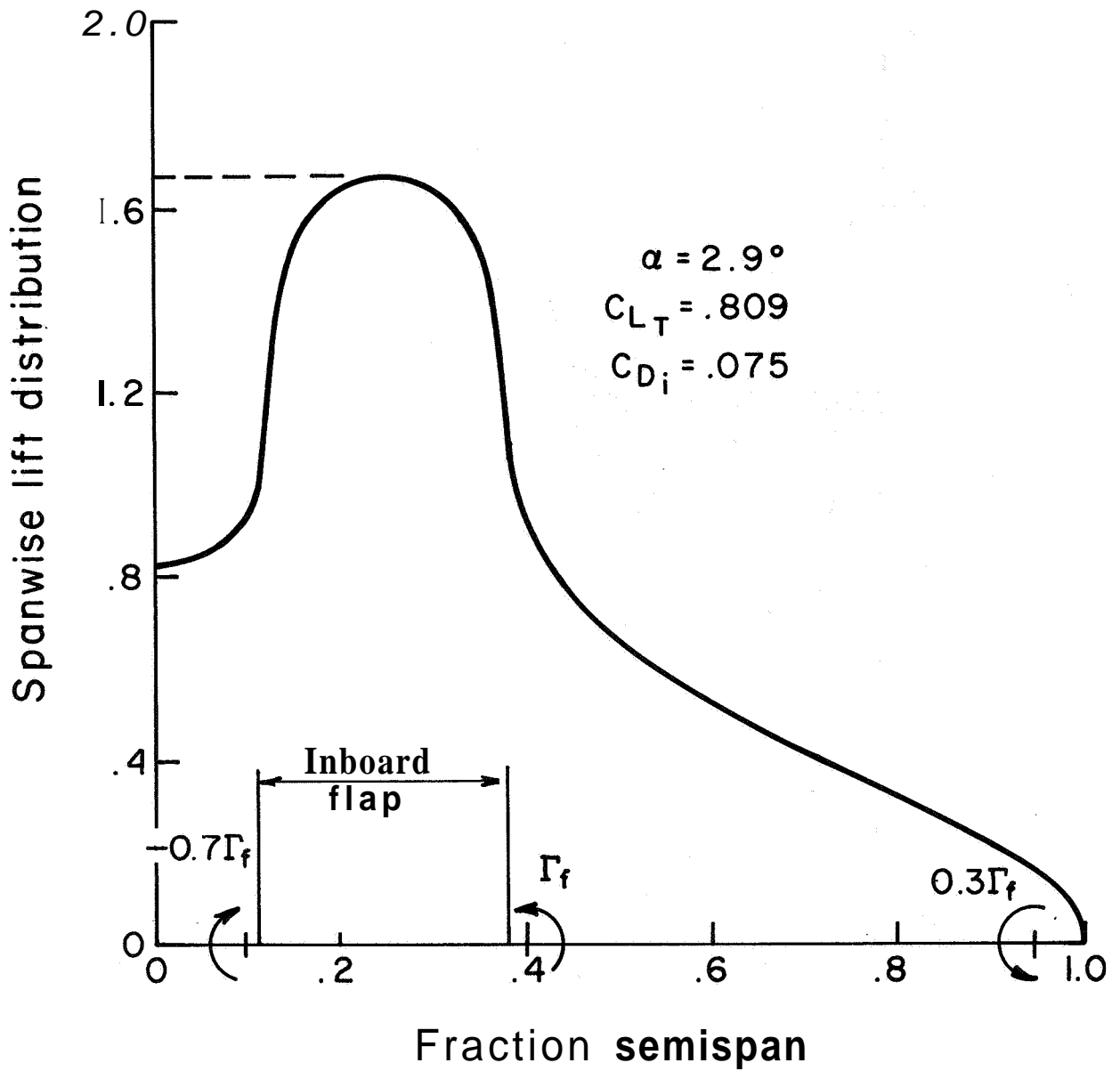
Figure 22.  Predicted spanwise lift distribution;  LDG/O
configuration (ref. 16).
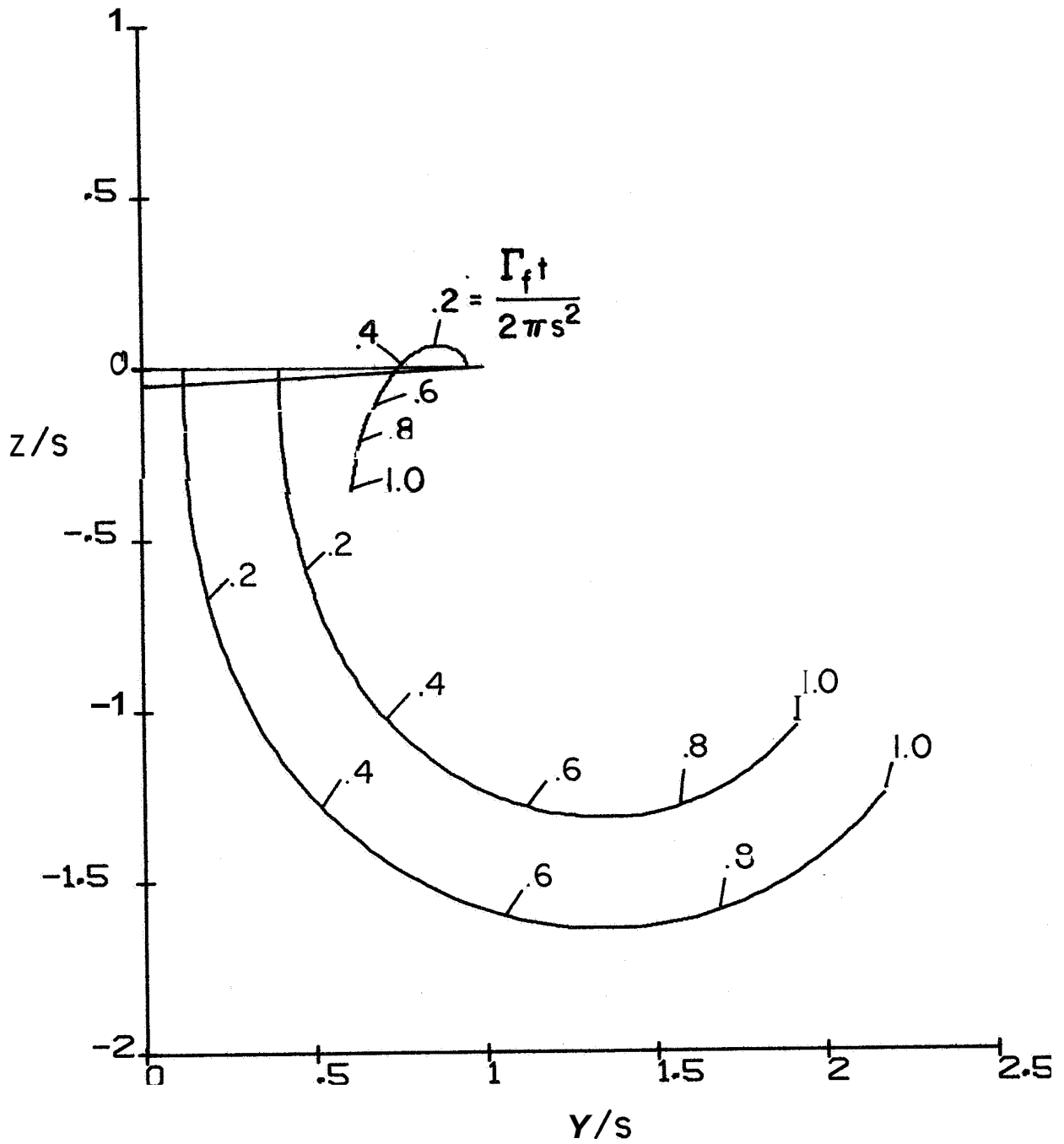
Figure 23.   Trajectories of the centroids of discrete vortices generated by the LDG/0 configuration (see fig. 22).

110
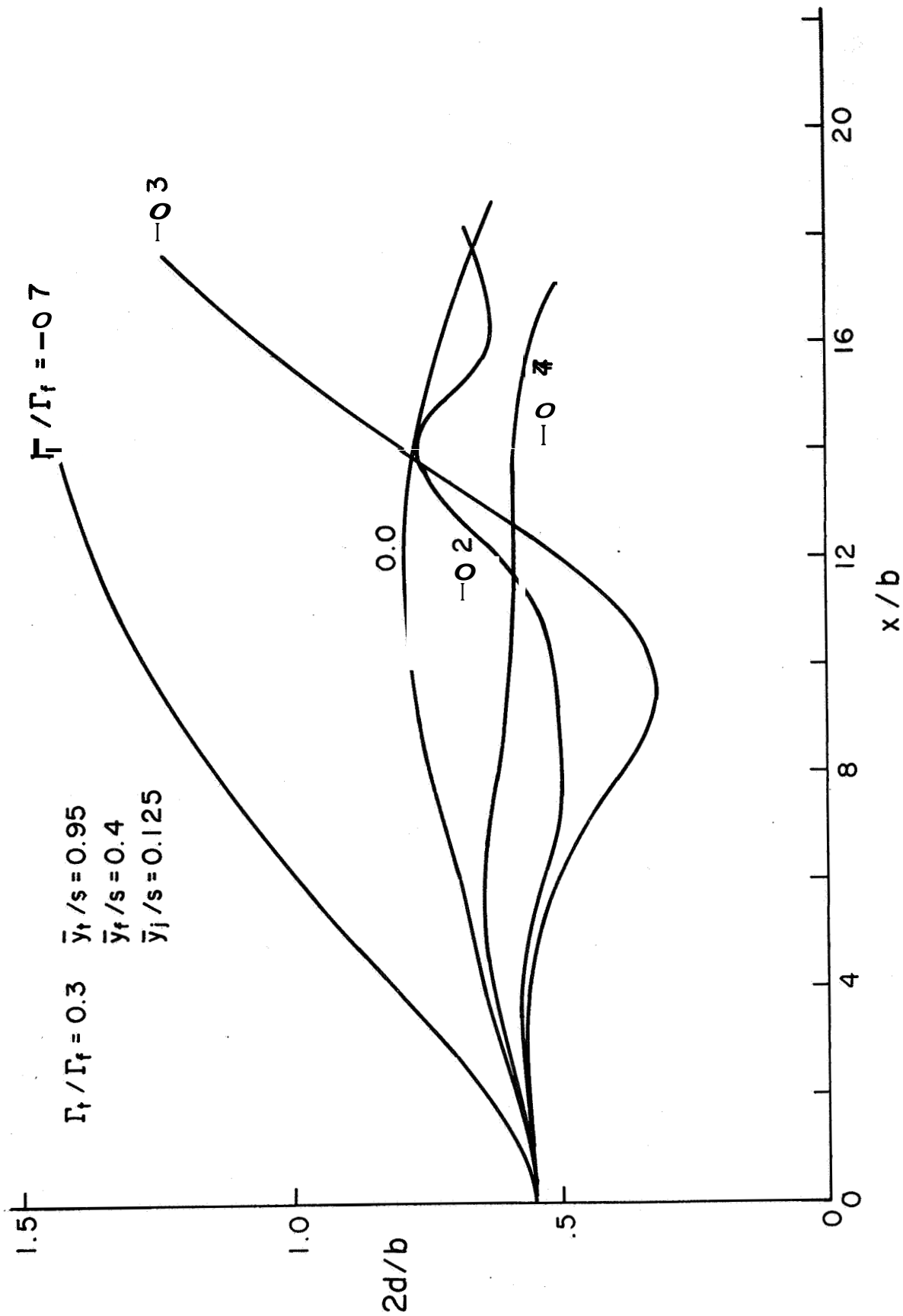
Figure 24. Sensitivity of the separation between tip and flap vortices as a function of the strength of the fuselage vortex $\Gamma_j$. The results for the LDG/O configuration shown in figure 22 are labeled $\Gamma_j = -0.7\Gamma_f$.

$\Gamma_t / \Gamma_f = 0.3$  $\dfrac{\overline{y}_t / s = 0.95}{\overline{y}_f / s = 0.4}$

$\Gamma_j / \Gamma_f = -0.47$

$\overline{y}_j / s = 0$

0.125

0.2

2d/b

1.0  .8  .6  .4  .2  0

$t\Gamma_f / 2\pi s^2$

0  .1  .2  .3  .4  .5  .6  .7
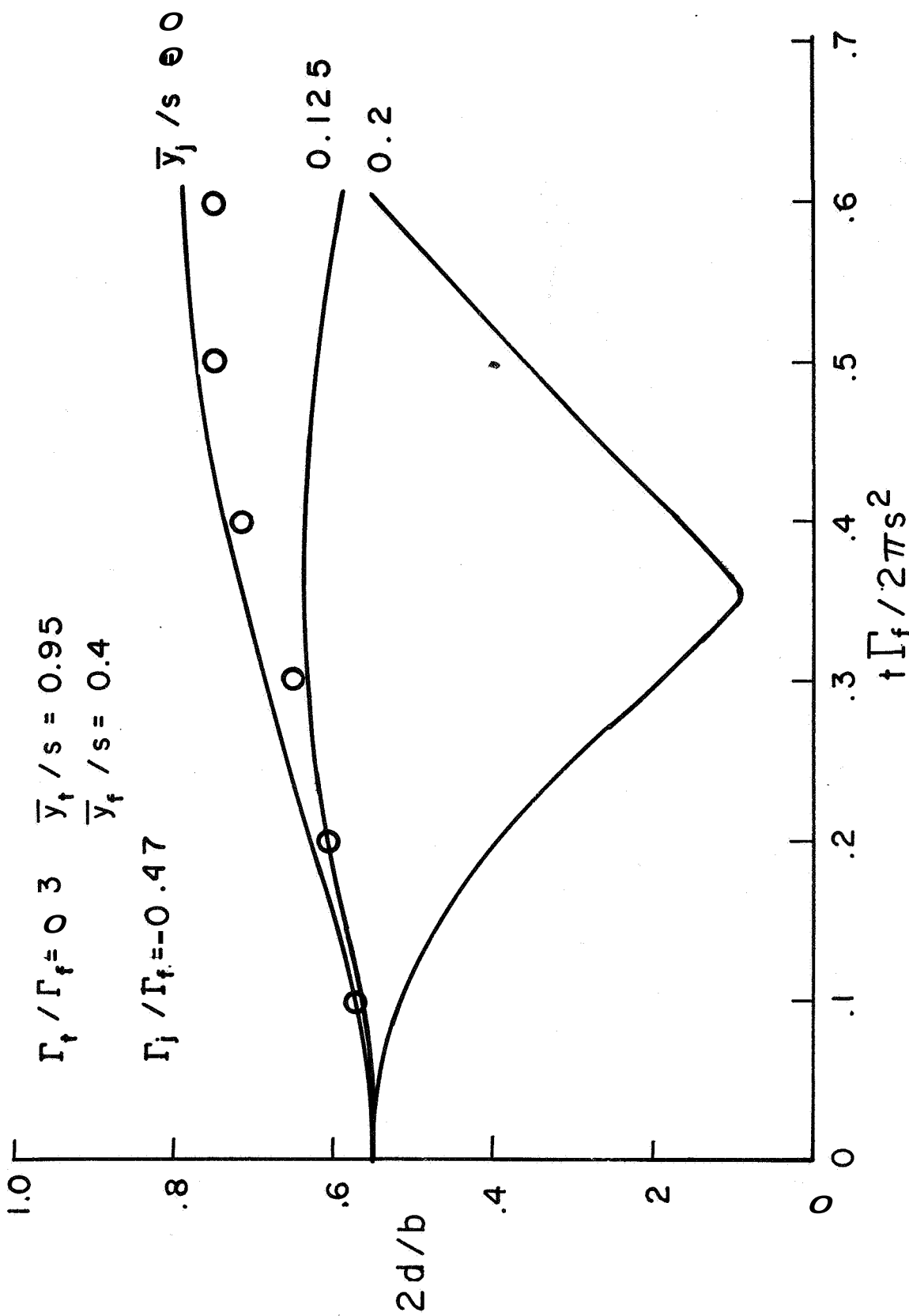
Figure 25.  Sensitivity of the separation between tip and flap vortices as a function of the initial position of the fuselage vortex $\overline{y}_j$.

112
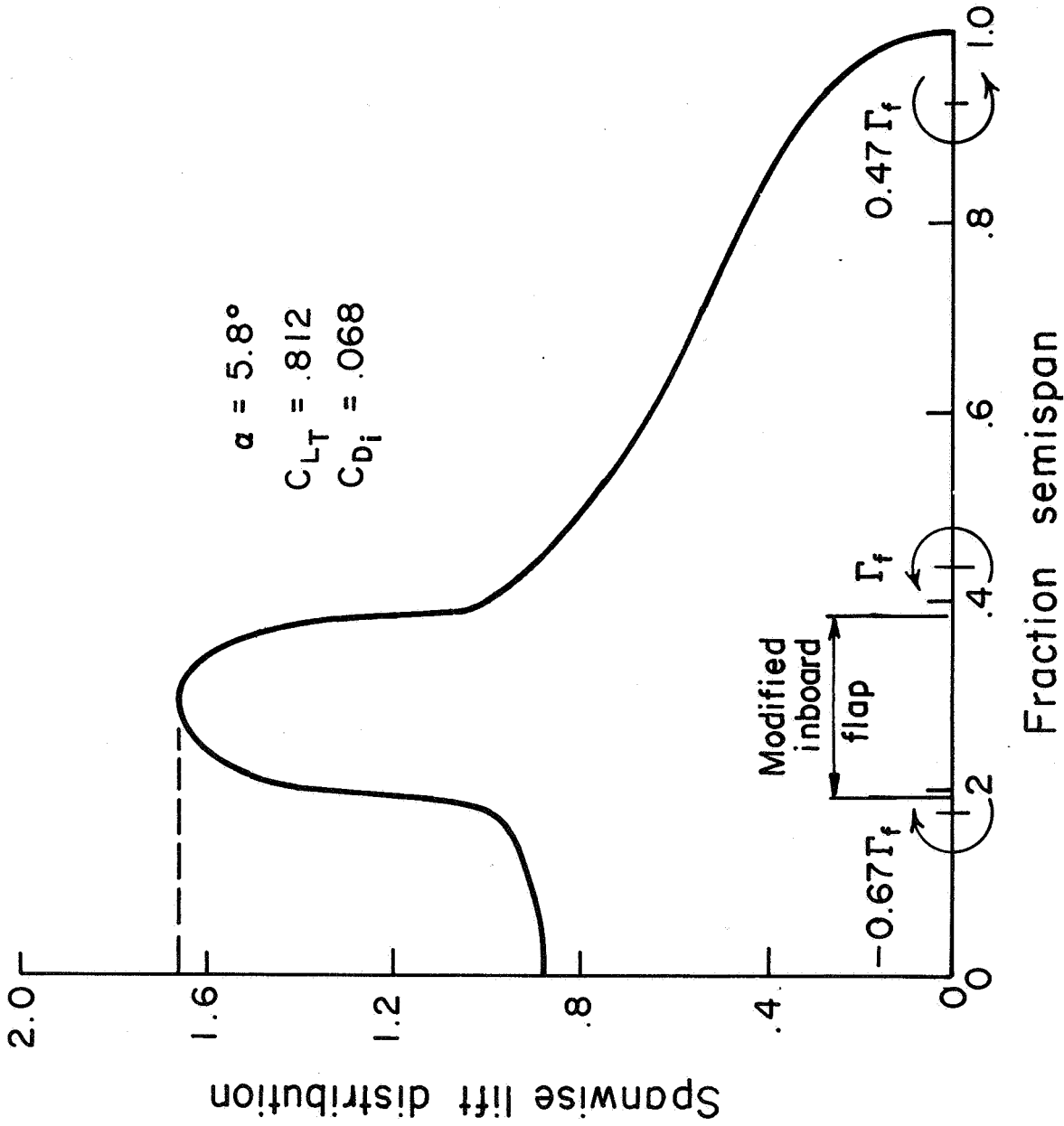
Figure 26.  Predicted spanwise lift distribution, modified LDG/O configurations (ref. 16)
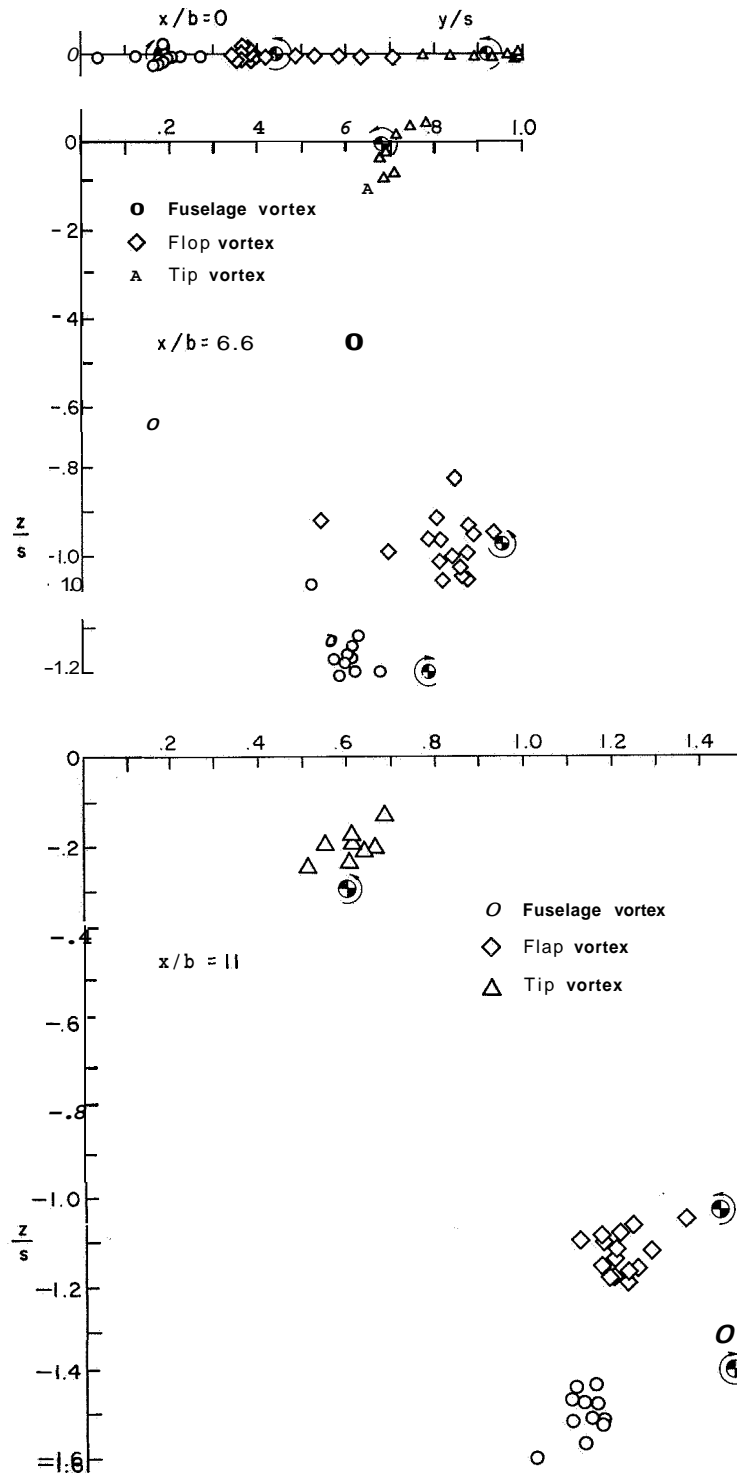
Figure 27. Comparison between using forty point vortices to represent the trailed sheet of vorticity and using three point vortices located at +,he centroid of the tip, flap, and fuselage vortices as shown in figure 26. ⊕ denotes centroid computed from the three-vortex computation.
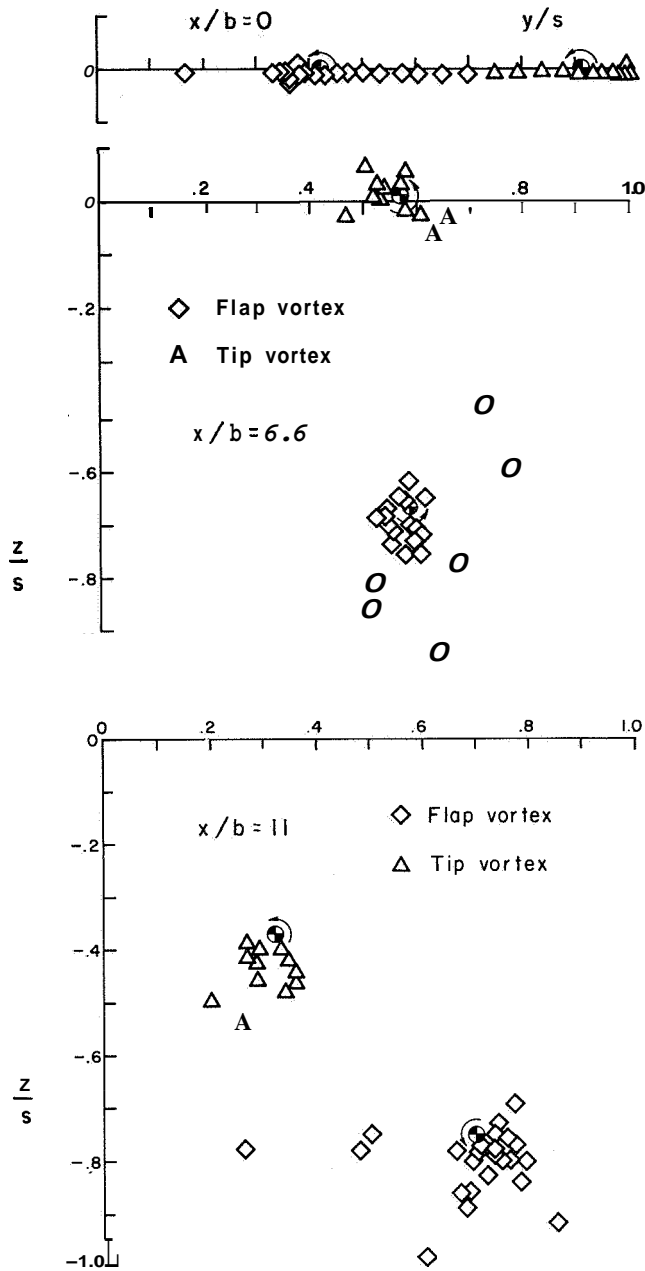
Figure 28. Comparison between using forty point vortices to represent the trailed sheet of vorticity and using two point vortices located at the centroid of the tip and flap vortices as shown in figure 26 (the fuselage vortex has been removed). ● denotes centroid computed from the two-vortex computation.
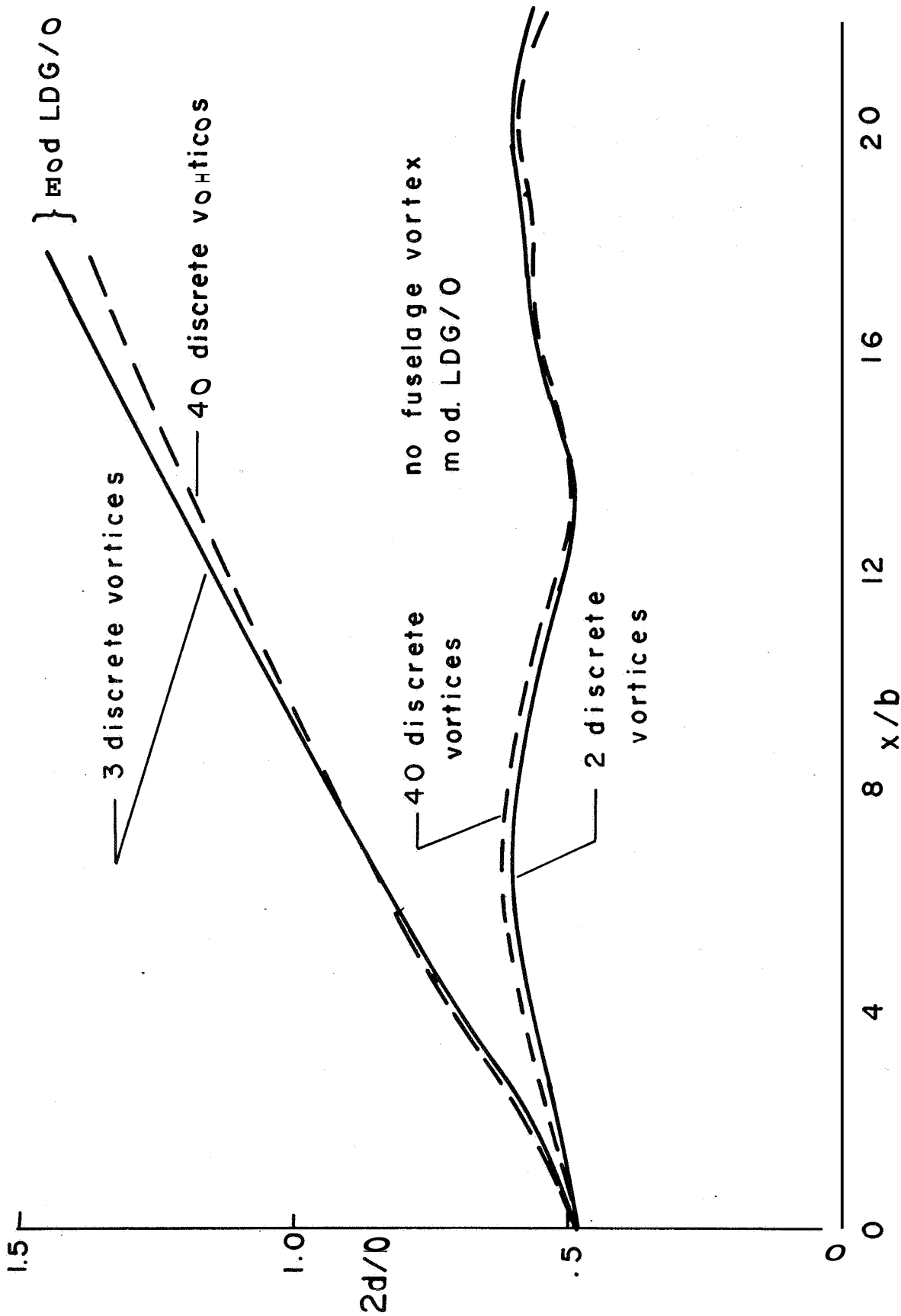
Figure 29. Comparison of the spacing between flap and tip vortices for the mod LDG/O configuration shown in figure 26.
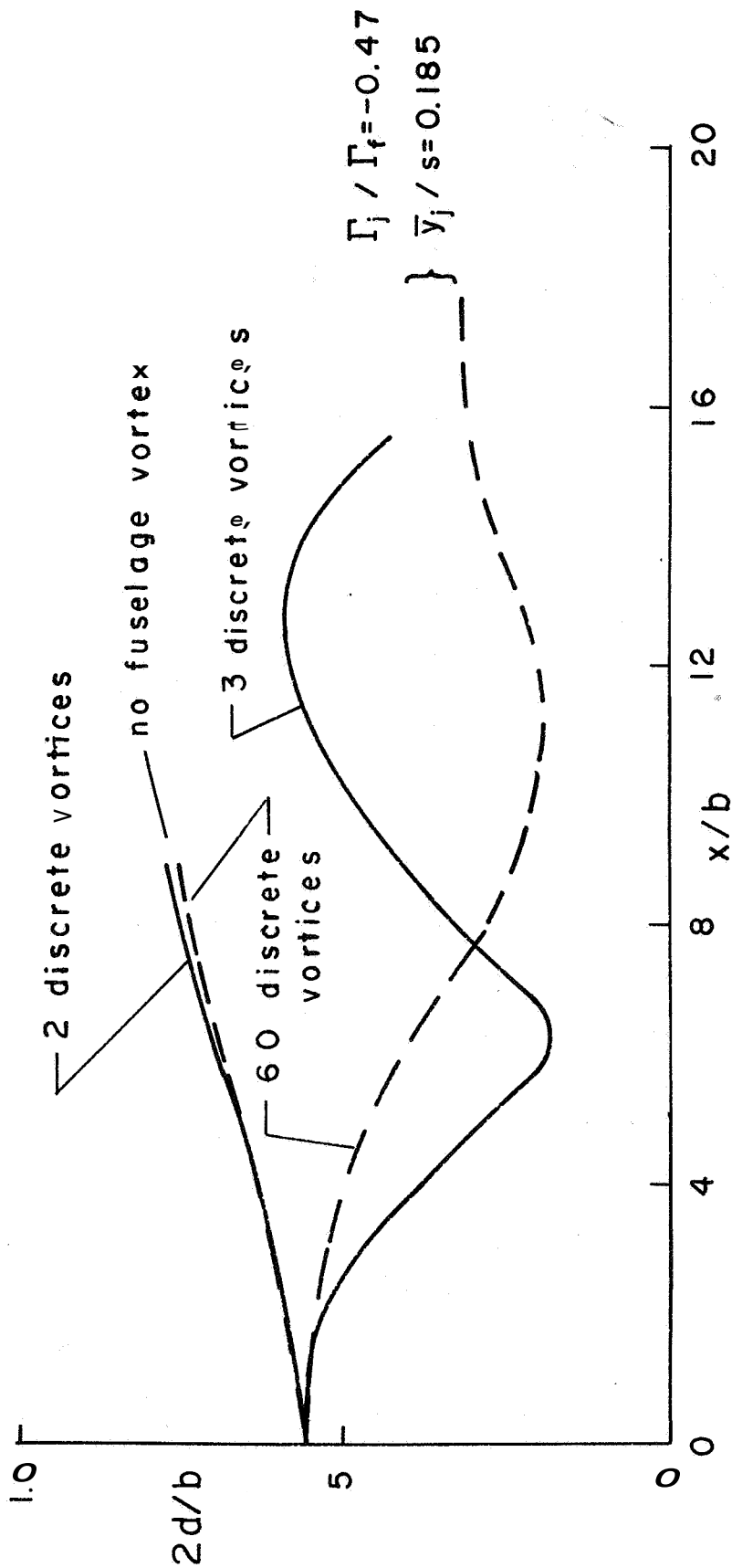
Figure 30   Comparison of the spacing between flap and tip vortices for an inboard altered LDG/O lift distribution.

117

$$\frac{\zeta 2\pi s'^2}{\Gamma}$$

$$\frac{\zeta 2\pi s'^2}{\Gamma} = \frac{2s'^2}{r_c^2} \exp\left(-\frac{r^2}{r_c^2}\right)$$

$r_c/s' = .4$

$r_c/s' = .8$

Initial vorticity
distribution along $z = 0$

$$\left(q\frac{2\pi s'}{\Gamma}\right)^2$$

Initial turbulence
distribution along $z = 0$

$$\left(q\frac{2\pi s'}{\Gamma^2}\right) = .3\exp\left(-\frac{r^2}{r_c^2}\right)$$
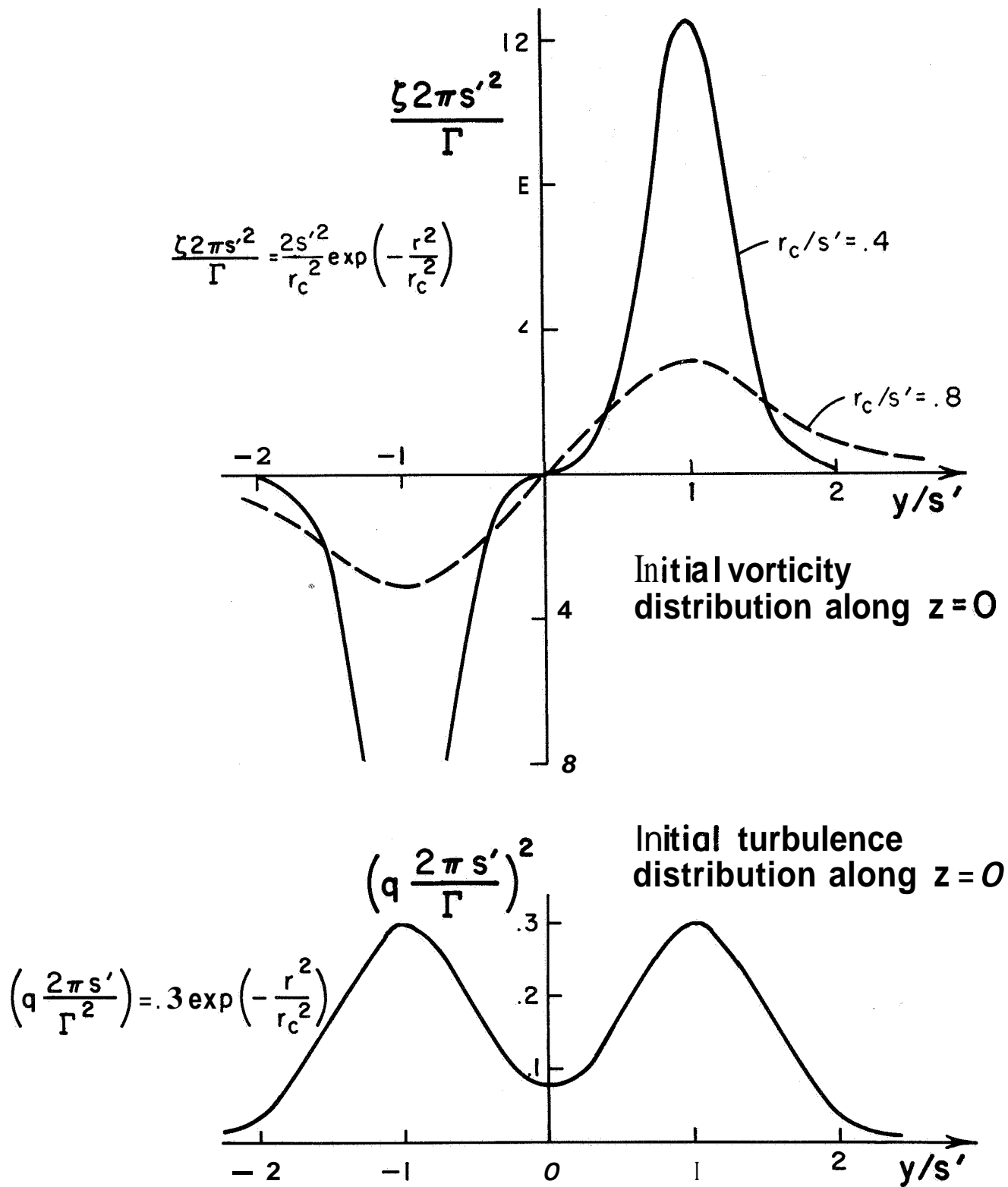
Figure 31.   Initial vorticity and turbulent kinetic energy
distributions used in the computation of the decay
of a vortex pair in a quiescent atmosphere,

118

## Half-Plane Circulation

$r_c/s' = .4$

$r_c/s' = .8$

$\dfrac{\Gamma}{\Gamma_0}$

$\left(\dfrac{x}{b'}\right)\left(\dfrac{b}{b'}\right)^2 \dfrac{C_L}{\pi A}$
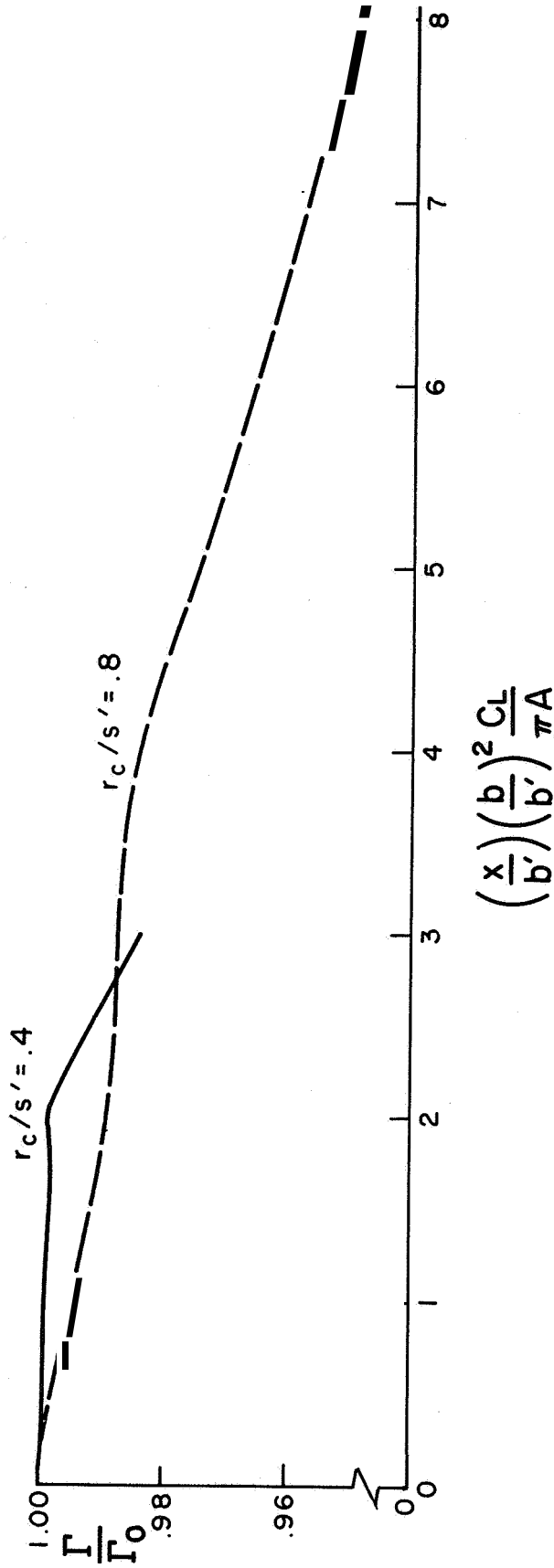
Figure 32. Comparison of the decay of circulation in a counter-rotating vortex pair for two different initial vortex core radii.

119
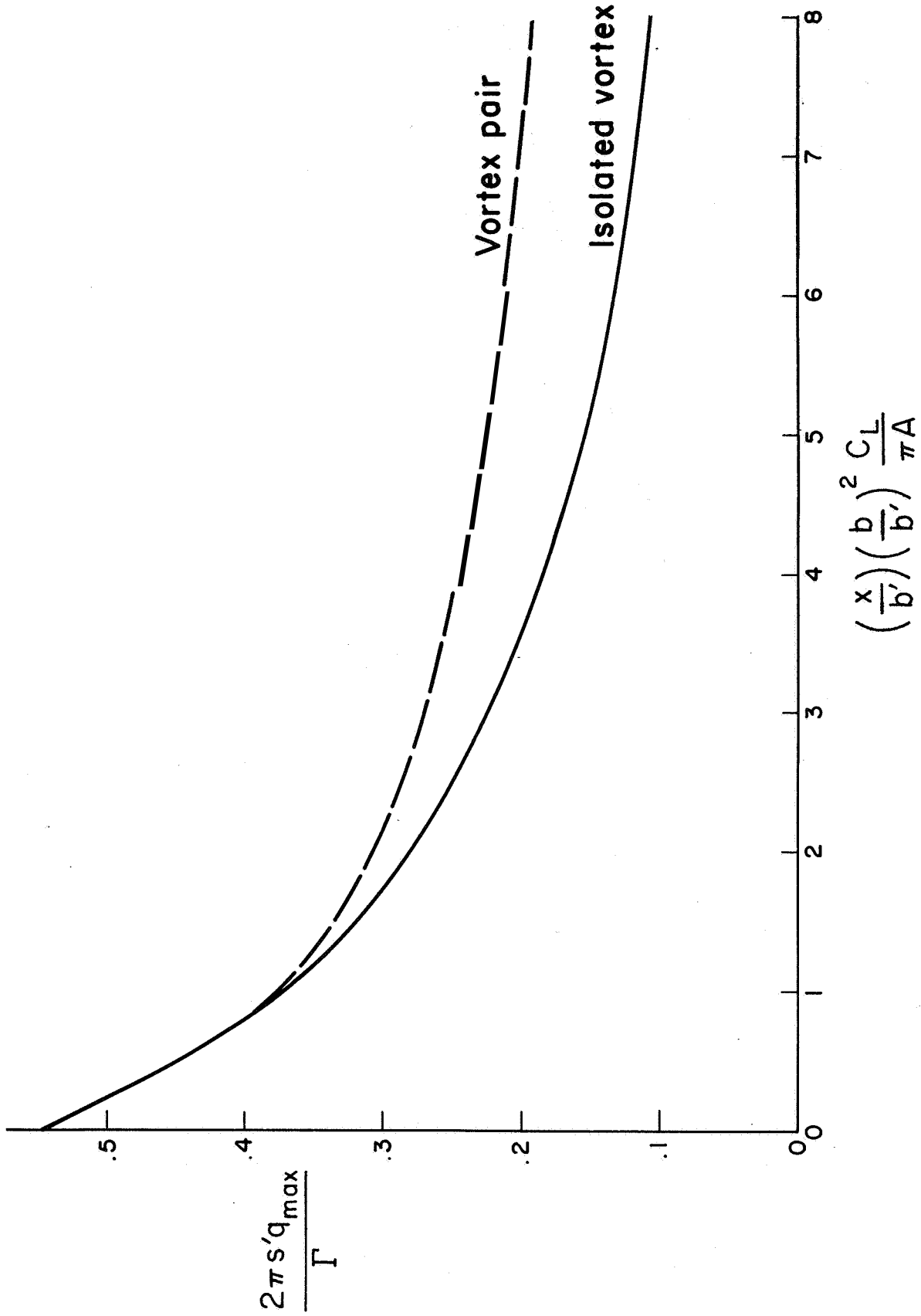
Figure 33    Comparison of the maximum root-mean-square turbulence level in a counter-rotating vortex pair and in an equivalent isolated vortex ($r_c/s' = 0.8$).
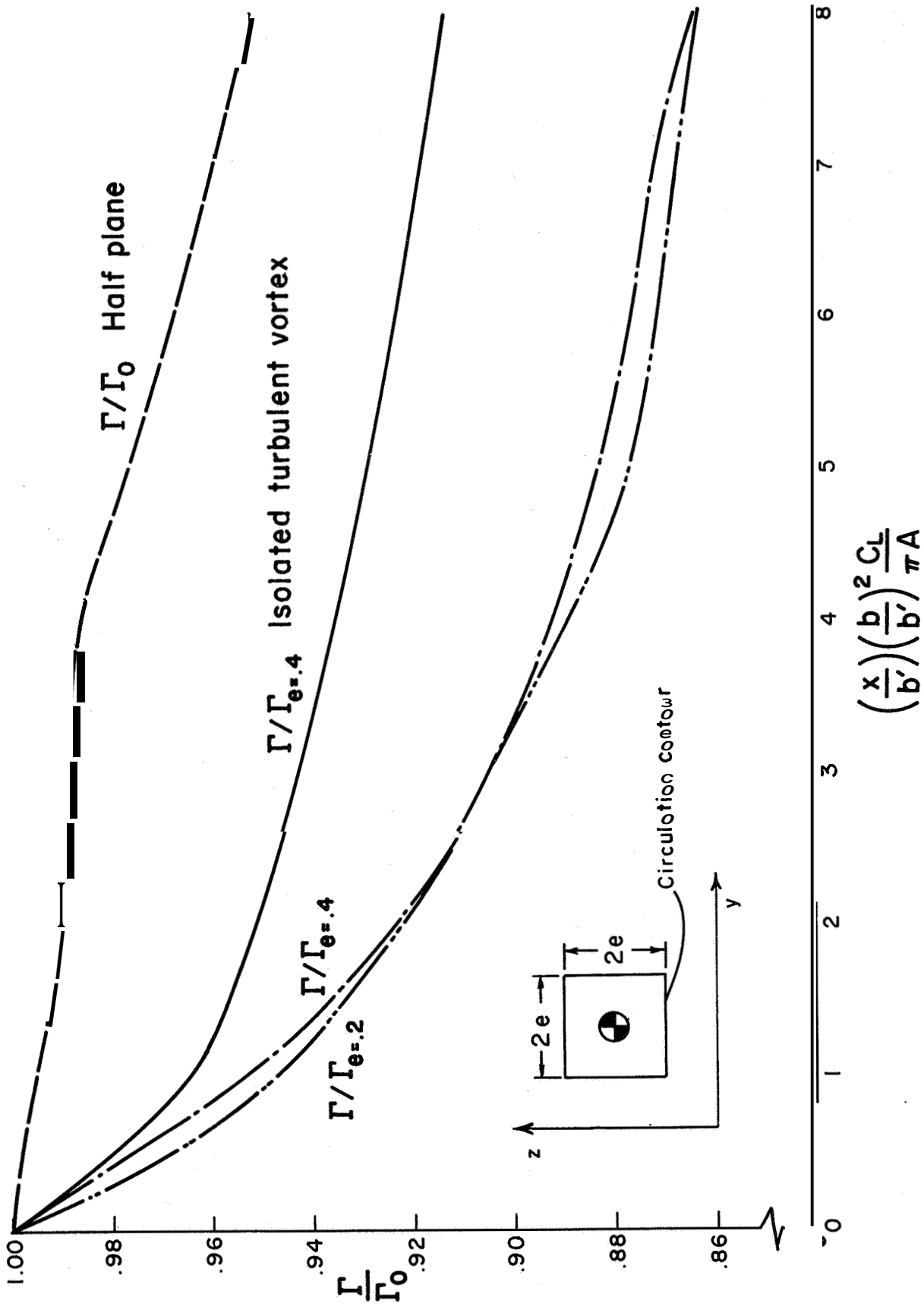
Figure 34. Decay of circulation in a counter-rotating vortex pair computed about square contours centered at the centroid of vorticity of the half-plane vorticity distribution ($r_c/s' = 0.8$).
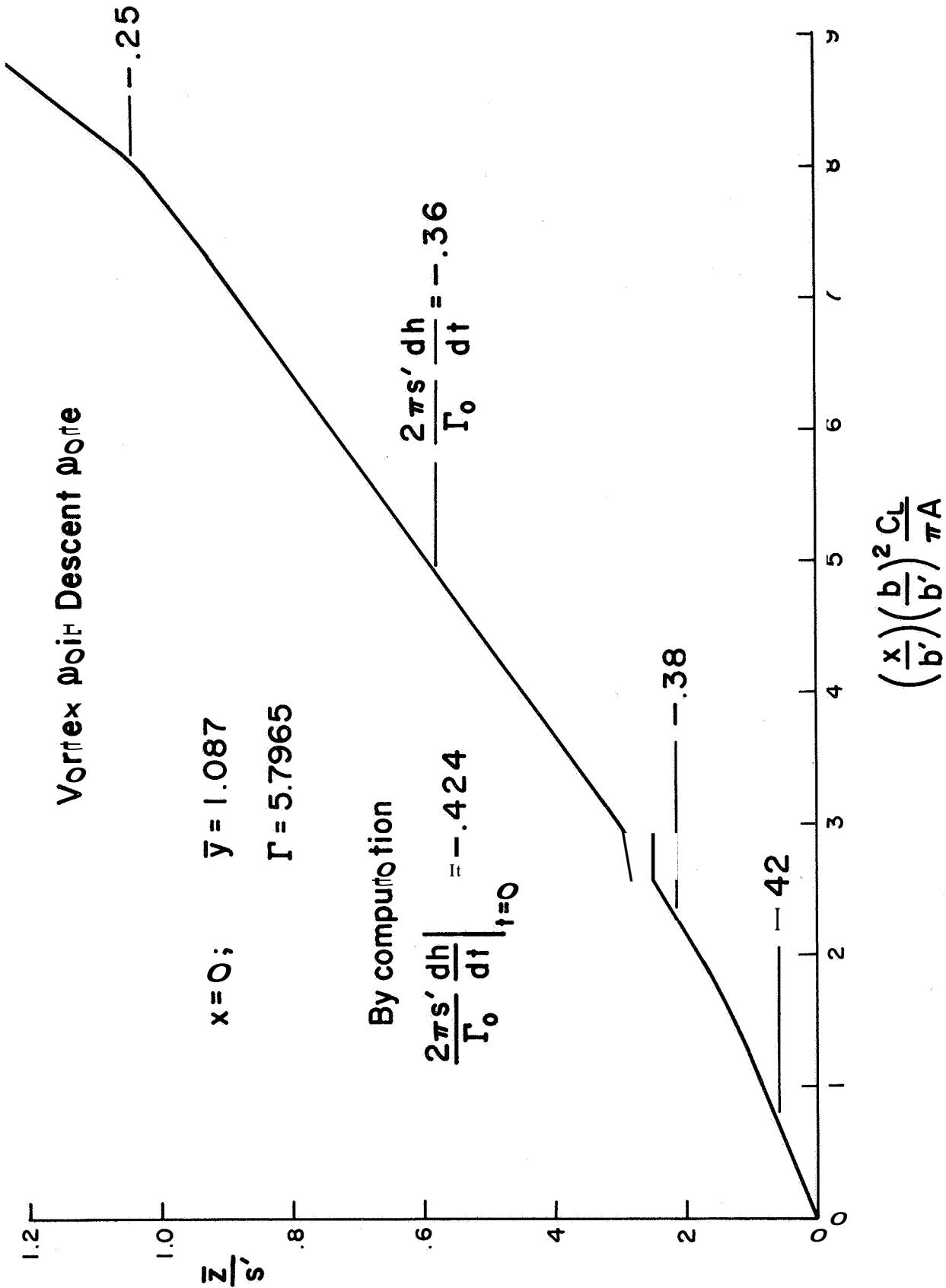
Figure 35. Descent rate of the counter-rotating vortex pair ($\kappa_C/s' = 0.8$)
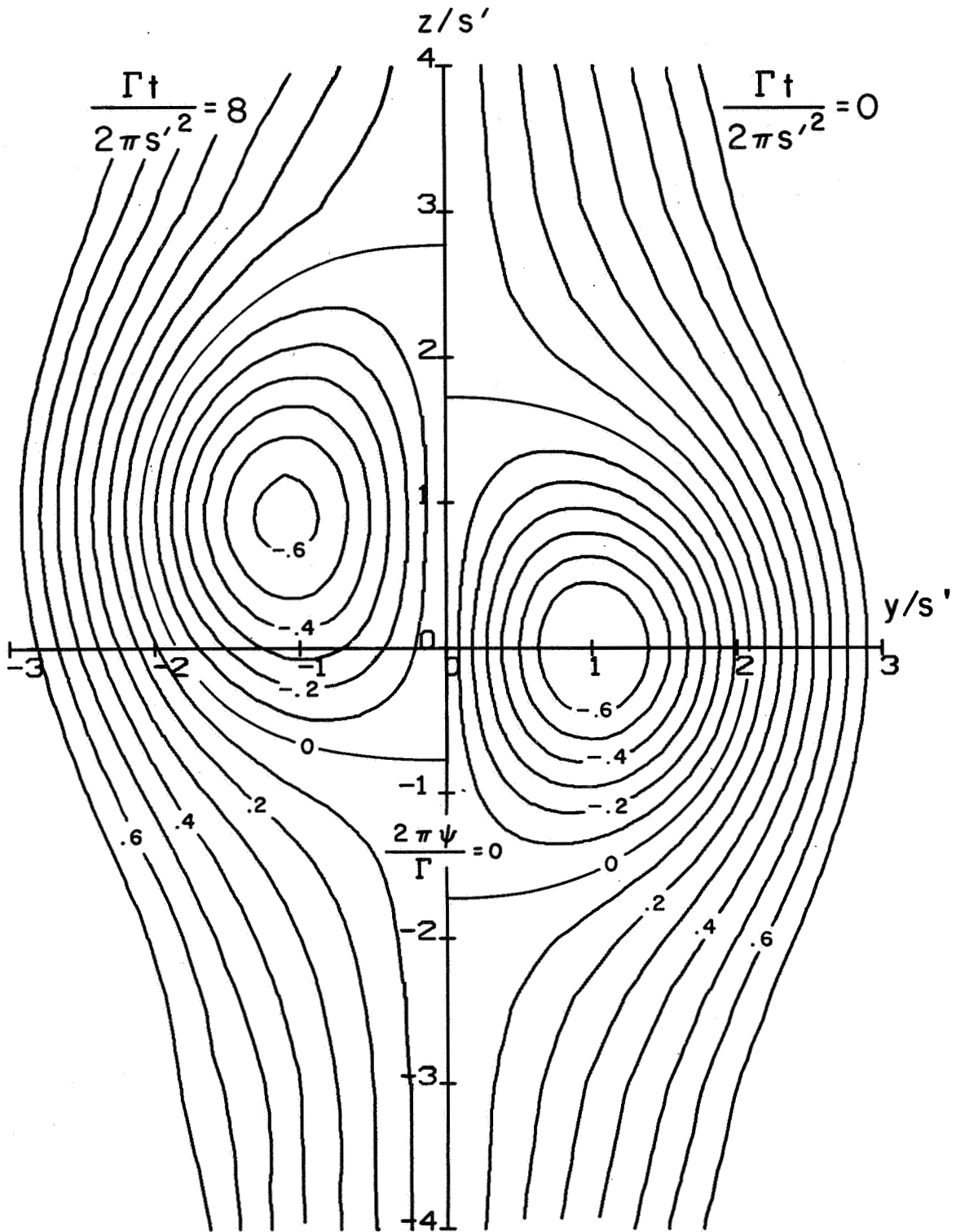
Figure 36. Instantaneous streamlines at $\Gamma t/2\pi s'^2 = 0.0$ and 8.0.
The descent of the pair is stopped by adding an upwash
of $\Gamma/4\pi s'$ . Streamlines shown for $\Gamma t/2\pi s'^2 = 8.0$ have
been reflected across the $y = 0$ axis.
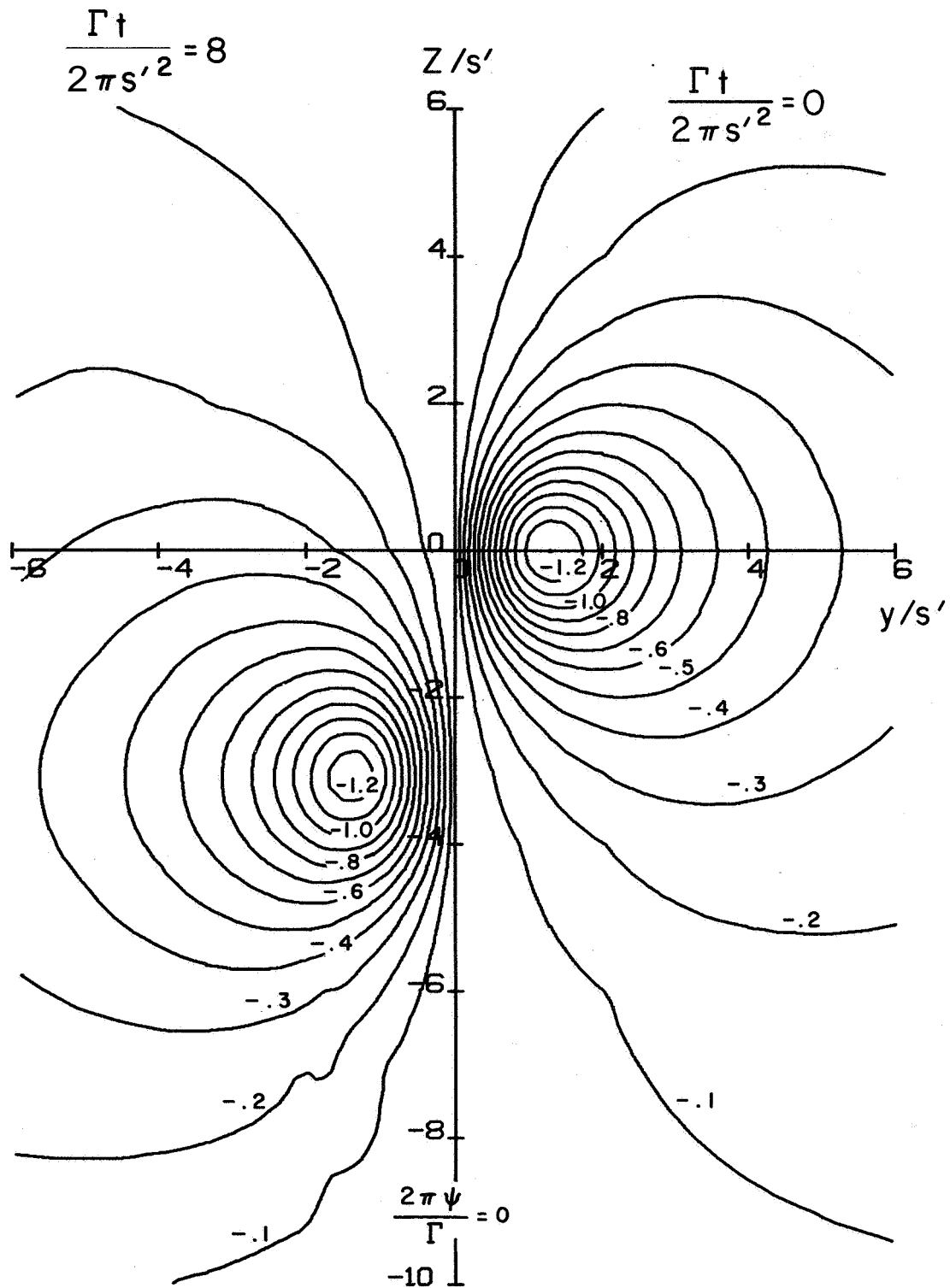
Figure 37.    Instantaneous streamlines at $\Gamma t / 2 \pi s'^2$ = 0.0 and 8.0. The upwash added in Figure 36 has been removed and the pair permitted to descend.  Streamlines shown for $\Gamma t / 2 \pi s'^2$ = 8.0 have been reflected across the  y = 0 axis.
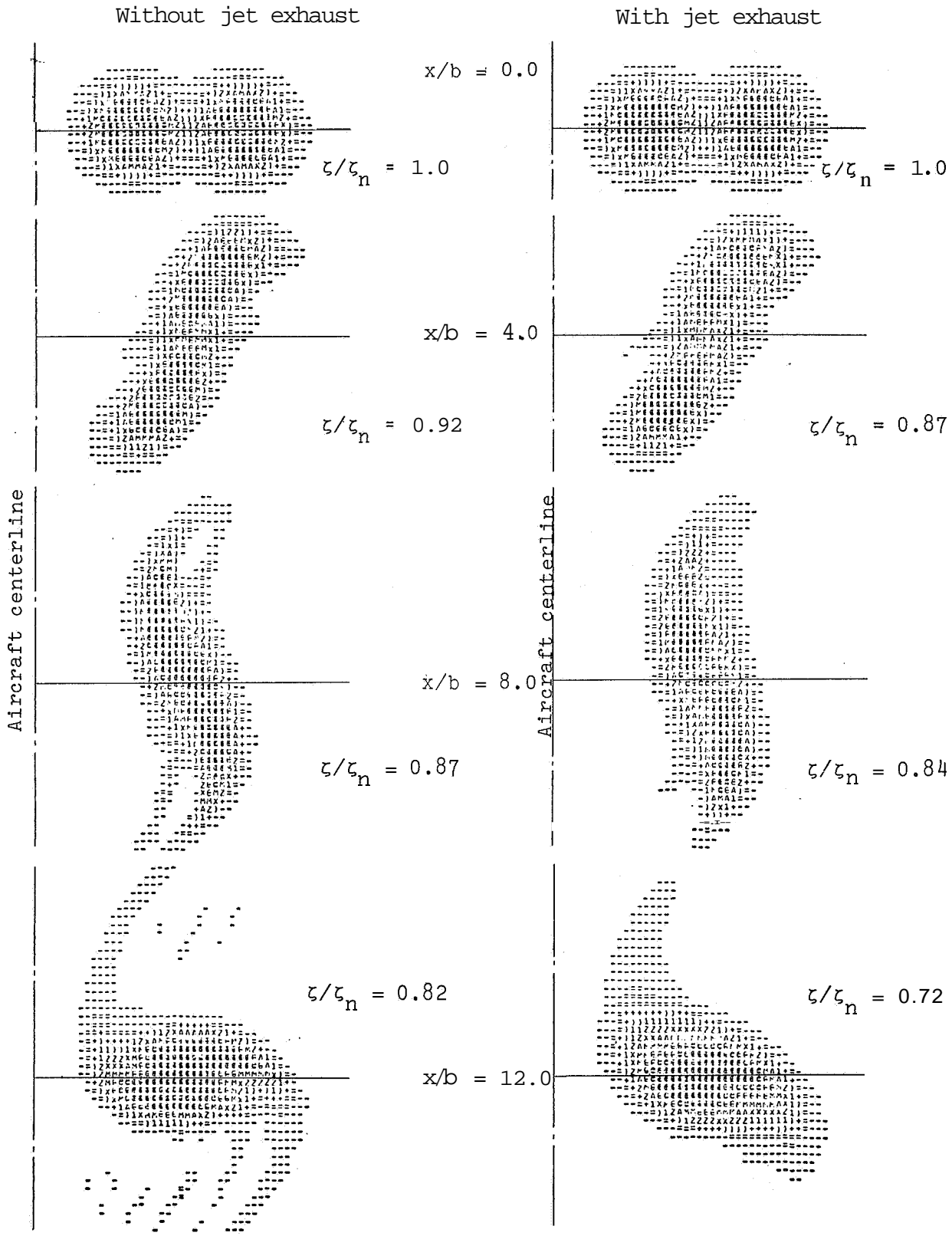
Figure 38. Intensity plots of the trailed vorticity $\zeta$. $\zeta_n = 48.5\Gamma/2\pi s2$ .

Without jet exhaust

With jet exhaust

$x/b = 0.0$

$q^2_{max}/q^2_n = 0.23$

$q^2_{max}/q^2_n = 0.26$

$x/b = 4.0$

$q^2_{max}/q^2_n = 0.29$

$q^2_{max}/q^2_n = 0.8$

$x/b = 8.0$

$q^2_{max}/q^2_n = 0.64$

$q^2_{max}/q^2_n = 1.0$

$q^2_{max}/q^2_n = 1.0$

$q^2_{max}/q^2_n = 0.82$

$x/b = 12.0$

$q^2_n = 0.044(\Gamma/2\pi s)^2$

$q^2_n = 2.5(\Gamma/2\pi s)^2$
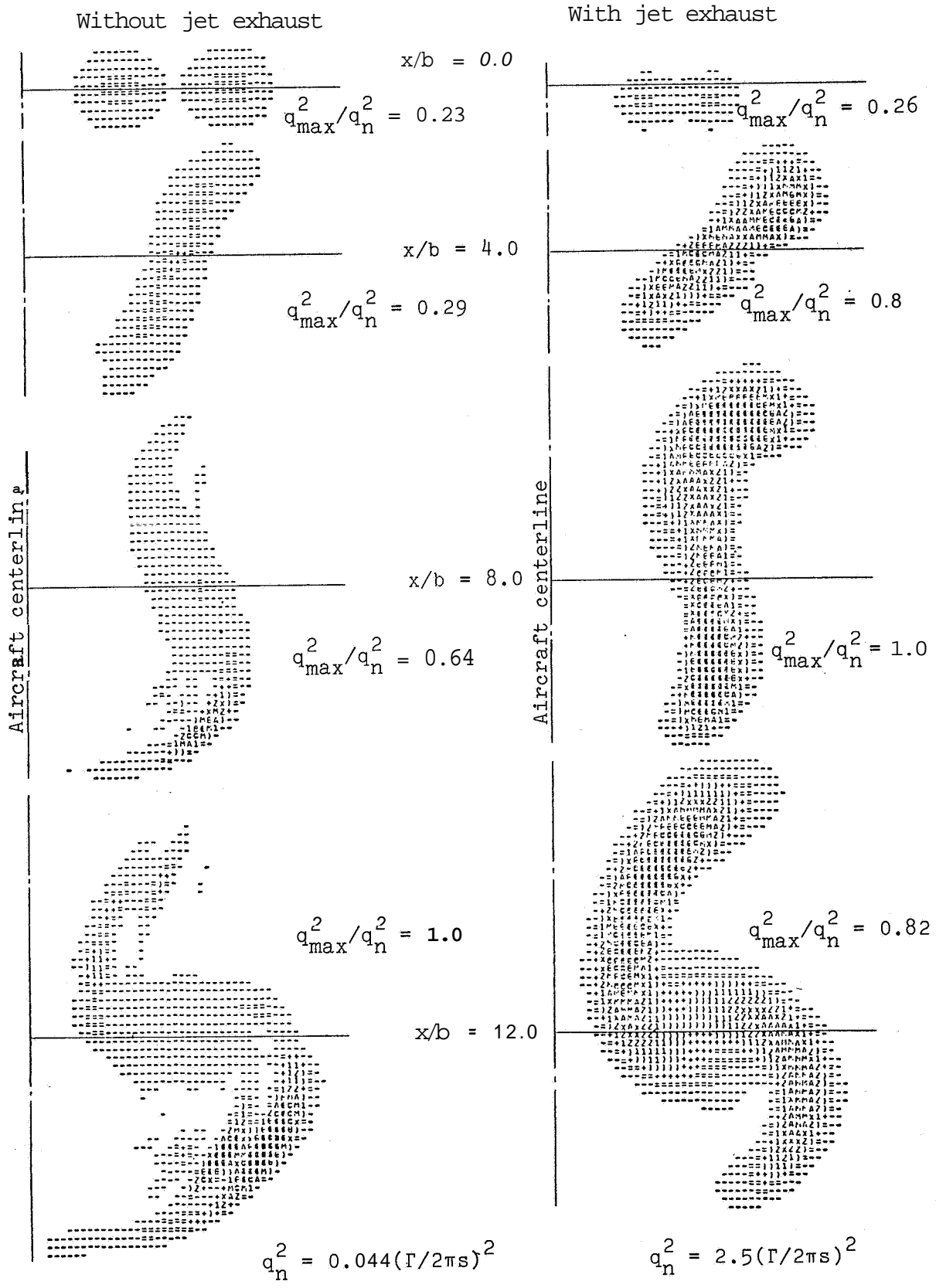
Figure 39.  Intensity plots of the turbulent kinetic energy.

$x/b = 0.0$

$\Delta U_{max}/\Delta U_n = 1.0$

$x/b = 4.0$

$\Delta U_{max}/\Delta U_n = 0.75$

Aircraft centerline

$x/b = 8.0$

$\Delta U_{max}/\Delta U_n = 0.45$

$x/b = 12.0$

$\Delta U_{max}/\Delta U_n = 0.3$
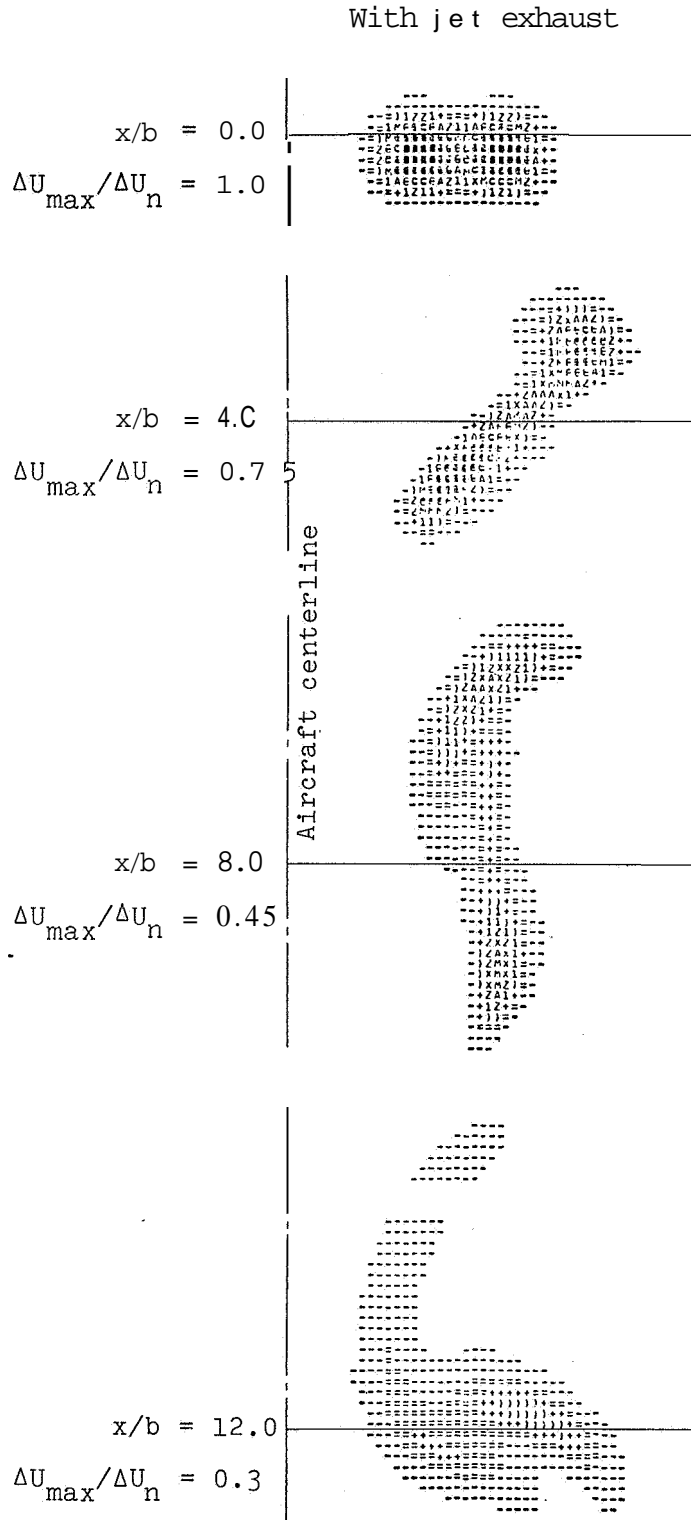
Figure 40.   Intensity plots of the jet exhaust axial velocity excess.   $\Delta U_n = 8.0\Gamma/2\pi s$ .

127
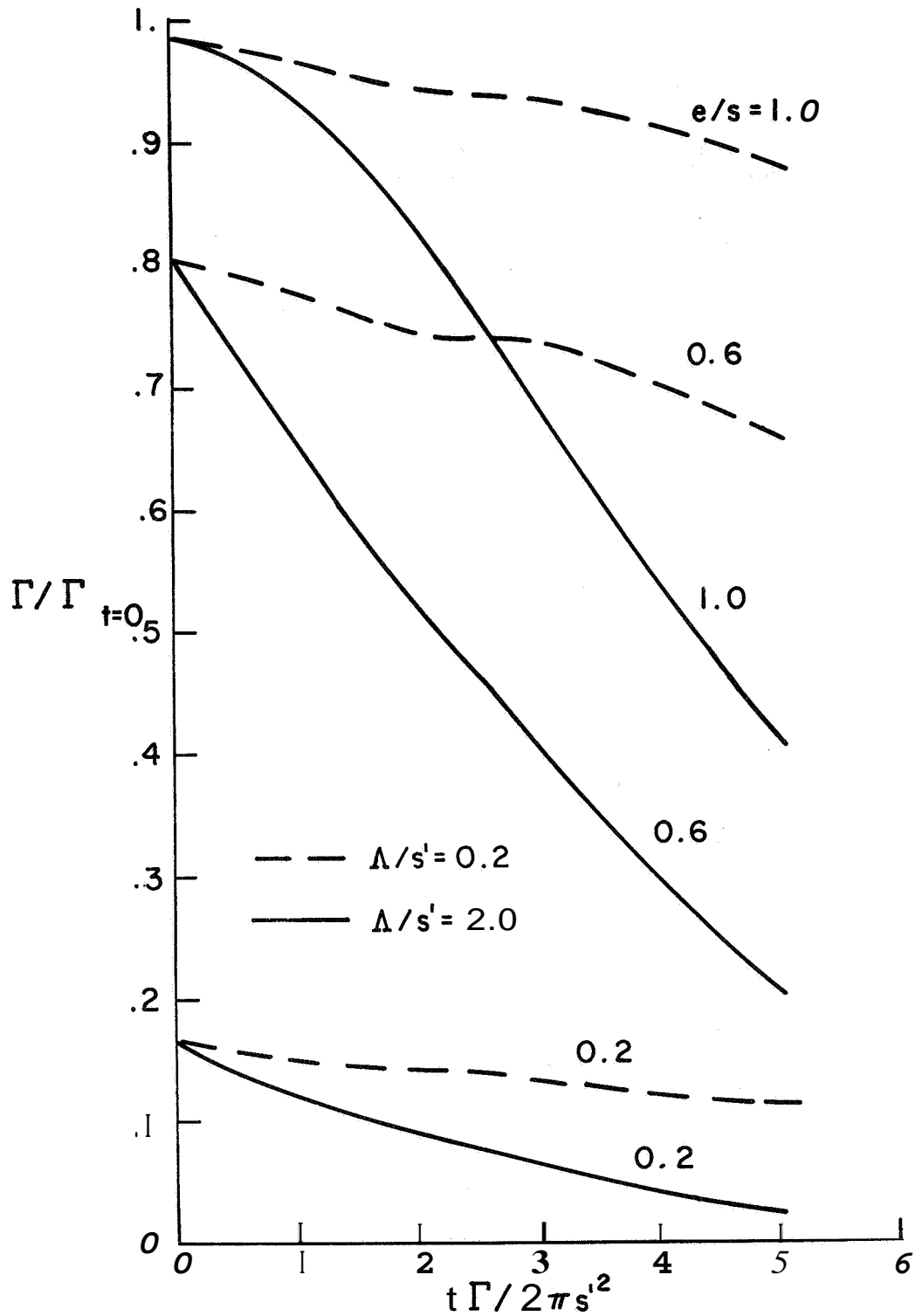
Figure 41. Decay of circulation in a counter-rotating vortex pair immersed in a turbulent atmosphere with constant turbulent dissipation rate ($E^{1/3} = 2$ $cm^{2/3}$/sec); see figure 34.

# GROUND-BASED FACILITIES FOR EVALUATING

# VORTEX MINIMIZATION CONCEPTS

Joseph W. Stickle

Langley Research Center


and


Mark W. Kelly

Ames 'Research Center

## SUMMARY

To determine the feasibility of altering the formation and decay of aircraft trailing vortexes through aerodynamic means, NASA used the test capabilities of two wind tunnels and two towing basins. This paper describes the facilities, common models, and measurement techniques that were employed in the evaluation of vortex minimization concepts.

## INTRODUCTION

The initial task of the NASA Wake Vortex Alleviation Program was to evaluate the many devices and concepts that had been proposed to alter vortex formation and decay. Facilities, therefore, were a major concern because the characteristics of the vortex system must be determined from the point of generation to points far downstream, representing in scale the area of interest to a following aircraft.

129

The problems, measurement techniques, and scaling of Reynolds number and viscosity effects were discussed among both Government and industry researchers in preparation for the evaluation program. It was generally agreed that evaluation testing should be limited to those facilities that can re-create, in model scale, an actual vortex penetration situation. It was further agreed that the facilities should have common models, standard measurement techniques, and be capable of providing a model Reynolds number on the order of 0.5 million or greater, based on the generating model chord. The facilities selected included the 40- by 80-ft wind tunnel at NASA's Ames Research Center, the vertical/short takeoff and landing (V/STOL) wind tunnel at Langley Research Center, and the Hydronautics Ship Model Basin in Laurel, Md. In addition, the inactive 549-m long towing basin at Langley was modified with a new overhead carriage system to provide a towing system using air as the test medium in lieu of water, as used at the Hydronautics facility. The new installation was designated the Langley Vortex Research Facility. The models selected include a 0.03-scale jumbo-jet transport generating aircraft and two trailing wing models representing, in span and aspect ratio, a small jet transport and business jet. Each facility had the capability to generate a vortex system and to measure directly the induced rolling moment of the vortex on the trailing models.

This paper describes the evaluation facilities and the standard measurement technique. It will also indicate the range of test capability including other measurement and visualization techniques that have been applied to the study of wake vortexes in these facilities.

It should be noted that reference 1 describes the development of a laser velocimeter for vortex flow analysis and the use of the water towing facility at the University of California, Berkeley. Although these were not part of the standard evaluation apparatus, they both contributed significantly to improved understanding of the complex nature of the aircraft trailing vortex system during the evaluation program.

$b_W$     wingspan of vortex generator model, m

c     local wing chord, m

$\bar{c}$     average wing chord, m

X     distance behind vortex generator model, m


## MODEL DESCRIPTIONS


### Vortex Generating Models

The generating aircraft model used in each of the facilities was a 0.03-scale jumbo jet transport, shown in figure 1. A sketch and pertinent geometric characteristics are given in figure 2. The initial model built for use in the Hydronautics Ship Model Basin was constructed of aluminum, stainless steel, and plastic. The three remaining models were molded of fiber glass, using molds constructed from the Hydronautics model. Mounting techniques varied between facilities and are discussed in subsequent facility descriptions; however, each generating model was equipped with a force balance to measure the performance impact of the vortex alleviation concepts. The generating models were equipped with two spanwise segments of triple-slotted trailing-edge flaps and full span leading-edge slats. Flap brackets were available to provide flap deflections for each of the spanwise segments.

The generating model used in the Ames 40- by 80-ft tunnel used flow-through nacelles and had no internal air ducting. The Hydronautics model had internal tubing for dye injection that can be pressurized for studies of vortex dissipation concepts with very low mass flow ($2.1 \times 10^{-4}$ $m^3/s$). For high mass flow studies, such as engine thrust effects, the Hydronautics facility incorporated an overhead scoop and centrifugal pump arrangement as shown in figure 3. Water is taken in through the scoop and pumped through' two streamlined struts positioned ahead of the model. The flow was scaled to

achieve the proper momentum and ratio of exit velocity to forward speed. The thrust of each strut was set to equal 25 percent of the generating model drag at the test lift coefficient. The lateral and vertical positions of the struts were varied to investigate the effects of engine placement.

The model used in the Langley Vortex Research Facility was equipped with high-pressure air (690 kPa (100 psi)) and internal tubing to simulate the engine thrust on all four engines. Flow rates have been adjusted to provide the appropriate thrust force; however, the ratio of model jet velocity to the model forward speed is higher than that .for full scale.

The V/STOL tunnel model also is equipped with high-pressure air (690 kPa (100 psi)) that can be used to simulate thrust in the manner similar to the Vortex Research Facility model. To date, mass flow tests in the V/STOL tunnel have involved only very-low-mass injection schemes and jettype spoilers.

Following Probe Models

The probe models are illustrated in figure 4 along with pertinent geometric characteristics. Each is a straight rectangular wing having the span (0.03 scale) and aspect ratio of a current day small jet transport aircraft and a business jet. The Hydronautics probe models are constructed of aluminum, although the other probe models are constructed of balsa wood. All of the probe models were instrumented with a single-component roll balance with the exception of the Hydronautics model, which also included lift and drag force measurement.

TEST PROCEDURES

The standard test procedure involves generation of a vortex system in the ground facility and surveying the flow field at various distances downstream using the roll-balance-equipped following model as a sensor. Although it is

recognized that this technique represents only one of many types of penetrations likely to occur in a real situation, it does represent one judged to be most hazardous from a pilot/control standpoint. It is also safe to assume that large reductions in the induced rolling moment will result in reductions in the severity of other upset situations. Figure 5 shows the test setup for each of the four facilities. The generating aircraft are mounted in the V/STOL and 40- by 80-ft tunnels in the most forward position of the test section, and the probe models are used to survey the vortex field at discrete downstream locations. Because the generating models in these facilities are stationary and the airstream is moving, the probe models can sense the vortex at a given position over a long period of time. Typical sample periods ranged from 10 to 40 s. Rolling-moment data in the V/STOL tunnel were sampled once per second and averaged over the sample period; data from the 40- by 80-ft tunnel were selected as only the highest peak within the sample period. Comparison of the two analysis techniques, using data from the V/STOL tunnel taken at 7.5 span lengths downstream with the large probe model, indicated approximately 10 percent higher values using the peak measurements over the averaged measurements, It would be expected that the difference measured with the smaller model, or at greater distances downstream with either model, would be greater because of the meandering of the vortex.

In the towing facilities, both models are moving and the data recording time is limited. A normal test run in the Hydronautics facility was approximately 25 s, which provides about 15 s for a single vertical survey through the vortex. In the Vortex Research Facility, the probe model is positioned prior to the run, and the sample time is approximately 2 s. In both Hydronautics and Vortex Research Facilities, the highest peak data per sample were used.

Figure 6 indicates the range of downstream distances in generating model span lengths that can be tested in the various facilities. The dark areas represent distances for which data have been obtained to date. It is worthwhile to note that figure 6 shows the test capability for the V/STOL tunnel extends well into the diffuser section. Trends of the rolling-moment data obtained in the diffuser and corrected for dynamic pressure change have been

found to be in general agreement with those at comparable distances from the Vortex Research Facility and from Hydronautics. Furthermore, reference **1** supports the diffuser results by comparing measurements made inside the test section behind a *1.22-m* straight wing model with measurements outside the test section, but at identical span lengths behind a *2.44-m* straight wing model.

## HYDRONAUTICS SHIP MODEL BASIN

The Hydronautics Ship Model Basin is a water–towing facility 95 m long and *8* m wide, with a water depth of *4* m. Two independently powered carriage systems are used to propel the vortex generating model and the following probe model. Maximum speed for conducting constant–speed runs is *6* m/s; however, the evaluation tests were conducted at a nominal *3.8* m/s, which corresponds roughly to the approach speed in span lengths per second of the full–scale aircraft. Test Reynolds number at this speed is approximately $1.0 \times 10^6$. The carriage system is shown in figure 7 for the generating model and in figure 8 for the following model. The generating model is attached with a pair of rigid faired struts that are mounted to a tilt table. The tilt table provides for a pitch attitude adjustment from $-4^o$ to $12^o$ relative to the model fuselage reference line. Vertical positioning is provided by substituting struts of different lengths. Normal test depth is 0.79 m below the surface; however, tests have been conducted at depths of 1.70 and *2.48* m. The latter depth places the generating model just under one span length above the tank floor for investigation of vortexes in ground effect.

Lateral adjustment of the generating model is ±0.71 from the tank centerline. The following model can be adjusted from the centerline to a position *2.28* m right of the centerline, giving a total lateral survey capability of *3* m. The following model has a motor–driven vertical scan system allowing a vertical survey of *0.46* m at a maximum rate of *0.04* m/s. In full scale, this would represent a climb rate slightly less than *30* m/min.

Separation distance between the two models was determined using the time differential for the two carriages to pass a point halfway down the tow tank and the measured speed of the carriages. For all tests, a sufficient number of vertical and lateral surveys were conducted to assure that the maximum imposed rolling moment present was measured at the various downstream distances. A sample time-history of data obtained during a test run is shown in figure 9. In the rolling-moment trace, the moment level builds and decays as the following model rises through the vortex. The maximum peak for each run is considered the maximum imposed rolling moment.

Prior to the vortex evaluation program, exploratory tests were made in the Hydronautics facility using hot wire anemometers and a vortex swirl meter to define vortex characteristics.

VORTEX RESEARCH FACILITY

A sketch of the Langley Vortex Research Facility is shown in figure 10. A gasoline-powered carriage is shown mounted on the 554-m overhead track, with the vortex-generating model blade mounted beneath the carriage. The following model is located 50 m downstream of the vortex generating model (a scale distance of 1.63 km (0.88 n. mi.)) through a series of trailers to measure the rolling moment induced by the vortex of the lead model.

The test section, constructed to isolate the wake of the carriage and trailers from the model wake, is 92 m long with a 0.05-m opening along the center of the ceiling to allow the model blade mounts to pass. The exterior of the building, shown at the entrance of the test section, encloses the entire length of the track.

The overhead track extends 308 m upstream of the entrance to the covered area where each test is initiated. After the carriage is launched, the automotive drive system accelerates through first and second gear to a velocity of 31 m/s, which is held constant by a cruise control throughout the length of the covered area. At the test position, 31 m inside the covered

area, smoke (vaporized kerosene) is deployed for flow visualization.   (See ref. *2.)*   At this point, high-speed motion picture and TV cameras are used to film the motion of the vortex produced by the generating model, while the aerodynamic forces experienced by the model are recorded.   After **1.6** s, the following model reaches this test point, measuring the vortex-induced roll.   Caliper brakes are applied as the vehicle leaves the covered area, bringing the vehicle to a 1-g stop over the next 77 m of track.

Figure **11** illustrates data trace taken from a typical run.   As the model enters the closed test section, downwash of the carriage is isolated from the vortex system and the vortex rises slightly into the path of the probe model indicated by the slight jump in rolling moment at time equal to 10 s.   Thirty-one meters, or **1** s later, the test sample begins and covers the next *2* s of data.   The maximum induced rolling moment is determined using the peak rolling moment during the test interval with the aid of video recording showing the position of the probe relative to the vortex core.   Normal test Reynolds number in the Vortex Research Facility is $4.7 \times 10^5$.

## V/STOL **WIND** TUNNEL

The V/STOL tunnel, located at NASA's Langley Research Center, has a test section *4.42* m high, 6.63 m wide, and *15.24* m long.   (See fig. *12.)*   It can be operated as a closed tunnel with slotted walls, or as one or more open configurations by removing the side walls and ceiling.   Tunnel speed is variable from 0 to 100 m/s *(200* knots).   In the vortex program, a majority of the tests were run at a free-stream dynamic pressure in the test section of 430.90 Pa, which corresponds to a velocity of *27.4* m/s.   The Reynolds number based on the generating model chord was approximately $4.7 \times 10^5$.   Investigations of the effect of Reynolds number on the rolling-moment data were conducted up to Reynolds numbers $1 \times 10^6$.   No significant effects were detected.   Blockage corrections were applied to the data by the method of reference 3.   Jet-boundary corrections to the angle of attack and to the drag were applied in accordance with reference *4.*   Basic aerodynamic data of lift, drag, and pitching-moment coefficients

for the generating model were obtained over an angle–of–attack range of $-4^o$ to $+24^o$.

The probe model was attached to a traverse mechanism capable of moving the model approximately 2 m laterally and vertically. The electric–powered traverse mechanism was positioned at various downstream distances and the flow field was surveyed. Contours of constant averaged rolling moment such as shown in figure 13 were produced. The location of single or multiple vortexes within the survey area were easily recognizable, particularly when using the smaller probe model. Other test capabilities used in the study of vortexes in the V/STOL tunnel include the three–component hot–wire anemometers and visual–ization techniques employing smoke and neutrally buoyant hydrogen soap bubbles.

## 40– BY 80–FT SUBSONIC WIND TUNNEL

The 40– by 80–ft subsonic wind tunnel is a closed–circuit wind tunnel used primarily for determining the low–speed aerodynamic characteristics of aircraft and spacecraft. The oval–shaped test section measures 12.19 m high by 24.38 m wide and is 24.38 m long. Airflow is produced by six variable–speed 12.19-m diameter fans, each powered by a 4.474 MW electric motor. Speed is continuously variable from 0 to 100 m/s (200 knots) at atmospheric pres–sure.

A photograph of the experimental setup for the vortex studies is shown in figure 4. The generator model is located at the forward end of the test section and the following model at the exit. The generator model is centrally located in the inlet and is attached by a single strut through a strain–gage balance to measure lift. The angle of attack of the generator is set remotely through an actuator and indicator. Downstream of the generator model 24.4 m a follower model is mounted on a single strut that can be remotely positioned vertically over a 3.05 m range and laterally over a 4.27 m range. The follower model is attached to its strut through a strain–gage balance to measure rolling moment. Full–scale range for the balance is such that adequate sensitivity would be provided for the rolling moment encountered on each model.

Figure 15 shows a typical record of rolling-moment variation with time. The source of the unsteadiness of the rolling-moment signals is the meander of the vortexes in the wind tunnel due to wind-tunnel turbulence. Earlier studies in the tunnel (ref. 5) have shown that single vortexes can move about as much as 1 m at this downstream location. The peak rolling-moment values shown on figure 15 are interpreted as corresponding to the times when the following model is alined with a vortex center. During the 38 s of data shown, the peak rolling moment was repeated three times.

The generator model was tested in both the upright and inverted positions to evaluate strut interference effects. It was found that for the conventional configurations, where the vortexes are shed primarily from the wingtip region, no strut interference could be found. However, for the configurations with the span-loading shifted inboard, in which vortexes are shed inboard of the wingtip, an inverted mounting of the generator model was required to avoid interference caused by the wake of the model mounting strut. Figure 14 shows the generator model in this inverted position.

Other test equipment used in the 40- by 80-ft tunnel for vortex study includes a hot-wire anemometer mounted on a rotating arm to survey the vortex flow field. The equipment and technique are described in reference 5.

## COMPARISON OF TEST DATA

Figure 16 presents curves of lift coefficient versus angle of attack for the four generating aircraft models in their respective facilities. In each case, the generating model was in the normal landing-flap configuration and the tail incidence was set at $0^o$. The curves indicate good agreement between facilities throughout the angle-of-attack range. A majority of the tests were conducted at a lift coefficient of 1.2 to approximate landing approach conditions and comparisons of data between facilities.

Figure 17 shows values of the induced rolling moment measured by the probe models with the generating aircraft in the normal landing flap configuration at a lift coefficient of 1.2. The data from the large probe model, figure 17(a), show a relatively consistent trend of rolling-moment coefficient with downstream distance if one neglects the data points taken in the diffuser section of the V/STOL tunnel. The data for the small probe model show a wider variation, with the V/STOL tunnel data well below that for the other facilities. The lower values of the rolling-moment coefficient may result from the data processing technique used in the V/STOL tunnel and its effect on the small model measurements.

The comparison of baseline data between facilities is intended to aid the reader in viewing results from other papers of this conference. The criterion for success of an alleviation concept was based on the ability of the concept to reduce the imposed rolling-moment coefficient at a downstream range of about 2 km (1 n. mi.) to a level that can be countered by the airplane's control system. For the small transport aircraft, the control induced rolling-moment coefficient capability is approximately 0.08; for the business jet, the value is about 0.05. If these values are applied in the Hydronautics facility, which had the highest test Reynolds number, the target alleviation at 1.9 km (1 n. mi.) represents a 32-percent reduction in rolling-moment coefficient for the large probe model and a 60-percent reduction for the small probe model. These reductions were considered in judging the effectiveness of concept in lieu of absolute values.

SUMMARY REMARKS

To determine the feasibility of alleviating the formation and decay of aircraft trailing vortexes through aerodynamic means, NASA used the test capabilities of two wind tunnels and two towing basins. The wind tunnels included the 40- by 80-ft subsonic wind tunnel at Ames Research Center and the V/STOL tunnel at Langley Research Center. An inactive towing basin at Langley (renamed the Vortex Research Facility) was converted to a high-speed (31 m/s)

139

towing basin using air as the test medium; and a contractor's water towing facility was used, the Hydronautics Ship Model Basin, in Laurel, Md. With common models and measurement techniques employed, each facility was capable of creating a scale model vortex system and measuring the imposed rolling moment on a probe model at various downstream distances. Comparison of the lift data for the baseline generating model (landing configuration) showed good agreement between facilities.

The imposed rolling moments on the probe models from the baseline model showed relatively good agreement between facilities for the large probe model. Agreement for the small probe model was not as good. Therefore, to evaluate vortex alleviation concepts, it was necessary to consider a percentage reduction in rolling-moment coefficient for each model at each facility in lieu of an absolute target level.

## REFERENCES

1.  Ciffone, D. L.; and Orloff, K. L.: Far-Field Wake-Vortex Characteristics of Wings. J. Aircraft, vol. 12, no. 5, May 1975.

2.  Patterson, J. C., Jr.; and Jordan, F. L., Jr.: A Static-Air Flow Visualization Method to Obtain a Time History of the Lift-Induced Vortex and Circulation. NASA TM X-72769, 1975.

3.  Herriot, John G.: Blockage Corrections for Three-Dimensional-Flow Closed-Throat Wind Tunnels, With Consideration of the Effect of Compressibility. NACA Rept. 995, 1950. (Supersedes NACA RM A7B28.)

4.  Gillis, Clarence L.; Polhamus, Edward C.; and Gray, Joseph L., Jr.: Charts for Determining Jet-Boundary corrections for Complete Models in 7- by 10-Foot Closed Rectangular Wind Tunnels. NACA WR L-123, 1945. (Formerly NACA ARR L5G31.)

5.   Corsiglia, V. R.; Schwind, R. K.;  and Chigier, N. A.:  Rapid-Scanning, Three-Dimensional Hot-wire Anemometer Surveys of Wing-Tip Vortices. J. Aircraft, vol. 10, no. 12, Dec. 1973, pp. 752-757.
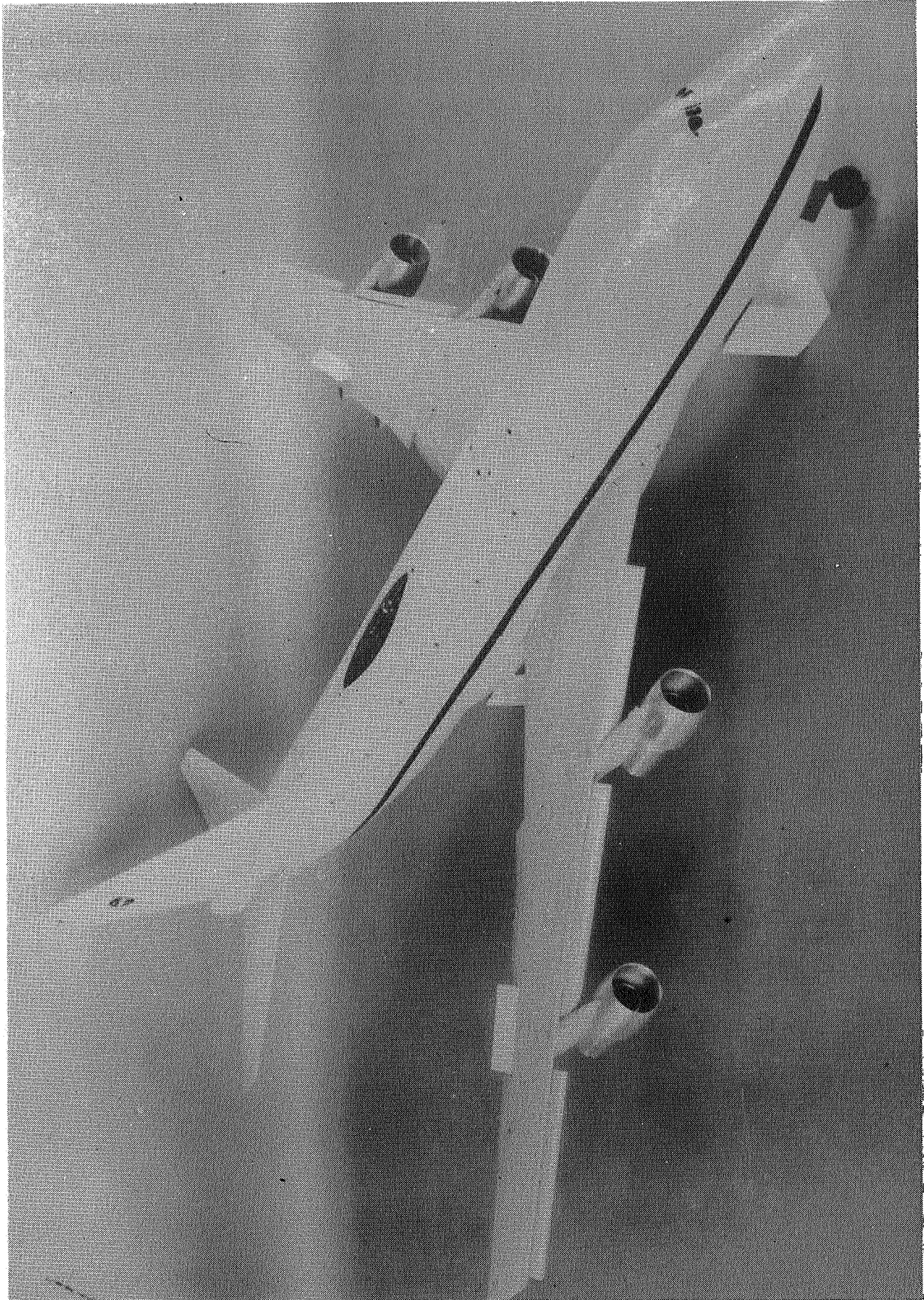
Figure 1.--Photograph of vortex generating model 1

142

Wing

| | |
|---|---|
| Span, m | 1.79 |
| Mean aerodynamic chord, m | 0.25 |
| Root chord, m | 0.497 |
| Tip chord, m | 0.121 |
| Sweepback at quarter chord, deg | 37.5 |
| Area, $m^2$ | 0.460 |
| Aspect ratio | 6.96 |

Fuselage

| | |
|---|---|
| Length, m | 2.06 |

Horizontal tail

| | |
|---|---|
| Span, m | 0.664 |
| Area, $m^2$ | 0.123 |
| Aspect ratio | 3.6 |
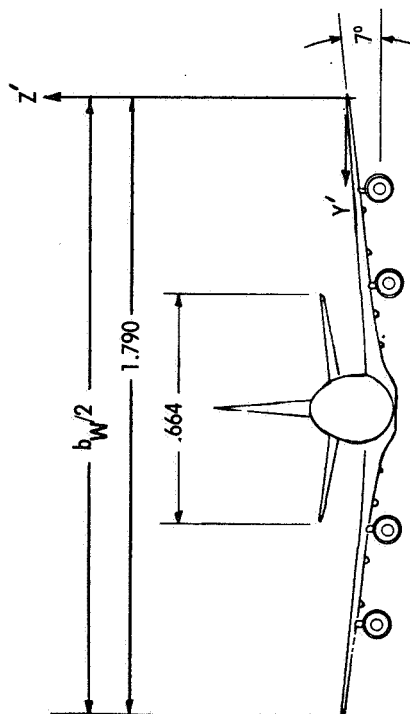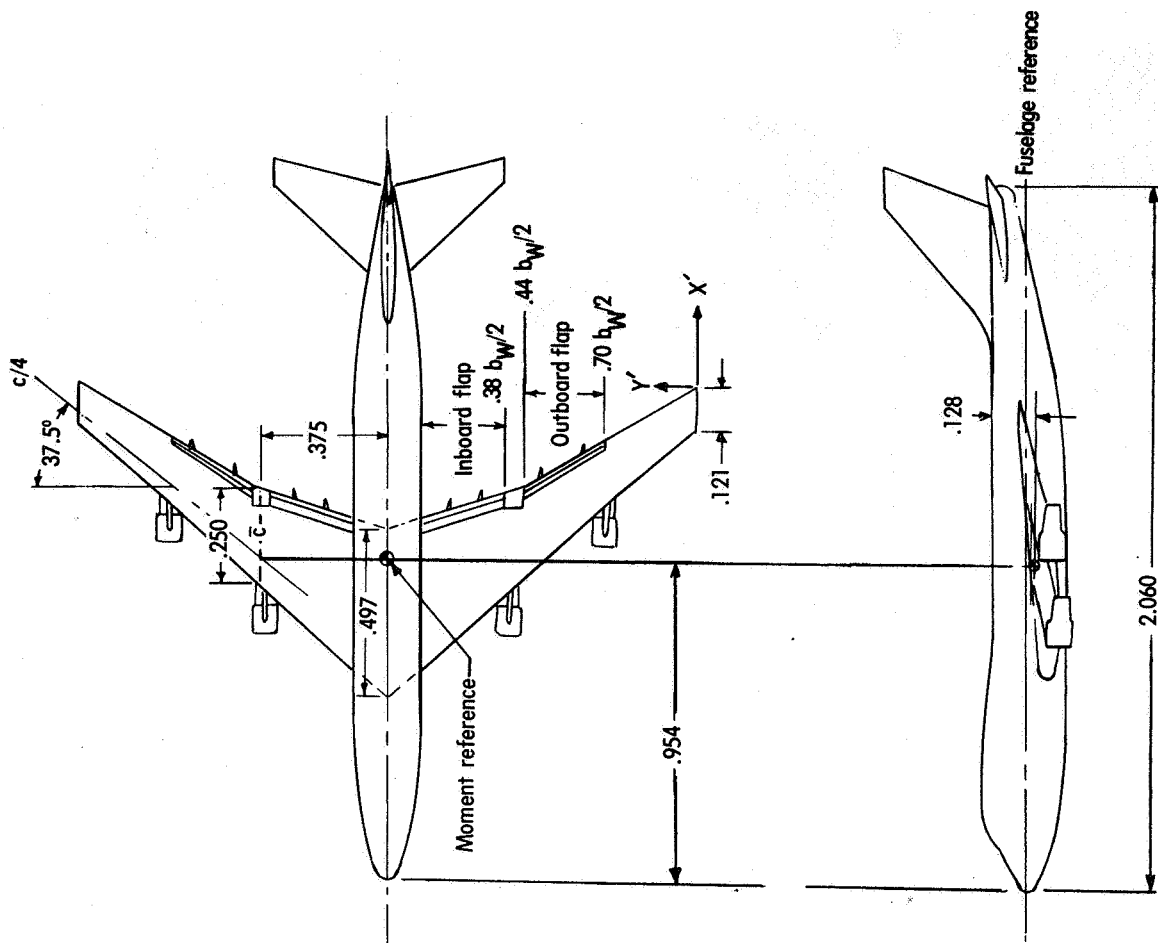
Figure 2.—Sketch and geometric characteristics of vortex generating model.

143
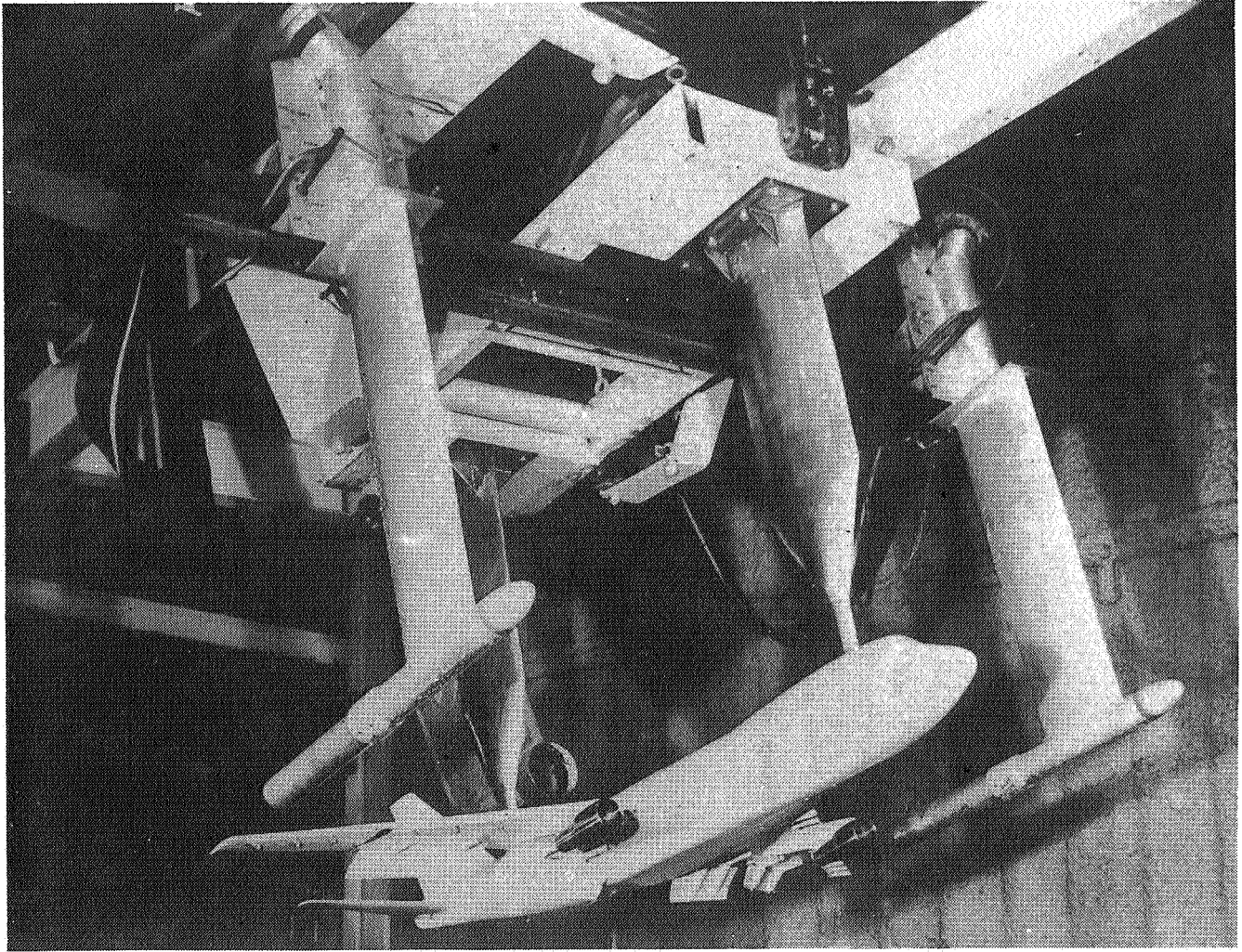
Figure 3.--Thrust simulation apparatus used in Hydronautics Ship Model Basin.

| Area, m² | 0.0199 |
| Span, m | .326 |
| Chord, m | .061 |
| Aspect Ratio | 5.45 |

(a)

| Area, m² | 0.0845 |
| Span, m | .853 |
| Chord, m | .099 |
| Aspect Ratio | 8.70 |

(b)
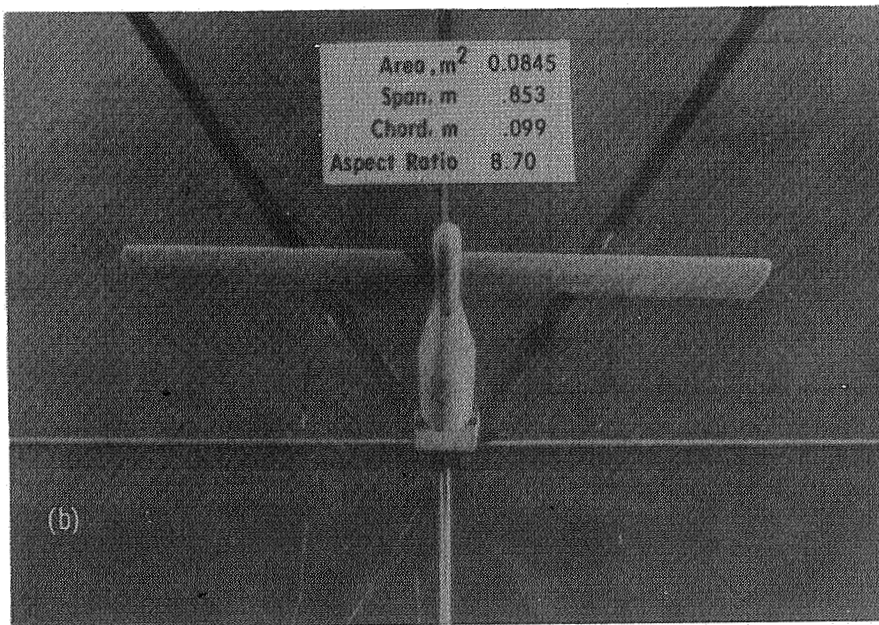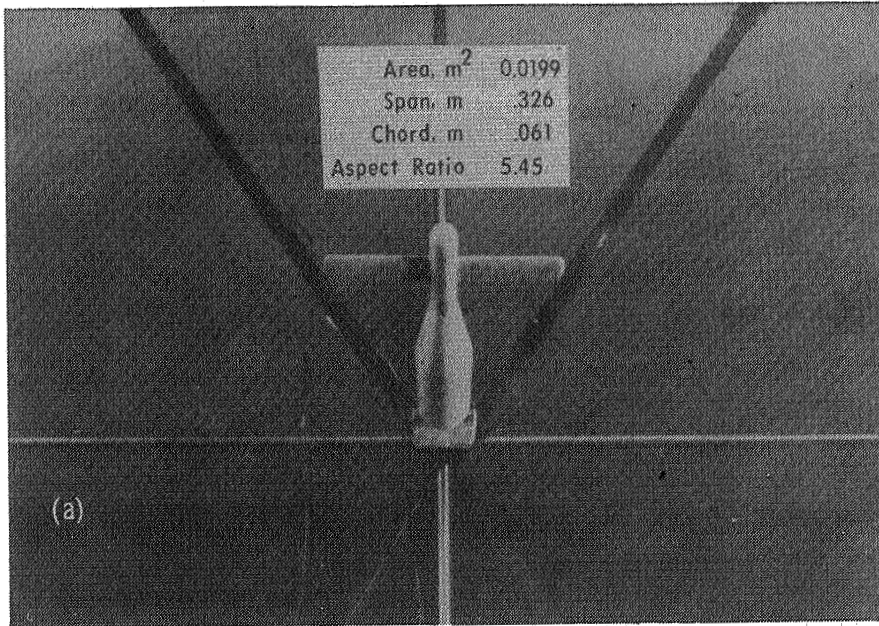
Figure 4.--Photograph of trailing **models.** (a) Small. (b) Large.

**40 BY 80 FOOT WIND TUNNEL**

FOLLOWING MODEL

GENERATING MODEL

MODEL 1

MODEL 2

24.4

.79

INSTRUMENT TOWER

DIMENSIONS IN METERS

**V/STOL TUNNEL**

Tunnel diffuser section

Tunnel test section

7.5 span lengths

15.0    20.0

Model mounted in forward bay

**VORTEX FLOW FACILITY**

5.2M

Generating Model

4.6M

50M

Prob Mode

**HYDRONAUTICS SHIP MODEL BASIN**

76.2 cm

Water surface

Generating model

Following model

Trailing vortex made visible by dye
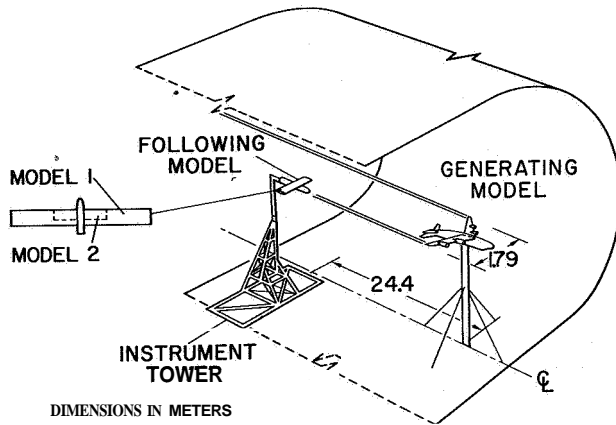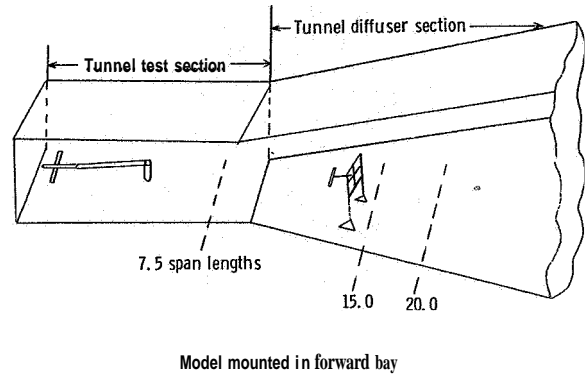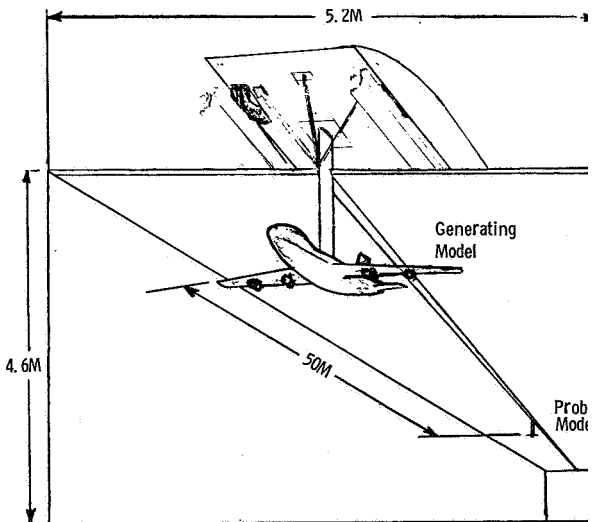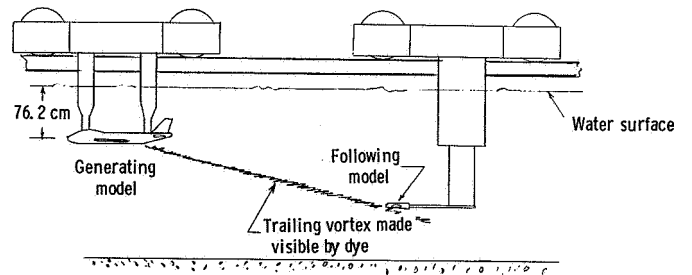
Figure 5.--Test arrangement in evaluation facilities.
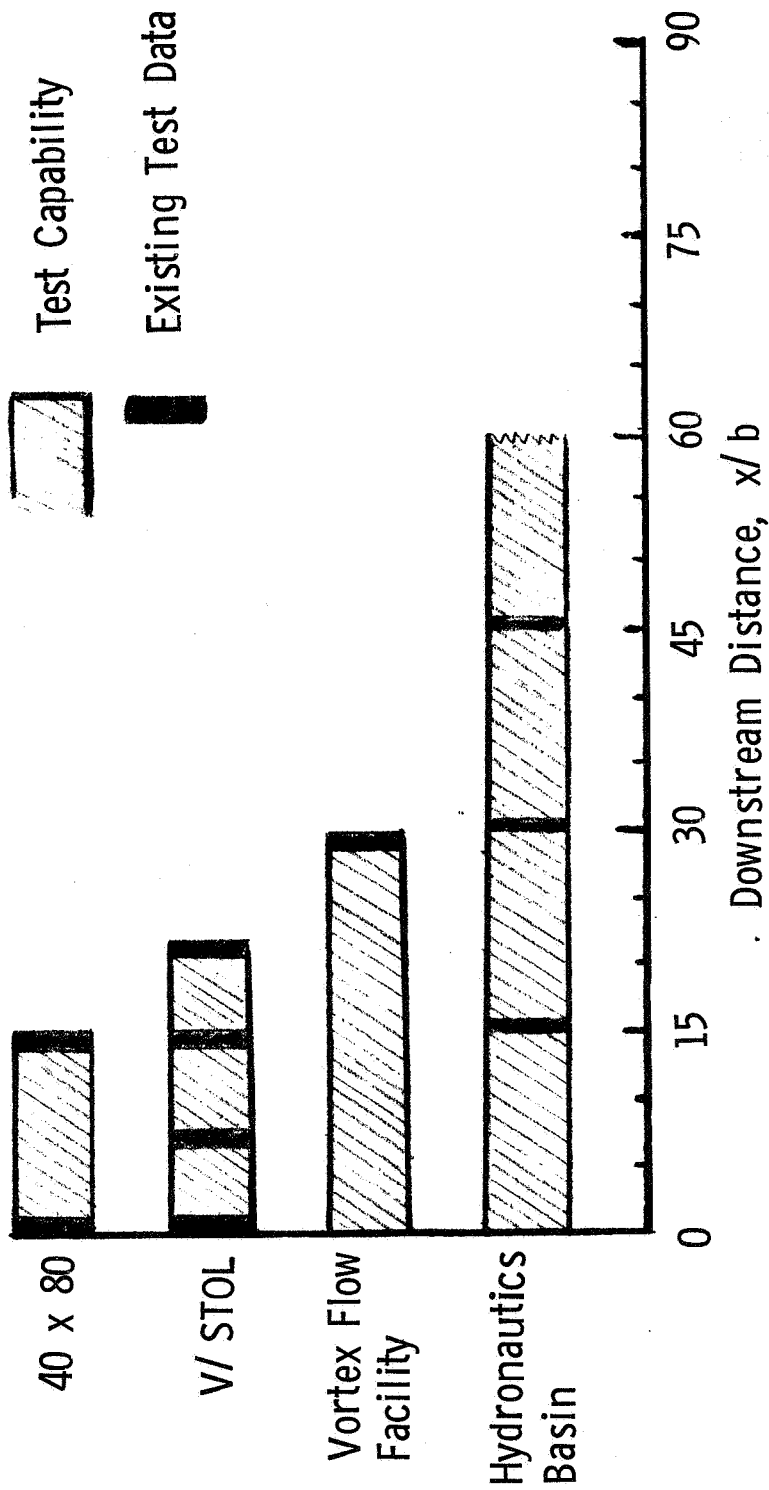
Figure 6 --Range of downstream test capabilities in evaluation facilities.
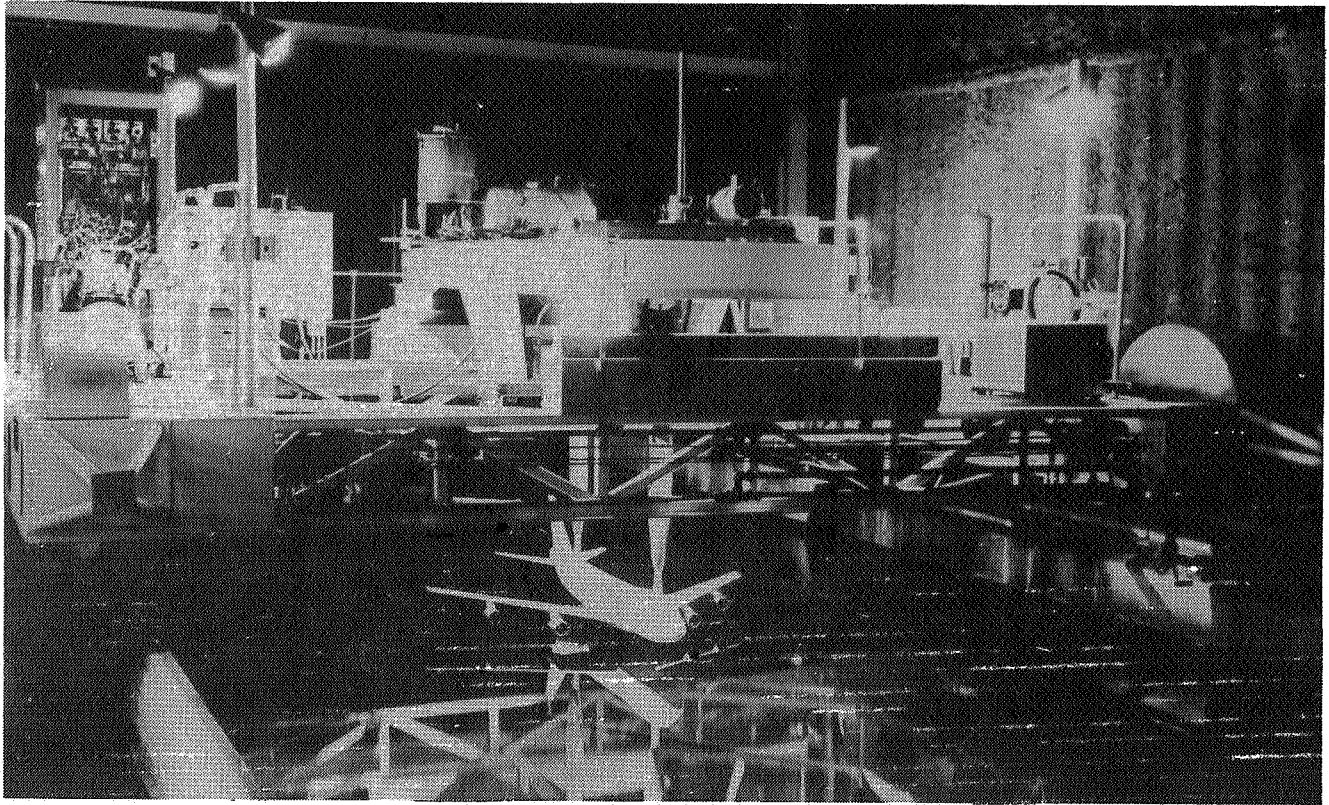
Figure 7.--Generating model carriage system--Hydronautics facility.
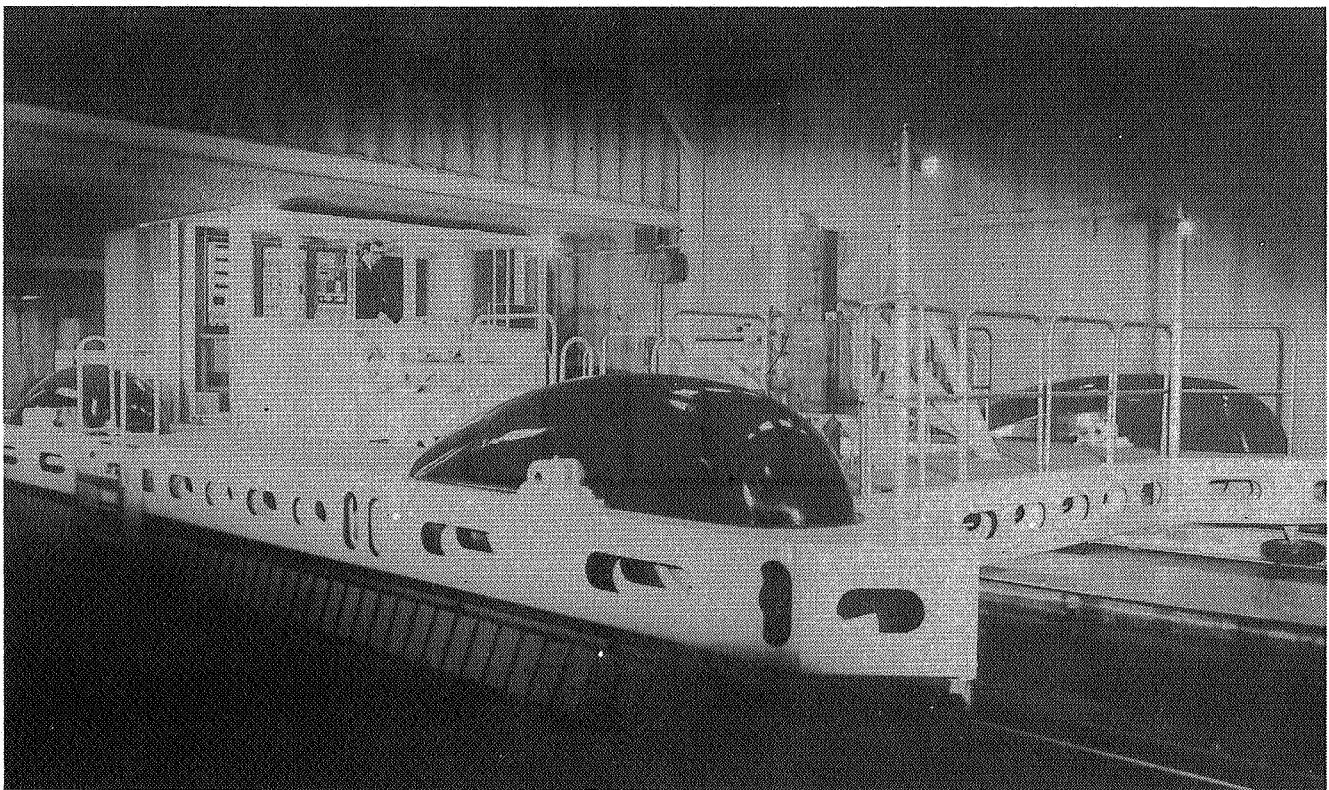


Figure 8.--Probe model carriage system--Hydronautics facility.

# Large probe model
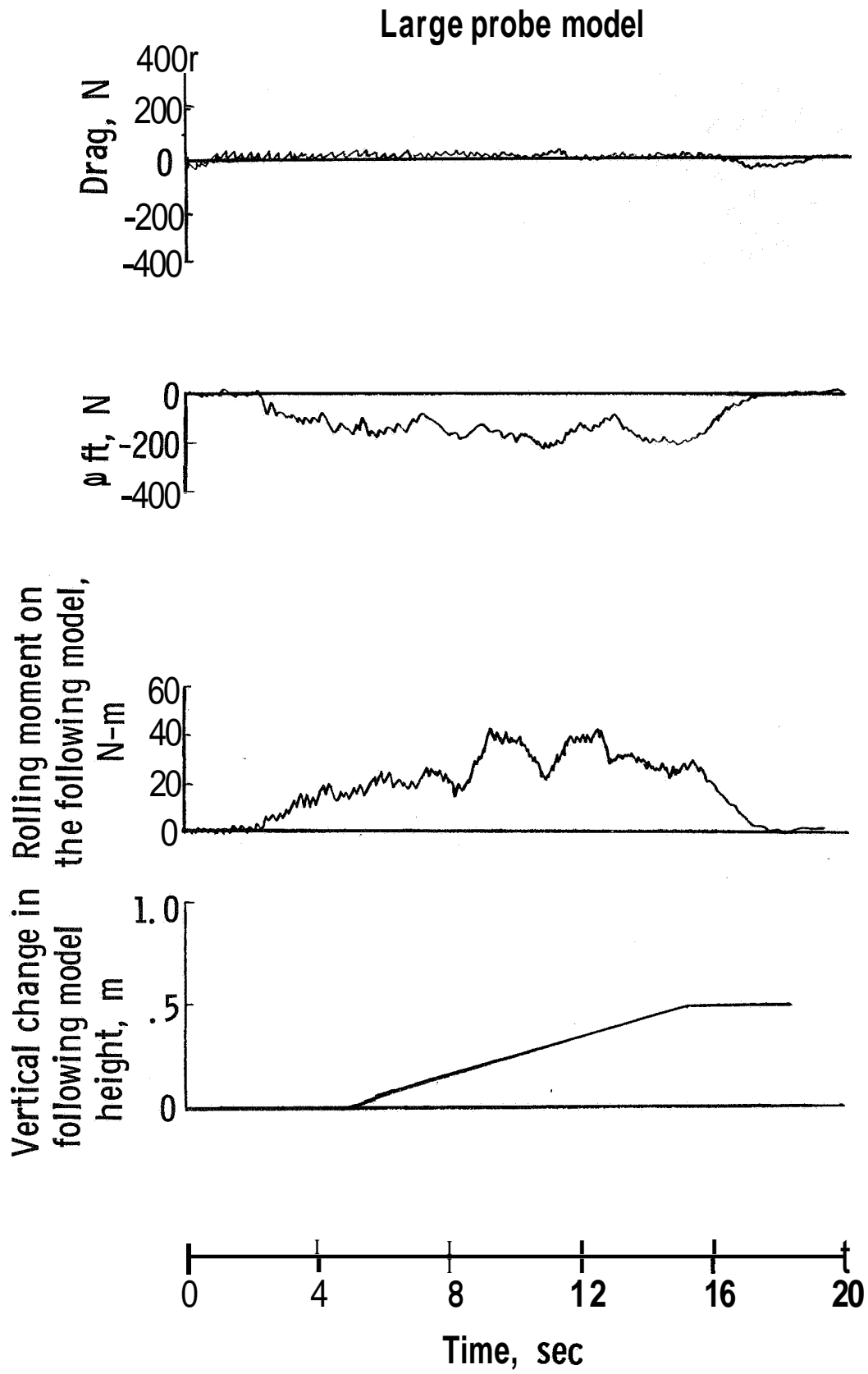


Figure 9.--Sample time history of vortex penetration--Hydronautics facility.
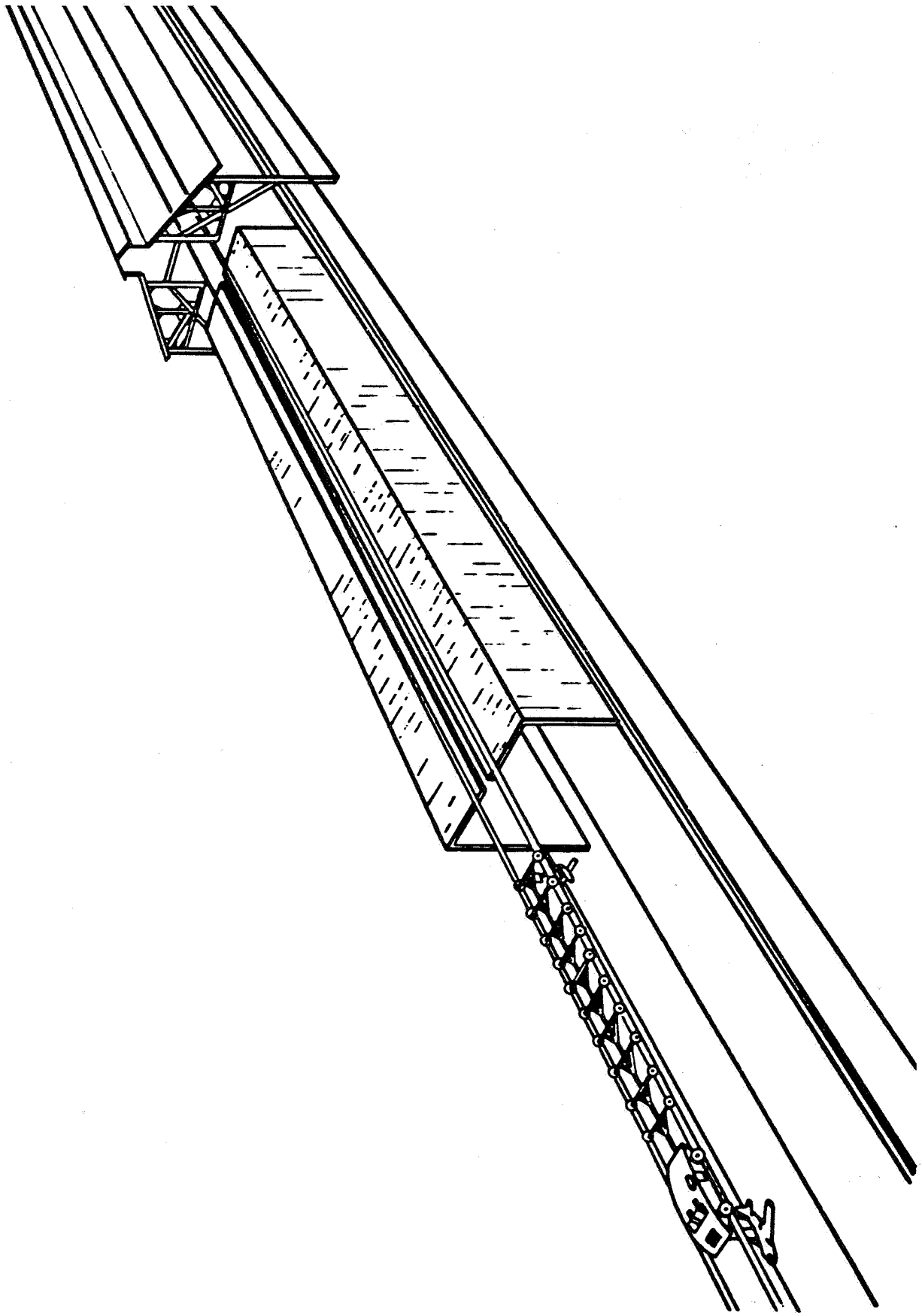
Figure 10.--Sketch showing the Langley Vortex Research Facility.
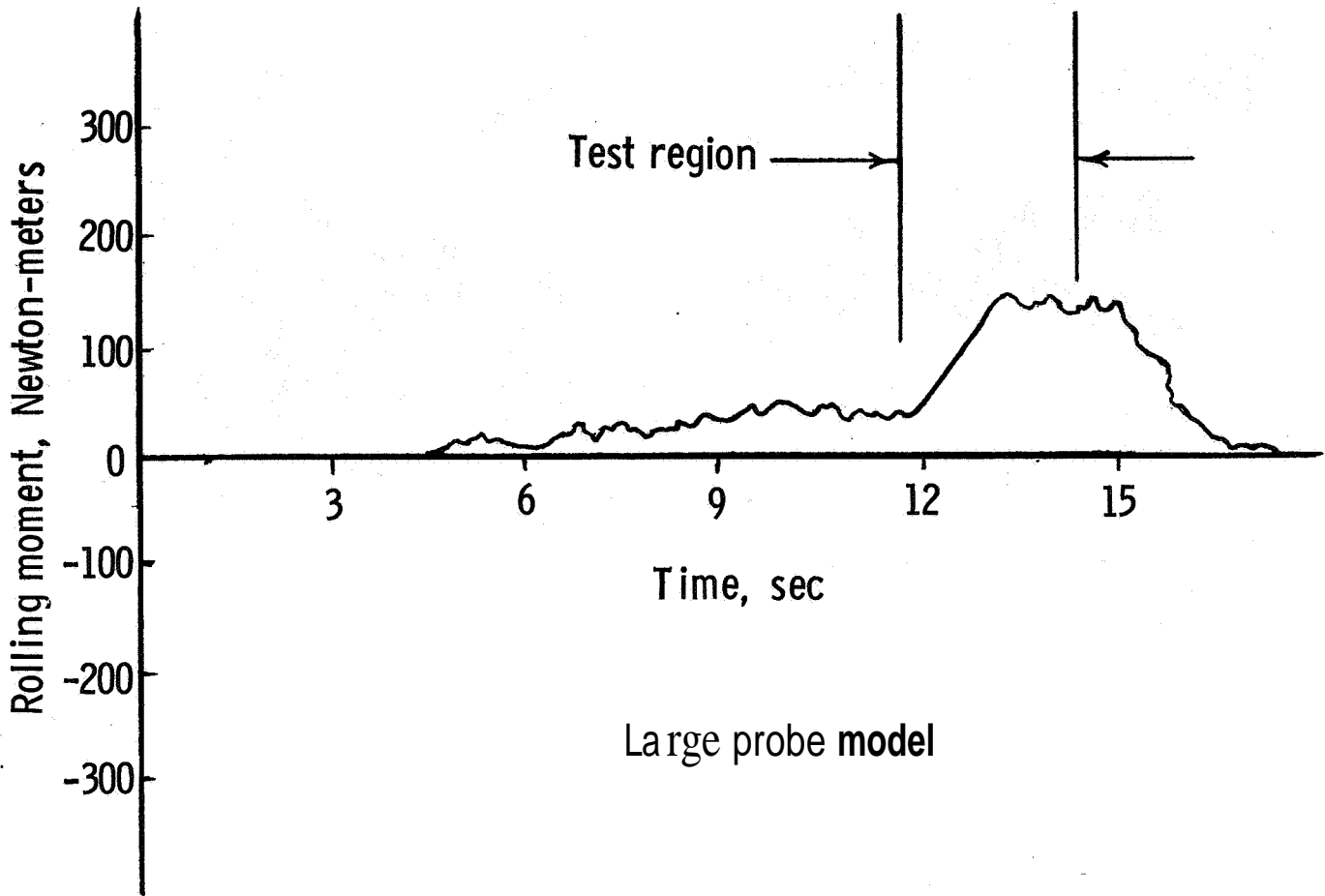
Figure 11.--Sample time history of vortex penetration--Vortex Research Facility.
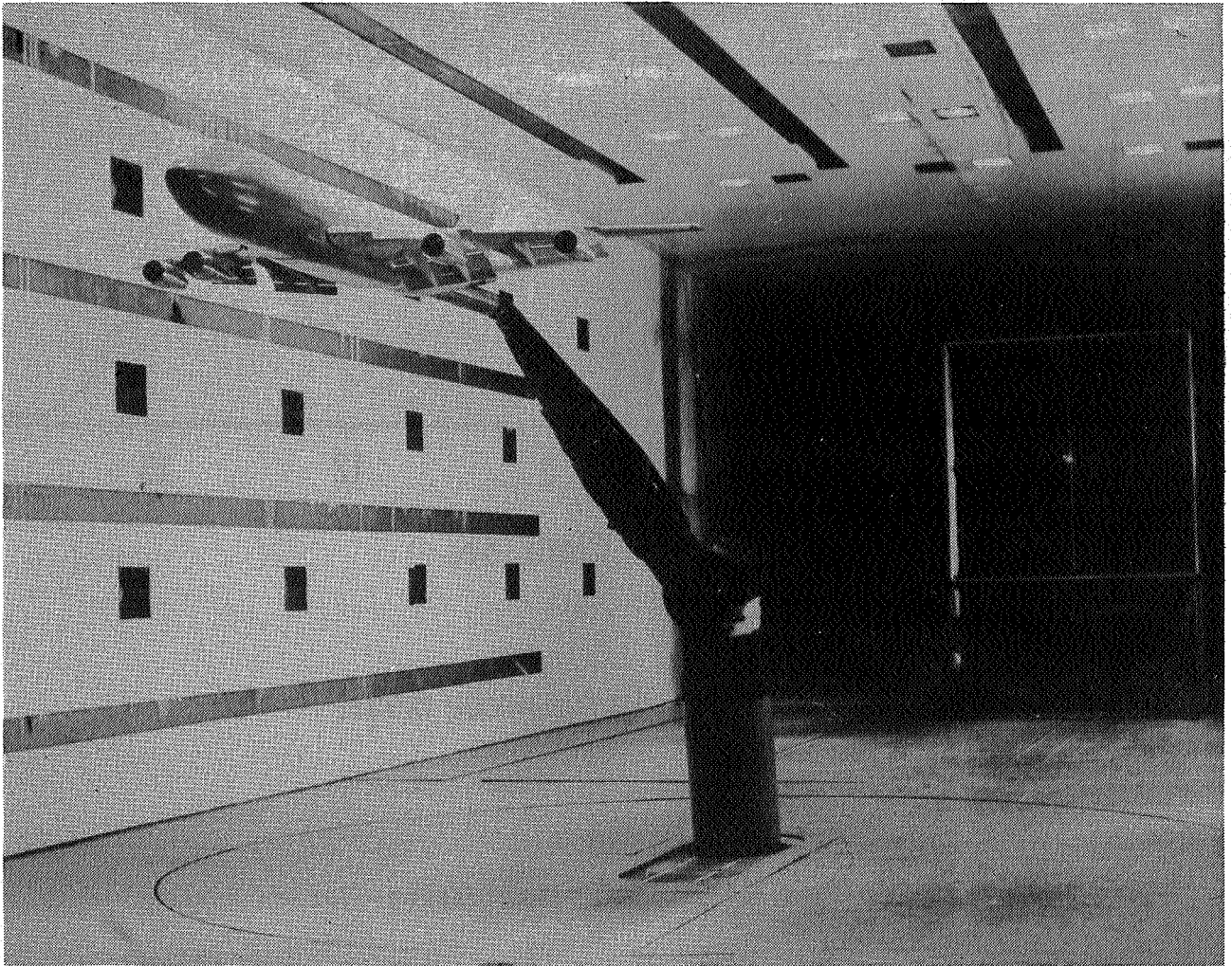
Figure 12.--Photograph of test apparatus in V/STOL tunnel.
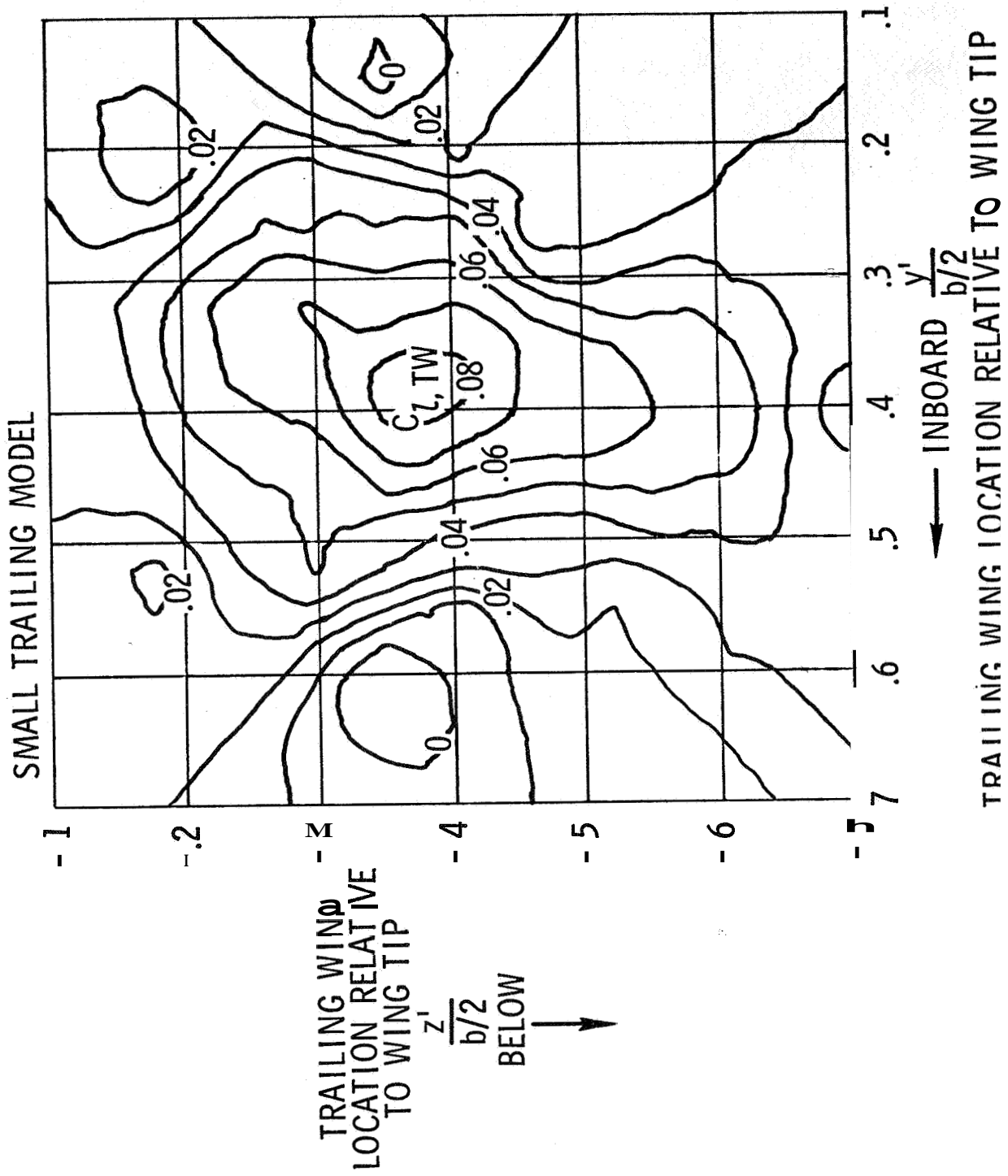
Figure 13.—Data sample showing rolling-moment contours—V/STOL tunnel.
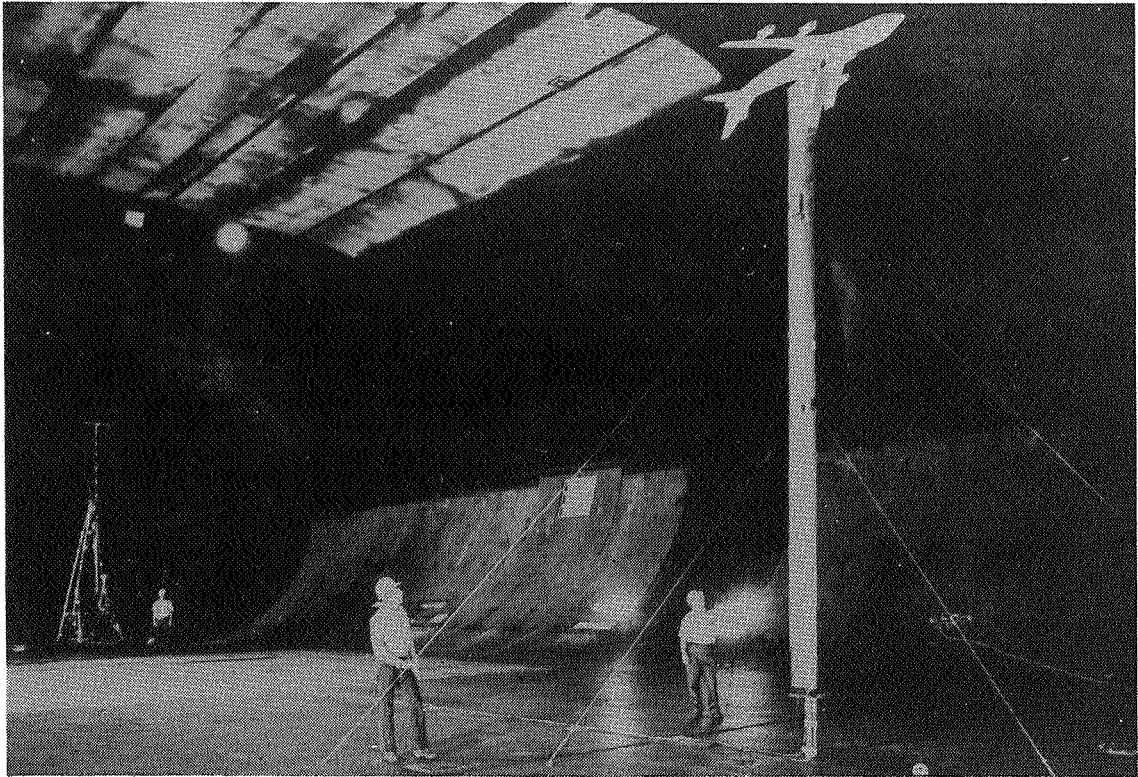
Figure 14.--Photograph of test setup in the 40- by 80-ft wind tunnel.
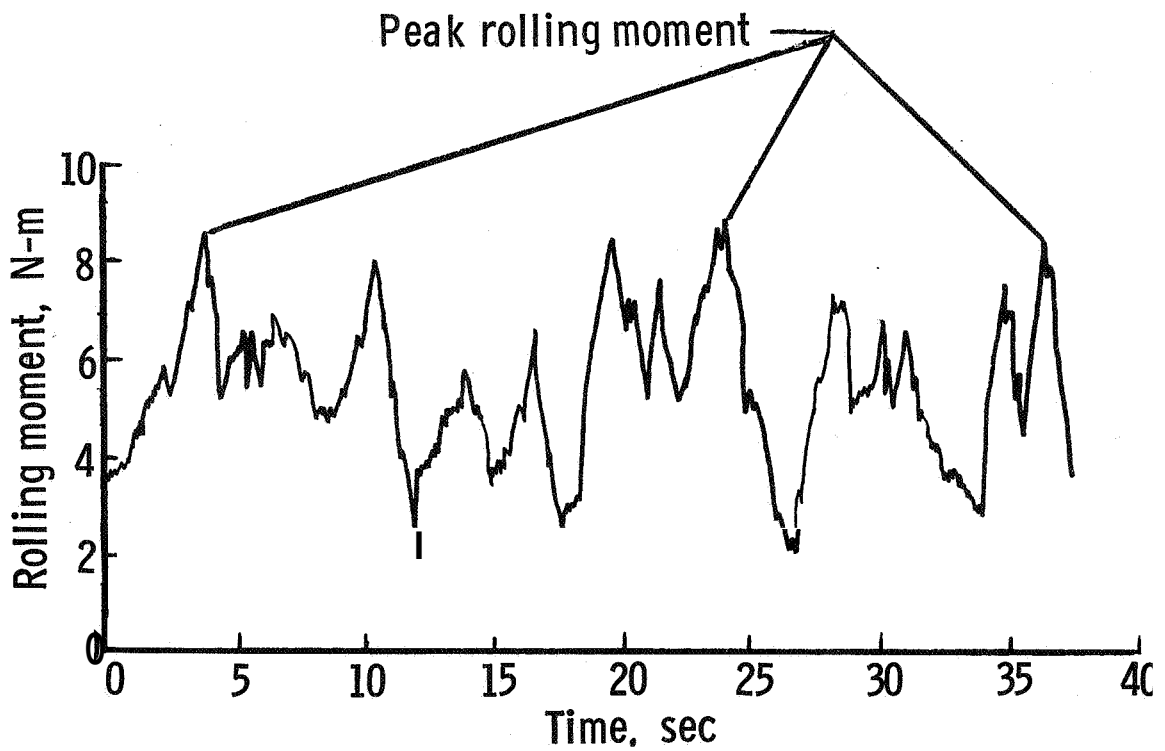


Figure 15.--Sample of rolling moment variation with time in the 40-by 80-ft tunnel.
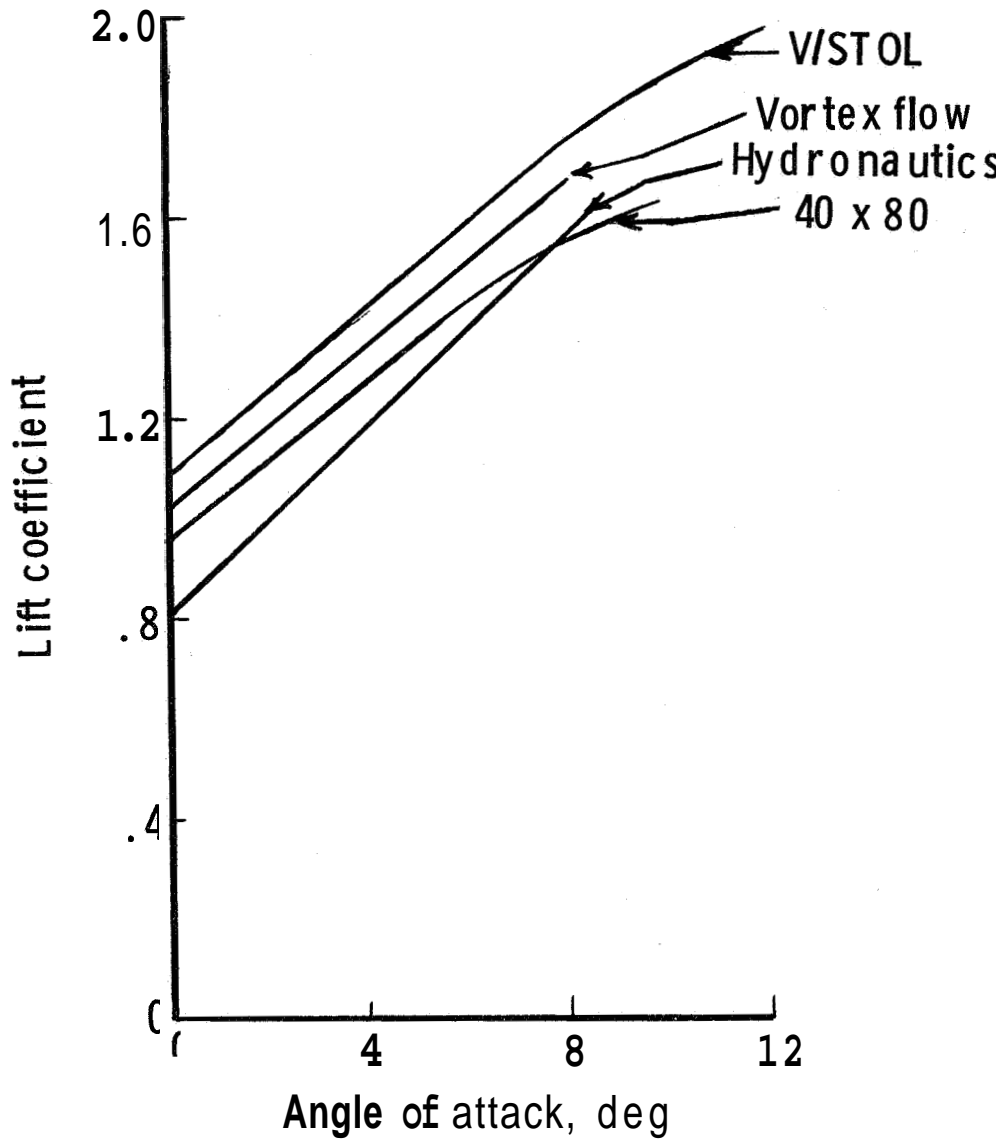
Figure 16.--Comparison of generating-model lift coefficient data from the evaluation facilities.



(a)  Span lengths behind generator aircraft

(b)  Span lengths behind generator aircraft
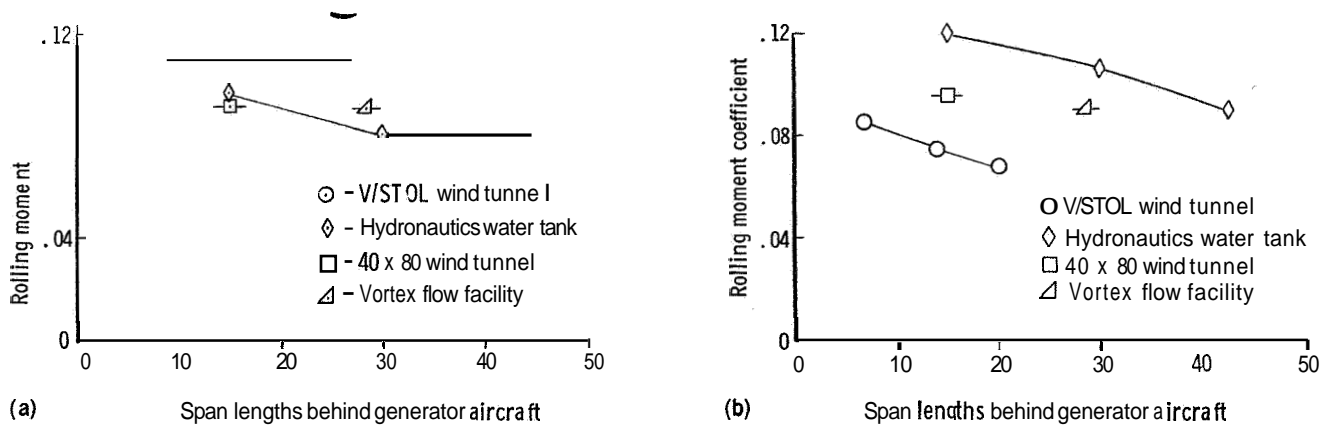
Figure 17.--Comparison of induced rolling-moment coefficients from the ·evaluation facilities.  (a) Large probe model.  (b)  Small probe model.

155

# APPLICATION OF LASER VELOCIMETRY TO AIRCRAFT WAKE-VORTEX MEASUREMENTS

Donald L. Ciffone and Kenneth L. Orloff

Ames Research Center

## SUMMARY

The theory and use of a laser velocimeter that makes simultaneous measurements of vertical and longitudinal velocities while rapidly scanning a flow field laterally are described, and its direct application to trailing wake-vortex research is discussed.  Pertinent measurements of aircraft wake-vortex velocity distributions obtained in a wind tunnel and water towing tank are presented.  The utility of the velocimeter to quantitatively assess differences in wake velocity distributions due to wake dissipating devices and span loading changes on the wake-generating model is also demonstrated.

## INTRODUCTION

**An** accurate, quantitative definition of the flow field associated with lift-generated wake vortices behind aircraft is essential if the fluid dynamics of these wakes are to be completely understood.  The recent, increasing number of both ground-based and flight experimental investigations of wake-vortex characteristics include flow visualization studies (refs. 1-8), measurements of induced rolling moments on following aircraft (refs. 5 and 9-12), and wake velocity measurements (refs. 13-28).  Flow visualization allows the investigator to view the structure of the wake, but leaves him to deduce the quantitative results of the fluid dynamic phenomena observed.  Following-aircraft rolling moment measurements allow the investigator to compare wake alleviation concepts, but once again the basic fluid-dynamic phenomena are "explained" deductively.  Only a direct measurement of the wake-velocity distributions provides a quantitative understanding of the flow field.  These measurements have been attempted using pressure probes (refs. 15 and 16), hot-wire anemometry (refs. 13, 14, 17, 18, and 27), and, more recently, with laser velocimetry (refs. 19-26 and 28).  The velocities obtained from a fixed hot wire or

157

pressure probe are subject to doubt because the probe may interfere with the structure of the vortex. It is questionable whether any mechanical probe can be placed near a small trailing vortex without significantly disturbing the flow. In addition, the meandering motion of vortices in test facilities complicates measurements using stationary probes (refs. 13-17). This vortex motion results in time averaging of velocity measured by a stationary probe, and a consequent loss of measurable detailed structure. The use of a high-speed rotating hot wire (ref. 18) represents one attempt to circumvent this vortex meander problem. Flight measurements have been performed using hot-wire anemometry in which an instrumented probe aircraft follows a generator aircraft to measure wake velocities. These measurements, however, are difficult to interpret and expensive to implement. The laser velocimetry measurement technique does not disturb the flow and has high spatial resolution. In addition, the processed signal from a laser velocimeter is linearly related to the velocity sensed and requires no calibration. The result is a quantitative definition cf the flow field which is easy to interpret. These properties of the laser velocimeter make it ideal for studying the fluid dynamics of aircraft trailing wakes.

A laser velocimeter developed at Ames Research Center, which makes simultaneous measurements of vertical and longitudinal velocities while rapidly scanning a flow field laterally, is discussed here. This instrument was developed specifically for wake-vortex measurements. The basic principles of laser velocimetry are reviewed briefly, and some of the more significant results from the application of this instrument to the measurement of aircraft wake-vortex characteristics is presented.

## NOMENCLATURE

AR      wing aspect ratio

b       wingspan, m

c       wing reference chord, m

$C_L$     lift coefficient

r       vortex radius, m

$U_\infty$      free-stream velocity, m/sec

$V_x$        streamwise velocity, m/sec

$V_\theta$        rotational velocity, m/sec

$V_{\theta_{max}}$        maximum rotational velocity, m/sec

$V_{\theta_p}$        maximum rotational velocity in plateau region, m/sec

$X$        downstream distance from trailing edge of wing, m

$\alpha$        angle of attack, deg

$\mu$        index of refraction

$\Gamma_o$        centerline circulation, $m^2$/sec

Subscripts

B        end of plateau region

P        plateau region


## LASER VELOCIMETRY TECHNIQUES

Not long after the introduction of the gas laser in the early 1960's,
scientists discovered a way to use the laser to measure the velocity of small
micron-sized particles entrained within a gas or liquid.  These particles are
assumed to move along the streamlines of the flow.  If the drag forces acting
on the particles dominate their inertia forces, then a measurement of their
velocity represents an accurate measurement of the fluid velocity at the loca-
tion of the particle.  This technique has become known as "laser velocimetry,"
and instruments designed to accomplish this measurement are called "laser
velocimeters."  The "dual-scatter" or "fringe" mode laser velocimeter has
gained widespread acceptance as a result of the ease with which it can be
optically aligned and the relatively high signal/noise ratios realized in the
measurement of the velocity of particles.  In this type of velocimeter, the
output beam of a laser is passed through a prism dividing it into two parallel,
coherent, beams of equal light intensity, which are then focused through a
convex lens to intersect at a point in the flow field where the velocity is to
be measured.  The velocimeter signal is generated from within the ellipsoidal

**159**

volume created by this intersection of the two light beams. This so-called probe volume varies in size from less than 50 microns in diameter in a small optical system to greater than 1 m for a velocimeter designed for atmospheric research. Because of the angle of intersection of the light beams, a pattern of evenly spaced, alternately light and dark interference fringes is formed within the probe volume. These fringes define a set of planes, each normal to the plane defined by the two crossed beams and parallel to the axis of the system (fig. 1). The spacing between the fringes, δ, is given by (ref. 29)

$$\delta = \frac{\lambda_o}{2\mu \sin (\theta/2)}$$ (1)

where $\lambda_o$ is the vacuum wavelength of the laser light, $\mu$ is the index of refraction of the fluid in which the beams intersect, and $\theta$ is the included angle between the laser beams. When a particle entrained within the moving fluid traverses the interference pattern, it alternately scatters laser light from the bright fringes at a measurable frequency, **f,** where

$$f = \frac{V \cos y}{\delta}$$ (2)

and $y$ is the angle at which a particle with velocity $V$ crosses the fringe pattern. Hence measured frequency is proportional to the component of flow velocity normal to the fringe planes and to the sine of the angle of intersection of the laser beams. The sign of the velocity remains undetermined.

Two-Dimensional, Scanning Laser Velocimeter

Figure 2 is a schematic diagram of a laser velocimeter developed by and currently being used at Ames Research Center. This instrument employs the crossed-beam concept described above, but uses the two brightest colors emitted at wavelengths of *4880* and *5145* Å from an argon-ion laser to simultaneously measure two components of the flow velocity. The two distinct colors from the laser makes the most efficient use of available laser power, especially where signal levels are expected to be low. The argon-ion laser was selected not only because it is a source having a multiple line emission spectrum, but also because it provides more response at the photodetector since the photocathodes of the detectors are generally more sensitive in the regions of the spectrum where argon emits radiation than in the longer wavelength region of the spectrum of He Ne lasers. The instrument shown in figure 2 is a crossbeam,

on–axis, backscatter laser velocimeter, where scattered laser light is collected by the same optical system that is used to focus the incident beams. This backscattering mode was selected over a forward–scattering instrument because difficulties in optical alignment are overcome, and not all test facilities have viewing stations on opposite sides of the test section. The two beamsplitters (BS) provide the scanning lens (LN) with two sets of parallel light beams (at *4880* and 5145 Å) orthogonal to each other.

A unique feature of this laser velocimeter is that the probe volume can be rapidly traversed (or scanned) along the optical axis of the system across the flow field while continuously acquiring velocity profiles. The scanning is accomplished by use of a simple "zoom–type" lens combination (LN and LP, see fig. 2). A small change in the position of the lens (LN) moves the probe volume over a much larger distance. The scanning arrangement is essentially a Galilean telescope operating in reverse. As shown in figure 3, the relationship for "scanning sensitivity," $dD/dS$, to focal length $f_{LP}$, and scan range, D, can be derived (ref. 30) from simple lens theory:

$$\frac{dD}{dS} = -\left(\frac{D - f_{LP}}{f_{LP}}\right)^2 \tag{3}$$

Figure 4 graphically illustrates the dependence of scanning sensitivity on scan range and focal length. Sensitivities near **30** have been found to be desirable when operating at scan ranges near 2 m. With this sensitivity, a change in lens spacing of 1 cm translates the probe volume 30 cm. The location of the probe volume is obtained from the output of a linear potentiometer that monitors the position of the scanning lens. The limits of the spatial scan are set to encompass the region of interest, and traverses are made continuously at speeds up to 1.6 m/sec with automatic reversal at preset limits. Since the system operates in the "confocal" mode (same optics used for both transmission and reception), the maximum scan rate is limited only by mechanical constraints and the method of signal processing.

The achromatic lens system permits the probe volume from the two colors to be coincident. Backscattered light that contains frequency data for both velocity components is collected by the lens system and is returned parallel to the outgoing laser beams. Mirrors (D and M in fig. 2) then separate the

light into the original colors and they, in turn, are focused onto photomultiplier tubes (PM) for processing.

## Signal Processing

The choice of signal processing electronics is based on the flow field to be measured and the expected characteristics of the velocimeter signals (ref. 31). Most of the initial laser studies of vortex wakes at Ames have used spectrum analyzers as the primary signal-processing electronics. These instruments are variable bandwidth filters with selectable sweep rates. The energy content of the signal within the bandwidth is displayed on a cathode ray tube as the filter sweeps through a selected frequency range. Two identical HP 8552/8553 spectrum analyzers operating at processing rates of 15 to 20 sweeps/sec monitored the two components of velocity. From the displayed power spectrum of the frequency (velocity) content of the velocimeter signal, the frequency at which the maximum signal occurs is taken as the average velocity of the flow. For greatest velocity sensitivity, it is desirable to have the range of expected signal frequencies span the acceptance band of the processing electronics. For example, at low velocities, it might be advantageous to increase the signal frequency by increasing the included crossbeam angle (eq. (2)). However, since the f number, $f_{LP/B}$, of the focusing lens, LP, decreases by increasing the included angle,

$$\frac{f_{LP}}{B} = \left[ 2 \left( \sqrt{- \frac{dD}{dS}} + 1 \right) \tan \frac{\theta}{2} \right]^{-1} \tag{4}$$

(under the constraint of low velocity) when larger included angles must be used, the focusing lens must have a low f number. This is illustrated in figure 5, where it is shown that, for a modest beam convergence angle of 6°, a representative scanning sensitivity of 30, and an incident laser light of 5000 Å, the resulting fringe spacing is 5 μ and the required focusing lens f number is 1.5. Spherical aberrations of lenses with low f numbers make optical scanning difficult and must be considered in the overall design and application of the optical system (ref. 30).

Figure 6 is a typical oscillograph trace from a single sweep of the spectrum analyzer during a scan through a vortex. The figure demonstrates how

162

the frequency information is extracted from the graphical record. The data are recorded on magnetic tape for later review. Typical simultaneously measured velocity distributions through a vortex are presented in figure 7. The streamwise profile provides information related to the drag of the generating model; the rotational distribution provides a measure of the strength of the wake and therefore some indication of the hazard it would present to an encountering aircraft. Several scans were made through the vortex from which mean curves were drawn through the data. Only when the scanning probe volume passes directly through the vortex core are data recorded. For these "core penetrations," the vertical velocity component is the same as the vortex rotational velocity and the longitudinal velocity component is the vortex streamwise velocity.

Spectrum analysis techniques cannot be interpreted without a great deal of difficulty when flows are unsteady or processed when a high level of turbulence is present. As a result, the signal-processing technique described above has recently been replaced by a Raytheon Model 15/55G two-channel frequency tracker to survey the multivortex wake behind a 1.83-m (6-ft) span wind-tunnel model of a Boeing 747 with flaps and landing gear (ref. 31). With the frequency tracker technique, whenever a signal is present above a preset threshold and within the bandwidth of the tracker (100 kHz), the tracker locks on and tracks the signal automatically in less than 3 msec. If the signal should "drop out," a variable time delay "hold" mode (adjustable between 0.1 and 100 msec) keeps the loop locked. After this time, if the signal does not reappear, an automatic "sweep" mode searches for the signal over the entire instrument range (0–15 MHz) in approximately 5 msec. This automatic sweep and lock-on feature of the tracker is important during optical traverses of multiple vortex wakes where there is a continual loss and reappearance of signal as the probe volume scans the wake. When a signal reappears, the signal/noise level can be quite different, and the frequency will often be a considerable distance from the "held" value. The tracker is then required to unlock, search, lock on, and track this new signal. The difference in velocity between the regions far from vortex centers and those near the vortices can produce signal frequencies that vary over a wide range, typically from about 0.5 to 5.0 MHz, in a short period of time. The frequency tracker is able to

track adequately under these conditions since it uses only a single broad frequency range that extends from approximately 0.05 to 15 MHz, with a slew rate capability in excess of 20 MHz/sec.

The data are stored in the core memory of a high-speed data acquisition system (ref. **31**) (transient capture device TCD) and can be handled in an on-line fashion, including plotting of fully reduced data or transferring to magnetic tape for storage and playback. Figure 8 shows a TCD record of a scan through the vortices from the inboard edge of the inboard flaps of the Boeing *747* model.

Directional sensitivity is accomplished by rotating the laser system 40° about the optical axis, thus biasing both channels of the velocimeter with a component of the free-stream velocity. The spatially compressed appearance of the wake structure on the right-hand side of the centerline results from the nonlinear scanning speed of the focal point for a constant motion of the scanning lens. Figure 9 shows the final processed (reduced and plotted) data corresponding to figure 8. The data are still being used to obtain relative strengths of the vortices in the wake, -turbulence intensity profiles, and to supply initial conditions for theoretical models that will predict the far-field wake characteristics.

Vortex Marking Techniques

Particulate scattering material is introduced into the test media to enhance the signal. For wind-tunnel experiments, smoke is introduced into the diffuser section of the wind tunnel by means of a mineral oil vapor generator. Recirculating the air provides a low-density concentration of the oil vapor throughout the wind tunnel *so* that velocity data can be gathered at any position in the test section. For water towing-tank studies, polystyrene copolymer latex solution is added to the water to provide scattering. The size distribution of these particles is between 2 and 15 μ. For wind-tunnel experiments, the size of the mineral oil particles is under investigation, but available literature (ref. **32)** suggests an upper limit of about 7 microns. For the flow measurements reported here, in which the mean values of the velocity (rather than turbulent fluctuations) are of interest, these particles can be expected

to accurately represent the fluid velocity. Since the particle sizes are not small compared to the wavelength of the incident laser light, their scattering properties are characterized by Mie scattering theory (ref. 33), which states that particle scattering cross section is a complex function of diameter, index of refraction, and the details of the measuring velocimeter (ref. 32). This, however, has not proven to be a liability when measuring the velocity in aircraft trailing wakes with the laser system described.

In wind-tunnel experiments, the centers of wake vortices are often visible because the core is seen as a dark region that lacks white smoke. As a result, reflections from the laser beams are significantly dimmer at the very center of the vortex because of the scarcity of light-scattering material. This makes it possible to observe visually when a traverse passes through the center of the vortex, and the event is marked on a separate recording channel of the magnetic tape. These "core penetration" events are transferred onto the oscillograph record from which the data are reduced. A small amount of core motion is acceptable when the probe volume of the velocimeter is well outside the vortex core region and the velocity gradients are low. However, acceptable traverses are limited to core penetrations in which no vortex movement is evident.

In the water tow-tank experiments, the vortex centerlines were marked by generating a thin sheet of air bubbles across the tank 1.5 m upstream (toward the starting end) of the test section location of the laser. The streamwise velocity defect in the vortex core region then acted in such a way as to drag some of these bubbles toward the passing airfoil; the radial pressure gradient associated with the rotational flow centered the bubbles in single file, producing a fine string of bubbles along the vortex centerline. As the vortex pair moved vertically in the tank, the laser system was also moved manually to keep the optical axis aligned with the vortex centerline. When the vortices could not be readily marked and visually located, the region of interest in the wake was mapped out by making continuous lateral traverses through the wake at different elevations.

A new technique of vortex marking in the water-tow tank (developed specifically for flow visualization studies, refs. 6 and 8) involves injecting

165

fluorescent dyes directly into the vortices from the wake-generating model and illuminating them with a system of lights (fig. 10). A separate, high-speed scan — short focal length — laser system with a high scan sensitivity is being developed for use with this flow visualization system to quantitatively assess the flow fields of multiple vortex wakes.

## VORTEX-VELOCITY MEASUREMENTS

The scanning, two-color, dual-beam, backscatter; argon-ion laser velocimeter described previously has been used to measure the vertical and streamwise velocity components in wakes containing vortices. The measurements have been made both in a wind tunnel (refs. 12-21, 24, and 31) and a water-towing facility (refs. 22, 23, 25, and 26). The need for a rapid scanning instrument differed for the two facilities. For the wind tunnel, the trailing vortices are fully established but may wander in a random manner. The center of the vortex does not remain stationary within the test section because large-scale eddies are convected through the wind tunnel. Hence the vortex must be traversed during a time which is short compared to the movement of the vortex. As discussed previously, the optical scanning is performed in a direction normal to the tunnel centerline. This is shown schematically in figure 11 for a semispan model and photographically in figure 12 for a 1.83-m (6-ft) span model of the Boeing 747. The model was mounted in an inverted position to minimize the interference of the support strut with the wake.

For the towing tank, rapid scanning at a given measurement station is required because of the time-dependent nature of the trailing vortices as the wing model is towed through the tank. The flow field does not have perturbations of the vortex velocity about a mean steady-state velocity, but rather a decaying shear flow. In this case, a meaningful time history of the vortex requires that the time for an optical traversal be short compared with vortex decay time, *so* that a mean "age" can be assigned to each measured profile. As the vortex pair moves in the tank due to its mutual influence, it is necessary that the velocimeter moves vertically while scanning to keep the optical axis alined with the vortex centerline. Spanwise continuous traversals of the

166

probe volume through the near-side wake are made with the automatic scan reversal set to encompass the area of interest (figs. 13 and 14).

## Wind-Tunnel Test Results

The first application of the laser velocimeter to measure the streamwise and rotational velocity distributions in vortices was to a square-tipped, 0.457-m chord, 1.218-m semispan wing mounted in the Ames 7- by 10-Foot Wind Tunnel (ref. 20). The airfoil section was an NACA 0015 and the planform was rectangular with no twist. Detailed velocity profiles were obtained at a scanning rate of 15 cm/sec (fig. 7) and were found to be in general agreement with data (ref. 18) obtained with a hot-wire probe mounted on the end of a rapidly rotating boom. This velocity information provides for a comparative evaluation of vortex alleviation schemes, as was demonstrated for a dissipator panel mounted on the rectangular wing. A square panel (4 percent of the semispan, 11 percent of the wing chord) was installed at the wing tip at the 1/4-chord position. A comparison of the measured velocity distributions showed a reduction in maximum rotational velocity and the development of a large streamwise velocity defect due to the panel.

The reduction in maximum rotational velocity, $V_{\theta_{max}}$, as a function of downstream distance is summarized in figure 15, together with the results obtained from the rapidly moving hot-wire data (ref. 18) of a geometrically similar configuration in the Ames 40- by 80-Foot Wind Tunnel at 55 chord lengths downstream. ($V_{\theta_{max}}$ was assumed to be the averagt maximum of the two peaks of the rotational velocity distribution (fig. 7).) From these results, it appears that the mechanism that alleviates the vortex develops with increasing downstream distance.

The need for experimental velocity distributions in the wakes of wings more representative of present-day transport aircraft was the rationale for the second series of wind-tunnel tests (ref. 21). Velocity profiles were obtained in the wake of a Convair-990 semispan wing (fig. 11). The effects of configuration buildup (including flaps, flow-through nacelles, and antishock bodies) and wingspan loading changes due to flap deflection and angle of attack were investigated. The effect of wingspan loading on the wake was

**167**

evident when a factor of 2 reduction in $V_{\theta max}$ was obtained at a constant lift coefficient by deploying the flaps and reducing the angle of attack.

## Water Tow–Tank Test Results

The wind–tunnel data on vortex streamwise and rotational velocity profiles are limited by the physical lengths of the wind–tunnel test sections.   What was lacking were measured velocity profiles that described the wake structure from several span lengths to hundreds of span lengths.   An integration of the measured rotational velocities across the wingspan of encountering aircraft would then yield an evaluation of the magnitude of the rolling moment induced by a vortex at more realistic downstream locations.   Therefore, tests were performed in the University of California's water tow–tank facility at Richmond, California.   In this method of testing, the model is towed under-water (figs. 13 and 14), generating a continuous wake that decays with time at each longitudinal point of the test gallery (fig. 10).   The test time ends when the vortex structure is altered by interference from boundaries of the water or the passage through the test section-of internal vortex waves, which arise from starting or stopping the model at the ends of the towing range.

*Effect of wing planform on wake* - The first sequence of tests (ref. 22) was designed to investigate the effects of wing planform on wake characteris- tics and to compare the results with near–field wake data obtained in wind tunnels with similar airfoils.   The three planforms tested are described in table I.   Typical data obtained which illustrate the effects of wing planform on vortex rotational velocity profiles are presented in figures 16 and 17, at 20 and 100 span lengths, respectively.

The diamond wing planform resulted in a lower concentration of vorticity in the core and diminished circumferential velocities in the adjacent regions. Both features are desirable in alleviating the wake hazard potential.   At 100 span lengths downstream, the velocity profiles were found to be quite similar, indicating that the effect of wing planform is no longer discernible.

The maximum rotational velocities (obtained by averaging the two peak values of velocity) identified two characteristic flow regions for their dependence on downstream distance (figs. 18 and 19).   The first, a "plateau"

region, with little change in maximum rotational velocity, extended from wake rollup to downstream distances as great as 100 span lengths, depending on span loading. This plateau is followed by a decay region in which the maximum rotational velocity decreases with downstream distance at a rate nominally proportional to the inverse half-power. This plateau did not come as a complete surprise since its existence is suggested in the turbulent shear-flow calculations of Donaldson (ref. *34)*. There was concern as to whether the initiation of the velocity decay was a real flow phenomenon or a consequence of starting and stopping waves. This possibility was explored experimentally and analytically and is discussed at length in reference 22. It was concluded that the test results were not affected by motion waves. The results indicate that inviscid vortex structure calculations should be applicable to downstream distances as great as *45* spans for rectangular wings at lower lift coefficients. A demonstration of the nearly inviscid nature of the flow field in the plateau region was made by Rossow (ref. 35), who used an inverse Betz technique to predict the span loading from the measured velocity profiles in this region.

Figure 18 presents the effect of span-load change due to angle-of-attack change for the rectangular wing planform. Also shown are results obtained from geometrically similar wings tested in the Ames *40-* by 80-Foot and 7- by 10-Foot Wind Tunnels (refs. 18 and 20). The agreement is seen to be reasonably good. Figure 19 shows span-loading effects due to wing planform at a common angle of attack of 5°. The data have been normalized by dimensionless circulation to eliminate effects due to differences in lift coefficient and aspect ratio of the wings. The vertical bars indicate the end of the plateau region.

A time history of streamwise velocity profiles for the rectangular wing at 8° angle of attack is presented in figure 20. These results characterize the radial diffusion of the streamwise velocity defect in the decay region. A profile obtained in the near field (ref. 20) $(X/b = 0.38)$ has been included to emphasize the initial concentration of streamwise momentum. The diffusion of the streamwise component of velocity can be traced in this way and its maximum value along the axis can be extracted and used in subsequent decay considerations.

Figure 21 shows how the maximum vortex-core streamwise velocity (in the towing direction) for the rectangular wing decreases with downstream distance

and angle of attack. The wind–tunnel data of references 14 and 20 and the water–tank data of references 36 and 37 are shown for comparison. The present data indicate a far–field maximum streamwise velocity decay that is inversely proportional to downstream distance to approximately the 1/4 power. Also shown in the figure are the streamwise velocity defect and rate of decay on the vortex centerline as computed (ref. 23) from the laminar theory of reference 38. The comparison is remarkably good and improves with decreasing angle of attack — believed to be a consequence of the approximation that $V_x \ll U_\infty$ in the analysis.

*Effect of flap deflections on wake* – In a second sequence of tests in the water tank (ref. 25), the swept-wing planform was fitted with seven flap segments on each half span. The flaps were used to achieve additional desired wingspan loadings. Four different span loadings at a lift coefficient of 0.70 were selected for investigation: (1) the wing with no flaps deflected? (2) a typical landing configuration, (3) a configuration tailored to reduce the gradient in the loading at the wingtip, and *(4)* a configuration with flaps deflected alternately ±15° in an attempt to create multiple spanwise spanload gradients (sawtoothing effect in the spanload distribution). These configurations are illustrated in figure 22. The flap schedules and test angles of attack to produce a common lift coefficient of 0.70 for all configurations are listed in table II.

A comparison of the effect of span loading on vortex rotational velocity distributions due to various combinations of flap deflections is presented in figures 23 and 24 at 25 and 95 span lengths downstream. All the data are at a common lift coefficient of 0.70. Much like the diamond wing planform, the tailored configuration yields lower rotational velocities in the core and adjacent regions and has a more diffuse velocity profile. However, once again, at 95 span lengths downstream in the decay region, the rotational velocity profiles are quite similar. At span lengths of 95, the dependence of the velocity profile on wingspan loading has lost most of its significance.

The downstream dependence of maximum rotational velocity for these configurations is summarized in figure 25. Although the limited amount of data precludes a positive identification of a plateau region for these flapped

configurations, the data suggest its presence. The decay region is readily apparent. Although a plateau region could never really be identified for the sawtooth configuration, the wake did eventually roll up (at 30 span lengths) and achieve rotational velocities almost comparable to the clean and landing configurations. At a lift coefficient of 0.7, there is little difference in the downstream characteristics of the maximum rotational velocities in the wake of the clean wing or the landing configuration. The results obtained with the tailored configuration are much like those obtained with the diamond wing planform. The maximum wake tangential velocities are less than half those of the other configurations, and the plateau region extends to 80 span lengths. Once again, this long plateau is instrumental in reducing the initial large differences in maximum rotary velocities to insignificant differences in the far wake.

A comparison of the measured radial distribution of streamwise velocity in the core of the vortices behind these swept-wing configurations at 75 span lengths downstream is presented in figure 26. The results show a streamwise velocity defect toward the model for all configurations.

*Plateau velocity correlation* - A correlation function based on the self-similar turbulent decay of a line vortex has been developed (ref. **39)** and utilized to substantiate the validity of using ground-based scale model data to predict high Reynolds number flight results. It was found that if the downstream dependence of vortex maximum rotational velocity is presented as a vortex velocity scaling parameter, $V_1 b / \Gamma_0 AR$, versus a distance scaling parameter, $(X/b)(\Gamma_0/U_\infty b)(AR)^2 f(\Gamma_0/\nu)$, the scale model and flight data collapse to a single curve. Presented in figure 27 are the results obtained when these scaling parameters are used to plot vortex maximum rotational velocity in the plateau region versus a corresponding downstream duration of this region obtained from the towing tank data presented previously (ref. 26). The line faired through the experimental points has a slope of -1, which implies the following inverse proportionality between the plateau velocity and extent of the plateau region:

$$\left(\frac{V_\theta}{U_\infty}\right)_P \left(\frac{X}{b}\right)_B = \frac{47}{AR \ f(\Gamma_0/\nu)} \tag{5}$$

The Reynolds number parameter, $f(\Gamma_o/\nu)$, was developed in reference **39** and is a function of vortex Reynolds number, $\Gamma_o/\nu = (\Gamma_o/U_\infty b)\,\mathrm{Re}(b)$. For $\Gamma_o/\nu \geq 3 \times 10^5$, $f(\Gamma_o/\nu) = $ **1**. Hence, for all flight conditions, $f(\Gamma_o/\nu) = $ **1**, and for most ground-based tests (including the water-tank tests of refs. 22 and 25), $f(\Gamma_o/\nu)$ is of order **1**.

Use of equation (5) and a −1/2 decay region downstream dependence of vortex maximum rotational velocity allows near-field wake velocity measurements in the plateau region (i.e., wind-tunnel data) to be used to estimate subsequent far-field vortex characteristics. The lines through the data in figures 18, 19, and 25 predict the downstream variation of maximum rotational velocity with this approach. The vertical bars indicate the predicted end of the plateau region. The predictions and measurements are seen to be in good agreement.

## CONCLUDING REMARKS

The theory and use of a laser velocimeter with high-speed spatial scanning capability has been described and its direct application to trailing wake vortex research has been presented. The scanning feature of this instrument minimizes the difficulties in velocity measurement due to what has been termed "vortex meander." Accurate vortex definition is achieved and the data are repeatable and consistent with other experimental results.

Measurements have been made of changes in wake rotational and streamwise velocity components due to span-loading changes of the wake-generating model. The results identified two characteristic flow regions for the dependence of vortex maximum rotational velocity on downstream distance. The first, a region of constant velocity, can extend from wake rollup to 80 span lengths downstream behind the generating wing, depending on span loading and angle of attack. This is followed by a decay region where $V_{\theta_{max}}$ varies approximately as $(X/b)^{-1/2}$. This implies that inviscid vortex structure calculations should be applicable to distances as great as 80 span lengths downstream for certain wing configurations.

It was shown that tailoring the wingspan loading by either planform shape or flap deflection (to reduce wing–tip vorticity by unloading the outboard sections of the wing) is equally effective in reducing the wake rotational velocities by factors of 2, broadening the vortex core, and extending the plateau region to 80 span lengths.

An orderly wake rollup was delayed to 40 span lengths downstream by introducing multiple vortices along the wingspan with alternate up–down flap deflections. These multiple vortices interacted with each other, resulting in large excursions in the wake and linking to form irregular loops. A plateau region was never achieved for this configuration.

A correlation of the water–tank results relates the magnitude of vortex maximum rotational velocity in the plateau region to the downstream extent of this region. With this knowledge, near–field wake velocity measurements in the plateau region (i.e., wind–tunnel results) can be used to estimate the far–field vortex characteristics.

## REFERENCES

1. Garodz, L. J.; Lawrence, D.; and Miller, N.: The Measurement of the Boeing 727 Trailing Vortex System Using the Tower Fly–By Technique, Rept. FAA–RD–74–90, Aug. 1974.

2. Tymczyszyn, J. J.; and Barber, M. R.: A Review of Recent Wake Vortex Flight Tests. 18th Annual Symposium of Society of Experimental Test Pilots, Los Angeles, Calif., Sept. 26, 1974.

3. Barber, M. R.; Kurkowski, L. J.; Garodz, L. J.; Robinson, G. H.; Smith, H. J.; Jacobsen, R. A.; Stinnett, G. W.; McMurtry, T. C.; Tymczyszyn, J. J.; Devereaux, R. L.; and Bolster, A. J.: Flight Test Investigation of the Vortex Wake Characteristics Behind a Boeing 727 During Two–Segment and Normal ILS Approaches, NASA TM X–62,398 and FAA–NA–75–151, Jan. 1975.

4. Huffaker, R. M.; Jeffreys, H. B.; Weaver, E. A.; Bilbro, J. W.; Craig, G. D.; George, R. W.; Gleason, E. H.; Marrero, P. J.; Reinbolt, E. J.; and Shirey, J. E.: Development of a Laser Doppler System for the

Detection, Tracking and Measurement of Aircraft Wake Vortices, Rept. FAA-RD-74-213, March 1975.
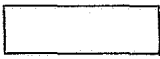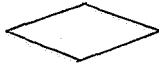
5. Corsiglia, V. R.; Rossow, V. J.; and Ciffone, D. L.:  Experimental Study of the Effect of Span Loading on Aircraft Wakes, NASA TM X-62,431, 1975.

6. Ciffone, D. L.; and Lonzo, C., Jr.:  Flow Visualization of Vortex Interactions in Multiple Vortex Wakes Behind Aircraft, NASA TM X-62,459, 1975.

7. Patterson, J. C., Jr.; and Jordan, F. L., Jr.:  A Static-Air Flow Visualization Method to Obtain a Time History of the Lift-Induced Vortex and Circulation, NASA TM X-72,769, 1975.

8. Ciffone, D. L.:  Vortex Interactions in Multiple Vortex Wakes Behind Aircraft, AIAA Preprint 76-72, Jan. 1976.

9. Croom, D. R.:  Low-Speed Wind-Tunnel Investigation of Various Segments of Flight Speed-Brake Spoilers as Trailing-Vortex Hazard-Alleviation Devices on a Transport Aircraft Model, NASA TN (to be published).

10. Patterson, J. C., Jr.; and Jordan, F. L., Jr.:  An Investigation of the Increase in Vortex Induced Rolling Moment Associated with Landing Gear Wake, NASA TM X-72,786, 1975.

11. Dunham, E. R., Jr.:  Model Tests of Various Vortex Dissipation Techniques in a Water Towing Tank, NASA TN (to be published).

12. Smith, H. J.:  A Flight Test Investigation of the Rolling Moments Induced on a T-37B Airplane in the Wake of a B-747 Airplane, NASA TM X-56,031, 1975.

13. Chigier, N. A.; and Corsiglia, V. R.:  Tip Vortices-Velocity Distributions, NASA TM X-62,087, 1971.

14. Chigier, N. A.; and Corsiglia, V. R.:  Wind-Tunnel Studies of Wing Wake Turbulence, J. Aircraft, vol. 9, no. 12, Dec. 1972, pp. 820-825.

15. Mason, W. H.; and Marchman, J. F., 111:  Farfield Structure of an Aircraft Trailing Vortex, Including Effects of Mass Injection, NASA CR-62,078, 1972.

16. Logan, A. H.: Vortex Velocity Distributions at Large Downstream Distances, J. Aircraft, vol. 8, no. 11, Nov. 1971, p. 930.

17. Corsiglia, V. R.; Jacobsen, R. A.; and Chigier, N. A.: An Experimental Investigation of Trailing Vortices Behind a Wing with a Vortex Dissipator, Aircraft Wake Turbulence and Its Detection, 1st ed., Plenum Press, New York, 1971, pp. 229-242.

18. Corsiglia, V. R.; Schwind, R. G.; and Chigier, N. A.: Rapid Scanning Three-Dimensional Hot Wire Anemometer Surveys of Wing Tip Vortices, J. Aircraft, vol. 10, no. 12, Dec. 1973, p. 762.

19. Grant, G. R.; and Orloff, K. L.: A Two-Color Dual-Beam Backscatter Laser Doppler Velocimeter, Appl. Optics, vol. 12, Dec. 1973, p. 2913.

20. Orloff, K. L.; and Grant, G. R.: The Application of Laser Doppler Velocimetry to Trailing Vortex Definition and Alleviation, NASA TM X-62,243, 1973.

21. Ciffone, D. L.; Orloff, K. L.; and Grant, G. R.: Laser Doppler Velocimeter Investigation of Trailing Vortice Behind a Semispan Swept Wing in a Landing Configuration, NASA TM X-62,294, 1973.

22. Orloff, K. L.; Ciffone, D. L.; and Lorincz, D.: Airfoil Wake Vortex Characteristics in the Far Field, NASA TM X-62,318, 1973.

23. Ciffone, D. L.; and Orloff, K. L.: Axial Flow Measurements in Trailing Vortices, AIAA J., vol. 12, Aug. 1974, pp. 1154-1155.

24. Orloff, K. L.; and Ciffone, D. L.: Vortex Measurements Behind a Swept-Wing Transport Model, J. Aircraft, vol. 11, no. 6, June 1974, pp. 362-364.

25. Ciffone, D. L.; and Orloff, K. L.: Far-Field Wake-Vortex Characteristics of Wings, J. Aircraft, vol. 12, no. 5, May 1975, pp. 464-470.

26. Ciffone, D. L.: Correlation for Estimating Vortex Rotational Velocity Downstream Dependence, J. Aircraft, vol. 11, no. 11, Nov. 1974, pp. 716-717.

27. Jacobsen, R. A.:  Hot Wire Anemometry for In-Flight Measurement of Air-
    craft Wake Vortices, 5th Annual Society of Flight Test Engineers
    Symposium, Anaheim, Calif., Aug. 8-10, 1974.

28. Baker, G. R.; Barker, S. J.; Bofah, K. K.; and Saffman, P. G.:  Laser
    Anemometer Measurements of Trailing Vortices in Water, J. Fluid Mech.,
    vol. 65, pt. 2, 1974, pp. 325-336.

29. Bossel, H. H.; Hiller, W. J.; and Meier, G. E. A.:  Noise-Cancelling
    Signal Difference Method for Optical Velocity Measurements, Rept. 7/71,
    Max-Planck-Institut für Strömungsforschung Göttingen, 1971.

30. Orloff, K. L.; and Biggers, J. C.:  Laser Velocimeter Measurement of
    Developing and Periodic Flows, International Workshop on Laser
    Velocimetry, Purdue Univ., March 1974.

31. Orloff, K. L.; Corsiglia, V. R.; Biggers, J. C.; and Ekstedt, T. W.:  The
    Application of Laser Velocimeter Signal Processing Electronics to Com-
    plex Aerodynamic Flows, LDA-Symposium, Technical University of Denmark,
    Lyngby, Denmark, 1975.

32. Orloff, K. L.; Myer, F. C.; Mikas, M. F.; and Phillips, J. R.:  Limita-
    tions on the Use of Laser Velocimeter Signals for Particle Sizing,
    International Workshop on Laser Velocimetry, Purdue Univ., Oct. 1975.

33. Grant, G. R.; and Donaldson, R. W.:  A Laser Velocity Measurement System
    for High-Temperature Wind Tunnels, NASA TM X-1976, 1970.

34. Donaldson, C. DuP.:  Calculation of Turbulent Shear Flows for Atmospheric
    and Vortex Motions, AIAA J., vol. 10, Jan. 1972, pp. 4-12.

35. Rossow, V. J.:  Prediction of Span Loading from Measured Wake-Vortex
    Structures - An Inverse Betz Method, J. Aircraft, vol. 12, no. 7,
    July 1975, pp. 626-628.

36. Olsen, J. H.:  Results of Trailing Vortex Studies In a Towing Tank, in
    Aircraft Wake Turbulence and Its Detection, edited by J. H. Olsen,
    A. Goldberg, and M. Rogers, Plenum, New York, 1971, p. 455.

37. Lezius, D. K.:  Study of the Far Wake Vortex Field Generated by a Rectan-
    gular Airfoil in a Water Tank, NASA TM X-62,274, 1973.

38. Moore, D. W.; and Saffman, P. G.:  Axial Flow in Laminar Trailing Vortices, Proc. Roy. Soc. (London), Sec. A, vol. **333, 1973,** pp. 491-508.

39. Inverson, J. D.:  Correlation of Turbulent Trailing Vortex Decay Data, J. Aircraft (to be published),

TABLE I.- MODEL GEOMETRY

|  | Rectangular wing | Diamond wing | Swept wing |
|---|---|---|---|
| Planform | | | |
| Span | 61 cm (24 in.) | 61 cm (24 in.) | 61 cm (24 in.) |
| Reference chord | 11.43 cm (4.5 in.) | 11.43 cm (4.5 in.) | 10.41 cm (4.1 in.) |
| Aspect ratio | 5.33 | 5.33 | 5.85 |
| Root chord | 11.43 cm (4.5 in.) | 22.86 cm (9.0 in.) | 18.21 cm (7.17 in.) |
| Leading edge sweep | 0° | 20.6' | 38.6° |
| Taper ratio | 1.0 | 0 | 0.25 |
| Section root | NACA 0015 | NACA 0015 | NACA 0011-64 (modified) |
| Tip | NACA 0015 | NACA 0015 | NACA 0008-64 (modified) |

| Configuration | Semispan flap settings,[a] deg | | $C_L$ | $\alpha$, deg |
|---|---|---|---|---|
| | (Inboard) | (Outboard) | | |
| Clean | 0/ 0/ 0/ | 0/ 0/ 0/ 0 | 0.70 | 6.8 |
| Landing | 20/20/ 20/ | 0/ 0/ 0/ 0 | .70 | 3.4 |
| Tailored | 10/10/ 0/ | -10/-15/-20/-30 | .70 | 7.5 |
| Sawtooth | -15/15/-15/ | 15/-15/ 15/-15 | .70 | 9.2 |

[a]Downward deflections are' positive.
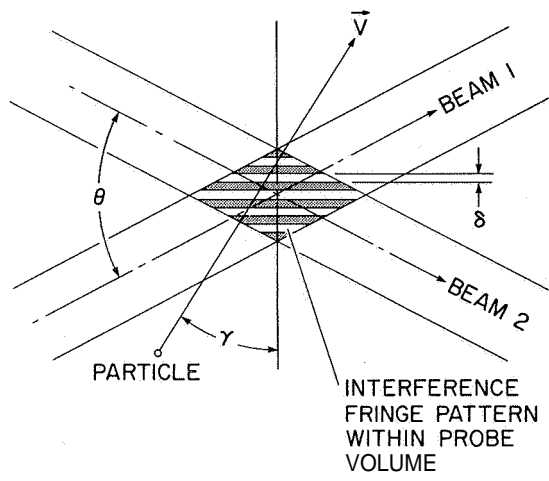
Figure 1.- Geometry of crossbeam system.



AL  ARGON-ION LASER (4 watts)
        EMITTING MULTIPLE COLORS
P   PRISM
M   MIRROR
A   APERTURE TO ELIMINATE ALL
        BUT TWO STRONG COLORS
BS  BEAM SPLITTER
D   DICHROIC MIRROR
LN  NEGATIVE SCANNING LENS
LP  POSITIVE FOCUSING AND
        COLLECTING LENS
L   LENS
PMV(PMH); PHOTOTUBE FOR RECEIVING
            VERTICAL (HORIZONTAL)
            VELOCITY SIGNAL

——— BLUE LASER LIGHT (4880 Å)
---- GREEN LASER LIGHT (5145 Å)
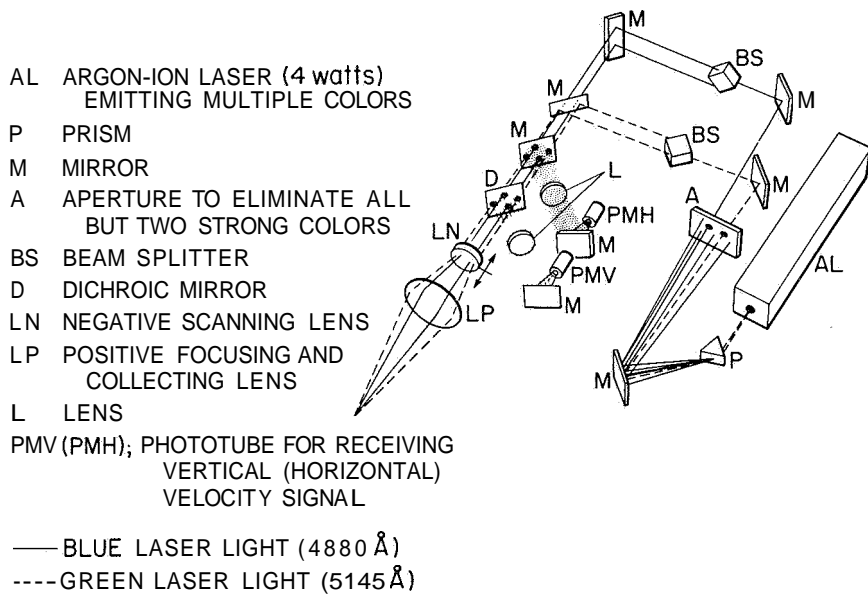
Figure 2.- Schematic representation of the Ames two-dimensional, backscatter,

scanning, laser velocimeter (ref. 20).
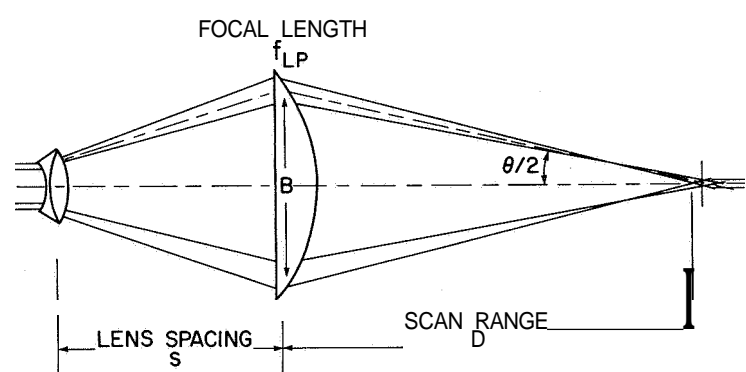


Figure 3.- Scanning lens system used for both transmission and reception

(ref. 30).
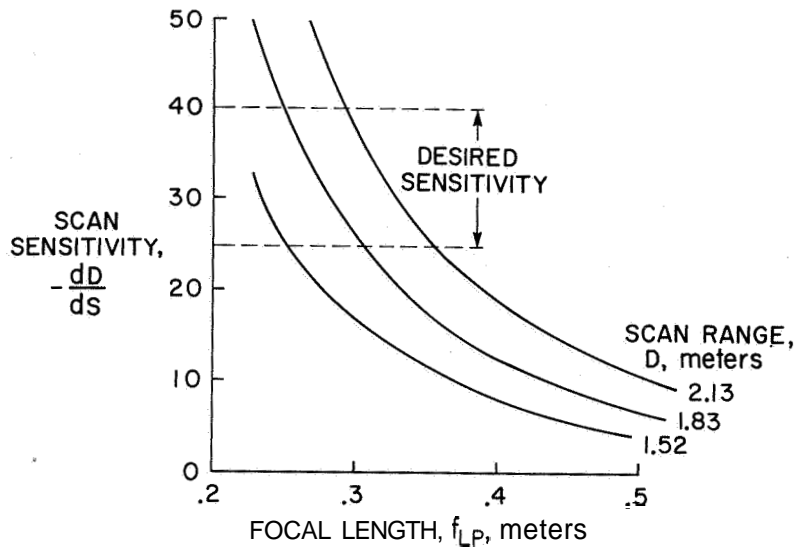
Figure 4.- Variation of scan sensitivity with focal length of focusing lens for several scan distances (ref. 30).
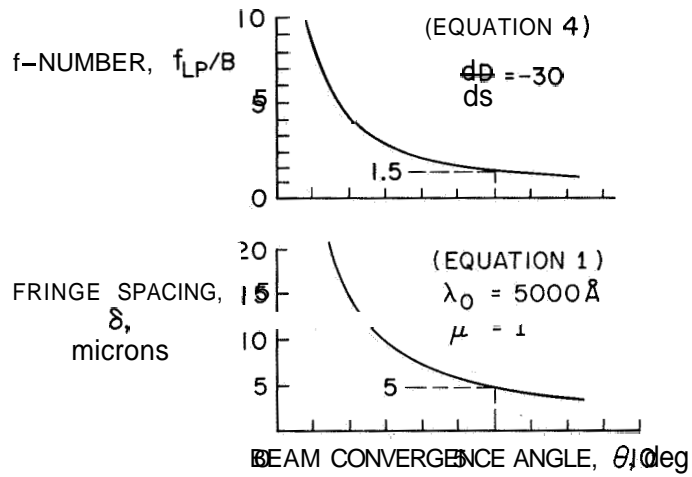


Figure 5.- Dependence of fringe spacing and required f number with beam convergence angle (ref. 30).
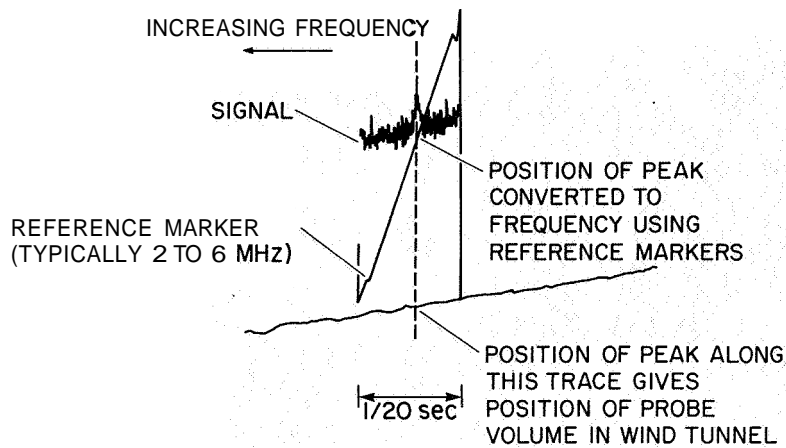
Figure 6.- Oscillograph trace of spectrum analyzer and lens carriage linear potentiometer outputs (ref. 20).
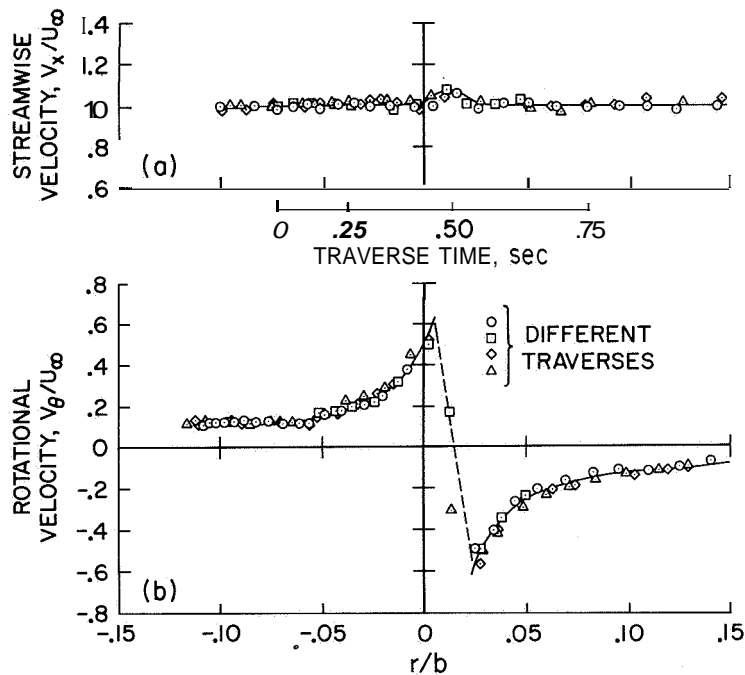


Figure 7.- Velocity distributions through wing-tip vortex of a semispan, square-tipped, rectangular wing with NACA 0015 airfoil; (a) streamwise velocity and (b) rotational velocity. $a = 11.1°$, $U_\infty = 22.8$ m/sec, $b = 2.44$ m, $X/c = 7.0$ (ref. 20).
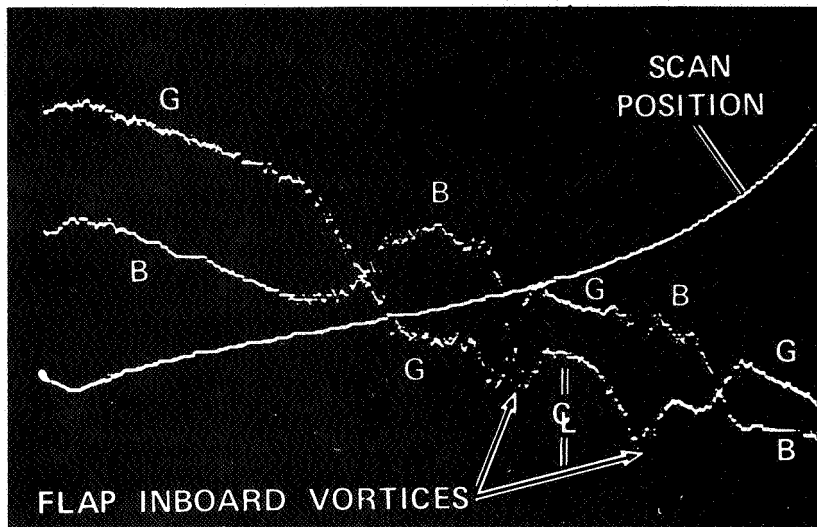
Figure 8.– Boeing 747 wake **TCD** record showing scan position of focal point, centerline of wind tunnel, and tracker outputs corresponding to the 4880 Å (B) and 5145 Å (G) channels of the velocimeter. This survey is through the vortex pair from the inboard edges of the inboard flaps. Inboard flaps deflected 30°, outboard flaps retracted? gear down; a = 8°, $U_\infty$ = 13.5 m/sec, b = 1.8 m, X/b = 1.5 (ref. 31).
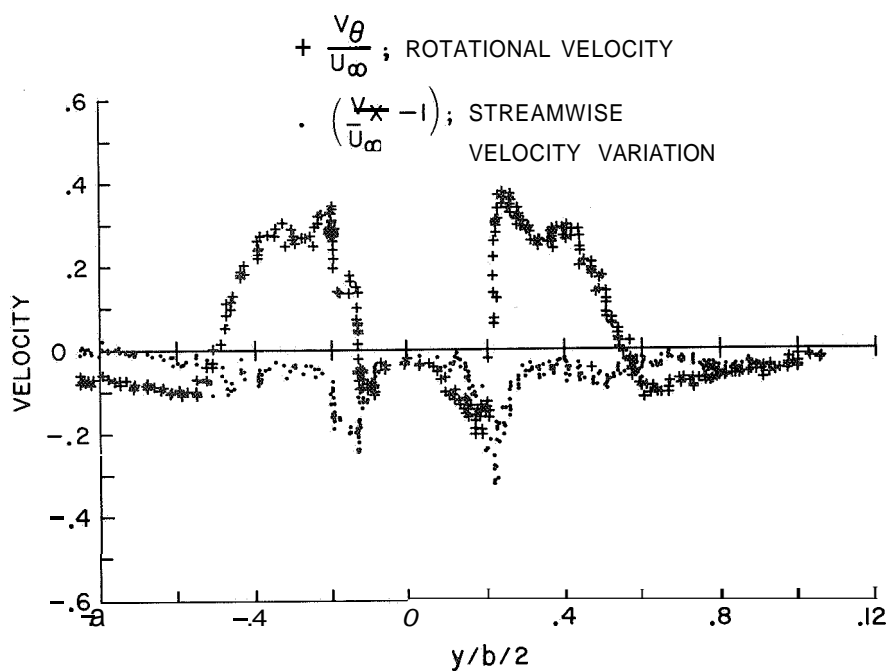


Figure 9.– Processed and plotted data from **TCD** record in figure 8 (ref. 31).
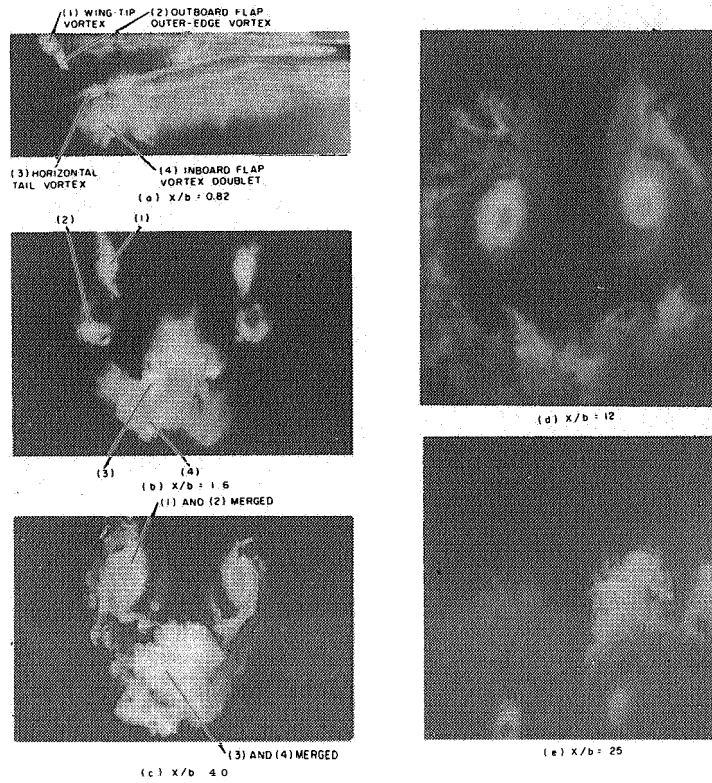
Figure 10.– Cross section of wake in light sheet; Boeing 747 landing configuration; $a = 2.9°$ (ref. 8).
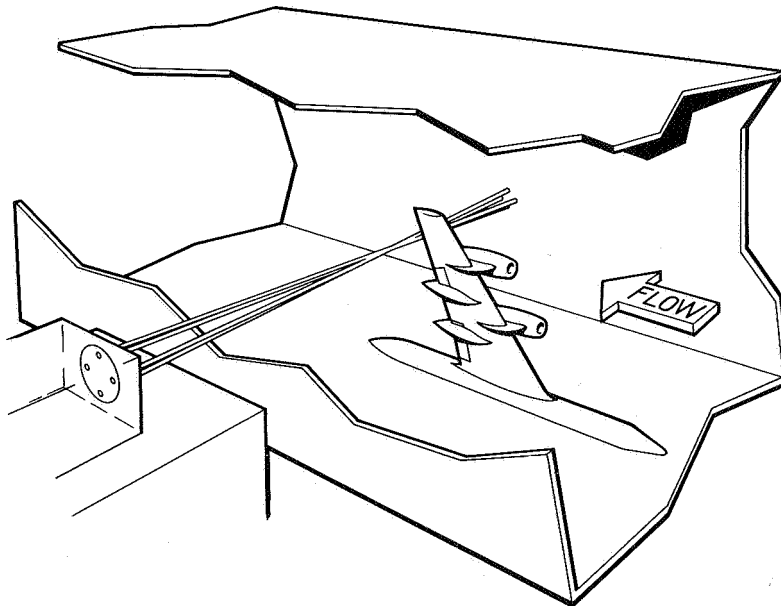


Figure 11.– Installation schematic drawing of semispan model in the Ames 7– by 10–Foot Wind Tunnel and location of scanning velocimeter (ref. 21).

183
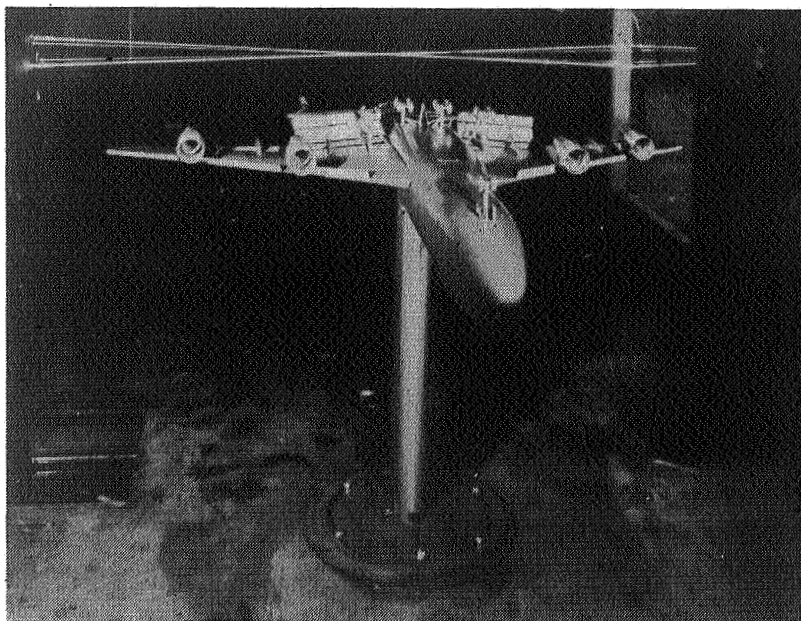
Figure 12.- Boeing 747 model installed in the Ames 7- by 10-Foot Wind Tunnel. Velocimeter scans behind the model at 1.5 wingspans (3 m) aft of the wing trailing edge (ref. 31).
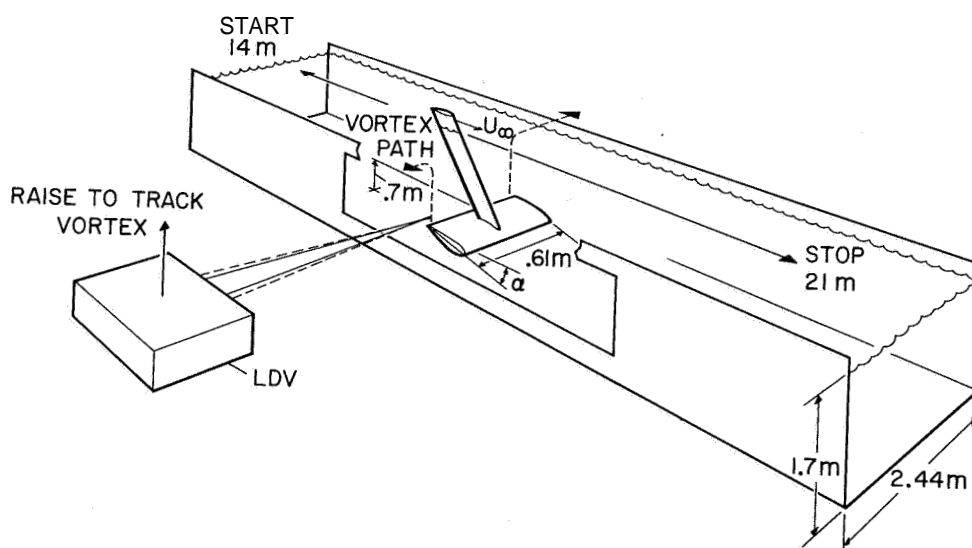


Figure 13.- Installation schematic drawing of model in water tow tank and vortex-tracking technique (ref. 22).

*184*
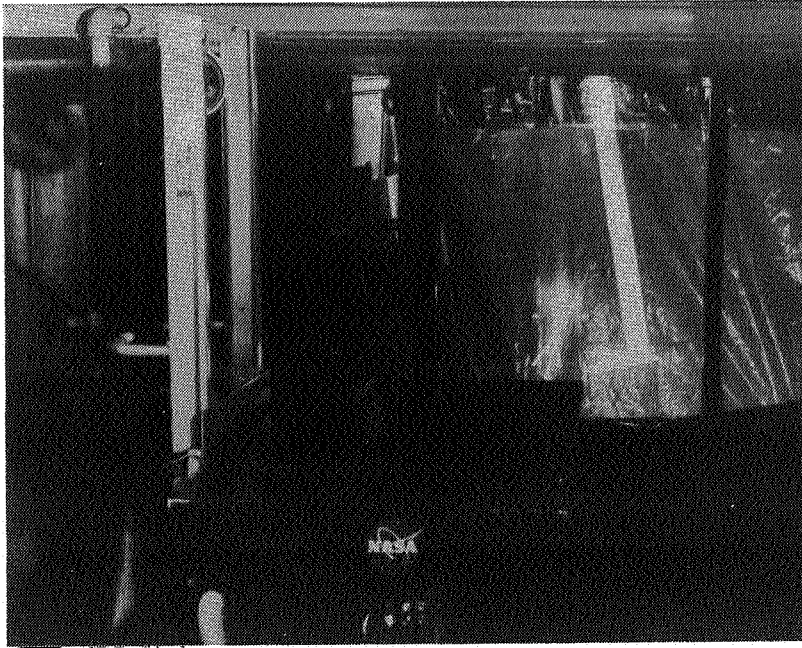
Figure 14.- Installation photograph, swept-wing model in test section of University of California water tow tank (ref. 25).
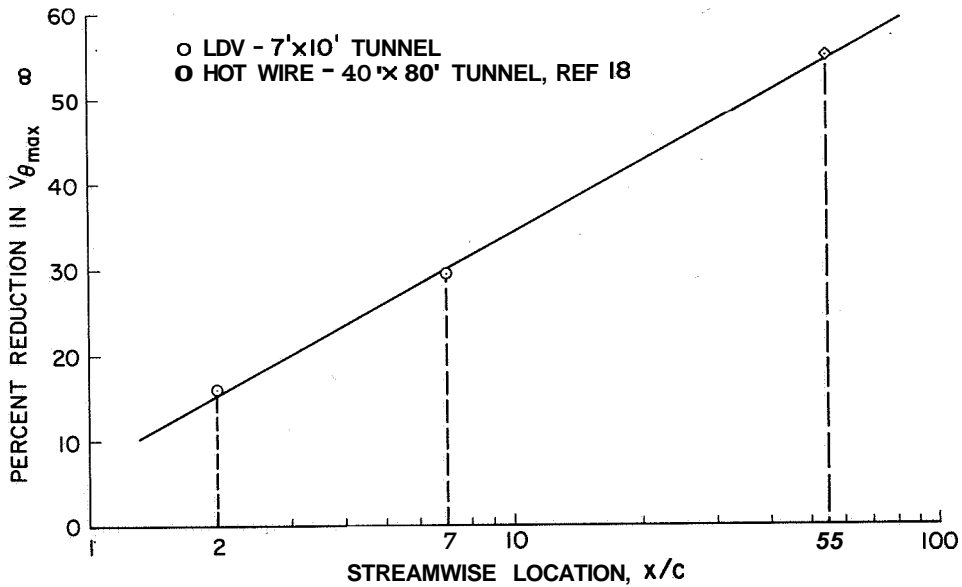


Figure 15.- Streamwise development of dissipator alleviation technique, $\alpha = 12°$ (ref. 20).
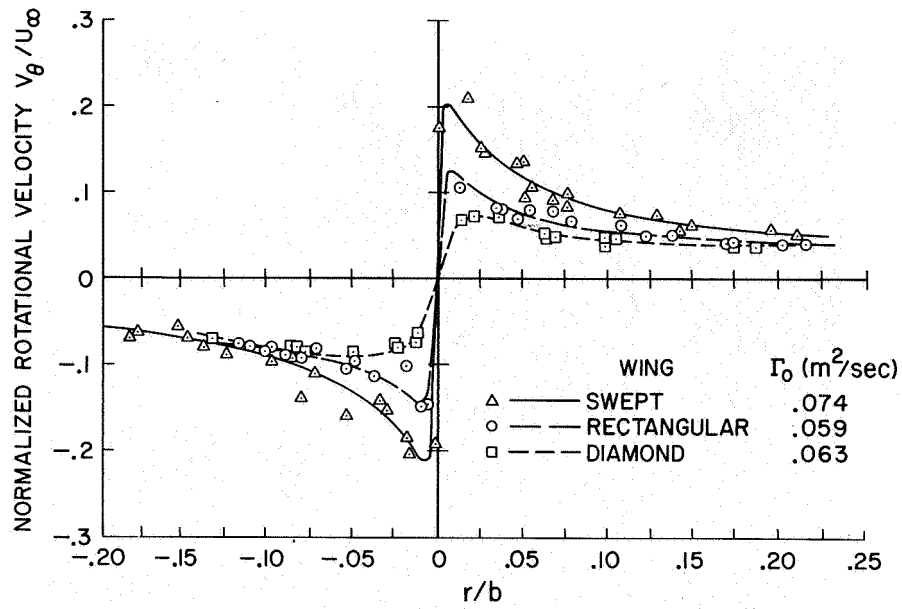
Figure 16.– Radial distribution of rotational velocity for different wing planforms at X/b = 20, $a = 5°$, U = 2.07 m/sec (ref. 22).
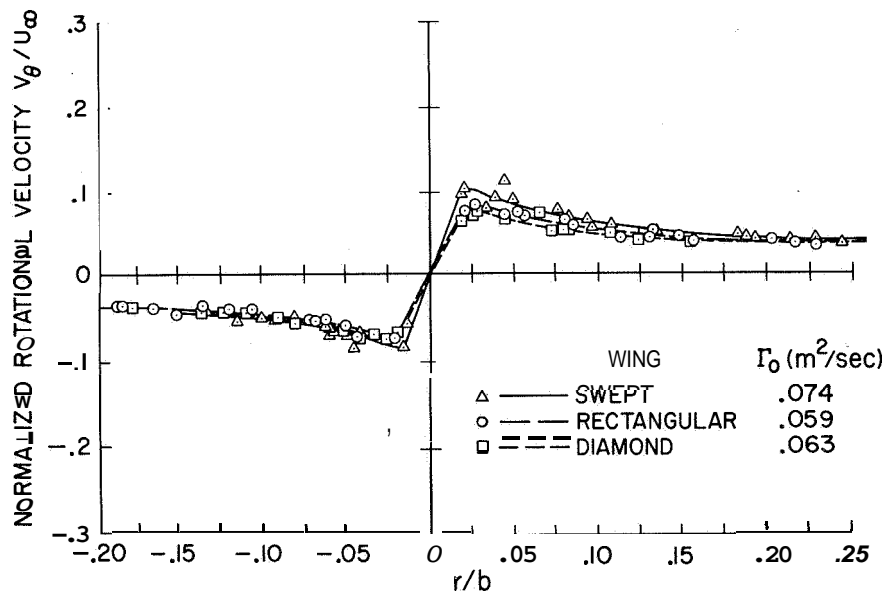


Figure 17.– Radial distribution of rotational velocity for different wing planforms at X/b = 100, $a = 5°$, $U_\infty$ = 2.07 m/sec (ref. 22).

186

**WATER TANK DATA, REF 25**

| $\alpha$, deg | $C_L$ | $U_\infty$ = 2.07 m/sec |
|---|---|---|
| ○ 4 | .28 | |
| □ 5 | .35 | |
| △ 8 | .56 | |

$$\frac{V_{\theta_{max}}}{U_\infty} \propto \left(\frac{x}{b}\right)^{-\frac{1}{2}}$$

**WIND TUNNEL DATA**

| $\alpha$, deg | $C_L$ | REF |
|---|---|---|
| ○ 4 | .28 | 20 |
| △ 8 | .56 | 20 |
| △ 8 | .56 | 18 |
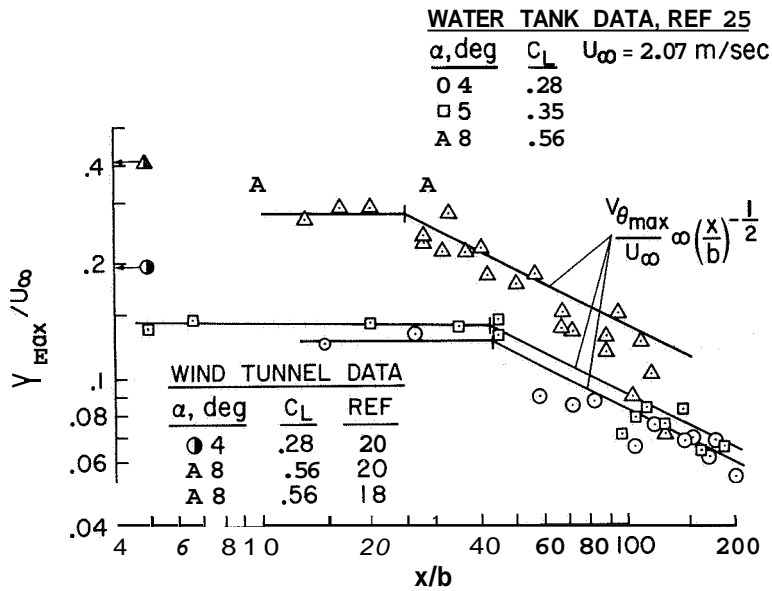
Figure 18.– Dependence of measured maximum rotational velocity on downstream distance and angle of attack, rectangular wing (ref. 26).



**WING PLANFORM** $(\Gamma_0/U_\infty b)$

| | $(\Gamma_0/U_\infty b)$ |
|---|---|
| ○ RECTANGULAR | 0.038 |
| △ SWEPT | .063 |
| □ DIAMOND | .050 |

$$\frac{V_{\theta_{max}}}{U_\infty} \propto \left(\frac{x}{b}\right)^{-\frac{1}{2}}$$
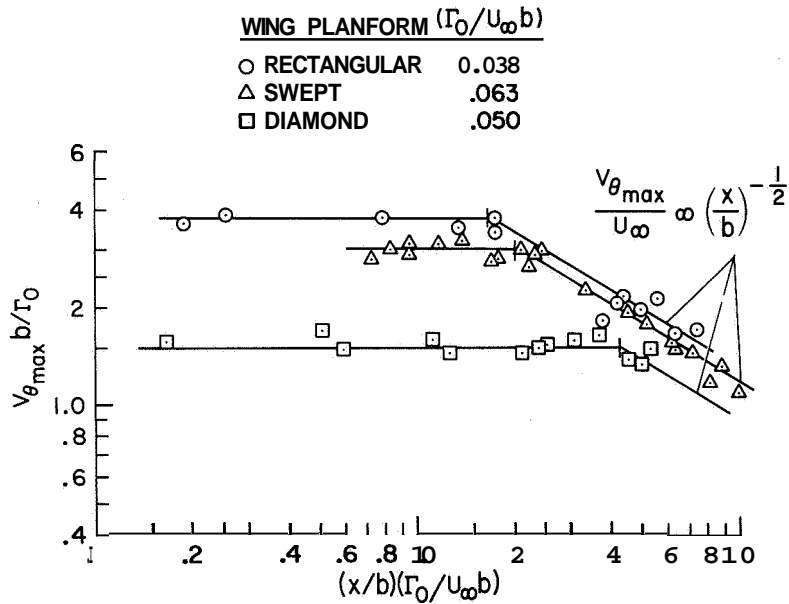
Figure 19.– Dependence of measured maximum rotational velocity on downstream distance and wing planform. Water tank data, $U_\infty$ = 2.07 m/sec, $\alpha$ = 5° (refs. 25 and 26).

187
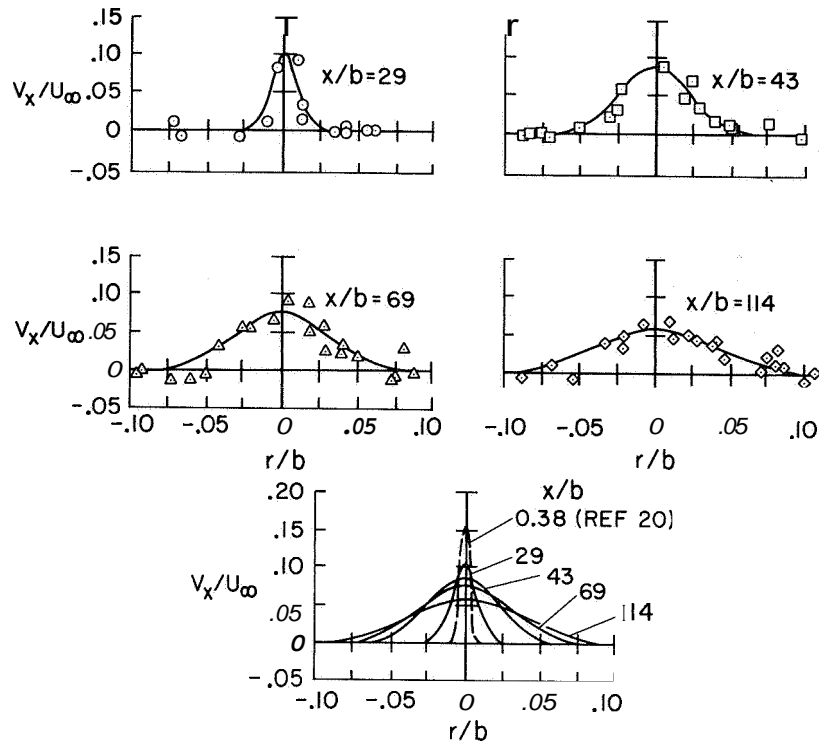
Figure 20.- Rectangular wing streamwise velocity-profile time histories,
$U_\infty = 2.07$ m/sec, $\alpha = 8°$. (ref. 25).

WATER TANK DATA
○ △ □    REF 23
── ● ──   REF 36
         REF *37*

WIND TUNNEL DATA
△    REF 20
▲    REF 14

THEORY
──  ──   REF *38*
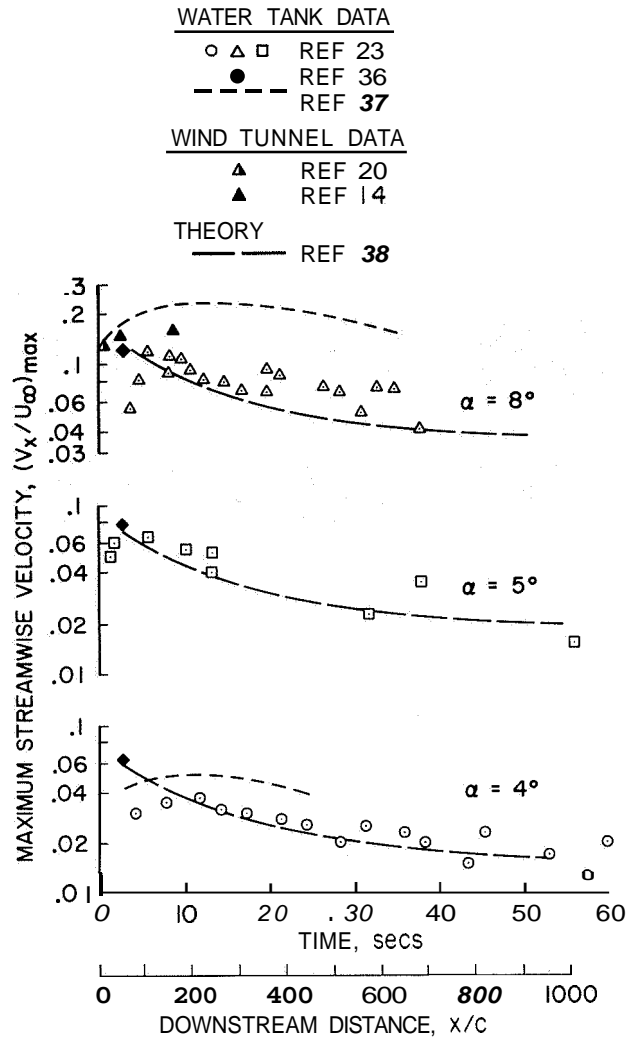
Figure 21.– Dependence of measured maximum streamwise velocity on downstream distance and angle of attack; rectangular planform; $U_\infty = 2.07$ m/sec (ref. **23**).
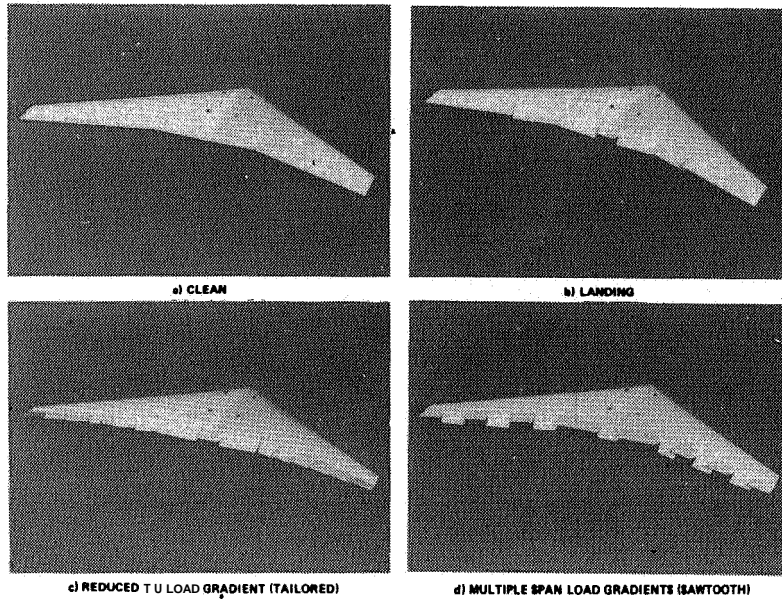
Figure 22.- Swept-wing model test configurations: (a) clean configuration, (b) landing configuration, (c) tailored configuration, (d) sawtooth configuration (ref. 25).
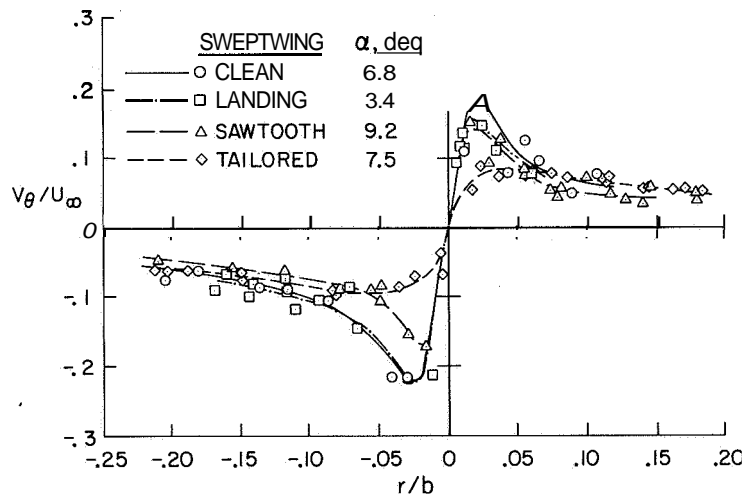


Figure 23.- Comparison of swept-wing configuration rotational velocity profiles; $U_\infty$ = 2.07 m/sec, $C_L$ = 0.7, X/b = 25 (ref. 25).
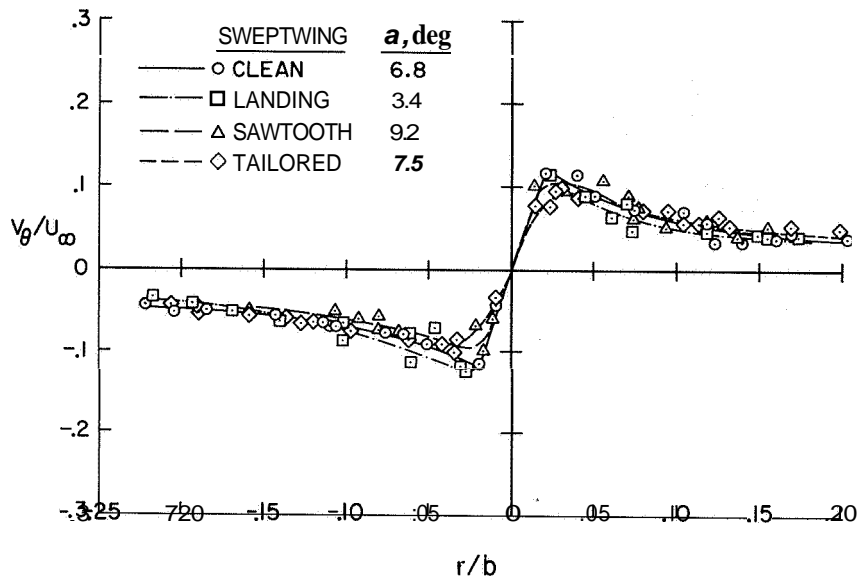
Figure 24.- Comparison of swept-wing configuration rotational velocity profiles; $U_\infty = 2.07$ m/sec, $C_L = 0.7$, X/b = 95 (ref. 25).
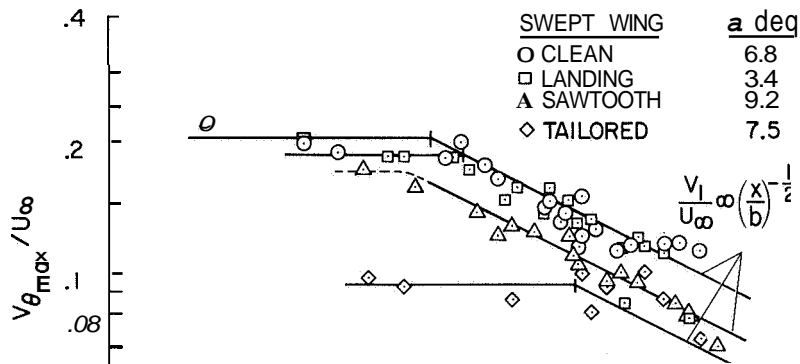


Figure 25.- Dependence of measured maximum rotational velocity on downstream distance and wingspan loading. Water tank data, $U_\infty = 2.07$ m/sec, $C_L = 0.7$ (refs. 25 and 26).

191
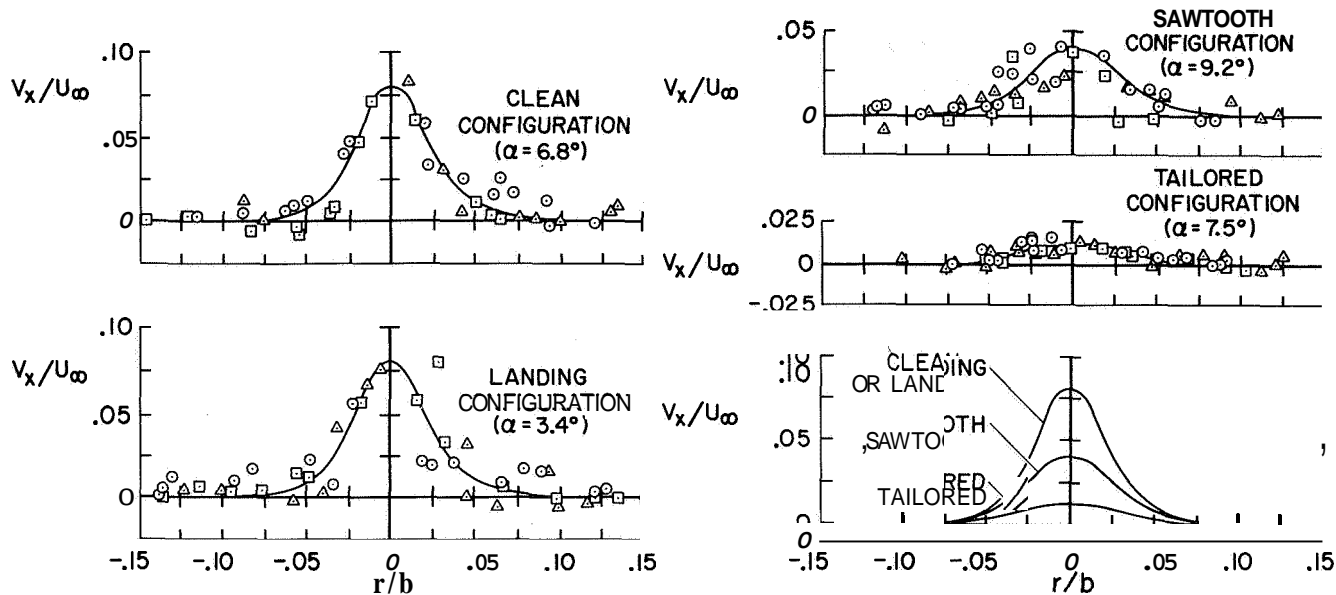
Figure 26.– Comparison of swept-wing configuration streamwise velocity profiles;
$U_\infty = 2.07$ m/sec, $C_L = 0.7$, X/b = 75 (ref. 25).
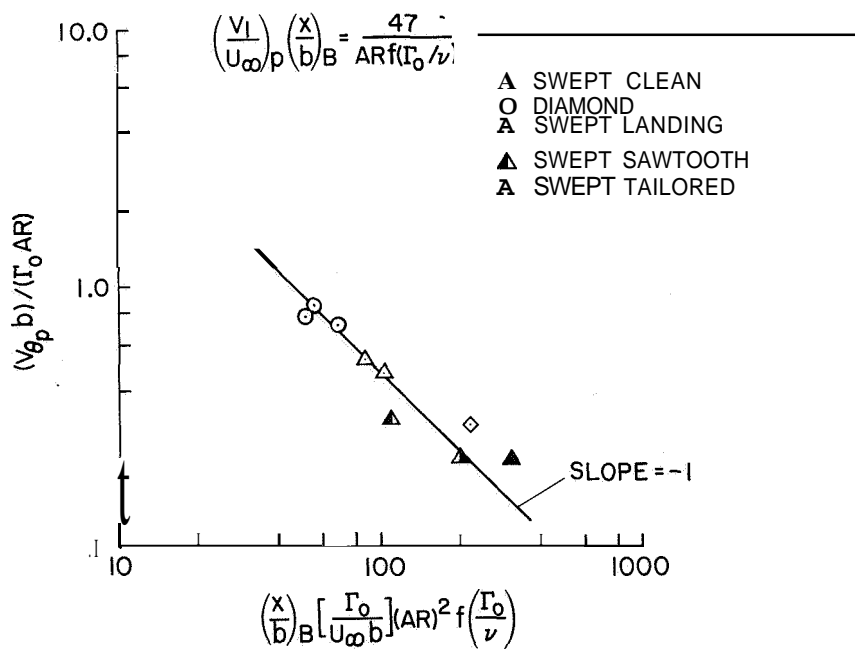


Figure 27.– Correlation of vortex maximum rotational velocity in plateau
region to downstream duration of this region (ref. 26).

192

# FLIGHT-TEST TECHNIQUES FOR WAKE-VORTEX MINIMIZATION STUDIES

Robert A. Jacobsen and M. R. Barber*

Ames Research Center

## SUMMARY

The flight-test techniques developed for use in the study of wake turbulence and used recently in flight studies of wake minimization methods are discussed. Flow visualization has been developed as a technique for qualitatively assessing minimization methods and is required in flight-test procedures for making quantitative measurements. The quantitative techniques are the measurement of the upset dynamics of an aircraft encountering the wake and the measurement of the wake velocity profiles. Descriptions of the instrumentation and the data reduction and correlation methods are given.

## INTRODUCTION

Flight tests have played an important role in the coordinated research program to develop vortex-wake alleviation techniques. The contribution of flight testing to this program lies in three important areas: to verify that the more flexible and less expensive to operate, ground-based research facilities are suitable for the development of vortex alleviation devices and techniques; to identify, under full-scale conditions, shortcomings of any alleviation technique that might not have been evident in the small-scale test environment; and to assess the operational feasibility of the developed techniques. The operational feasibility phase has two facets. The first is the influence of the alleviation device on the operation of the generating aircraft, but this subject is outside the scope of this paper. The second facet is to demonstrate the level of alleviation attained in the operational situation.

Recent flight experience has emphasized the importance of flight tests in complementing and focusing the research efforts in the ground-based facilities. As a result of wind-tunnel studies at Ames and Langley Research Centers, it

---

*Flight Research Center.

was discovered that raising the outboard flap segment in the landing configuration of a Boeing 747 markedly reduces the rolling moments induced on a following model (ref. 1).   Flight tests confirm that the vortex-induced upset can be reduced substantially through this flap modification.   However, the flight-test results show that the alleviation is greatly diminished when the landing gear is extended (ref. 2).   This effect of gear was unexpected and hence had been overlooked in the wind tunnels.   The flight test, therefore, had two important effects ▪ confirming that the wind-tunnel test results were meaningful and focusing future research on configurations that provide alleviation in the presence of a lowered landing gear.

Three flight-test techniques for wake turbulence research have evolved. The development of these techniques was initiated before the wake-vortex alleviation program so that the hazards associated with the vortex systems could be documented from a number of jet aircraft.   The three techniques are flow visualization, upset measurements of encountering aircraft, and velocity profile measurements.

Flow visualization is useful in comparisons of various alleviation configurations.   However, the primary value of flow visualization is to make it feasible for the pilot of a probe aircraft to locate the vortex and to penetrate its core so that the other two techniques can be applied.  Historically, the first flow visualization simply relied on the entrainment of the jet exhaust in the vortices.   This system was marginally successful for the tightly rolled-up vortex systems generated by transport aircraft in the cruise configuration and, for some aircraft, in the landing configuration.   However, for most aircraft in the landing configuration, with or without alleviation, specially developed flow visualization techniques must be used.  As might be expected, the more effective an alleviation technique is in eliminating or spreading the organized flow within the wake, the more difficult it becomes to mark the wake effectively.

Techniques for evaluating the hazard due to a wake vortex by measuring the upset of a penetrating aircraft were well developed before the alleviation program was initiated.   Early efforts included measurements of the wakes of large jet aircraft (such as the C-5A), with a number of smaller aircraft ranging in size from a Convair CV-990 to a Cessna 210 (refs, 3- 6).  Response

measurements were used in the earliest flight-test program to'assess the effect of an alleviation device.

This experiment was conducted at Ames in 1970 using a spoiler on the wingtip of the CV-990 (ref. 7). This device had been developed in the wind tunnel on the basis of tuft-grid studies. In flight, the effect of the spoiler was determined by mounting it on one wingtip while leaving the other tip clean. The Ames Learjet was used to probe the wake from one wingtip and then the wake from the other. The pilots could not discern any effect of this device. However, data reduction did indicate that there was some alleviation effect. The principal result of this flight program was to convince research-ers at Ames that more definitive flight-test techniques were needed to effec-tively evaluate the alleviation techniques.

The desire for a more definitive technique led to the development of methods for measuring velocity profiles. Such measurement had been made in flight earlier at Langley using angle of attack and sideslip vanes (see ref, 8). However, it was felt necessary to develop instruments with higher fre-quency response characteristics than vanes. There are several advantages to measuring the velocity profile in the wake. First, it may provide more insight into the processes actually occurring in the flow field leading to vor-tex dissipation. Second, unlike response measurements that cannot be extrapo-lated to other sizes of aircraft, a velocity profile can be used to estimate the rolling moment imposed on any aircraft, Finally, these measurements, along with simultaneous measurements of aircraft response, can be used to verify response calculation and to develop improved methods of making these calculations.

In the following sections, the current state of development of each flight-test technique is discussed in greater detail.

## FLIGHT-TEST TECHNIQUES

### Flow Visualization

Flow visualization has been a primary concern throughout the development of wake turbulence flight-test techniques. Not only is it a useful tool for observing the mechanisms of vortex decay, it is also a necessary element in

195

any of the probe aircraft work. The visualization provides a target for the pilot of the probe aircraft to increase the probability that the wake encounters provide the maximum information possible. Without the target provided by the visualization, an extremely large number of passes through the estimated location of the wake would be required to provide a significant number of encounters. Even then, there would be no assurance that the strongest portion of the wake had been measured. In fact, it has proven difficult to develop flow visualization that defines the wake well enough at separation distances of 2 to 10 nautical miles to enable a large percentage of the probe aircraft encounters to penetrate the core region of the vortex.

The visualization used for most of the vortex alleviation flight tests has been provided by "smoke generators" built for NASA by Frank Sanders Aircraft Co. (Long Beach, Calif.). Figure 1 shows one of these devices — an aluminum cylinder approximately 25 cm (10 in.) in diameter and 1.4 m (4.5 ft) long with a 0.7-m (2.2-ft) tailpipe. The "smoke" generated by this device is actually small droplets of mineral oil created when oil vapor expelled by the smoke generator is condensed by the cooler ambient air. A combustor contained within the cylinder generates the heat used to vaporize the mineral oil. The oil is sprayed into the exhaust of the combustor in the tailpipe extending behind the cylinder. The fuel for the combustor and the mineral oil are contained in tanks located within the cylinder. The self-contained tankage provides for 20 min of operation with ambient air being used to support the combustion. At the approach speeds used for much of the wake turbulence testing, the operation of the combustor on ambient air is marginal. The device was modified recently to allow engine bleed air to be used in the combustor. This change greatly improved the "smoke" production, but the operating time is reduced to 10 min.

In a typical installation on a research aircraft, one or more smoke generators is mounted under the wing at each spanwise location where a discrete vortex is expected to form (fig. 2). These locations typically include the wingtip, edges of the flap segments, and the wing/fuselage junction. The two most recent installations have both been on a B-747 used for the wake alleviation program at Flight Research Center (Edwards Air Force Base, Calif.). In the first of the two installations (fig. 2), a single smoke generator was

mounted at the tip, one at the outboard edge of the outboard flap segment and one at the outboard edge of the inboard flap segment of each wing. The flow visualization provided by this installation was often marginal and improvements were made to the system before the next series of tests on that aircraft. Those improvements included doubling the number of smoke generators at each of the previous six locations and adding two at the inboard edge of each inboard flap. Each of these 16 smoke generators had bleed air from the jet engines ducted to their inlets to further improve their performance. This installation has produced excellent results. An example of the flow visualization produced by this arrangement is demonstrated in figure **3.**

A second type of flow visualization has been used which also performed adequately for either flow-field observation or for marking the wake to facilitate probing. The wake in this case was marked with an inert powder blown into the airstream at any location of interest. The inert powder used is finely ground diatomaceous earth. Figure *4* is a diagram of a typical installation. The powder is contained in tanks located in the aircraft fuselage with tubing extending along or inside the wing to the desired location. When visualization is desired, the tanks are pressurized using bottled gas that expels the powder out the tubes. This system is easy to install and is aerodynamically clean, but the visualization period is relatively short. The powder is bulky and, for the size of tanks and delivery lines used, it is expelled in about *90* sec. The tanks must then be refilled (which can be done in flight) before additional visualization can be accomplished. This type of flow visualization was used on a DC-3 and a DC-10 in programs at Flight Research Center (ref. 5) and on the Augmentor Wing Jet STOL Research Aircraft at Ames (ref. 9). Figure 5 shows the installation of an inert powder system on a DC-10 and figure *6* shows the visualization of the wake of a DC-3 using a similar system.

## Flight Measurements

Flight tests to determine the relative strengths of vortex systems have been made by penetrating the wake to measure either the upset imparted to a probe aircraft or the flow velocities within the wake. As noted previously, either technique requires flow visualization. In addition, both techniques require that the distance between the probe and wake-generating aircraft be

197

known, and that limits be placed on this distance to ensure that structural limit loads are not exceeded.

Three different methods have been used in wake turbulence flight programs conducted by NASA to measure the distance between the probe aircraft and the aircraft that generated the wake. The first technique requires the use of two ground radars. By tracking each aircraft to establish its position in space as a function of time, the distance between the two aircraft can be determined. This technique has been used in NASA programs at Edwards and Vandenberg Air Force Bases. The information is communicated to the probe aircraft pilot to aid him in controlling the experiment. The second technique used when radar facilities were not available is to conduct the flight test while flying a radial toward (or away from) a distant Distance Measuring Equipment (DME) ground station. The probe aircraft pilot calls out his distance to that station as he encounters the wake. At that time, the pilot of the wake-generating aircraft calls out his distance to the station and the difference in the two is the separation between the aircraft. Both of these techniques are inconvenient in that extensive ground facilities are required or a communication link is required that can, at times, be confusing.

To overcome these difficulties, a third system was developed: a pair of airborne DME's was modified (by Sierra Research Corp., Buffalo, New York) so that one of the pair performed as a beacon and the other as an interrogator of that beacon. The beacon is mounted in the lead aircraft and the interrogator is mounted in the probe aircraft. A direct and continuous measurement of separation distance is obtained completely independent of ground facilities. This system has been used in all of the recent wake turbulence programs.

Concern for the structure of the probe aircraft makes it necessary to place limits on the probing technique, especially as separation distances are reduced. Three methods have been used to assure the safe operation of the probe aircraft. The first method is to limit the airspeed of the probe aircraft to a value that will prevent the loads on any aerodynamic surface from reaching their limits. For this calculation, each surface is assumed to be stalled at 1.3 times the maximum lift coefficient for that surface to allow for the "dynamic stall" effect. Knowing the limit load capability of that surface then allows a maximum allowable airspeed to be computed. This procedure is

followed for each surface and the lowest airspeed is used as the operational limit. It is then assured that any aerodynamic situation encountered will not cause structural damage. This method has been used at Ames Research Center to assure the safe operation of their Learjet probe aircraft in wake turbulence testing.

The second method for assuring safe operation is to monitor the loads in the critical locations of the probe aircraft structure and telemeter that information to the ground. At each separation distance where probing is done, enough. encounters are obtained to ensure that the maximum loads possible at that location have been imposed on the probe aircraft. If these maximum loads are less than a predetermined percentage of the yield loads, then the separation distance can be reduced. Once the measured loads exceed that predetermined percentage of the yield load, no probing is performed at a closer separation distance. This technique has been used at Flight Research Center with their T-37 probe aircraft.

The third technique used to establish a lower limit on the separation distance for probe encounters is the subjective opinion of the pilot of the probe aircraft. If, at any time, the pilot feels that continued probing at closer separation distances or at that same separation distance cannot be done safely, that series of encounters is stopped.

*Upset measurements* - Measurements taken to derive the moments induced on an aircraft subjected to wake turbulence have become known as "upset measurements." Actually, it is necessary to measure more than simply the upset of the probe aircraft. The control inputs, angular rates, airspeed, and angles of attack and sideslip must be known to account for those angular accelerations resulting from the aerodynamic characteristics of the probe aircraft. The separation distance between the two aircraft and the encounter altitude are also required to correlate the data.

Upset measurements are taken with the flight path of the probing aircraft nominally parallel to the wake axes (hence the name "parallel probes") (fig. 7). When probing the wake of an unfamiliar configuration, the initial encounter with the wake is made at a separation distance large enough to ensure that the resulting forces will not severely load the structure of the aircraft. This is an additional precaution to the safe operation procedures previously

described.  As the probe aircraft encounters the wake, the pilot performs his
task in one of two modes.  He can hold the controls fixed, allowing the upset
to remove the aircraft from the wake, or he can attempt to hold the probe air-
plane as nearly centered in a vortex as possible.  Either action produces the
desired data, but the pilot may obtain more subjective information by using a
combination of the two.  This procedure is repeated several times at each sepa-
ration distance to increase the probability that the maximum possible induced
accelerations of the probe aircraft were achieved.

The instrumentation used to obtain the data required to derive the induced
moments is, generally, that which would be typical for a study of handling
qualities.  The three-dimensional aircraft dynamics are measured by angular
accelerometers, rate and attitude gyros, and linear accelerometers.  The deflec-
tions of the control surfaces are measured as are airspeed, altitude, angles
of attack and sideslip, and separation distance.  Typical roll axis data are
shown in figure 8.

Figure 9 is a block diagram of the data-reduction process.  During an
encounter, the velocity gradients in the flow field to which the probe aircraft
is being subjected can be quite high.  As a result, the angles of attack and
sideslip measured on the nose boom or at any single point on the aircraft can-
not be considered representative of the effective flow-field angularity to
which the whole airframe is subjected.  Consequently, it is necessary to com-
pute an effective angle of attack and sideslip from the measured linear accel-
erations and angular rates.  The angular accelerations that would have been
caused in still air by the aerodynamic forces and control inputs are computed.
When subtracted from the measured angular accelerations, the accelerations
induced by the vortex flow are derived.  Computed aerodynamic and control
accelerations and net acceleration due to the vortex flow are shown in figure
10 for the same encounters shown in figure 8.  The measured roll acceleration
is repeated.

A roll acceleration parameter, convenient for comparative purposes, was
developed to relate the vortex-induced roll acceleration, $\dot{p}_{vortex}$, to the max-
imum roll acceleration capability of the aircraft using maximum aileron deflec-
tion $\dot{p}_{\delta a_{max}}$.  The ratio $\dot{p}_{vortex}/\dot{p}_{\delta a_{max}}$ indicates how severe the induced
moment was.  The physical meaning of this parameter is that, when a value of

200

unity is reached, the pilot could exactly counter the vortex-induced roll acceleration with maximum deflection of the ailerons. Similar parameters can be determined for accelerations in the pitch and yaw axes. For each encounter behind a given configuration, the peak values of this roll-acceleration parameter are plotted against the separation distance at which they occurred (fig. 11). Assuming that the highest values at each distance represent the maximum upset expected at that location, an upper bound to the data is constructed. The separation distance defined by the intersection of that boundary and the line for a unity roll acceleration parameter is used in comparisons with values obtained in a similar manner from data obtained during tests of other aircraft or configurations. An example of how these comparisons are made is shown in figure 12, where the separation distance for unity roll acceleration parameter is plotted against the gross weight of the wake-generating aircraft for several sizes of probe aircraft. This figure demonstrates that the upset received by a given probe aircraft is decreased as the gross weight of the wake-generating aircraft is decreased. Similar comparisons can be made for the flight-test results of wake-vortex alleviation methods.

*Velocity profile* measurements - The need for more definitive information on the vortex-wake phenomenon led to the development of another flight-test technique. Use of this technique results in measurements of the velocity profiles in the wake, which will allow comparisons of the wake structure with theories (ref. 10). This can be especially useful in the wake alleviation work by more clearly defining the changes in the wake structure caused by an alleviation technique.

These measurements require a completely different technique in procedure, instrumentation, and data reduction. The flow velocities must be measured by sensors with higher frequency response characteristics than normally used in handling qualities research, and the aircraft motion must be measured for use in correcting the velocity data. The separation distance is again required to correlate the data.

The flight-test procedure used to obtain velocity profile data is considerably different from that used during upset measurements (fig. **13**). The flight path of the probing aircraft is across the wake to effectively traverse the flow field with the velocity-measuring probe. Ideally, the flight path

201

should be in a plane perpendicular to the wake axes to minimize the motion excursions for which corrections must be made. The limited capability of the flow visualization systems to mark the wake results in an inability to see the wake well enough from right angles to enable the pilot of the probe aircraft to penetrate the vortex cores consistently. As the crossing angle is reduced, the apparent density of the flow visualization medium is increased, thereby allowing consistent core penetrations. Local atmospheric conditions and the angle of the sun relative to the two aircraft affect visualization as well. Experience has shown that crossing angles of from $25^o$ to $45^o$ are adequate for this task, These lower crossing angles have the additional advantage of allowing a shorter time between crossihgs because a turn of only $50^o$ to $90^o$ is required to traverse back across the wake. This saving of time between wake crossings allows more data to be obtained in the amount of time allowed by the flow visualization system.

As with the upset measurement procedures, wake encounters are begun at separation distances large enough to assure safe operations. A zigzag flight path is flown while the separation distance is continually reduced until a predetermined minimum separation distance is reached. This minimum separation distance is set for safety reasons and, as for upset measurements, is based on computed loads, extrapolated load measurements, or probe pilot decisions. Once the minimum separation distance is reached, a $360^o$ turn is initiated which sets the probe aircraft up for additional data at a larger separation distance. This procedure is repeated several times until adequate data are acquired for that wake-generating aircraft configuration.

The frequency content of the velocity data being recorded as the probe aircraft traverses the wake is considerably higher than that normally seen in aircraft dynamics work. Assuming reasonable values for the probe aircraft velocity and the vortex core size of 120 m/sec (400 ft/sec) and 3 m (10 ft), respectively, the apparent frequency of the approximately sinusoidal input recorded as the vortex core is penetrated is 40 Hz. This frequency is higher than conventional research aircraft flow angularity sensors are able to measure reliably. Three types of sensors have been used to this purpose. Angle of attack and sideslip vanes (fig. 14) have been used by Langley Research Center on a T-33 research aircraft (ref. 8). A five-hole pitot tube (fig. 15) has been used at Flight Research Center on a T-37 probe aircraft. At Ames

Research Center, a three-component, hot-wire anemometer (fig. 16) has been used on a Learjet probe aircraft (ref. 11). The instrumentation system and data-reduction technique described below is that for the hot-wire anemometry sensors and is typical of the data-reduction technique required for the others as well. In addition to the high-frequency velocity measurements, information on the probe aircraft dynamics is required. These are measured by angular and linear accelerometers and angular rate and attitude gyros. The range between the aircraft whose wake is being studied and the probe aircraft is measured directly by a pair of modified DME's as in the upset measurements.

The data-reduction process is indicated by the flow chart in figure 17. The airborne-recorded analog data are digitized at the rate of 1000 samples/sec. (This rate is necessary because of the high-frequency content of the data.) The wake velocities are first computed from the hot-wire data in an axis system aligned with the body axes of the aircraft, and corrections are made for the vertical velocity and pitch rate of the aircraft. Corrections are also made for the apparent vertical and lateral velocities that result from the effective angles of attack and sideslip generated as the aircraft reacts to the induced forces. The three components of velocity are then resolved into an axis system aligned with the axis of the vortex using the relative heading for each pass across the wake. The flight path of the probe is computed from the initial airspeed and the measured vertical accelerations and pitching excursions. In this way, a velocity distribution along a known path in space is determined.

The velocity profile measured at a separation distance of 2.9 nautical miles behind a B-747 in its normal landing configuration is presented in figure 18. All three components of velocity are shown, the top one being the vertical velocity component defined as positive upward, the middle trace is the lateral component defined as positive to the left, and the bottom trace is the axial velocity component defined positive toward the aircraft that generated the wake. Comparing these data with that of the next figure demonstrates the ability of this system to show the effects of vortex-wake alleviation in the measured flow field. A comparison of figures 18 and 19 indicates the reduction in the three components of velocity in the wake of the B-747 at 2.2 nautical miles with the outboard flaps retracted.

Another purpose for which these data can be used is to understand, or at least dacument., the changes in the vortex structure as it ages. Since no two traverses of the wake are the same, these comparisons are best made by fitting data of various ages with a mathematical model and observing the changes in the model parameters as the vortex ages. For the initial attempts at modeling these data, a pair of Lamb vortices was selected. This representation is convenient because the formulation is analytic. Matching the computed velocities to the measured data along the actual flight path was accomplished using the locations of the two vortices, the circulation of each vortex, and their core size as parameters. The match was done in a least squares sense on the vertical and lateral velocity components simultaneously. A result of that matching procedure is seen in figure 20, where the velocities computed from the model as they would have been measured along the flight path are compared with the measured data. If the wake can be adequately represented by a single pair of vortices, this procedure results in a satisfactory match. Modeling the wake at various separation distances and comparing the results can show the decay of the velocities in the vortex (fig. 21). The reduction of maximum velocity is seen as the separation distance increases.

An application of this mathematical modeling technique to the wake alleviation work is shown in figure 22, where a model of the tangential velocity profile of the B-747 wake at separation distances up to 3.1 nautical miles in normal landing configuration is compared with that for the same airplane's wake at distances as close as 1.0 nautical mile with the outboard flap segment retracted. Even though the profiles for the latter case are at closer separation distances, the peak tangential velocity is reduced and the effective core size increased.

## REFERENCES

1. Corsiglia, V. R.; Rossow, V. J.; and Ciffone, D. L.: Experimental Study of the Effect of Span Loading on Aircraft Wakes. NASA TM X-62,431, 1975.
2. Smith, H. J.: A Flight Test Investigation of the Rolling Moments Induced on a T-37B Airplane in the Wake of *a* B-747 Airplane. NASA TM X-56,031, 1975.

3. Andrews, W. H.: Flight Evaluation of the Wing Vortex Wake Generated by Large Jet Transports. NASA FWP-18, presented at Boeing/AFOSR Symposium on Aircraft Wake Turbulence, Seattle, Wash., Sept. 1970.

4. Andrews, W. H.; Robinson, G. H.; and Larson, R. R: Exploratory Flight Investigation of Aircraft Response to the Wing Vortex Wake Generated by Jet Transport Aircraft. NASA TN D-6655, 1972.

5. Andrews, W. H.; Tymczyszyn, J. J.; Jacobsen, R. A.; and Drinkwater, F. J., III: Flight Investigation of the Response of Wide-Body Tri-Jet Aircraft to the Wing Vortex Wake Generated by Large Transport Aircraft. NASA Flight Research Center Working Paper FWP-35, Feb. 1973.

6. Barber, M. R.; Kurkowski, R. L.; and Garodz, L. J.: Flight Test Investigation of the Vortex Wake Characteristics Behind a Boeing 727 During Two-Segment and Normal ILS Approaches. NASA TM X-62,398, 1975.

7. Corsiglia, V. R.; Jacobsen, R. A.; and Chigier, N: An Experimental Investigation of Trailing Vortices Behind a Wing with a Vortex Dissipator. Presented at Boeing/AFOSR Symposium on Aircraft Wake Turbulence, Seattle, Wash., Sept. 1970.

8. Verstynen, H. A., Jr.; and Dunham, R. E., Jr.: A Flight Investigation of the Trailing Vortices Generated by a Jumbo Jet Transport. NASA TN D-7172, 1973.

9. Jacobsen, R. A.; and Drinkwater, F. J., III: Exploratory Flight Investigation of Aircraft Response to the Wing Vortex Generated by the Augmentor Wing Jet STOL Research Aircraft. NASA TM X-62,387, 1975.

10. Kuhn, G. D.; and Jacobsen, R. A: Analysis of Wake Vortex Flight Test Data Behind a T-33 Aircraft. NASA CR-137,669, 1975.

11. Jacobsen, R. A.: Hot-wire Anemometry for In-Flight Measurements of Aircraft Wake Vortices. Paper presented to SFTE, Aug. 1974.

205
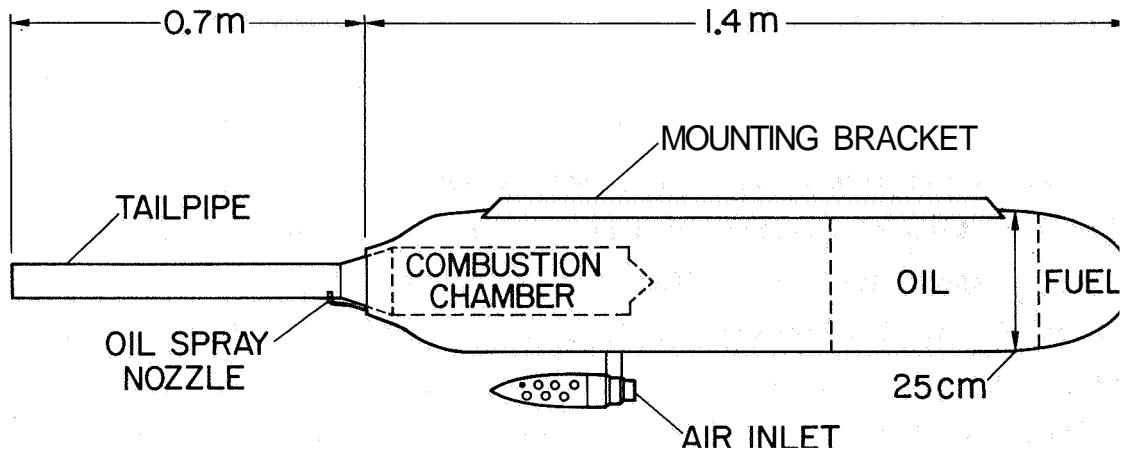
Figure 1.- Self-contained smoke generator.
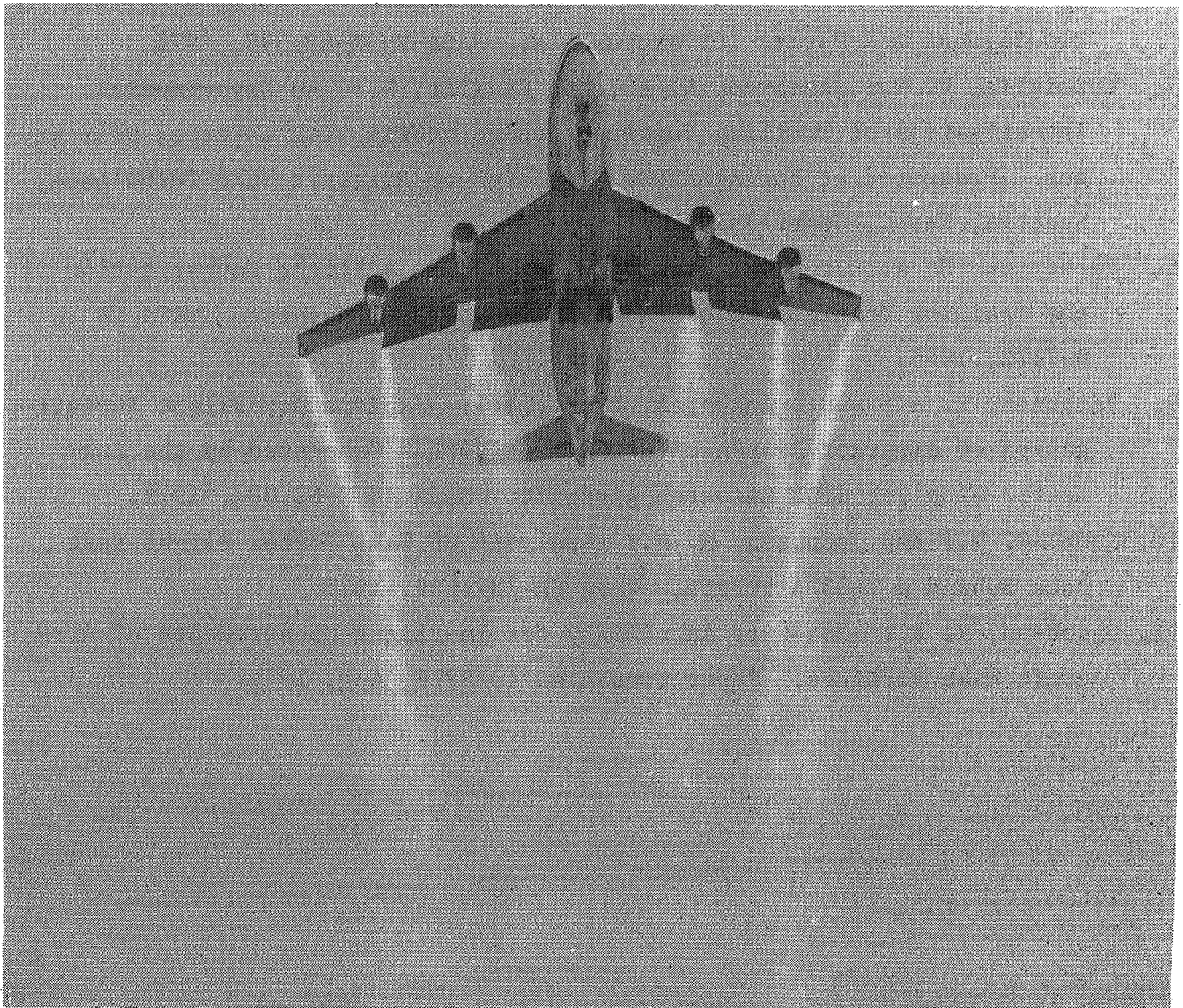


Figure 2- B-747 with six smoke generators used to mark its wake.

206

Figure **3.-** B-747 with 16 smoke generators used to mark its wake.
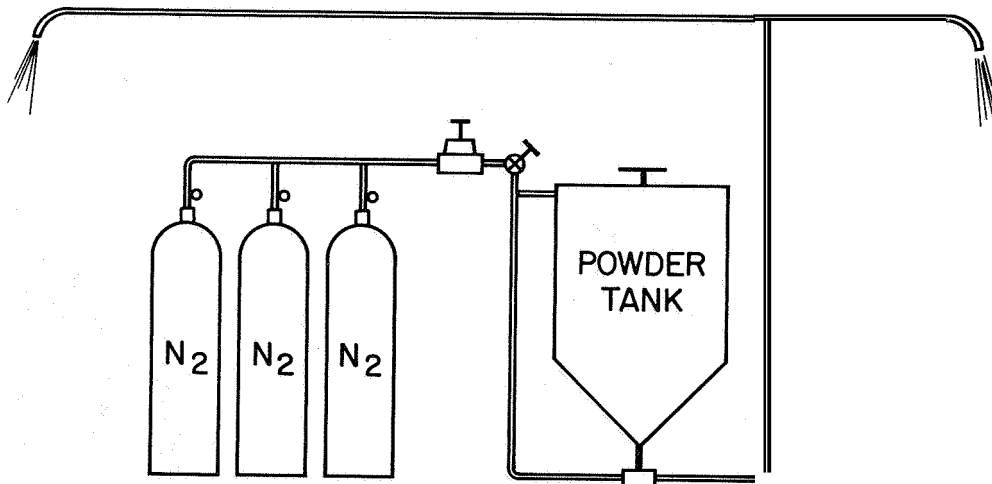


Figure *4.-* Diagram of inert powder flow visualization system.
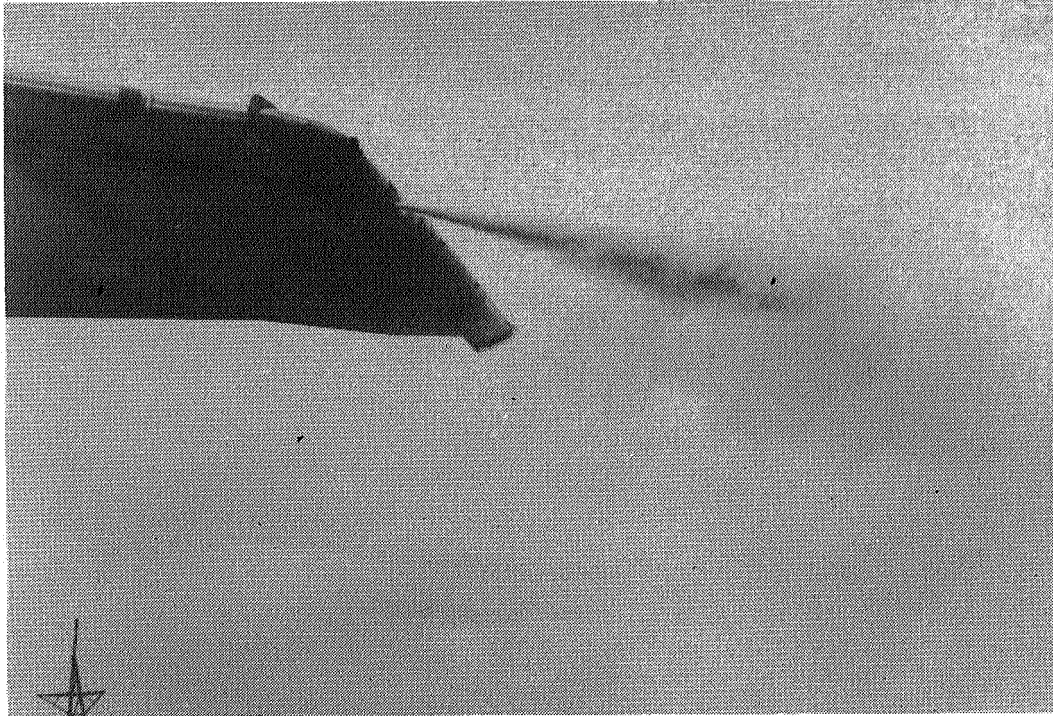
Figure 5.- Inert powder flow visualization system on DC-10.



Figure 6.- Inert powder flow visualization system on DC-3.
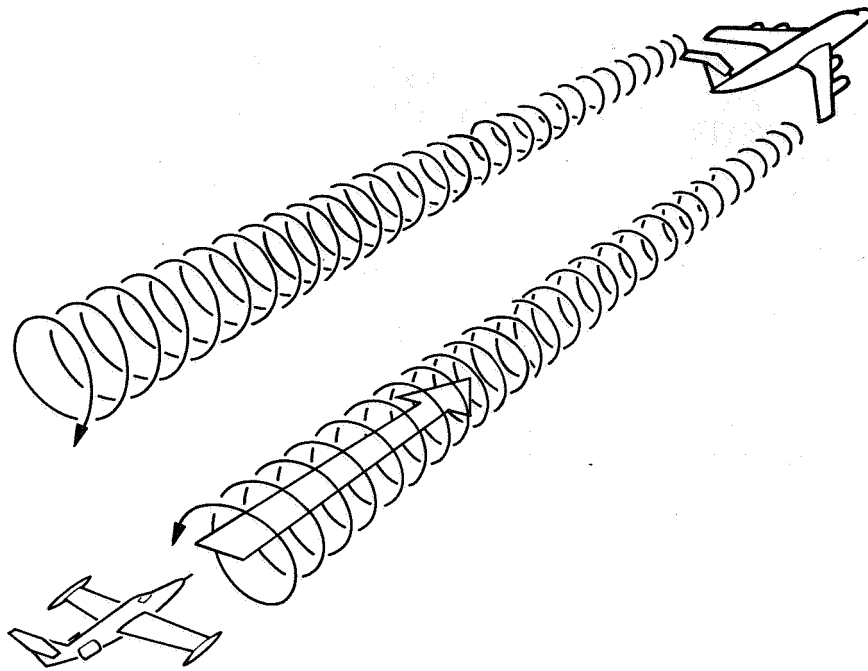
Figure 7.–.Probe aircraft flight path during upset measurements of vortex wake.



TIME, sec
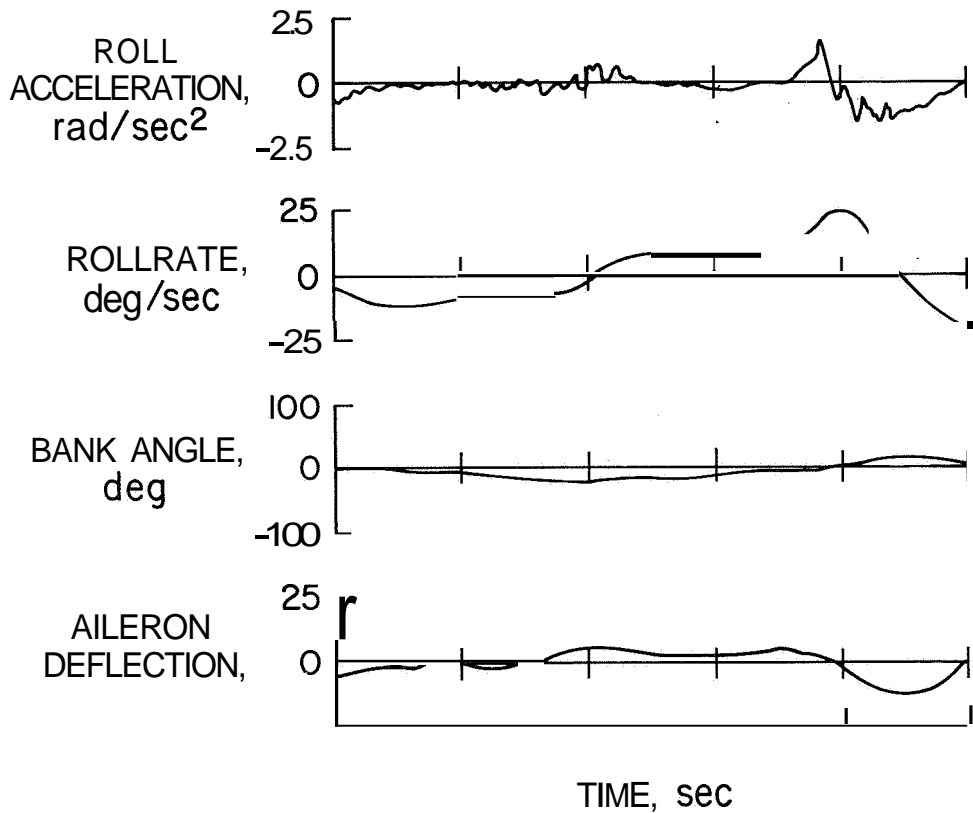
Figure *8.–* Time histories of the Learjet. roll axis responses to the B–747 wake,
vortex;,. separation distance of 4.7 nautical miles; B–747 with landing flaps,
gear up, thrust for level flight.
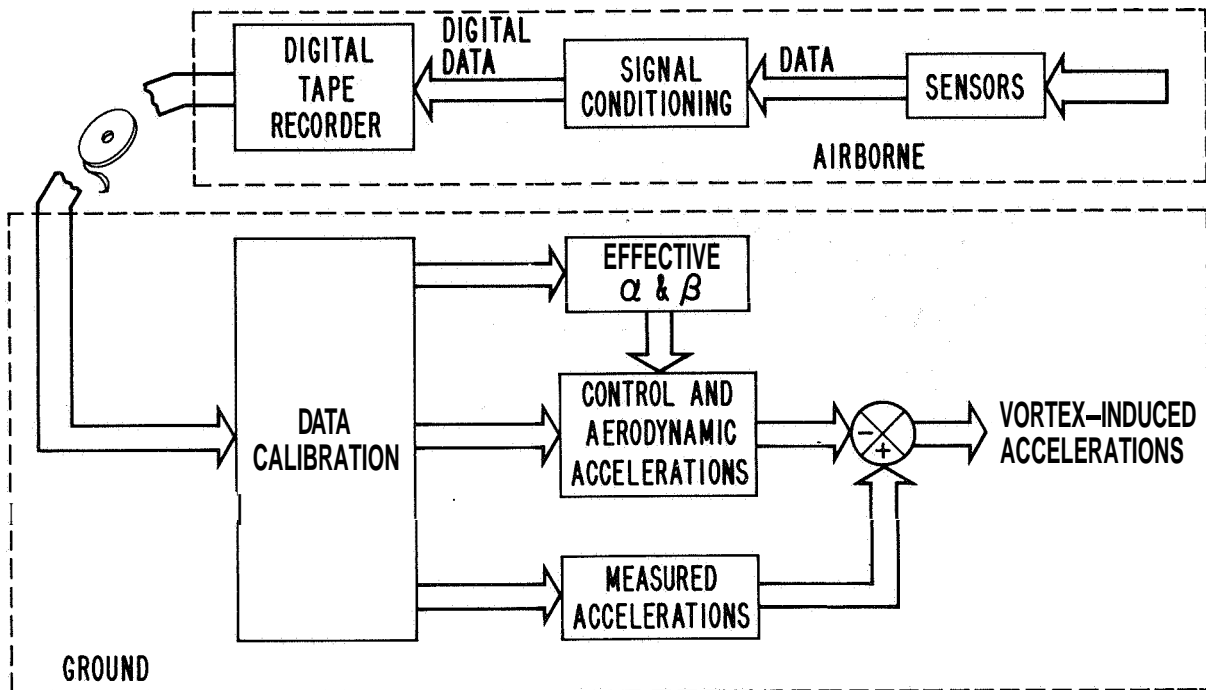
Figure 9.- Block diagram of data-reduction system used for upset measurements.
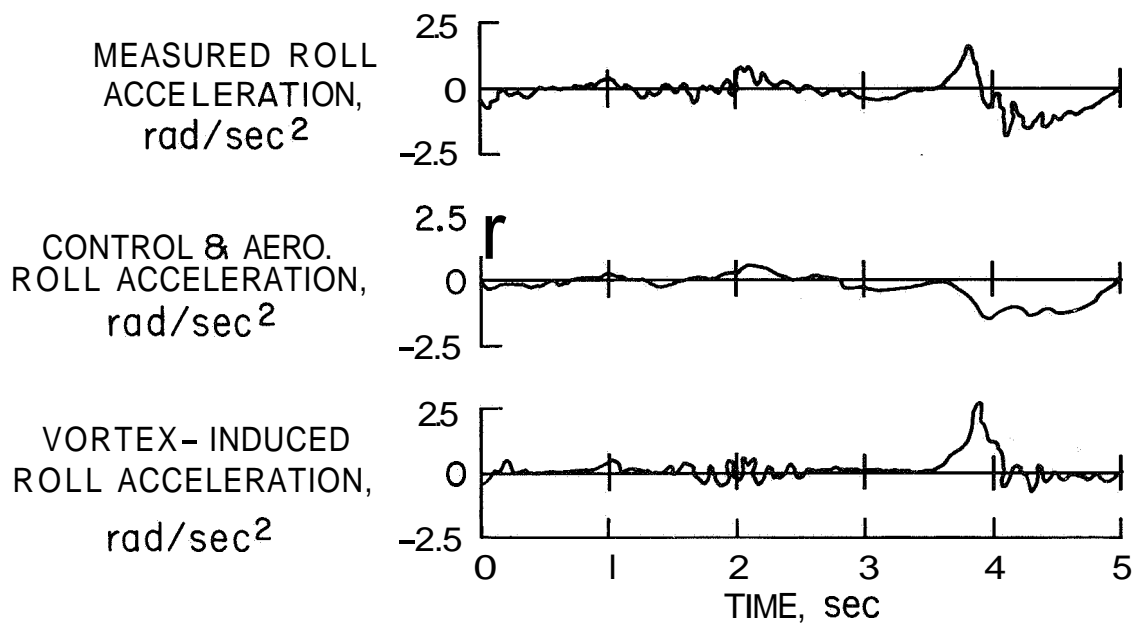


Figure 10.- Time histories of the computed control and aerodynamic roll axis
acceleration and the resulting vortex-induced roll acceleration of the
Learjet for the encounter in figure 8.
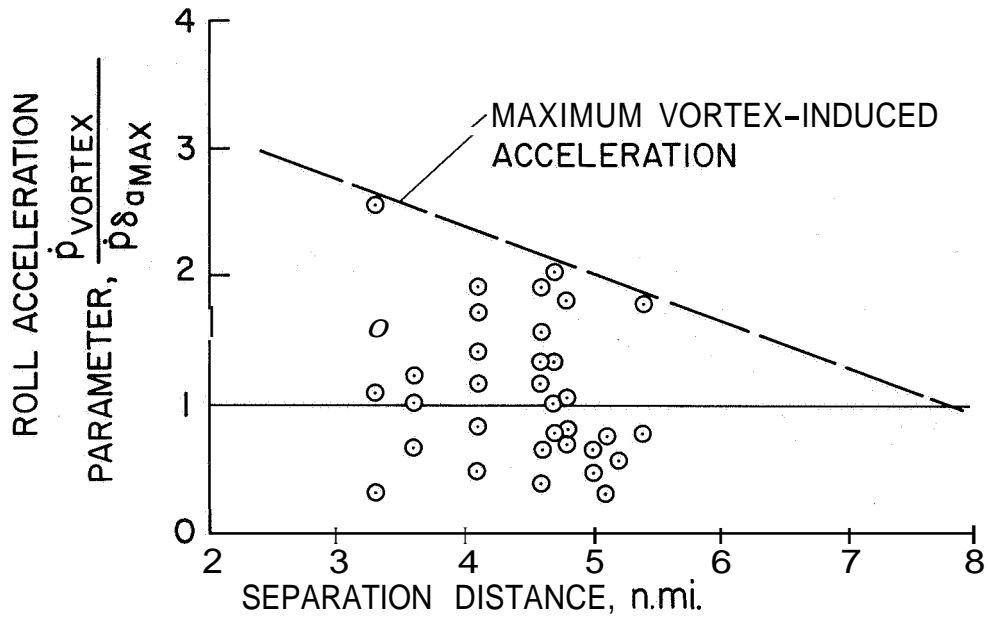
Figure 11.– Roll acceleration parameter versus separation distance for LearJet in the *B-747* wake; *B-747* with flaps down, gear up, thrust for level flight, $C_L = 1.4$.
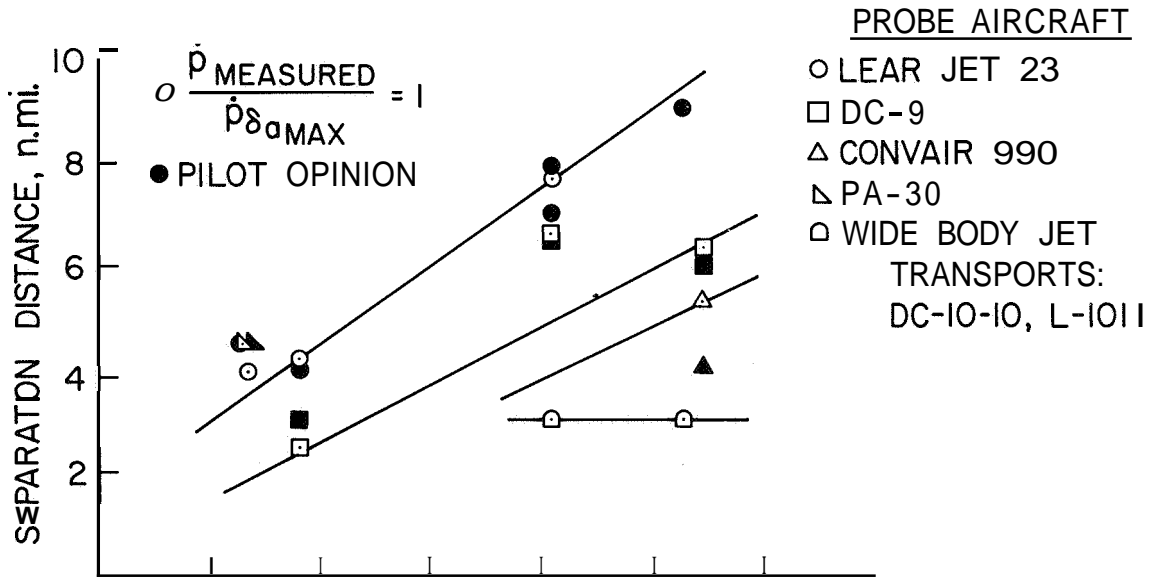


Figure 12.– Comparison of the minimum separation distances based on roll control criteria, for an operational encounter of wake vortices for several probe aircraft.
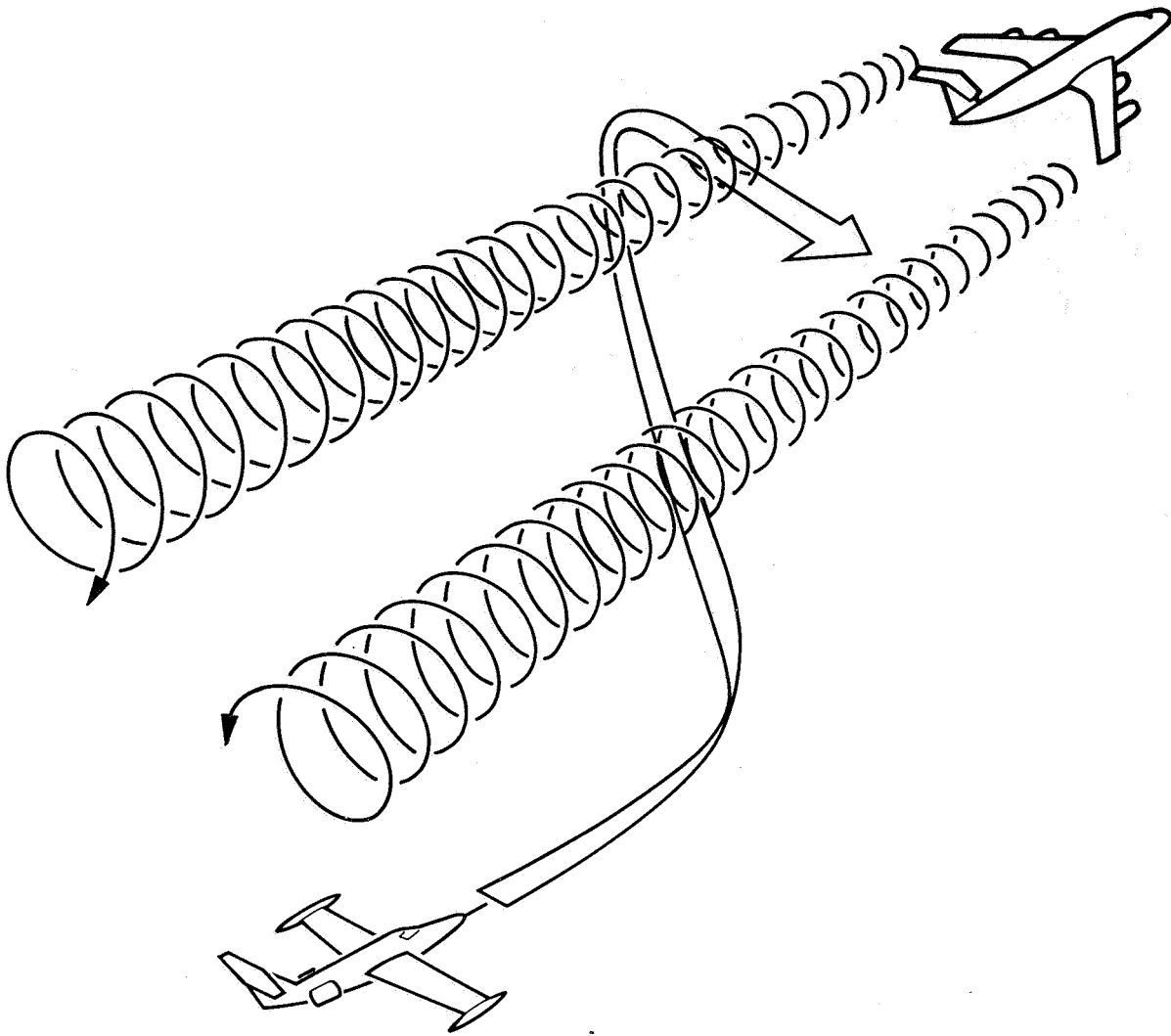
Figure 13.– Probe aircraft flight path during velocity profile measurements of vortex wakes.
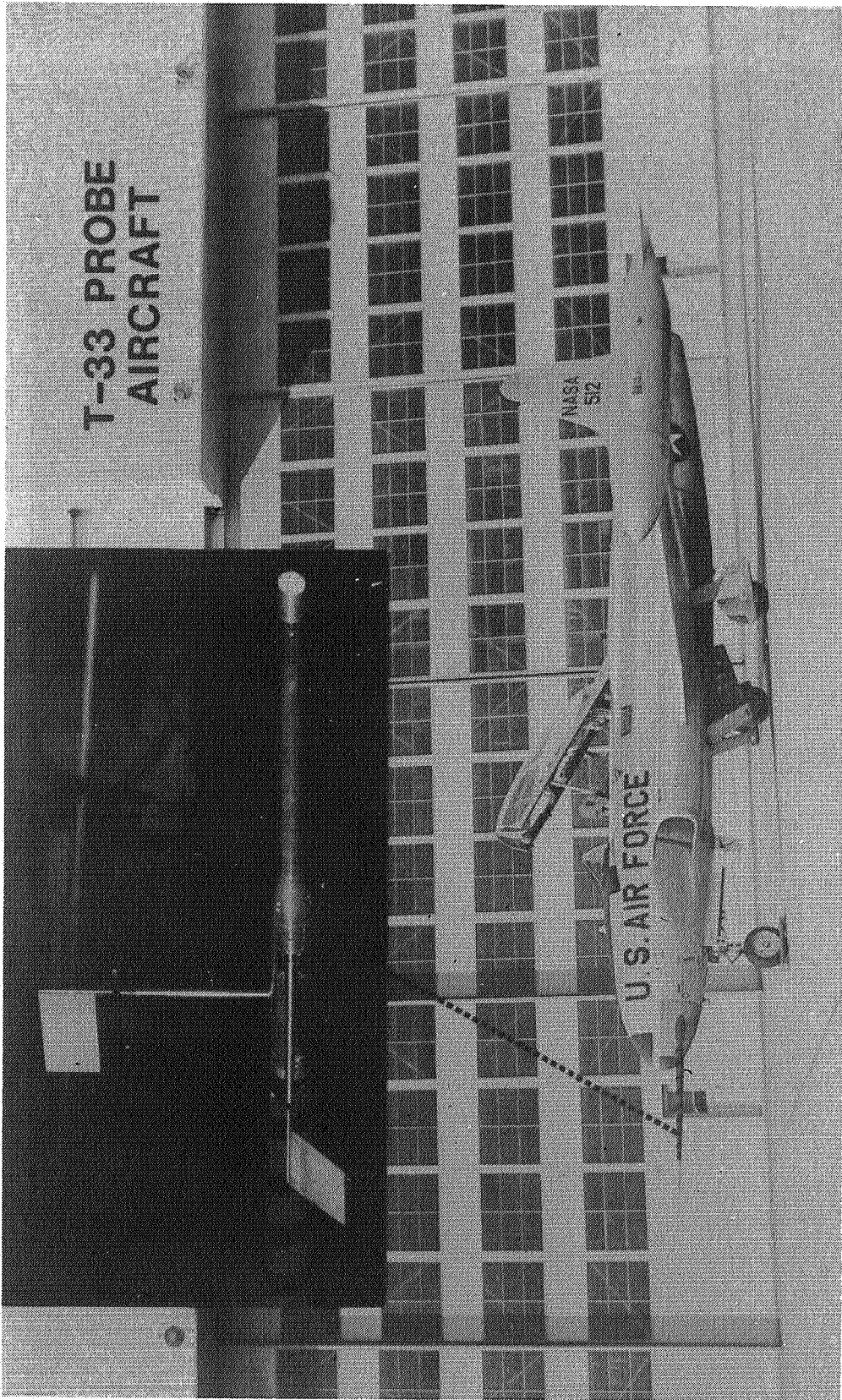
Figure 14.– Flow angularity vanes on nose boom of T-33 probe aircraft.
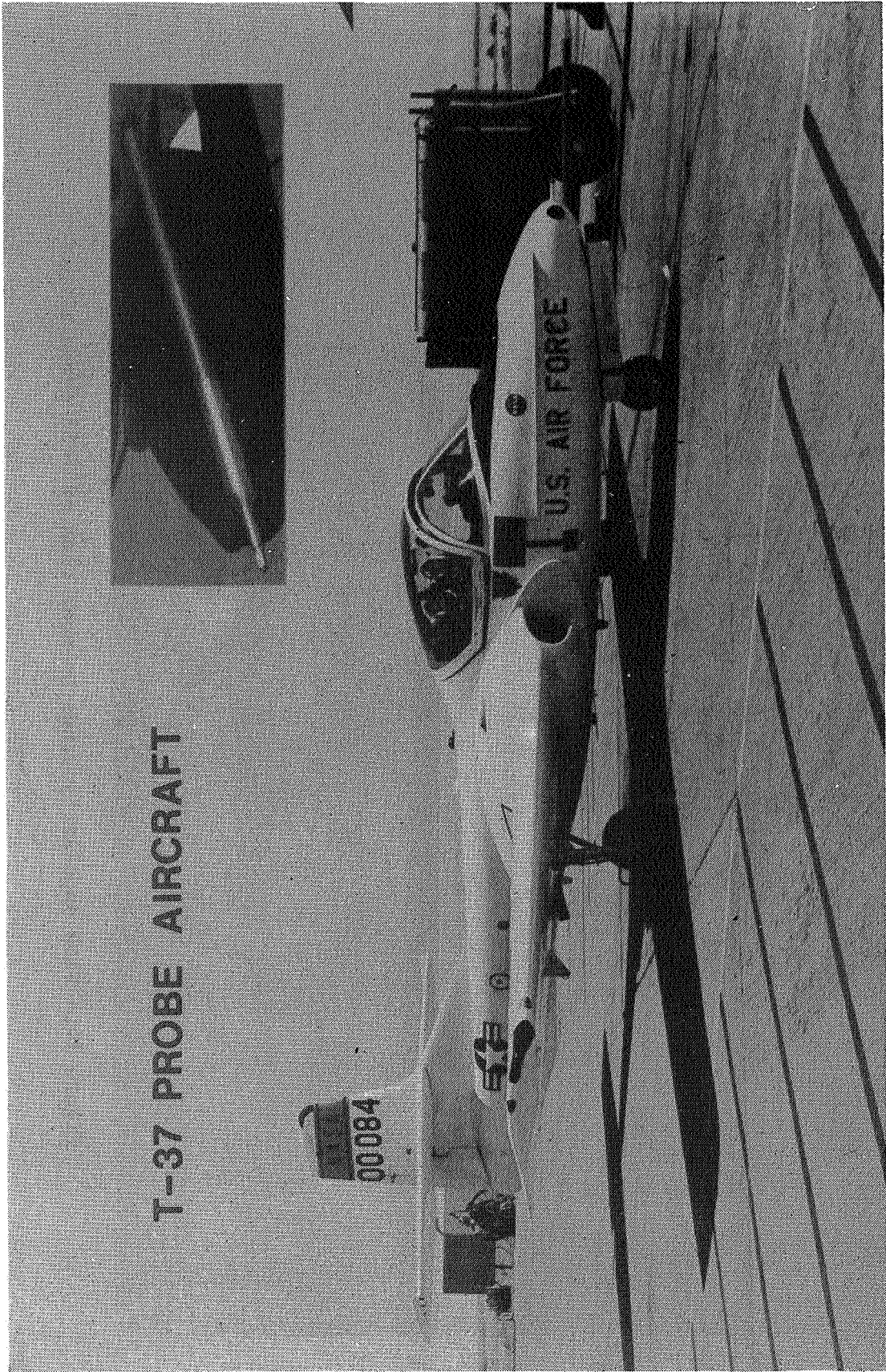
Figure 15.- Five-hole pitot tube on nose boom of T-37 probe aircraft.
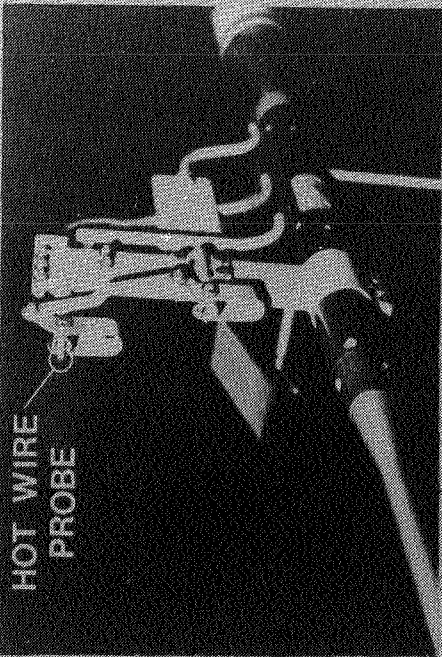
LEARJET PROBE AIRCRAFT
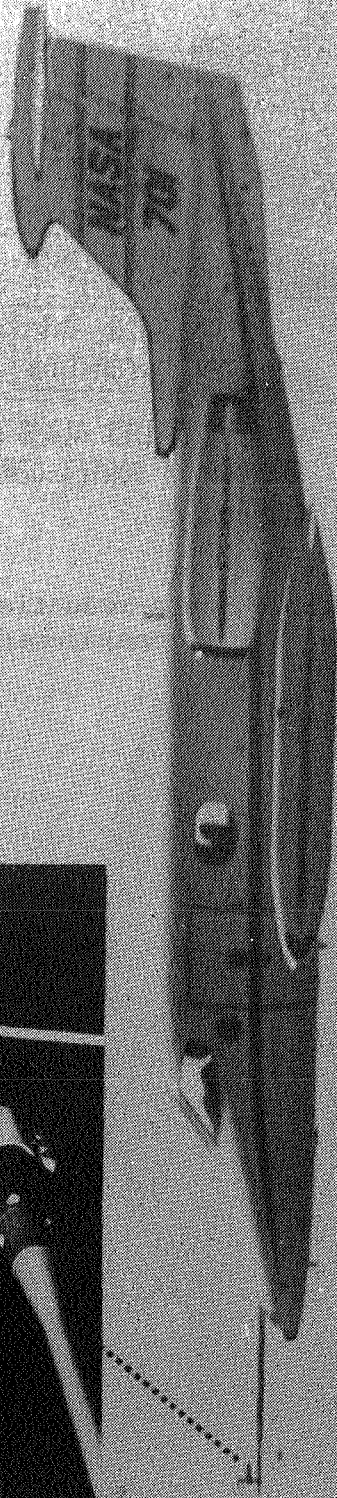
HOT WIRE PROBE

Figure 16.- Hot-wire anemometry probe mounted on nose boom of Learjet probe aircraft.
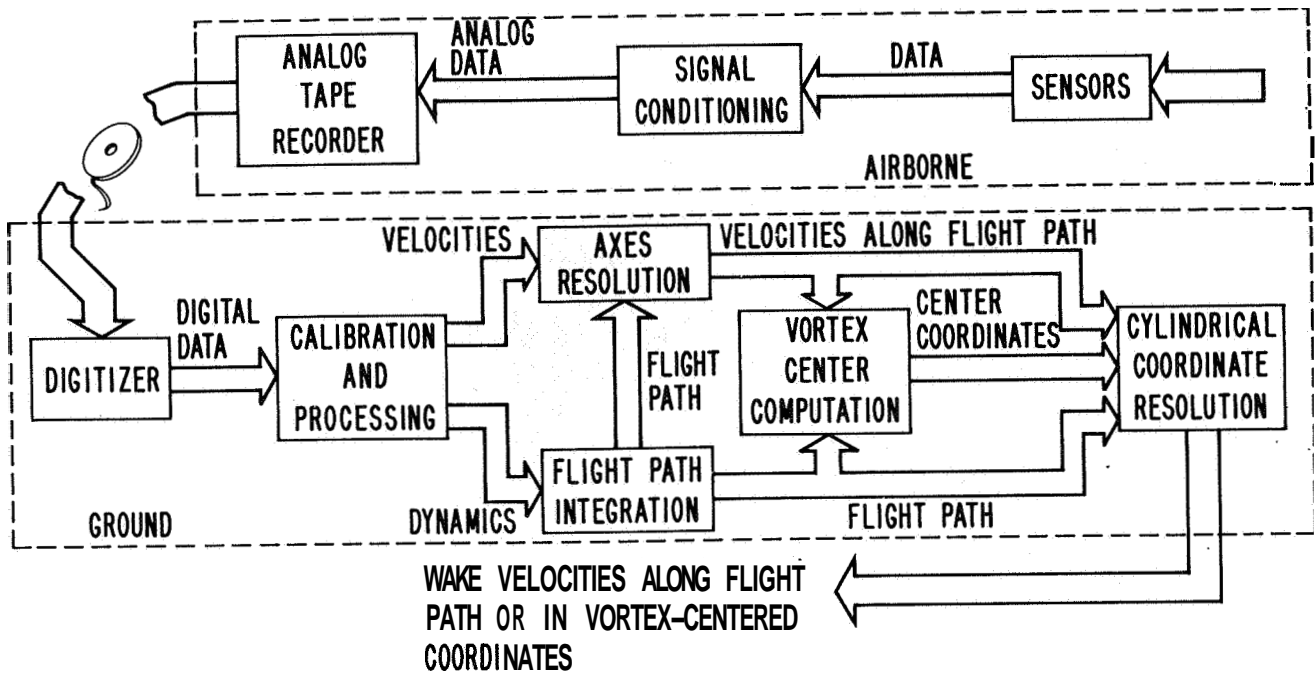
Figure 17.-  Block diagram of data-reduction system used for velocity profile
measurements.

216
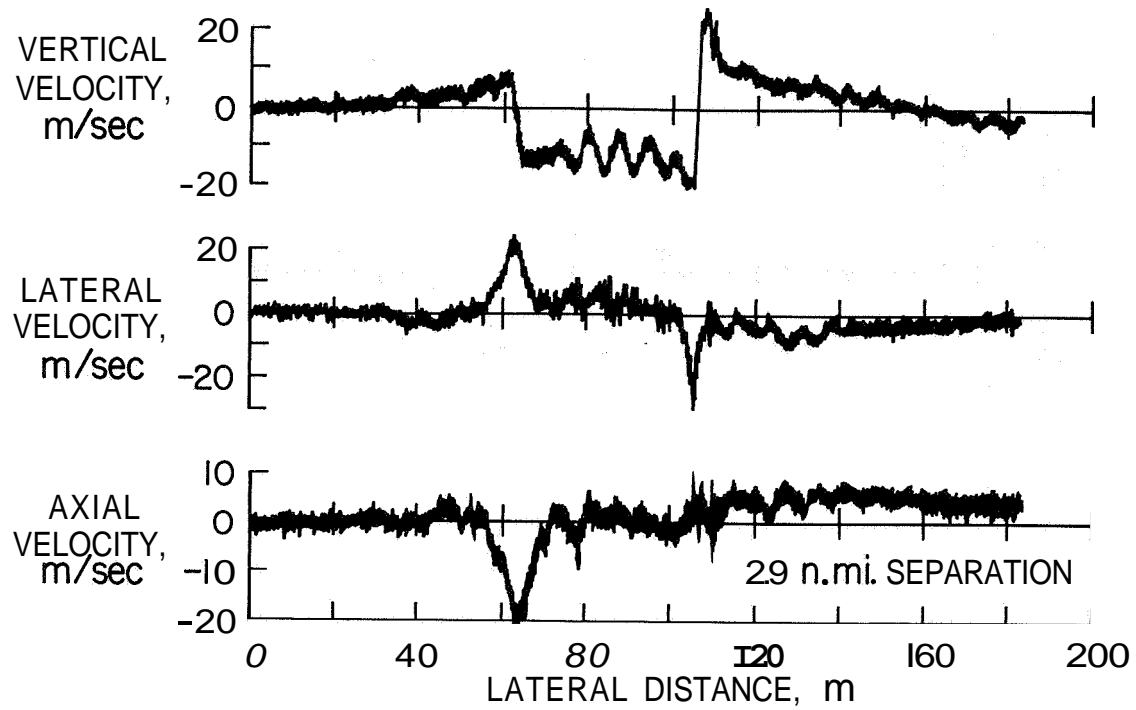
Figure 18.– Vertical, lateral, and axial velocity components in the wake of a B–747 in landing configuration.
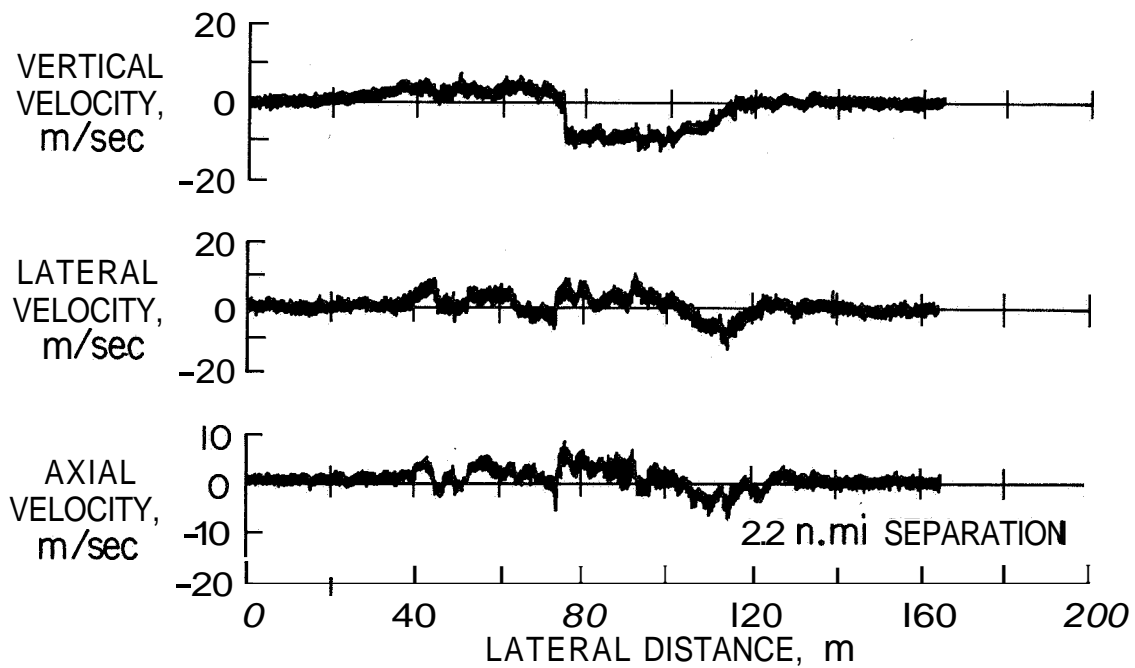


Figure 19.– Vertical, lateral, and axial velocity components in the wake of a B–747 with outboard flap retracted.

217
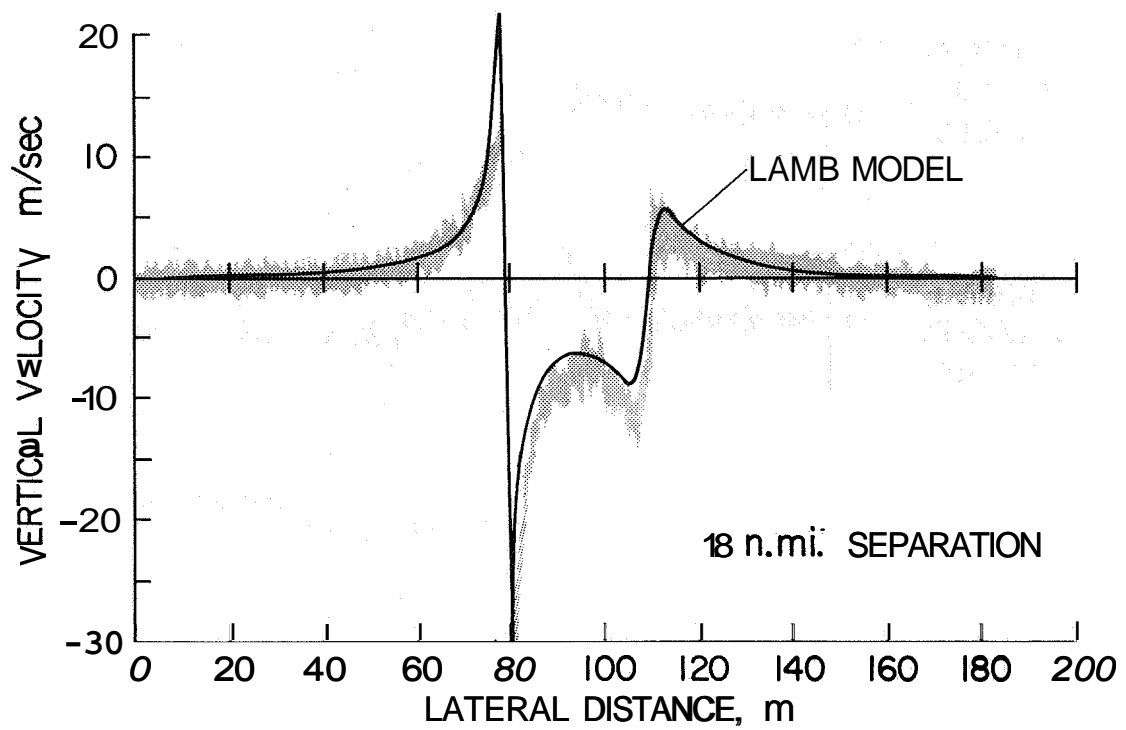
Figure 20.- Vertical velocity distribution measured along the probe aircraft flight path in the wake of a B-727 in takeoff configuration compared to the results of a mathematical model. of a Lamb vortex pair matched to the data.
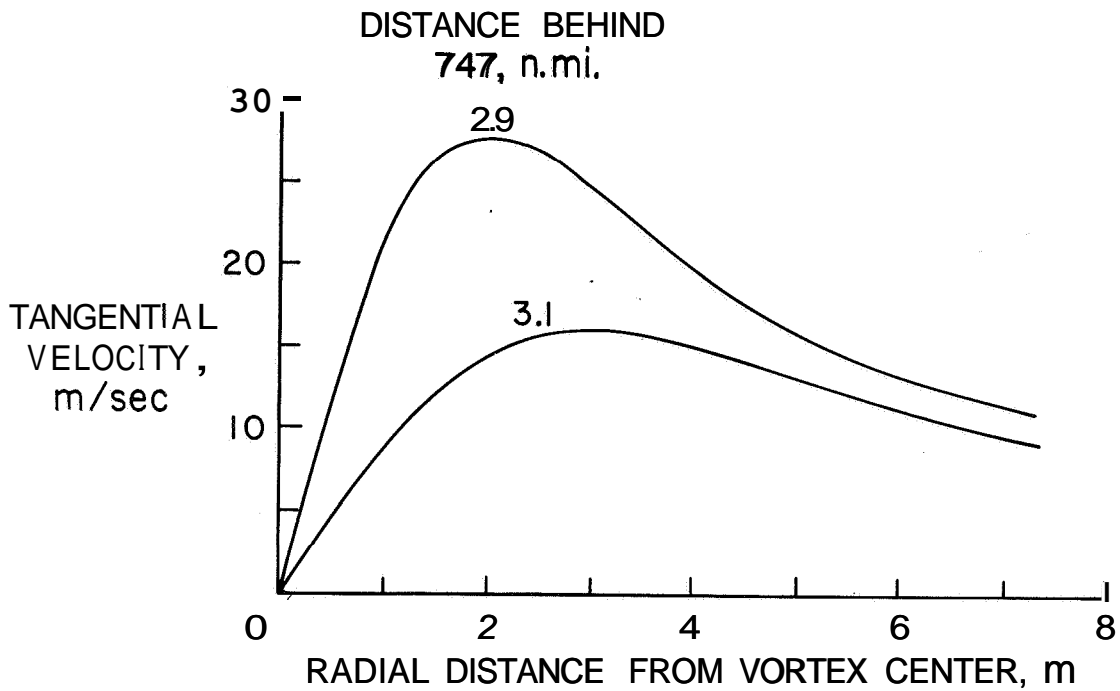
Figure 21.- Decay of a vortex in the wake of a B-747 in landing configuration as indicated by a Lamb vortex model matched to the measured velocities.
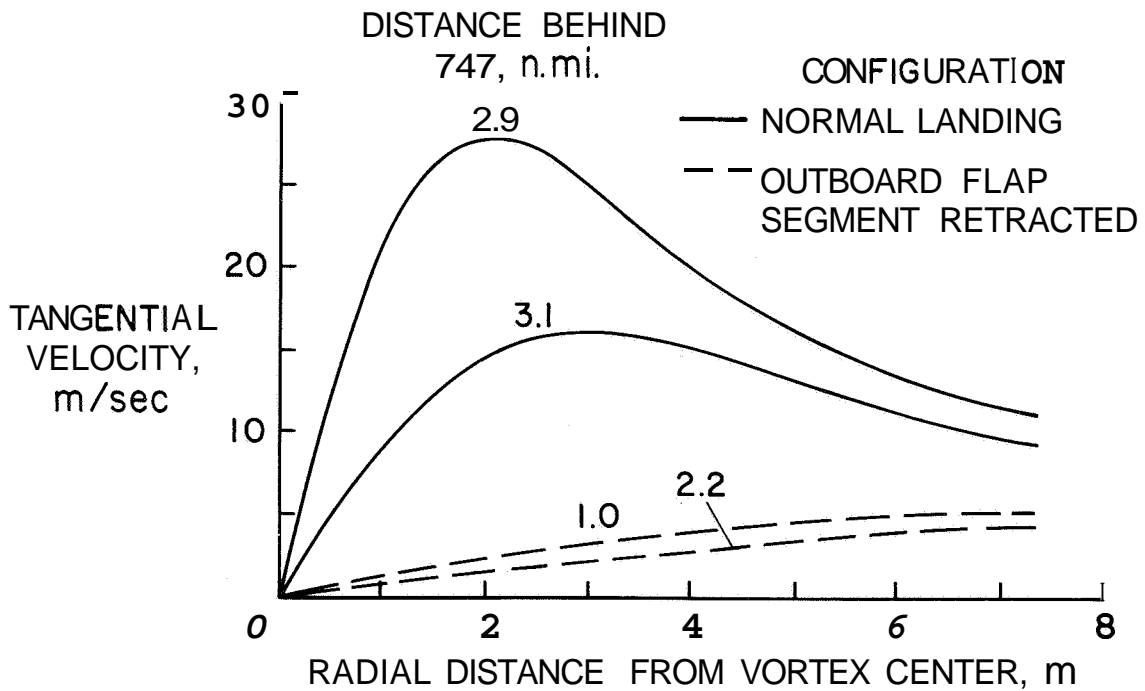


Figure 22.- Alleviation of the velocities in the wake of a B-747 resulting from retraction of the outboard flap segment as indicated by a Lamb vortex model matched to the measured velocities.

# UNSUCCESSFUL CONCEPTS

# FOR AIRCRAFT WAKE VORTEX MINIMIZATION

R. Earl Dunham, Jr.

NASA Langley Research Center

## ABSTRACT

This report describes exploratory concepts investigated by the National Aeronautics and Space Administration to achieve a reduction in the vortex-induced rolling upsets produced by heavy aircraft trailing vortexes. The initial tests included the use of mass injection, oscillating devices, wingtip shape design, interacting multiple vortexes, and end plates. Although later refinements of some of these concepts were successful, initial test results did not indicate a capability of these concepts to significantly alter the vortex-induced rolling upset on a following aircraft.

## INTRODUCTION

The National Aeronautics and Space Administration has been conducting an extensive program to find methods for the reduction of the operational constraints imposed by trailing vortexes from large jet aircraft during terminal-area operations. The research program has involved model tests (refs. 1 to 11), theoretical studies (refs. 12 to 16), and flight tests (refs. 17 to 20) of concepts and techniques that would reduce the rolling upset on a smaller following aircraft. During the course of the research program, several areas were identified as having some success in reducing the

upset on a following aircraft. The injection of turbulence into the vortex has been shown to alter the vortex structure by premature aging and dissipation (refs. 17 and 21). The combined effects of the turbulence and momentum impulse from jet engines have been shown to change the vortex structure (ref. 22). In addition to turbulence injection, the far–field structure of trailing vortexes can be affected by alteration of the span–load distribution to shed multiple vortexes (refs. 9, **23,** and 24), which mutually interact to reduce the vortex strength. The combined effects of turbulence injection and span–load alteration were investigated through the use of spoilers (refs. 9, 10, 20, and 25).

During the development of these promising techniques, several concepts and ideas investigated were shown to alter the trailing vortex structure in varying degrees without significantly altering the upset experienced by a following aircraft. This paper summarizes the numerous concepts investigated that did not meet the primary program objective of achieving a reduction in the vortex–induced rolling upset on a following aircraft.

## SYMBOLS

$b_f$   wingspan of following model used to measure rolling moment, m

$b_g$   wingspan of vortex generator model, m

c   local wing chord, m

$C_{\ell,f}$   rolling-moment coefficient on following model, $2M/\rho S_f b_f V_0^2$

$C_{\dot{m}}$   mass rate coefficient, $\dot{m}/\rho S_g V_0$

$C_\mu$   momentum coefficient, $2\dot{m}V_j/\rho S_g V_0^2$

$\dot{m}$   mass rate, kg/s

M   measured rolling moment, N–m

r   distance from center of vortex, m

$S_f$   wing area of following model used to measure rolling moment, $m^2$

$S_g$   wing area of vortex generator model, $m^2$

$V_j$   jet velocity, m/s

$V_0$   free–stream velocity, m/s

$V_\theta$    tangential velocity in a vortex, m/s

X    downstream distance behind the vortex generator model, m

$\rho$    fluid density, $kg/m^3$

## PRESENTATION OF RESULTS

In general, the investigation of a particular concept began with a preliminary evaluation through the flow visualization of the vortex pattern with and without the vortex–alleviation concept. All of the test facilities used in the vortex minimization program (wing tunnels and water and air tow facilities (ref. 26)) provided an adequate visual assessment of the vortex alleviation capabilities of a particular concept. If the initial flow visualization indicated a change in the vortex structure, a quantitative assessment of the effectiveness was undertaken. The quantitative assessment was obtained by detailed velocity measurements or, as described in reference 26, by a determination of the vortex–induced rolling moment imposed on a trailing wing model.

It was assumed during flow–visualization studies that, in order for a concept to be effective in reducing the vortex rolling upset on a following aircraft, a large visual change in the vortex flow would be detectable. Several concepts were eliminated from further consideration on their inability to visually alter the vortex flow pattern. Conversely, some concepts were found to visually alter the flow while causing a measurable change in the vortex velocity distribution, without significantly reducing the rolling upset on a trailing wing. Additionally, certain techniques that were evaluated on straight wings were found to be less effective when applied to the multiple, diffuse vortex system shed by a flapped, swept, large transporttype wing.

Many of the concepts described in this paper, although unsuitable for minimization of the vortex hazard behind a large transport aircraft, may have other vortex–related aerodynamic benefits. Two possible benefits are the reduction of vortex–induced helicopter blade loads caused by the impingement of the preceding–blade vortex (blade slap) and the reduction of aircraft cruise drag. It may be possible to further refine some of the techniques described

223

to achieve an acceptable reduction in vortex–induced upset. In fact, some of the unsuccessful concepts explored were later refined to the stage of successful application.

The concepts and techniques describe have been divided into two broad categories for discussion: (1) active devices and (2) passive devices. The active devices attempted to alter the vortex by emitting either a sheet or jet of air at various positions on the wing, or through oscillating devices to create an instability in the shed vortex sheet. The passive devices attempted to alter the vortex by controlling or altering the flow about the wing.

## Active Devices

### *Blowing Concepts*

Use of mass injection or air blowing was explored in many different forms. The simplest form of blowing consisted of an air jet located so as to inject air in the vortex axial direction. This concept, as it was evaluated on a straight wing, is shown in figure 1. Flow visualization studies conducted during the initial evaluation of this concept (ref. 27) indicated a visual alteration in the vortex structure as blowing increased. Hot–wire anemometer measurements of the vortex tangential velocity distribution, with and without blowing, are shown in figure 2. The data indicate a significant reduction in peak tangential velocity; however, rolling-moment measurements of the vortex–induced roll on a following model, using the technique described in reference 26 and shown in figure 3, indicated no apparent reduction as blowing increased. Although a significant reduction in the vortex imposed rolling moment could not be achieved with this concept, the achievable reduction in peak vortex tangential velocity (fig. 2) may be significant when applied to the vortex impingement blade–slap problem of helicopters.

The jet blowing concept was evaluated on a swept–wing transport model. It was envisioned that the jet would be provided by a small engine located

on the wingtip. The wingtip–mounted engines, shown on the transport model in figure *4,* were **small** compared to the propulsion engines and would provide only about 8 to 10 percent of the thrust required for cruise. No detectable reduction in vortex–imposed rolling moment was measured during the evaluation of the wingtip–mounted engines. Because the large mass flow and thrust levels of the jet engines of transport aircraft have been shown to alter the character of the trailing vortex system (ref. 22), one of the reasons for the inability of the wingtip–mounted engines (fig. *4)* or the jet blowing (fig. 1) to reduce the vortex hazard was the relatively low mass flow and momentum coefficients used for these tests ($C_{\dot{m}} = 0.0008$ and $C_{\mu} = 0.02$).

Several techniques for blowing a sheet of air from a wingtip to inhibit the formation of the vortex have been tried. Figure 5 illustrates two techniques that were evaluated on a straight–wing model to inhibit the wingtip vortex formation. Figure 5(a) illustrates the means by which a chordwise sheet of air was blown downward from the wingtip, while figure 5(b) shows how a tube was extended from the trailing edge of the wingtip to blow a sheet of air downward in the spanwise direction. Vortex–induced rolling–moment measurements obtained on a following model 7.5 span lengths behind the generating model, with these two techniques, are shown in figure 6. Spanwise blowing was found to be the most effective. The results of a detailed study of the spanwise blowing concept (fig. 5(b)) are described in reference 28. As reported in reference 28 and shown in figure 7, the spanwise blowing provided a significant improvement in the wing lift/drag ratio.

The spanwise tip blowing concept was evaluated on a large jet transport model in the manner illustrated in figure 8. The spanwise blowing concept was found to provide an improvement in the clean wing (cruise configuration) lift-to-drag ratio of the jet transport model, as shown in figure 9. However, the measured improvement in lift–to–drag ratio was not as large as that found for the straight–wing tests of reference 28. In addition, no significant change in the lift–to–drag ratio of the flaps–down (landing approach) configuration of the transport model due to spanwise blowing was noted. The vortex–induced rolling moment on a small–wing model ($b_f/b_g = 0.182$) behind the transport model, for both the flap–down and clean–wing configuration, as a function of

increased spanwise blowing is shown in figure 10. The data show a small reduction in rolling moment as blowing is increased for the cruise configuration; however, no effect was noted for the flap-down configuration. Because the flap-down configuration creates a complex vortex structure made up of wingtip and flap vortexes, it was expected that spanwise blowing at only the wingtip might not influence the large flap vortex. Some tests were conducted using a crude implementation of the spanwise blowing concept on the outboard edges of the flaps. These tests did not show a reduction in rolling moment for the flap-down configuration.

Other variations of blowing techniques have been investigated and are illustrated in figure 11. Hot-wire measurements behind these configurations (ref. 6) indicated a reduction in the peak tangential velocity for the cruise configuration, but no reduction was noted for the flaps-down configuration. The inability of the configurations shown in figure 11 to alter the vortex structure for the flap-down configuration is probably due to the low momentum and mass flow used and the implementation of these concepts at the wingtip.

*Oscillating Devices*

Introduction of a cyclic disturbance into the shed vortex sheet was investigated in an attempt to trigger a dynamic instability within the flow field that would lead to its collapse. Velocity measurements of the jet mass-injection technique (fig. 2) indicated an ability to alter the details of the vortex core, and effects of cyclically varying the jet by turning it on and off with a highly responsive valve were investigated. The jet could be pulsed to provide a jet on time of 2 to 14 wingspans behind the model and a jet off time of between 2 and 60 span lengths behind the model. The mass flow and momentum of the jet for the time the valve was open were similar to those used in the test setup of figure 1. The pulsating jet did not appear to induce a visual instability in the vortex.

Tests were conducted of a small oscillating spoiler on a large transport model, as illustrated in figure 12. The spoiler could be cyclically deployed

226

4

so as to introduce a disturbance wave of 1.5 to **13** spans behind the vortex generator model. This spoiler was located in a different position and was smaller than the successful spoiler concept reported in reference 25. The oscillating spoiler was found ineffective in altering the vortex pattern shed by the transport model in a flaps–down landing approach configuration. Apparently, because of its position on the wing, the disturbance shed by the spoiler was not being introduced into the vortex system for the flap–down configuration. The oscillating spoiler altered the vortex pattern shed by the transport model in a flaps–up cruise configuration, as illustrated in figure 13. While the spoiler was deployed, the vortex core diameter was apparently increased; and while the spoiler was down, the vortex core was unaffected. **As** shown in figure **13,** the oscillating spoiler produced a vortex of varying core diameter immediately behind the aircraft. The effects of the spoiler were washed out beyond about six spans behind the aircraft. The rolling moment on a trailing aircraft model was found to be reduced over the test range of 6 to *45* spans behind the transport aircraft; however, the reduction was independent of the frequency of oscillation. The same reduction also could be achieved by leaving the spoiler in the deployed position. Tests were unsuccessful in exciting a vortex instability.

These two oscillating techniques introduced longitudinal disturbances in the vortex. Cyclic variation of the load distribution, so as to oscillate the centroid of vorticity of the wing to produce a variation of the vortex spacing and provide a lateral disturbance, has been investigated. The results of these tests are presented in reference 29. As reported in reference 29, the Crow instability (ref. 30) can be initiated. It is felt that for the modest shifts in load distribution that can be obtained on operational aircraft, the shift in vortex spacing would be small and the time required for the instability to continue to linking and vortex breakup would be too long to significantly alter the vortex hazard.

## Passive Devices

The use of end plates and variations of the end-plate concept have been investigated. Figure 14 shows three end-plate concepts evaluated. During flow visualization studies, the basic end plate (fig. 14(a)) was found to slightly inhibit the rollup of the vortex sheet shed by the wing; however, after the rollup was complete, the vortex structure did not appear to be different than without the end plate. A variant of the end plate is the body of revolution (fig. 14(b)) that had an opening in the center to allow a mixing of the flow which passed through the center with the exterior flow. This device was observed to alter the vortex only slightly. To increase the mixing between the fluid that passed through the body of revoluion and exterior flow, turning vanes (fig. 14(c)) were placed inside the body of revolution to impart a swirl opposite the vortex. The turning vanes did not visibly alter the vortex.

A very efficient end-plate design known as a "winglet," which was developed for improved cruise efficiency, was evaluated to determine its effect on the trailing vortex structure. Figure 15 is a photograph of winglets as installed on the large jet transport model. Results indicate that for their intended design a reduction of cruise drag of about 8 percent was achieved on a second-generation transport model. Tests conducted in the Langley Research Center's Vortex Research Facility (ref. 26) indicated that the winglets reduced the rolling moment on a trailing wing 10 to 15 percent for the transport in a clean-wing cruise configuration. Tests conducted with the transport model in a flaps-down landing approach configuration showed no reduction of the vortex system due to the wingtip-mounted winglets. No attempt was made to implement the winglets on the flap system of the transport aircraft.

Reduction of the loading gradient at the wingtip has been investigated using the wingtip design (ogee tip) shown in figure 16. Figure 17 shows the reduction in peak tangential velocity measured at one span behind the ogee tip. Simple strip-theory calculations from the vortex velocity distribution (fig. 17) of the vortex-imposed rolling moment on a trailing aircraft showed

very little reduction in rolling moment. Consequently, the concept was not considered suitable for minimization of the wake vortex hazard. However, the ogee tip, along with other concepts that reduce the vortex–peak tangential velocity without reducing significantly the vortex imposed rolling moment on a trailing aircraft, may have other vortex–related applications. In particular, the blade–slap problem for helicopter operations is related to the passage of a rotor blade through the large velocity gradients associated with the vortex from a preceding blade. The ogee tip has shown some promise in reducing helicopter blade slap.

Another technique investigated for vortex alleviation was to extract rotational energy from the vortex system by trailing a set of large fixed-crossed blades attached to the wingtip to inhibit the vortex rotation (fig. 18). Velocity distributions obtained 2.5 spans behind the crossed blades are shown in figure 19. The alteration in vortex velocity distribution (fig. 19) would not produce a significant reduction in the vortex–imposed rolling moment on a trailing aircraft.

Initial tests of wingtip devices and vortex generators to produce multiple vortexes that will interact have been conducted (fig. 20). Flow visualization studies on a straight–wing model, of the two techniques shown in figures 20(a) and 20(b), indicated little beneficial effect from the interaction of multiple vortexes. Rolling–moment measurement obtained on a model behind the multiple vortex system, shown in figure 20(c), indicated no reduction in the vortex hazard. Later, more successful tests of the interaction of multiple vortex systems, obtained by alteration of the lift distribution (ref. 24), indicate a requirement to maintain the proper vortex strength and spacing to produce successful interactions of vortexes. The theoretical efforts described in reference 16 provide an indication as to the required relationship for spacings and strengths of multiple vortexes to achieve vortex merging and dissipation.

## CONCLUDING **REMARKS**

During the conduct of the NASA program to develop vortex minimization schemes, numerous concepts were evaluated that were not capable of achieving a significant reduction of the vortex–imposed rolling moment on a trailing aircraft. Early tests indicated that the use of mass injection at momentum and mass flow levels significantly lower than that used for cruise propulsion would not significantly reduce the vortex hazard. Initial tests also indicated that the beneficial interaction of multiple vortexes required the proper relationship between spacing and strength. Although several concepts were not capable of achieving a significant reduction of the vortex hazard, they were shown to be capable of reducing the induced drag for cruise performance improvement. Tests to date have been unable to excite a dynamic instability of the vortex system by using a cyclic–disturbance input.

## REFERENCES

1.   Chigier, N. A.; and Corsiglia, V. R.:  Tip Vortices – Velocity Distribution.  NASA TM X–62087, 1971.

2.   Chigier, N. A.; and Corsiglia, V. R.: Wind–Tunnel Studies of Wing Wake Turbulence.  J. Aircraft, vol. 9, no. 12, 1972, pp. 820–825.

3.   Corsiglia, V. R.; Schwind, R. K.; and Chigier, N. A.:  Rapid Scanning Three–Dimensional Hot–wire Anemometer Surveys of Wingtip Vortices.  J. Aircraft, vol. 10, no. 12, 1973, pp. 752–757.

4.   Orloff, K. L.; and Grant, G. R.:  The Application of a Scanning Laser Doppler Velocimeter to Trailing Vortex Definition and Alleviation.  AIAA paper 73–680, 1973.

5.   Corsiglia, V. R.; Jacobsen, R. A.; and Chigier, N. A.:  An Experimental Investigation of Trailing Vortices Behind a Wing With a Vortex

Dissipator. Aircraft Wake Turbulence and Its Detection, J. Olsen, A. Goldberg, and M. Rodgers, eds., Plenum Press, Inc., 1971, pp. 229–242.

6.  Kirkman, K. L.; Brown, C. E.; and Goodman, A.: Evaluation of Effectiveness of Various Devices for Attenuation of Trailing Vortices Based on Model Tests in a Large Towing Basin. NASA CR–2202, 1973.

7.  Croom, Delwin R.: Low–Speed Wind–Tunnel Investigation of Forward–Located Spoilers and Trailing Splines as Trailing Vortex Hazard–Alleviation Devices on an Aspect–Ratio–8 Wing Model. NASA TM X–3166, 1975.

8.  Rossow, V. J.; Corsiglia, V. R.; Schwind, R. G.; Frick, J. K. D.; and Lemmer, O. J.: Velocity and Rolling Moment Measurements in the Wake of a Swept–Wing Model in the 40– by 80–Foot Wind–Tunnel. NASA TM X–62414, 1975.

9.  Croom, D. R.; and Dunham, R. E., Jr.: Low–Speed Wind–Tunnel Investigation of Span–Load Alteration, Forward–Located Spoilers, and Splines as Trailing Vortex Hazard Alleviation Devices on a Transport Aircraft Model. NASA TN D–8133, 1975.

10. Croom, D. R.: Low–Speed Wind Tunnel Investigation of Flight Spoilers as Trailing Vortex Hazard–Alleviation Devices on a Transport Aircraft Model. NASA TN D–8162, 1976.

11. Patterson, J. C., Jr.: Vortex Attenuation Obtained in the Langley Vortex Research Facility. J. Aircraft, vol. 12, no. 9, Sept. 1975, pp. 745–749.

12. Rossow, V. J.: On the Inviscid Rolled–up Structure of Lift–Generated Devices. J. Aircraft, vol. 10, Feb. 1973, pp. 86–92.

13. Brown, C. E.: Aerodynamics of Wake Vortices. AIAA J., vol. 11, Apr. 1973, pp. 531–536.

14. Rossow, V. J.: Theoretical Study of Lift–Generated Vortex Wakes Designed to Avoid Rollup. AIAA J., vol. 13, no. 4, Apr. 1975, pp. 476–484.

15. Rossow, V. J.: Inviscid Modeling of Aircraft Trailing Vortices. Wake Vortex Minimization. NASA SP–409, 1977.

16. Bilanin, A. J.; Teske, M. E.; Donaldson, C. duP., Snedeker, R. S.: Viscous Effects in Aircraft Trailing Vortices. Wake Vortex Minimization. NASA SP–409, 1977.

17. Hastings, E. C., Jr.; Patterson, J. C., Jr.; Shanks, R. E.; Champine, R. A.; Copeland, W. L.; and Young, D. C.: Development and Flight Tests of Vortex Attenuating Splines. NASA TN D–8083, 1975.

18. Smith, H. J.: A Flight Test Investigation of the Rolling Moments Induced on a T–37B Airplane in the Wake of a B–747 Airplane. NASA TM X–56031, 1975.

19. Tymczyszyn, J. J.; and Barber, M. R.: Recent Wake Turbulence Flight–Test Programs. Paper presented at the 18th Annual Symp. Soc. Experiment Test Pilots (Beverly Hills, Calif.), Sept, 26, 1974.

20. Barber, M. R.; Hastings, E. C., Jr.; Champine, R. A.; and Tymczyszyn, J. J.: Vortex Attenuation Flight Experiments. Wake Vortex Minimization. NASA SP–409, 1977.

21. Patterson, J. C., Jr.; Hastings, E. C., Jr.; and Jordan, F. L., Jr.: Ground Development and Flight Correlation of the Vortex Attenuating Spline Device. NASA SP–409, 1977.

22. Patterson, J. C., **Jr.**; and Jordan, F. L., **Jr.**: Thrust–Augmented Vortex Attenuation, Wake Vortex Minimization. NASA **SP–409, 1977.**

23. Ciffone, D. **L.**; and Lonzo, C., **Jr.**: Flow Visualization of Vortex Interaction in Multiple Vortex Wakes Behind Aircraft. NASA TM **X–62459, 1975.**

24. Corsiglia, V. **R.**; and Dunham, R. E., **Jr.**: Aircraft Wake–Vortex Minimization by Use of Flaps. Wake Vortex Minimization. NASA **SP–409, 1977.**

25. Croom, D. R.: The Development and Use of Spoilers as Vortex Attenuators. Wake Vortex Minimization. NASA **SP–409, 1977.**

26. Stickle, **J.** W.; and Kelly, M. W.: Ground–Based Facilities for Evaluating Vortex Minimization Concepts. NASA **SP–409, 1977.**

27. White, **R.** P., **Jr.**; and Balcerak, **J.** C.: An Investigation of the Mixing of Linear and Swirling Flows. -Report **72–04,** Rochester Applied Science Associates, Inc., Feb. **1972.**

28. Yuan, **S.** W.; and Bloom, A. M.: Experimental Investigation of Wingtip Vortex Abatement. Ninth Congr. Int. Council Aeronaut. Sci., Haifa, Israel, Aug. **25–30, 1974.**

29. Bilanin, A. **J.**; and Widnall, S. E.: Aircraft Wake Dissipation by Sinusordial Instability and Vortex Breakdown. AIAA paper **73–107,** 11th Aerosp. Sci. Meeting, Jan. **1973.**

30. Crow, **S.** C.: Stability Theory for a Pair of Trailing Vortices. AIAA J., vol. **8,** Dec. **1970,** pp. **2172–2179.**
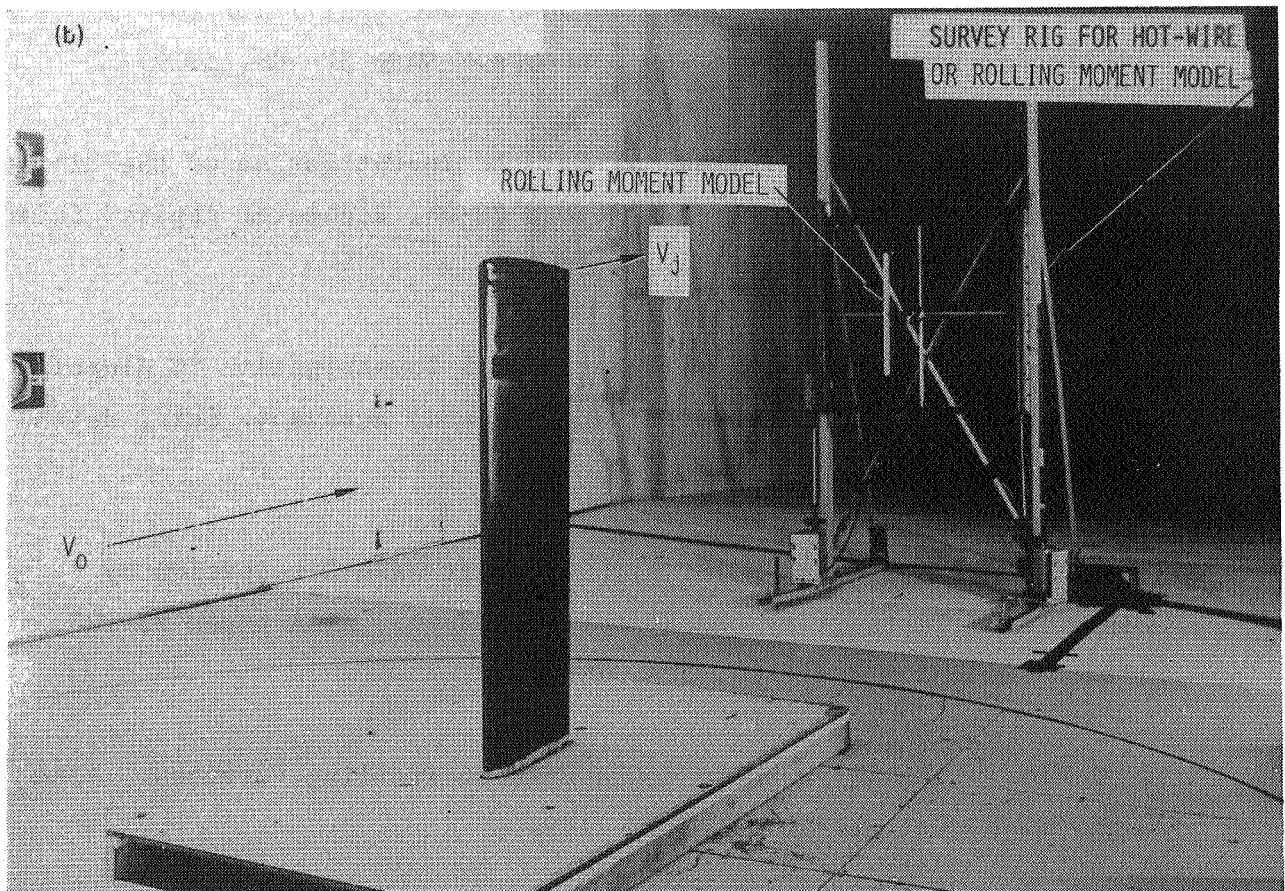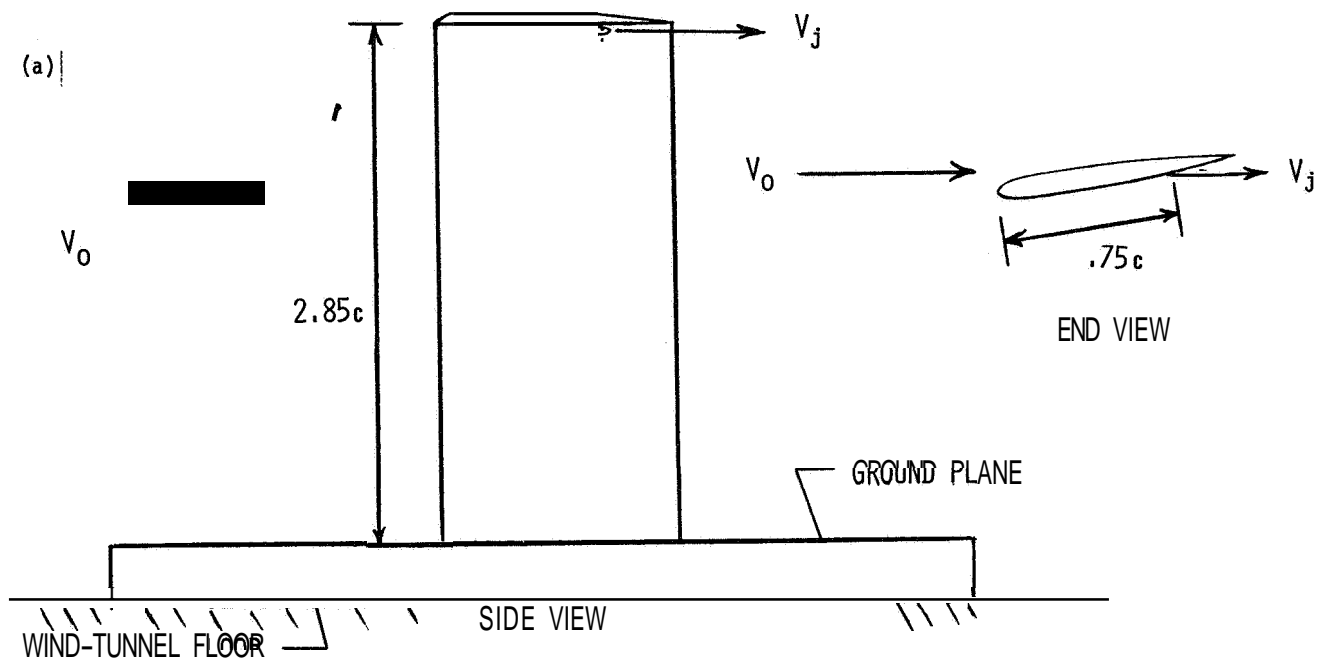
Figure 1.--Model and test setup used for the evaluation of axial mass injection.
(a) Diagram of model. (b) Photograph of test setup.

234
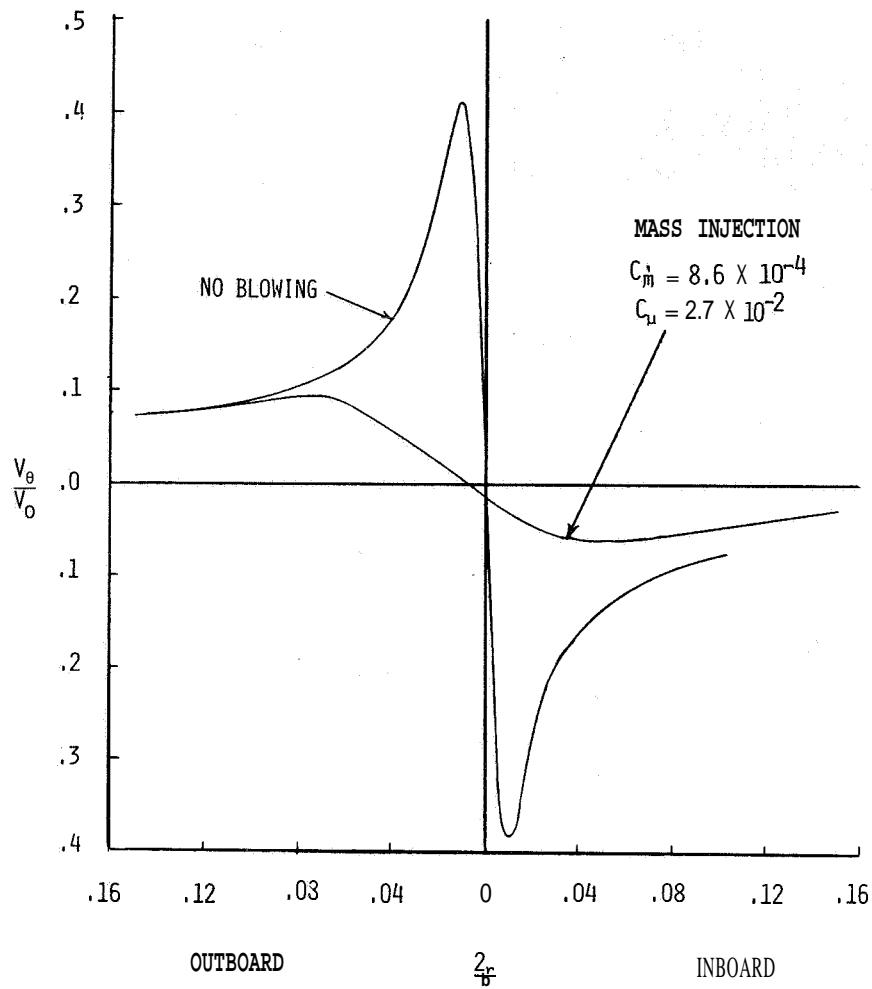
Figure 2.--Effect of mass injection on vortex velocity distribution.
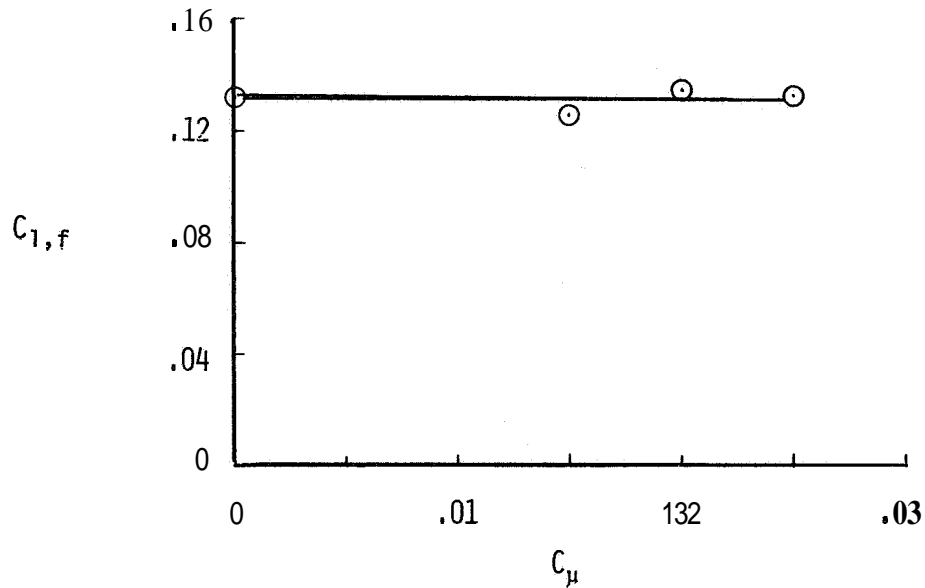


Figure 3.--Measured rolling moment on a following wing model as mass injection is increased. Lift coefficient = 0.73 on the vortex generator; $b_f/b_g = 0.18$; $X/b_g = 6.67$.
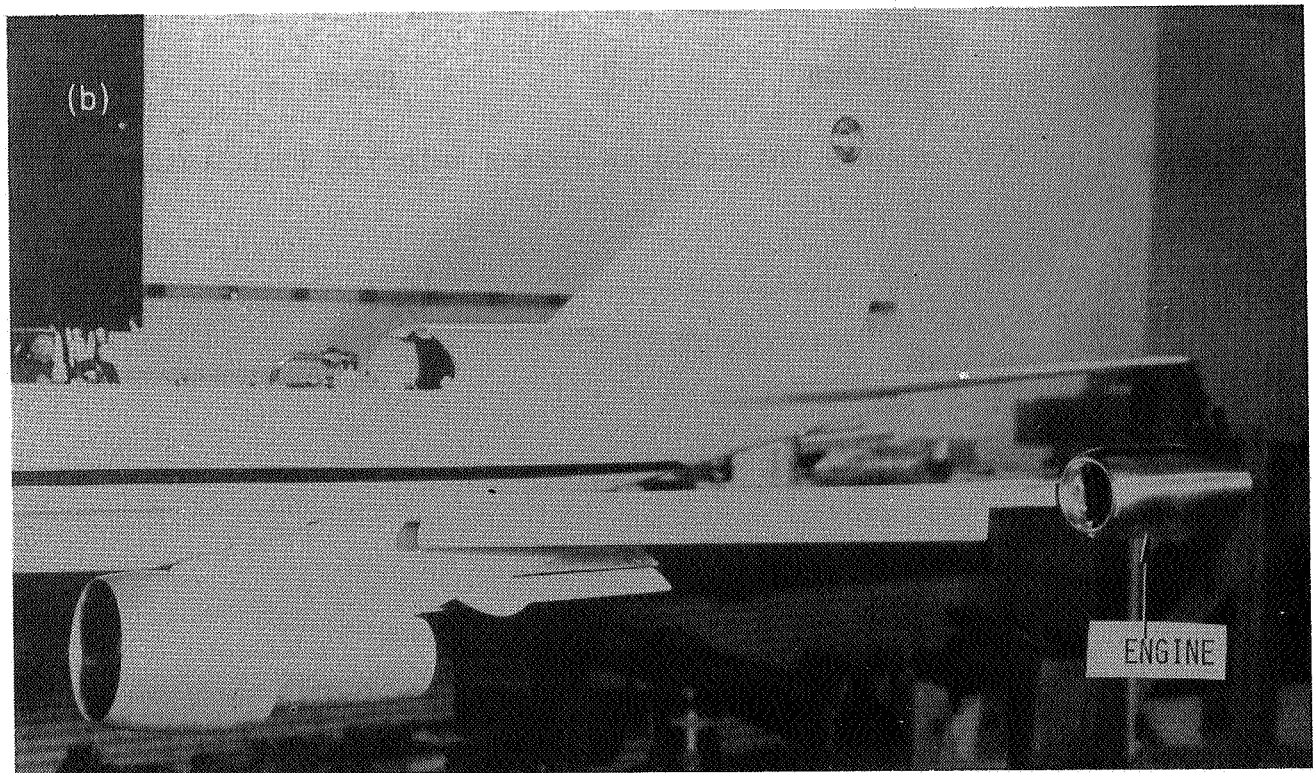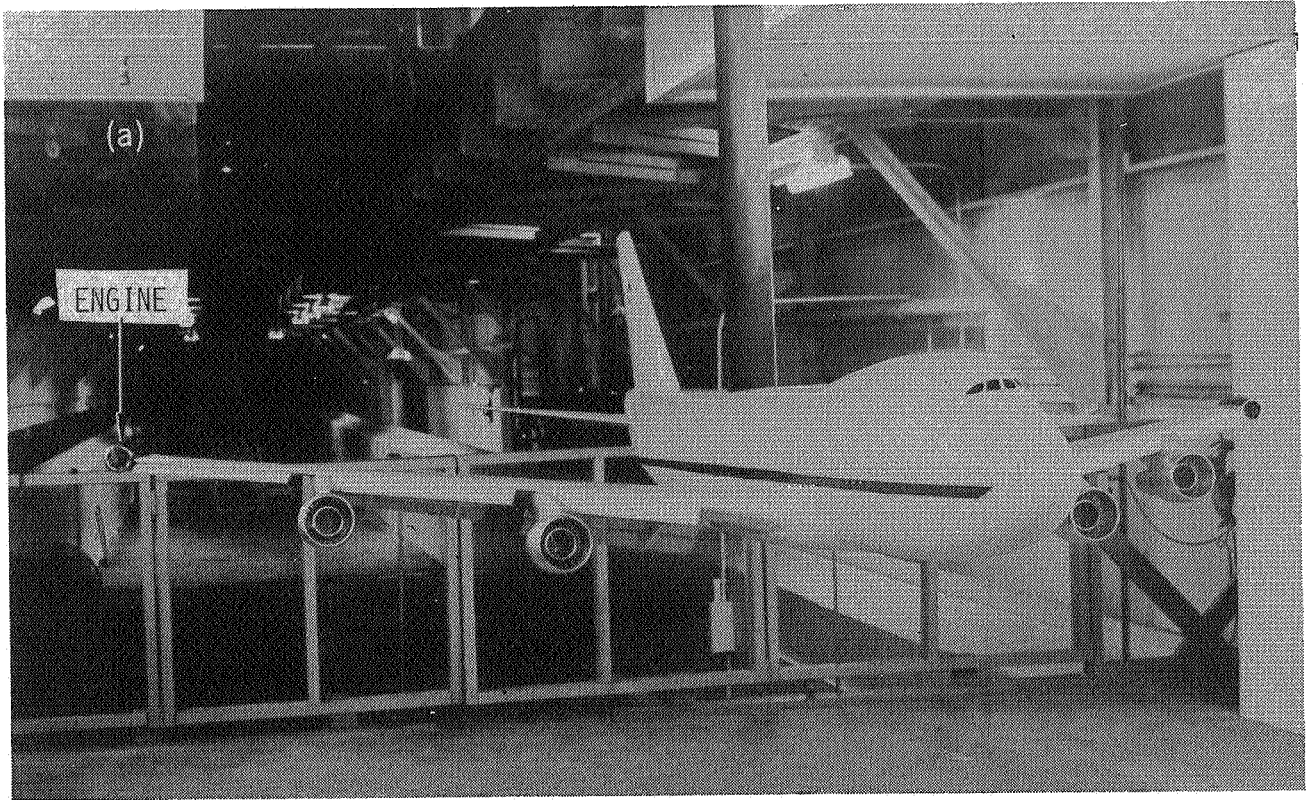
Figure 4.--Photographs of wingtip-mounted engines on transport model. (a) Front
view. (b) Side view.
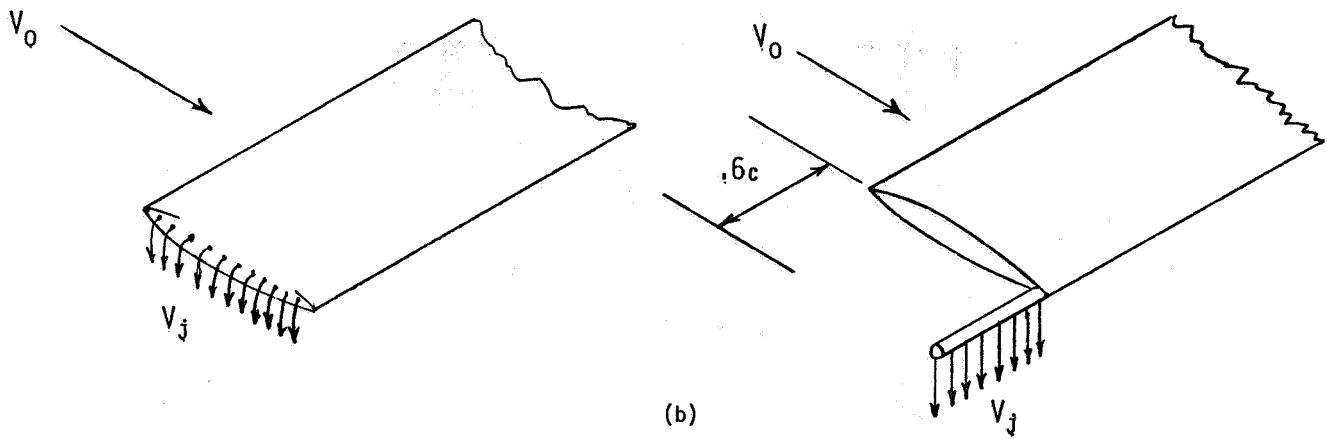
Figure 5.--Two techniques used to direct a sheet of air downward from the wingtip. (a) Chordwise blowing downward from a rounded wingtip. (b) Spanwise blowing downward from an extended tube.

**TEST CONDITIONS**

**ROUNDED WINGTIP WITH CHORDWISE BLOWING (FIG. 5(a))**

⊙ $C_\mu = 0$

▣ $C_\mu = .018$

**SPANWISE BLOWING FROM A TUBE (FIG. 5(b))**

◇ $C_\mu = 0$

△ $C_\mu = .018$
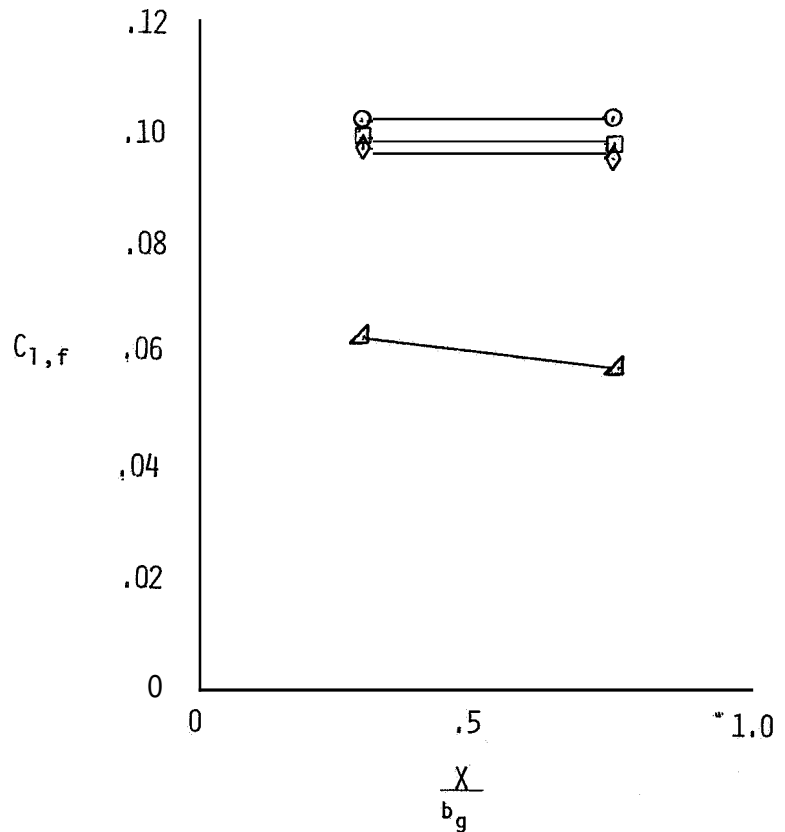


Figure 6.--Rolling moment measurements behind a straight wing of aspect ratio 6.8.

237
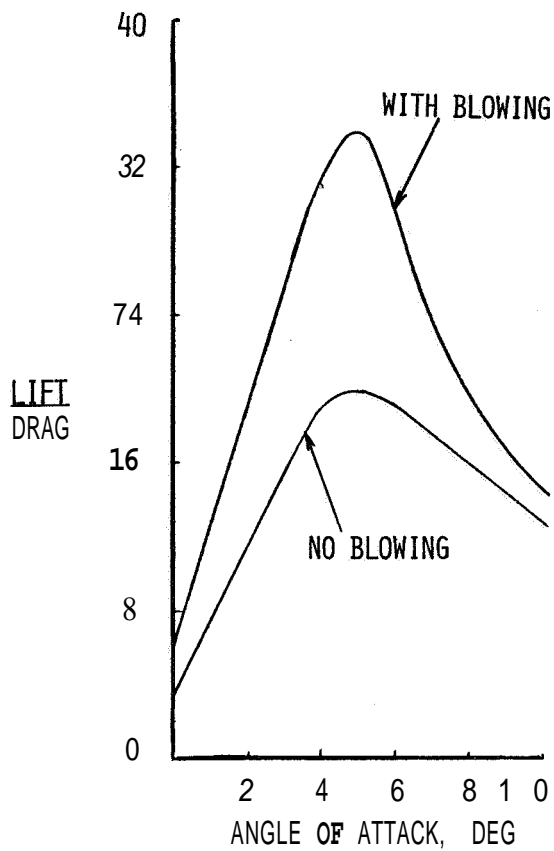
Figure 7.--Change in lift-drag ratio with spanwise blowing (fig. 5(b)). (Data from ref. 28.)
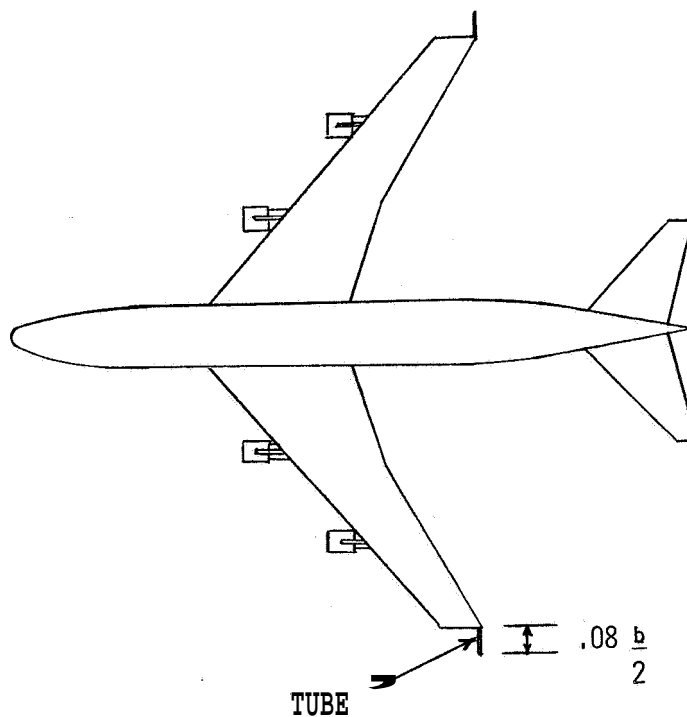


Figure 8.--Spanwise downward blowing at the wingtip of a transport aircraft model.
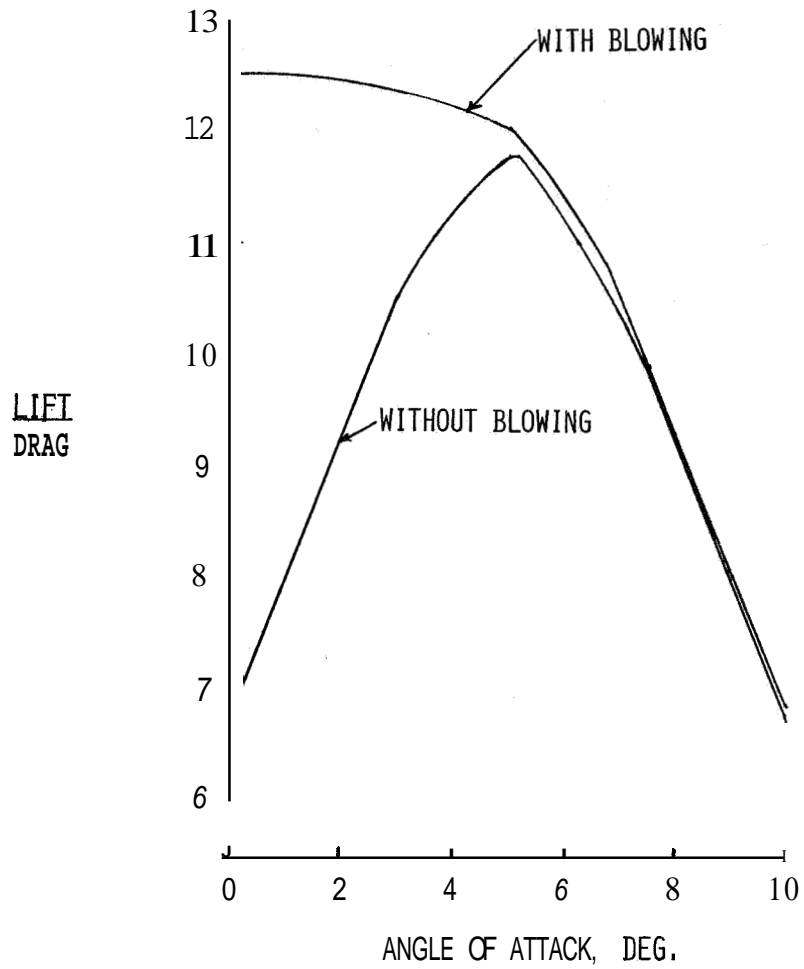
Figure 9.--Change in lift-drag ratio with spanwise downward blowing at transport model wingtip in cruise configuration.

.10

FLAPS EXTENDED LIFT COEFFICIENT OF 1,

.08

.06

$C_{l,f}$

.04

.0

FLAPS RETRACTED LIFT COEFFICIENT OF .8

0

0                    I02              ,04

$C_\mu$
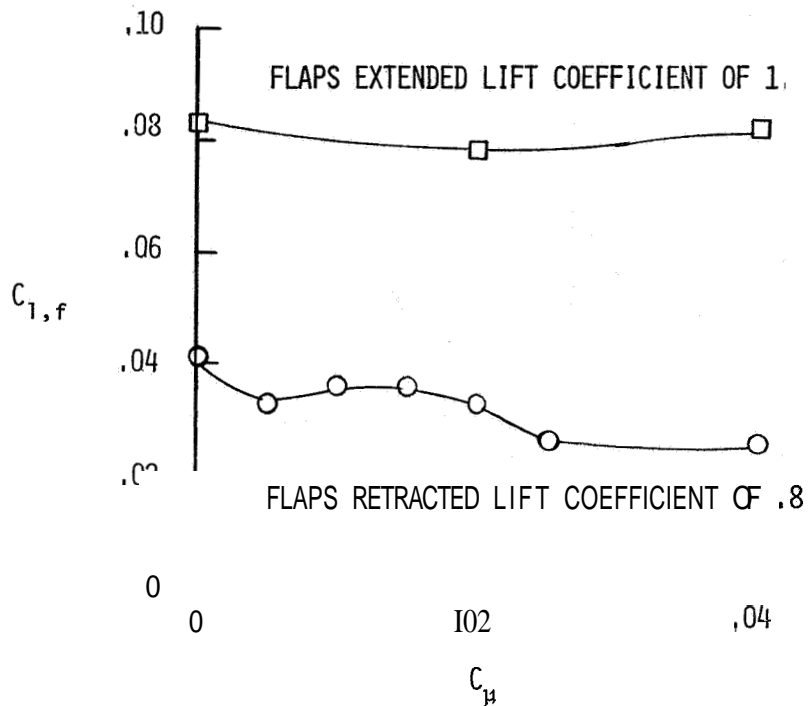
Figure 10.--Rolling moment measured by small-wing model $(b_f/b_g = 0.182)$ at 7.5 spans behind a transport-aircraft model with spanwise downward blowing at the wingtip (fig. 8).

(a)

JET ←

JET ←

(b)

WINGTIP

JET →

JET →

(c)

WINGTIP

JET

70°

#INGTIP

JET SHEET

(d)
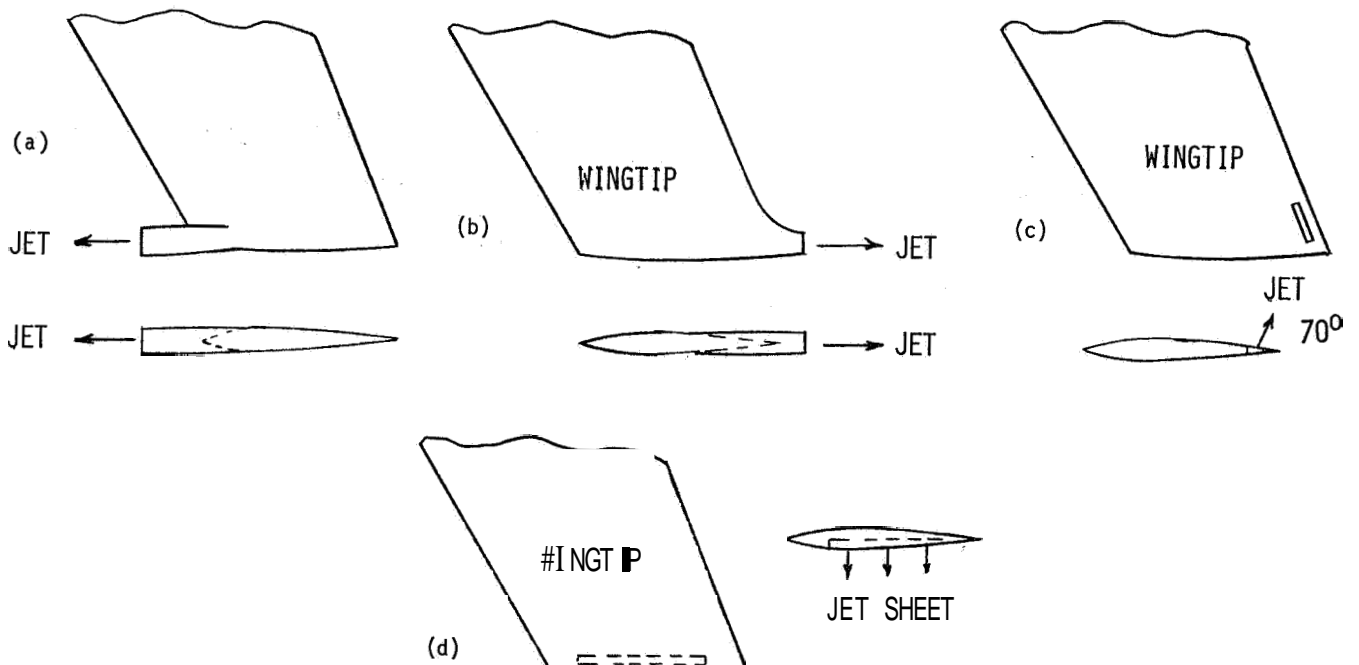
Figure 11.--Blowing devices investigated on the wingtip of a large transport model. (a) Forward blowing jet. (b) Rearward blowing jet. (c) Upward deflected jet. (d) Downward jet sheet.

OSCILLATES FROM 0 TO 90 DEGREES

.1 c

SECTION A-A

.6c

.96 $\frac{b}{2}$

.83 $\frac{b}{2}$

A          A
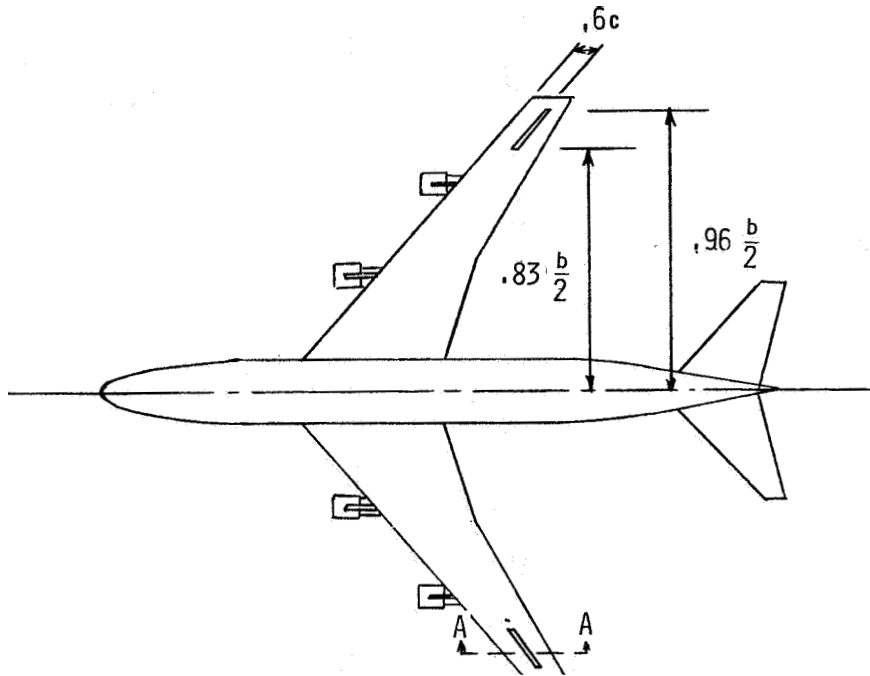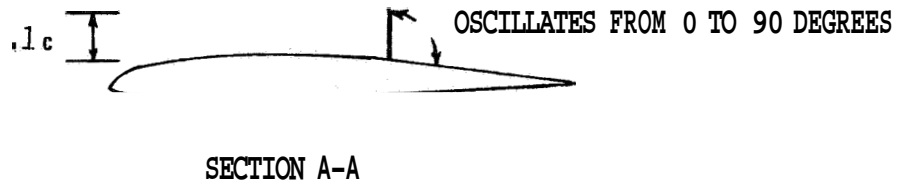
Figure 12.--Oscillating spoiler device on large transport model.

VARIATION IN CORE SIZE

≈6 SPANS
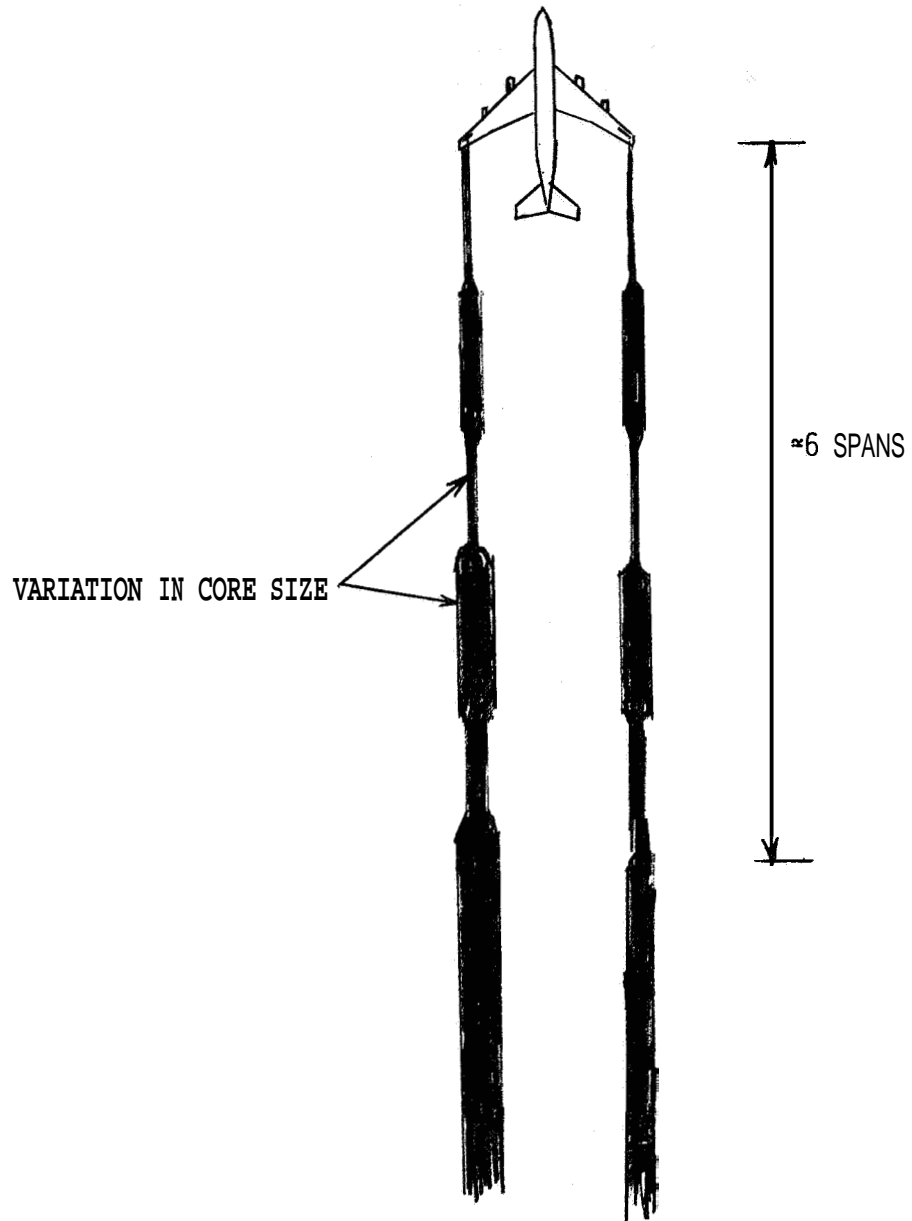
Figure 13.--Effect on an oscillating spoiler on transport-model trailing
vortices, in cruise configuration.
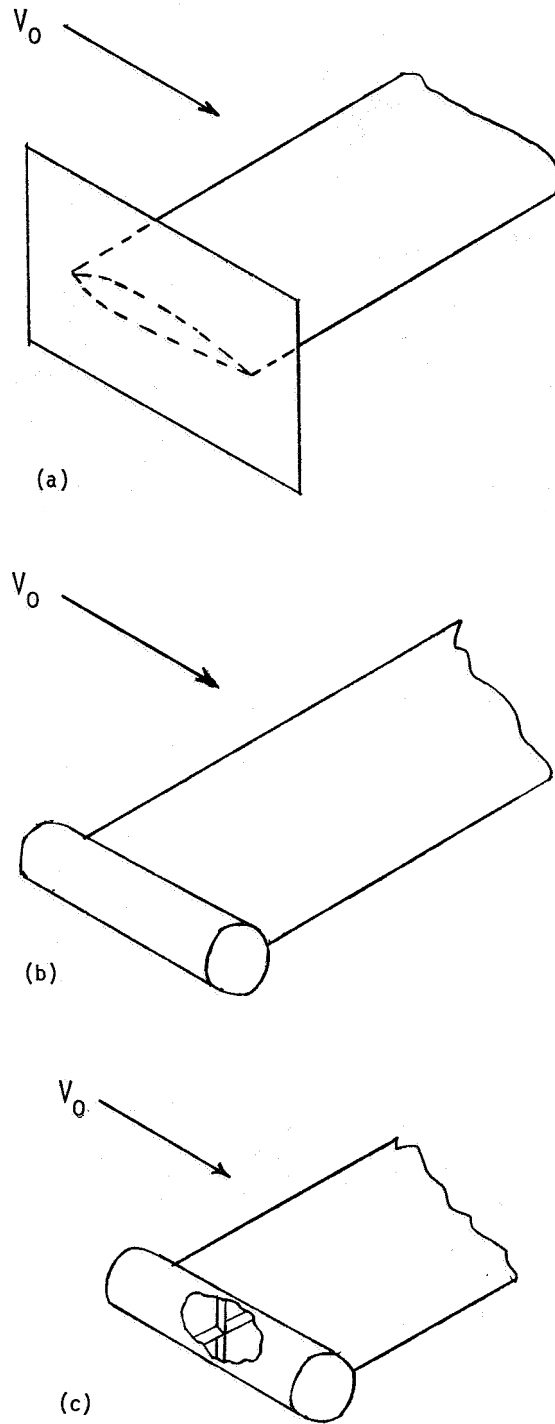
Figure 14.--The three types of wingtip end plates evaluated. (a) Sheet end
  plate. (b) Body of revolution with flow through center. (c) Body of revolu-
  tion with turning vanes in center.
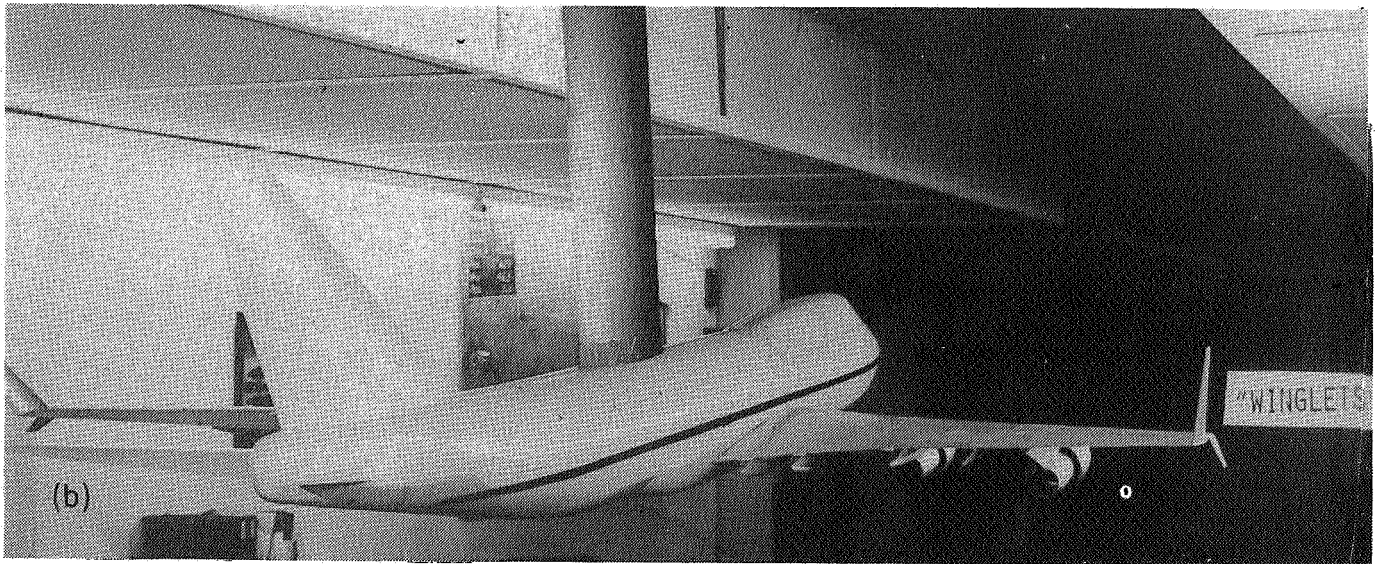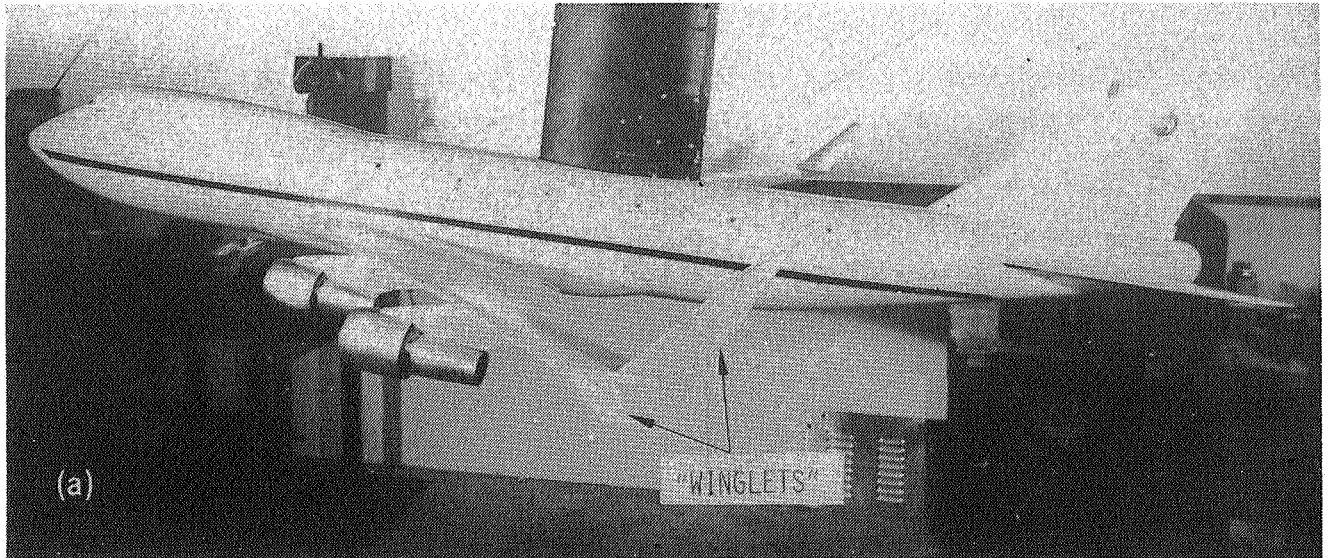
Figure 15.--Photographs of wingtip-mounted winglets on transport model. (a)
Side view. (b) Rear view.
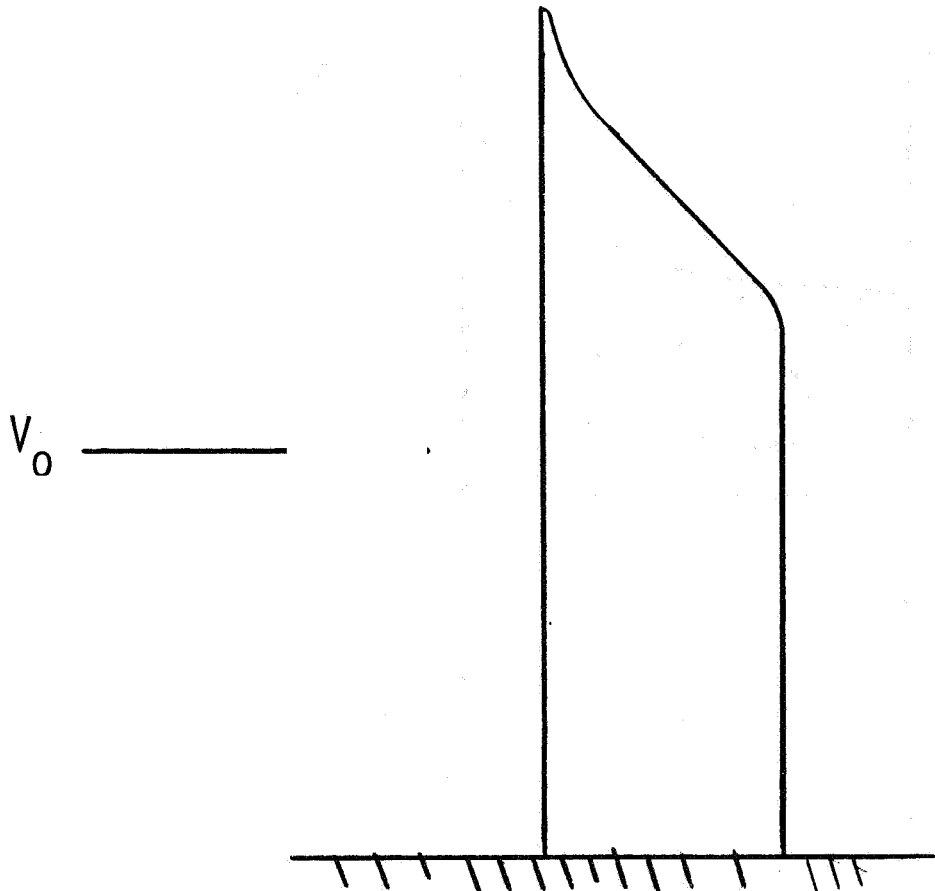
Figure 16.--Modified wingtip shape (ogee tip).
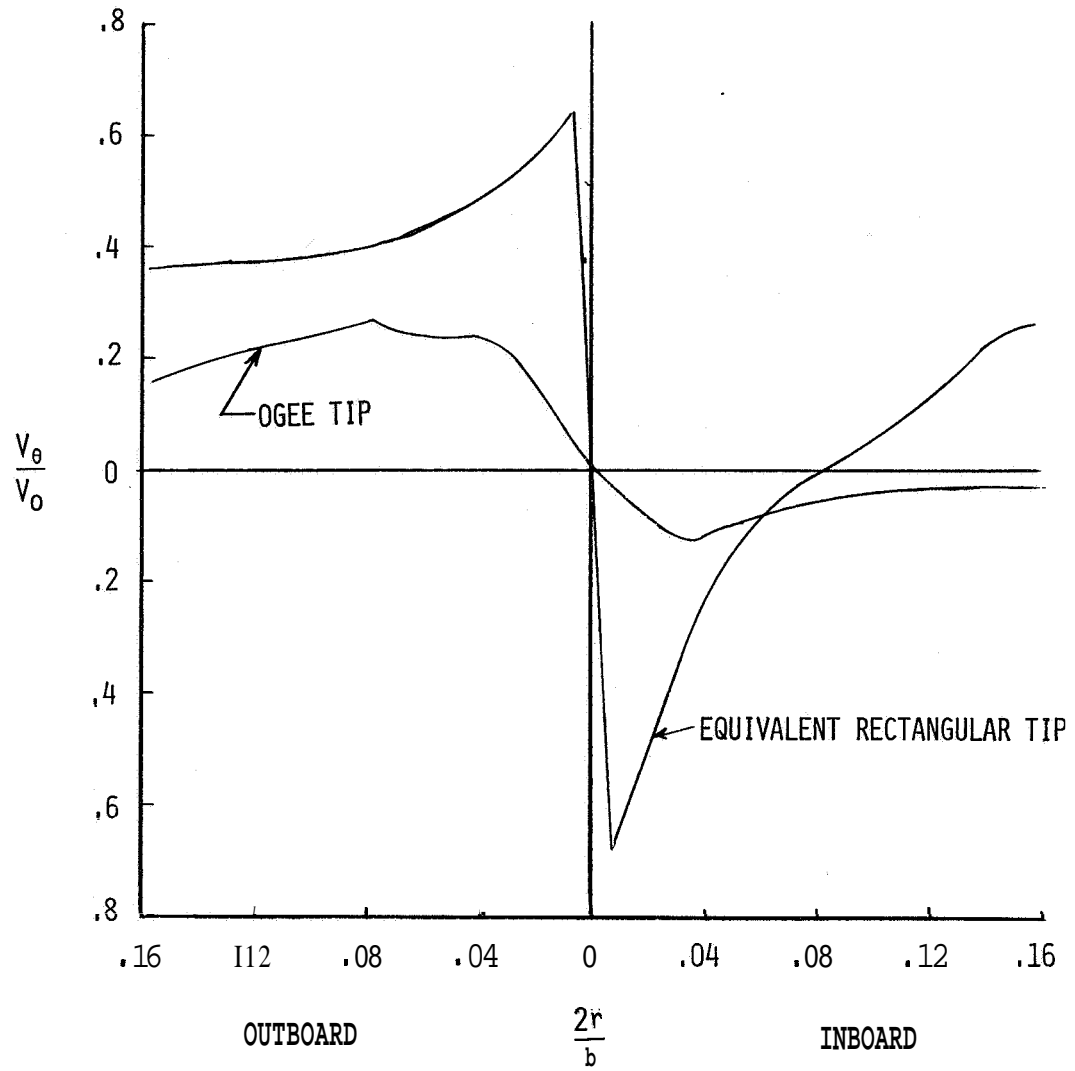
Figure 17.——Effect of modified wingtip, shape (ogee tip) on vortex dissipation.
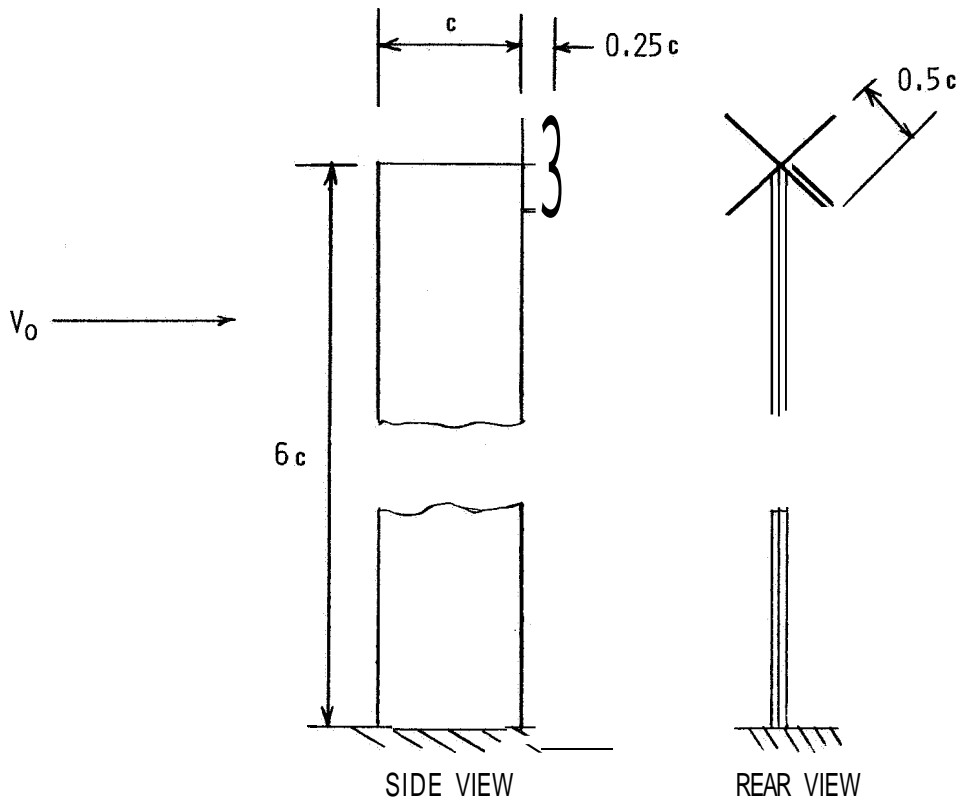
Figure 18.--Arrangement of crossed blades to inhibit vortex rotation.
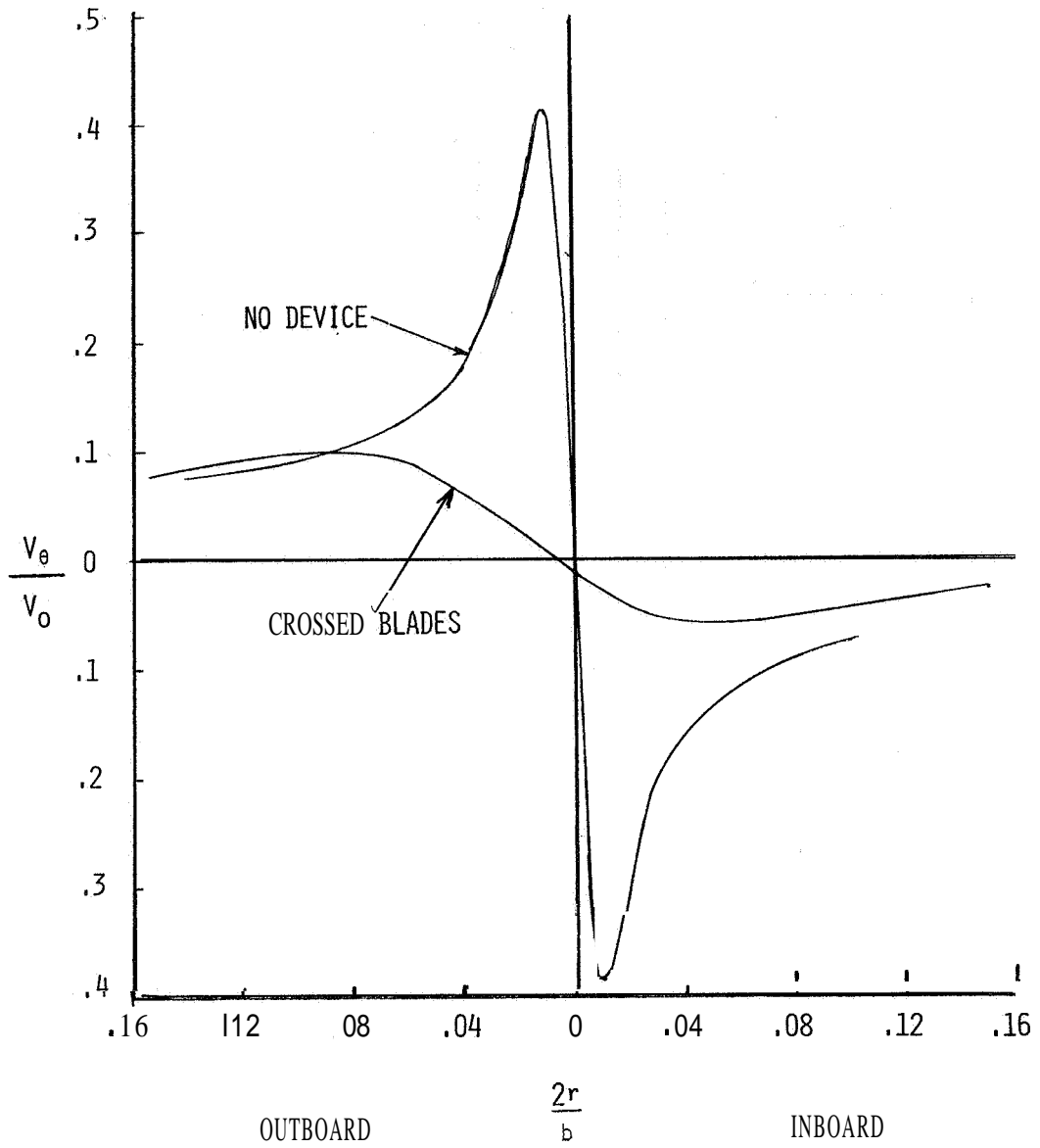
Figure 19.--Effect of crossed blades (fig. 18) on vortex velocity distribution.
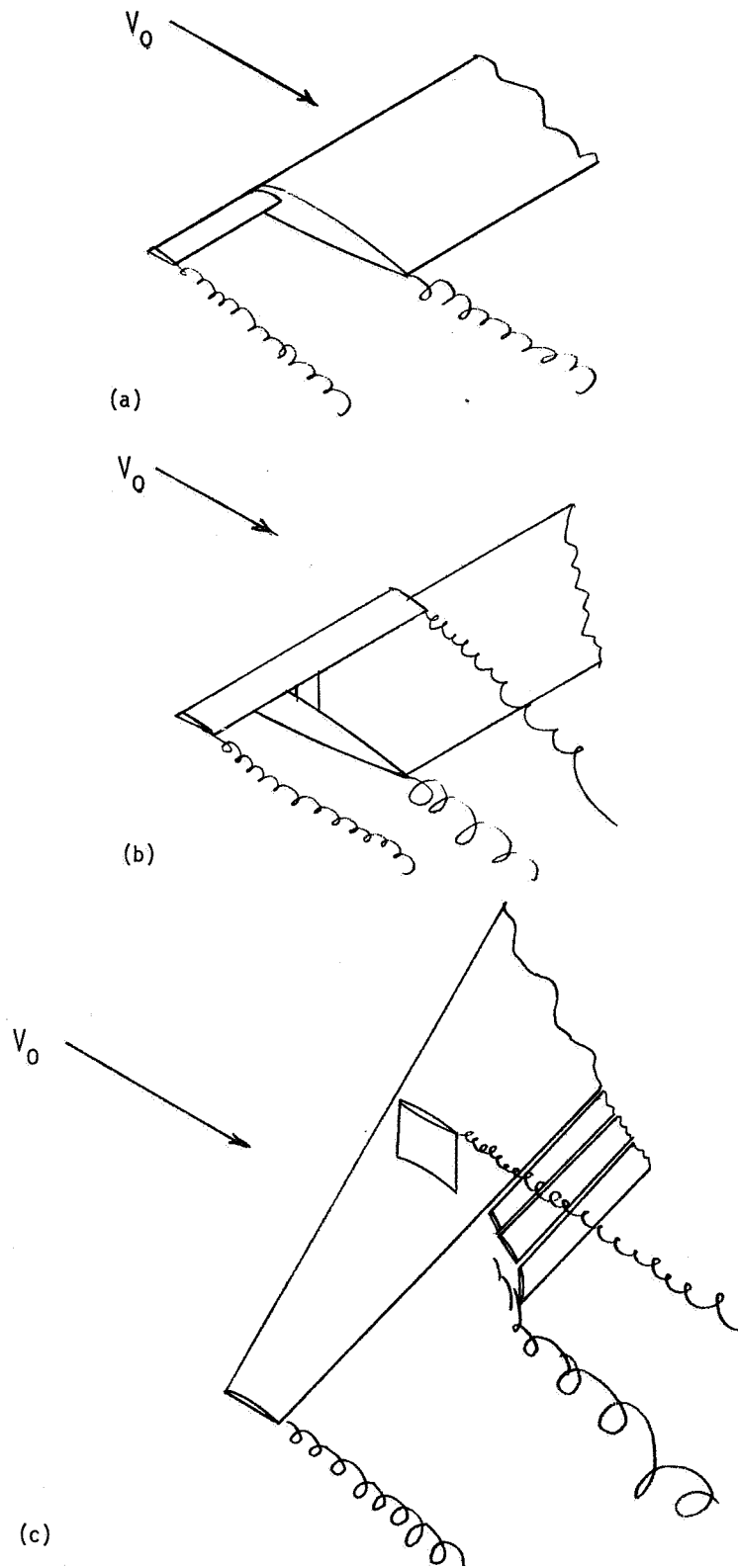
Figure 20.--Techniques used to investigate interaction of multiple vortices. (a) Wingtip extension. (b) Biplane wingtip. (c) Large vortex generator on transport aircraft model.

# THRUST-AUGMENTED VORTEX ATTENUATION

James C. Patterson, Jr., and Frank L. Jordan, Jr.
NASA Langley Research Center

## SUMMARY

An experimental investigation has been conducted in the Langley Vortex Research Facility to determine the vortex attenuating effect of engine thrust. Tests were made using a 0.03-scale model of the Boeing 747 transport aircraft as a vortex-generating model. A Learjet-class probe model was used to measure the vortex-induced rolling moment at a scale separation distance of 1.63 km (0.88 n. mi.). These tests were conducted at a lift coefficient of 1.4 at a model velocity of 30.48 m/s.

The data presented in this paper indicate that engine thrust is effective as a vortex attenuating device when the engines are operated at high thrust levels and are positioned to direct the high-energy engine wake into the core of the vortex. The greatest thrust vortex-attenuation is obtained by operating the inboard engine thrust reversers at one-quarter thrust and the outboard engines at maximum forward thrust.

## INTRODUCTION

The lift-induced wingtip vortex associated with the large wide-body jet transport aircraft of today has become a major problem in the terminal area resulting from the large upset rolling moment induced on smaller following aircraft. The persistent nature of this type of flow has also resulted in an unseen hazard during cruise flight long after the generating aircraft has passed. The wingtip vortex, the strength of which is a function of lift for a particular aspect ratio and wing planform, has been in existence since the beginning of flight, becoming an ever-increasing problem as the weight of each succeeding

251

generation of aircraft has increased. A NASA-wide research effort is now underway to reduce or possibly eliminate this lift-induced vortex by some means that could be retrofitted to existing aircraft to cope with the vortex persistence problem.

The high-energy wake produced by the large jet engines required for the wide body transports of today has been proposed as a means of attenuating the lift-induced vortex. Results of tests conducted to determine the vortex attenuation due to engine thrust level, thrust position, and the effect of reverse thrust are presented here. Visual data indicating the effect of thrust on the circulatory field surrounding the vortex as well as the effect on the vortex are included with the vortex-induced rolling–moment measurements made at 1.63-km (0.88-n.-mi.) scale distance behind the vortex generating model.

## APPARATUS AND PROCEDURE

### Facility Description

An overall view of the internal modification made to the towing tank in the transition from the model towing basin to a Langley Vortex Research Facility is shown in figure 1. The carriage is shown mounted on the 548.64-m overhead track with a transporttype vortex-generating aircraft model blade mounted beneath this carriage. A vortex probe model is located at 48.77 m, a scale distance of 1.63 km(0.88 n. mi.) downstream of the vortex-generating model. By using the flow visualization system discussed in reference 1, the position of this model relative to the vortex core is determined visually during each test, while the induced rolling moment is recorded in the facility test section.

The test section, constructed to isolate the wake of the carriage and trailers from the model wake, is 91.44 m long, 5.49 m wide, and 4.27 m high with a 5.10–cm opening along the center of the ceiling to allow the model

blade mounts to pass.   The exterior of the building shown at the entrance of the test section encloses the entire length of the track.

## Test Models

The vortex-generating model in figure 2 is a 0.03-scale model of the B-747 jet transport aircraft and is shown blade mounted on an internal six-component strain-gage balance.   High-pressure air is piped from a bottle field onboard the vehicle down the rear portion of the model blade mount to each engine nacelle for thrust simulation.   The thrust of each engine is individually controlled to allow a difference in thrust level between the inboard and outboard engines.   The model is equipped with both leading- and trailing-edge flaps to simulate the landing configuration.

The probe models used to measure the roll induced by the vortex of the E-747 model are shown in figure 3.   The smaller of the two models is in the Learjet class; the other is similar in scale size to the DC-9 transport. The models include two swept and tapered wings plus two unswept untapered research wings having the same span and aspect ratio as the swept wings.   The vertical and lateral position of the following model may be varied to fix this model in the vortex generated by the E-747 model.   This position of the roll model is recorded by a television camera to allow an instant replay of each test to determine the degree of vortex core penetration.   The internal strain-gage balance used with these models is also shown in this figure.   All models were constructed of fiber glass and aluminum.

## PRESENTATION OF RESULTS

A sequence of photographs of the vortex flow created by a E-747 model in the Langley Vortex Research Facility is shown in figure 4.   These photographs were taken at approximately 0.5-s intervals while the model traversed a distance of approximately nine wing spans between each photograph.

The moment the vortex-generating model penetrates the smoke screen, the vortex system produced by this model becomes visible and may be observed for some time after the model has passed. The wing-tip vortex and the vortex produced by the outer edge of the outboard flap are shown for each wing panel in the first photograph. These two vortexes produced by each wing panel orbit about a common axis forming a single vortex within four wing spans behind the model. This results in the classical vortex sheet emanating from a lifting wing rolling into a single vortex in the vicinity of each wingtip, shown in the sequential photographs. These two vortexes move downward under the influence of the wing downwash, and the vortex cores become visible with time as a portion of the smoke material is induced upstream along the periphery of the vortex core. This movement of the smoke along the vortex core possibly results from the lower pressure associated with the more recently formed wake upstream of the smoke screen. Beyond the radius of the rotational flow of the vortex core, the irrotational potential flow region can be seen. In the effort to reduce or eliminate the vortex hazard through a reduction in vortex flow, it should be kept in mind that the circulation flow shown can only be eliminated by canceling the total lift to the aircraft. By converting the angular momentum of the persistent vortex flow into linear momentum or turbulent flow, the vortex-circulatory wake system may possibly be caused to dissipate more rapidly.

Thrust Effect

The rolling moment induced by the vortex is obtained with the probe model as it penetrates the vortex shown in the last photograph of figure *4* taken 1.6 s after the vortex-generating model had passed the test position. The lift-induced vortex is responsible for *40* to *50* percent of the cruise drag in the form of induced drag and approximately 70 percent of the drag during landing. This large amount of energy associated with the vortex will require a large energy input to cause the vortex to break down. It has been shown in references **2** and **3** that by forcing a mass of air forward into the vortex the axial flow in the vortex core is disrupted such that the vortex

becomes unstable and breaks down as shown in reference **4.** The jet exhaust wake of the large engines employed on today's transport is a source of high energy that when properly directed into the vortex core may trigger this same dissipating effect on the vortex.

Tests have been conducted with the model engine simulators on the **B-747** model operated at a static gross sea level thrust comparable to the maximum thrust obtainable by the full-scale transport **aircraft.** The landing gear is extended for all tests as a result of the unexpected increase in vortex strength discovered as a result of extending the landing gear. (See ref. 5.) The visual data of the effects of engine thrust on the vortex formation are presented in figure 5. The wingtip and flap vortexes do not appear as distinct as for the zero thrust case when the high-energy jet engine exhaust from the inboard and outboard engines is introduced on either side of the final vortex rollup position. This final position was found to be approximately 55 percent of the wing semispan during the investigation of the spline vortex attenuating device (ref. **2).** The attenuating effect of the thrust should be greater than that of the spline device because of the continued injection of an air mass from the engines into the vortex formed at a particular position along the flightpath, The amount of engine exhaust that reaches the vortex, of course, decreases as the separation distance between the aircraft and this position increases. The downwash produced by the wing is apparent in this figure as well as the circulatory field in the vicinity of each wingtip.

The effect of thrust on the rolling-moment coefficient induced on the Learjet class aircraft probe model by the vortex of the **B-747** transport model with full landing flaps is presented in figure 6. The jet engine wake has an attenuating effect on the vortex that reduces the measured rolling moment by approximately 20 percent of the zero thrust case at the separation of 1.63 km (0.88 n. mi.).

The results of flight tests conducted by the Flight Research Center using the **B-747** jet transport aircraft indicate the similar thrust attenuating effect on the induced vortex (ref. 6). At a separation distance of approximately 9 km (5 n. mi.), the vortex-induced rolling moment measured by

255

the small jet aircraft (Learjet class) was increased on an average by approximately 40 percent when the thrust was reduced from that required for level flight with full flaps deployed, to an idle thrust level. More recent flight tests at a separation distance of approximately 6.5 km (3.5 n. mi.) also indicate this same reduction in vortex strength resulting from the dissipating effect of the engine thrust on the vortex.

## Engine Location

Neither of the engines on one wing panel of this model configuration is directly aligned with the vortex spanwise-rollup position. The outboard engine is located at the 70-percent semispan station, and the inboard engine is at 40 percent. As stated, the position of final vortex rollup is approximately 55 percent of the semispan for this model; therefore, it should be expected that the effect of thrust shown here is not the maximum.

In an attempt to increase the vortex attenuation resulting from engine thrust, the outboard engine on the vortex B-747 model was moved inward along the wing leading edge to the 55-percent semispan station. The induced rolling-moment model results obtained with the outboard engine in this new position, with and without thrust, are presented in figure 7. The vortex induced roll value for the thrust-off case is slightly higher than with the engine at the 70-percent semispan position, possibly resulting from the reduced underwing fencing effect offered by the engine-pylon combination located further out along the wing span. Interruption of the spanwise flow under the wing would tend to reduce the strength of the vortex, as an associated change in span load would indicate. Applying maximum thrust with the outboard engines at the 55-percent semispan position results in an additional 50-percent reduction in vortex-induced rolling moment. This result demonstrates not only the vortex attenuating effect of engine thrust, but also the importance of properly directing this energy.

## Thrust Reversers

Because the high engine thrust levels required to obtain an appreciable reduction in vortex strength may not be applicable to the landing case, it has been suggested that the jet engine thrust reversers might be employed as a vortex attenuating device. The reversers on the B-747 operate by directing the fan flow and primary flow of the fan-jet engines approximately $26^o$ forward of the vertical plane, resulting in approximately 42 percent of the total engine thrust reversed.

Model tests were conducted using an annular structure at the model engine fan exit to turn the fan flow 120" simulating the full-scale engine reverser. The vortex-induced rolling moment results obtained with the two outboard or two inboard engine thrust reversers deployed, operating at 25-percent maximum forward thrust, and with the nonreversed engines operating at full thrust are presented in figure 8. The inboard engine reversers are approximately three times as effective as the outboard reversers, resulting in a 60-percent reduction in the measured vortex rolling moment. The visual data for the inboard reverser configuration are presented in figure 9. Comparison of these data with those of figure 4, basic configuration without thrust, indicates that the vortex core has been eliminated while the accompanying circulation has been greatly reduced. Full-scale flight tests of reverser effectiveness have been conducted recently using the B-747 airplane without landing flaps deployed. A significant reduction in the actual roll upset of the probe aircraft was achieved by operating the outboard engine reversers at idle thrust while the inboard engines developed maximum thrust.

## Multivortex System

Tests were conducted to determine the effect of a variation in span lift loading on vortex dissipation. The span load was altered by retracting the outboard flaps, resulting in the vortex system shown by the visual data presented in figure 10. These data indicate that for the zero-thrust case there is a distinct wingtip and flap vortex system. The vortexes that form on the inner edge of each inboard flap tend to dissipate each other as a

result of their opposite senses of rotation and proximity aided by the end-plate effect of the nearby fuselage. Vortexes that formed at the flap outer edges orbited with the wingtip vortexes until the flap vortex flow broke down at approximately 0.78 km (0.43 n. mi.) downstream from the model. The wingtip vortex persisted long after that, as indicated by the well-defined vortex in the last photograph of the figure at a separation distance of 1.63 km (0.88 n. mi.).

The effect of thrust on the multivortex system resulting from deploying only the inboard flaps is presented visually in figure 11. The core of each vortex is visually dissipated and circulation has been reduced as shown previously as a result of the engine wake.

The measured rolling–moment coefficient increased from a value of approximately 0.03 to 0.04 when the full engine thrust was applied to the inboard flap configurations. This result was unexpected and had not been experienced in previous engine thrust tests. In reviewing the videotaped visual data, it was apparent that in the zero-thrust case, the wingtip vortex had moved into such a position relative to the probe model at the scale distance of 1.63 km (0.88 n. mi.) that its influence tended to reduce the rolling moment induced by penetration of the flap vortex. The dissipating effect of thrust on the wingtip vortex reduced the favorable effect of this vortex on the probe model, resulting in the larger flap vortex-induced roll.

There was some indication during the full-scale flight tests of this mutual effect of the vortexes on the probe aircraft in multivortex systems. These effects have been .associated with a change in separation distance between the generating and probe aircraft that alters the relative position of each vortex to the probe aircraft.


CONCLUDING REMARKS


An experimental investigation to determine the dissipating effect of engine thrust on the lift-induced vortex of a model B-747 transport aircraft

indicated that--

(1) The strength of the lift-induced vortex of the B-747 may be attenuated by the thrust of the large fan-jet engines employed by this transport.

(2) The thrust-augmented vortex attenuation may be maximized by proper engine location relative to the vortex.

(3) Deploying the thrust reverser on the inboard engines at low thrust levels is a very effective method of achieving a large degree of vortex attenuation.

(4) The mutual effect of the vortexes in a multivortex system may enhance as well as attenuate the rolling moment induced on a following aircraft as a result of the relative position of each vortex to the probe aircraft,

## REFERENCES

1. Patterson, J. C., Jr.; and Jordan, Frank L., Jr.: A Static-Air Flow Visualization Method to Obtain a Time History of the Lift-Induced Vortex and Circulation. NASA TM X-72769, 1975.

2. Patterson, J. C., Jr.: Vortex Attenuation Obtained in the Langley Vortex Research Facility. J. Aircraft, vol. 12, no. 9, Sept. 1975, pp. 745-749.

3. Hastings, E. C., Jr.; Patterson, J. C., Jr.; Shanks, R. E.; Champine, R. A.; Copeland, W. L.; and Young, D. C.: Development and Flight Tests of Vortex-Attenuating Splines. NASA TN D-8083, 1975.

4. Hall, M. G.: Vortex Breakdown. Annual Review of Fluid Mechanics. Vol. 4, M. Van Dyke, W. G. Vincenti, and J. V. Wehausen, eds., Annual Reviews, Inc., 1972, pp. 195-218.

5. Patterson, J. C., Jr.; and Jordan, F. L., Jr.: An Investigation of the Increase in Vortex Induced Rolling Moment Associated With Landing Gear Wake. NASA TM X-72786, 1975.

6,    Smith, H. J,:   A Flight Test Investigation of the Rolling Moments In-
        duced on a T–37B Airplane in the Wake of a B-747 Airplane.   NASA
        TM X-56031, 1975,

COVERED AREA

TRAILER

FOLLOWING MODEL

VEHICLE

VORTEX GENERATING MODEL

Figure 1.—Arrangement of the Langley Vortex Research Facility.

261
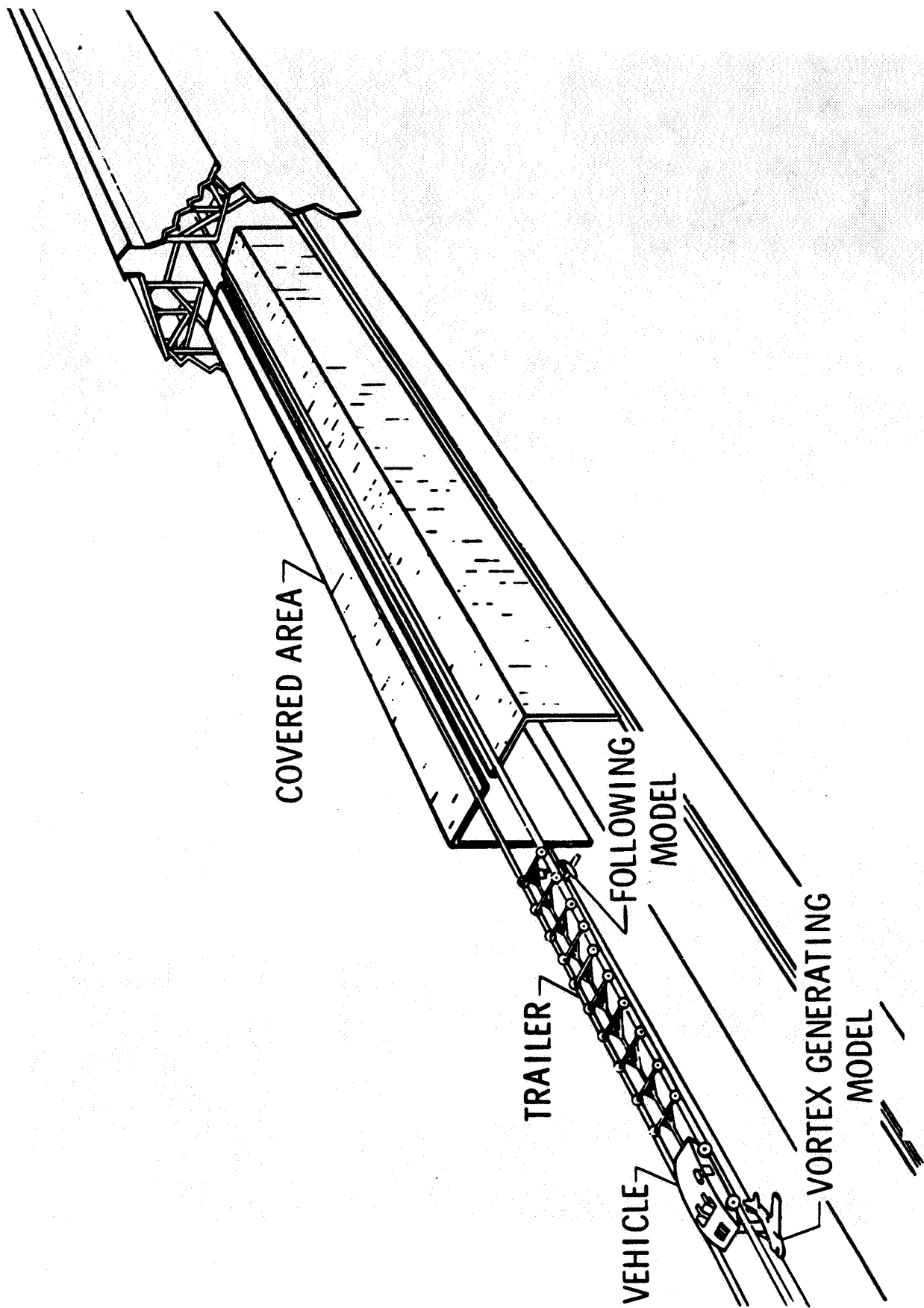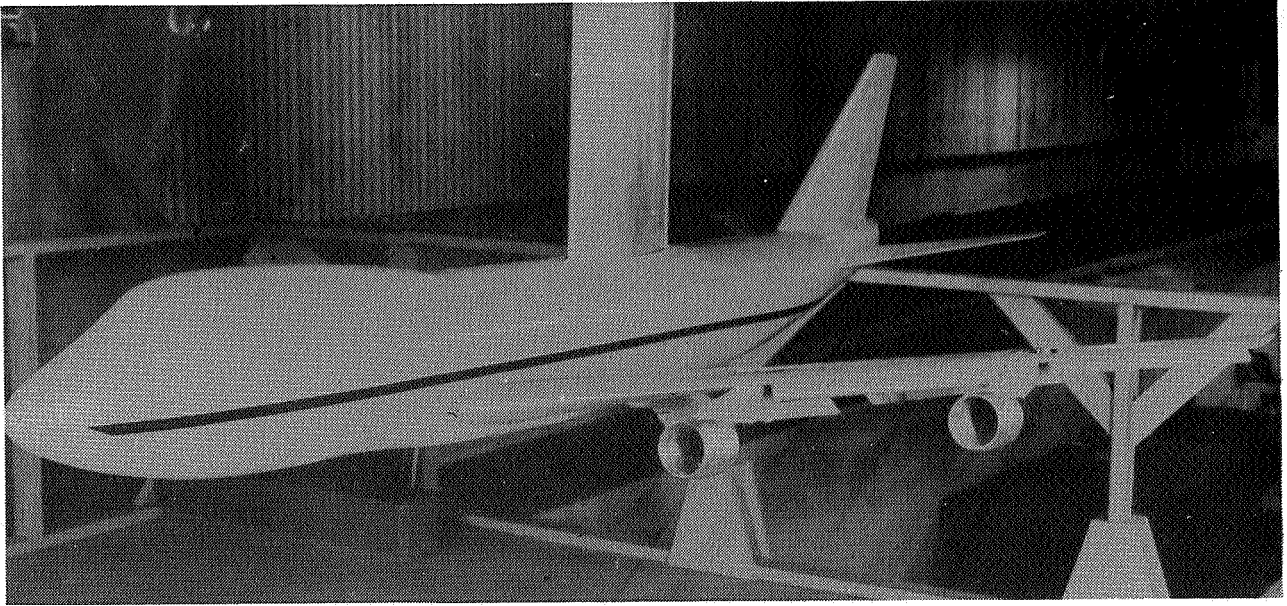
Figure 2.--Photograph of the 0.03-scale-model wide-body jet transport aircraft used as vortex generating model.
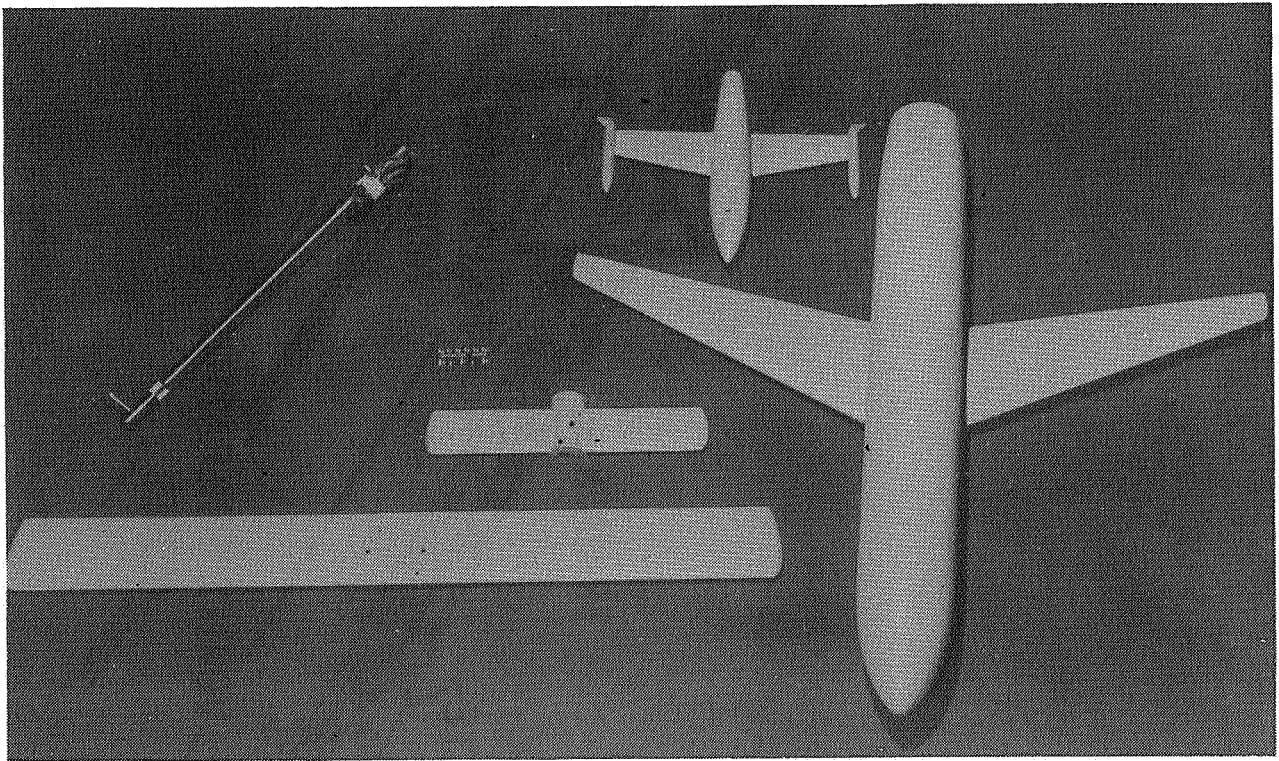


Figure 3.--Photograph of the 0.03-scale-model DC-9 and Learjet-class aircraft used as vortex probe models.
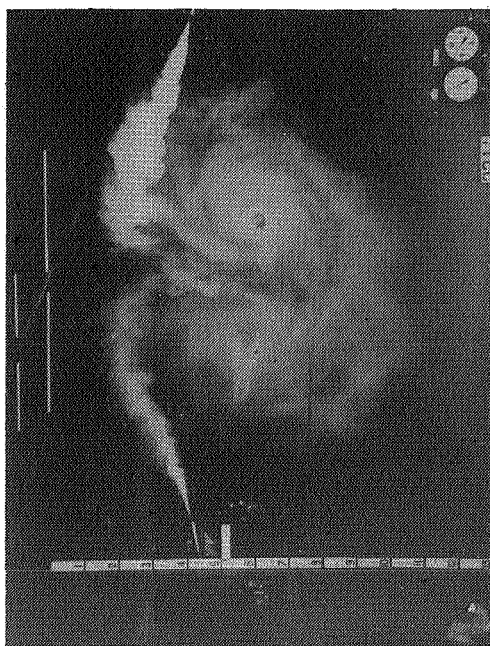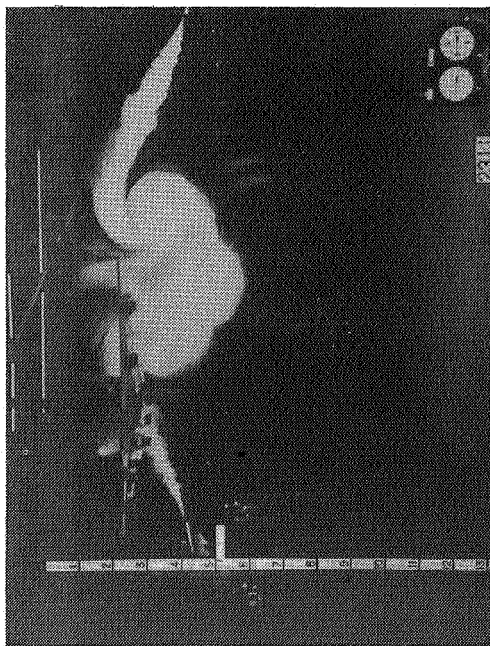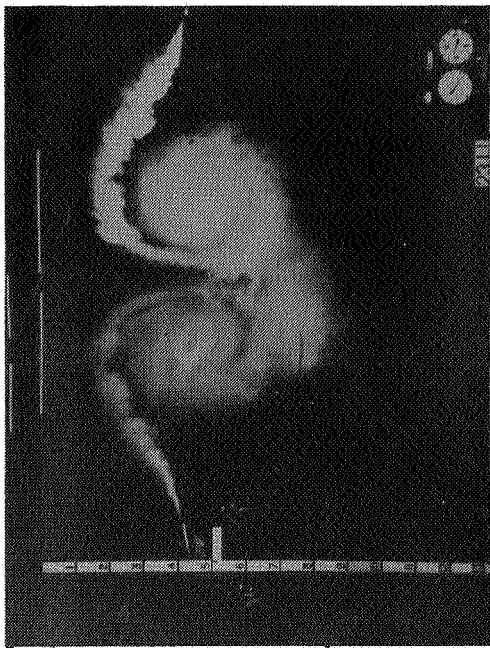
Figure 4.—Lift-induced vortex system created by 0.03-scale-model of jet transport aircraft (flaps deflected 30°). Photographic sequence rate corresponds to a separation distance of 0.54 km. Following model is centered in vortex in lower right photograph. Lift coefficient = 1.40; velocity = 30.48 m/s.
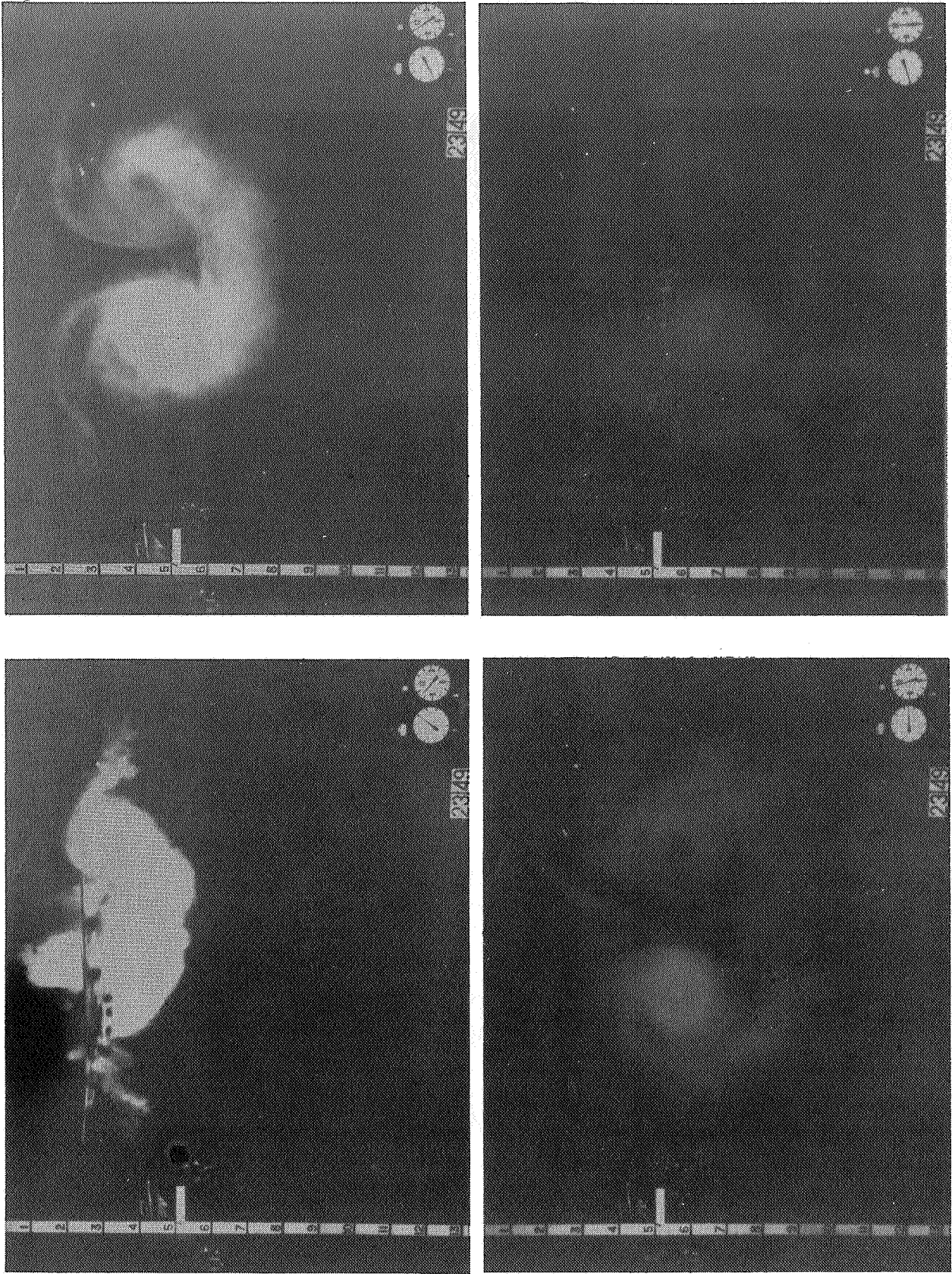
Figure 5.--Effect on maximum engine thrust on vortex system of transport aircraft model in figure 4 (flaps deflected 30°).
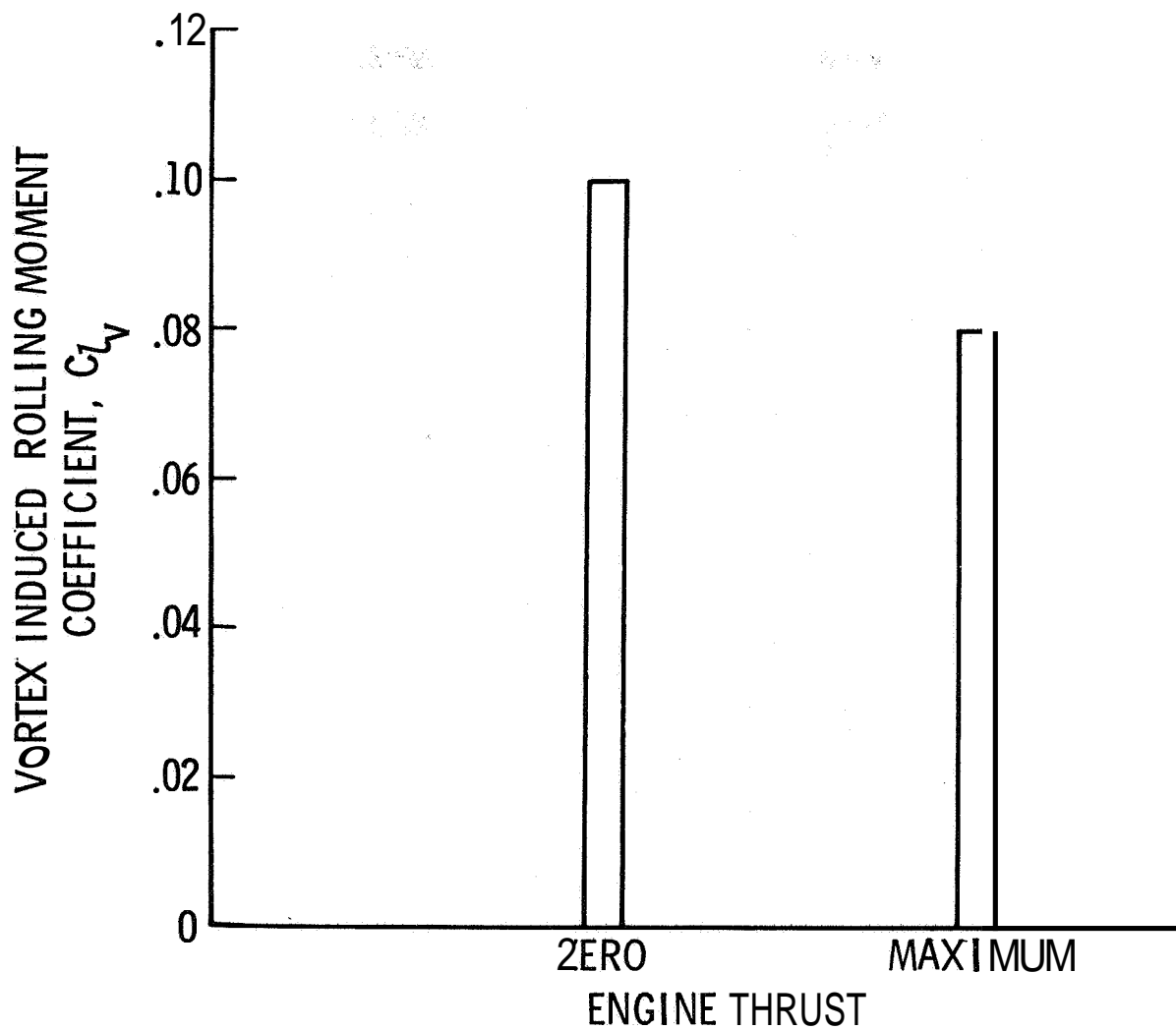
Figure 6.--Effect of engine thrust on vortex-induced rolling moment coefficient with Learjet-class chase model. Lift coefficient = 1.40; separation distance = 1.63 km (0.88 n. mi.).

VORTEX INDUCED ROLLING MOMENT COEFFICIENT, $C_{l_V}$

.12

.10

.08

.06

.04

.02

0

ZERO

MAXIMUM
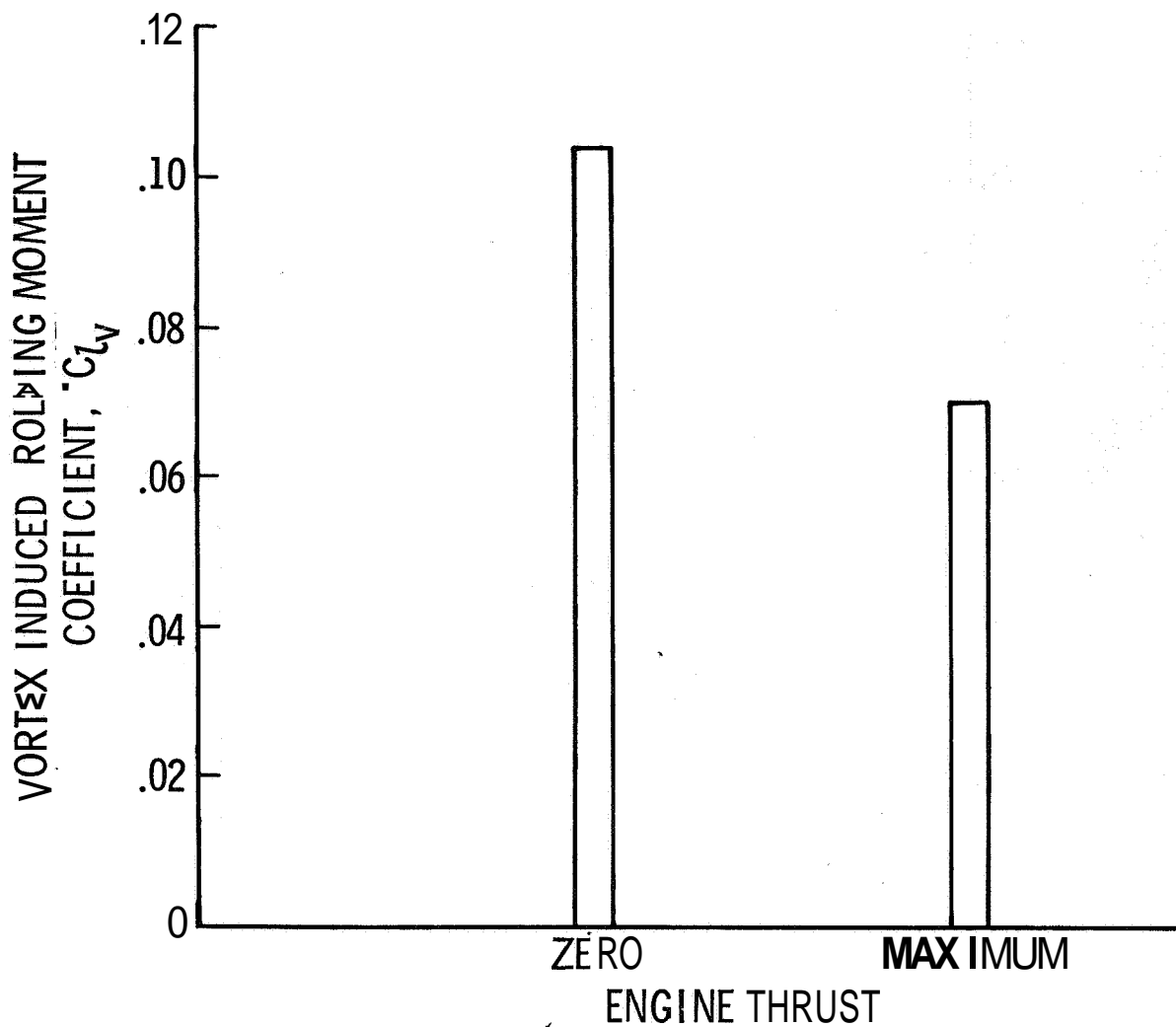
ENGINE THRUST

Figure 7.--Effect of engine thrust on vortex–induced rolling moment coeffi–
cient with outboard engines located at 55 percent of wing semispan and
Learjet–class chase model. Lift coefficient = 1.40; separation distance =
1.63 km (0.88 n. mi.).
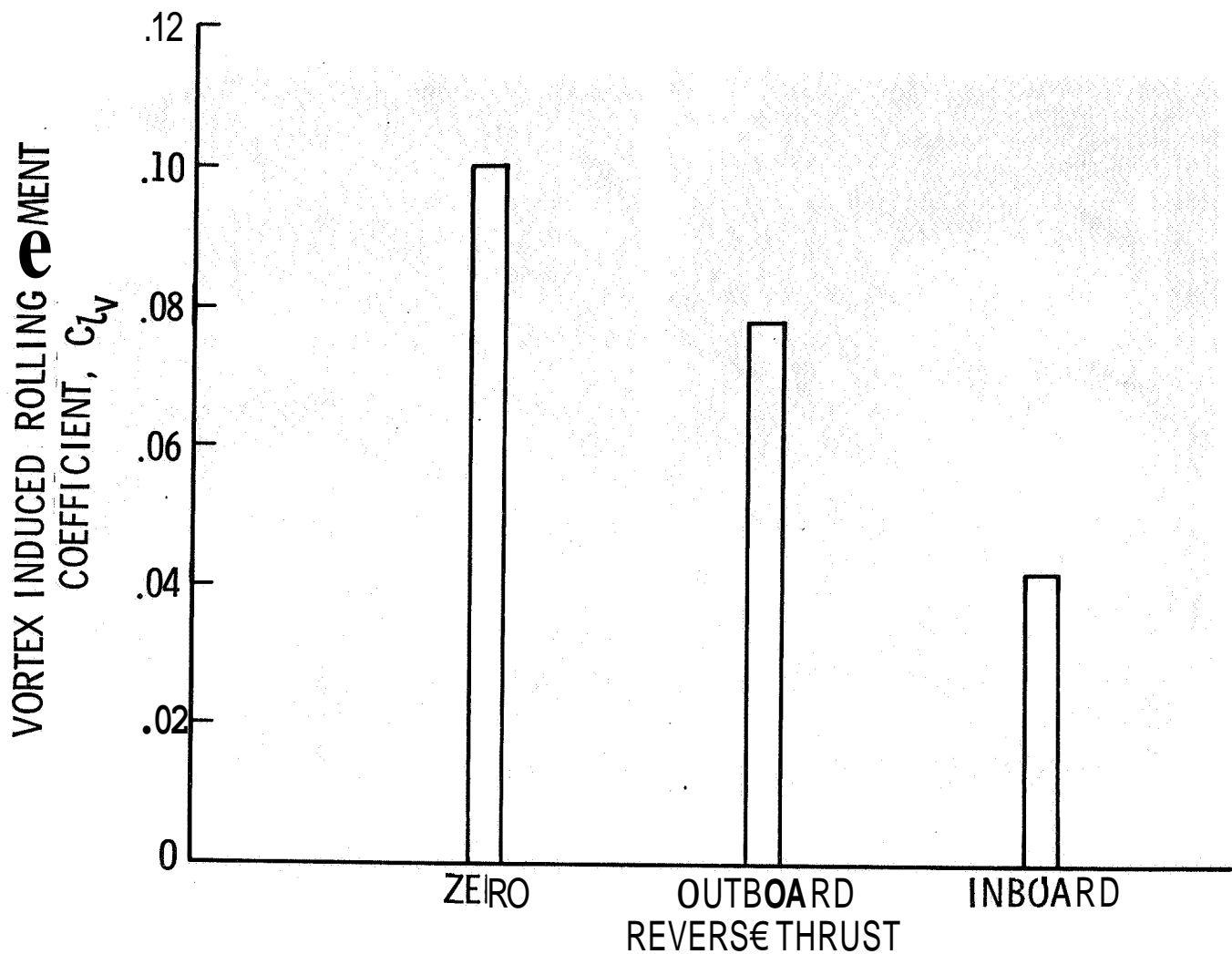
Figure 8.--Effect of engine reverse thrust on vortex-induced rolling-moment coefficient with Learjet-class chase model. Lift coefficient = 1.40; reverse thrust, 1/4 maximum; forward thrust, maximum; separation distance = **1.63** km (0.88 n. mi.).
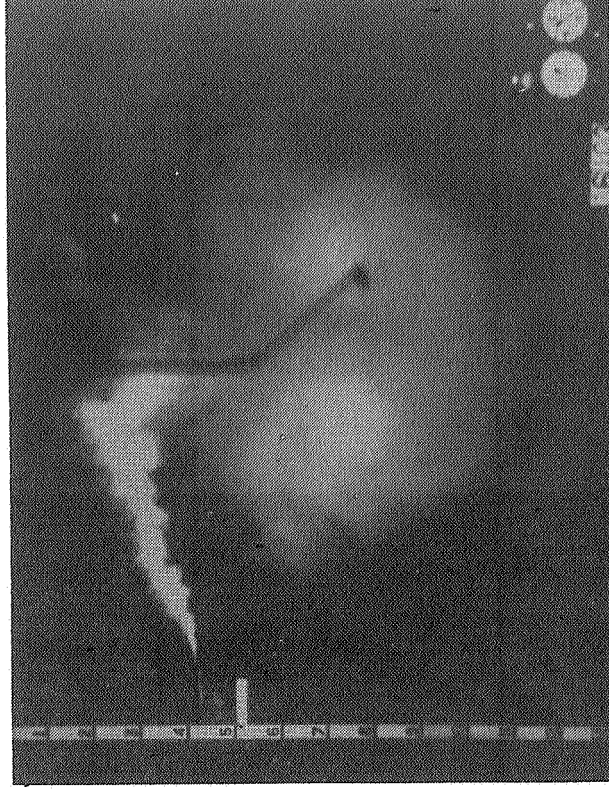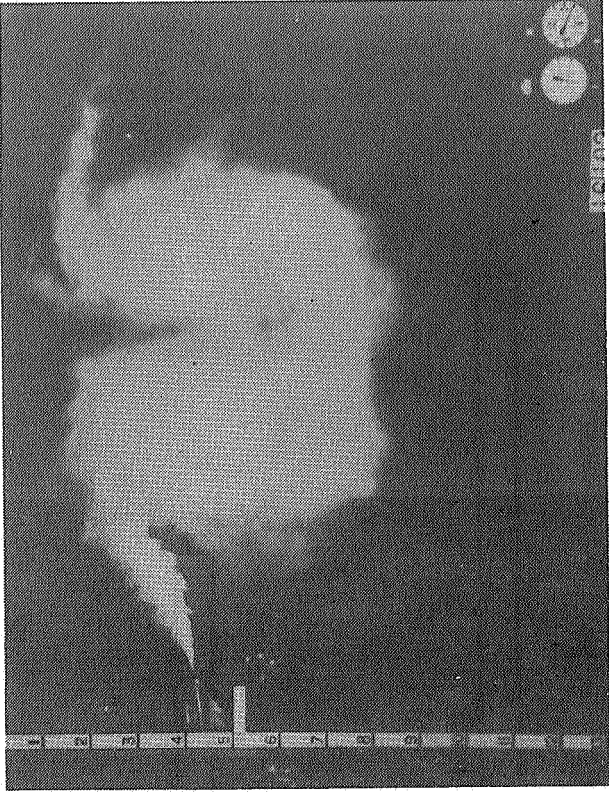
Figure 9.—Effect of inboard engine reverse thrust on vortex system of wide-body jet transport aircraft model in figure 4 (flaps deflected 30°)
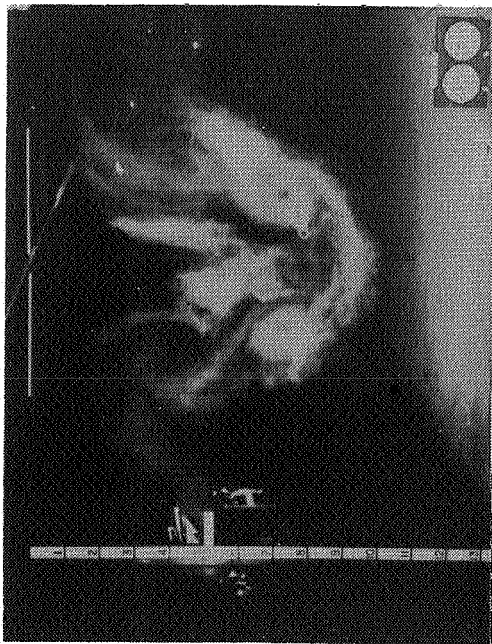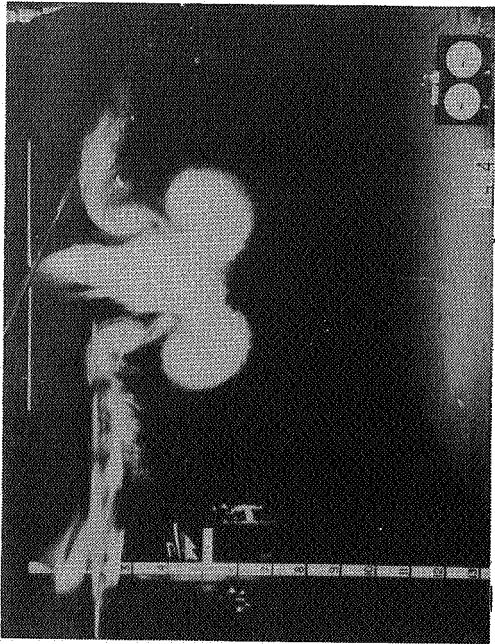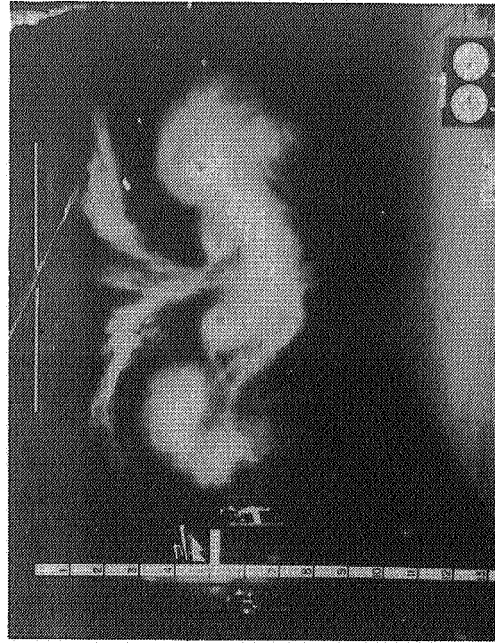
Figure 10.--Lift-induced vortex system created by 0 03-scale model of the wide-body jet transport aircraft (inboard flaps deflected 30°). Photographic sequence rate corresponds to a separation distance of 0 54 km. Following model is centered in vortex in last photograph. Lift coefficient = 1.20; velocity = 30.48 m/s.

269
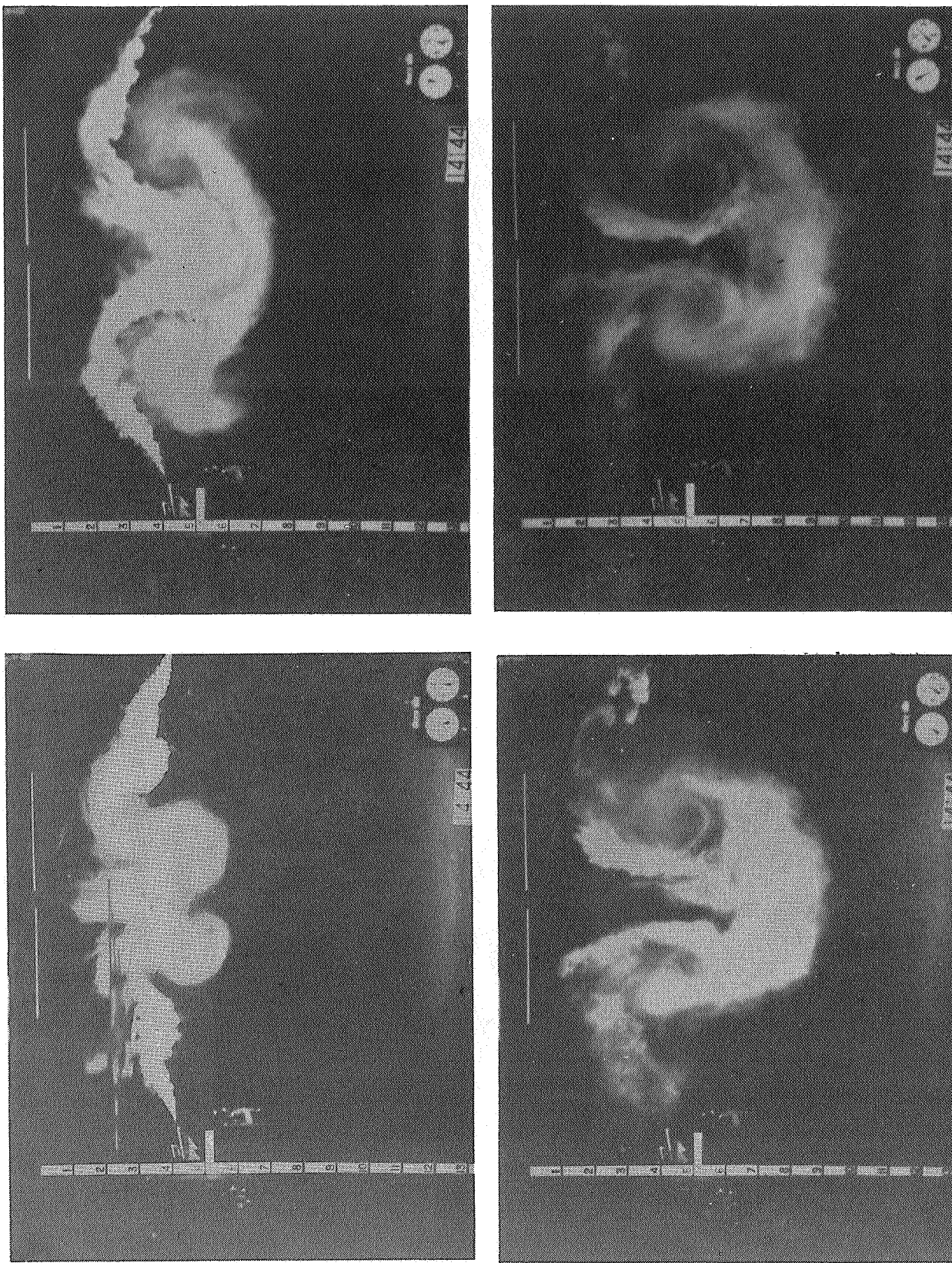
Figure 11.—Effect of maximum engine thrust on (fig 10) vortex system of wind-tunnel jet transport aircraft model (inboard flaps deflected 30°).

# GROUND DEVELOPMENT AND FLIGHT CORRELATION

## OF THE VORTEX ATTENUATING SPLINE DEVICE

James C. Patterson, **Jr.**, Earl C. Hastings, **Jr.**,

and Frank L. Jordan, **Jr.**

NASA Langley Research Center

## SUMMARY

The data presented in this report indicate that the wing-mounted spline is a effective vortex-attenuating device.  A comparison of the vortex-induced rolling moment results at a separation scale distance of 0.70 km (0.38 n. mi,) obtained in the Langley Vortex Research Facility with those measured in full-scale flight indicate good agreement for the unattenuated vortex configuration. The comparison also indicates that the spline effectiveness in flight was greater than in the ground facility test.  The results of an applications study show that, for the heavy commercial jet aircraft studied, use of the splines does result in some degradation of the climb gradient and rate of climb, but the aircraft should meet certification requirements.

## INTRODUCTION

The introduction of large, wide-body transport aircraft has resulted in an additional safety problem in the terminal area because of the strength and persistence of the lift-induced vortex.  Because vortex strength is a

271

function of the lift for a particular aspect ratio and wing platform, the vortexes produced by the heavy transport aircraft that are now in service have become a hazard to following aircraft. The persistent nature of the vortex flow prolongs this unseen hazard to long after the vortex–generating aircraft has passed. NASA is engaged in a broad research program to increase understanding of vortex behavior and to develop methods of attenuating the trailing vortexes.

This paper presents the results of some of the experimental research and development at Langley Research Center of a vortex–attenuating device referred to as a spline. The areas of research discussed include the development of the spline device in the Langley Vortex Research Facility, a correlation of full–scale and small–scale test results, and results of an applications study to evaluate the impact of employing splines on a modern, heavy jet transport aircraft.

## SYMBOLS

$b$    wing span, m

$\bar{c}$    mean geometric chord, m

$C_{l_P}$    rolling moment due to rolling velocity, $\partial C_l/\partial(pb/2U)$ per rad

$C_{l_r}$    rolling moment due to yawing velocity, $\partial C_l/\partial(rb/2U)$ per rad

$C_{l_v}$    vortex–induced rolling-moment coefficient

$C_{l_\beta}$    rolling moment due to sideslip, $\partial C_l/\partial\beta$ per rad

$C_{l_{\delta}}$    rolling moment due to total aileron deflection, $\partial C_l/\partial\delta_a$ per rad

$C_{\ell_{\delta_r}}$    rolling moment due to rudder deflection, $\partial C_{\ell}/\partial \delta_r$ per rad

$I_{xx}$    moment of inertia about longitudinal body axis, kg-m$^2$

$I_{yy}$    moment of inertia about lateral body axis, kg-m$^2$

$I_{zz}$    moment of inertia about vertical body axis, kg-m$^2$

$J_{xz}$    roll-yaw product of inertia, kg-m$^2$

L    rolling moment, m-N

P    angular rate about longitudinal body axis, rad/s

q    dynamic pressure, N/m$^2$

q'    angular rate about lateral body axis, rad/s

r    angular rate about vertical body axis, rad/s

S    wing area, m$^2$

U    velocity component along the longitudinal body axis, m/s

$\beta$    angle of sideslip, rad

$\delta_a$    total aileron deflection, rad

$\delta_r$    rudder deflection, rad

$\theta$    pitch attitude in Earth reference system, rad

$\phi$    roll attitude in Earth reference system, rad

$\psi$    heading relative to Earth reference system, rad


## TESTS IN THE LANGLEY VORTEX RESEARCH FACILITY

### Preliminary Vortex Research

Early vortex research that led to the spline concept was conducted in a pilot version of the Langley Vortex Research Facility. This pilot facility used a stationary airflow visualization method allowing a greater insight

into the actual motions of the wingtip vortex. The flow visualization method (ref. 1) developed in the pilot Vortex Research Facility is based on the fact that the air molecules affected by the wingtip are set into circular motion with no longitudinal flaw, with the exception of those molecules in the vortex core itself. To make this circular vortex motion visible, a screen of smoke is produced through which a model is propelled. As the model passes through the smoke screen, and for some time afterward, it is possible to photograph the entire life span of the vortex. (Although this same relative motion is present in the conventional wind tunnel, the test section usually is not of sufficient length to observe the full development of the vortex.

The first tests were conducted using a wing panel mounted on the monorail catapult system in the Langley towing basin. Preliminary runs were made that illustrated the vortex–alleviating effect of a number of configurations. These configurations were essentially geometric modifications of the wingtip, such as end plates, tip planform variations, tip extensions, flow-through nacelles, and many others that had only a small effect on the far-field vortex flow, and were, therefore, not solutions to the vortex persistence problem.

It was proposed that an unfavorable or positive pressure gradient applied just downstream of the wingtip might force the vortex to dissipate. This pressure gradient was applied by a decelerating chute at each wingtip, which virtually eliminated the vortex flow in both the near and far field. The mechanism behind the success of this approach is believed to be the result of disrupting the vortex axial flow plus the shearing stress between the rotational vortex flow and the linear flow of the mass of air forced forward into

each vortex core by the decelerating chutes. As a more practical application of this idea, the spline concept was tested and found to produce the same vortex attenuating effect as the decelerating chute. The spline configuration has the advantage that it can be readily retracted during cruise flight and deployed for landing.

## Langley Vortex Research Facility Description

The later small-scale, spline vortex attenuation tests described in this paper were conducted in the Vortex Research Facility. In this new facility the stationary airflow visualization method was again employed as in the earlier investigations. It was possible to determine the aerodynamic forces associated with the vortex generating model, and by positioning a second model in this vortex core downstream of the lead model it was possible to determine the vortex-induced rolling moment. An overall view of the Vortex Research Facility is shown in figure 1. The carriage is mounted on the 548.64-m overhead track, with a vortex-generating aircraft model blade mounted beneath this carriage, and a following vortex probe model located 48.77 m downstream (a scale distance of 0.70 km), through a series of trailers to measure the induced rolling moment resulting from the lead model vortex.

The test section, constructed to isolate the wake of the carriage and trailers from the model wake, is 91.4 m long with a 5.08-cm opening along the center of the ceiling to allow the model blade mounts to pass. The exterior of the building shown at the entrance of the test section encloses the entire length of the track.

## Test Model Description

Photographs of the two models used in the spline vortex attenuation investigation are shown in figures 2 and *3*. These are 0.07-scale models of the generating aircraft and probe aircraft used in the full-scale flight tests discussed later in this paper.

The model of the vortex generating aircraft with the spline device installed on the wingtip was blade mounted beneath the carriage on an internal six-component strain-gage balance. The three-bladed model propellers were free to rotate as the model moved through the test facility. The effect of thrust was determined by powering each model propeller with a small reciprocating engine capable of producing the scale thrust level of an engine on the full-scale generating aircraft, The effects of thrust were negligible.

The 0.07-scale model of the low wing, single engine vortex probe aircraft is shown in figure *3*. At this scale, the mean geometric wing chord of this model is *11.43* cm, resulting in a Reynolds number of 230 000 at the test velocity of approximately *30.48* m/s. Although low Reynolds number lift data are not available for this type of aircraft, it was doubtful, based on the data from the low Reynolds number test of reference 2, that the flow over the model wing was attached at the angles of attack induced by the vortex. During early tests the roll measurements made were unusually constant throughout the length of the test section. The probe aircraft model was in one fixed position relative to the wingtip of the vortex generating model during each run, and as a result of the vortex meander, this model was not perfectly centered in the vortex at all times throughout the entire length of the test

276

section.  The induced rolling moment measured by the probe model therefore varied with the degree of vortex penetration.  The constant rolling moment measured, therefore, indicated that the wing of the probe model was, indeed, stalled and that the vortex–induced roll was probably greater than that measured at this low Reynolds number.

To avoid this reduced performance for the following model, the wing panels of the probe model were deflected in a manner to reduce the relative vortex–induced angle of attack.  When penetration of the vortex produced by the left wing of the generating model occurs, an upflow is imposed on the left wing of the probe model and a downflow on the right wing.  By reduction of the angle of attack of the left wing and increase of that of the right wing by physically deflecting each wing panel separately, the vortex tangential velocity relative to each wing panel is reduced, such that the induced angle of attack is below the angle at which wing stall occurs at the test Reynolds number.  The wing panel deflection angle resulting in the greatest measured vortex induced–rolling moment was found to be $\pm 3^{o}$.

Transition was fixed by applying a 100–grit Carborundum strip of 0.254 cm width on all upper and lower surfaces at the 5–percent local chord position.

## TEST RESULTS

### Effect of Spline Spanwise-Position

The formation of the lift–induced vortex occurs near the tip of a lifting wing having a constant span load over a  large percent of the span,

such as that theoretically associated with a wing that is not tapered, twisted, or swept. The wing of the generating model used in this investigation was tapered and twisted; therefore, the final rollup of all the small vortexes formed along the span of the wing with each change in lift, plus the vortex created at the wingtip, coalesce inboard of the wing tip. Model tests were conducted to determine this rollup position, using the flow visualization technique of reference 1. The spline device was positioned at this location and at other spanwise locations along the wing span while the resulting rolling moment was measured by the probe model to determine the spanwise position that produces the maximum vortex alleviation. These rolling moment values induced on the probe model at a separation distance of 0.23 km are presented in figure 4.

The basic data of figure 4 show the maximum rolling moment induced by the generating model without vortex attenuation. The reduction in vortex–induced rolling moment attributed to the wingtip–mounted spline device is approximately 28 percent of the maximum. The attenuating effect becomes progressively greater as the spline is moved inboard, reaching a maximum roll reduction at approximately the 75–percent semispan position. The induced rolling moment at this point is reduced approximately 36 percent below that for the configuration without splines. These force data also indicate that the attenuating effect of the spline decreases as the spline is moved further inboard. The spline was tip mounted for the full–scale flight test because of structural considerations; therefore, the flight rolling–moment measurements presented here are considered somewhat conservative.

Visual data for the unattenuated configuration presented on figure 5 indicate the formation of the vortex system as this model moves through the smoke screen. The distinct vortex cores, the surrounding circulatory field, and the wing downwash may readily be seen as well as the growth and movement of the vortex system with time. The final photograph is of the probe model as it penetrates the vortex produced by the left wing panel of the generating model.

Visual data obtained for the generating model with tipmounted splines presented in figure 6 indicate that the high-energy vortex core produced by the basic unattenuated model is eliminated by the flow field of the spline device and the circulation around the core is greatly reduced. The vortex probe model shown in the final photograph measures the rolling moment induced by this altered vortex. Visual data obtained with the spline device located at the various spanwise positions (not shown) indicate a more dispersed flow pattern than shown here. As the splines are moved inboard along the span there is a tendency for the tip vortex to form, but it is rapidly dissipated as it moves into the flow field produced by the spline.

Visual data of the wake at separation distances several kilometers (miles) downstream from the vortex generating model indicate that there is a tendency for the vortex to reform possibly as a result of the remaining circulation. This same result was also noted during flight test, although the large diameter vortex that did reform when penetrated by the probe aircraft induced very little roll.

## Effect of Spline Diameter

Preliminary qualitative results obtained in the pilot facility (ref. **1)** indicate that the required spline diameter for vortex attenuation below the hazard level was approximately 55 percent of the wing mean geometric chord. The effect of spline diameter on the vortex–induced rolling moment measured in the Vortex Research Facility by the following model is presented in figure 7. These data indicate that the vortex attenuation of the spline device is a function of the exposed area as would be expected. However, reducing the diameter from 55 to 35 percent $\bar{c}$ resulted in only a small change in the reduction in induced rolling moment. Wind tunnel tests have shown that the drag associated with the spline is a direct function of frontal area, there– fore, the 35–percent $\bar{c}$ diameter spline would have substantially less drag than the 55–percent diameter spline. Therefore, the 40–percent–diameter spline would probably be optimum, considering both vortex attenuation and drag. The smallest diameter spline tested (27 percent $\bar{c}$) resulted in a sizable decrease in vortex attenuation while the largest spline tested (65 percent $\bar{c}$) resulted in an increase in vortex attenuation that extended much farther downstream and prevented the vortex from reforming. However, it would be expected that this larger spline would cause significant increase in drag.

The effect of spline diameter on the development of the lift–induced vortex is shown visually on figure 8. These data were obtained approximately 0.23 km (0.13 n. mi.) downstream from the vortex generating model. The results for the smallest diameter spline (upper left–hand photograph) indicate the vortex is beginning to reform at this short separation distance. As the

spline diamater is increased, it can be seen that vortex development is further retarded.

## Effect of Spline Chordwise Position

The spline position behind the wing trailing edge was based on experimental wind tunnel tests (not reported) such that the impingement of the spline pressure field on the wing surfaces causes a minimum loss in lift and increase in drag.  The increase in drag during landing is not considered as significant as any loss of lift might be.

## FLIGHT TEST DESCRIPTION

Detailed descriptions of the aircraft, systems, and procedures used in these tests are presented in reference 3 and summarized briefly here.

The aircraft shown in figure 9 was used as the generating aircraft because it was available and could be adapted for tip splines without undue time or expense.  Some additional characteristics of the generating aircraft used are as follows:

Empty operational mass, kg ($1b_m$) . . . . . . . . . . . . . . . 22 294 (49 *150)*

Wing area, $m^2$ ($ft^2$). . . . . . . . . . . . . . . . . . . .     135.8 (1462.0)

Wing mean aerodynamic chord, m (ft) . . . . . . . . . . . . . . . .4 (13.61)

Wing aspect ratio . . . . . . . . . . . . . . . . . . . . . . . . . . . .     9.44

Wing incidence (root), deg . . . . . . . . . . . . . . . . . . . . . . . . . .     4

Wing incidence (tip) deg . . . . . . . . . . . . . . . . . . . . . . . . . .     1

Horizontal tail area, $m^2$ $(ft^2)$ . . . . . . . . . . . . . . . . . 30.2 (324.9)

Vertical tail area, $m^2$ $(ft^2)$ . . . . . . . . . . . . . . . . . 16.7 (179'.3)

Engine . . . . . . . . . . . . . . . . . . . . .          Pratt and Whitney 2000 D-5

Propeller data:

    Type . . . . . . . . . . . . . . . . . Hamilton standard constant speed

    Gear ratio. . . . . . . . . . . . . . . . . . . . . . . . . . . . . . 2:1

    Blade activity factor . . . . . . . . . . . . . . . . . . . . . . . 100

    Diameter, m (ft) . . . . . . . . . . . . . . . . . . . . . . 3.97 (13.0)

For these tests, the basic aircraft was modified by the installation of the splines (see fig. 10), a spline jettison system, and a flow visualization system for vortex marking. As previously noted, tests in the Vortex Research Facility indicated that splines located inboard of the wing tips would be more effective than splines located at the tips. (See fig. 4.) With flaps down, the optimum spline location would have been further inboard. However, because the extensive structural modifications required to locate the splines inboard precluded anything but a tip-mounted location, the flight tests were made with the splines at the wing tips and with the flaps retracted. Inflight motion pictures showed that this configuration positioned the splines in a location to interact with the tip vortexes, even though optimization of the spline location was not possible.

A diagram of the probe aircraft is shown in figure 11. For these tests, the probe aircraft was equipped with onboard distance measuring equipment (DME); an S-band radar tracking beacon, and a fixed 16-mm motion picture camera. Additional information on the characteristics of the probe aircraft

include the following:

**Mass :**

Empty operation, kg ($1b_m$) . . . . . . . . . . . . . . . . . 799 (1761)

Gross takeoff, kg ($1b_m$) . . . . . . . . . . . . . . . 1009 (2225)

Inertias (approximate):

$I_{xx}$, kg-m$^2$ (slug-ft$^2$) . . . . . . . . . . . . . . . . . 1356 (1000)

$I_{yy}$, kg-m$^2$ (slug-ft$^2$) . . . . . . . . . . . . . . . . 1900 (1401)

$I_{zz}$, kg-m$^2$ (slug-ft$^2$) . . . . . . . . . . . . . . . . 2700 (1991)

$J_{xz}$, kg-m$^2$ (slug-ft$^2$) . . . . . . . . . . . . . . . . . 67.6     (50)

Wing data:

Area, m$^2$ (ft$^2$) . . . . . . . . . . . . . . . . . . . . 14.9   (160)

Span, m (ft) . . . . . . . . . . . . . . . . . . . . . 9.14    (30)

Chord, m (ft) . . . . . . . . . . . . . . . . . . . . 1.6   (5.3)

Aileron data:

Span, m (ft) . . . . . . . . . . . . . . . . . . . . . 1.6   (5.3)

Chord, m (ft) . . . . . . . . . . . . . . . . . . . . . 0.305   (1.0)

Engine type . . . . . . . . . . . . . . . . . . . . . . . . Lycoming 0-360-A3A

On a typical penetration flight, the two aircraft would rendezvous and
establish the desired airspeeds, headings, and altitudes.  The probe aircraft
records, DME, and camera were turned on, and the vortex-marking system in the
generating aircraft was activated,  When the desired separation distance
between the two aircraft was established, the probe aircraft approached the
vortex trail along'a parallel course.  Shallow-angle penetrations were then
made from just above or below the trail.  For flights without splines, pene-
trations were made at separation distances between 9.26 km (5 n. mi.)  and

3.70 km *(2* n. mi.). With splines installed, penetrations were made as close as *0.6* km *(0.32* n. mi.). All penetrations were made in the flaps–up configuration at a nominal altitude of *2100* m *(7000* ft) and indicated airspeeds of 50±5 m/s (90±10 knots). The test Reynolds number, based on these nominal values and the $\bar{c}$ of the probe aircraft, was *4.364* × $10^6$.

In comparing vortex attenuation results from flight tests with those from ground facilities, a difference in testing technique should be noted. In these flight tests (as in flight tests in general) it was often difficult to precisely position the probe aircraft in the vortex core. Some factors that contributed to this difficulty were small vortex core, meander of the vortex because of atmospheric disturbances, and the tendency of the probe aircraft to roll away from the core. (In these tests, this problem was less severe with the attenuated (splines–deployed) vortex because the core size was larger and the vortex less intense.) Data presented from the Vortex Research Facility, however, were determined when it was certain that the probe model was within the vortex core.

To minimize this difference in test technique, the flight tests involved a large number of penetrations to increase the probability that the maximum possible induced–roll accelerations of the probe aircraft were achieved. The validity of this technique is discussed later in this paper.

## DATA ANALYSIS AND RESULTS

One of the parameters used to evaluate vortex attenuation effectiveness was the maximum roll acceleration $\dot{p}_{max}$ derived from measured rate data recorded

by the probe aircraft during penetrations with controls as nearly neutral as possible. Many penetrations were made to provide a large statistical sampling. The maximum values obtained (ref. 3) are shown in figure 12. Data are presented for the generating aircraft without splines, and with the 2.28-m splines installed. It is evident that the splines were effective in attenuating the vortex effects over the range of distances shown.

As noted in reference 3, these results include the effects of small aileron deflections. To provide a comparison of the flight data with data from the Vortex Research Facility, additional analyses were conducted to express the flight results in terms of the rolling-moment coefficient resulting from vortex alone.

The equation of motion in roll (see ref. 4, ch. 3) is given by

$$L = \dot{p}I_{xx} - \dot{r}J_{xz} + q'r(I_{zz} - I_{yy}) - pqJ_{xz} \tag{1}$$

where a dot above a symbol denotes a derivative with respect to time.

The linearized equation, expressed in terms of rolling-moment coefficients (ref. 4), is

$$\frac{I_{xx}\ddot{\phi}}{qSb} - \frac{J_{xz}\ddot{\psi}}{qSb} - \frac{\dot{\phi}b}{2U}C_{\ell_I} - \frac{\dot{\psi}b}{2\bar{u}}C_{\ell_r} - C_{\ell_\beta}\beta = C_{\ell_{\delta_a}}\delta_a + C_{\ell_{\delta_r}}\delta_r \tag{2}$$

where

$$\dot{\phi} = p + q' \sin\phi \tan\theta + r \cos\phi \tan\theta \tag{3}$$

and

$$\psi = (q' \sin \phi + r \cos \phi) \sec \theta \tag{4}$$

Equation (2) was used as the basis of this analysis because a computer program was available and sample cases showed less than a 4 percent difference in the results from the complete and linearized (computer) methods.

Adding a term $C_{\ell_V}$ for the vortex effect, and transposing terms in equation (2), gives the relationship used in this analysis:

$$C_{\ell_V} = \frac{I_{xx}\ddot{\phi}}{qSb} - \frac{J_{xz}\ddot{\psi}}{qSb} - \frac{\dot{\phi}b}{2U} C_{\ell_P} - \frac{\dot{\psi}b}{2\bar{u}} C_{\ell_r} - C_{\ell_\beta} B - C_{\ell_{\delta_a}} \delta_a - C_{\ell_{\delta_r}} \delta_r \tag{5}$$

Equation (5) was used to determine values of $C_{\ell_V}$ at 0.1-s time intervals during each vortex penetration of interest, and the maximum values are presented as the flight test $C_{\ell_V}$ values in this report. In the solution of equation (5), the inertias, wing area, and wing span of the probe aircraft were used. Aerodynamic and control derivatives were those obtained in earlier Langley Research Center flight test and simulator tests with this aircraft:

$C_{\ell_P}$, rad$^{-1}$ . . . . . . . . . . . . . . . . . . . . . . . . . . . . . . . . -0.2741

$C_{\ell_r}$, rad$^{-1}$ . . . . . . . . . . . . . . . . . . . . . . . . . . . . . . . . .07

$C_{\ell_\beta}$, rad$^{-1}$ . . . . . . . . . . . . . . . . . . . . . . . . . . . . . . -.045

$C_{n_{\delta_a}}$, rad$^{-1}$ . . . . . . . . . . . . . . . . . . . . . . . . . . . . . . -.0365

$C_{\ell_{\delta_r}}$, rad$^{-1}$ . . . . . . . . . . . . . . . . . . . . . . . . . . . . . -.014

Airspeed, dynamic pressure, control position, attitude, and rate information were determined from measurements recorded during the vortex penetrations.

An indication of the accuracy of this procedure was shown, using the results of flight tests with the probe aircraft in which aileron rolls were performed in undisturbed air ($C_{\ell_V} = 0$). Data as listed for probe aircraft and flight-test data were used with equation (5), and $C_{\ell_V}$ histories were calculated for a number of rollmaneuvers. In all cases, the maximum calculated values of $C_{\ell_V}$ were between 0 and 0.003. This indicated that the error resulting from the analytical method was much smaller than the vortex-induced values.

Maximum values of $C_{R_V}$ from this analysis are shown in figure 13. The maximum aileron rolling moment coefficient, $C_{\ell_{\delta_a}} 6_{a_{max}}$ is also shown. The data show that for the unattenuated (no spline) vortex, the vortex-induced roll was larger than the maximum aileron roll at separation distances closer than 8 km (4 n. mi.) and was about 60 percent above that value at 4.11 km (2.22 n. mi.). For the attenuated (splines-on) case, the vortex-induced roll coefficient was always less than the roll capability of the aileron under the same conditions.

## GROUND FACILITY/FLIGHT TEST CORRELATION

A comparison of the results obtained in the Langley Vortex Facility with those obtained in flight is presented in figure 14. The rolling moment induced by the lift-induced vortex of the 0.07-scale generating model was measured at a scale distance of 0.70 km (0.38 n. mi.) downstream of this model, although the flight data are presented at separation distances ranging

from 4.11 to 9.09 km.  The flight data in this figure has been corrected to the same value of  $U/U_f$  (where  $U_f$  is the velocity of the following aircraft) as the 0.07  scale tests.

A flight rolling moment coefficient of the 0.058  is obtained for the basic configuration at a separation distance of 0.70  km using the straight line extrapolation shown.  This extrapolation is based on flight test results presented by Marvin R. Barber, et al, in this report.  There is reasonable agreement between the "no splines" data based on this extrapolation.  This indicates that the test techniques employed in the ground and the flight experiments were valid for this configuration.

The attenuated rolling-moment coefficients (splines on) presented in figure 14 are for the wing-tip mounted spline device with a diameter equal to 55 percent of the mean geometric wing chord.  It was possible during the flight test to probe as close as 0.60 km behind the vortex-generating aircraft allowing a direct comparison between flight and model test results.

The tip-mounted spline reduced the vortex-induced rolling moment in flight approximately 72 percent at a separation distance of 0.70  km while the model results indicate a vortex roll reduction of approximately 27 percent at this same separation distance.  These data indicate that a greater vortex attenuating effect is derived from the spline device in flight than in the ground facility. Although the reason for this discrepancy has not yet been determined it might be conjectured then that Reynolds number may have a large affect on the flow field developed by the spline device reducing its vortex attenuating effect at model scale.  The model visual data indicate that the well-organized vortex core is nearly eliminated while the circulation outside of the core remains and produces the rolling moment measured by the following model.  The lower velocities associated with the circulation would be affected by model scale.

## APPLICATIONS STUDY

During these flight tests, the performance of the generating aircraft with splines attached was evaluated and found to be acceptable (ref. 3). However, because this generating aircraft was not a representative commercial aircraft, a preliminary study was conducted for NASA by the Boeing Co. to evaluate the performance of the aircraft shown in figure 15. Results are presented in reference 5.

In summary, it was concluded that for splines deployed only on approach, the concept appears feasible from the standpoint of structures, stability and control, performance, and operations. The largest spline effects are decreases in landing climb gradient and climb rate, and an increase in approach noise. Even with these penalties, the aircraft would meet certification requirements. Effects on other parameters such as takeoff, cruise, range, approach speed, and so forth, were indicated to be insignificant.

## CONCLUDING REMARKS

The results obtained during this investigation indicate that--

(1) The spline device is effective in reducing the strength of the lift-induced vortex.

(2) A comparison of the vortex-induced rolling moment obtained in the Langley Vortex Research Facility with full-scale flight results indicate good agreement for the unattenuated aircraft configuration. This implies that the test techniques employed on the ground and in flight experiments were valid.

(3) A comparison of data at 0.70 km indicates that the vortex attenuation achieved in flight was greater than was obtained in the ground facility, indicating that the ground facility was conservative with this device.

(4) A preliminary study indicated that the installation of splines on current commercial jet aircraft would be feasible. Significant penalties would result in the landing phase climb capability and approach noise. Even with the penalties, however, this aircraft would meet current certification requirements.

## REFERENCES

1. Patterson, J. C., Jr.; and Jordan, F. L., Jr.: A Static–Air Flow Visualization Method to Obtain a Time History of the Lift–Induced Vortex and Circulation. NASA TM X–72769, 1975.

2. Jacobs, E. N.; and Sherman, A.: Airfoil Section Characteristics as Affected by Variation of Reynolds Number. NACA TR–586, 1937.

3. Hastings, E. C., Jr.; Patterson, J. C., Jr.; Shanks, R. E.; Champine, R. A.; Copeland, W. L.; and Young, D. C.: Development and Flight Tests of Vortex Attenuating Splines. NASA TN D–8083, 1975.

4. Blakelock, J. H.: Automatic Control of Aircraft and Missiles. John Wiley & Sons, Inc., Apr. 1965.

5. Tracey, P. W.; and Berger, John H.: The Effects of Installing Vortex Attenuation Devices on the Design, Performance, and Operations of a Heavy Commercial Jet Transport. Boeing Report Number D6–37174, 1975.

COVERED AREA

TRAILER

FOLLOWING MODEL

VEHICLE

VORTEX GENERATING MODEL
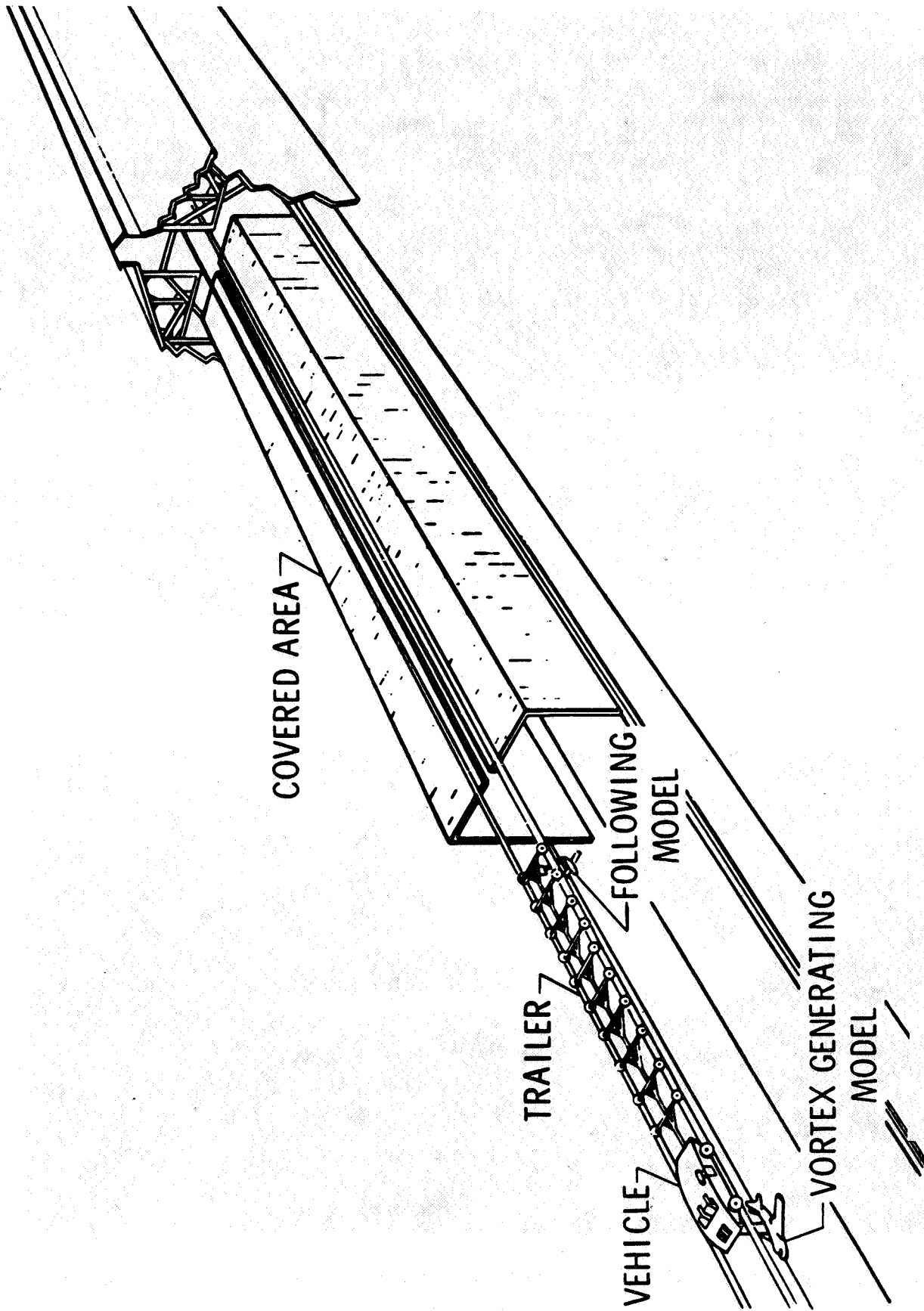
Figure 1.—Arrangement of the Langley Vortex Research Facility.
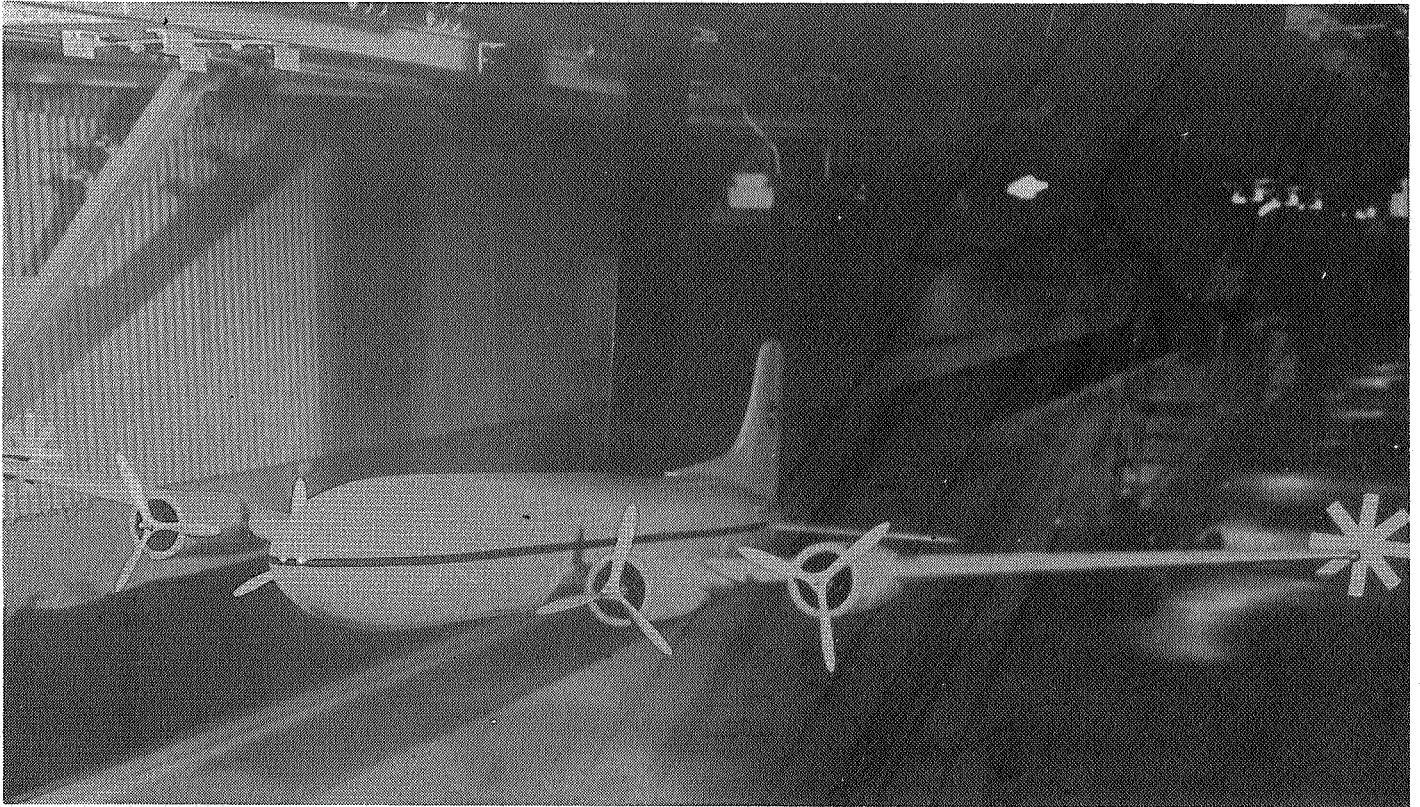
Figure 2.--Photograph of 0.07-scale model of propeller driven transport aircraft used as the vortex-generating model.
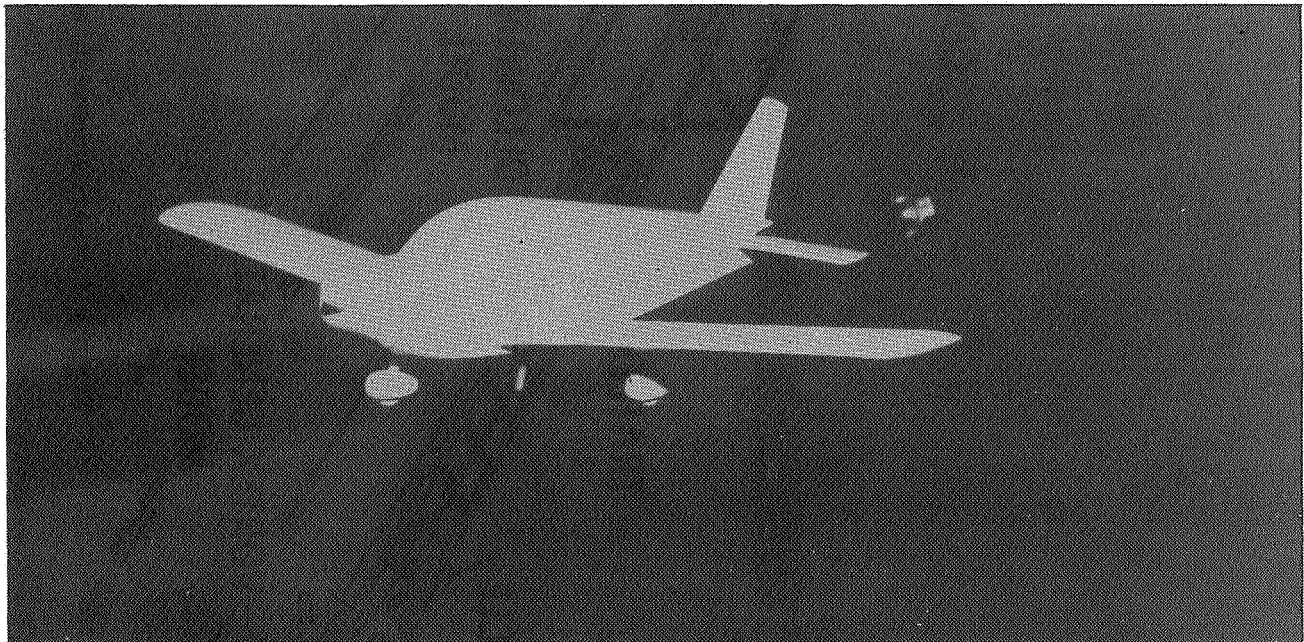


Figure 3.--Photograph of 0.07-scale model of single engine light aircraft used as the vortex probe model.
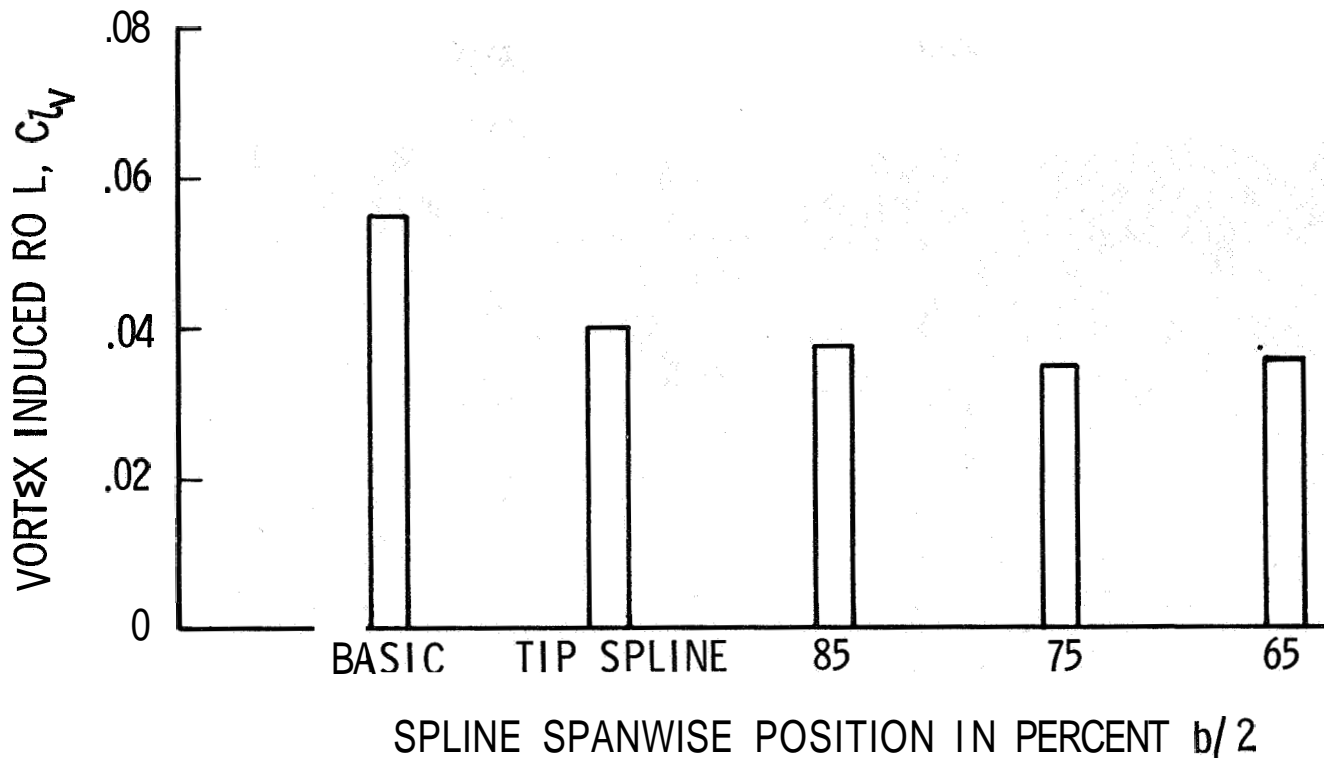
Figure 4.--Effect of spline spanwise position on vortex attenuation.
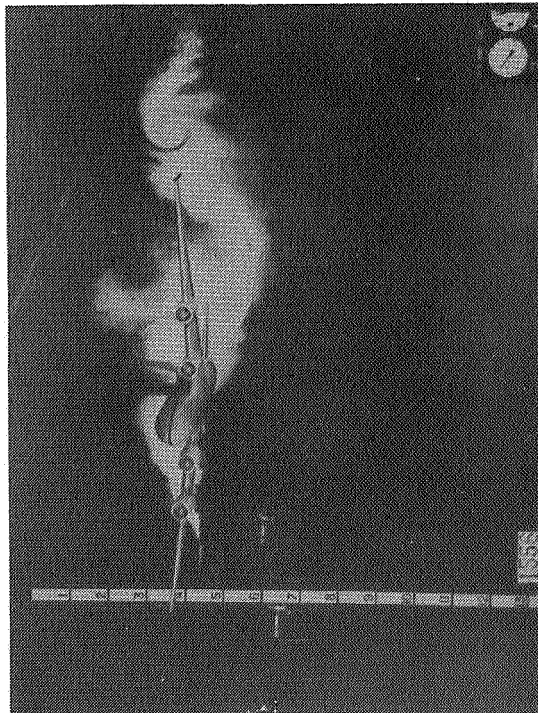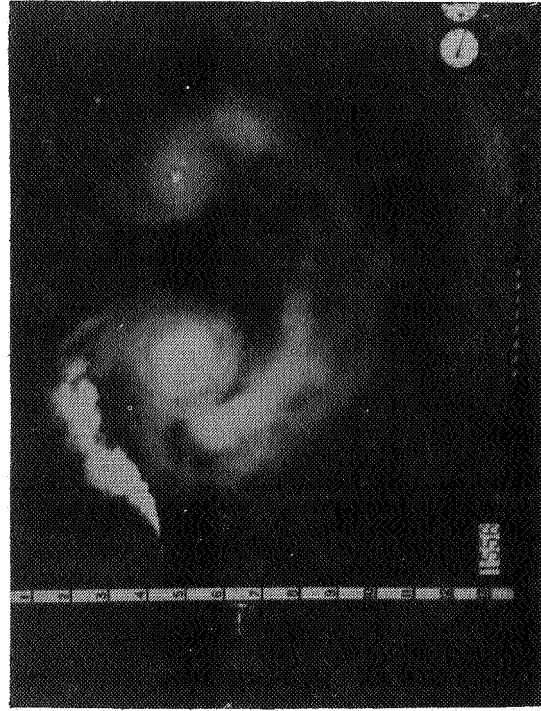
Figure 5 —Lift-induced vortex system created by 0.07-scale model of transport aircraft. The photographic sequence corresponds to a separation distance of 0 23 km. The following model is centered in the vortex in the last photograph. Lift coefficient = 0.9, velocity = 30.48 m/s.
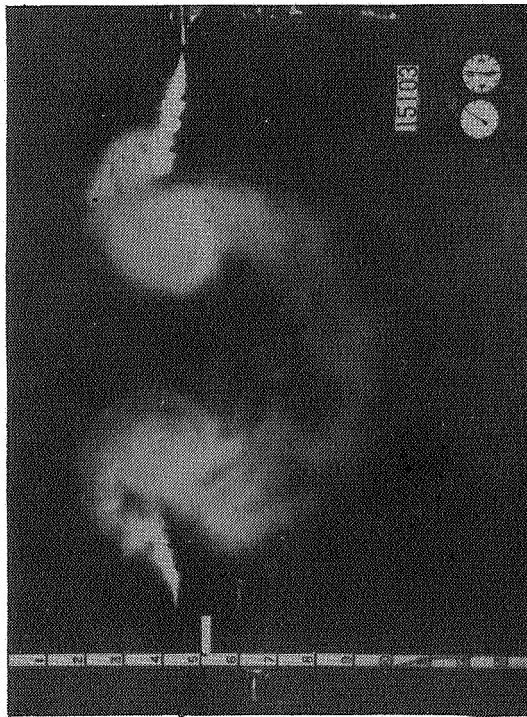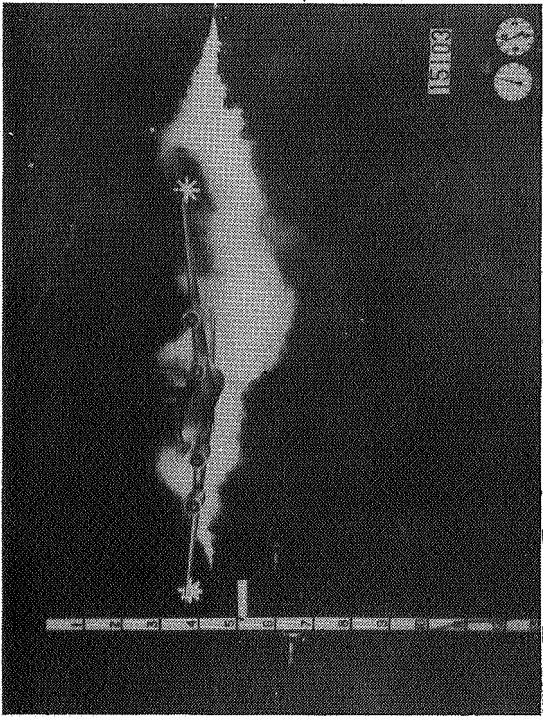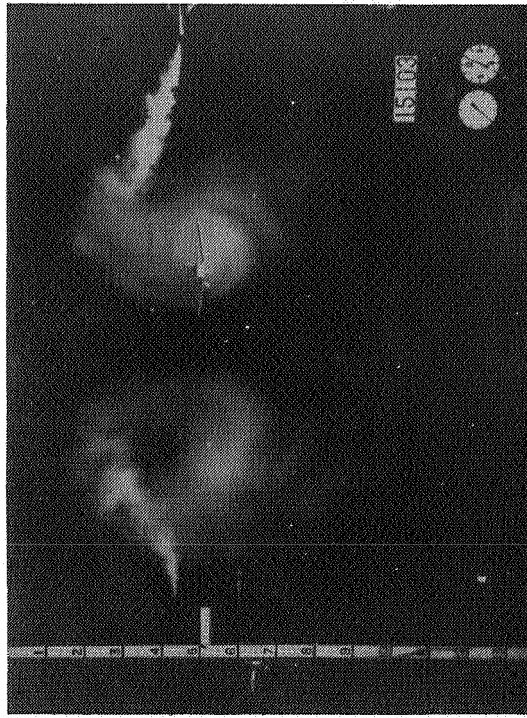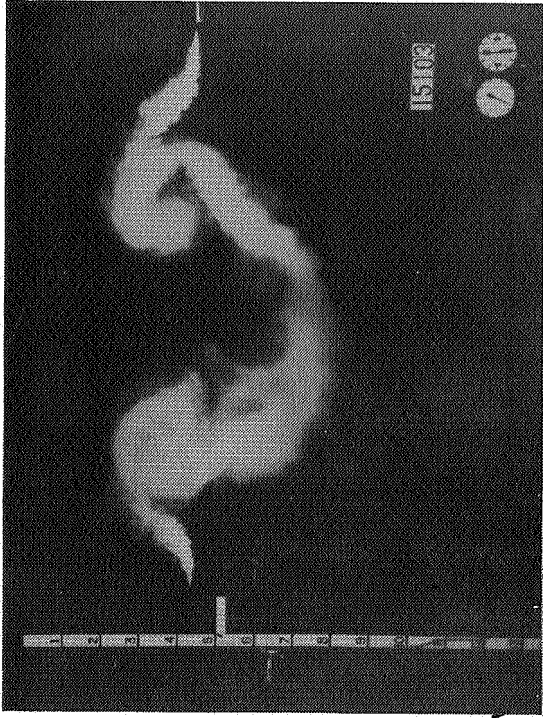
Figure 2.—Effect of the spline vortex attenuating device on the vortex system of transport aircraft The photographic sequence corresponds to a separation distance of 0 2₃ km. The following model is centered in the vortex in the last photograph. Lift coefficient = 0.8; velocity = 30 48 m/s
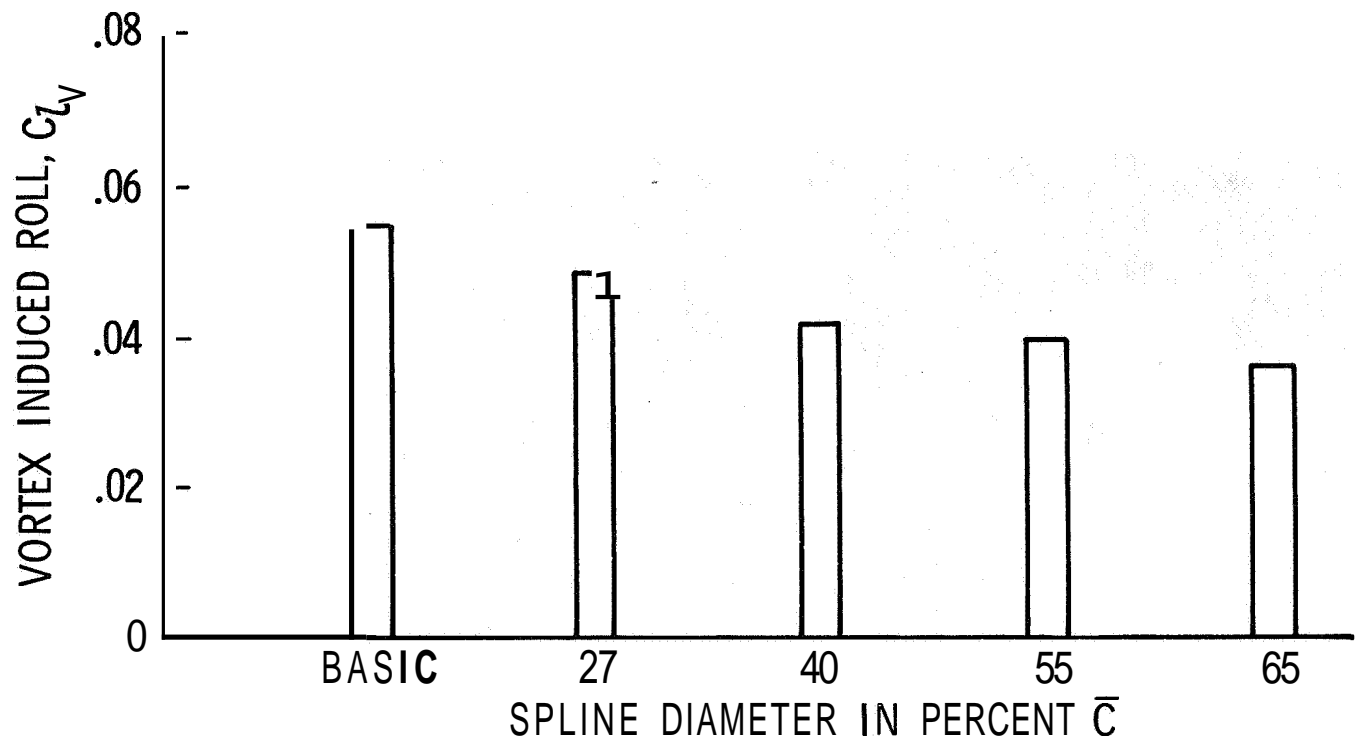
Figure 7.--Effect of spline diameter on the vortex attenuation of wingtip-
mounted spline.
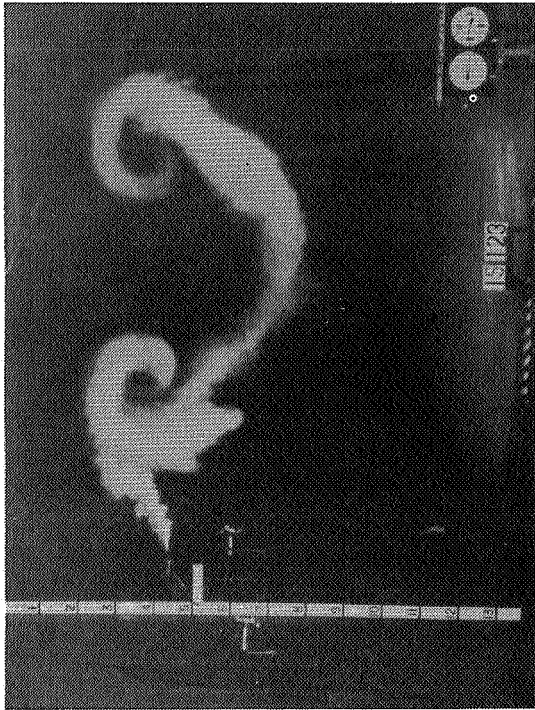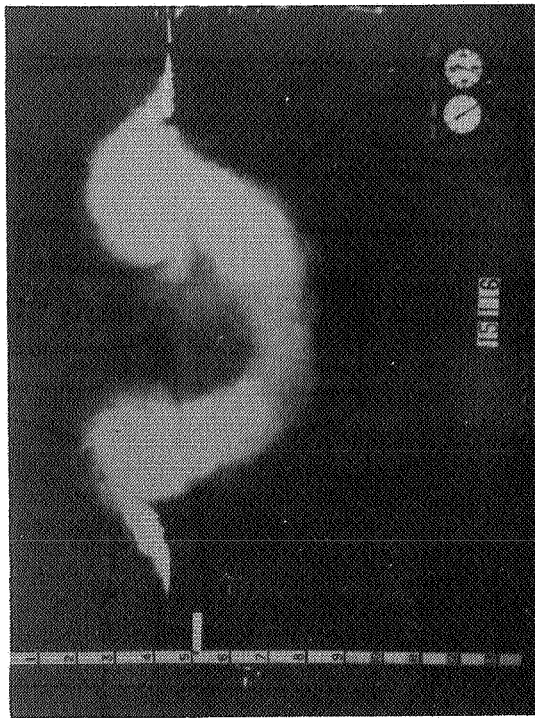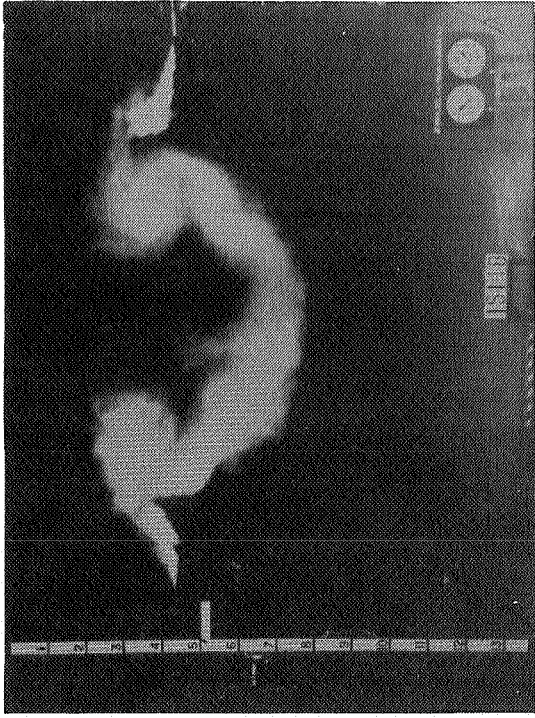
Figure 8 —Effect of spline diameter on vortex system from the transport aircraft at a separation distance of 0 23 km. Spline diameters at upper left are 25 percent of mean geometric chord; lower left, 50 percent; lower right, 60 percent.
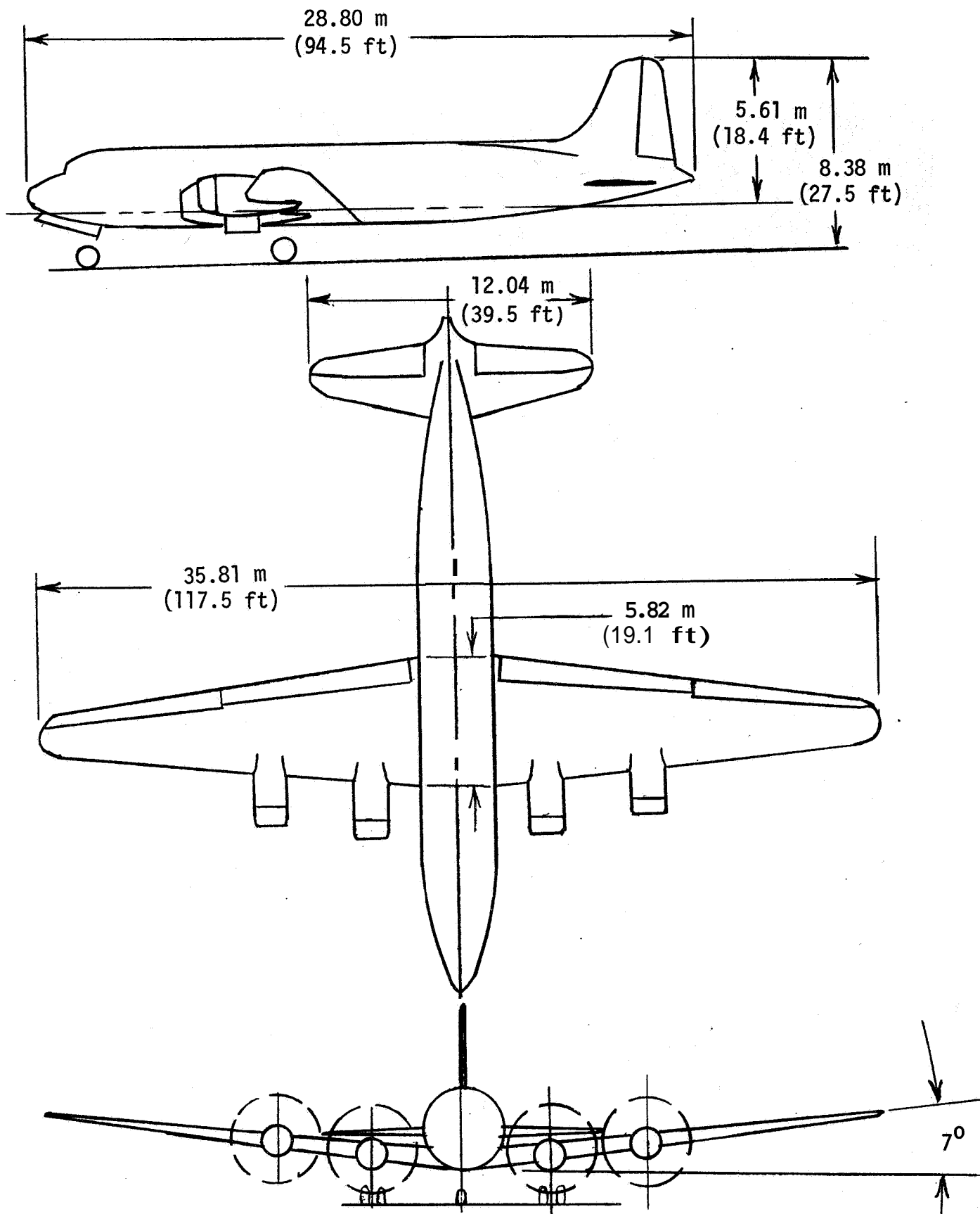
Figure 9.--Diagram of unmodified generating aircraft.

298
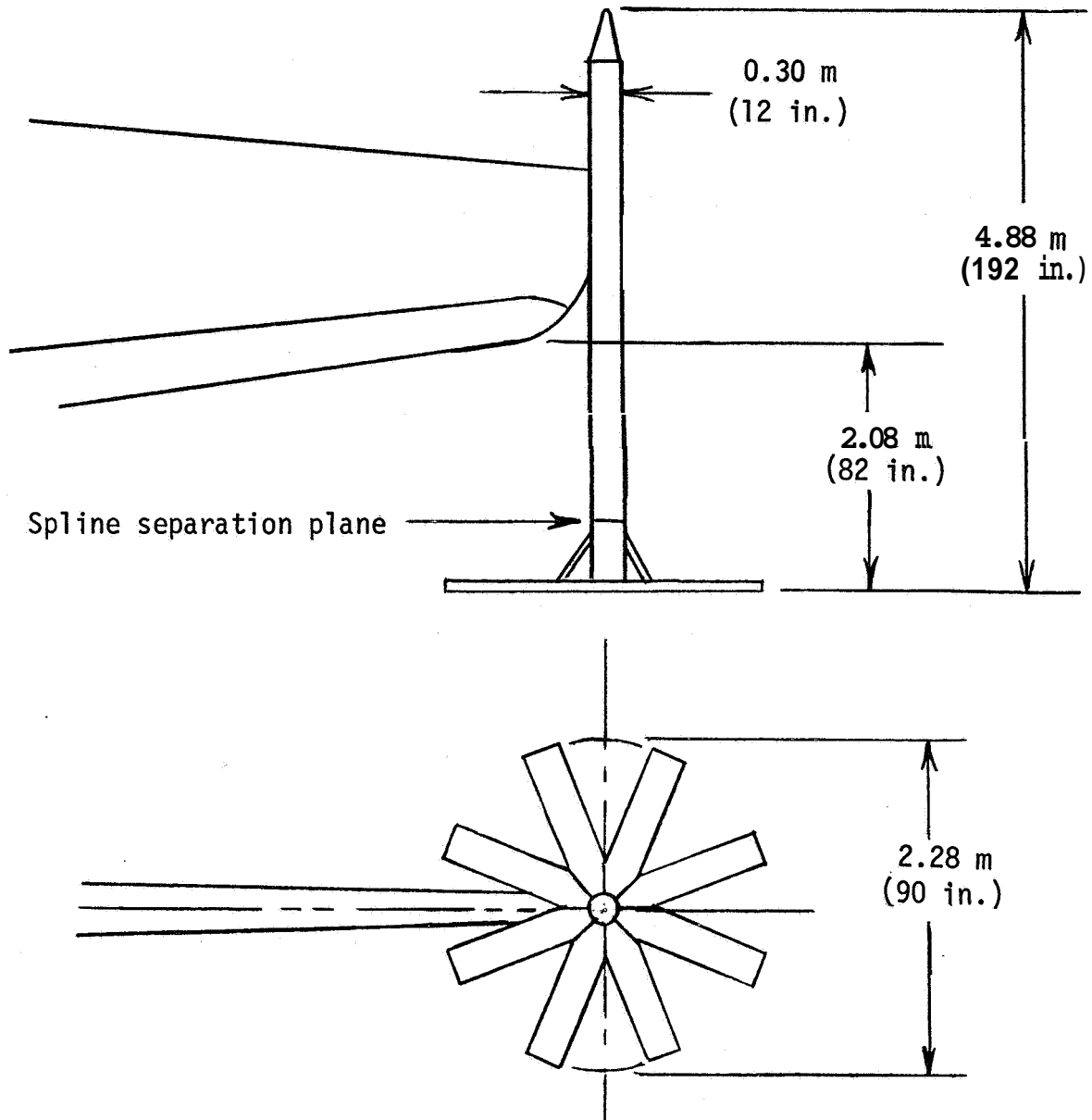
Figure 10.--Sketch of spline assembly at wingtip.
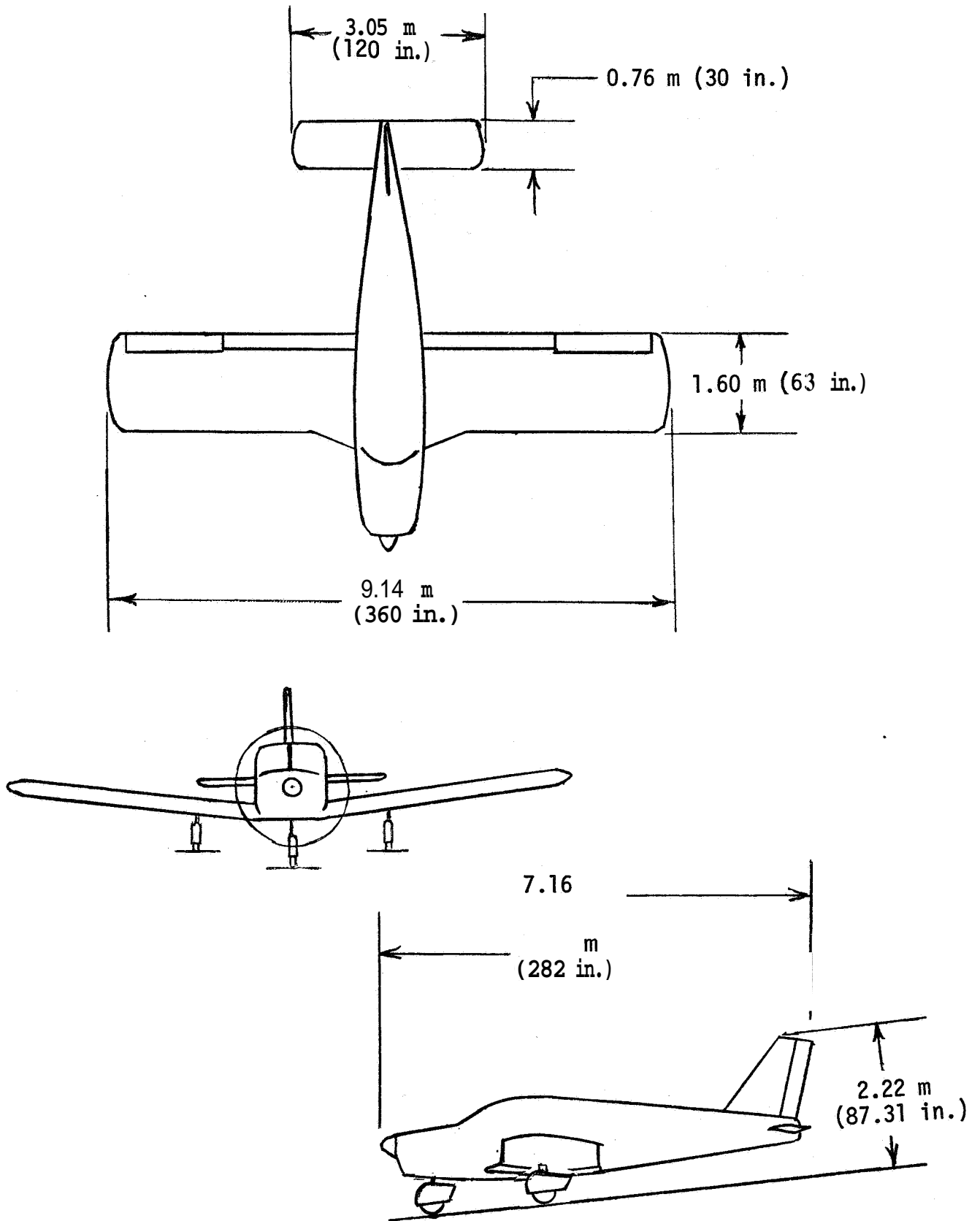
Figure 11.--Diagram of probe aircraft.

300
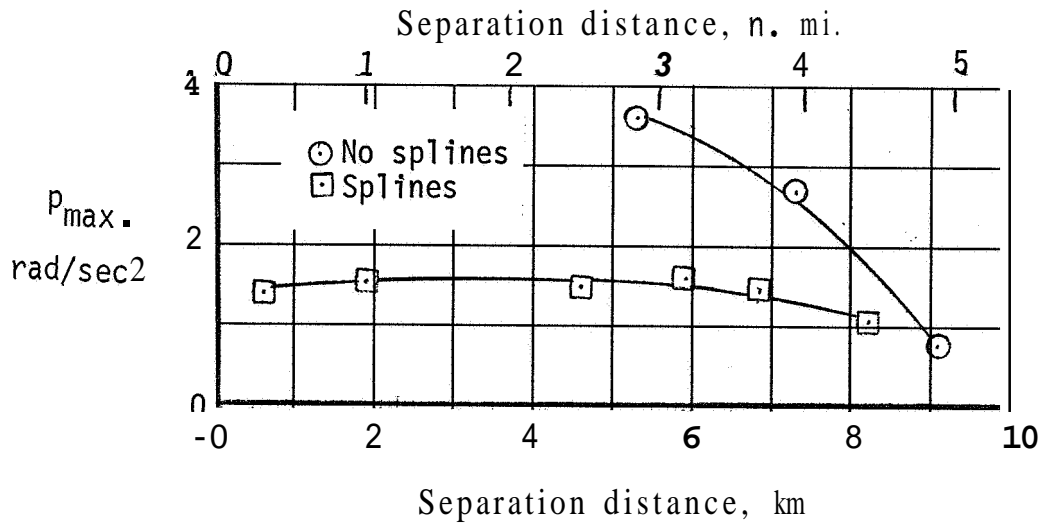
Figure 12.--Maximum roll acceleration.
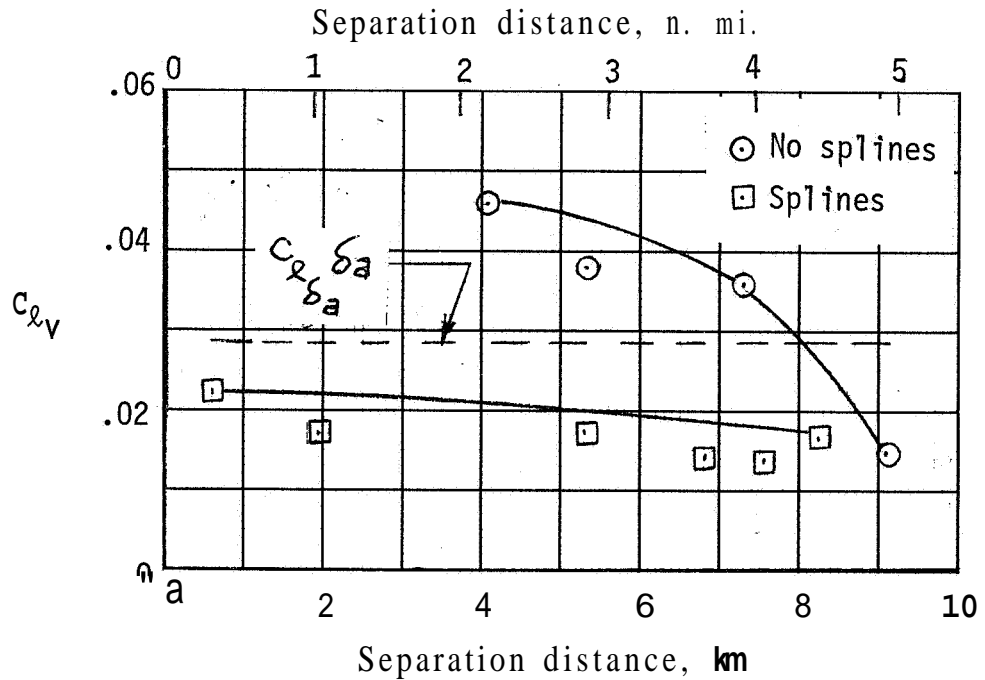


Figure 13.--Maximum vortex-induced rolling moment coefficient from flight tests.

301

Separation distance, n mi

O No splines
□ Splines

Extrapolated

.07 scale

Note: Flight II-Qa corrected for $U/U_\infty$, $\beta$, $\dot{\phi}$, $\dot{\psi}$, $l_a$ and $\delta_r$

$C_{\ell_V}$

Flight (corrected)

$C_{\ell_{\delta_o}}^{la}$

$C_{\ell_{\delta_o}}^{la}$

Separation distance, km
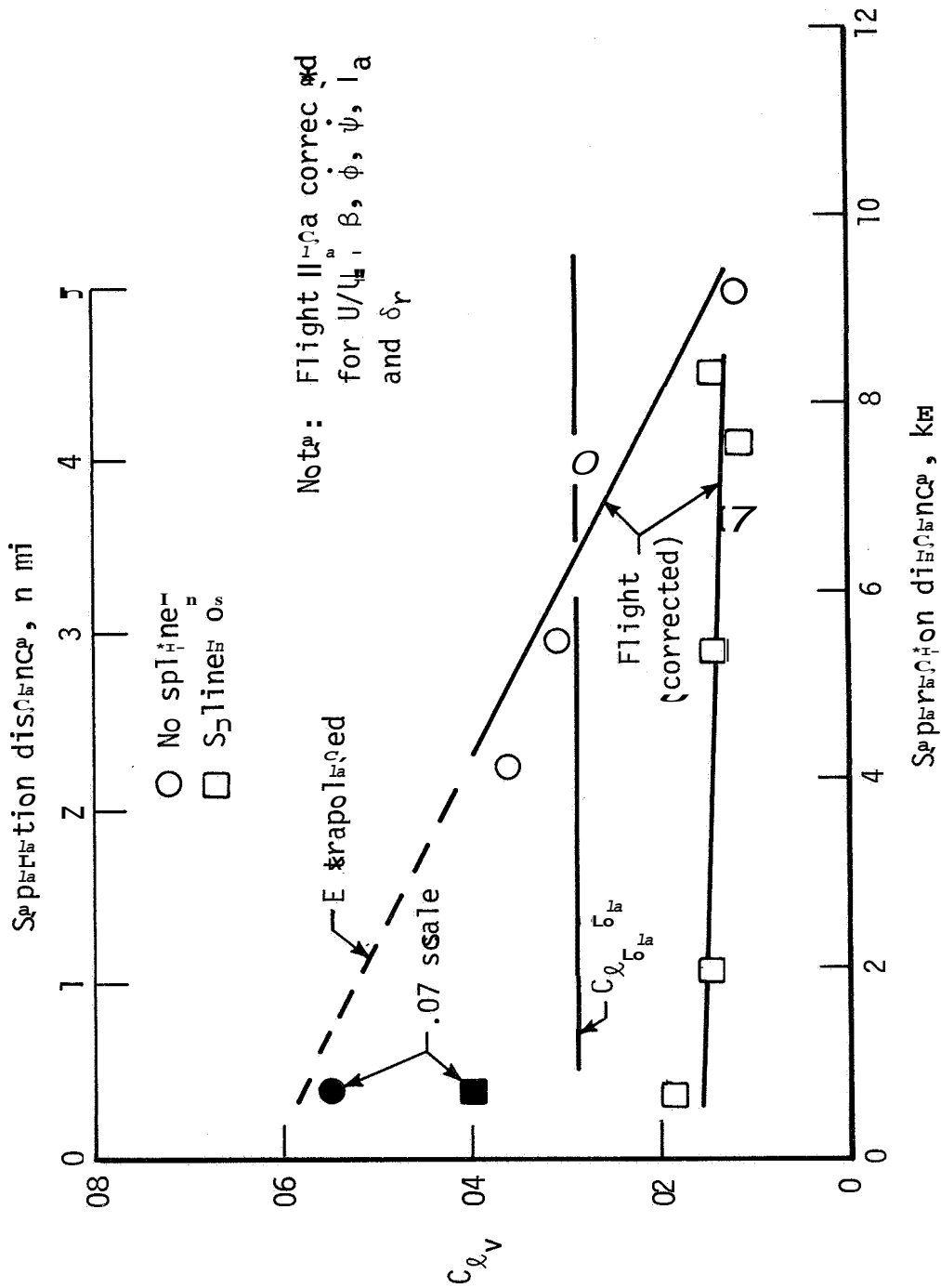
Figure 14.—Correlation of the vortex-induced rolling moment results obtained in flight and in the ground-based facility. Lift coefficient = 0.8.

Inboard flap track fairing

Spline pod

1.17 m. dia. (3.83 ft.)

6.43 m (21.08 ft)

3.40 m (11.17 ft)

Outboard flap track fairing

Insert

0.91 m (3.00 ft)

5.09 m. dia. (16.7 ft.)

See insert for details

$\frac{b}{2}$

.549
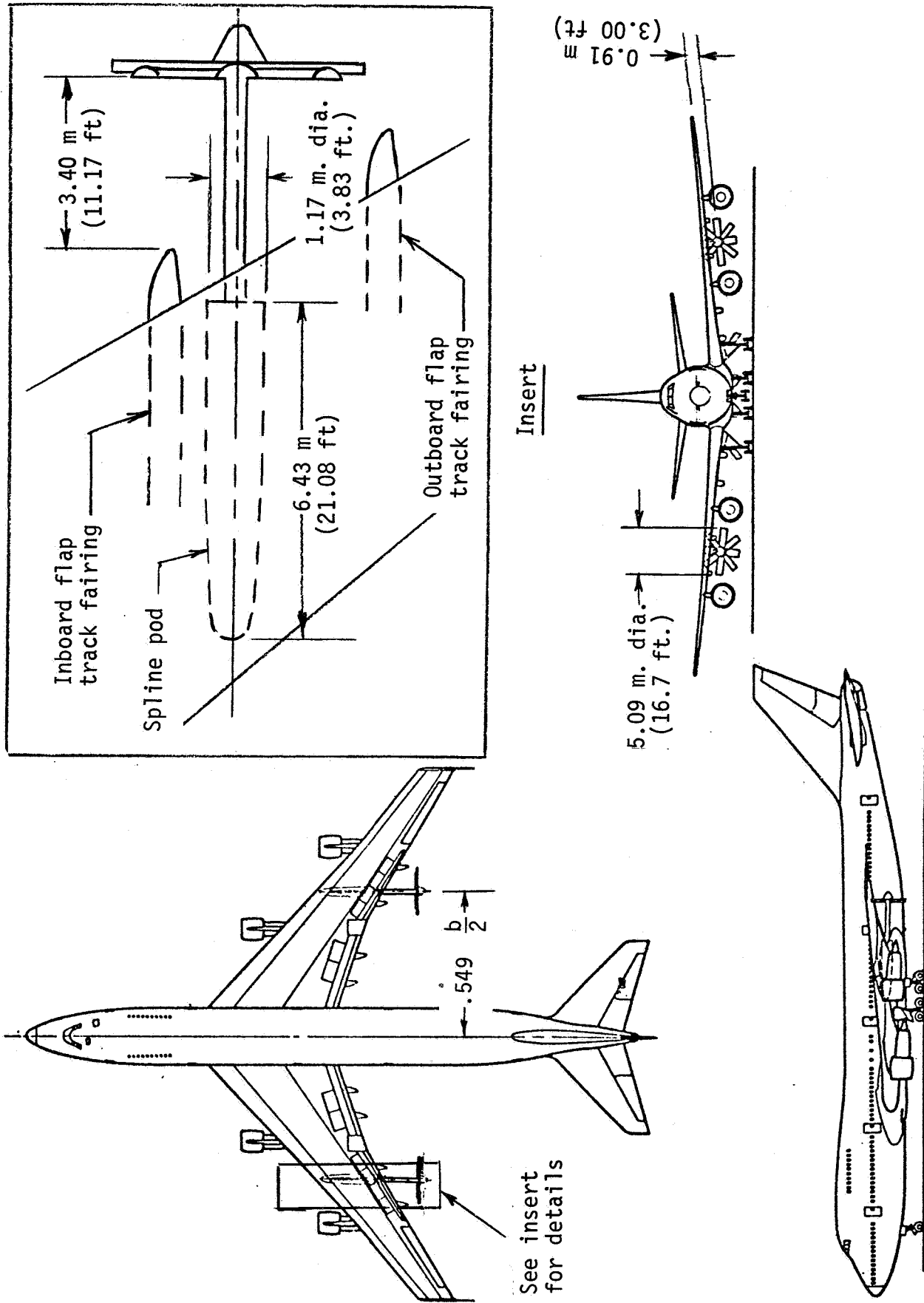
Figure 15.--Spline system installation on heavy commercial jet aircraft.

303

# AIRCRAFT WAKE–VORTEX MINIMIZATION BY USE OF FLAPS

Victor R. Corsiglia and R. Earl Dunham, Jr.*

Ames Research Center

## SUMMARY

A survey is made of research on the alleviation of the trailing vortex hazard by altering span loading with flaps on the generator airplane. Flap configurations of the generator that shed multiple vortices were found to have wakes that dispersed by vortex merging and sinusoidal instability. Reductions of approximately 50 percent in both the wake rolling moment imposed on a following aircraft and the aircraft separation requirement were achieved in the ground–based and flight–test experiments by deflecting the trailing–edge flaps more inboard than outboard. Significantly, this configuration did not increase the drag or vibration on the generating aircraft compared to the conventional landing configuration. Ground–based results of rolling–moment measurement and flow visualization are shown, using a water tow facility, an air tow facility, and a wind tunnel. Flight–test results are also shown, using a full–scale B–747 airplane. General agreement was found among the results of the various ground–based facilities and the flight tests. Some progress has been made in identifying configurations that alleviate the wake; however, more research is required before a configuration acceptable for airline operation is found.

## INTRODUCTION

The objective of the NASA wake–vortex alleviation program is to reduce the intensity of the lift–generated vortices shed by large subsonic transport aircraft so that separation distances between aircraft can be reduced during landing and takeoff. One aspect of this program has been devoted to investigating the effect on the wake of turbulence injection into the vortices

---

*Langley Research Center.

(refs. 1-14). In these studies, a variety of spoiler sizes and locations were considered, as well as various spline configurations. Although some of the turbulence injection devices were effective in reducing wake intensity, the penalties associated with their drag, lift, unsteady loads, and installation made them unacceptable solutions to the wake-vortex problem. Recently, however, the use of the existing spoilers on the *B-747* airplane has been found to be effective (refs. 15 and 16), and an effort is underway to reduce the associated penalties to a tolerable level (ref. 17).

An alternate approach to wake-vortex minimization is to distribute the lift on the wing so that a very diffuse wake results. This approach is attractive in that lower levels of wing profile drag would be expected compared to the use of drag devices such as a spoiler or spline. This lower drag is especially important for takeoff and the climb phase of flight. This paper discusses the use of flaps as a technique to alter span loading and includes work performed by the **NASA** Ames, Flight, and Langley Research Centers.

## NOTATION

| | |
|---|---|
| $b$ | wingspan |
| $c$ | wing local chord |
| $\bar{c}$ | wing average chord |
| $c_\ell$ | local lift coefficient |
| $c_l$ | rolling-moment coefficient |
| $C_D$ | total drag coefficient |
| $C_L$ | total lift coefficient |
| $C_M$ | total pitching-moment coefficient |
| $D$ | vortex spacing (see fig. 11) |

$i_t$       horizontal stabilizer incidence

$r$         vortex radius

$t$         time

$\Delta t$        time increment

$U_\infty$        free-stream velocity

$V_\theta$        vortex swirl velocity

$x$         downstream distance

$Y$         spanwise distance

$a$         angle of attack

$\eta$         $= 2y/b_g$

$30°/0°$     indicates inboard flap deflected 30" and outboard flap deflected
            $0°$ typically

Subscripts

$f$         follower model

$g$         generator model

RELATIONSHIP BETWEEN SPAN LOADING AND VORTEX-WAKE INTENSITY

Theoretical

Significant progress was made in understanding the relationship between
span loading on the generating wing and the structure of the downstream vortex
wake when the Betz method (ref. 18) was adopted by several investigators.   The
wake rollup procedure described by Betz in 1932 received little attention
until Donaldson (refs. 19 and 20) showed that the swirl velocity distribution
calculated in this way compared favorably with measurements.   Mason and
Marchman (ref. 21) applied the Betz method to a series of tapered wings and

307

concluded that the trailing vortex became more intense as the vorticity was concentrated on the outer portion of the wing. A similar conclusion was drawn by Brown (ref. 22), who applied the Betz theory to a parabolically loaded wing. Rossow (ref. 23) applied the Betz method to a wide range of wing span loadings. Figure 1 is a sample of his results. The swirl velocity is seen to be significantly reduced in panels (b), (c), and (d) of the figure as compared to panel (a), which corresponds to elliptic span loading. Rossow (ref. 24) then extended his analysis to more complicated configurations by use of a time–dependent point–vortex model that also satisfied the Betz invariants. He found that (i) span loadings could be tailored to produce a very diffuse wake and (ii) by shedding multiple vortices in the wake, strong interactions between vortices could occur which would disperse the vorticity.

## Experimental

Rorke, Moffitt, and Ward (ref. 25) found that vortex swirl velocity in the wake of a rectangular wing could be significantly reduced by installing an ogee wingtip that reduced the wingtip loading. A similar conclusion was obtained by McCormick and Padakannaya (ref. 26) in their study of the effect of a drooped wingtip. Rossow et al. (ref. 12) showed that swirl velocities could be reduced by tailoring for an optimum span loading by use of a seg–mented trailing–edge flap on a swept wing (fig. 2). However, the rolling moment imposed on a following model alined with the vortex was found, in some cases, to be increased as a result of tailoring the loading, depending on the span of the follower relative to the span of the generator. Ciffone and Orloff (ref. 27) conducted further studies using the same design of swept wing as in reference 12. They found that when multiple vortices were shed in the wake, strong interactions occurred between some vortices. However, other vortices persisted in the wake and resulted in swirl velocities as high as those found in the wake of conventional configurations.

## USE OF FLAPS ON THE B–747 AIRPLANE

To coordinate the activities of the various NASA centers in the wake–vortex minimization effort, a common objective was adopted. The generating

wing was agreed to be that of a *B-747* airplane and the following wings would be representative of a Learjet and a DC-9 airplane for the lightweight (<12,500 lb) and medium-sized followers, respectively. Particular interest was focused on those modifications of the generator which were sufficiently minor to be regarded as retrofit modifications.

In view of research work on the effect of span loading (discussed previously), an obvious possibility for consideration on the generator was to retract the outboard flap with the inboard flap left at the landing setting (figs. 3 and *4*). The generator was equipped with two spanwise segments of triple-slotted, trailing-edge flaps capable of high lift. Figure 5 shows the span loadings produced by various flap settings of the generator using a vortex lattice method for the wing and flaps, including the effect of camber and twist, but without fuselage or tail. Note that the conventional flaps 0" and takeoff configurations have approximately elliptical span loadings and hence would be expected to shed a single vortex from each wingtip. With the conventional landing configuration, some additional sharp gradients in loading are evident at the flap edges from which discrete vortices might originate. However, with the outboard flap retracted (30°/0°),[1] these gradients are more pronounced and three vortices from each wing would be expected, that is, one from each flap edge and one from the wingtip.

Ground-Based Measurement

*Flow visualization* - Dunham (ref. 9) conducted experiments in a water-tow facility (owned and operated by Hydronautics Inc. under contract to Langley Research Center) where the generator model was towed underwater along a long channel. He observed (fig. 6) that when the outboard flap was retracted, the wingtip and flap outboard vortex interacted and merged to form a single diffuse vortex pair aft of about 15 spans downstream. Additional flow visualization studies (refs. 28-32) were conducted using an

---

[1]The notation 30°/0°, for example, is used to indicate 30" inboard flap deflection and 0" outboard flap deflection; 30" is the nominal angle used to designate the configuration for landing (5" for takeoff). The actual deflection of the various flap panels appears in figure **3.**

air–tow channel, water–tow channel (owned and operated by the Univ. of Cali –
fornia under contract to Ames Research Center) (fig. 7), wind tunnel, and
full–scale flight test (fig. 8). From all these studies, the picture of the
wake appearing in figure 9 emerged. With the conventional landing configu –
ration aft of about 2 spans downstream, the wake consisted of two intense
counterrotating cores that very slowly diffused their vorticity. In contrast,
the wake of the configuration with the outboard flap retracted and the inboard
flap set to the landing deflection consisted of three vortices per side, one
from each flap edge and one from the wingtip. The vortex that was most
intense and well defined originated at the flap outboard edge. The two
weaker vortices left the wingtip and flap inboard edge, respectively. The
pattern rotated as it moved downstream, with the tip vortex passing over the
flap vortices so that, by about 13 spans downstream, it had moved to a posi –
tion between the flap vortices. The flap and tip vortices ultimately merged.
Following this merger, a very diffuse wake remained. In addition to the
vortices shown in figure 9, Ciffone and Lonzo (ref. 29) noted that the hori –
zontal tail vortices rapidly merged with the flap vortices.

   *Vortex merging* - The vortex merging phenomenon is a mechanism for
dispersing the vorticity in the wake. It was generally observed, for example,
that a single vortex pair in isolation persisted as an organized vortex with
a small core, whereas it was found that the wake would disperse rapidly if
(i) multiple vortex pairs were shed with initially large spacing and (ii) the
self–induced wake velocities convected these vortices into close proximity.
As shown in figure 7, the wingtip and flap vortices are convected into close
proximity between $x/b_g = 1.5$ and $x/b = 13$. Next the vorticity of the
weak vortex (tip) is convected into an annulus around the strong vortex
(flap). This convection is sketched schematically in figure 10. Here the
vortical region of the weak vortex is taken to be circular at time zero. In
the time increments shown, this region is distorted because of the velocity
of the strong vortex. When the two vortices are of comparable strength, the
core region is elongated in both vortices. Furthermore, the elongation of
the core will result in additional distortion because of self–induced
velocities (ref. *33).*

The rolling moment on a following airplane for fully merged vortices would be expected to be below that for the conventional configuration at the same lift Coefficient of the generator. For example, consider the **two** idealized span loadings sketched in figure **11.** For the modified configuration, the wingtip and flap vortices are assumed to merge into a single circular vortex core with uniformly distributed vorticity (i.e., Rankine vortex). The circulation and core diameter of this merged vortex can be obtained from vortex invariants (ref. 18). The rolling-moment coefficient on the follower in the wake of this merged vortex, as well as in the wake of the single vortex of the conventional configuration, can be computed by use of the method discussed in reference 12 or 24 for a given lift coefficient of the generator. This result is shown in figure **11** as a function of the spacing between the two vortices of the modified configuration. For vortex spacing in excess of **0.3** of the semispan, the reduction in the rolling-moment coefficient behind the modified configuration compared with the conventional configuration is substantial. This simplified example illustrates one mechanism for dispersing the wake. **In** an actual wake, the vortices before merger have distributed vorticity, and there are vortices of opposite sense from the inboard edges of the flap and the horizontal stabilizer. All these vortices must be considered in predicting the downstream wake and rolling moment on a follower. Rossow (ref. **33)** has conducted additional theoretical research on the conditions for the merger of multiple vortices.

*Rolling moment on the follower* - Experiments were conducted in the Ames 40- by 80-Foot Wind Tunnel in which the rolling moment was measured on a following model held fixed in the wake of the generator model (figs. **3** and 12). Figure **13** shows the variation of the rolling-moment coefficient with the circulation of the trailing vortex for the conventional flap settings of the generator (ref. **30)** at **13.6** spans downstream of the generator. Also shown is the corresponding measurement in the wake of a supersonic transport model (ref. 34). The rolling moment increases nearly linearly with $\Gamma/b_g U_\infty$, as predicted (ref. 12) for the case when the vorticity distribution remains unchanged and only the magnitude changes. This result is expected because the shape of the span-load distribution is nearly independent of lift over the range of angle of attack tested and, for these configurations, the vortex

structure is determined by the span-load distribution (ref. 18). For figure 13, $\Gamma/b_g U_\infty$ was obtained from $C_{L_g}$ by assuming elliptic loading. Note in figure **13** that the various configurations lie on approximately the same curve, which implies that the change in the vortex structure for the configurations shown is sufficiently small that the change in rolling moment could not be detected. When the outboard flap of the B-747 model was retracted (figs. 14(a) and (b)), a greater than 50-percent reduction in rolling moment was measured for the smaller follower model. With the larger follower model, the reduction in rolling moment was less. For comparison, typical values for the roll control capability for the Learjet and DC-9 are also presented in figure 14 and, at $C_{L_g} = 1.2$, the imposed rolling-moment coefficient about equals the capability of the Learjet and slightly exceeds the capability of the DC-9. The nominal value of $C_{L_g}$ for the B-747 in the conventional landing configuration lies between 1.2 to 1.4.

Experiments were also conducted in the Hydronautics Inc. water-tow facility (ref. 9) using follower and generator models identical to those used in the wind-tunnel tests discussed previously. In these water-tow experiments, the follower and generator models were towed at the same speed, with the follower model held fixed at various lateral and vertical positions in the wake. By use of this technique, substantially greater downstream . distances could be obtained compared to the wind-tunnel experiments. Results for the variation of $C_{l_f}$ with downstream distance appear in figures 14 (c) and (d). **Also** shown are comparable wind-tunnel and air-tow facility data. There is general agreement on the effectiveness of retracting the outboard flap as a technique to reduce the wake rolling moments. However, the water-tow facility data show that the effectiveness for the smaller follower (fig. 14(c)) occurs farther downstream compared with the wind-tunnel results. This difference may result from either a higher turbulence level in the wind tunnel as compared to the water-tow facility or the effect of the water tank boundaries on the paths of the vortices.

*Drag, angle of attack, and pitching moment on the generator* - The forces and moments on the generator were measured for the 30°/30° and 30°/0° configurations (ref. 14) (fig. 15). The effect of retracting the outboard flap

on drag was small. The change in angle of attack to maintain a lift coef-
ficient $C_{L_g} = 1.2$ was about 3.5" (trimmed). In aircraft operation, however,
this lift loss due to the 30°/0° configuration would require compensation by
either an increase in aircraft angle of attack or airspeed or a combination
of these variables. The effect of retracting the outboard flap on the
pitching-moment characteristics is to require an additional 5° of tail
incidence for trim and to reduce longitudinal static stability, $(-\partial C_M/\partial C_{L_g})$,
about 13 percent at $C_{L_g} = 1.2$. In airline operation, this effect on the
pitching-moment characteristics would probably require that the aft limit of
the center-of-gravity location be moved forward from its present location.

## Flight Test

As a result of the ground-based studies discussed above, flight tests
were conducted using a full-scale B-747 airplane to generate the wake and a
Learjet and T-37B airplanes to probe the wake (refs. 31, 32, and 35).
Figure 16 is a summary of pilot qualitative separation requirement for the
follower airplane. With the landing gear retracted to correspond to the
ground-based experiments, the separation requirement was reduced substantially
for the 30°/1° configuration[2] compared to the 30°/30° configuration (fig.
16(a)). Lowering the landing gear, however, increased the separation require-
ment for all configurations and especially for the 30°/1° configuration.
Sideslip was also found to adversely affect the wake alleviation when the
landing gear was up (fig. 16(b)).

Flow visualization obtained during the flight test provided some insight
into the cause of the landing gear effect. Figure 17 shows the smoke trails
from the B-747 airplane for the 30°/1° configuration with the landing gear
both up and down. With the landing gear up, a well-defined vortex pair was
shed from the inboard edge of the flaps and these vortices underwent large-
amplitude sinusoidal interactions. With the landing gear deployed, these
same vortices appeared to be more diffuse, and no such interactions were seen.

---

[2]For certain mechanical reasons, the outboard flap of the B-747 airplane was
retracted only to 1° instead of 0°. It is felt that this difference is
insignificant.

313

The flap inboard vortex with the landing gear up did not appear as sharp in any of the ground-based visualization experiments as it appears in figure 17. However, this apparent lack of agreement with the model tests is probably not significant since the effect of the landing gear was also measured in the ground-based experiments. Recently, Leonard (ref. *36)* modeled this flow using a three-dimensional, time-dependent inviscid calculation with six concentrated vortices. His results, using a similar configuration (fig. 18), indicate that the sinusoidal oscillations observed in flight also appear in the computed results.

The rolling moment imposed on the following aircraft was obtained by subtracting the effects due to ailerons, sideslip, etc., from the measured roll acceleration during a vortex encounter. This result (ref. 32) for the configuration with the landing gear up appears in figure 19. Also shown for comparison are the results from the ground-based facilities presented above, which correspond to a rectangular wing follower whose span and aspect ratio were scaled to the aircraft used in the flight tests. Excellent agreement was obtained for the configuration with the outboard flap retracted. With the conventional landing configuration (flaps 30°/30°), the ground-based rolling moment lies in the lower range of the flight-measured values, depending on the procedure used to extrapolate the ground-based results to the downstream distances tested in flight.

## INTERFERENCE OF LANDING GEAR WITH WAKE ALLEVIATION

The basic factors that cause the landing gear to interfere with the vortex wake are still not fully understood. As discussed above, it appears from figure 17 that the effect of the landing gear is to diffuse the flap inboard vortex. Therefore, a vortex generator (figs. *4* and 20) which was designed to shed a strong vortex at the same location and sense as each of the flap inboard vortices when the landing gear was down was tested in the Hydronautics Inc. water tow facility. The results without the vortex generator installed (fig. 21) show a substantial increase in rolling moment due to the landing gear for the 30°/0° flap configuration similar to those achieved in the flight tests. With the vortex generator installed, the

314

rolling–moment reduction due to flaps was insensitive to the presence of the landing gear. Patterson and Jordan (ref. 28) (fig. 22), in their air–tow facility studies, were able to produce an increase in rolling moment, with the landing gear removed, equal to the gear effect by either placing end plates at the inboard edges of the flap or by extending the flap inboard across the fuselage. A possible explanation of these results is that both the end plate and the fuselage flap diffused the flap inboard vortex. Further research is required to directly measure the flap inboard vortex axial and swirl velocities to determine the actual role of this vortex on the alleviation of the wake. Ciffone and Lonzo (ref. 29) observed in their water–tow studies that the concentrations of dye and the vortex trajectories were different between landing gear up and down with the 30°/0° flap configuration. They then studied an alternate configuration that appeared to alleviate the wake and to be insensitive to the presence of the landing gear. This configuration was obtained by setting both the inboard and outboard flaps to 30" deflection and removing the inboard 30 percent of the inboard flap. Studies of this configuration are continuing.

## CONCLUDING REMARKS

Certain span–load distributions produce less intense wakes than others. An approximately 50–percent reduction in both the wake rolling moment imposed on a following aircraft and aircraft separation requirement was achieved in the ground–based and flight–test experiments by deflecting the trailing–edge flaps more inboard than outboard. Significantly, this configuration did not increase the drag or vibration on the generating aircraft compared to the conventional landing configuration. However, further research is required to obtain a configuration with an alleviated wake that is acceptable for airline operation.

Another major conclusion derived from the investigations summarized here is that wake–vortex experiments conducted in ground–based facilities produce results that correlate well with full–scale flight–test results. It was found that there was general agreement in both the flow visualization and the

rolling moment imposed on a following aircraft between flight-test and ground-based experiments.

## REFERENCES

1. Chigier, N. A.; and Corsiglia, V. R.:   Tip Vortices-Velocity Distributions, NASA TM X-62, 087, 1971

2. Chigier, N. A.; and Corsiglia, V. R.:   Wind-Tunnel Studies of Wing Wake Turbulence.   J. Aircraft, vol. 9, no. 12, 1972, pp. 820-825.

3. Corsiglia, V. R.; Schwind, R. K.; and Chigier, N. A.:   Rapid Scanning Three-Dimensional Hot-wire Anemometer Surveys of Wing-Tip Vortices, J. Aircraft, vol. 10, no. 12, 1973, pp. 752-757.

4. Orloff, K. L.; and Grant, G. R.:   The Application of a Scanning Laser Doppler Velocimeter to Trailing Vortex Definition and Alleviation. AIAA Paper 73-680, 1973 (see also NASA TM X-62,243, 1973).

5. Orloff, K. L.:   Trailing Vortex Wind-Tunnel Diagnostics with a Laser Velocimeter, J. Aircraft, vol. 11, no. 8, 1974, pp. 477-482.

6. Corsiglia, V. R.; Jacobsen, R. A.; and Chigier, N. A.:   An Experimental Investigation of Trailing Vortices Behind a Wing With a Vortex Dissipator.   Aircraft Wake Turbulence and Its Detection, edited by J. Olson, A. Goldberg, and M. Rogers, Plenum Press, New York, 1971, pp. 229-242.

7. Wentz, W. H., Jr.:   Evaluation of Several Vortex Dissipators by Wind Tunnel Measurements of Vortex-Induced Upset Loads.   Wichita State Univ. Aeronautical Rept. 72-3, 1972.

8. Kirkman, K. L.; Brown, C. E.; and Goodman, A.:   Evaluation of Effectiveness of Various Devices for Attenuation of Trailing Vortices Based on Model Tests in a Large Towing Basin, NASA CR-2202, 1973.

9. Dunham, E. R., Jr.:   Model Tests of Various Vortex Dissipation Techniques in a Water Towing Tank, Langley Working Paper, LWP-1146, Jan. 1974.

10. Hastings, E. C., Jr.; Shanks, R. E.; Champine, R. A.; Copeland, W. L.; and Young, D. C.: Preliminary Results of Flight Tests of Vortex Attenuating Splines. NASA TM X-71,928, 1974.

11. Croom, Delwin R.: Low-Speed Wind-Tunnel Investigation of Forward-Located Spoilers and Trailing Splines as Trailing-Vortex Hazard-Alleviation Devices on an Aspect-Ratio-8 Wing Model. NASA TM X-3166, 1975.

12. Rossow, V. J.; Corsiglia, V. R.; Schwind, R. G.; Frick, J. K. D.; and Lemmer, O. J.: Velocity and Rolling-Moment Measurements in the Wake of a Swept-Wing Model in the *40-* by 80-Foot Wind Tunnel. NASA TM X-62,414, 1975.

13. Patterson, J. C., Jr.: Vortex Attenuation Obtained in the Langley Vortex Research Facility. J. Aircraft, vol. 12, no. 9, Sept. 1975, pp. 745-749.

14. Croom, D. R.; and Dunham, E. R., Jr.: Low-Speed Wind-Tunnel Investigation of Forward-Located Spoiler, and Trailing Splines as Trailing-Vortex Hazard-Alleviation Devices, NASA TN D-8133, 1975.

15. Croom, D. R.: Low-Speed Wind-Tunnel Investigation of Various Segments of Flight Spoilers as Trailing-Vortex Hazard-Alleviation Devices on a Transport Aircraft Model, NASA TN D-8162, 1976.

16. Croom, D. R.: The Development of the Use of Spoilers as Vortex Attenuators. NASA Symposium on Wake Vortex Minimization, Washington, D.C., Feb. 25-26, 1977.

17. Corsiglia, V. R.; and Rossow, V. J.: Wind-Tunnel Investigation of the Effect of Porous Spoilers on the Wake of a Subsonic Transport Model, NASA TM X-73,091, 1976.

18. Betz, A.: Behavior of Vortex Systems, NACA TM 713, **Z**. Angew. Math. Mech. transl., vol. XII, *3*, 1932.

19. Donaldson, C. du P.: A Brief Review of the Aircraft Trailing Vortex Problem, Rept. AFOSR-TR-71-1910, July 1971.

20. Donaldson, C. du P.; Snedeker, R. S.; and Sullivan, R. D.: A Method of Calculating Aircraft Wake Velocity Profiles and Comparison With Full-Scale Experimental Measurements, J. Aircraft, vol. 11, Sept. 1974, pp. 547-555.

21. Mason, W. H.; and Marchman, J. F., III: Far-field Structure of an Aircraft Trailing Vortex, Including Effects of Mass Injection. NASA CR-62,078, 1972.

22. Brown, C. E.: Aerodynamics of Wake Vortices. AIAA J., vol. 11, no. 4, April 1973, pp. 531-536.

23. Rossow, V.: On the Inviscid Rolled-up Structure of Lift-Generated Vortices. J. Aircraft, vol. 10, no. 11, Nov. 1973, pp. 647-650.

24. Rossow, V. J.: Theoretical Study of Lift-Generated Vortex Wakes Designed to Avoid Rollup. AIAA J., vol. 13, no. 4, April 1975, pp. 476-484.

25. Rorke, J. B.; Moffitt, R. C.; and Ward, J. F.: Wind-Tunnel Simulation of Full-scale Vortices. A.H.S. Paper 623, May 1972.

26. McCormick, B. W.; and Padakannaya, R.: The Effect of a Drooped Wing Tip on Its Trailing Vortex System. Aircraft Wake Turbulence and Its Detection, edited by J. Olson, A. Goldberg, and M. Rogers, Plenum Press, New York, 1971, pp. 157-70.

27. Ciffone, D. L.; and Orloff, K. L.: Far-Field Wake-Vortex Characteristics of Wings, J. Aircraft, vol. 12, no. 5, May 1975.

28. Patterson, J. C., Jr.; and Jordan, F. L., Jr.: An Investigation of the Increase in Vortex Induced Rolling Moment Associated with Landing Gear Wake. NASA TM X-72,786, 1975.

29. Ciffone, D. L.; and Lonzo, C., Jr.: Flow Visualization of Vortex Interactions in Multiple Vortex Wakes Behind Aircraft. NASA TM X-62,459, 1975 (see also Vortex Interactions in Multiple Vortex Wakes Behind Aircraft, Preprint 76-62, 14th Aerospace Sciences Meeting, Jan. 26-30, 1976, Washington, D.C.).

30. Corsiglia, V. R.; Rossow, V. J.; and Ciffone, D. L.: Experimental Study of the Effect of Span Loading on Aircraft Wakes, NASA TM X–62,431, 1975.

31. Barber, M. R.: Vortex Attenuator Flight Experiments, NASA Symposium on Wake Vortex Minimization, Washington, D.C., February 25–26, 1977.

32. Smith, H. J.: A Flight Test Investigation of the Rolling Moments Induced on a T 37B Airplane in the Wake of a B–747 Airplane. NASA TM X–56,031, 1975.

33. Rossow, V. J.: Inviscid Modeling of Aircraft Trailing Vortices. NASA Symposium on Wake Vortex Minimization, Washington, D.C., February 25–26, 1977.

34. Rossow, V. J.; Corsiglia, V. R.; and Phillippe, J. J.: Measurements of the Vortex Wakes of a Subsonic– and a Supersonic–Transport Model in the 40– by 80–Foot Wind Tunnel, NASA TM X–62,391, 1974.

35. Tymczyszyn, J. J.; and Barber, M. R.: Recent Wake Turbulence Flight Test Programs. Paper presented-at the 18th Annual Symposium of the Society of Experimental Tests Pilots, September 26, 1974, Beverly Hills, Calif.

36. Leonard, A.: Numerical Simulation of Interacting, Three–Dimensional Vortex Filaments, Proceedings of the 4th International Conference on Numerical Methods in Fluid Dynamics, Boulder, Colorado, June 24–28, 1974, pp. 245–250; also published in Lecture Notes in Physics, vol. 35, Springer·Verlag, Berlin, 1975.

SPAN
LOAD

SWIRL
VELOCITY

0   .5   I   15
$\eta$

(a) ELLIPTIC LOADING

SPAN
LOAD

SWIRL
VELOCITY

0   .5   I   15
$\eta$

(b) PARABOLIC LOADING

SPAN
LOAD

SWIRL
VELOCITY

0   .5   I   15
$\eta$

(c) TRIANGULAR LOADING

SPAN
LOAD

SWIRL
VELOCITY

0   .5   I   15
$\eta$

(d) $(1-n^2)^2$
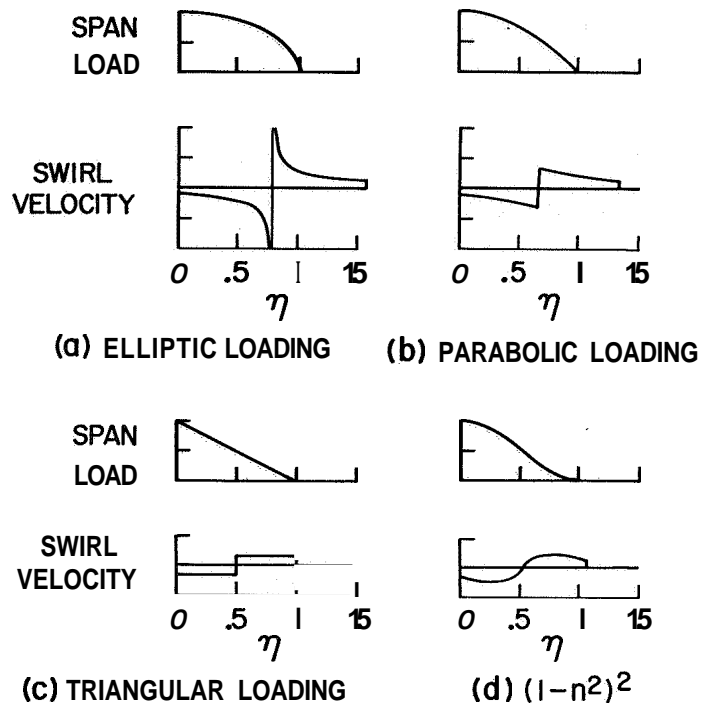
Figure 1.–,Predicted swirl velocity in the downstream wake for various span–
load distributions using the Betz method (ref. 18) by Rossow (ref. *23).*
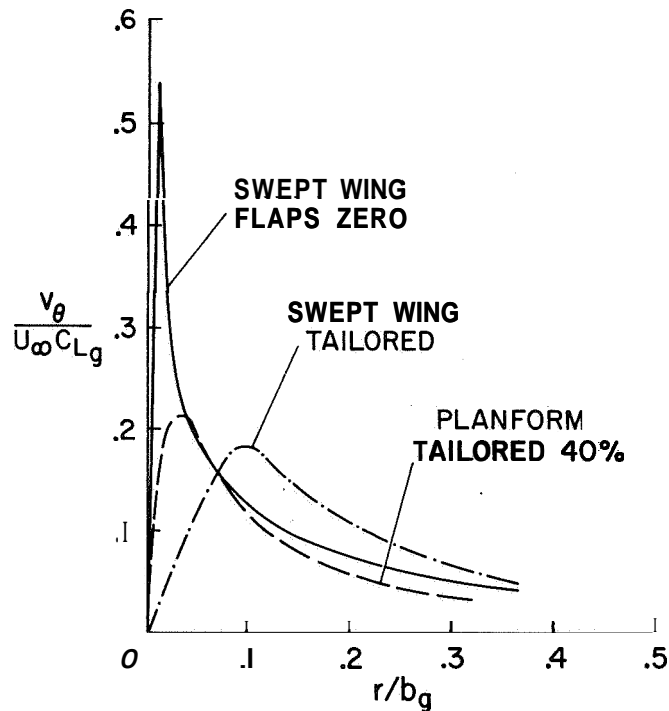


Figure *2.* – Measured swirl velocity distribution in the downstream vortex for
two configurations whose span loadings have been tailored according to the
method described in reference *24* to produce a diffuse vortex as compared
to a swept wing with flaps undeflected (ref. 12).

FLAPS ZERO

TAKE-OFF
(DESIGNATED 5°)

LANDING
(DESIGNATED 30°)
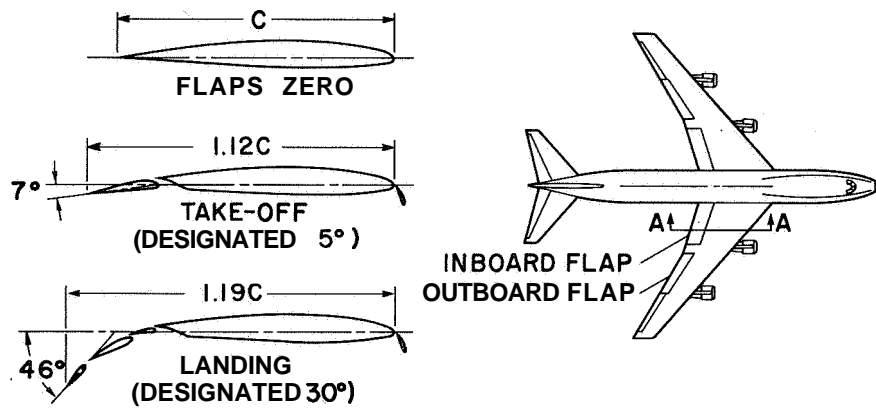
SECTION A-A DETAILS

INBOARD FLAP
OUTBOARD FLAP

Figure 3.- Sketch of the B-747 model.
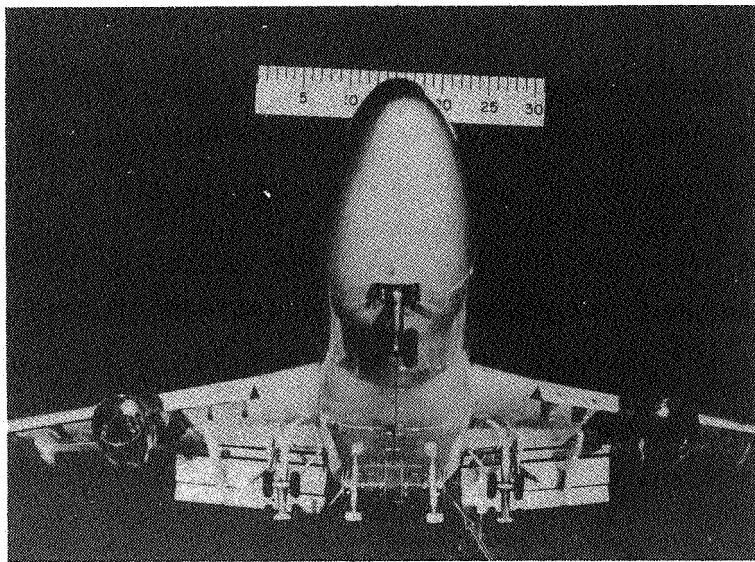


VORTEX GENERATOR AT
~45° TO VERTICAL

Figure 4.- Photograph of the B-747 model (dimensions in cm).
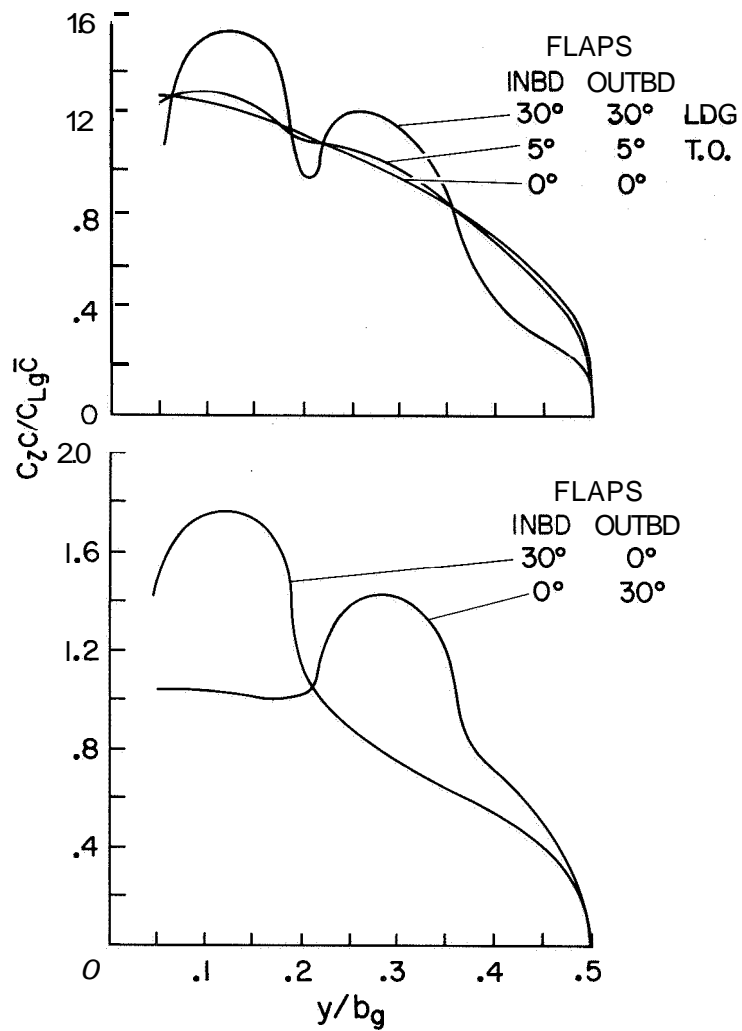
Figure 5.– Predicted variation of span loading on the *B-747* model for various settings of the inboard and outboard trailing–edge flaps (ref. 30).
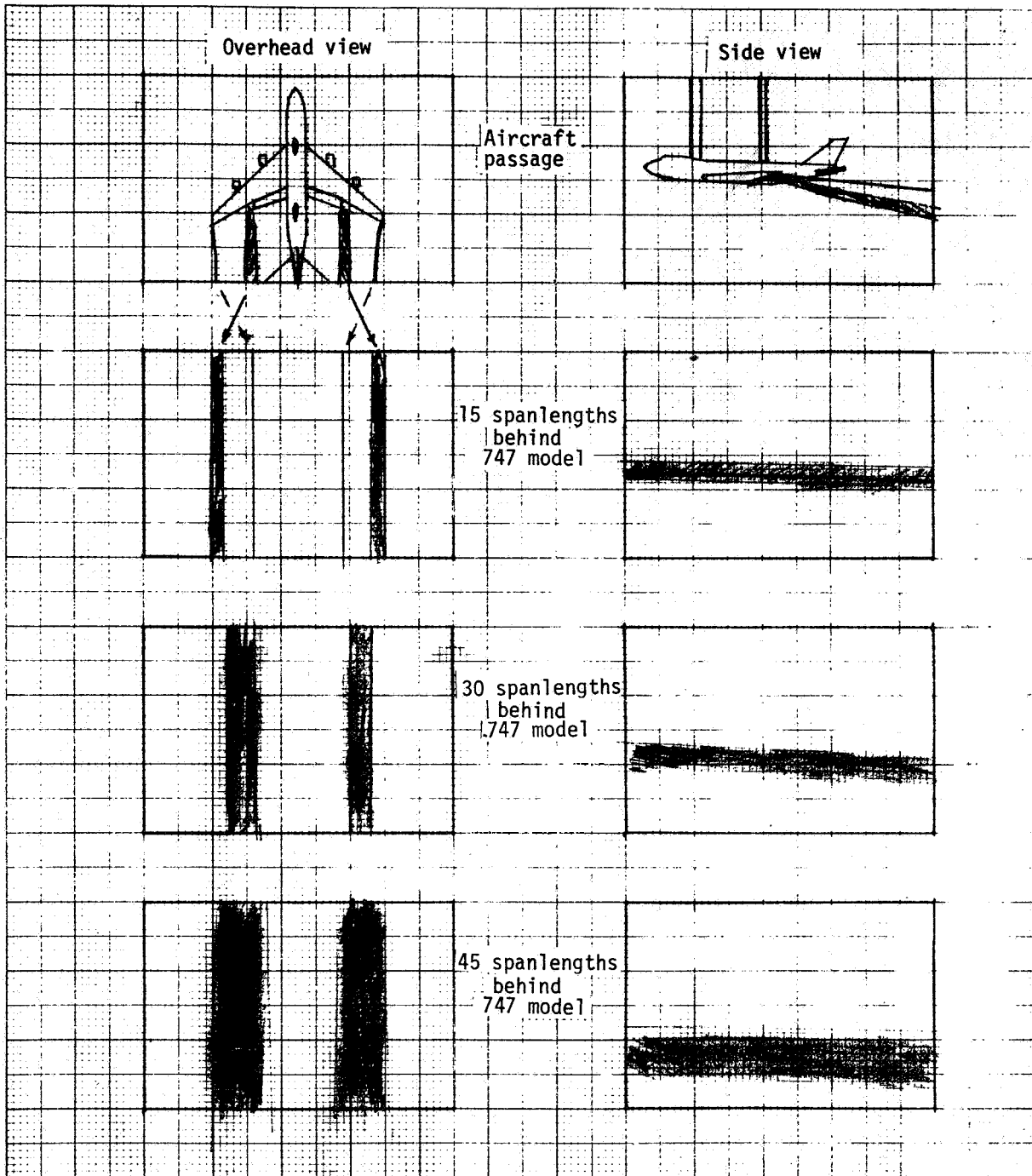
Figure *6.-* Illustration of the merger of the wingtip and flap outboard vortices for the 30°/0° flap configuration, as observed in the Hydronautics Inc. water-tow facility (ref. 9).
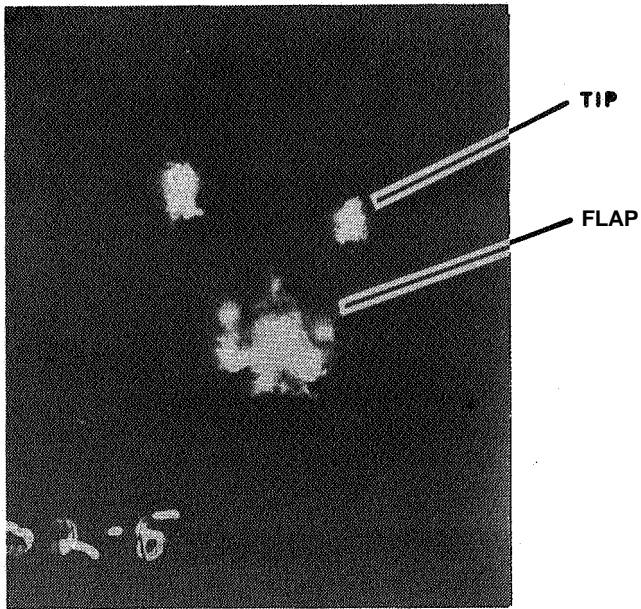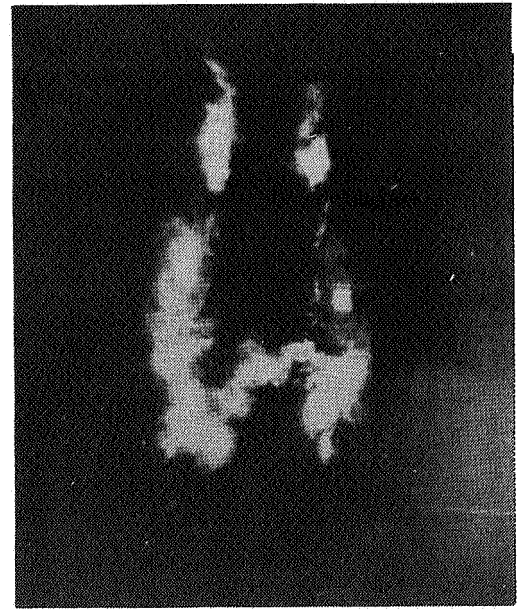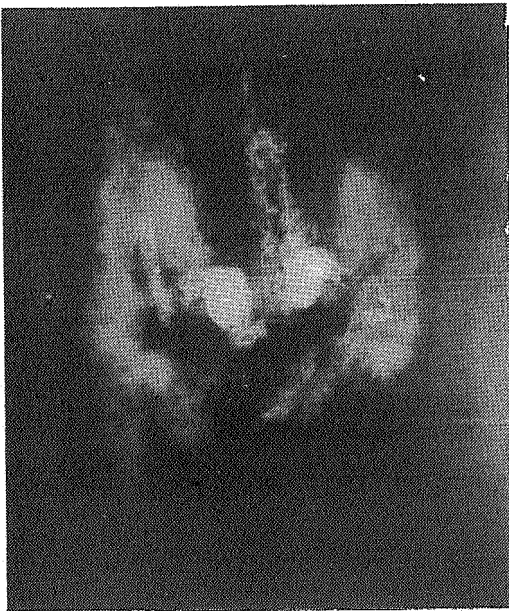
Figure 7.--Light slit photographs of dye traces in the water tow facility, generator flaps:  Ldg/0°, $\alpha$ = 5.8°, $U_\infty$ = 1 m/sec (3.3 ft/sec).

324

**FLAPS: 30°/30°**                    **FLAPS: 30°/0°**

Figure 8.– Photographs of smoke trails from the *B-747* test airplane showing the vortex interactions from reference **31.**
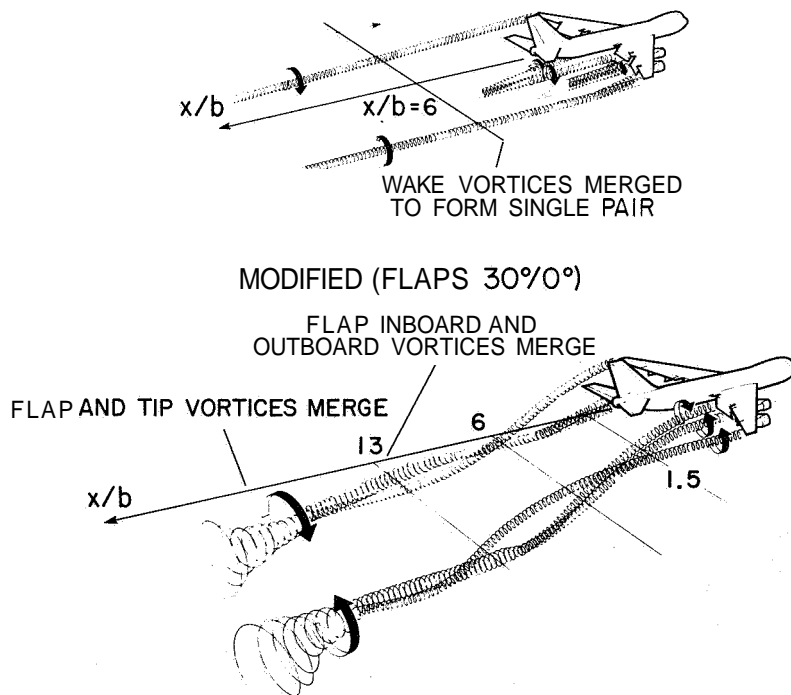


Figure 9.– Sketch of the interaction of the various vortices in the wake of the *B-747* model for the **30°/30°** and **30°/0°** flap configurations.
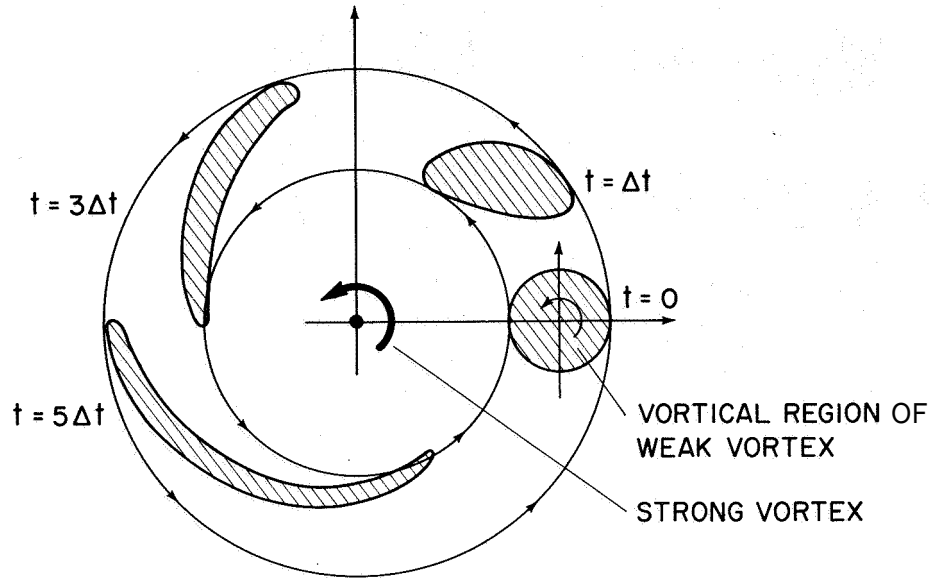
Figure 10.– Sketch of the idealized convective merging of a weak vortex with a strong one.



b) ROLLING-MOMENT RATIO
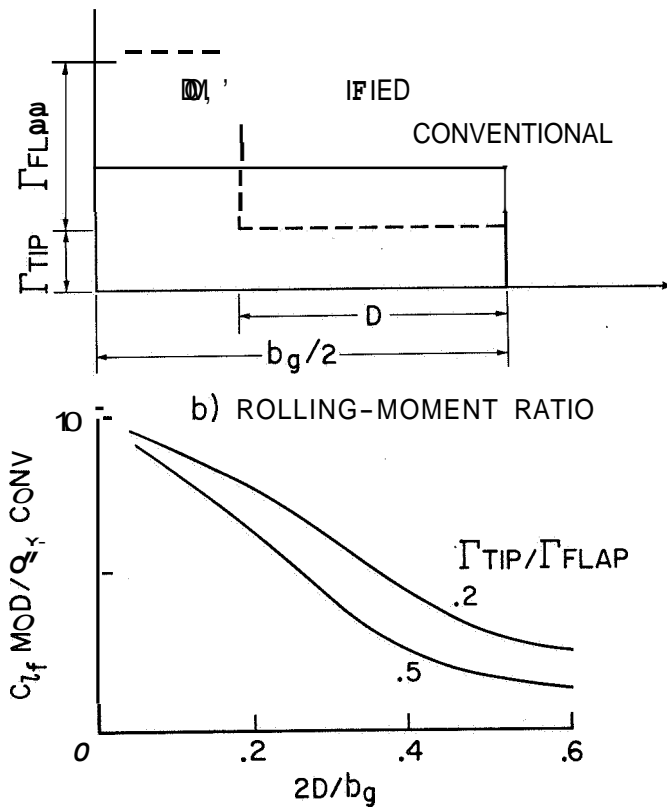
Figure 11.– Idealized example of the effect of merging two vortices into a single Rankine vortex on the rolling–moment coefficient on a follower as compared to a single vortex wake at the same lift and span; $b_f/b_g = 0.2$.
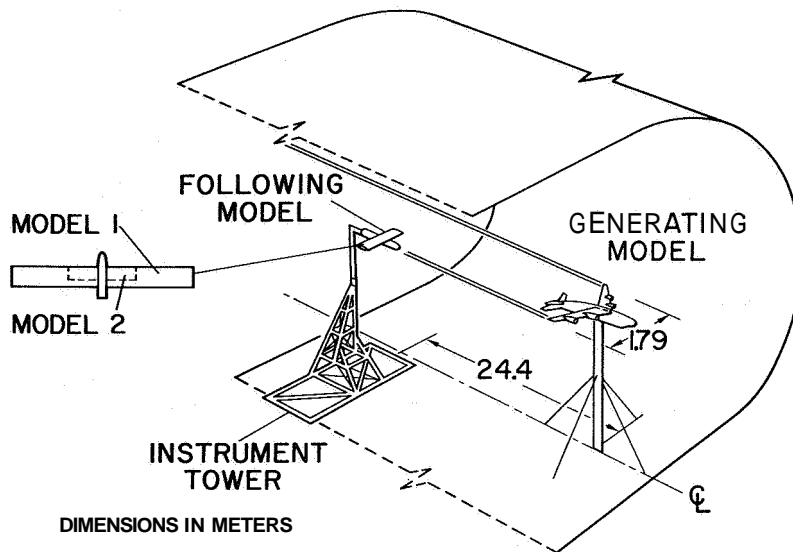
Figure 12.- Experimental setup in the Ames *40-* by 80-Foot Wind Tunnel.
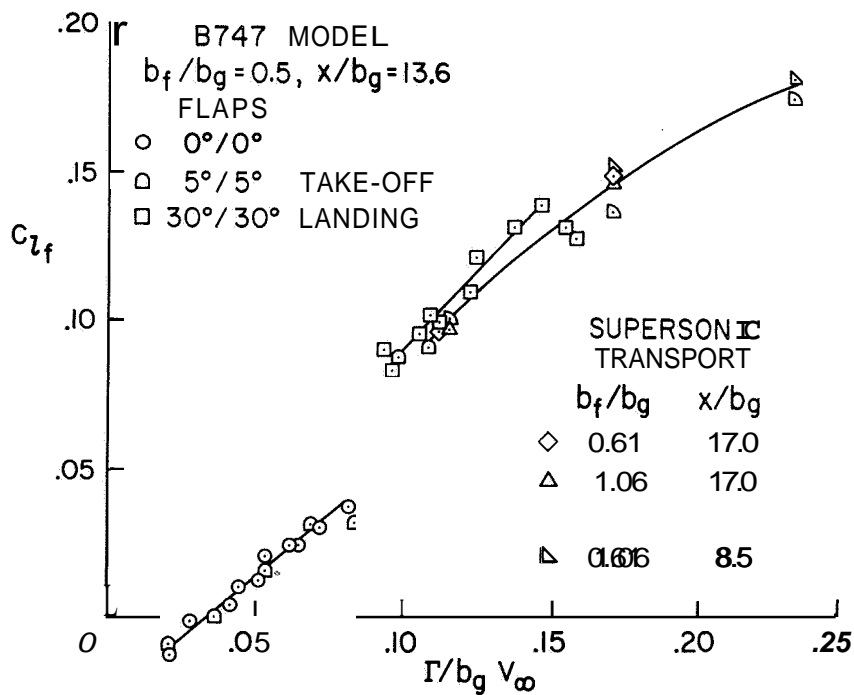


Figure 13.- Variation of the peak rolling-moment coefficient on the following
models for the *B-747* model with conventional flap settings (ref. 30) and
for a supersonic transport model with flaps undeflected (ref. 34), as
measured in the Ames *40-* by 80-Foot Wind Tunnel.
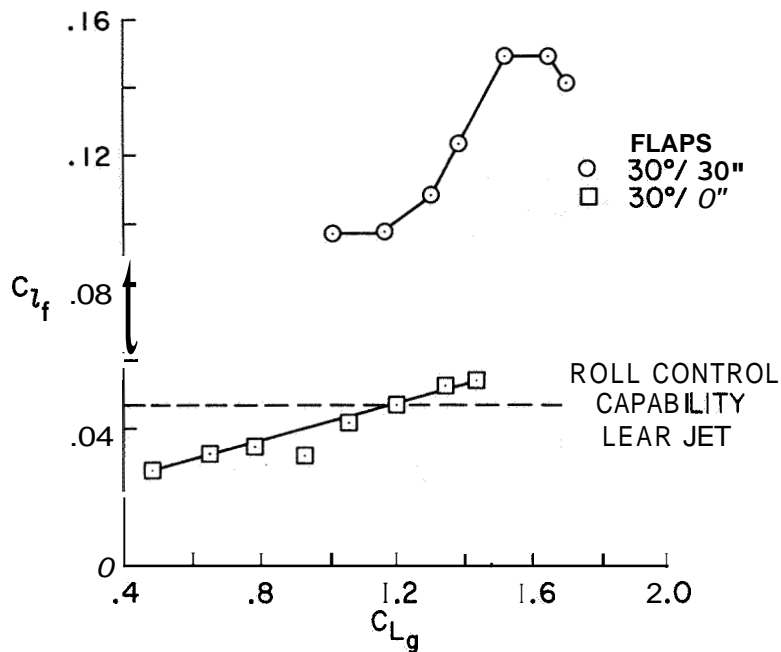
(a) $x/b_g = 13$, $b_f/b_g = 0.2$, Learjet size follower, Ames 40- by
80–Foot Wind Tunnel (ref. 30).
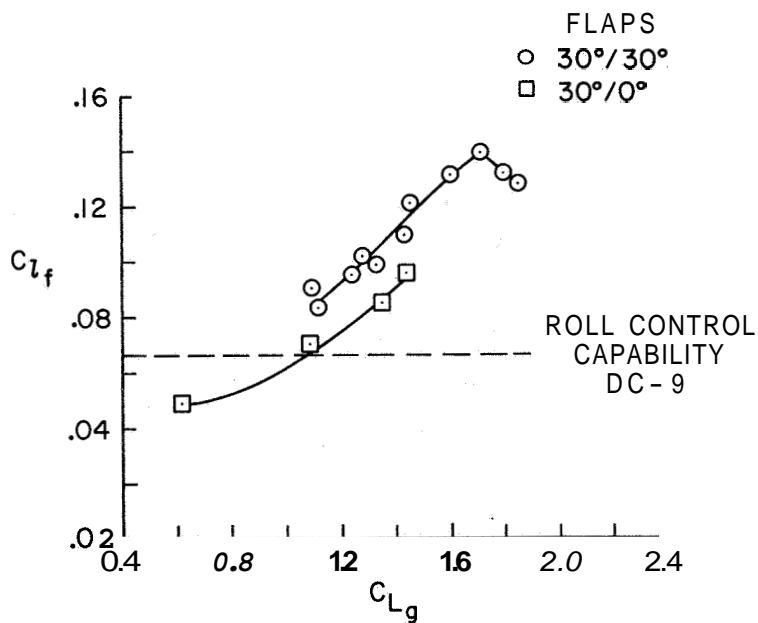


(b) $x/b_g = 13$, $b_f/b_g = 0.5$, DC–9 size follower, Ames 40- by
80–Foot Wind Tunnel (ref. 30).

Figure 14.– The effect of retracting the outboard flap of the B-747 model on
the rolling moment imposed on the following model, landing gear up.

FLAPS
O 30°/30°
△ 30°/0°
●▲ CORSIGLIA et al.[30]
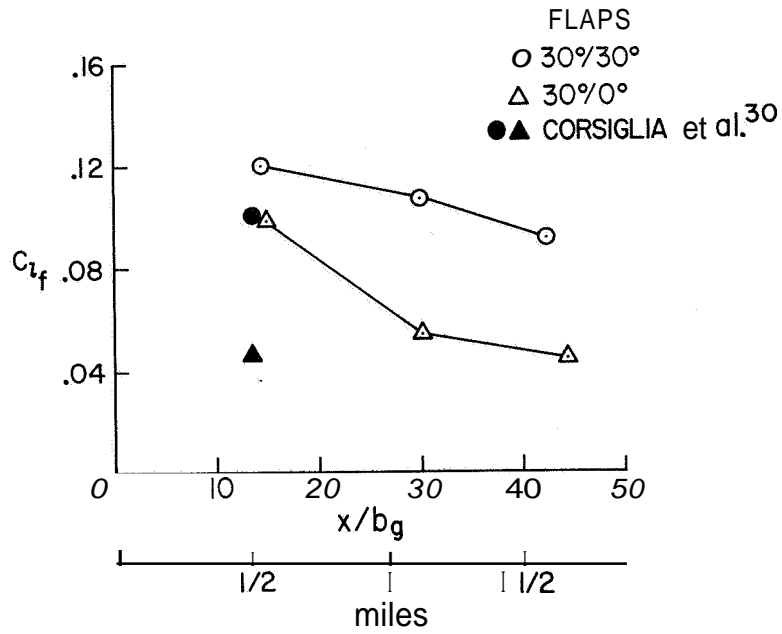
(c) $C_{L_g}$ = 1.2, $b_f/b_g$ = 0.2, Learjet size follower, Hydronautics Inc. water-tow facility.



FLAPS
O 30°/30°
A 30°/0°
●▲ CORSIGLIA et al.[30]
ⵀ△ PATTERSON & JORDAN[28]
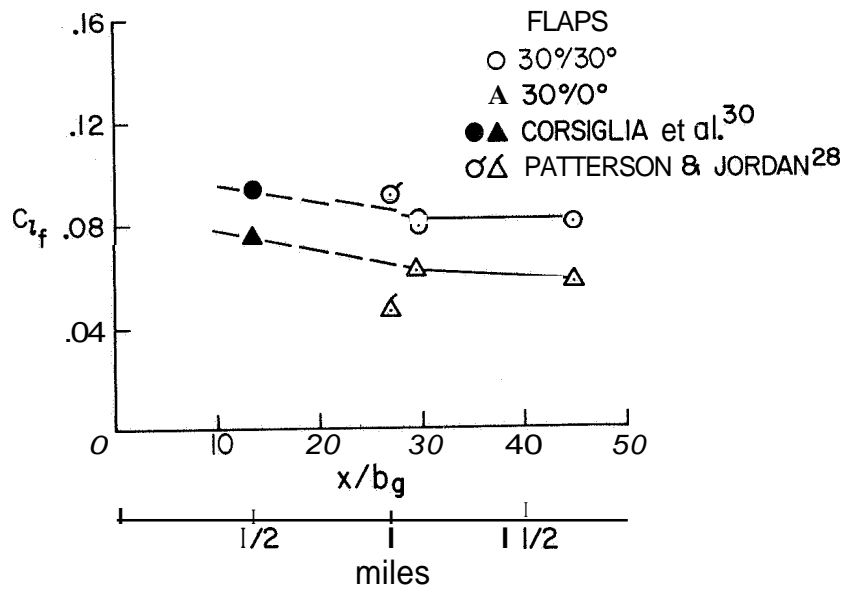
(d) $C_{L_g}$ = 1.2, $b_f/b_g$ = 0.5, DC-9 size follower, Hydronautics Inc. water-tow facility.

Figure 14.- Concluded.
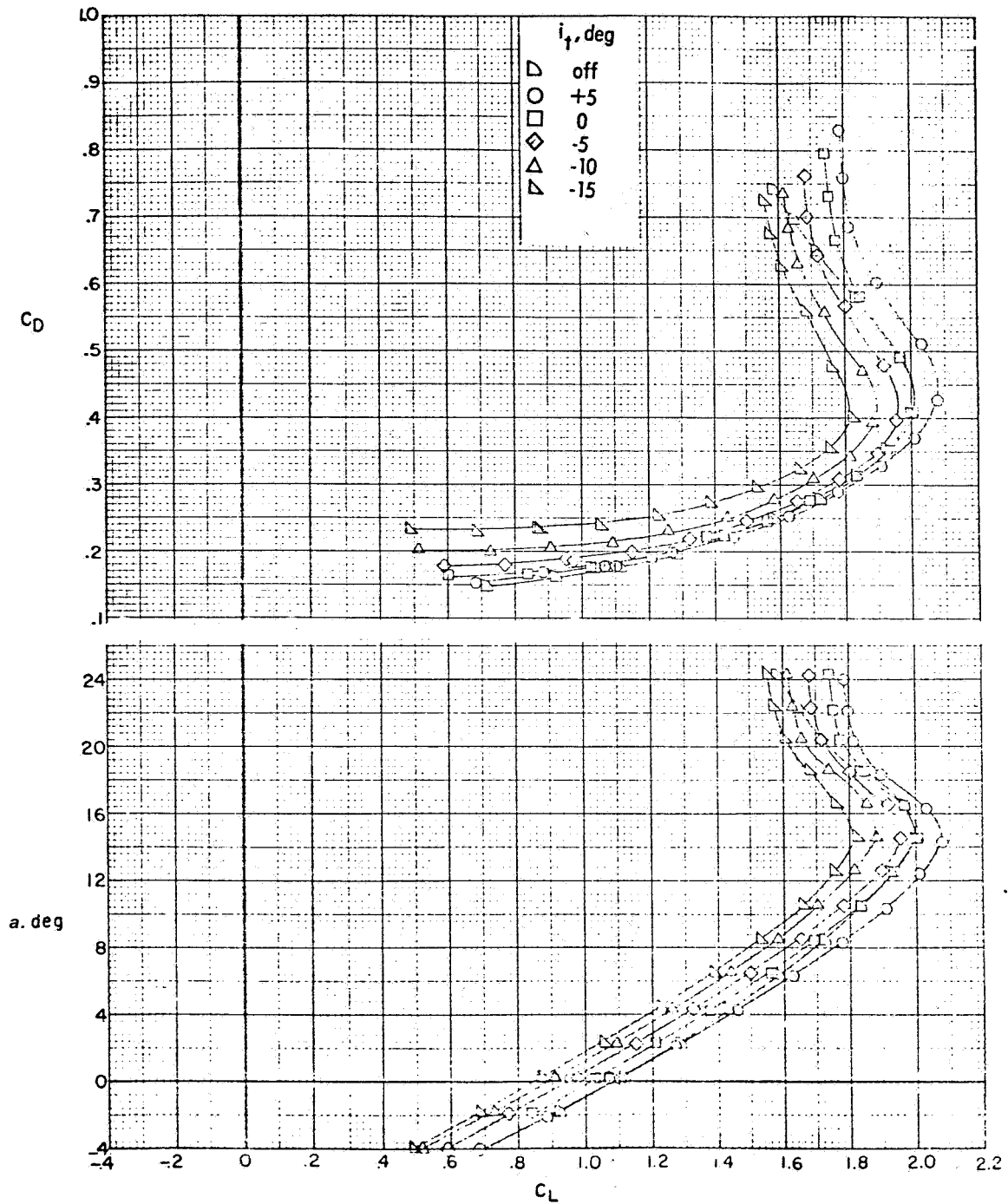
(a) Drag coefficient and angle of attack, flaps 30°/30°, conventional landing configuration.

Figure 15.– Effect of the horizontal–tail incidence on the longitudinal aero-dynamic characteristics of the B–747 model, as measured in the Langley V/STOL Wind Tunnel; landing gear up (ref. 14). Moment center at 25 percent mean aerodynamic chord.
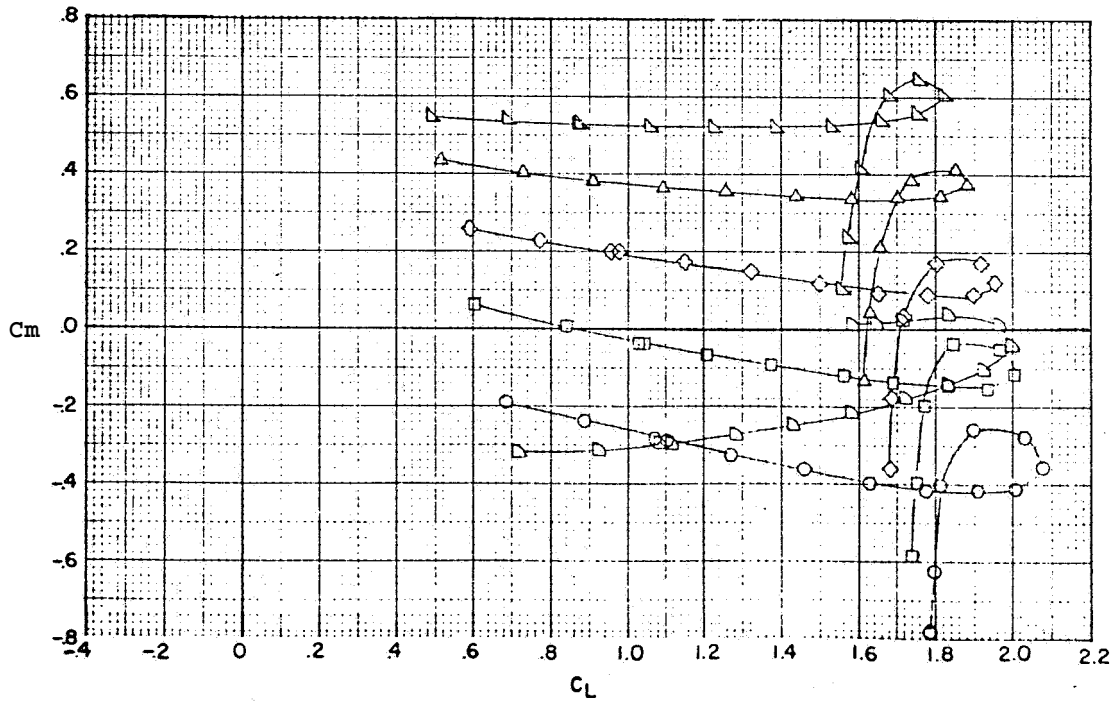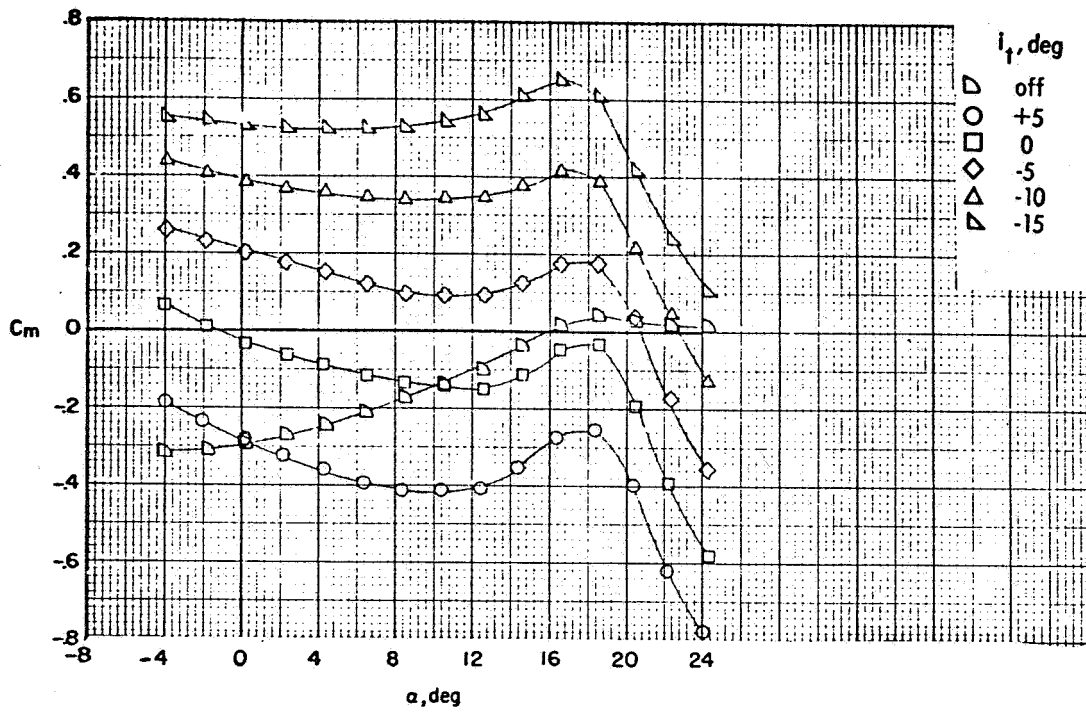
(b) Pitching-moment coefficient, flaps 30°/30°,
conventional landing configuration.

Figure 15.- Continued.
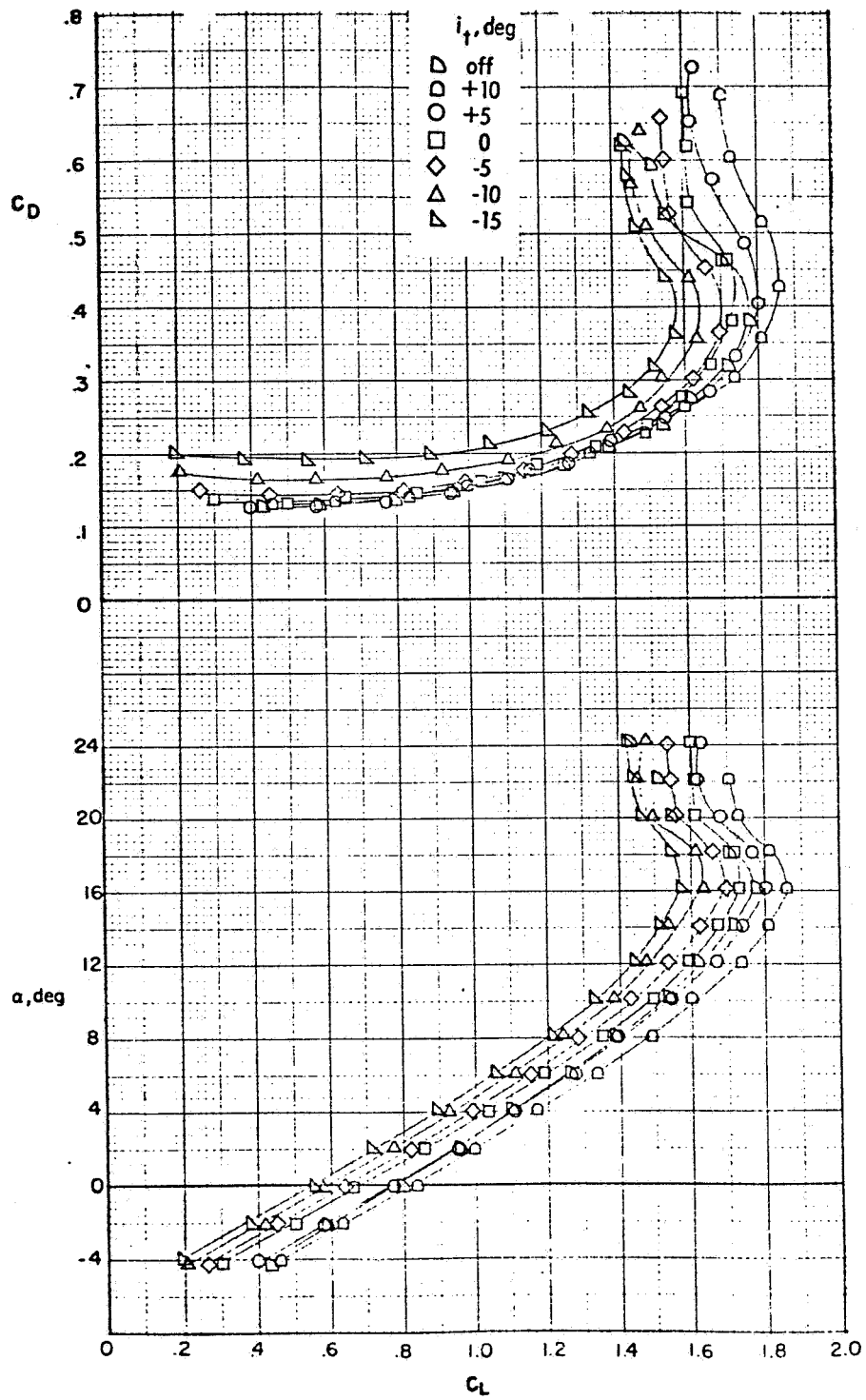
(c) Drag coefficient and angle of attack, flaps 30°/0°, outboard flap retracted.

Figure 15.– Continued.
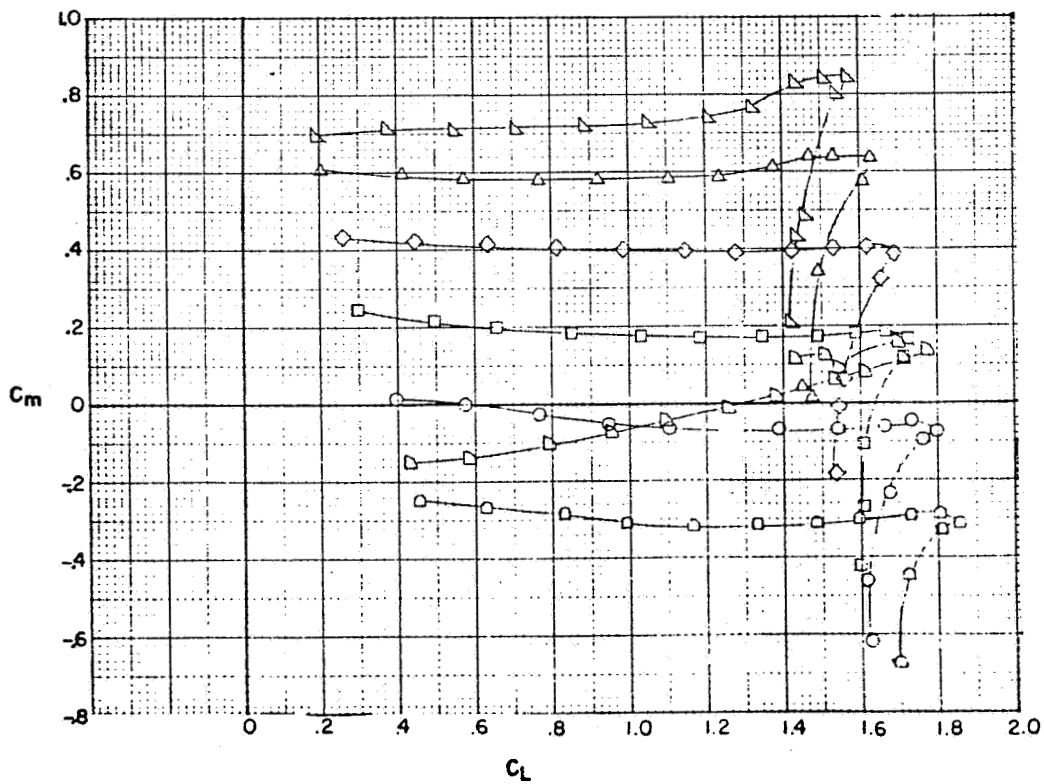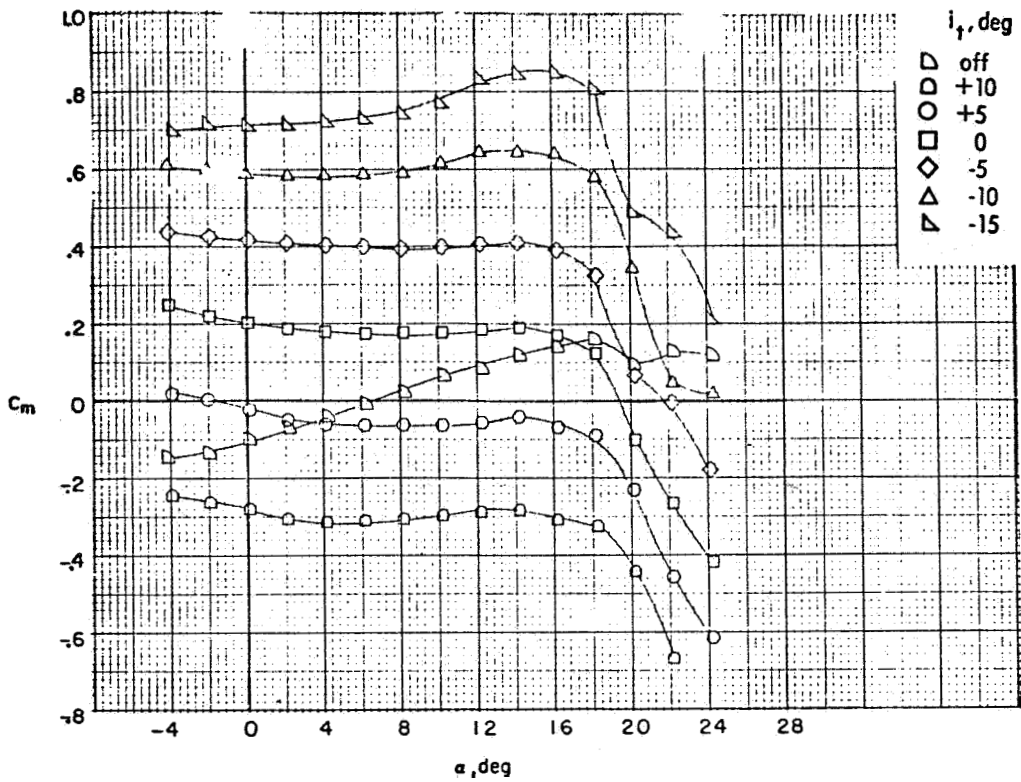
(d) Pitching-moment coefficient, flaps 30°/0°, outboard flap retracted.

Figure 15.- Concluded.
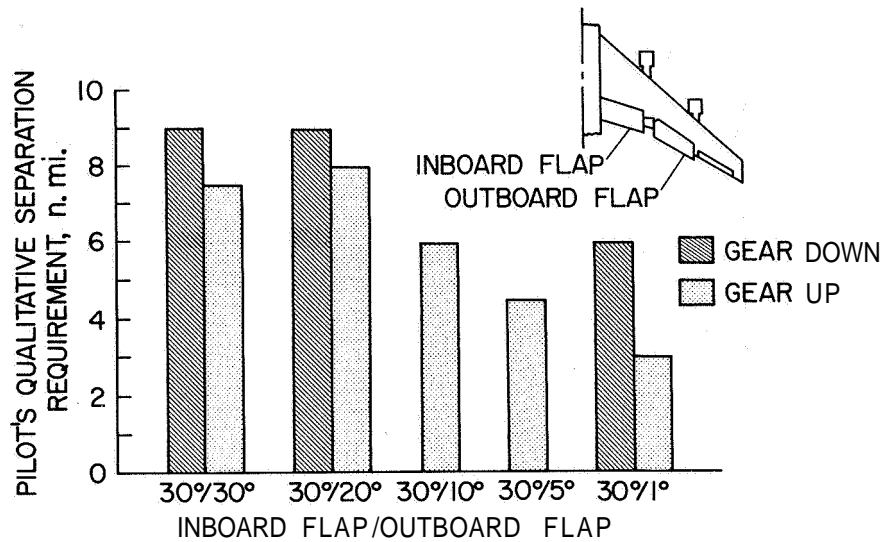
(a) Variation with outboard flap deflection, no yaw.
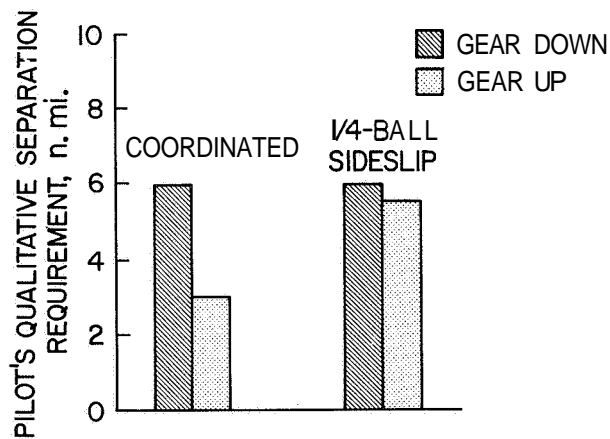


(b) Variation with yaw on the generator airplane, flaps $30°/1°$.

Figure 16.- Pilot qualitative separation requirement for a Learjet or T-37B airplane following a B-747 airplane; level flight (ref. **35**).
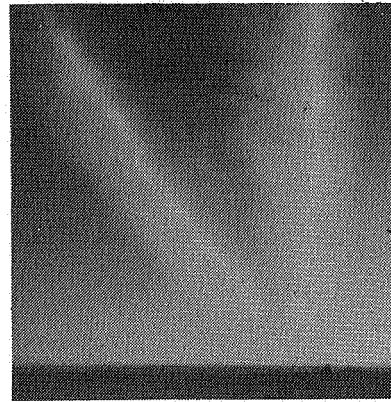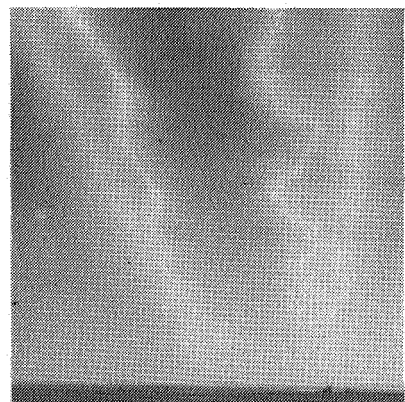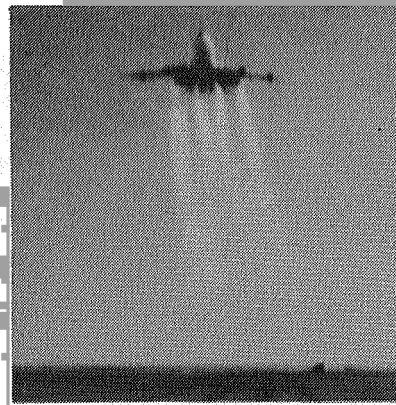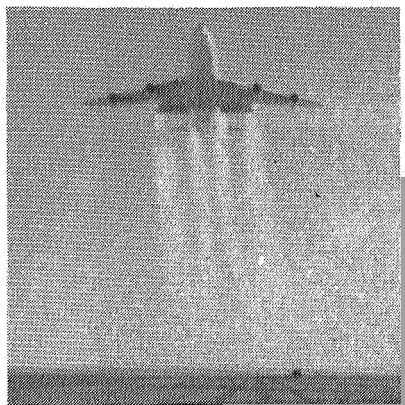
**LANDING GEAR UP**  **LANDING GEAR DOWN**

Figure 17.– Flow visualization photographs from flight tests of the B-747 airplane in the 30°/1° configuration showing the effect of the landing gear on the flap inboard vortices (ref. 31).
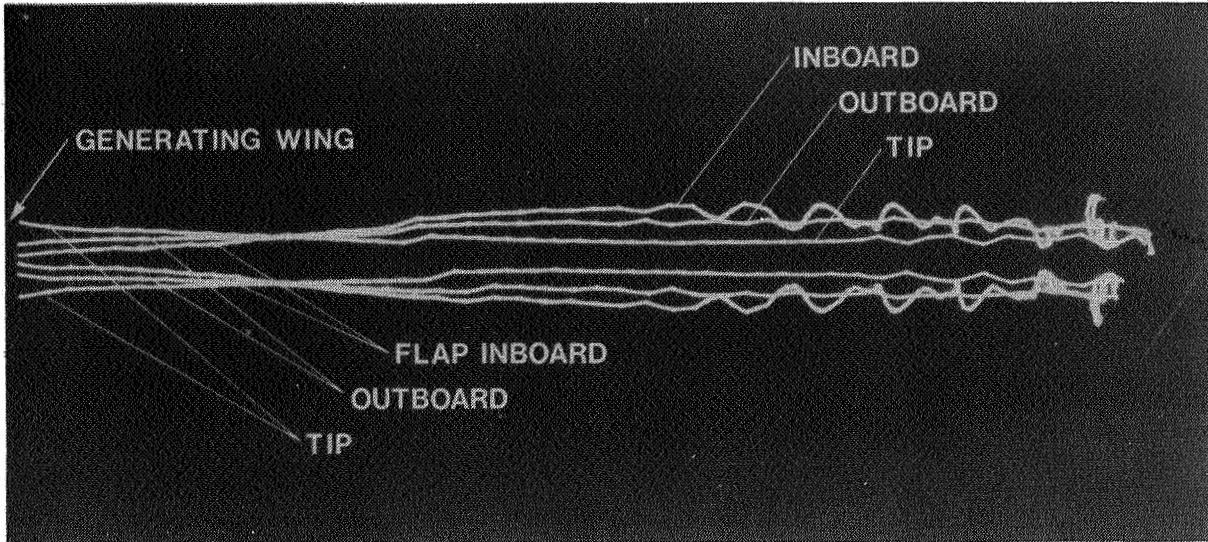
Figure 18.- Computer graphics display of the results of a three-dimensional
   time-dependent inviscid calculation of the wake vortex interaction behind
   a configuration with a three vortex pair wake with landing gear up
   (ref. **36).**
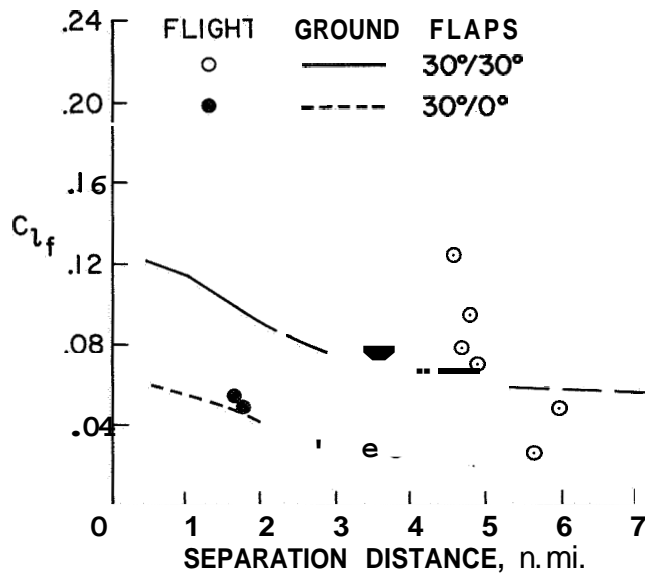


Figure 19.- Comparison of the flight-measured rolling-moment coefficient
   imposed on the **T-37B** airplane with the ground-based measured values from
   reference **32.**

336
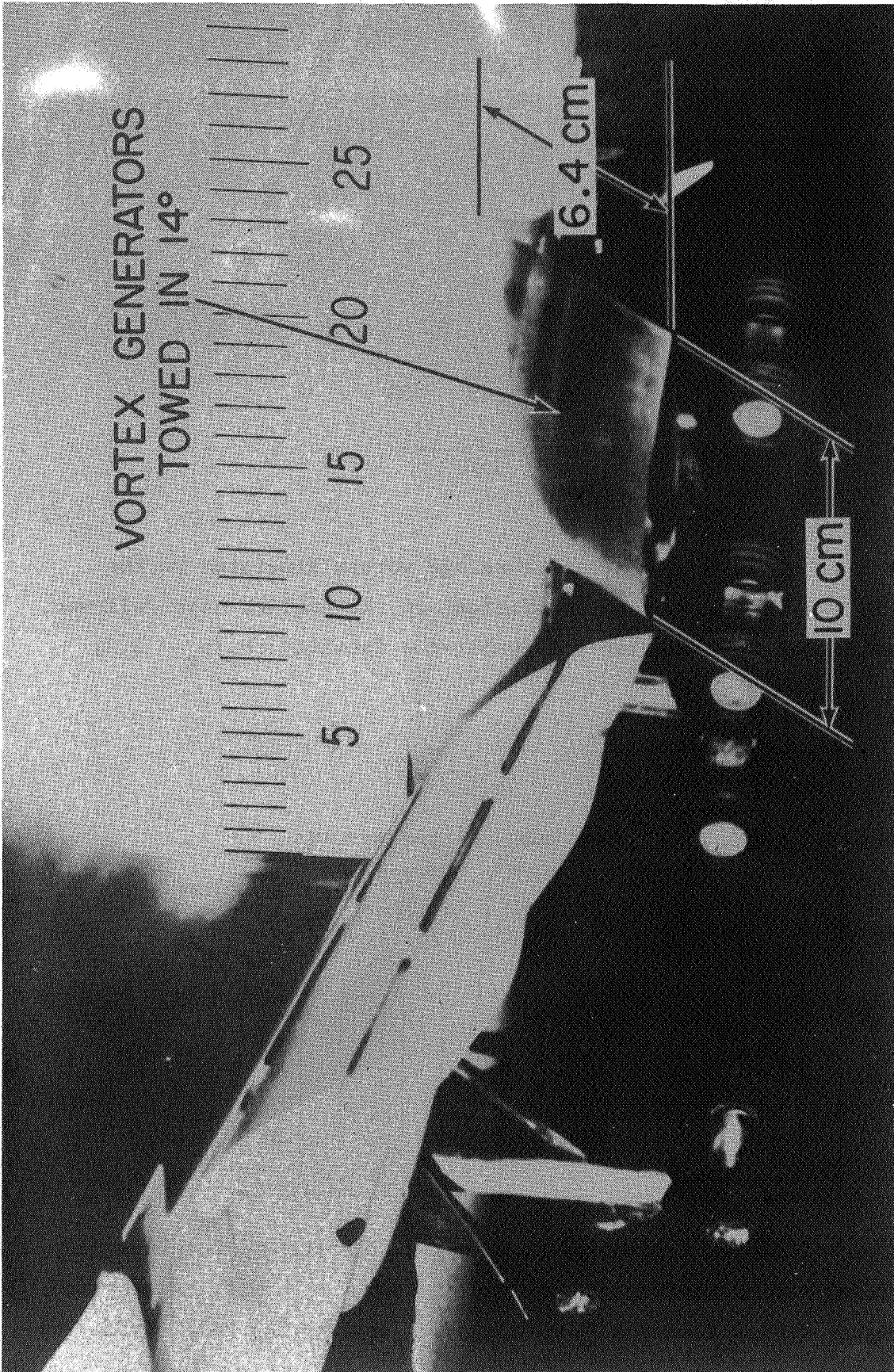
Figure 20 - Photograph of the B-747 model used in the Hydronautics Inc rotor-
tow facility tests     the fuselage vortex generator (dimensions in cm).

| | FLAPS | LANDING GEAR | FUSELAGE VORTEXGENERATOR |
|---|---|---|---|
| O | 30°/30° | OFF | OFF |
| △ | 30°/0° | OFF | OFF |
| ◇ | 30°/0° | ON | OFF |
| ● | 30°/0° | ON | ON |
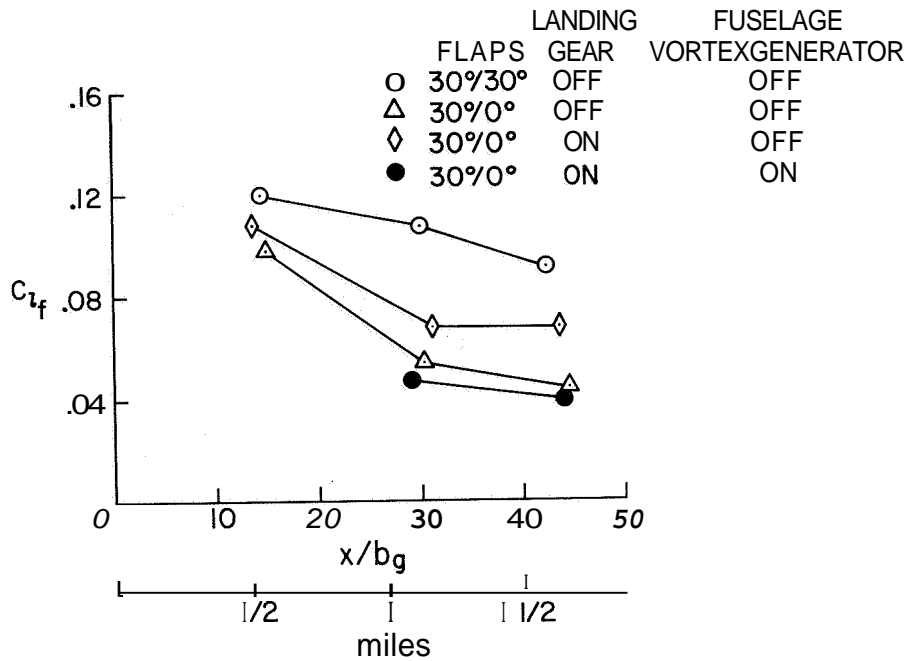
Figure 21.– Effect of landing gear and fuselage vortex generator on the variation of the rolling–moment coefficient on the Learjet size follower, as measured in the Hydronautics Inc. water–tow facility; $b_f/b_g = 0.2$, $C_{L_g} = 1.2$.
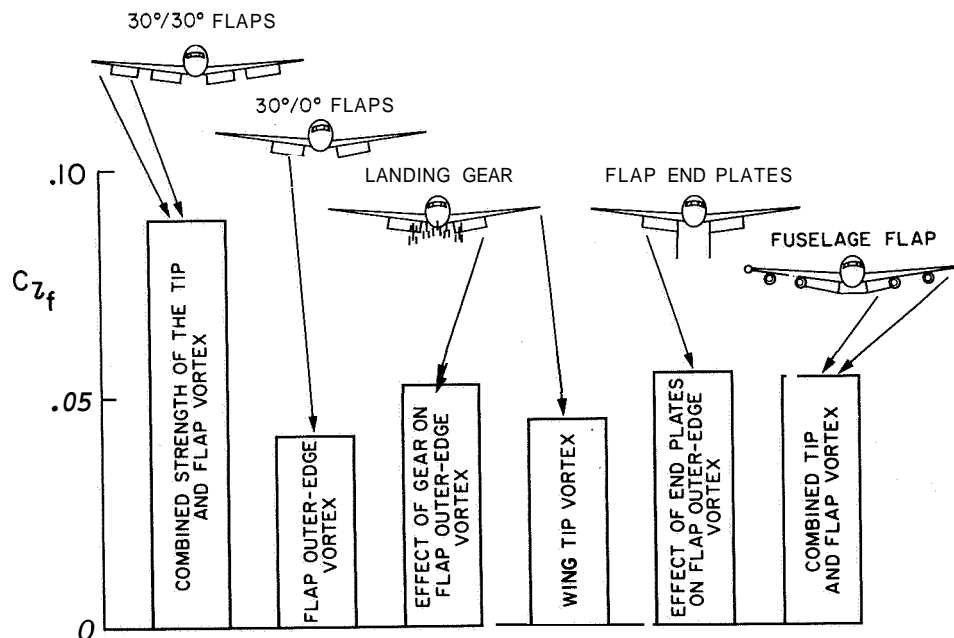


Figure 22.– The effects of landing gear, flap en plates, and fuselage flap on the rolling–moment coefficient on the DC–9 size follower, as measured in the Langley Vortex Research Facility; $b_f/b_g = 0.5$, $C_{L_g} = 1.2$ (ref. 28).

338

# THE DEVELOPMENT AND
# USE OF SPOILERS AS VORTEX ATTENUATORS

Delwin R. Croom

NASA Langley Research Center

## SUMMARY

This paper presents the results of groundbased and flight investigations performed at NASA to develop spoilers as trailing vortex alleviation devices. Based on the results obtained in these investigations, it was found that the induced rolling moment on a trailing model can be reduced by spoilers located near the midsemispan of a vortex–generating wing. Substantial reductions in induced rolling moment occur when the spoiler vortex attenuator is located well forward on both unswept and swept wing models. In addition, it was found that existing flight spoilers on the jumbo–jet transport aircraft can be effective as trailing vortex attenuators.

## INTRODUCTION

The strong vortex wakes generated by large transport aircraft are a potential hazard to smaller aircraft. NASA is involved in a program of model tests, flight tests, and theoretical studies to determine the feasibility of reducing the hazard by aerodynamic means. This hazard is defined schematically in figure 1. One phase of this program has been devoted to experimental investigations of spoilers as a possible method of trailing vortex attenuation because spoilers can inject turbulence in the wake, and they are also an effective way to alter the span load distribution. This paper briefly covers NASA activity in development of spoilers as vortex attenuators.

$b$        wing span, m

$c$        wing chord, m

$\bar{c}$        wing mean aerodynamic chord, m

$C_L$        lift coefficient, $\dfrac{\text{lift}}{qS_W}$

$C_{L,\,trim}$        trimmed lift coefficient

$C_{\ell,\,TW}$        trailing wing rolling-moment coefficient

$$\cong \frac{\text{trailing wing rolling moment}}{qS_{TW}b_{TW}}$$

$C_m$        pitching-moment coefficient $= \dfrac{\text{pitching moment}}{qS_W\bar{c}_W}$

$C_\mu$        momentum coefficient

$q$        dynamic pressure, Pa

$S$        wing area, m$^2$

$V$        velocity, m/s

$V_j$        jet velocity, m/s

$V_\infty$        free-stream velocity, m/s

$Y$        lateral dimension, m

$a$        angle of attack, deg

$\delta_j$        jet deflection, deg

Subscripts:

max        maximum

TW        trailing wing model

W        generating model

## EARLY SPOILER INVESTIGATIONS

In 1970, the NASA Ames Research Center performed wind-tunnel and flight investigations of a wingtip-mounted spoiler (refs. **1** and **2**). The wind-tunnel results shown in figure **2** indicated that a downstream distance of 10 wing chord lengths, the circumferential was reduced because of the spoiler by approximately one-half, while the core diameter was approximately doubled. These results were interpreted as significantly altering the vortex structure in a manner that would contribute to a more rapid dissipation of the vortex and an accompaying reduction in vortex intensity. Subsequent to the wind-tunnel test, wingtip spoilers were mounted on the left wingtip of a Convair 990 aircraft for evaluation in flight. In the flight program, a Learjet **23** airplane was used to probe the vortexes from both the right and left wingtip of the Convair 990. The roll response of the Learjet was used as an index of the intensities of the vortexes. Several short encounters with each vortex were made by the probe aircraft, and the pilot reported that he could tell no difference between the modified and unmodified vortexes from the dynamic response of the aircraft. **It** was concluded, therefore, that further research was required to determine an effective technique in the use of spoilers for vortex attenuation.

## RECENT SPOILER INVESTIGATIONS

In 1971, experimental work was initiated at the NASA Langley Research Center to further investigate spoilers as a possible vortex abatement device. In the first phase of this study, a semispan wing was used in a study to determine the proper location for a spoiler to be installed on the wing to cause the largest apparent alteration to the trailing vortex. The semispan wing was mounted on the Langley tow tank carriage and propelled through a smoke screen, and observations were made of the behavior of the smoke entrained in the vortex. After several hundred observations of the smoke patterns with the spoilers positioned at practically every conceivable location on the wing, it was determined that a spoiler of about 8-percent chord projection located

between the 50- and 75-percent spanwise location near the 30-percent chord line would cause the most alteration to the vortex system, and, in general, the observed vortex motion became essentially nonexistent after a very short time. Based on these observations, a wind-tunnel investigation was made using an unswept aspect-ratio-8 wing model with a spoiler having an 8-percent projection located along the 30-percent chord line between the 50- and 75-percent semispan station as shown in figure 3. The three-quarter span flaps used on this model were appended to the wing as is shown in figure 3. Figure 4 is a photograph of the aspect-ratio-8 model mounted in the Langley V/STOL tunnel.

The spoiler effectiveness was evaluated using the trailing model technique to determine the maximum rolling-moment coefficient (fig. 5) induced by the generating model. It can be seen that the spoiler was effective in reducing the induced rolling-moment coefficient on the following model by about 25 percent throughout the range of downstream distances investigated. The complete results of this investigation were reported in reference 3.

Because the prime concern was the vortex-wake problem behind very large transport aircraft, a decision was made to concentrate ground-based studies on the jumbo-jet class of aircraft. Therefore, a 0.03-scale model of a jumbo-jet transport (fig. 6) was used for subsequent tests in the Langley V/STOL tunnel. Results of this investigation are reported in reference 4. Figure 7 is a photograph of the generating aircraft model mounted in the V/STOL tunnel with all landing flaps extended 30°; also shown downstream is the traverse rig for mounting the trailing model.

Two sizes of unswept trailing wing models were used during the investigations (fig. 8). One had a span and aspect ratio equivalent to a small business jet aircraft; the other had the span and aspect ratio equivalent to a medium size jet transport aircraft. These trailing models are referred to on the figures as the small and the large trailing models.

The first spoiler configuration investigated as a vortex attenuator on the generating model was a plain vertical projection spoiler located along the 30-percent chord line between the 50- and 75-percent semispan stations as is

342

shown in figure 9. Figure 10 is a photograph of the spoilers mounted on the wing of the generating model. Figure 11 shows the effect of spoiler projection on the induced rolling-moment coefficient, measured on the small trailing wing model located at 6.74 spans downstream of the generating model. It can be seen that the maximum reduction in rolling moment was achieved with about an 8-percent spoiler projection. Therefore, subsequent tests were made with the spoiler projected to 8 percent.

The effectiveness of the spoilers in reducing the trailing wing rolling-moment coefficient for the two sizes of trailing models downstream of the generating model is shown in figure 12. It can be seen that the induced rolling-moment coefficient on the large trailing model downstream of the generating model was larger than those induced on the small trailing model. The reduction in induced rolling-moment coefficient on the small trailing model was about 35 to 40 percent over the range of downstream distances investigated; whereas, the reduction in induced rolling-moment coefficient on the large model was on the order of 15 to 25 percent.

Data obtained in the Hydronautics, Inc., water towing tank on the generating model with and without spoilers is shown in figure 13. This facility allows for data to be taken at a greater downstream distance than can be obtained in the V/STOL tunnel. Even though the magnitude of the measured trailing wing rolling-moment coefficients does not agree with those obtained in the V/STOL tunnel, the trends do agree, and the effectiveness of the spoiler as a vortex attenuator is substantiated over the extended downstream range available in the towing tank.

A jet spoiler was also investigated (fig. 14) on the generating model. Holes were drilled into a wing pressure chamber at various angles to the wing upper surface so that various jet-sheet angles could be investigated. In this investigation it was found that when the jet sheet was directed vertically ($\delta_j = 90^o$) or inclined forward ($\delta_j = 120^o$), at relatively low values of $C_\mu$ the jet spoiler was effective in reducing the induced trailing wing rolling moments on the small trailing model. When the jet sheet was inclined to the rear ($\delta_j = 60^o$ or $\delta_j = 75^o$), the induced rolling moments were not reduced until much larger values of $C_\mu$ were reached. A possible reason for this is shown by

the data in figure 15. It can be seen that for the vertical- and forward-inclined jet spoiler ($\delta_j = 90^o$ and $\delta_j = 120^o$) at a $C_\mu$ value of 0.05, there is a reduction of lift-curve slope generally associated with the separated region that is expected aft of a forward-located spoiler. When the jet was inclined rearward, there was entrainment of the flow, and no extensive separation region was noted. The jet spoiler in this case acted similarly to a boundary-layer control device.

Even though the spoiler concepts discussed so far did show promise as possible vortex attenuators on the full-scale airplane, their use would require extensive modifications to the airplane. It became apparent that the normal flight spoilers already on the airplane should be studied as possible vortex attenuators. Therefore, exploratory wind-tunnel tests were made in the V/STOL tunnel during March 1975 using wooden wedges to represent the various of the flight spoilers noted on figure 16. These exploratory results were encouraging; therefore, the model wing was modified so that the flight spoilers would be more representative of those on the full-scale transports. Over the section of the wing immediately forward of the outboard flaps, spoilers were con-structed that would operate similarly to the actual flight spoilers--when retracted, the spoilers made the contours of the upper surface of the wing and when deflected, a large gap was formed forward of the flap. The spoiler segments identified on figure 16 as 1, 2, 3, and 4 were investigated in the following combinations: 1 and 2 (fig. 17); 2 and 3 (fig. 18); 3 and 4 (fig. 19); and 1 and 4 (fig. 20).

The results obtained for these various combinations of flight spoilers are presented in figure 21. (Complete test results are available in ref. 5.) It can be seen that with either of these various combinations of flight spoiler segments deflected to $45^o$, there was a large decrease in the trailing rolling-. moment coefficient induced on the small trailing wing model. Two of these configurations (1 and 2, and 1 and 4) were investigated over a spoiler deflectio range. The results shown in figure 22 indicate that essentially all the spoiler effectiveness was obtained at a deflection angle of about $30^o$.

Data obtained in the V/STOL tunnel using the large trailing model (fig. 23) indicate that the induced rolling-moment coefficient is attenuated,

however, to a lesser extent than was noted for the smaller trailing model. Data obtained in the Hydronautics, Inc., water towing tank with the small trailing model (fig. 24) confirmed the foregoing results and also indicated that the large reduction in induced rolling-moment coefficient on the small trailing model was also realized at much greater downstream distance than was obtainable in the Langley V/STOL tunnel.

Tests were also made in the Langley Vortex Research Facility of the various flight spoilers as vortex attenuators on a genarating model, and the results (fig. 25) essentially agree with those obtained in both the Langley V/STOL tunnel and the Hydronautics, Inc., water tank facility.

As a result of the findings in the ground-based facilities, a flight program was made at the Hugh L. Dryden Flight Research Center that used the existing flight spoilers on a NASA-owned B-747 aircraft as the vortex attenuating device. A T-37 aircraft is used to penetrate the trailing vortex. Penetrations behind the B-747 airplane in its landing configuration were limited to about 13 km (7 n, mi.), with appropriate deflection of the 3-747 flight spoilers, penetration as close as about 4 km (2 n. mi.) were made. These flights results (ref. 6) have verified the trends obtained in the ground-based facilities.

## CONCLUDING REMARKS

Results obtained in these investigations showed that the induced rolling moment on a trailing model can be reduced by spoilers located near the midsemispan of a wing. Substantial reductions in induced rolling moment occur when the spoiler vortex attenuator is located well forward on both unswept and swept wing models. In addition, it was found that the existing flight spoilers on the jumbo-jet transport aircraft model are effective as trailing vortex attenuators.

# REFERENCES

1. Corsiglia, Victor R.; Jacobsen, Robert A.; and Chigier, Norman: An Experimental Investigation of Trailing Vortices Behind a Wing With a Vortex Dissipator. Aircraft Wake Turbulence and Its Detection, Plenum Press, Inc., 1971, pp. 229-242.

2. Dunham, R. Earl, Jr.; Verstynen, Harry A., Jr.; and Benner, Margaret S.: Progress Report on Wing Trailing Vortex Studies. NASA SP-270, 1971, pp. 101-113.

3. Croom, Delwin R.: Low-Speed Wind-Tunnel Investigation of Forward-Located Spoilers and Trailing Splines as Trailing Vortex Hazard Alleviation Devices on an Aspect-Ratio-8 Wing Model. NASA TM-X-3166, 1975.

4. Croom, Delwin R.; and Dunham, R. Earl, Jr.: Low-Speed Wind-Tunnel Investigation of Span Load Alteration, Forward-Located Spoilers, and Splines as Trailing-Vortex Hazard Alleviation Devices on a Transport Aircraft Model. NASA TN D-8133, 1975.

5. Croom, Delwin R.: Low-Speed Wind-Tunnel Investigation of Various Segments of Flight Spoilers as Trailing-Vortex-Alleviation Devices on a Transport Aircraft Model. NASA TN D-8162, 1976.

6. Barber, Marvin R.; Hastings, Earl C., Jr.; Champine, Robert A.; and Tymczyszyn, Joseph J.: Vortex Attenuation Flight Experiments. NASA SP-409, 1977.
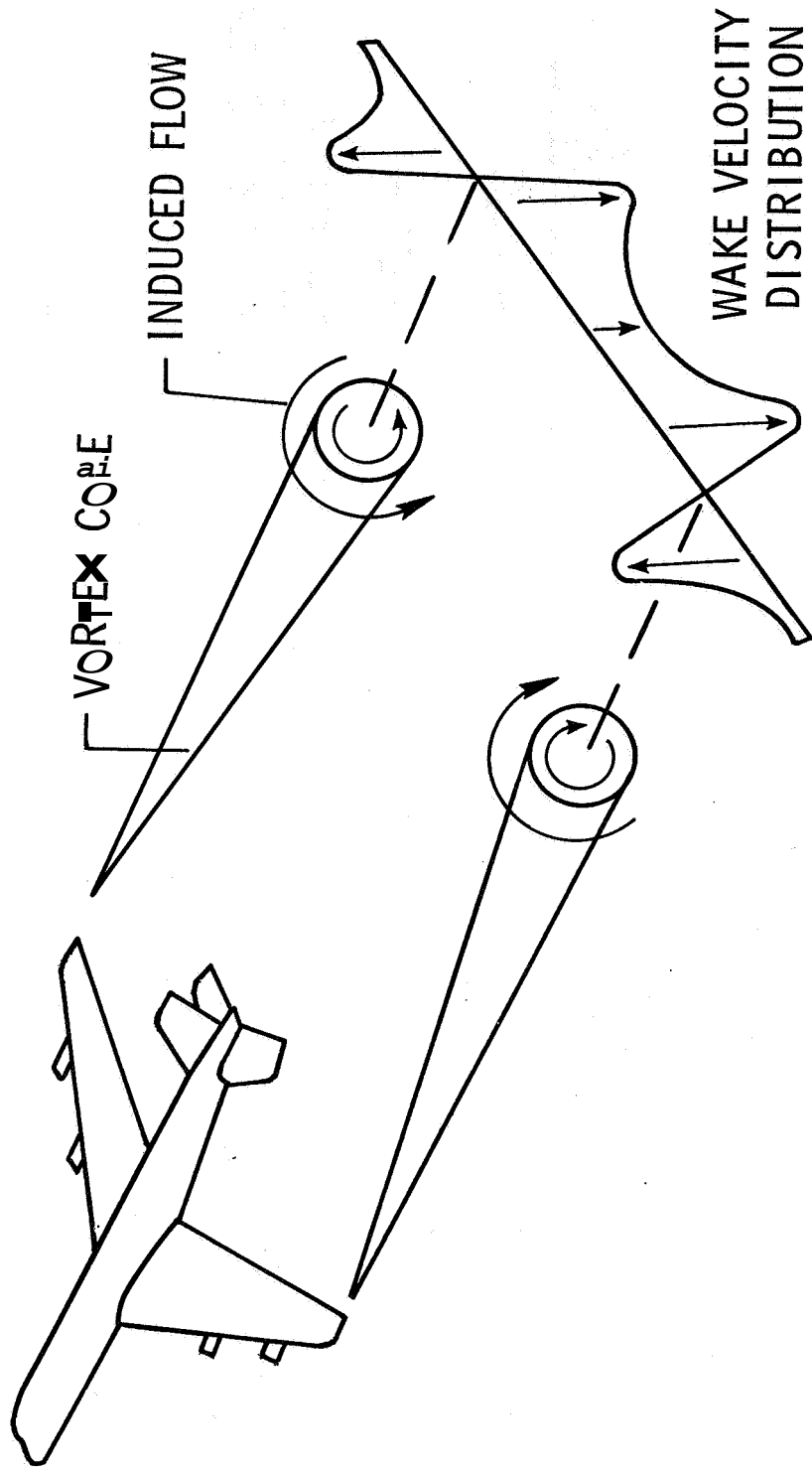
Figure 1 —Aircraft vortex wake hazard
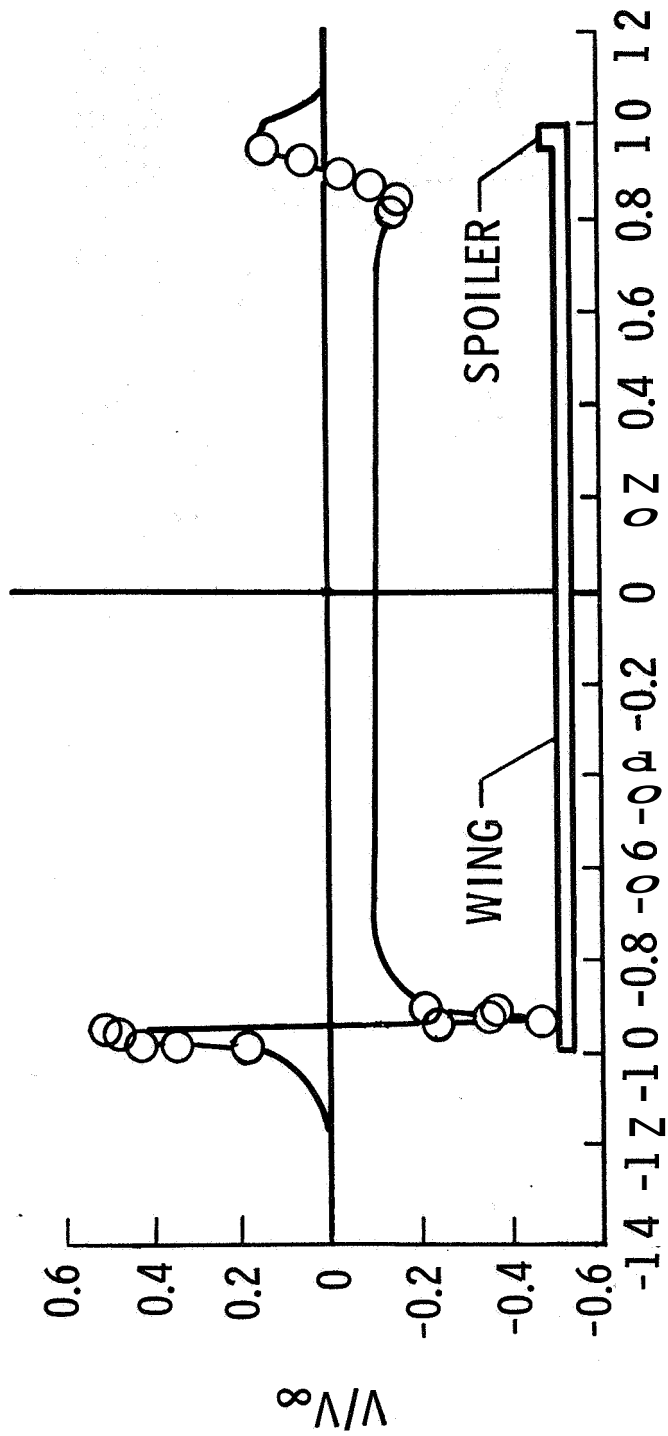
Figure 2.—Tangential velocity components for trailing vortex (left tip) and displaced vortex (right tip). x/c = 10.

.75 b/2

FLAP SPAN

FLAP ARRANGEMENT

.015c →‖← .015c

30°

.3c

SECTION A-A

A    A

.5 b/2

MIDSPAN SPOILER

.75 b/2

.3c →    .083c

c

SPOILER ARRANGEMENT
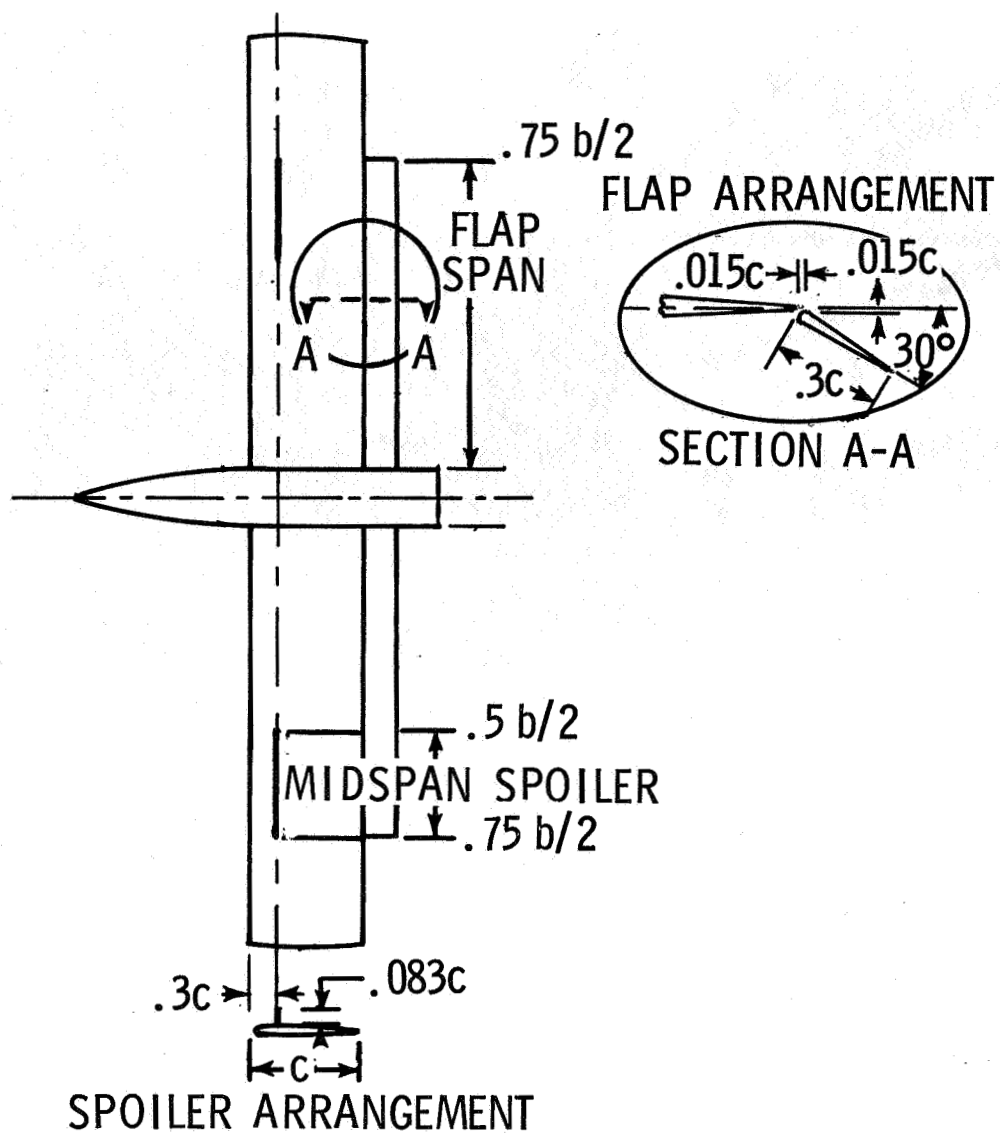
Figure 3.--Sketch of aspect−ratio−8 models.

3
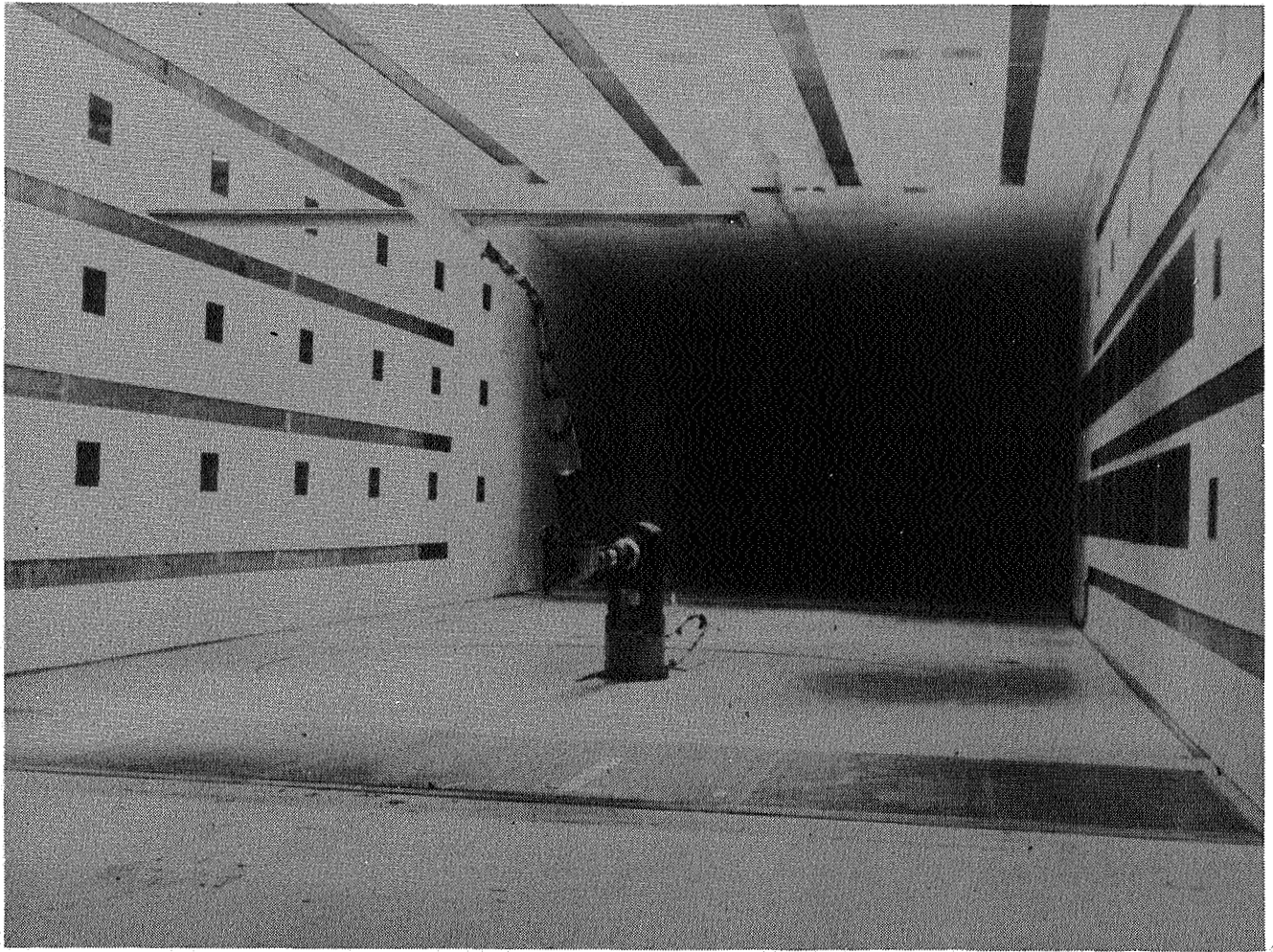
Figure 4.--Aspect-ratio-8 model in Langley **V/STOL** tunnel.
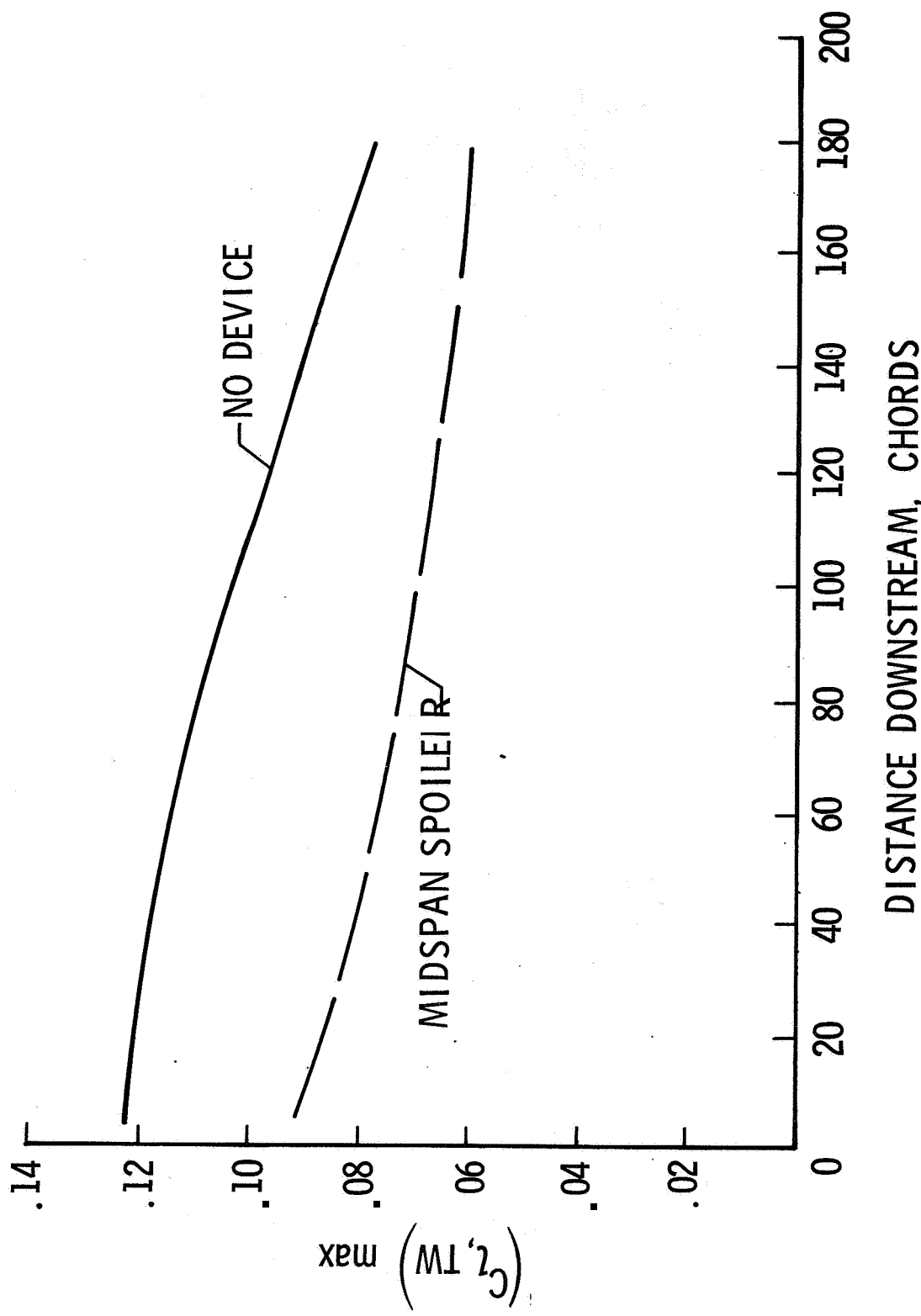
Figure VI -Effect of spoiler on aspect-ratio-8 model. $C_L = 1.25$; $b_{TW}/b = 0.25$.
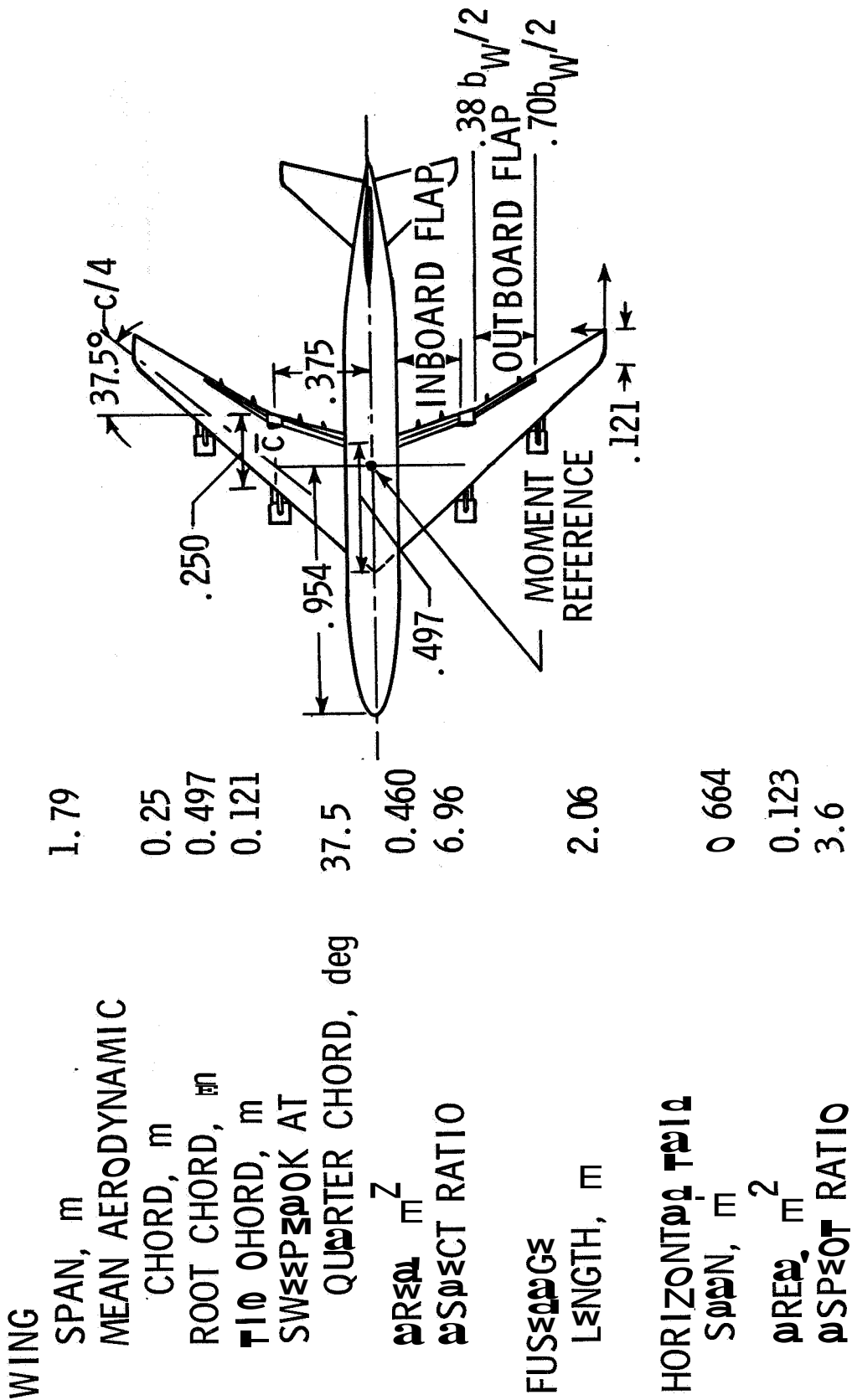
Figure 6 —-Plan view of transport aircraft model.

WING

| | |
|---|---|
| SPAN, m | 1.79 |
| MEAN AERODYNAMIC CHORD, m | 0.25 |
| ROOT CHORD, m | 0.497 |
| TIP CHORD, m | 0.121 |
| SWEEP AT QUARTER CHORD, deg | 37.5 |
| AREA, $m^2$ | 0.460 |
| ASPECT RATIO | 6.96 |

FUSELAGE

| | |
|---|---|
| LENGTH, m | 2.06 |

HORIZONTAL TAIL

| | |
|---|---|
| SPAN, m | 0.664 |
| AREA, $m^2$ | 0.123 |
| ASPECT RATIO | 3.6 |

352
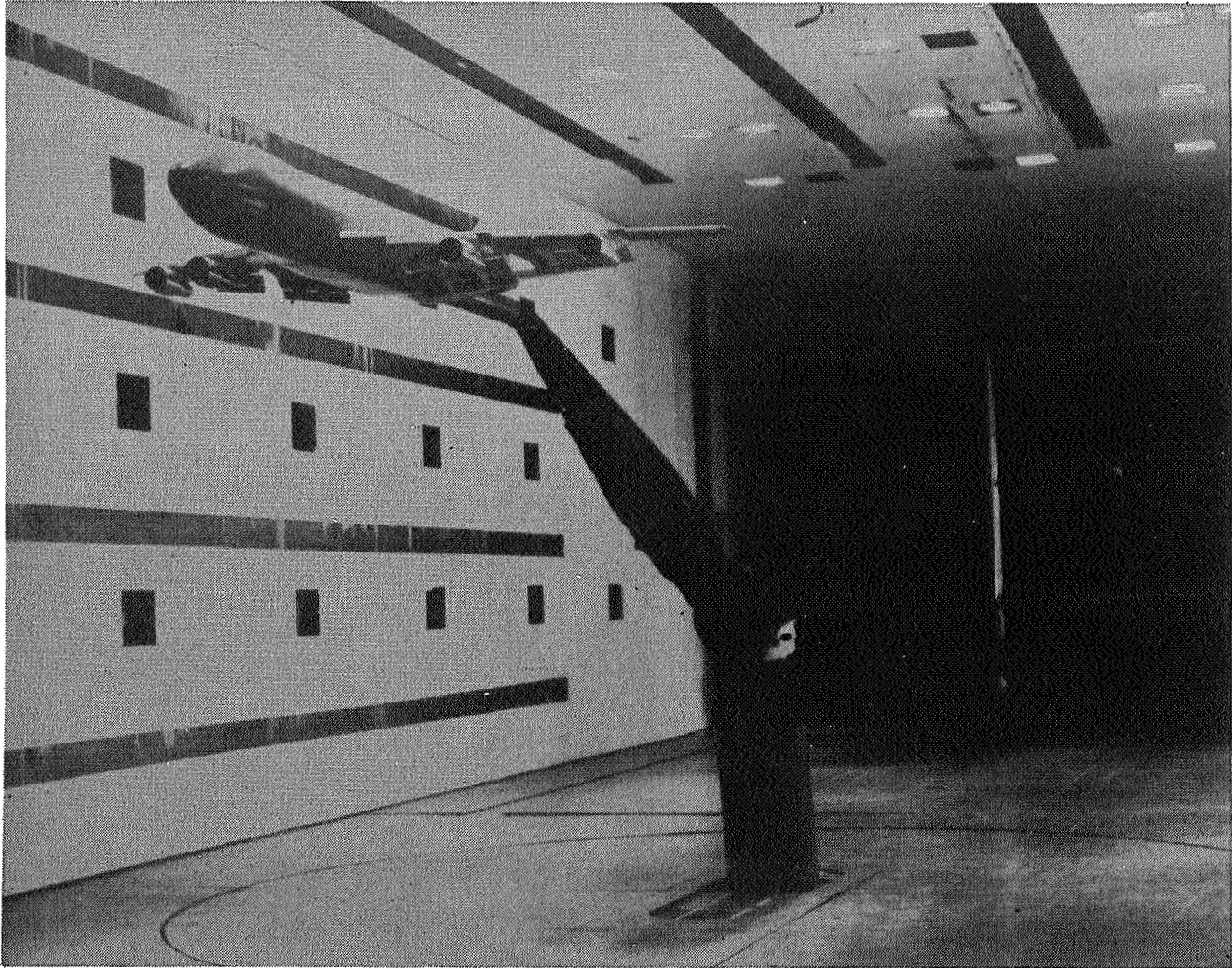
Figure 7.--Transport model with flap configuration 30°/30° in V/STOL tunnel.

| AREA, $m^2$ | 0.0199 | | AREA, $m^2$ | 0.0845 |
|---|---|---|---|---|
| SPAN, m | .326 | | SPAN, m | .853 |
| CHORD, m | .061 | | CHORD, m | .099 |
| ASPECT RATIO | 5.45 | | ASPECT RATIO | 8.70 |
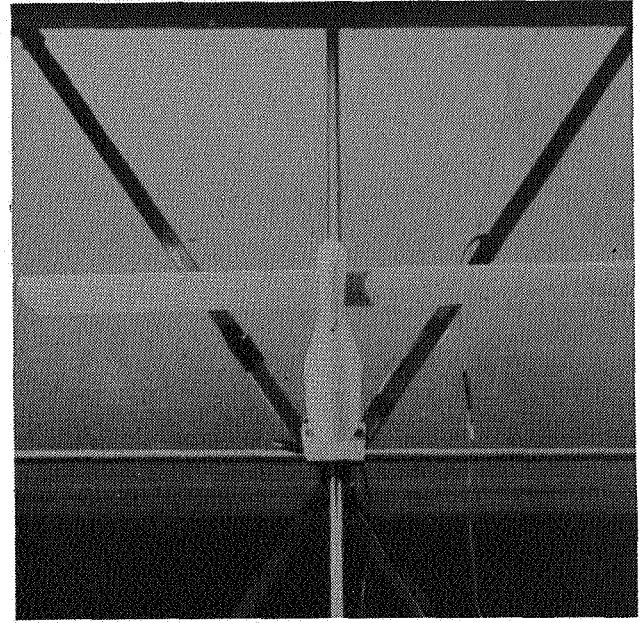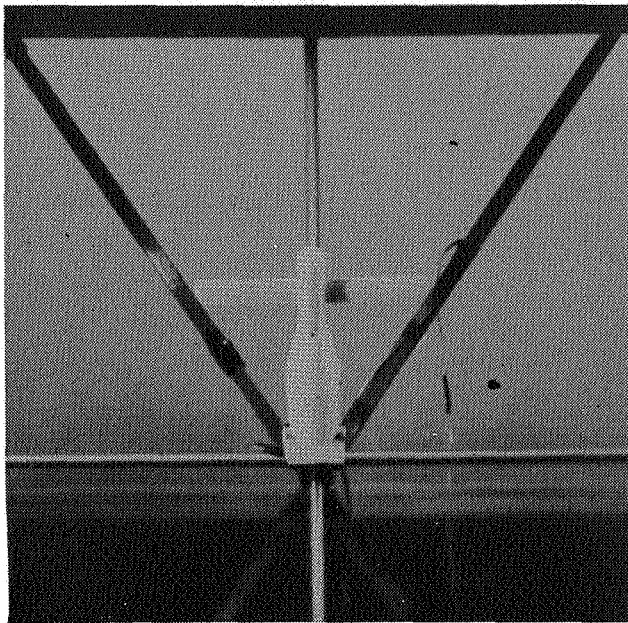


**SMALL TRAILING MODEL**      **LARGE TRAILING MODEL**

Figure 8.--Unswept trailing wing models on traverse mechanism.
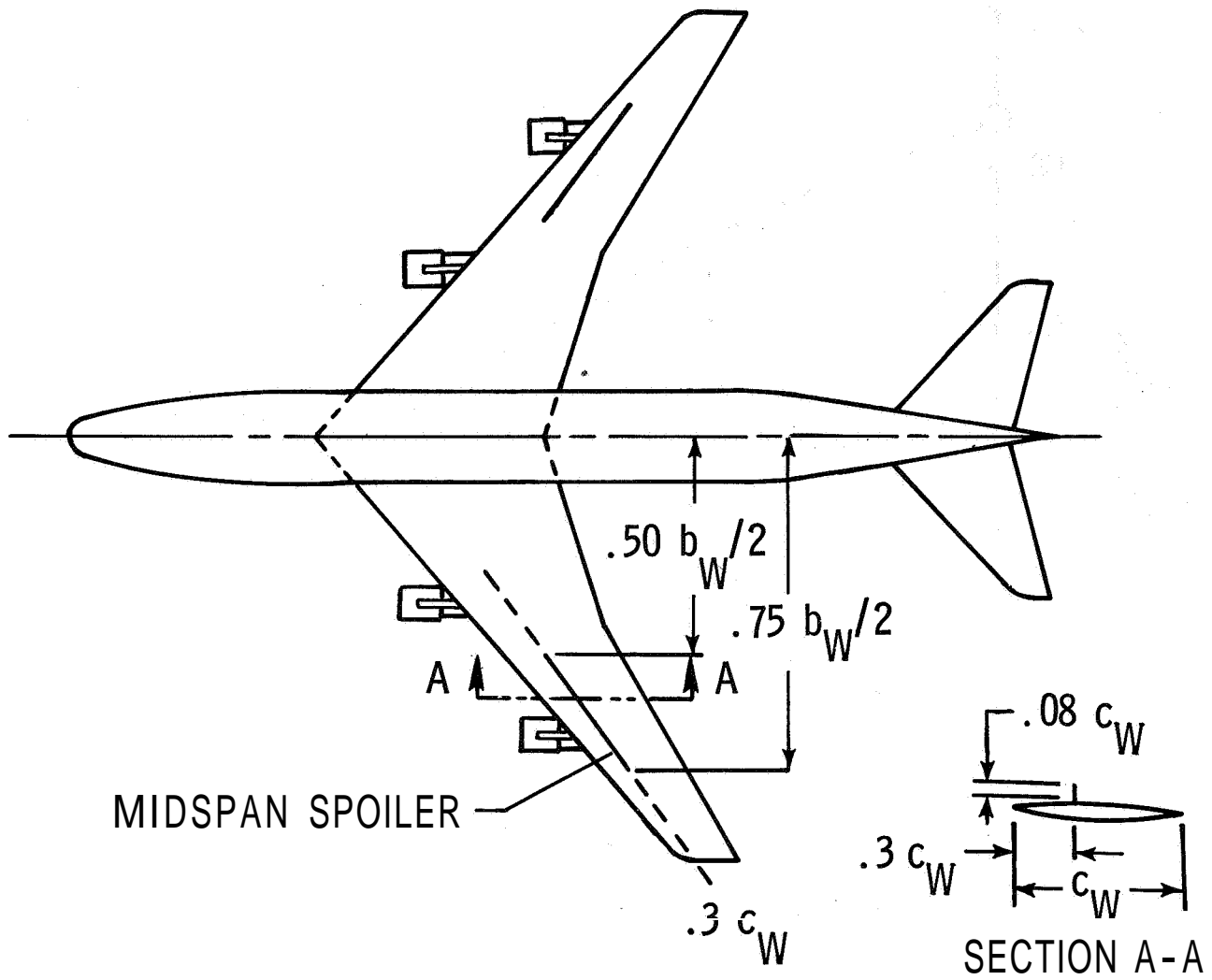
Figure 9.--Midspan spoiler configuration details.
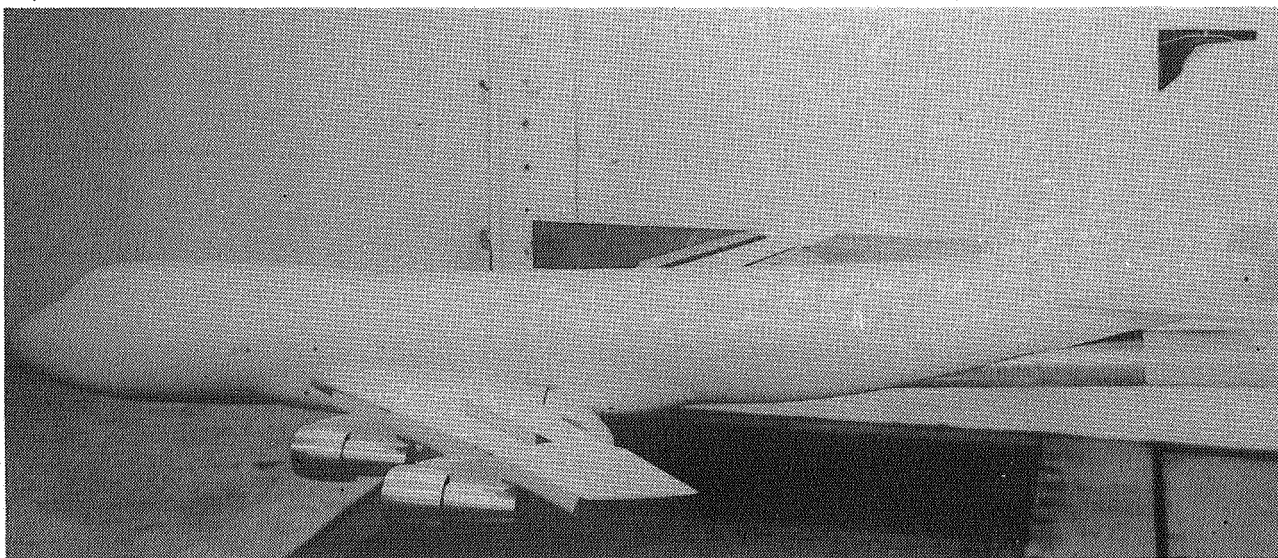


Figure 10.--Midspan spoiler on transport model.

355

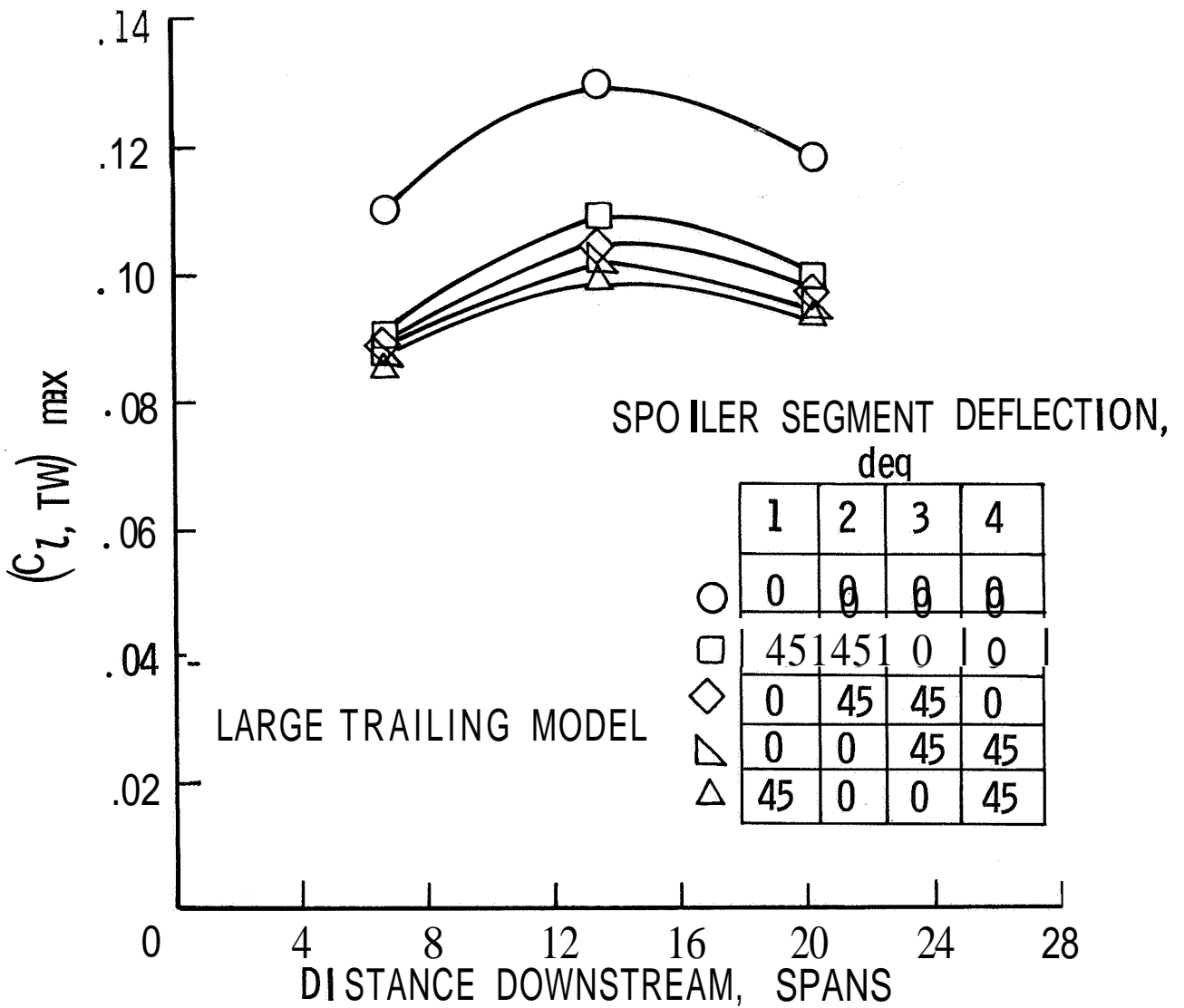Figure 11,--Transport model with forward-located midspan spoiler. $C_{L,trim} = 1.2$; 6.74 spans downstream.
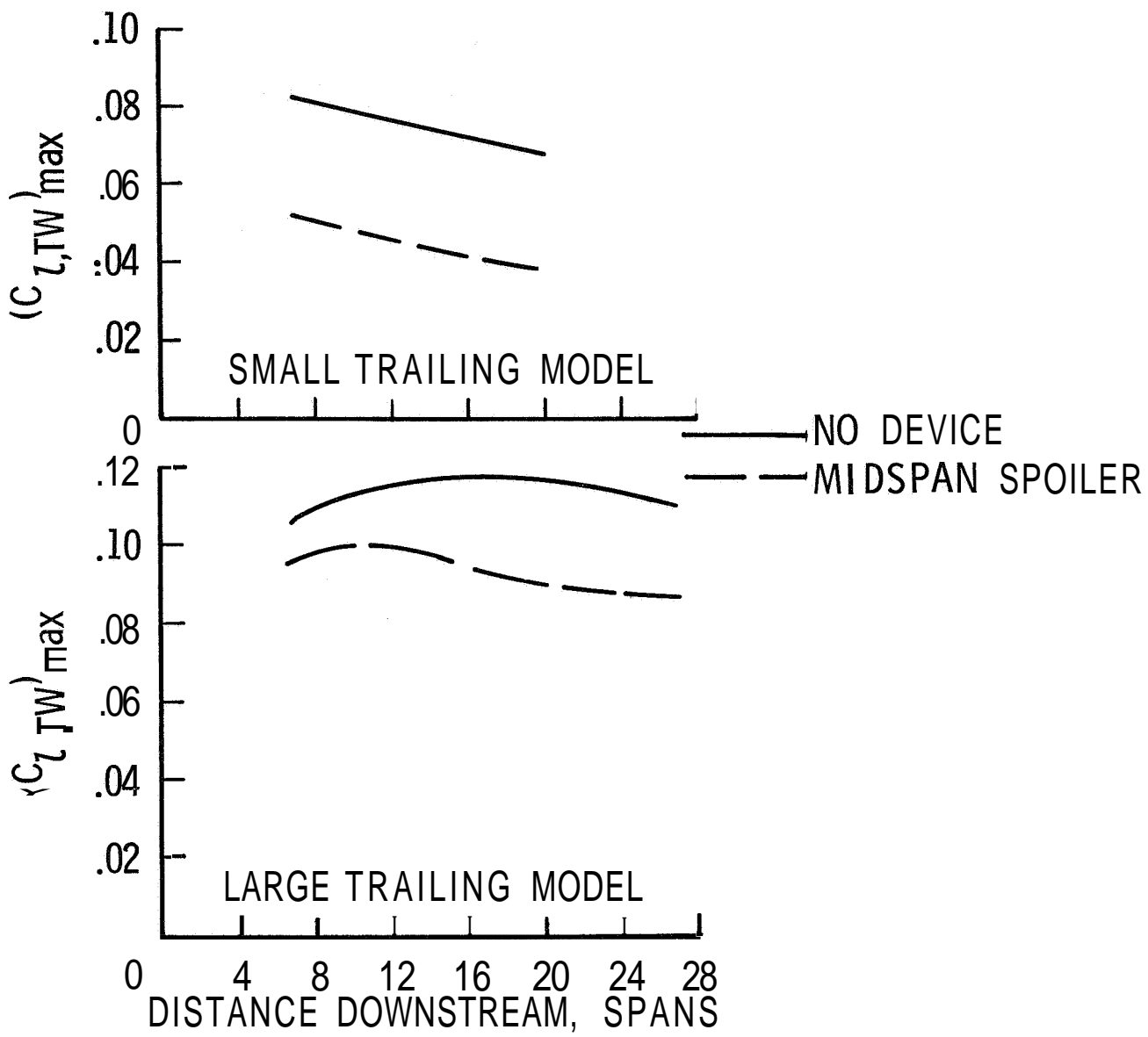
Figure 12.--Variation of trailing wing, rolling-moment coefficient with distance downstream from transport model--V/STOL tunnel. Midspan spoiler; $C_{L,trim} = 1.2$.

357
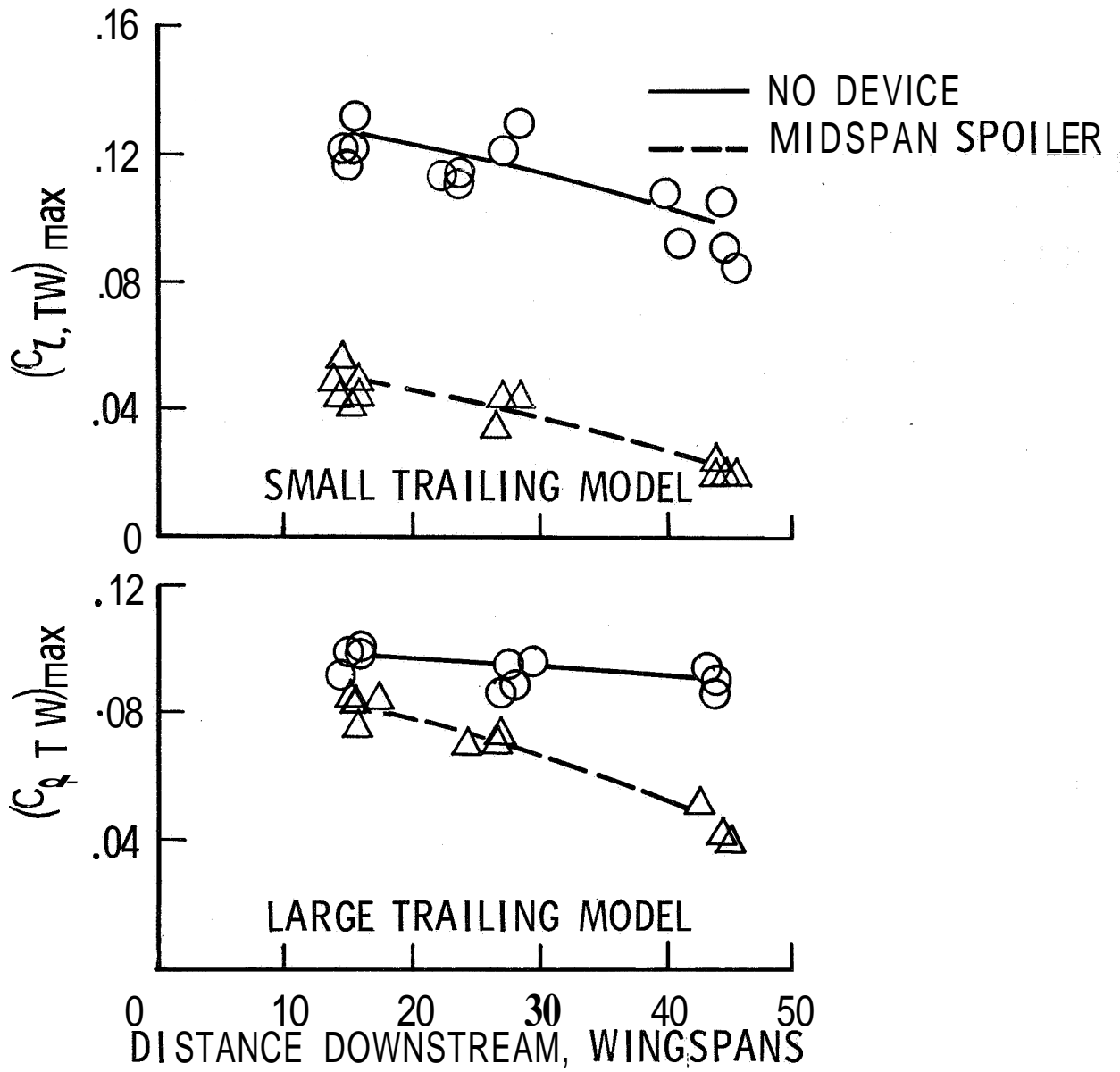
Figure 13.--Variation of trailing wing, rolling-moment coefficient with distance downstream from transport model--water tank. Midspan spoiler; $C_{L,trim} = 1.2.$
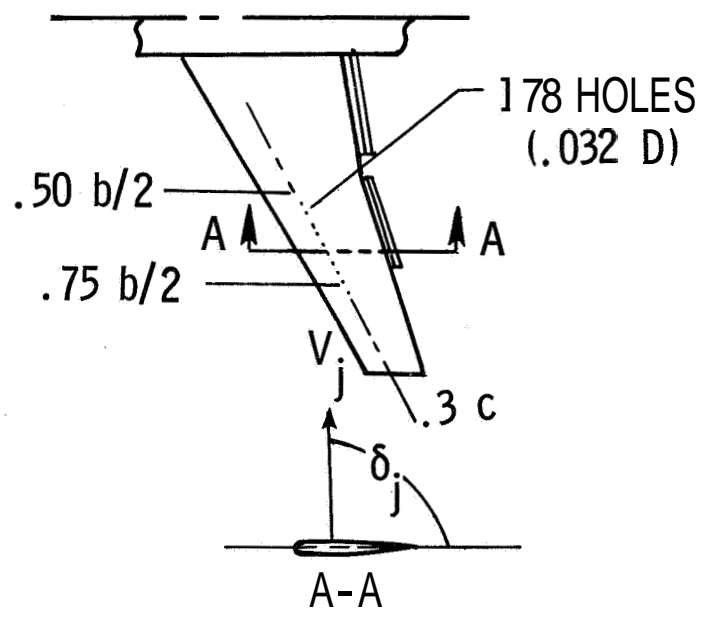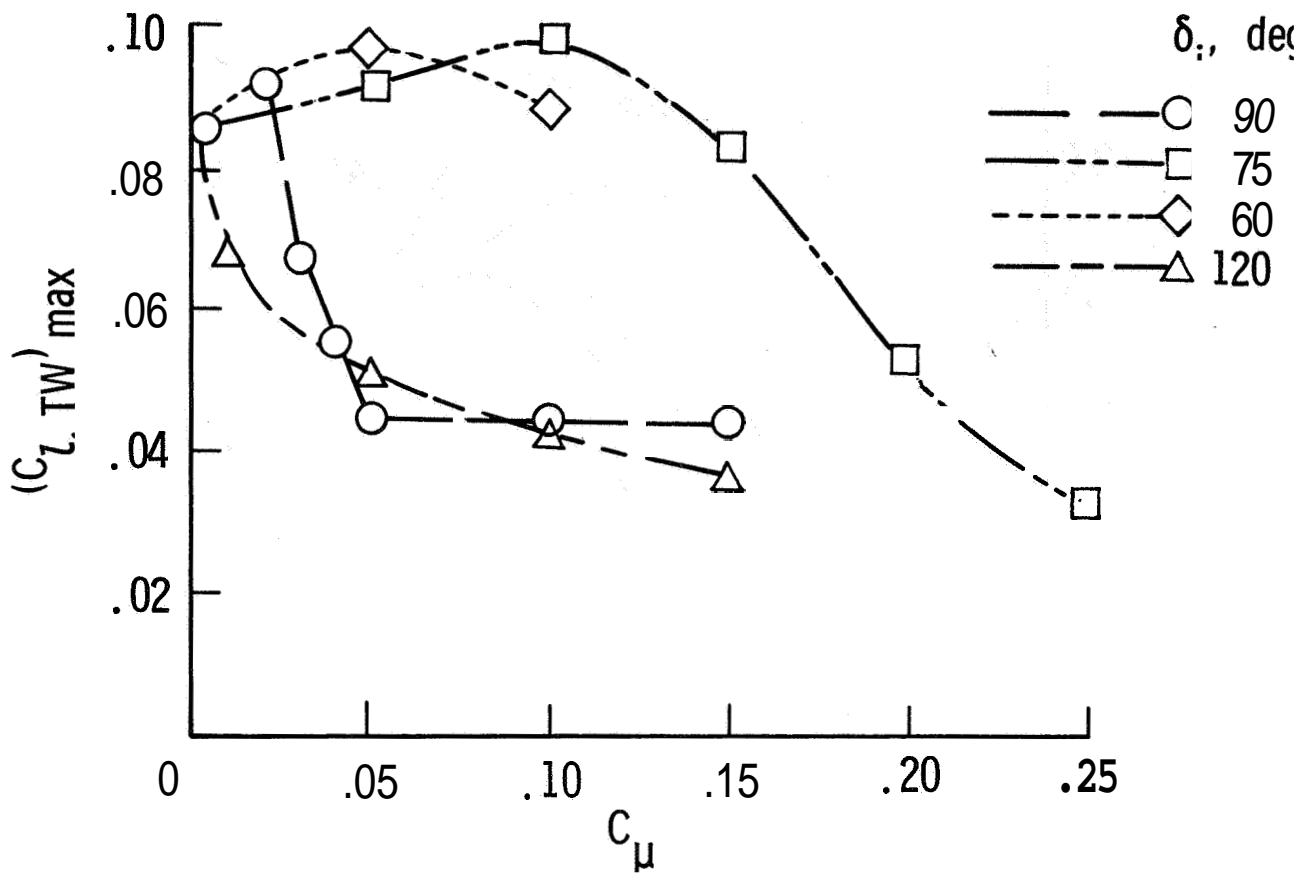
Figure 14.--Transport model with jet spoiler, small trailing wing 6.74 spans downstream. $C_{L,trim} = 1.2$; $C_M = 0$.
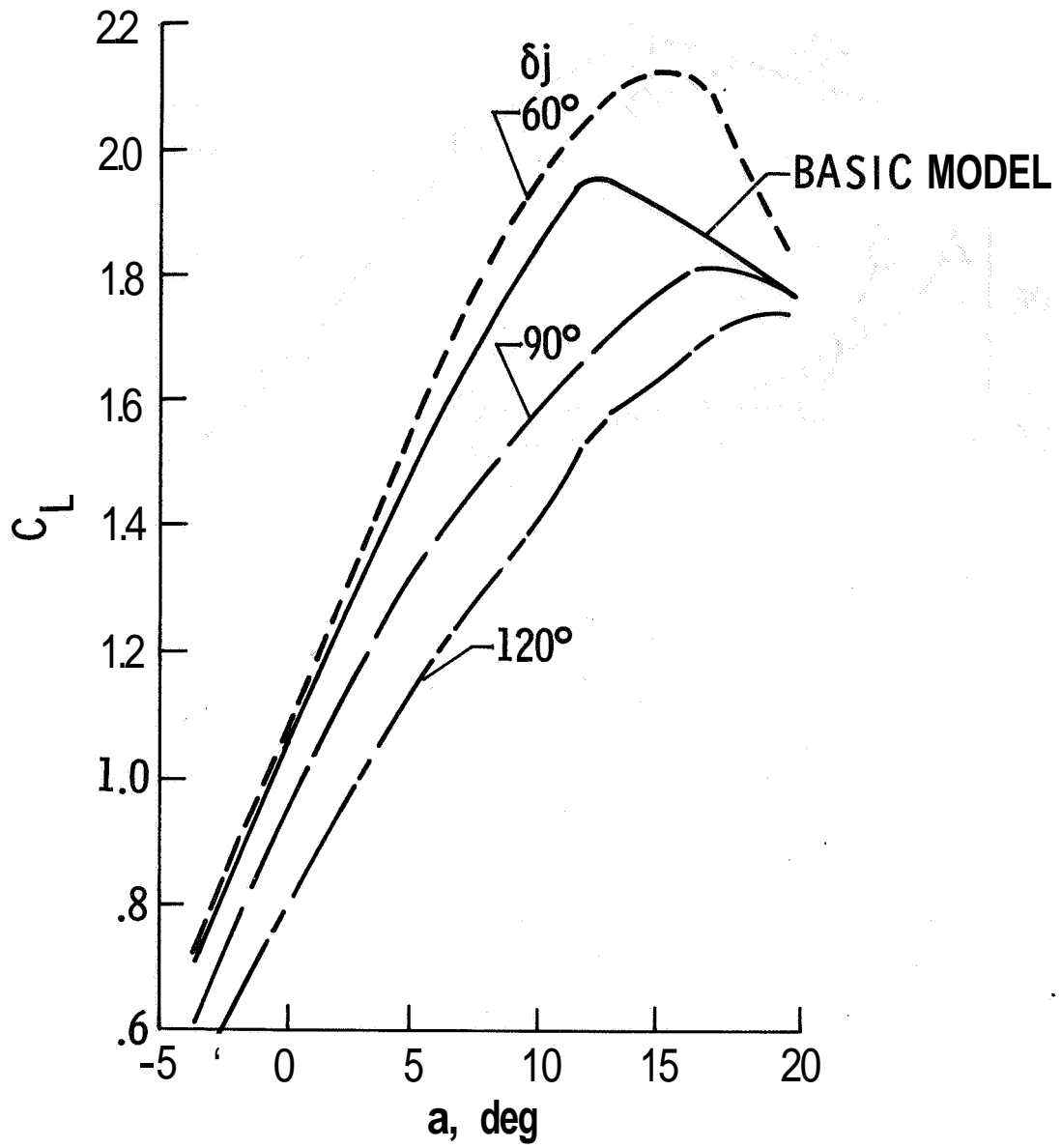
Figure 15.--Transport model with jet spoiler, C = 0.05.
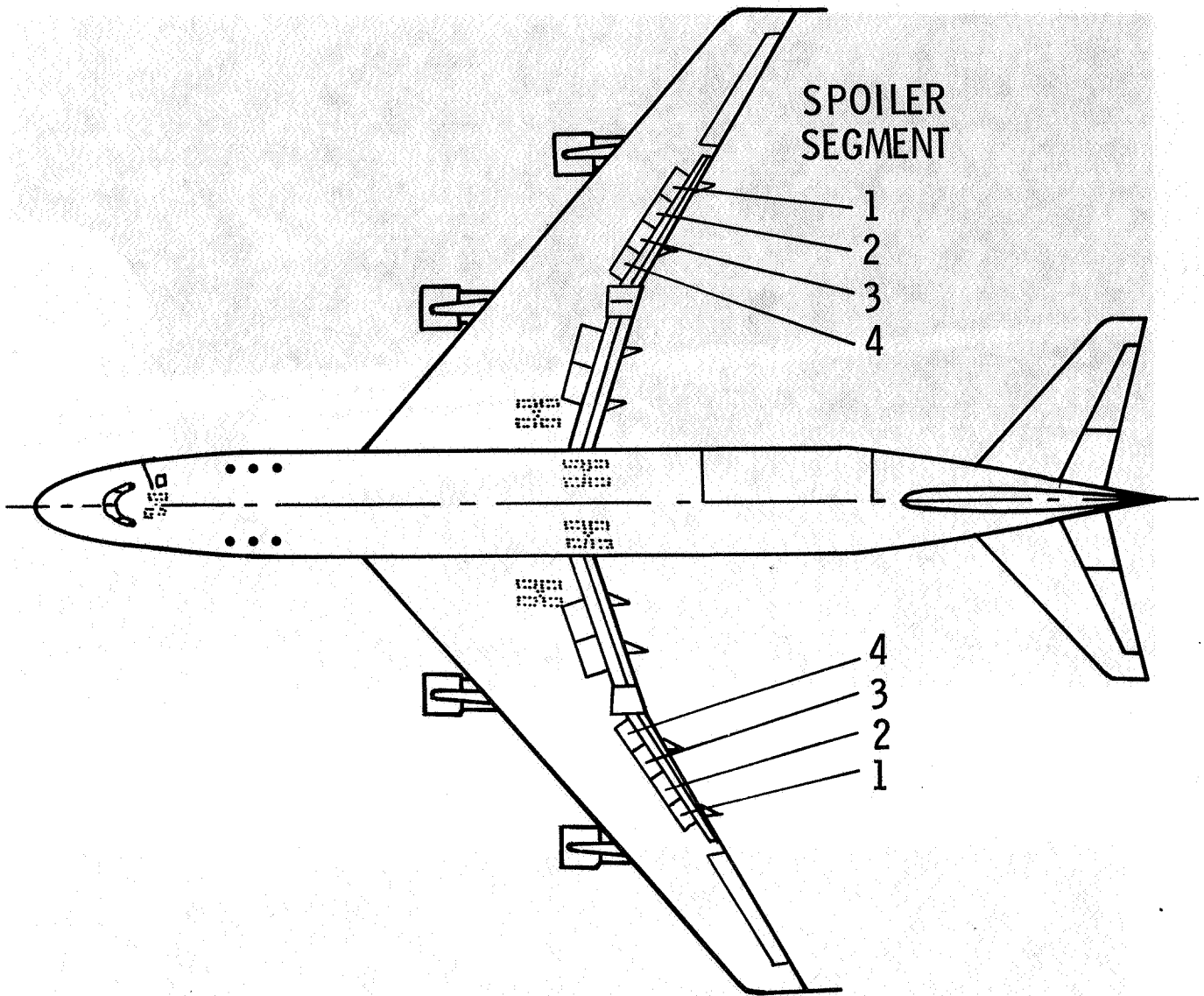
Figure 16.--Flight spoilers on the B-747 model.
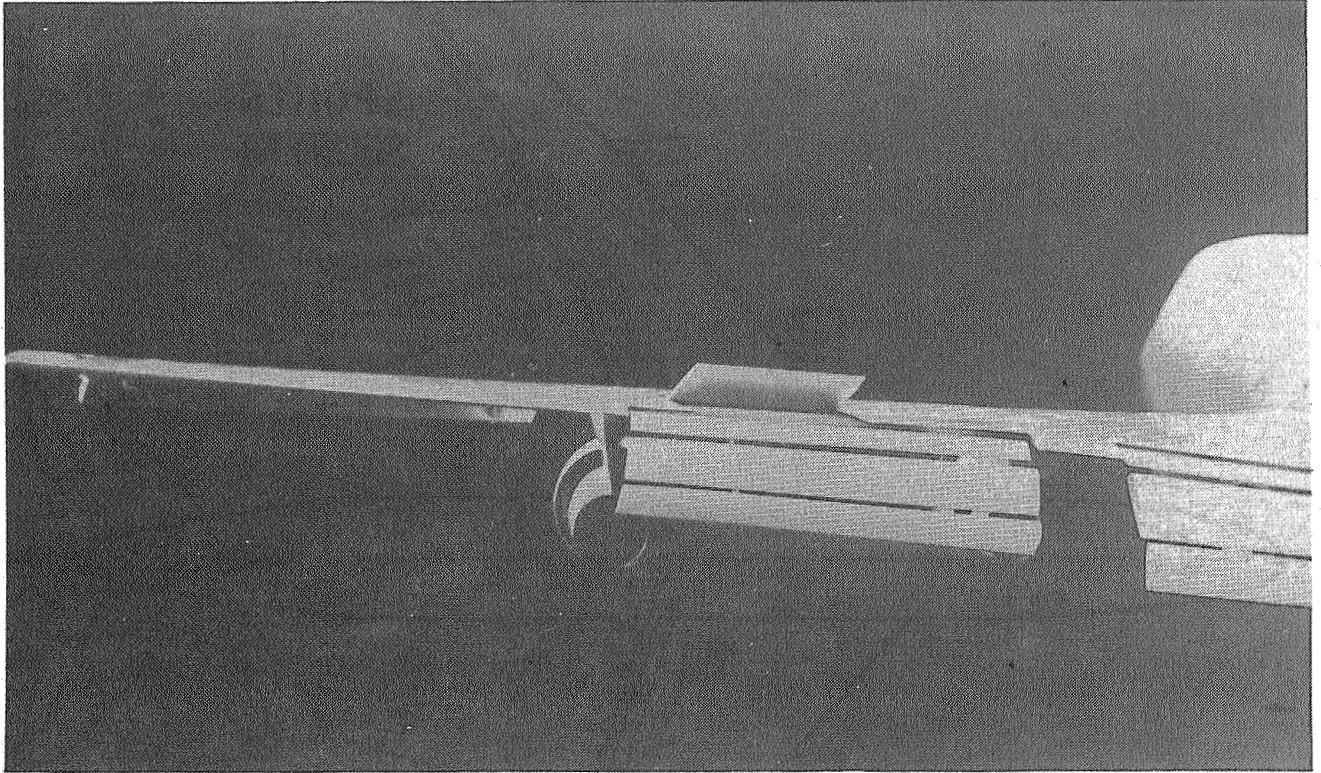
Figure 17.--Flight spoilers **1** and 2 on transport model.
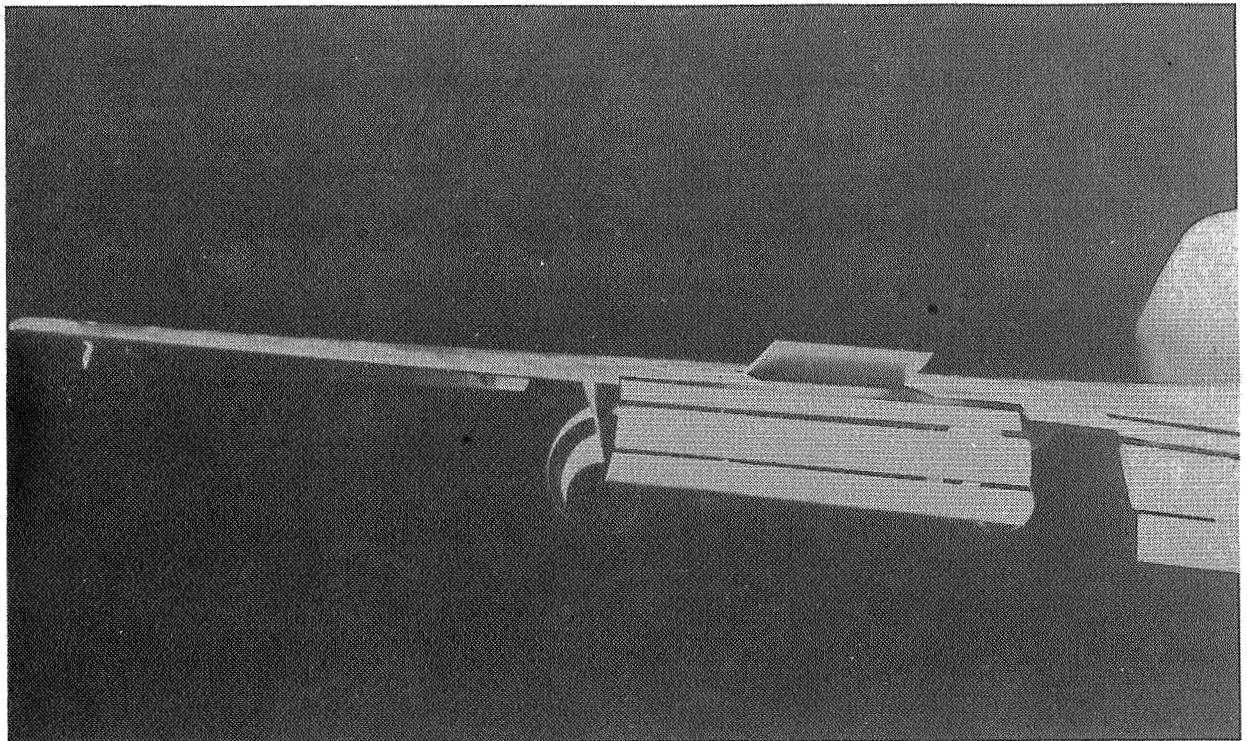


Figure 18.--Flight spoilers 2 and **3** on transport model.
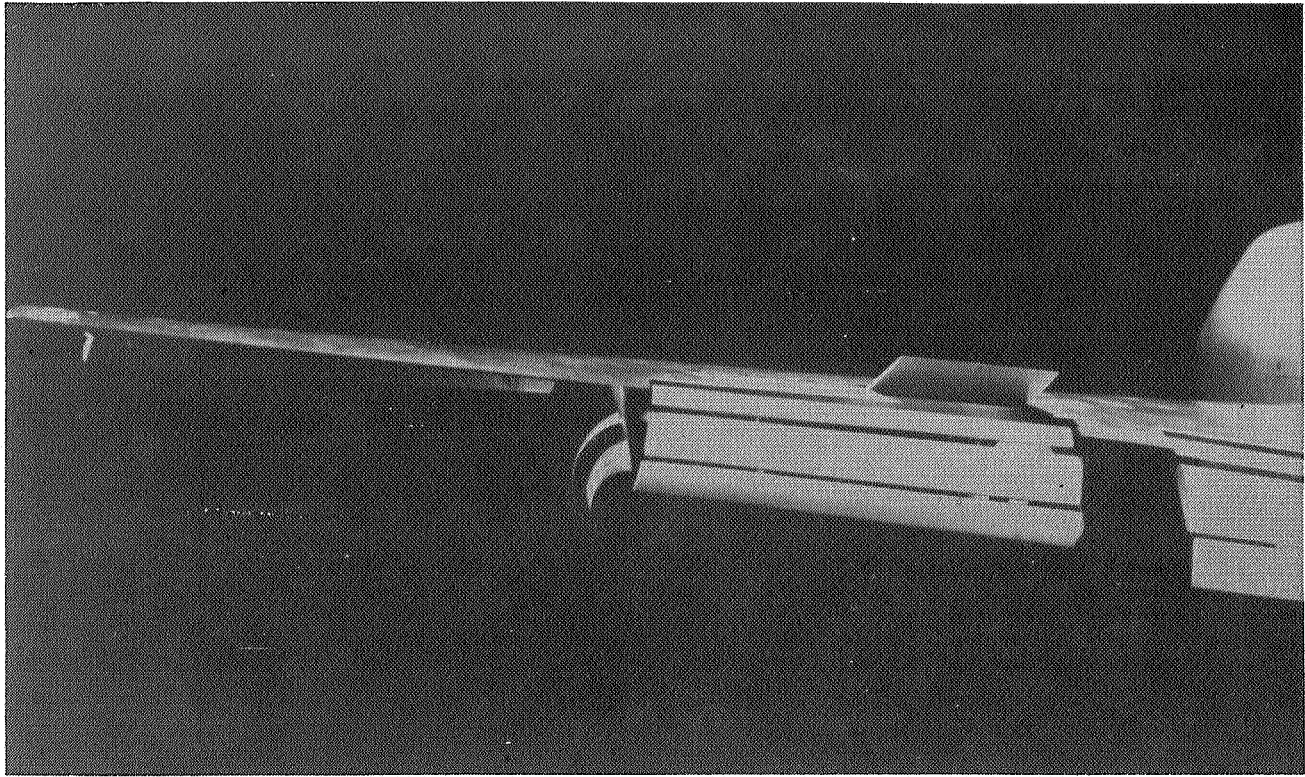
Figure 19.--Flight spoilers 3 and 4 on transport model.
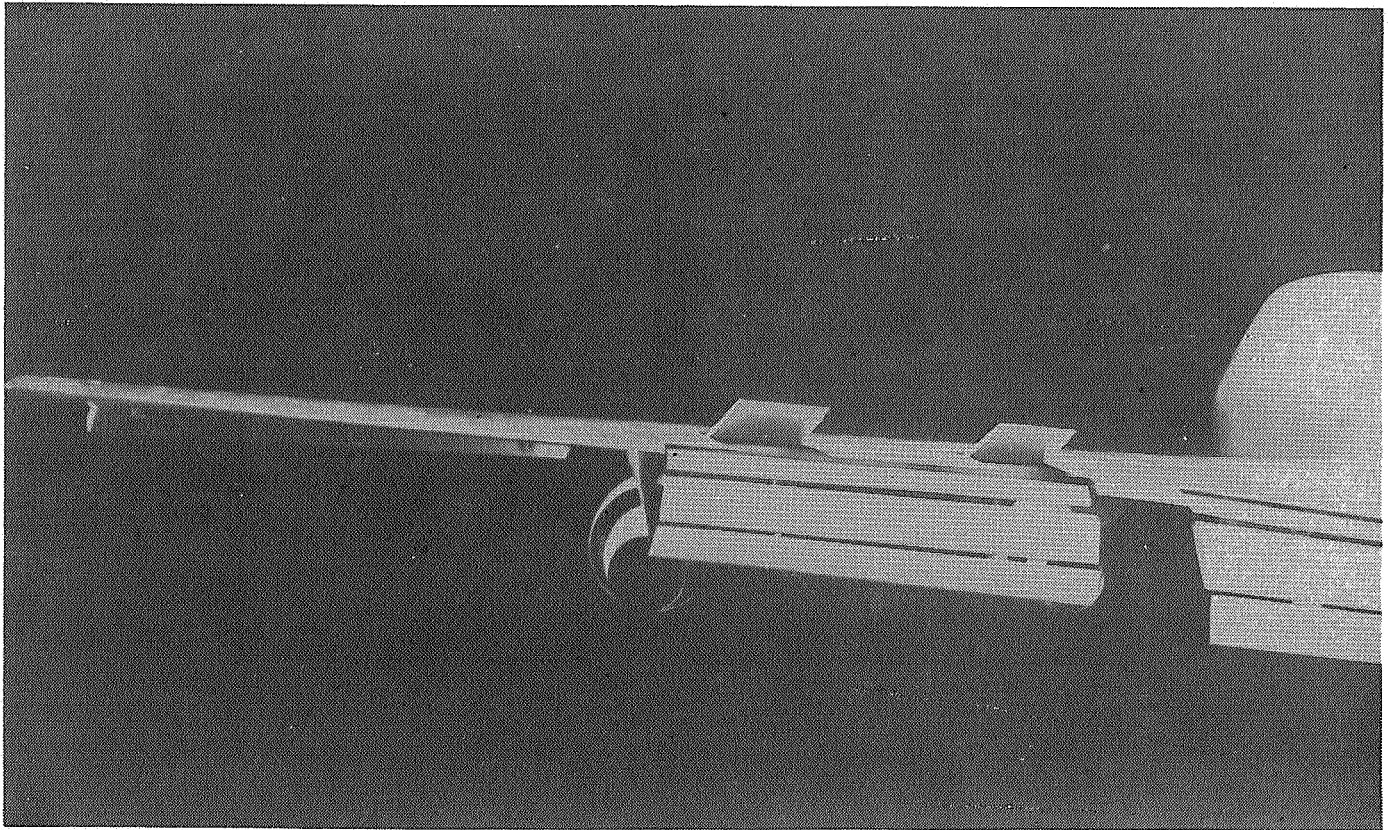


Figure 20.--Flight spoilers 1 and 4 on transport model.
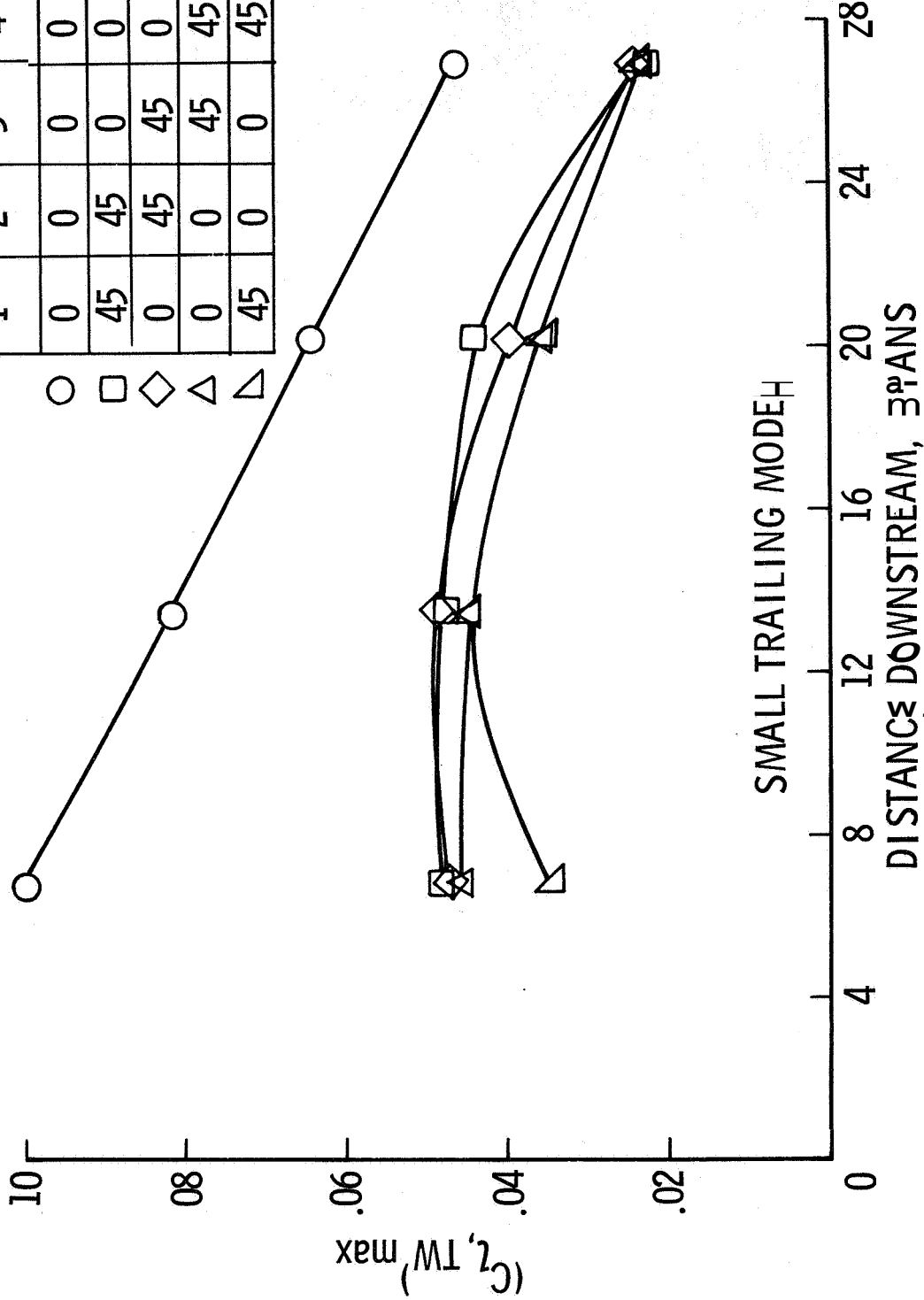
Figure 21.--Variation of trailing wing, rolling-moment coefficient with distance downstream from transport model. Flight spoilers; $C_{L,trim} = 1.2$
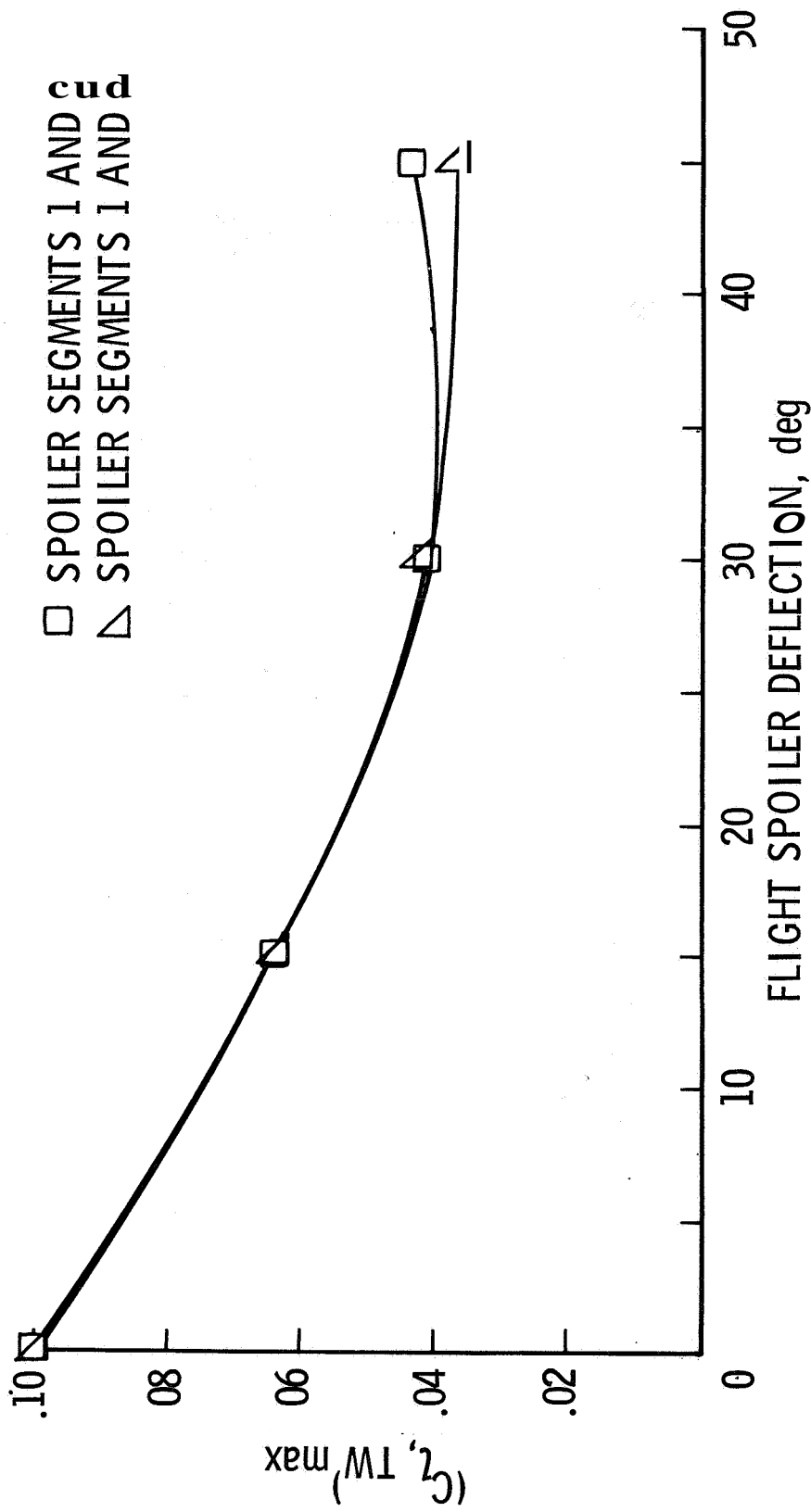
Figure 22.--Variation of trailing wing, rolling-moment coefficient with spoiler deflection. Flight spoilers; $C_{L,trim} = 1.2$; $6.7$ spans downstream.

Figure 23.--Variation of trailing wing, rolling-moment coefficient with distance downstream from transport model. $C_{L,trim} = 1.2$,
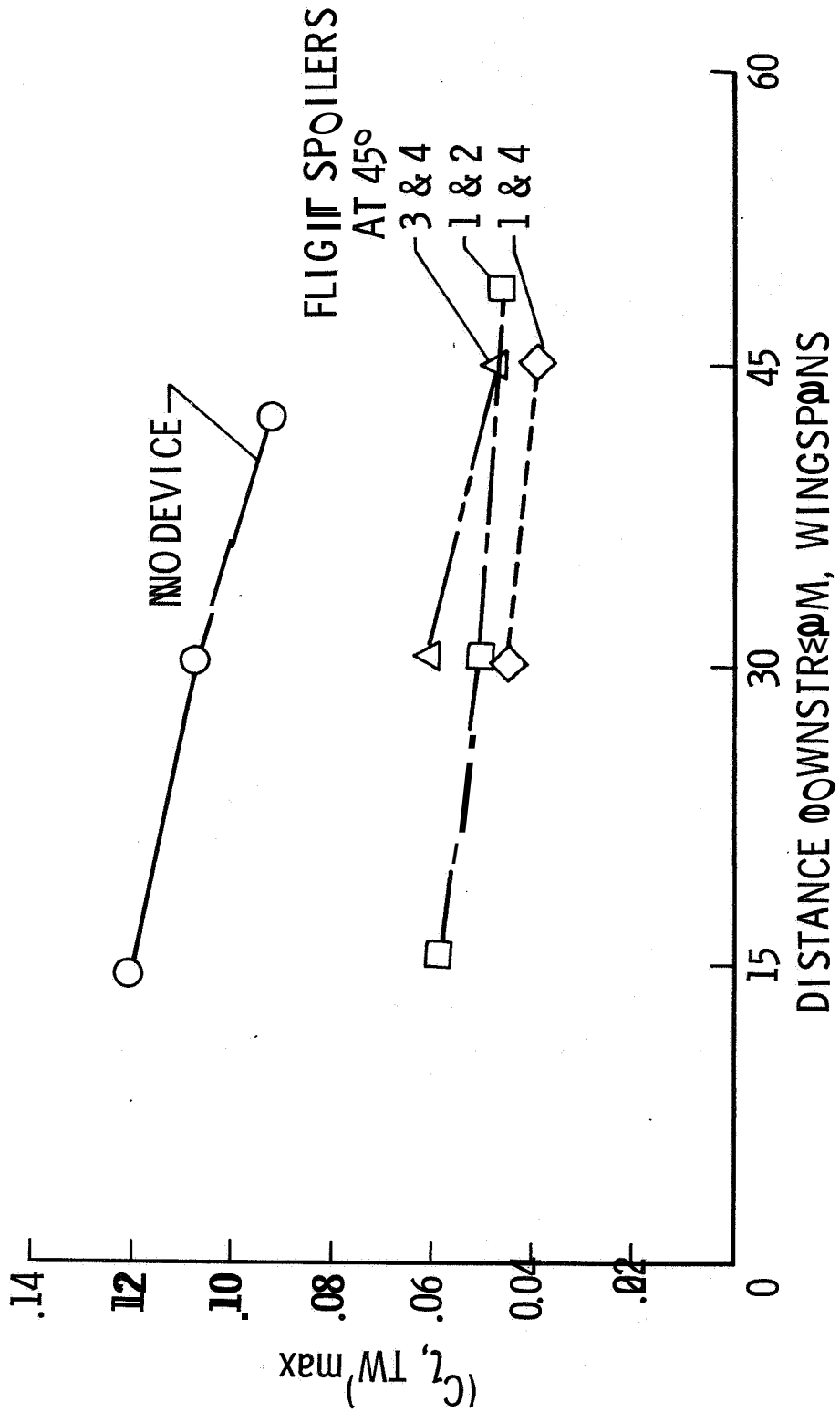
Figure 24.--Transport model flight spoiler, water towing tank, small trailing model. $C_L = 1.2$.
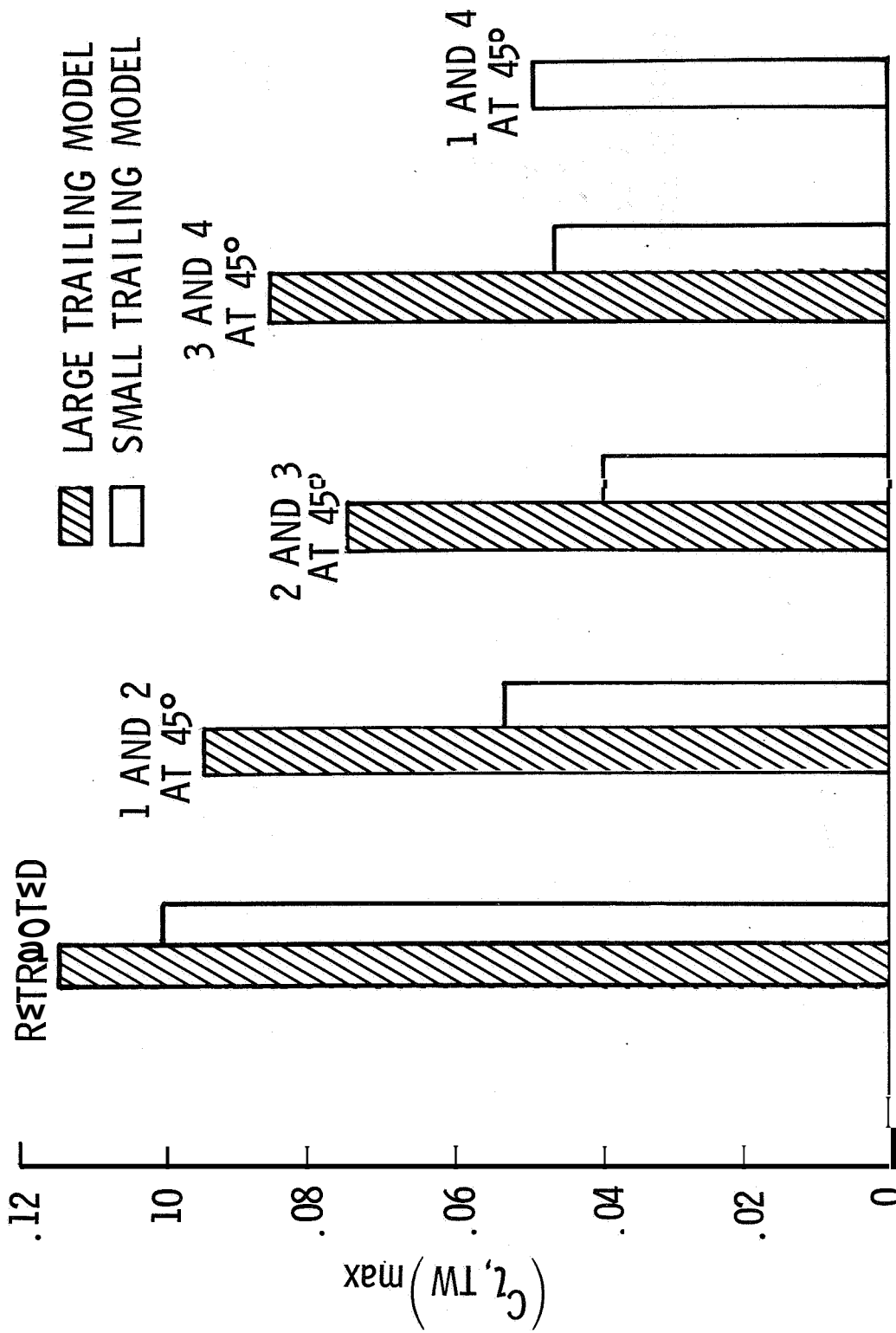
Figure 25.—Transport model flight spoilers, Langley Vortex Research Facility.

$C_L = 1.45$; 27 spans downstream.

# VORTEX ATTENUATION FLIGHT EXPERIMENTS

Marvin R. Barber, Earl C. Hastings, Jr.,[*]
Robert A. Champine,[*] and Joseph J. Tymczyszyn[†]

Dryden Flight Research Center

## SUMMARY

Flight tests evaluating the effects of altered span loading, turbulence ingestion, combinations of mass and turbulence ingestion, and combinations of altered span loading and turbulence ingestion on trailed wake vortex attenuation were conducted in several NASA flight test programs. Span loadings were altered in flight by varying the deflections of the inboard and outboard flaps on a B–747 aircraft. Turbulence ingestion was achieved in flight by mounting splines on a C–54G aircraft. Mass and turbulence ingestion was achieved in flight by varying the thrust on the B–747 aircraft. Combinations of altered span loading and turbulence ingestion were achieved in flight by installing a spoiler on a CV–990 aircraft and by deflecting the existing spoilers on a B–747 aircraft.

The characteristics of the attenuated and unattenuated vortexes were determined by probing them with smaller aircraft. Acceptable separation distances for encounters with the attenuated and unattenuated vortexes are presented.

## INTRODUCTION

Flight tests evaluating the effects of altered span loading, turbulence ingestion, combinations of mass and turbulence ingestion, and combinations of altered span loading and turbulence ingestion on trailed wake vortex attenuation were conducted

---

[*]Langley Research Center.
[†]Federal Aviation Administration, Western Region.

in several **NASA** flight test programs.  The programs were initiated .because ground facility (wind tunnel and water tank) measurements indicated that certain configuration changes offered potential for vortex attenuation, with a resultant increase in safety and airport capacity.

Table **1** summarizes the vortex attenuation flight experiments.  The table also lists the aircraft involved in each experiment and gives some idea of the magnitude and timing of the programs.

Span loadings were altered in flight by varying the deflections of the inboard and outboard flaps on a Boeing B-747 aircraft.  Figure **1**(a) shows the B-747 airplane'flying with a conventional or **30/ 30** landing flap configuration (i .e. , inboard flap deflected 30° and outboard flap deflected 30°).  Figure 1(b) shows the airplane flying with the 30/1 flap configuration (inboard flap deflected 30°, outboard flap deflected 1°) . The following combinations of inboard/outboard flap deflections were tested:  30/30, 30/20, 30/10, 30/5, 30/1, and **5/30.**  The minimum outboard flap deflection was 1° so that the leading-edge flaps could be kept extended (the leading-edge flap deflections are programed according to trailing-edge flap deflections) . Various span loads were tested because of the attenuation potential forecast by the wind-tunnel tests reported in reference **1.**  The results of the flight tests of span loading alterations are reported in references 2 and **3.**

Turbulence was created and ingested into the vortexes in flight by mounting splines on a McDonnell Douglas C-54G aircraft and by varying the thrust of the engines on the B-747 aircraft.  Figure 2 shows the splines on the aircraft in flight, and figure **3** shows details of the splines.  These tests were preceded by wind-tunnel tests which are reported in conjunction with the flight tests in reference 4.

The inboard and outboard engines of the B-747 airplane are alined directly in front of the outboard edges of the inboard and outboard flaps, respectively. Figure **1** illustrates the engine/flap alinement . This alinement naturally caused curiosity about the effects of changes in engine thrust on the wake vortexes of the B-747 airplane in the normal landing configuration and in attenuated configurations. Therefore, the effects of engine thrust were evaluated on numerous occasions throughout the B-747 vortex attenuation flight tests.

The combined effects of altered span loading and turbulence ingestion were tested in flight by installing a fixed spoiler on the wingtip of a Convair CV-990 aircraft and by deflecting the existing spoilers on the B-747 airplane.  Figures 4(a)

and 4(b) show the CV-990 wingtip spoiler from a distance and close up. Wind-tunnel tests of this configuration were conducted and reported in conjunction with flight tests in reference 5.

Figure 5 is a sketch of the B-747 spoiler/speed brakes, referred to herein as spoilers. The effects of various spoiler segment combinations on vortex attenuation were tested thoroughly in the Langley V/STOL wind tunnel (ref. 6). These results were sufficiently promising to warrant flight test verification. Therefore, the effects of deflecting these spoilers on vortex attenuation are being evaluated in flight tests.

All the B-747 flight tests were conducted with the NASA B-747 space shuttle carrier aircraft, and because the airplane was not always available, some of the tests could not be made before this writing. The scheduling problem also prevented many of the quantitative data from being processed in time for this paper. This .paper therefore summarizes the qualitative assessment of the vortex attenuation pro-vided by some of the B-747 configurations,

## SYMBOLS

| | |
|---|---|
| $\lvert \dot{p} \rvert_{(measured)}$ | roll axis angular acceleration measured during vortex encounter |
| $\lvert \dot{p} \rvert_{\delta_{a_{max}}}$ | maximum roll axis angular acceleration that can be generated by ailerons |
| $C_{l_v}$ | vortex-induced rolling-moment coefficient |
| $C_{l_{\delta_a}} \delta_{a_{max}}$ | maximum rolling-moment coefficient that can be generated by ailerons |
| $\bar{c}$ | mean aerodynamic chord |

## TEST TECHNIQUES

The technique of vortex attenuation flight testing has been described in detail in the paper by Jacobsen and Barber earlier in this conference. However, a review of the techniques from the pilot's standpoint is believed to be appropriate.

The most significant test in a qualitative evaluation of the vortex hazard to a trailing aircraft consists of probing the vortex as it would most likely be encountered in a real landing approach situation. To simulate this situation, the vortexes are probed with as small a penetration angle as possible. This type of probe is referred to as a parallel probe (i.e. , the probing aircraft's flight path is approximately parallel to the vortex). The probe aircraft may enter the vortex wake from below, from above, or from either side. The probes result in pitch, roll, and yaw upsets that are representative of those that would be experienced by trailing aircraft in real situations. Qualitative assessments of these upsets enable the probe pilot to select separation distances (or times) behind a generating aircraft that result in acceptable levels of vortex-induced hazard.

The only limitation on a simulation of real vortex encounter situations is test altitude. Statistically it is known that most accidents attributed to trailed wake vortexes occur on landing approach at relatively low altitudes. Unfortunately, flight test experience to date has not resulted in sufficient confidence in either predictive techniques or the repeatability of flight test results to permit testing at altitudes less than those required for comfortable recovery from inverted flight. In practice, this means the tests must be conducted no lower than approximately 1500 meters (5000 feet) above ground level.

Therefore, the probe pilot is evaluating an upset hazard at high altitudes above ground level and attempting to extrapolate his evaluation to low altitudes. This shortcoming has become more and more significant as the attenuated vortex configurations have enabled vortex encounters at closer separation distances, thereby increasing the need to verify the acceptability of the configuration.

In the past, probe pilots have estimated minimum separation distances by determining the separation distance at which the vortex-induced upsets would cause them to decide to execute a missed approach if they were performing an IFR approach. As noted, these determinations were made during parallel probes made approximately 1500 meters (5000 feet) above ground level.

Figure 6 summarizes the data that were obtained from tests reported in references 7 to 10. The correlation of the data throughout the numerous test programs is relatively good and illustrates that the pilots' opinions obtained by using the previously discussed technique agree remarkably well with the minimum separation distances that were established by using the roll control criterion discussed by

372

Jacobsen and Barber. These data and the techniques for obtaining them were the baseline from which the vortex attenuation flight tests to be discussed herein were initiated. Experience gained in the vortex attenuation flight tests show some short-comings in these data and indicate areas where present techniques are inadequate.

## TEST RESULTS

### Altered Span Loading

Span loadings were altered in flight by varying the deflections of the inboard and outboard flaps on a B-747 aircraft as shown in figures 1(a) and 1(b). Seventeen flights were flown by the B-747 airplane to complete these tests, and the Cessna T-37B and Learjet-23 (LR-23) aircraft were utilized as the probe aircraft. Both parallel and cross-track probes were performed during this test series. Most of the tests were preceded by the wind-tunnel tests reported in reference 1, and were partially reported in references 2 and 3.

The results of these tests are summarized in figure 7, which presents the pilots' qualitative assessments of the alleviation provided by retracting the outboard flap on the B-747 airplane. The landing-gear-up data show that a significant amount of attenuation was provided by retracting the outboard flap. These data agree with wind-tunnel data obtained from a model that did not have a landing gear. When the landing gear on the airplane was extended, a significant amount of the attenuation was lost.

An assessment of the correlation between the pilots' qualitative separation requirements and the requirements that would be dictated by the roll control criterion can be obtained by comparing figure 7 with figures 8(a) and 8(b). In general, these data show that the quantitative and qualitative requirements are in agreement.

During these tests it was also noted that engine thrust and aircraft sideslip had a significant effect on the attenuation provided by the altered span loadings. These effects are illustrated in figures 9 and **10.**

The differences in the B-747 trailed vortex system with and without the outboard flap extended can be evaluated by reviewing the photographs in figures 11(a) to 11(j) and figures 12(a) to 12(g). A comparison of figure 11(a) and figure 12(a) indicates that with the outboard flap extended the dominant vortex is the vortex shed from

the outboard edge of the outboard flap.  With the outboard flap retracted, the dominant vortex is that shed from the outboard edge of the inboard flap.  In both cases, the wingtip vortex interacts with the dominant vortex.  The effects of configuration on vortex life can also be compared.  The unattenuated vortex persists for at least 45 seconds, when the cameraman ceased taking pictures.  The attenuated vortex disappears completely in 30 seconds,  After these tests, the vortex marking system was modified to include smokers at the inboard edge of the inboard flap to try to determine why the landing gear reduced the attenuation.  The photographs in figures 13(a) and 13(b) show that the landing gear diffuses a powerful vortex at the inboard edge of the inboard flap, significantly reducing the attenuation provided by the 30/1 flap configuration.  Though not available in the photographic record at this time, visual observations of the inboard vortex showed that it intermingled with the vortex off the outboard edge of the inboard flap when it was not diffused by the landing gear.

Although interesting from a research standpoint, the vortex attenuation afforded by the 30/1 flap configuration was disregarded for obvious operational reasons when the degrading effects of the landing gear were discovered.  It should be noted that this configuration also imposed a center-of-gravity limitation on the B–747 airplane.

A flight evaluation of the vortexes 4 nautical miles to 6 nautical miles behind the B–747 airplane in the 5/30 flap configuration was short and conclusive.  Whereas the 30/1 flap configuration produced marked attenuation, the 5/30 vortex resulted in T–37B encounters that were even more violent than those caused by the conventional 30/30 landing configuration at 6 nautical miles.  One encounter at 6 nautical miles produced a violent double snap roll which far exceeded the capability of the roll rate data acquisition system and also caused an engine flameout.  These tests showed the correct approach to vortex attenuation to be increasing the inboard span loading,

## Turbulence Ingestion

The ingestion of turbulence into the vortexes in flight was accomplished by mounting splines on the wingtips of a C–546 aircraft (figs. 2 and 3).  The Piper Cherokee (PA–28) airplane was used as the probe aircraft for these tests.  The vortex attenuation results of these tests are shown in figure 14, which compares the probe aircraft's roll accelerations in the attenuated and unattenuated vortexes. The data show that the PA–28 airplane has insufficient roll control power to overcome

the vortexes of the basic **C-54G** airplane at a separation distance of approximately **4** nautical miles, and that maximum roll control power is never required to oppose the vortex attenuated by splines. The data generally correlate with the pilots' opinions of the attenuation, which was that roll control became insufficient approximately **2.5** nautical miles behind the unattenuated **C-54G** airplane but that it was sufficient throughout the entire range of separations tested for the attenuated configuration. The unattenuated data represent the **C-54G** airplane in the clean configuration and therefore are not directly comparable to the data presented in figure 6, which are for the normal landing configuration.

The effects of the splines on the performance, handling qualities, and noise of the **C-54G** airplane were also measured. It was concluded that although the splines significantly reduced the rate of climb of the C-54G airplane, the airplane's four-engine performance was acceptable for this test program. (It should be noted that the splines were not retractable, as they would be for any configuration seriously proposed for operation.) The splines caused no noticeable changes in the handling qualities of the **C-54G** airplane. Finally, the maximum overall sound pressure level of the **C-54G** airplane during landing approach with splines on was approximately **4** decibels higher than with splines off.

The vortex attenuation potential of the splines should not be too easily discounted because of what may seem to be rather complex operational problems. An unpublished study concerning the feasibility of producing retractable splines concluded that the concept is practical.

## Combinations of Mass and Turbulence Ingestion

Flight tests were conducted with the **B-747** airplane to evaluate the effects of engine thrust on vortex attenuation. In general, most of the **B-747** testing has been conducted with thrust for level flight at altitudes of approximately **3000** meters (**10,000** feet), because a level flightpath makes it easier for the probe pilots to find and encounter the vortexes. However, considerable testing has been performed for all the attenuated and unattenuated configurations wherein the thrust was reduced from that required for level flight to that required for a -3° flightpath angle and further to flight idle (approximately -6° flightpath angle, depending on spoiler, flap, and gear configuration). To date, a detailed comparison of the pilots' qualitative assessments of the effects of engine thrust with quantitative data has not been

completed. In general, however, it appears that reducing the thrust from that required for level flight to flight idle adds approximately 2 nautical miles to the required separation distance. This generalization is true for both the 30/30 and 30/1 flap configurations (fig. 9).

Tests wherein the inboard and outboard engine thrust levels have been varied alternately have been conducted, but the data are not yet available. Tests to determine the effects of engine thrust on the attenuation provided by deflecting various spoiler segments are yet to be completed.

### Combinations of Span Loading Alteration and Turbulence Ingestion

Wind-tunnel tests made as early as 1969 indicated that the character of the trailing vortex system could be changed significantly by adding a spoiler to the wing in the area of the vortex formation (ref. 5). Flight tests of a spoiler on the wingtip of a CV-990 aircraft (fig. 4) were conducted in 1970 as a result of these wind-tunnel tests. Unfortunately, at that time in-flight vortex marking systems were not available, and therefore the tests were rather inconclusive.

More recently, however, wind-tunnel tests have shown that extending various combinations of the B-747 spoilers is effective in attenuating its vortexes (ref. 6). Figure 5 shows that the four outboard spoiler panels on the B-747 airplane are in the vicinity of the outboard flap, where the dominant vortex is shed (fig. 11). Therefore, it is not surprising that extending these spoilers affects the resulting vortex system.

These tests were paced by wind-tunnel tests (ref. 6). In flight, the spoilers were deflected in the following combinations:

| Spoiler panel | | | | | | | | | | | |
|---|---|---|---|---|---|---|---|---|---|---|---|
| 1 | 2 | 3 | 4 | 5 | 6 | 7 | 8 | 9 | 10 | 11 | 12 |
| Spoiler panel deflection, deg | | | | | | | | | | | |
| -- | -- | 37 | 37 | -- | -- | -- | -- | 37 | 37 | -- | -- |
| 41 | 41 | -- | -- | -- | -- | -- | -- | -- | -- | 41 | 41 |
| 25 | 25 | -- | -- | -- | -- | -- | -- | -- | -- | 25 | 25 |
| 45 | -- | -- | 45 | -- | -- | -- | -- | 45 | -- | -- | 45 |
| -- | 45 | 45 | -- | -- | -- | -- | -- | -- | 45 | 45 | -- |

The deflection angles were chosen as a result of the flight crew's concern about the level of buffet induced by the spoilers and limitations of the control system on the production B-747 airplane. The 37° deflection for spoilers 3, 4, 9, and 10 and the 41° deflection for spoilers 1, 2, 11, and 12 were used because of the crew's concern about the safety of accepting a higher level of buffet. The 25° limit for the deflection of spoilers 1, 2, 11, and 12 was established because it caused the highest buffet level that the flight crew felt passengers would tolerate. The 45° deflections for the spoiler combinations (1, 4, 9, 12) and (2, 3, 10, 11) were limited primarily by the control system. It is interesting to note that the flight crew felt that the buffet level with a spoiler deflection of 45° was excessive for spoiler combination (2, 3, 10, 11), but acceptable for the spoiler combination (1, 4, 9, 12).

Figure 15 summarizes the pilots' qualitative separation requirements from the spoiler flight tests. The data illustrate that with spoilers 1, 2, 11, and 12 deflected 41°, significantly more attenuation is provided than with any other configuration. In fact, it would appear from these data that the 41° deflection of spoilers 1, 2, 11, and 12 could be proposed as an operational configuration that would allow light aircraft to be spaced as close as 3 nautical miles behind heavy aircraft. Therefore, a series of tests was developed to investigate the operational feasibility of using this configuration. This investigation was to include actual landings of the B-747 airplane with the spoilers extended and probes of its vortex at landing flare altitudes by the T-37B airplane.

Landing the B-747 airplane with the spoilers extended was accomplished in a relatively straightforward manner, and the pilots indicated that the spoilers did not significantly detract from the airplane's landing performance.

The proposed low altitude probes with the T-37B airplane required a reevaluation of the criteria on which probing was based at altitude. As discussed in TEST TECHNIQUES, the probe pilots used as a criterion the level of upsets which would force them to abandon an approach either on instruments or after breaking out at the bottom of an overcast. Among other factors, a bank angle limit of approximately 30° for the T-37B airplane at altitude was considered as a baseline (with lower limits for aircraft with larger wingspans). The adequacy of this partial criterion was questioned, however, when actual landings were proposed; lower control power, proximity to stalls or spins at low altitude, and the thrust required

to overcome the downwash of the generating airplane became additional items of concern.

Intentional probes of the downwash area between the B-747 vortexes were made with the B-747 airplane with spoilers 1, 2, 11, and 12 deflected. The T-37B airplane probed this area to less than 2 nautical miles and found only light to moderate turbulence with an incremental downwash of approximately 150 meters per minute (500 feet per minute). The problem of adequate climb performance at low speeds in the landing configuration had to be considered, even when roll control power was adequate to overcome the vortex-induced roll. An additional unknown was the variation of vortex strength and life as a function of altitude and ground effect. Tests using ground-based sensors were conducted to evaluate the normal and attenuated vortex characteristics, but the results are not yet available.

Another question pertinent to the problem of separation distance is the effectiveness of attenuating devices for following aircraft that have considerably larger wingspans than the T-37B and LR-23 airplanes. Wind-tunnel and water tank tests on a McDonnell Douglas DC-9 scale model indicate a definite reduction in induced roll, but not as large a reduction as models of smaller wingspan experienced. This effect is due to the better fit of an airplane with a larger wingspan in the larger attenuated vortex.

All T-37B probe pilots agree that the attenuated vortex is much larger in diameter, is less well defined, and has lower tangential velocities than the usual, well-formed vortex tube. A DC-9 airplane is being instrumented and is to be test flown to determine the degree of effectiveness of vortex attenuation on an airplane with a significantly larger wingspan than the T-37B and LR-23 aircraft.

A comparison of the photographs presented in figures 16(a) and 16(b) with those shown in figures 17(a) and 17(b) will provide the reader with an illustration of the differences in the formation of the B-747 vortex systems with and without spoilers 1, 2, 11, and 12 extended.

## CONCLUDING REMARKS

Flight tests made to evaluate the effects of altered span loading, turbulence ingestion, combinations of mass and turbulence ingestion, and combinations of altered span loading and turbulence ingestion on trailed wake vortex attenuation

showed aerodynamic attenuation to be possible and probably operationally practical. This conclusion is based on the fact that three of the methods tried provided significant levels of wake vortex attenuation.

## REFERENCES

1. Corsiglia, Victor R.; Rossow, Vernon J.; and Ciffone, Donald L.: Experimental Study of the Effect of Span Loading on Aircraft Wakes. NASA TM X-62431, 1975.

2. Tymczyszyn, Joseph J.; and Barber, Marvin R.: Recent Wake Turbulence Flight Test Programs. SETP 1974 Report to the Aerospace Profession — Eighteenth Symposium Proceedings. Soc. Exp. Test Pilots, Sept. 1974, pp. 52-68.

3. Smith, Harriet J.: A Flight Test Investigation of the Rolling Moments Induced on a T-37B Airplane in the Wake of a B-747 Airplane. NASA TM X-56031, 1975.

4. Hastings, Earl C.; Patterson, J. C., Jr.; Shanks, Robert E.; Champine, Robert A.; Copeland, W. Latham; and Young, Douglas C.: Development and Flight Tests of Vortex-Attenuating Splines. NASA TM X-8083, 1975.

5. Corsiglia, Victor R.; Jacobsen, Robert A.; and Chigier, Norman: An Experimental Investigation of Trailing Vortices Behind a Wing With a Vortex Dissipator. Aircraft Wake Turbulence and Its Detection, John H. Olsen, Arnold Goldburg, and Milton Rogers, eds., Plenum Press, 1971, pp. 229-242.

6. Croom, Delwin R.: Low-Speed Wind-Tunnel Investigation of Various Segments of Flight Spoilers as Trailing-Vortex-Alleviation Devices on a Transport Aircraft Model. NASA TN D-8162, 1976.

7. Andrews, William H.; Robinson, Glenn H.; and Larson, Richard R.: Exploratory Flight Investigation of Aircraft Response to the Wing Vortex Wake Generated by Jet Transport Aircraft. NASA TN D-6655, 1972.

8. Robinson, Glenn H.; and Larson, Richard R.: A Flight Evaluation of Methods for Predicting Vortex Wake Effects on Trailing Aircraft. NASA TN D-6904, 1972.

9. Andrews, William H.; Robinson, Glenn H.; and Larsdn, Richard R.: Aircraft
Response to the Wing Trailing Vortices Generated by Large Jet Transports.
NASA Aircraft Safety and Operating Problems—Volume 1. NASA SP–270, 1971,
pp. 115-126.

10. Barber, M. R.; Kurkowski, R. L.; Garodz, L. J.; Robinson, G. H.;
Smith, H. J.; Jacobsen, R. A.; Stinnett, G. W.; McMurtry, T. C.;
Tymczyszyn, J. J.; Devereaux, R. L.; and Bolster, A. J.: Flight Test
Investigation of the Vortex Wake Characteristics Behind a Boeing 727 During
Two–Segment and Normal ILS Approaches. NASA TM X–62398, 1975,

TABLE 1.—VORTEX ATTENUATION FLIGHT EXPERIMENTS

| Method of attenuation | Means of attenuation | Vortex-generating aircraft | Vortex-probing aircraft | Number of test flights | Time period for test flights |
|---|---|---|---|---|---|
| Altered span loading | Altered inboard/outboard flap deflections | B-747 | Learjet-23 (LR-23) Cessna T-37B | ≈17 | 1974 |
| Turbulence ingestion | Splines | C-54G | Piper Cherokee (PA-28) | ≈20 | 1973 |
| Mass and turbulence ingestion | Altered inboard/outboard engine thrust levels | B-747 | LR-23 T-37B | ≈2 | 1974/1975 |
| Altered span loading and turbulence ingestion | Wingtip-mounted spoiler | CV-990 | LR-23 | ≈2 | 1969 |
| | Altered spoiler deflections | B-747 | LR-23 T-37B McDonnell Douglas DC-9 | ≈15 | 1975/1976 |

*(a)  30/30 flap configuration.*



*(b)  30/1 flap configuration.*

*Figure 1.  B-747 span Zoad test configurations.*
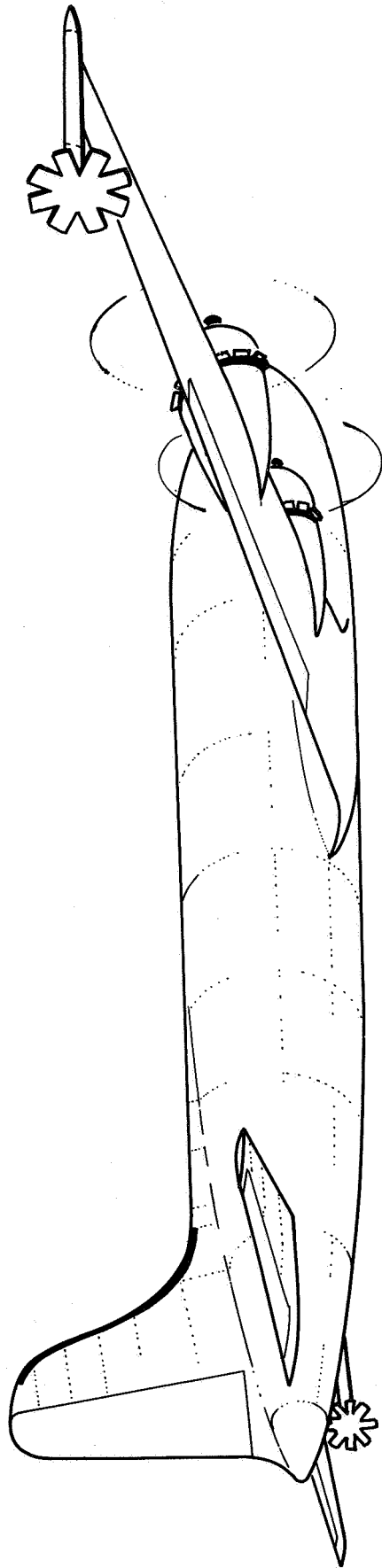
*Figure 2. C-54G aircraft with splines installed.*

383'
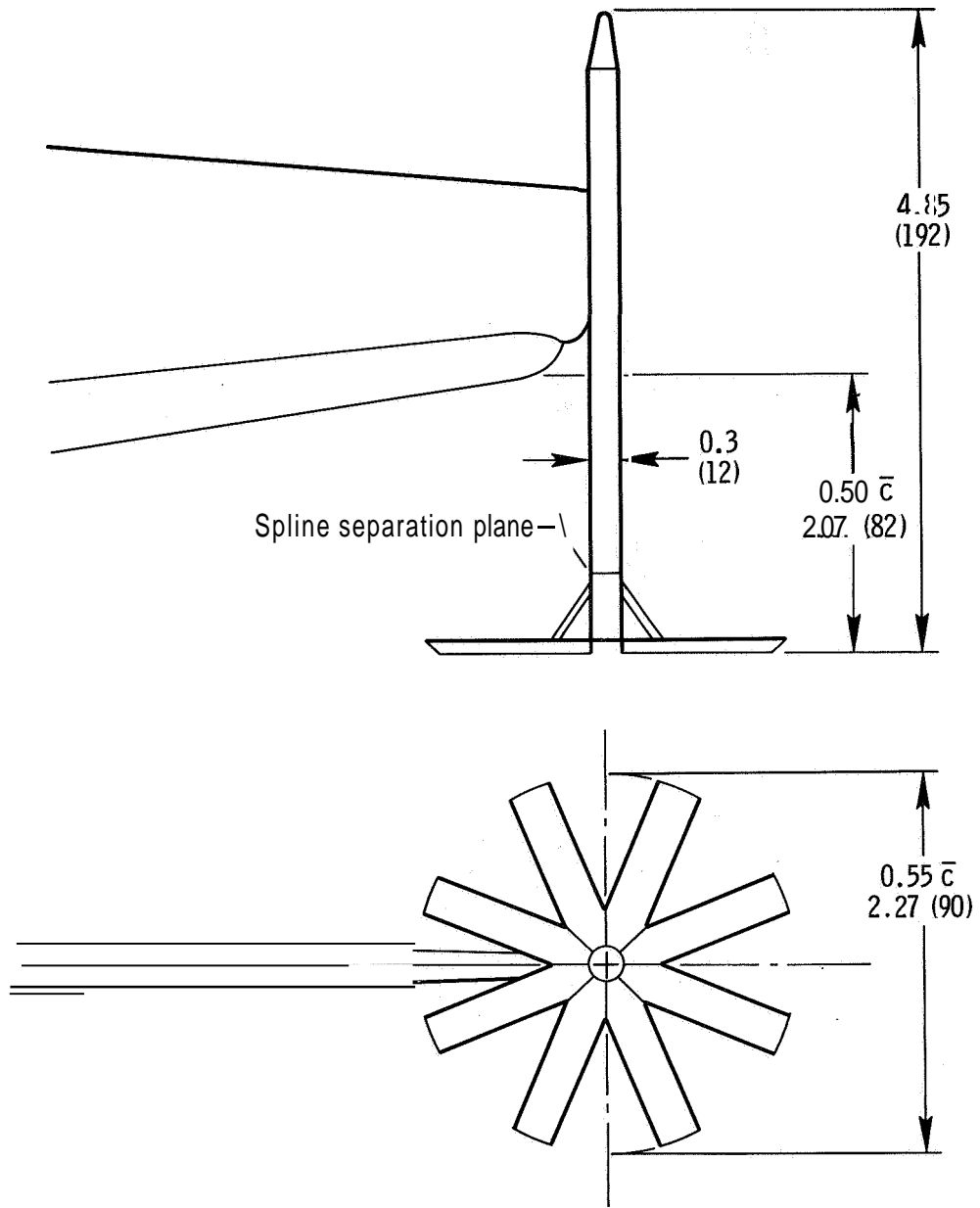
*Figure* **3.** *Diagram* of *spline arrangement. Dimensions in meters (inches).*
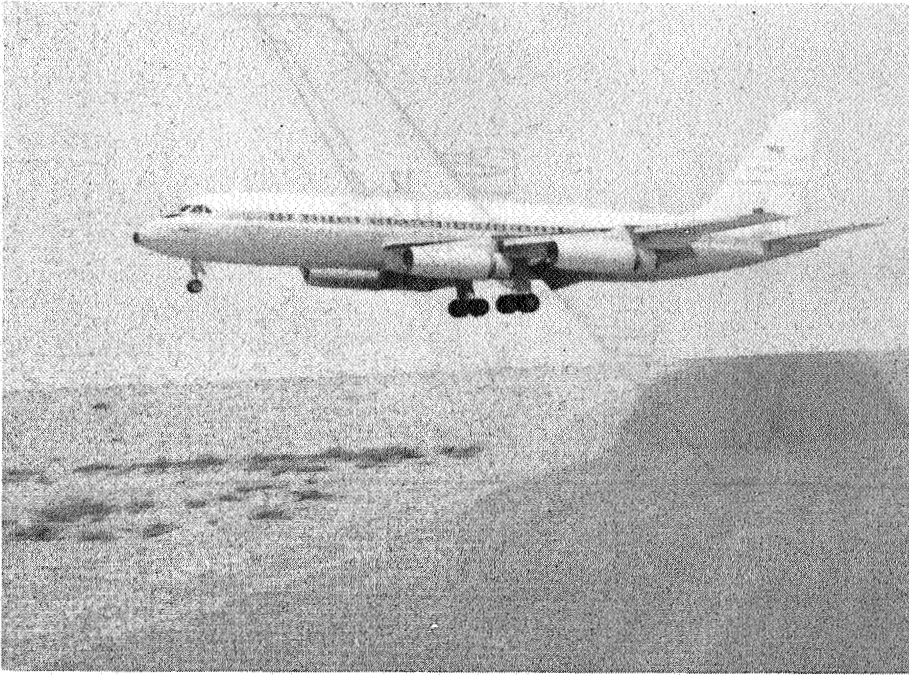
(a) *From a distance.*
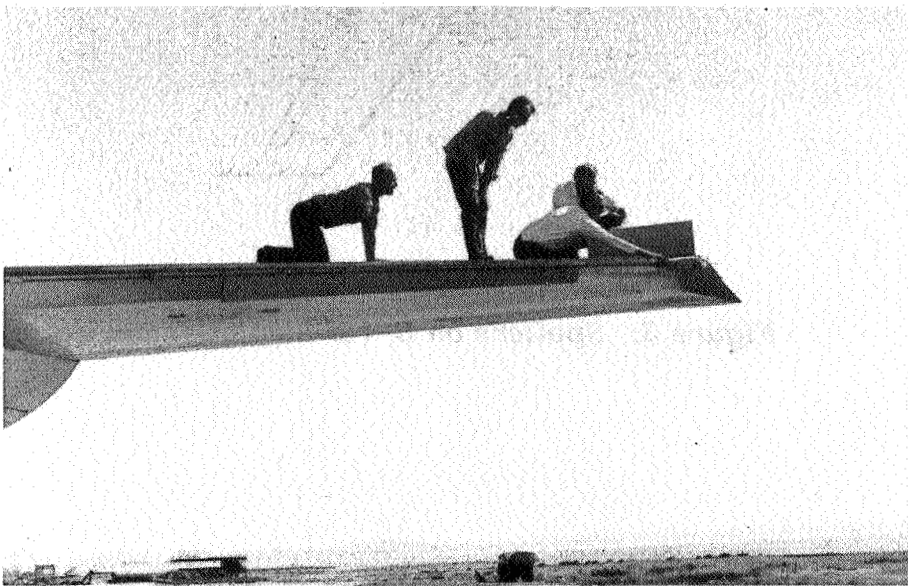


(b) *Close up.*

*Figure 4. CV-990 wingtip spoiler.*
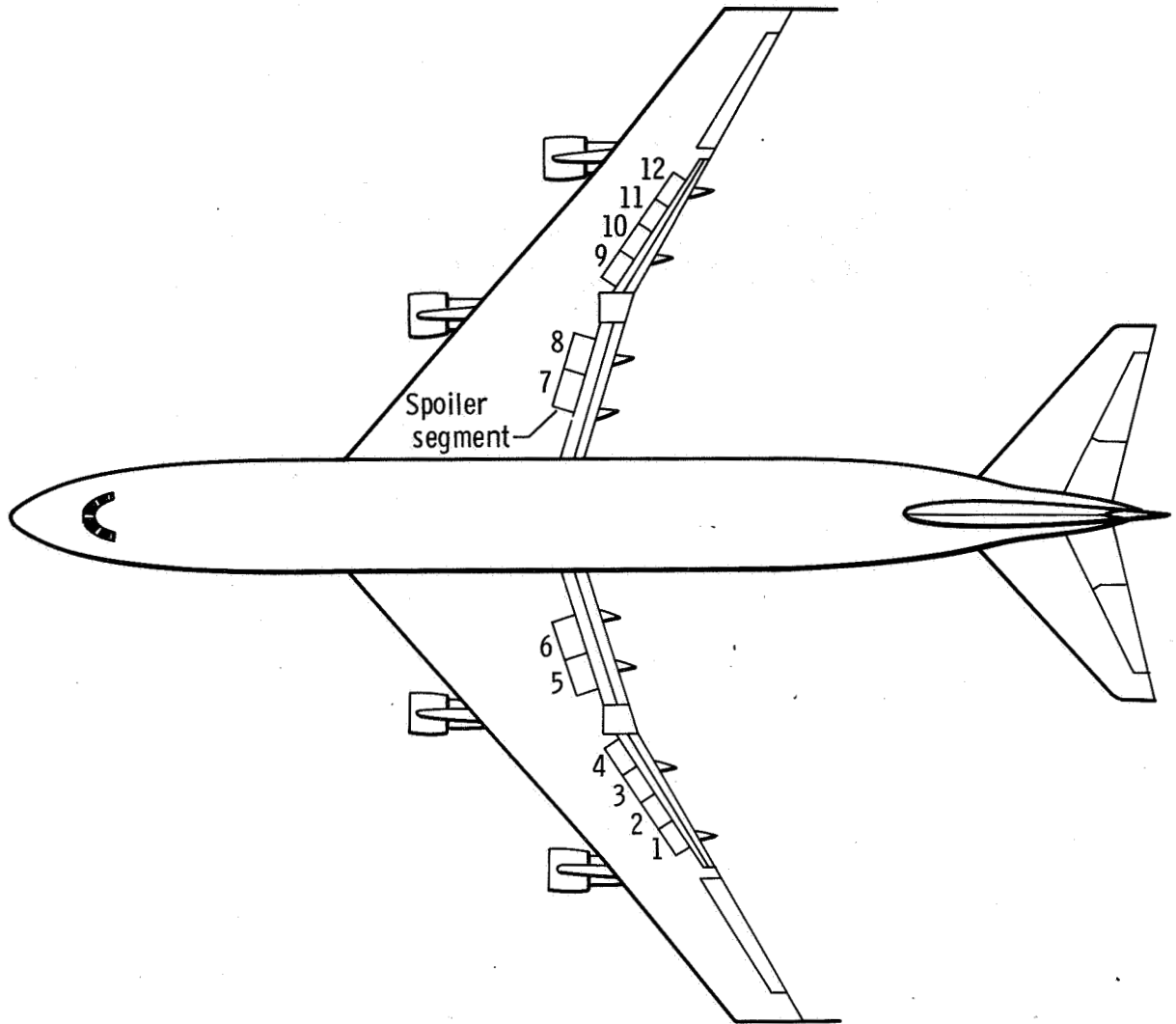
*Figure 5.  Spoilers on B-747 airplane.*
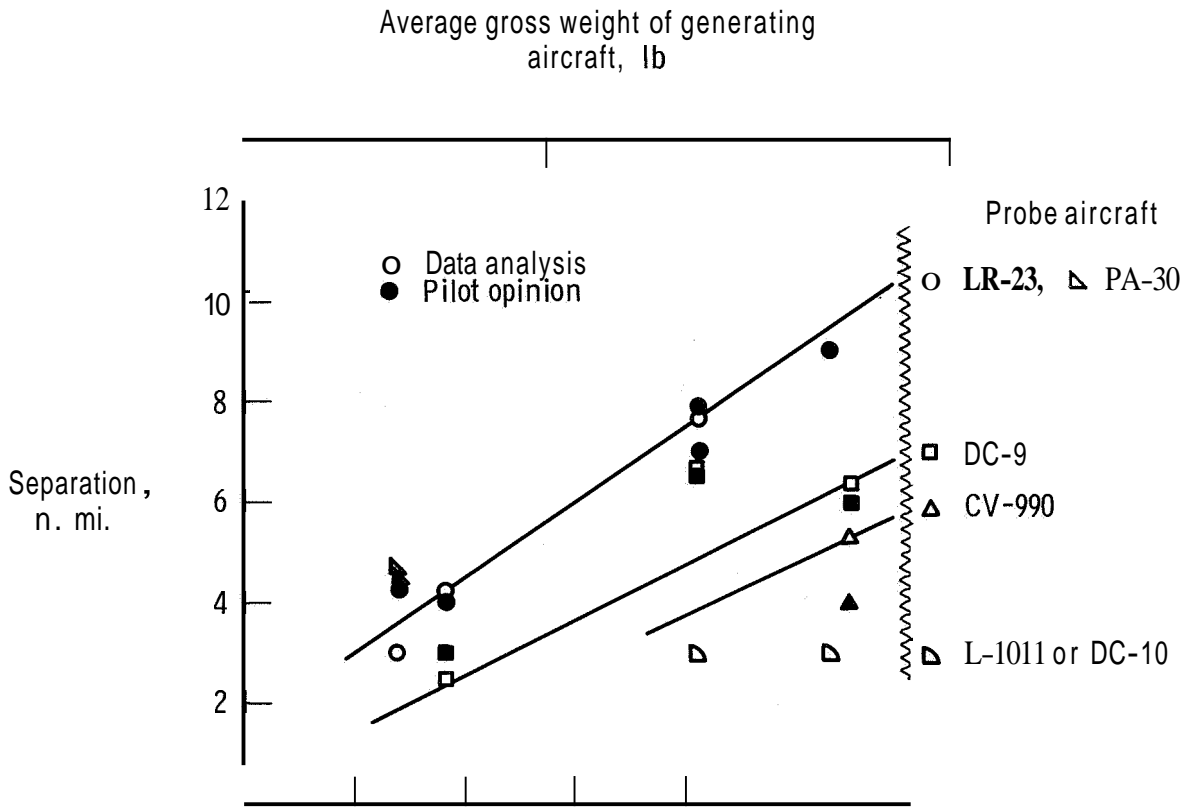
*Figure 6. Minimum separation distance based on pilot opinion and roll control criterion. Generating aircraft in Zanding configuration;* $\dfrac{|\dot{p}|_{measured}}{|\dot{p}|_{\delta_{a_{max}}}} = 1.$
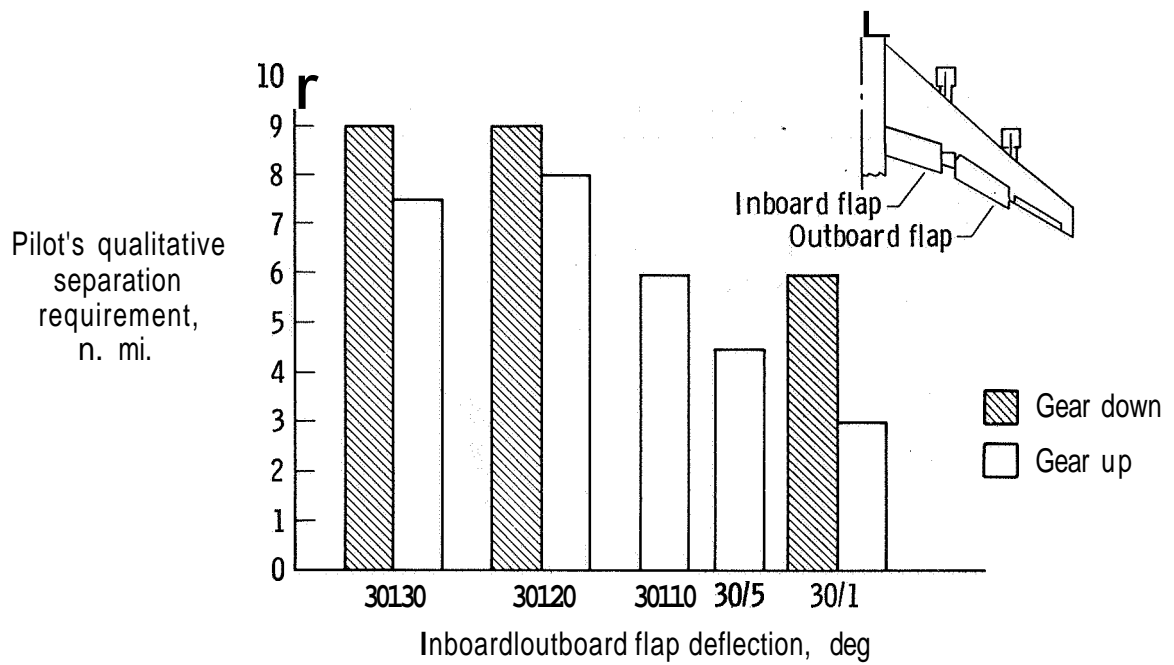
*Figure 7. Effect of outboard flap and landing gear on wake vortex alleviation. B-747 airplane; thrust for level flight.*
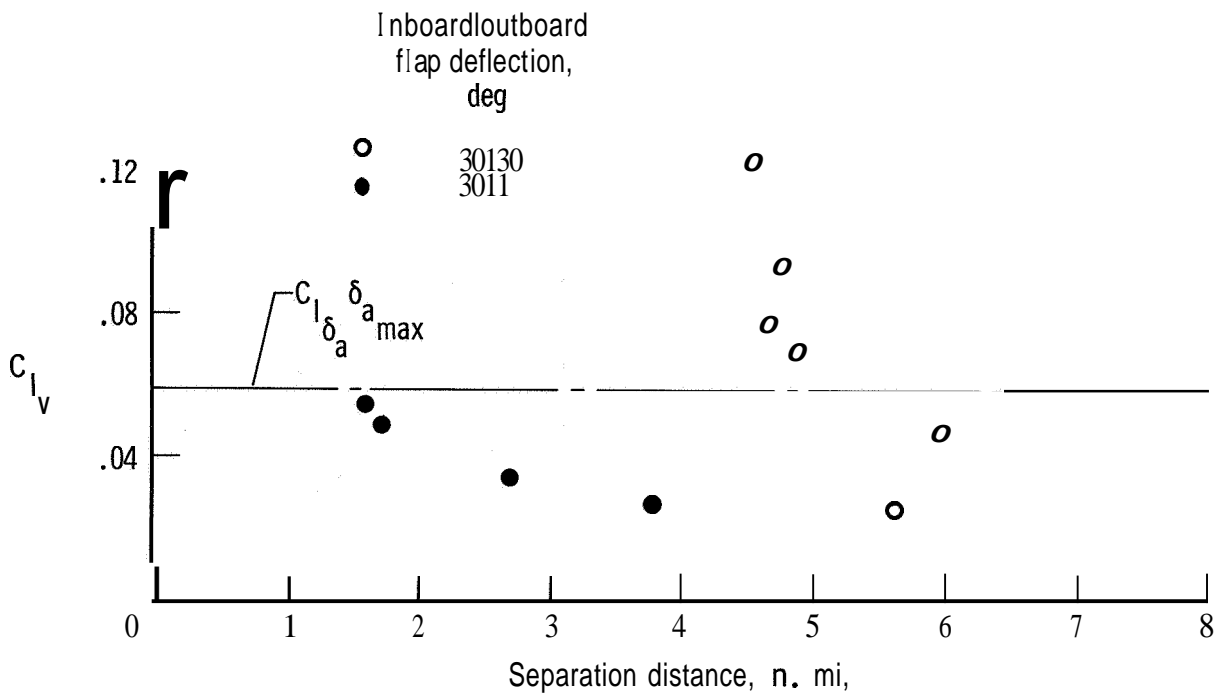
*(a) Measured by T-37B airplane. B-747 lift coefficient = 1.2.*
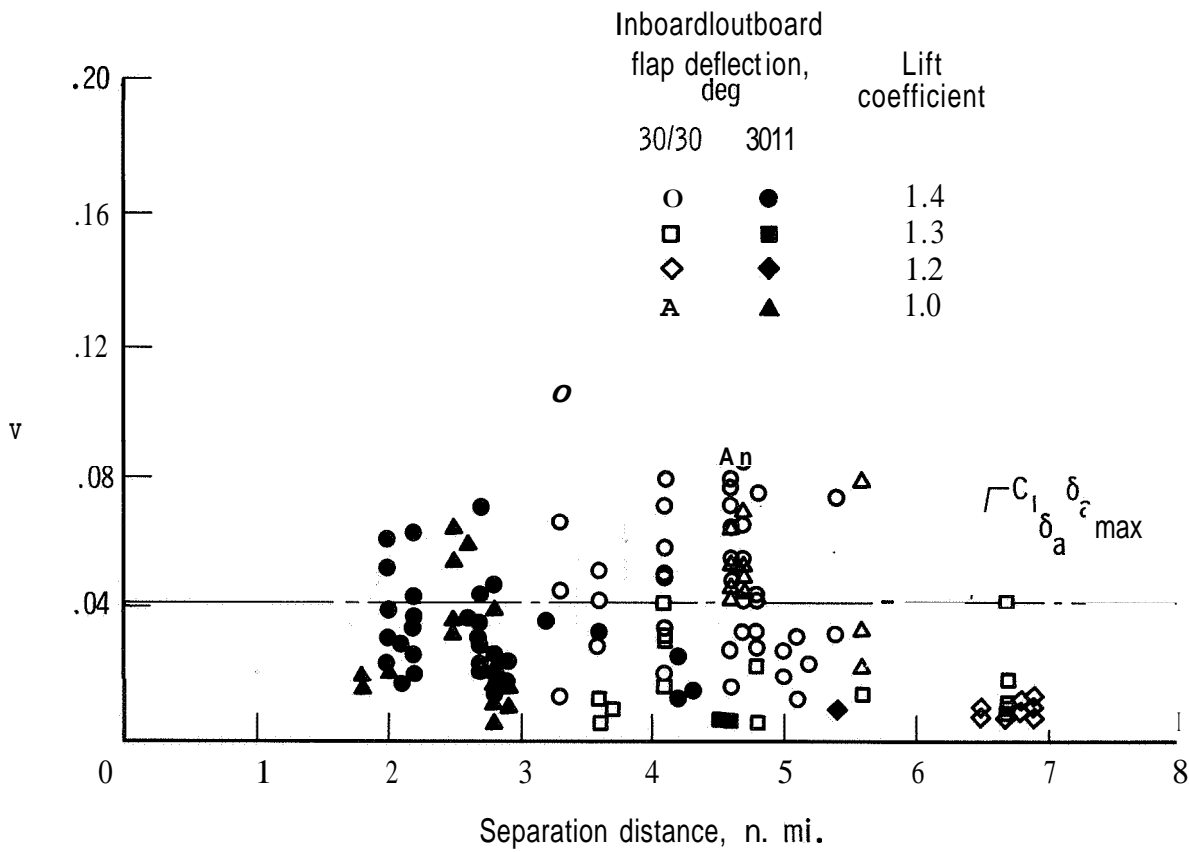


*(b) Measured by LR-23 airplane.*

*Figure 8. Effect of B-747 flap configuration on vortex-induced rolling moments. €3-747 gear up; thrust for level flight.*
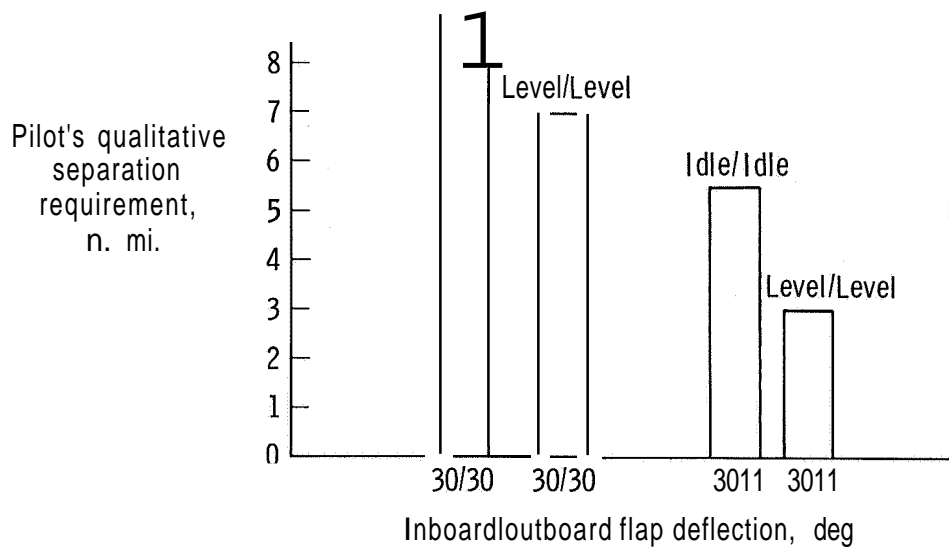
*Figure 9. Effect of thrust on wake vortex alleviation. B-747 airplane; gear up.*
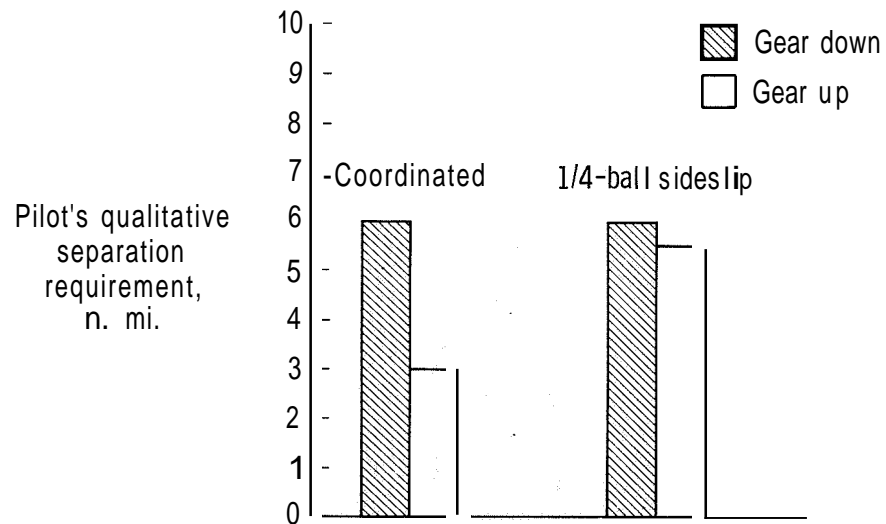


*Figure 10. Effect of sideslip on wake vortex alleviation. B-747 airplane; 30/1 flap configuration; thrust for level flight.*
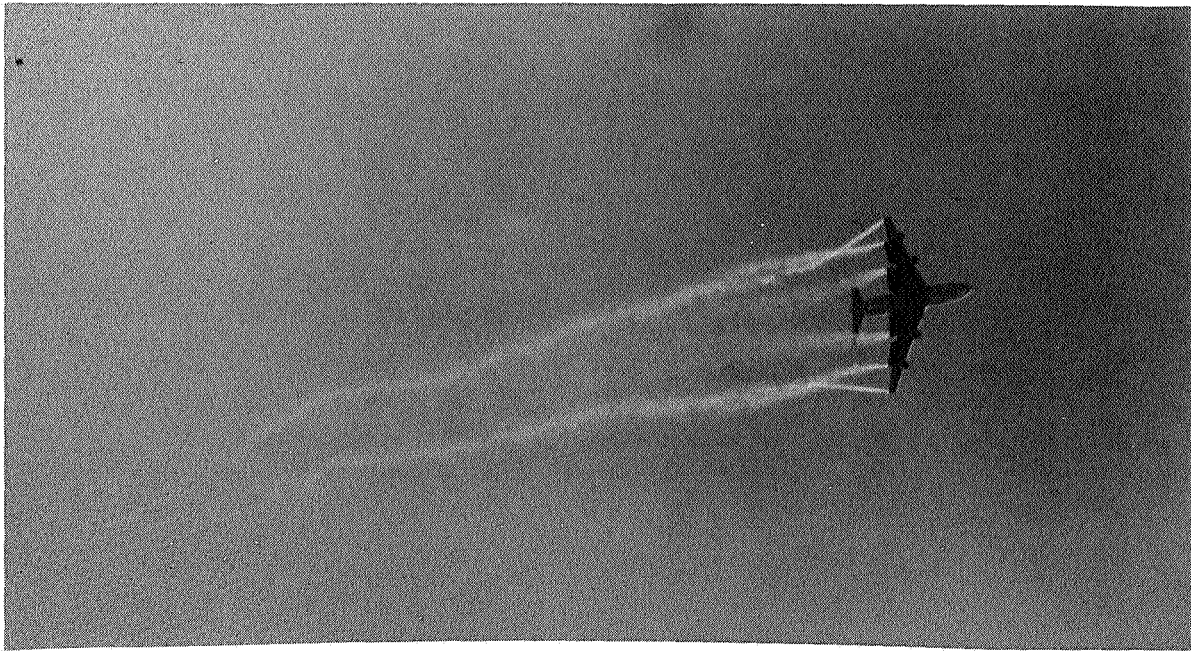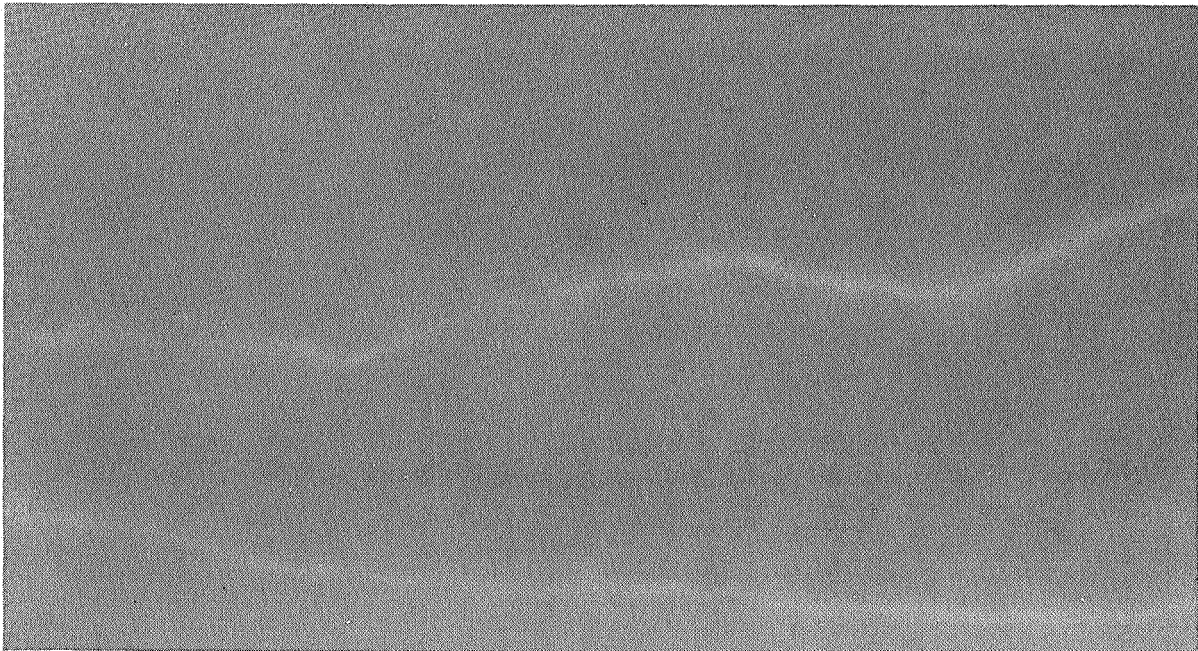
*(a) Time = 0 second.*
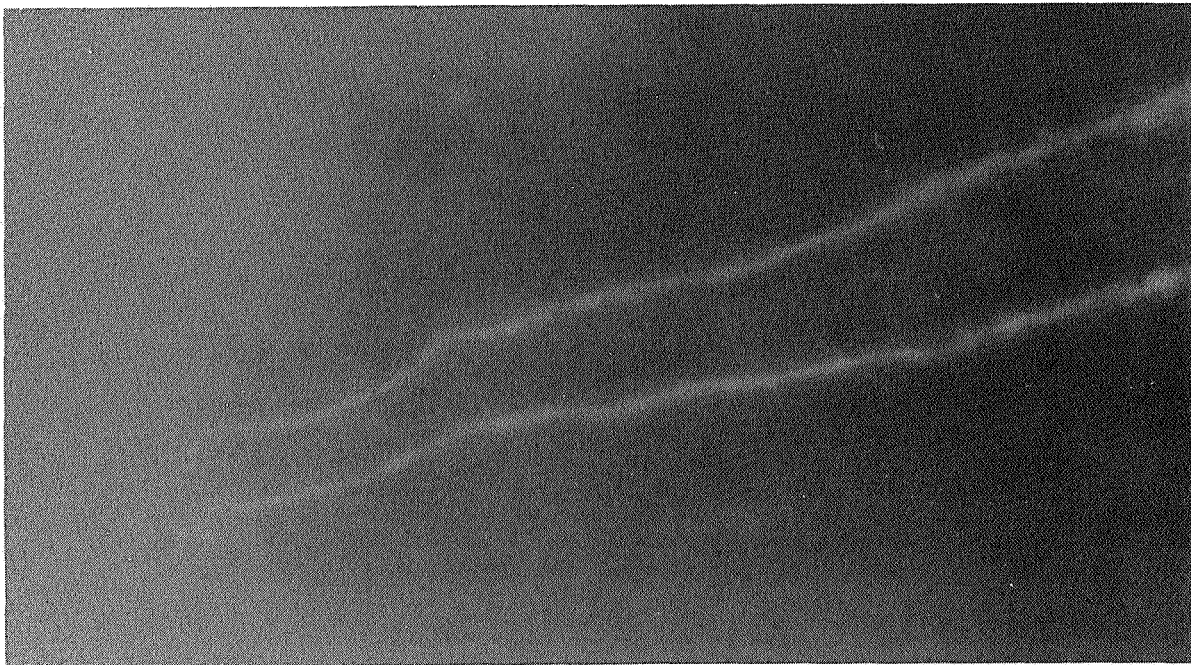


*(b) Time = 5 seconds.*

*Figure 11.* B-747 *wake vortex characteristics. 30/30 flap configuration; gear up; weight = 276,000* kg *(607,000* lb*); airspeed = 150 knots.*
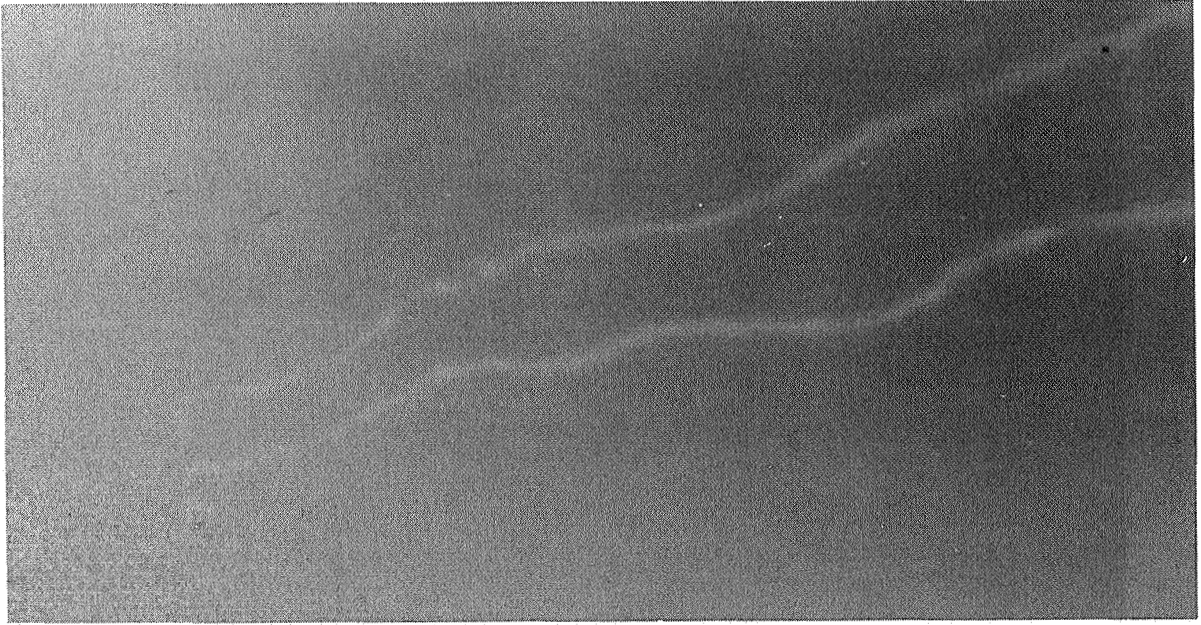
*( c )  Time = 10 seconds.*



*(d)  Time = 15 seconds.*

*Figure 11.  Continued.*
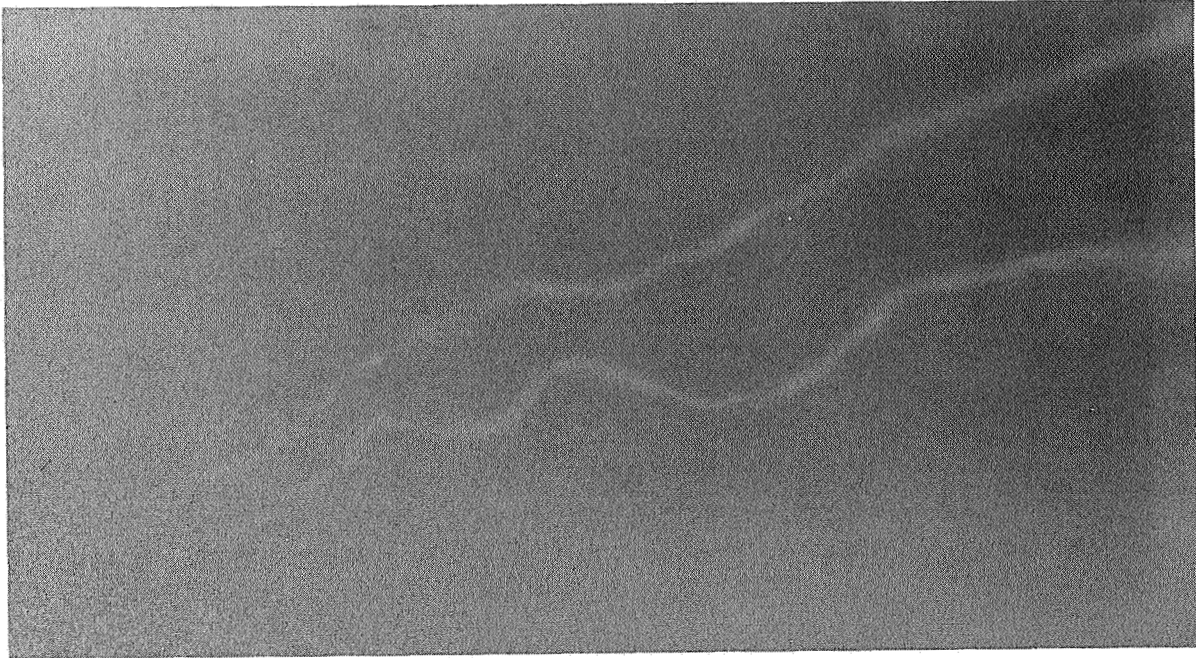
*(e) Time = 20 seconds.*
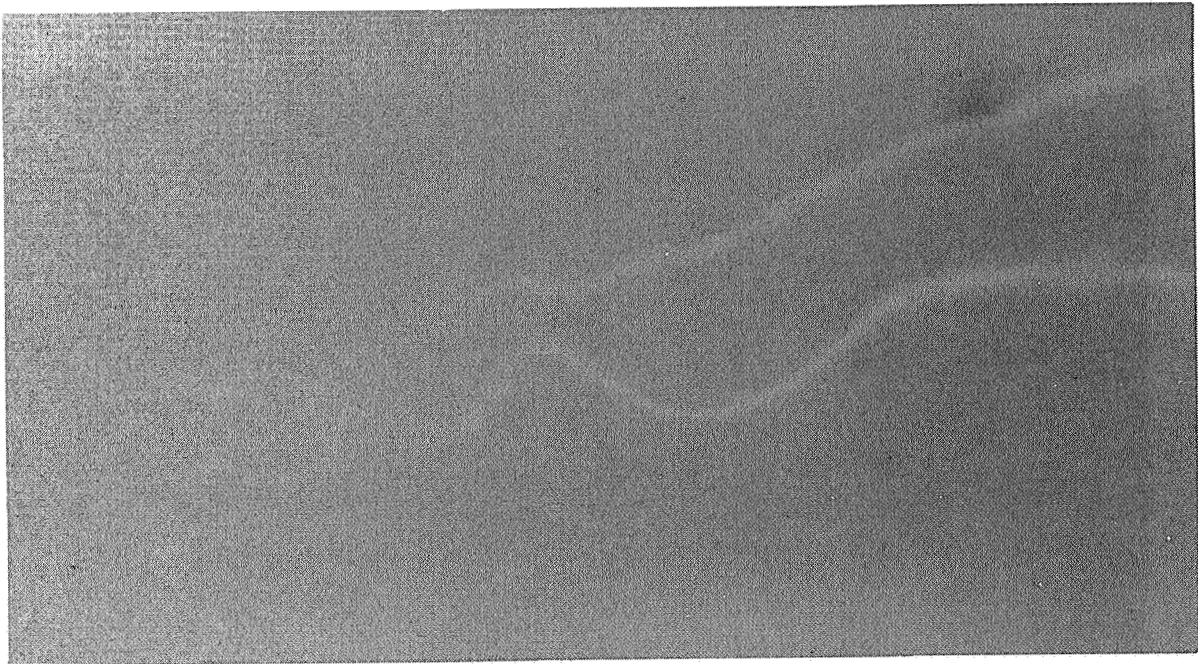


*(f) Time = 25 seconds.*

*Figure 11. Continued.*
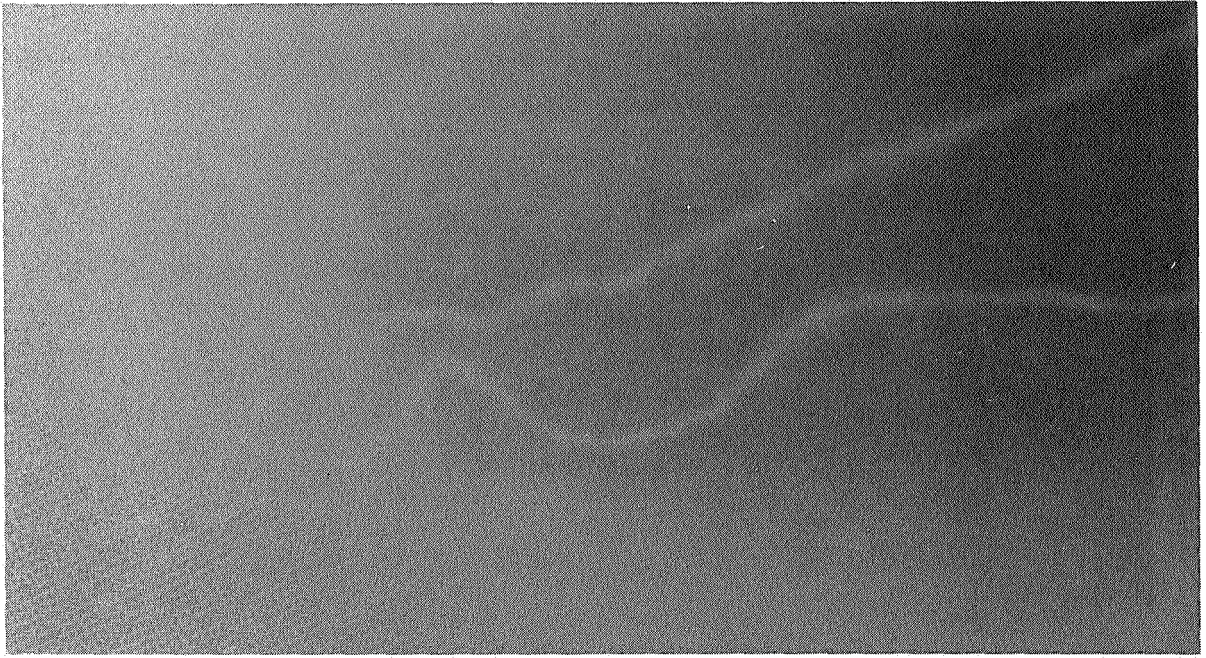
(g)  Time = **30** seconds.
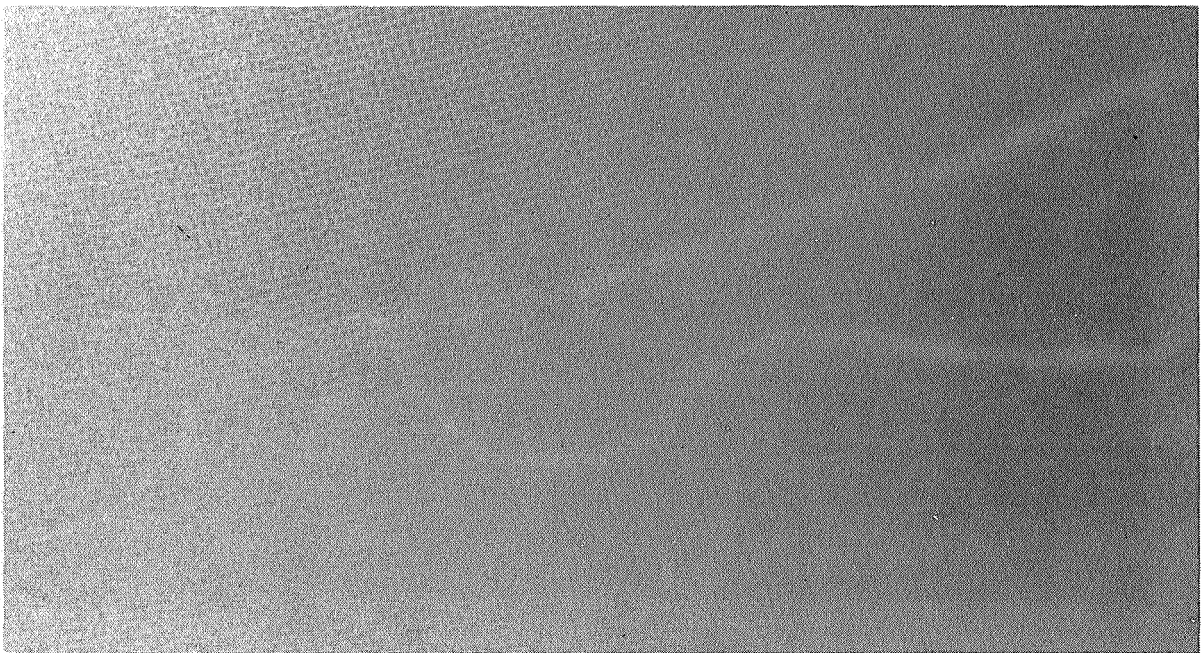


(h)  Time = **35** seconds.

Figure 11.   Continued.
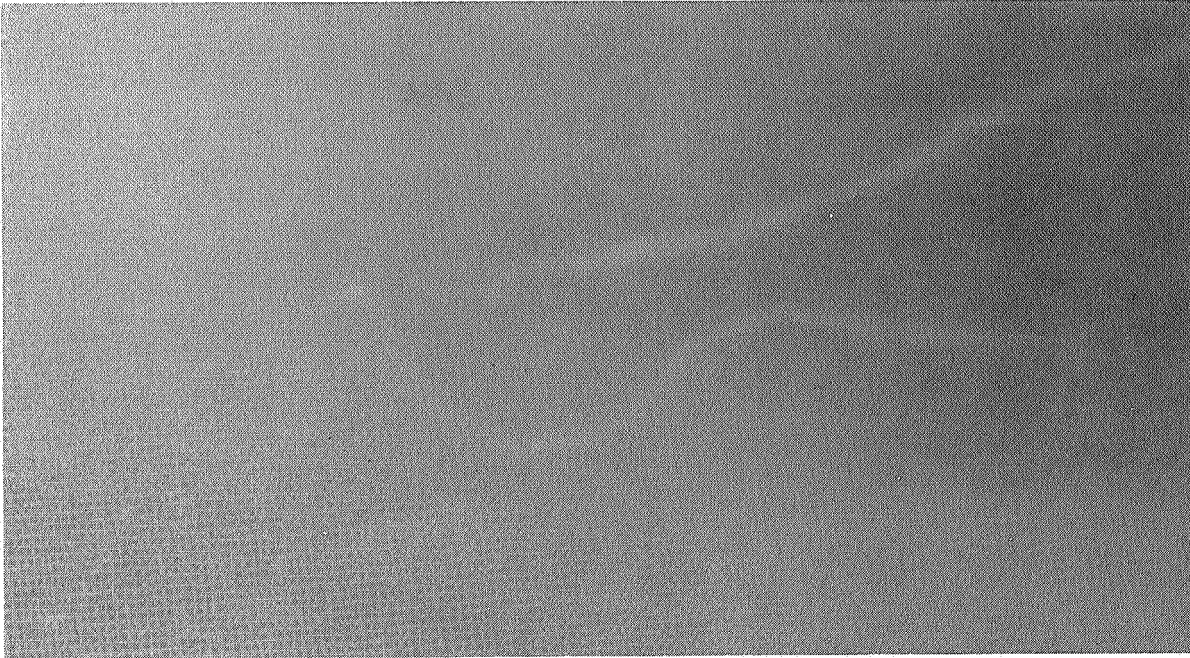
*(i)  Time = 40 seconds.*
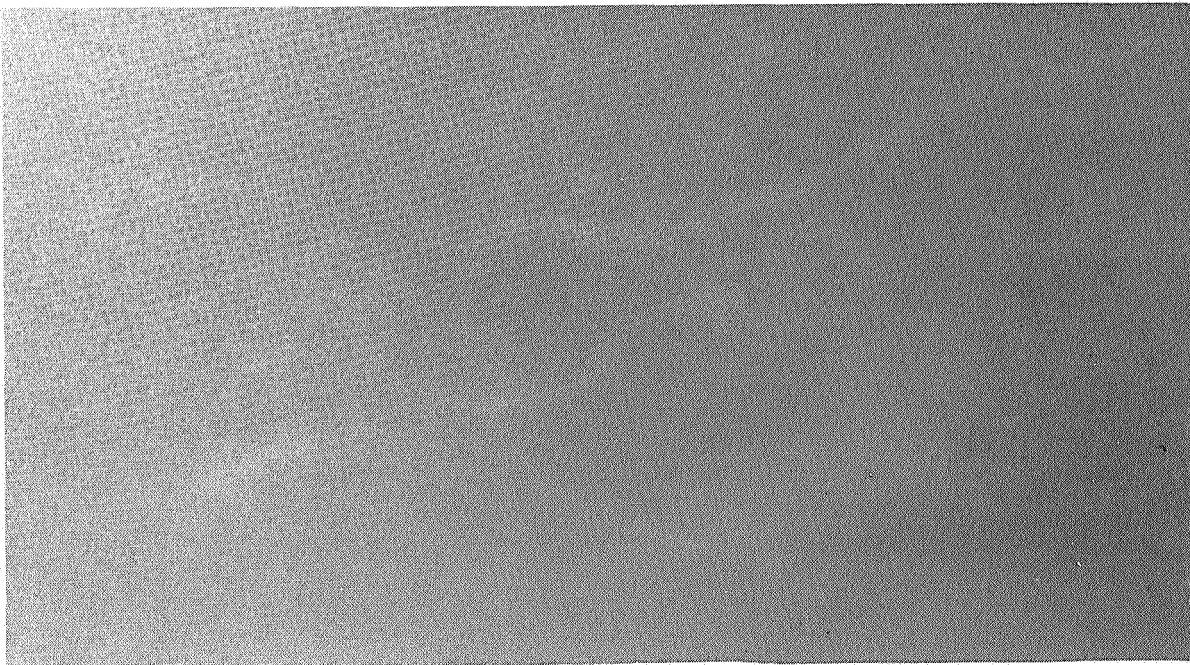


*(j)  Time = 45 seconds.*

*Figure 11.  Concluded.*
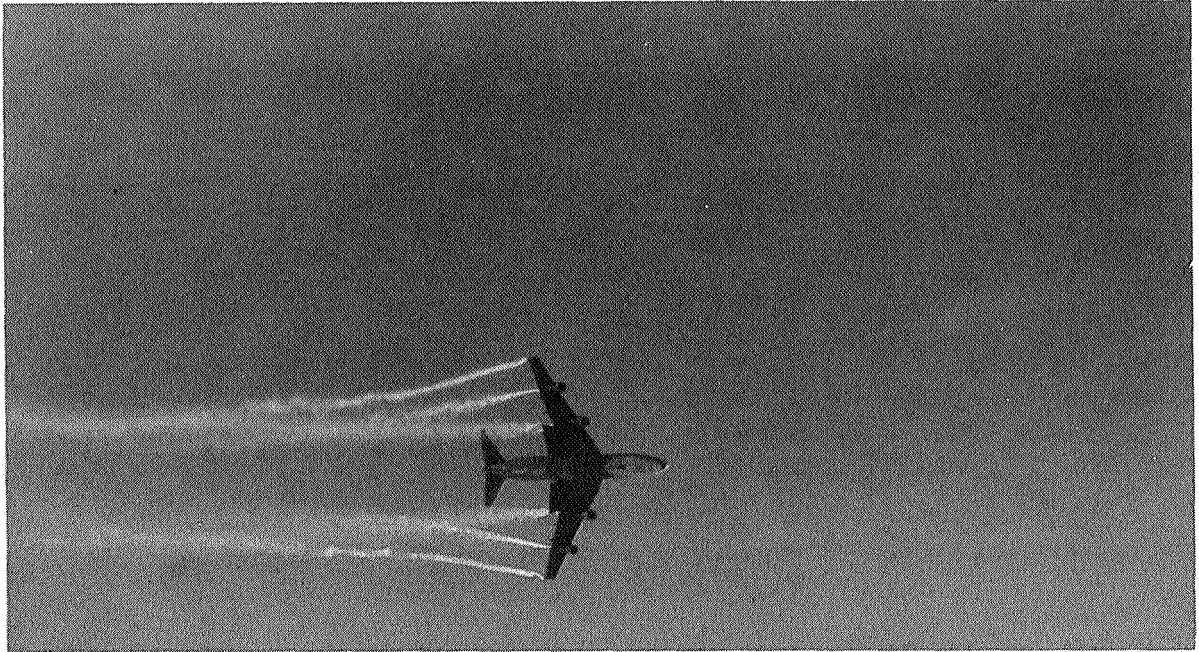
*(a)  Time = 0 second.*
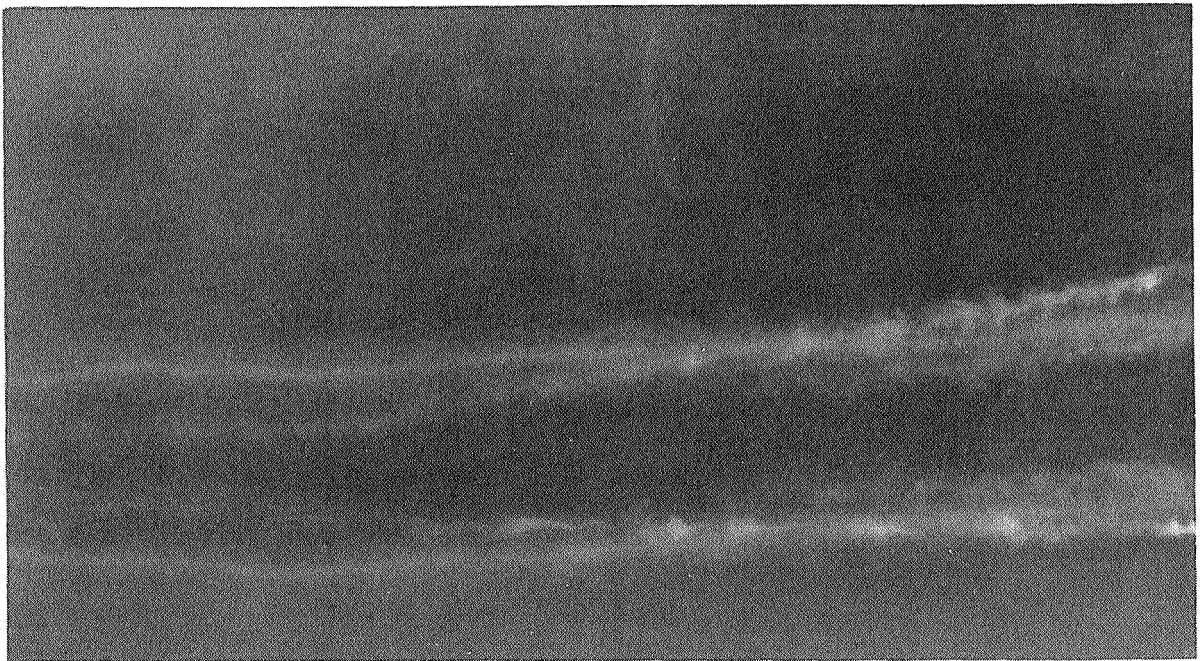


*(b)  Time = 5 seconds.*

*Figure 12.  B-747 wake vortex characteristics.   30/1 flap configuration;
gear up; weight = 263,000 kg (578,000 lb);  airspeed = 150 knots.*

(c) *Time = 10 seconds.*



(d) *Time = 15 seconds.*

**Figure** *12. Continued.*
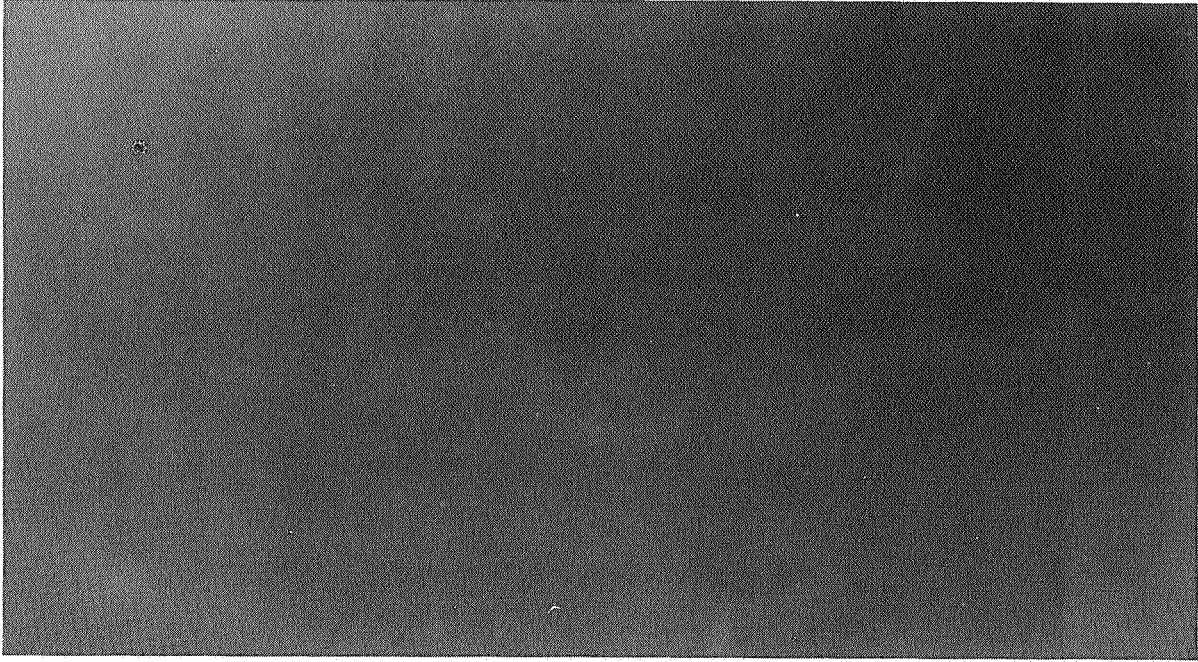
397
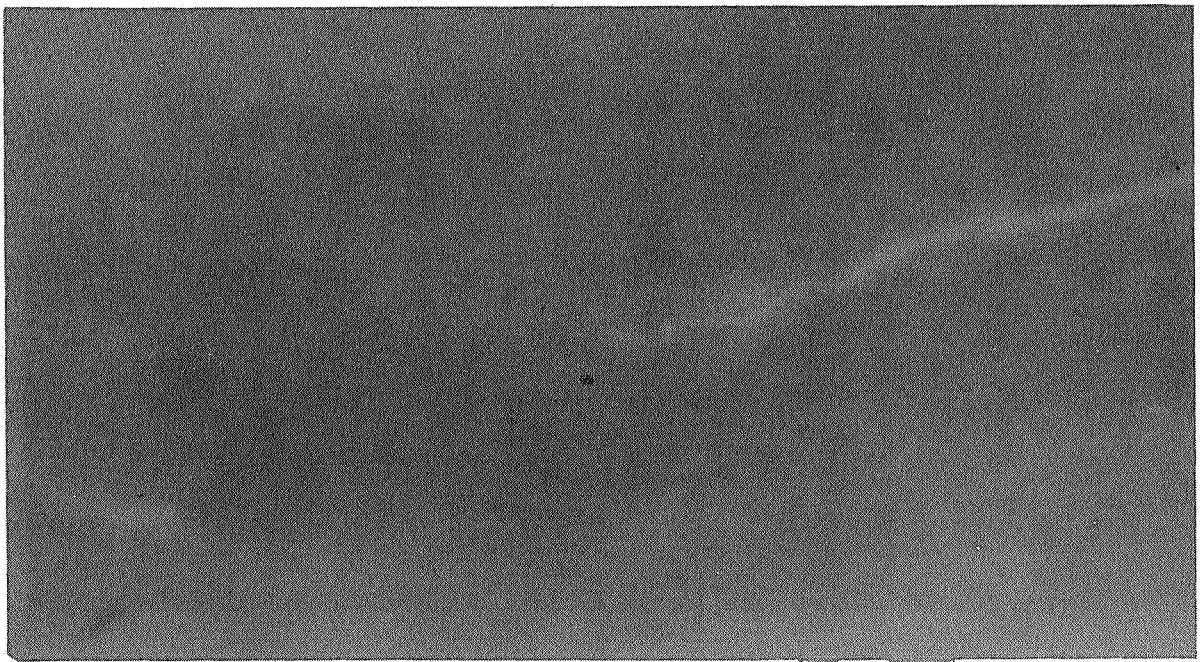
*( e )  Time = 20 seconds.*



*(f)  Time = 25 seconds.*

*Figure 12.  Continued.*

*(g)  Time = 30 seconds.*

*Figure 12.  Concluded.*

*(a) Landing gear extended.*



*(b) Landing gear retracted.*

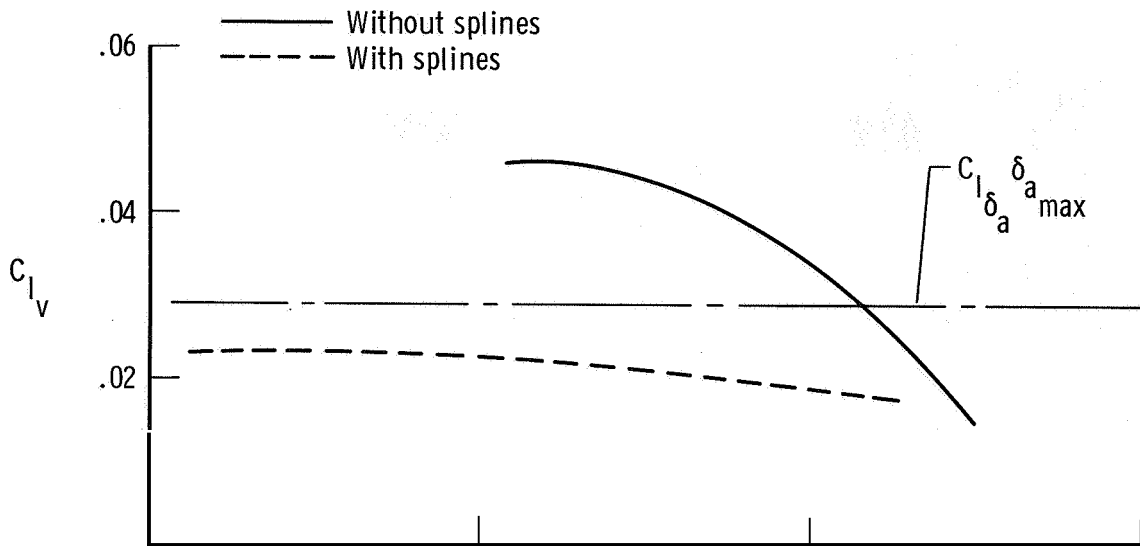*Figure 13. Effect of landing gear extension on vortex for B-747 30/1 flap configuration.*

*Figure 14. Effect of splines on vortex attenuation. C-54G generator aircraft, gear and flaps up, thrust for level flight; PA-28 probe aircraft.*
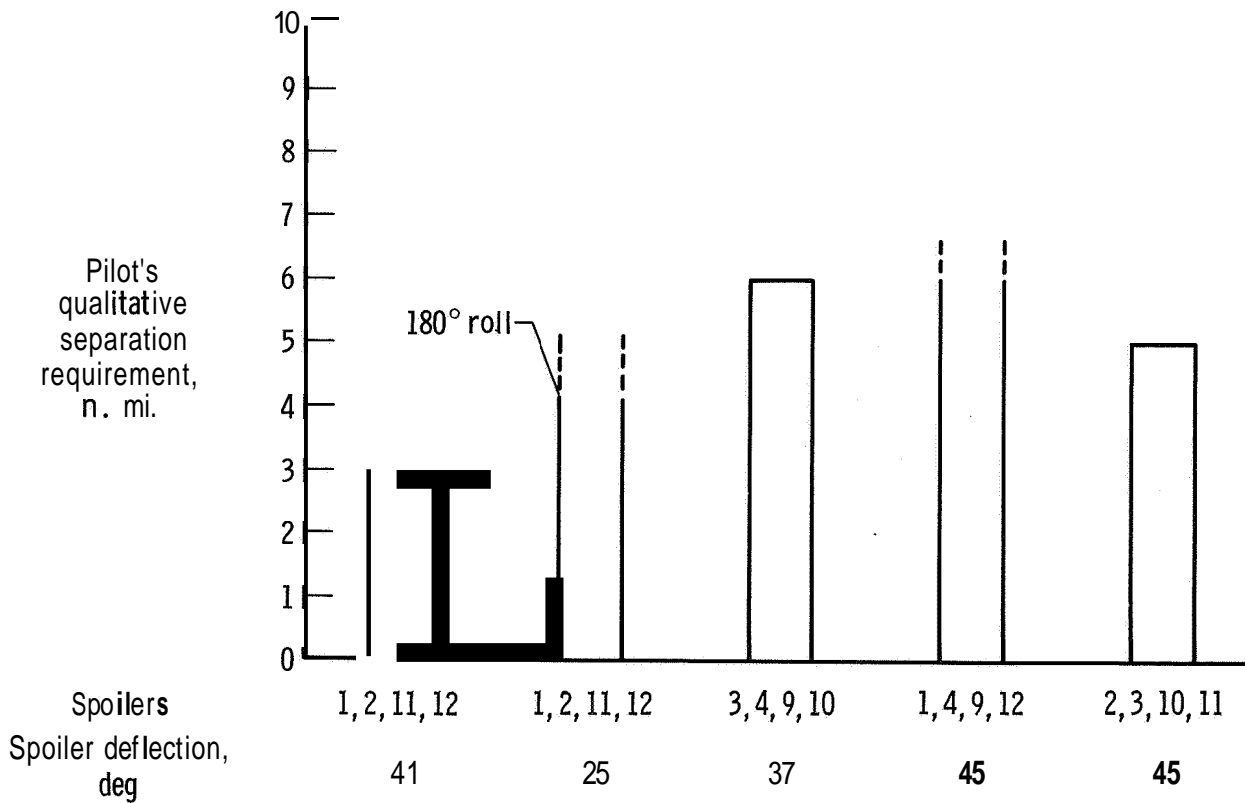


*Figure 15. Effect of spoilers on wake vortex attenuation. B-747 airplane; thrust for 3° flightpath; 30/30 flap configuration; gear down; weight ≈250,000 kg (≈550,000 lb).*

*(a) Front view.*



*(b) Rear view.*

*Figure 16.  Formation of B-747 wake vortexes.  Conventional landing configuration.*

*(a) Front view.*



*(b) Rear view.*

*Figure 17. Formation of B-747 wake vortexes. Conventional landing configuration with spoiler segments 1, 2, 11, and 12 deflected 41°.*